NASA/TM-20240008586

SUPIN: A Tool for the Aerodynamic Design and Analysis of Supersonic Inlets

John W. Slater
Glenn Research Center, Cleveland, Ohio

October 2024

NASA STI Program Report Series

Since its founding, NASA has been dedicated to the advancement of aeronautics and space science. The NASA scientific and technical information (STI) program plays a key part in helping NASA maintain this important role.

The NASA STI program operates under the auspices of the Agency Chief Information Officer. It collects, organizes, provides for archiving, and disseminates NASA's STI. The NASA STI program provides access to the NTRS Registered and its public interface, the NASA Technical Reports Server, thus providing one of the largest collections of aeronautical and space science STI in the world. Results are published in both non-NASA channels and by NASA in the NASA STI Report Series, which includes the following report types:

- TECHNICAL PUBLICATION.
  Reports of completed research or a major significant phase of research that present the results of NASA programs and include extensive data or theoretical analysis. Includes compilations of significant scientific and technical data and information deemed to be of continuing reference value. NASA counterpart of peer-reviewed formal professional papers but has less stringent limitations on manuscript length and extent of graphic presentations.

- TECHNICAL MEMORANDUM.
  Scientific and technical findings that are preliminary or of specialized interest, e.g., quick release reports, working papers, and bibliographies that contain minimal annotation. Does not contain extensive analysis.

- CONTRACTOR REPORT.
  Scientific and technical findings by NASA-sponsored contractors and grantees.

- CONFERENCE PUBLICATION.
  Collected papers from scientific and technical conferences, symposia, seminars, or other meetings sponsored or cosponsored by NASA.

- SPECIAL PUBLICATION.
  Scientific, technical, or historical information from NASA programs, projects, and missions, often concerned with subjects having substantial public interest.

- TECHNICAL TRANSLATION.
  English-language translations of foreign scientific and technical material pertinent to NASA's mission.

Specialized services also include organizing and publishing research results, distributing specialized research announcements and feeds, providing information desk and personal search support, and enabling data exchange services.

For more information about the NASA STI program, see the following:

- Access the NASA STI program home page at http://www.sti.nasa.gov

NASA/TM-20240008586

SUPIN: A Tool for the Aerodynamic Design and Analysis of Supersonic Inlets

John W. Slater
Glenn Research Center, Cleveland, Ohio

National Aeronautics and
Space Administration

Glenn Research Center
Cleveland, Ohio 44135

October 2024

This work was sponsored by the Advanced Air Vehicles Program
at the NASA Glenn Research Center.

Level of Review: This material has been technically reviewed by technical management.

This report is available in electronic form at https://www.sti.nasa.gov/ and https://ntrs.nasa.gov/

NASA STI Program/Mail Stop 050
NASA Langley Research Center
Hampton, VA 23681-2199

Contents

SUPIN: A Tool for the Aerodynamic Design and Analysis of Supersonic Inlets

John W. Slater
National Aeronautics and Space Administration
Glenn Research Center
Cleveland, Ohio 44135

Abstract

The Supersonic Inlet Design and Analysis Tool (SUPIN) is a computational program that performs geometric modeling and aerodynamic design and analysis of a set of supersonic inlets whose types include the axisymmetric pitot, three-dimensional pitot, axisymmetric, two-dimensional, two-dimensional bifurcated-duct, and streamline-traced inlets. The inlets are modeled by dividing the inlet flowpath into components that start at the freestream and ends at the engine face. The primary components of the inlet include the external supersonic diffuser, throat section, and subsonic diffuser. Each component is characterized by a set of inputs that include geometric and aerodynamic factors. Examples of the geometric factors are angles, lengths, area ratios, and coordinates that describe the geometry of the components. Examples of the aerodynamic factors are Mach numbers, flow ratios, and pressure ratios that set constraints or desired aerodynamic properties of the component. These input factors are specified within a text-based input data file that is read into SUPIN. SUPIN is a Fortran 95 program that performs the inlet design and analysis as a batch or non-interactive process. SUPIN writes output data files describing the inlet geometry and aerodynamic performance. SUPIN uses analytic, empirical, and numerical methods to perform the inlet design and analysis. The inlet geometry is constructed using planar and three-dimensional geometry constructs and is represented by coordinates, angles, areas, profiles, and surfaces. Surfaces are output in the form of a Plot3D surface grid file. SUPIN does have some capability to automatically generate planar and three-dimensional, multi-block, structured grids for computational fluid dynamics (CFD) analysis. The aerodynamic analysis performed by SUPIN computes quasi-one-dimensional properties, such as Mach numbers, pressures, and temperatures, through the inlet flowpath. Planar aerodynamic properties, such as those for shock and Mach waves, are computed for the supersonic compression of the external supersonic diffuser and throat section. The inlet performance is characterized by the inlet flow rates, total pressure recovery, and inlet drag. The primary intent of this document is to describe the usage of SUPIN. The methods used within SUPIN are documented and may serve as a useful reference for understanding the aerodynamic design and analysis of supersonic inlets.

Nomenclature

Roman Symbols

a	Acoustic speed; semi-major axis length
A	Area
AR	Aspect ratio
b	Semi-minor axis length
c	Acoustic speed for method-of-characteristics equations
C_D	Drag coefficient
C_p	Pressure coefficient
CR	Contraction Ratio
d	Distance
D	Diameter; drag
D_{ref}	Reference dimension used for normalization of several inlet dimensions (ft)
e	Specific internal energy
F, f	Factor; constant; input
g	Gravitational constant, $g = 32.174 \frac{lbm\ ft}{lbf\ s^2}$
h	Height or altitude; specific enthalpy
H	Height
i, j, k	Indices
K	Flag or constant
L	Length
M	Mach number; mode for four-point NURBS
N	Number; amount; normal
p	Static pressure; shape parameter for a super-ellipse
q	Dynamic pressure
Q	Bleed sonic coefficient; heat transfer
r	Radius
R	Gas constant, air $R = 1716.246 \frac{lbf-ft}{slug\ \ {}^{\circ}R}$
s	Specific entropy
T	Temperature
u,v,w	Velocity components
V	Velocity magnitude
w	Width
W	Flow rate
WR	Flow ratio
X,Y,Z	Coordinates in planar coordinate system
x,y,z	Cartesian coordinate for inlet global coordinate system

Greek Symbols

α	Angle-of-incidence
β	Angle-of-sideslip; shock angle; wave angle
δ	Total pressure ratio; boundary-layer thickness; deflection
μ	Mach angle
ξ	Circumferential angle along streamline-traced inlet leading edge
η_C	Adiabatic compression efficiency
η_{KE}	Kinetic energy efficiency
υ	Prandtl-Meyer function
Δ	Increment
ρ	Static density
π	Pi
γ	Ratio of specific heats, $\gamma = 1.4$ for air
Γ	Gamma function
ϕ	Flow function; circumferential angle
Φ	Bleed region porosity
ψ	Stream function; static temperature ratio
θ	Total temperature ratio; surface angle; streamwise angle; ray angle

Subscripts

0	Freestream or reference conditions
1	Cowl lip station
2	Engine face
C	Corrected flow rate for sea level conditions=
b	Bleed
B	Boundary
bang	Bleed hole incidence angle
bbeg	Beginning of a bleed region
BEF	Bottom of engine face
bend	End of a bleed region
bexit	Bleed exit property
bext	Bleed spatial extent
bleed	Bleed flows
bloc	Bleed location within the inlet
bot	Bottom entity
bplen	Bleed plenum
bpor	Bleed porosity
breg	Bleed region
bseg	Bleed segment
btyp	Type of bleed region
bypass	Bypass flows
cap	Capture

cb	Centerbody
cbsh	Centerbody shoulder
cbsha	Start of the centerbody shoulder
cbshb	End of the centerbody shoulder
clex	Cowl lip exterior
clflow	Flow property at the cowl lip
clin	Cowl lip interior
clip	Cowl lip
comt	Component
CP	Calorically perfect gas
cps	Control points
cw	Cowl
cwex	Cowl exterior
δ	Property at edge of the boundary layer
DS	Downstream of a terminal shock wave
EF	Engine face
eff	Effective
ent	Entity
eq	Equivalent
EX	End of the external supersonic compression
exd	External supersonic diffuser
exit	Exit property, such as bleed plenum exit
g	Geometric
HEF	Hub of the engine face
hub	Hub property
IN	End of the internal supersonic compression
int	Internal
k	Index for row of total pressure engine-face rake
L	Local; length
max	Maximum value
min	Minimum value
nose	Nose
N	Normal
NS	Conditions downstream of a normal shock or terminal shock structure
other	Other flows
p	Property is evaluated at constant pressure
prp	Property
r	Radial direction
ref	Reference
region	Property of a region
sd	Subsonic diffuser
SD	Start of the subsonic diffuser
sh	Shoulder

sonic	Sonic conditions ($M = 1$)
spillage	Spillage
spin	Spinner
SSL	Standard Sea Level
stbot	Bottom of cross-section of a streamline-traced inlet
stcl	Cowl lip profile for the streamline-traced inlet
stex	Streamline-traced supersonic diffuser exit
stgs	Stages of the external supersonic diffuser
stle	Leading edge of a streamline-traced inlet
stsh	Shoulder of the streamline-traced inlet
sttop	Top of cross-section of a streamline-traced inlet
strunc	Truncation of the streamline-traced supersonic diffuser
subd	Subsonic diffuser
sub	Subsonic
TC	Coordinate of minimum area on cowl lip interior
TEF	Top of engine face
TH	Station for the geometric throat of the inlet
top	Top entity
thrt	Throat section
TP	Thermally perfect gas
t	Total or stagnation conditions
thrt	Throat section
typ	Type of inlet
v	Property is evaluated at constant volume
var	Variation
wid	Width
x	Axial direction
y	Transverse direction

1.0 Introduction

This document describes the methods and usage of the NASA Supersonic Inlet Design and Analysis (SUPIN) computational tool developed at the NASA John H. Glenn Research Center. This document also presents some of the basic features of inlets and aspects of the aerodynamic design and analysis of inlets. Several key terms and phrases are denoted in ***bold italics***. This introductory section starts with a discussion of the role of the inlet within the air-breathing propulsion system for an aircraft in Subsection 1.1. Subsections 1.3 to 1.5 presents a historical overview of various inlets and their application in aircraft over the last eighty years. The historical overview starts with a look at pitot inlets for subsonic jet aircraft and continues with external and mixed-compression inlets for supersonic and hypersonic aircraft. Subsection 1.7 provides an overview of SUPIN. Subsection 1.7 provides a roadmap for the contents of the remainder of this document.

1.1 Role of the Inlet

The ***inlet*** is the component of an ***airbreathing propulsion system*** for an ***aircraft*** through which the air enters the propulsion system. The other two major components of the propulsion system are the ***engine*** and ***nozzle***. The inlet captures airflow and ducts the airflow to the engine where fuel is mixed with the airflow and combustion is performed. The choice of engines for an airbreathing propulsion system include ***turbojet***, ***turbofan***, ***turbo-ramjet***, ***ramjet***, and ***scramjet engines***. The combusted airflow/fuel mixture then leaves the engine and enters the nozzle which forms an exhaust jet that is expelled to provide ***thrust*** for the aircraft. The inlet, engine, and nozzle work together as a system to perform a ***thermodynamic cycle*** involving compression, heat addition, and expansion in which the air is the working fluid and thrust is produced. Reference 1 provides a basic discussion of propulsion cycle analysis. Reference 2 provides an intermediate discussion of propulsion systems.

The aerodynamic design and analysis of an inlet depend on 1) the state of the flow presented to the inlet and 2) the demands of the engine for which the inlet provides the airflow. The general ***inlet design and analysis problem*** can be stated as designing and performing aerodynamic analysis of an inlet that takes in airflow at a certain state and delivers the airflow to the engine at a desired state. The state of the airflow approaching the inlet can be considered the ***upstream boundary condition*** for the inlet design and analysis problem. The desired state of the airflow for the engine can be considered the ***downstream boundary condition*** for the inlet design and analysis problem. The state of the airflow approaching the inlet and the desired state of the airflow for the engine are established by the ***mission*** of the aircraft.

1.1.1 Aircraft Mission

An aircraft is designed to perform a certain ***aircraft mission***. A list below discusses several generic aircraft missions. An ***aircraft mission profile*** can be established which precisely defines the consecutive ***phases of the mission***. Examples of the phases include take-off, climb, cruise, descent, and landing. The junctures at the start and end of each phase of the mission profile are designated with numbers starting with 1 at the start of the mission and incrementing by one until the end of the mission. One or more key junctures or phases along the mission are selected as conditions for which the aircraft and propulsion system are to be designed and analyzed. These key junctures or phases are referred to as the ***design points*** or ***reference points***. However, the aircraft and propulsion system are required to perform in an acceptable and stable manner throughout the mission at all ***operating points***. Reference 3 provides an introduction to aircraft design. References 3 and 4 provide further information regarding the aircraft mission.

The mission profile establishes the altitude, speed, and attitude at which the aircraft is to operate. These specifications establish the kinetic and thermodynamic properties of the flow approaching the aircraft, which is referred to as the ***freestream***. The kinetic properties are the speed and orientation of the freestream flow. In the reference frame of the aircraft, the speed of the freestream flow approaching the aircraft is equal to the speed of the aircraft. The thermodynamic properties of the freestream are established from the altitude of the aircraft. The discussions of this document consider inlets for aircraft operating from subsonic through the hypersonic speed range. A limit of Mach 5 is imposed on the discussions so as not to consider very high temperature effects associated with dissociation of air molecules. Reference 5 provides further information on propulsion systems for hypersonic vehicles.

The manner of the integration of the propulsion system with the aircraft may result in the freestream flow interacting with the forward portions of the aircraft prior to encountering the start of the inlet. This portion of the flow is referred to as the ***approach flow***. The interactions of the approach flow with the aircraft can change the flow properties as they approach the start of the inlet. The state of the flow at the start of the inlet is referred to as the ***approach flow conditions***. The ***location of the start of the inlet*** within the aircraft is established based on such considerations as aircraft weight distribution, aerodynamic shielding of the inlet, and flow features of the approach flow. The approach flow conditions and the location of the start of the inlet form the ***upstream boundary conditions*** for the inlet design and analysis problem.

Several general types of aircraft missions of interest in this document are summarized in the list below:

- ***Transport Mission***. This mission involves delivery of passengers and cargo over a desired range and can involve both commercial and military aircraft. The aircraft has a conventional take-off and landing from a runway. The climb and descent occur rather gradually, and the aircraft is not expected to experience high rates of maneuvering. Most of the mission is spent cruising at a certain speed and altitude. The propulsion system likely uses turbojet or turbofan engines and is designed to provide high levels of efficiency at the cruise condition while providing the necessary thrust at take-off and climb.
- ***Attack Mission***. This mission involves military aircraft expected to engage a target. The aircraft has a conventional take-off and landing from a runway and is expected to experience high rates of acceleration and maneuvering as it engages a target. The propulsion system likely involves turbojet and turbofan engines but could involve the use of ramjets. The propulsion system is designed for robustness to operate at the extreme conditions while providing thrust at all operating conditions.
- ***Missile Mission***. This mission is similar to the attack mission in that the aircraft engages a target and can experience high rates of maneuvering. A difference is that the missile is expected to be air-launched from a parent aircraft or boosted to a take-over speed by a solid rocket. While the propulsion system is also designed for robustness, requirements for simplicity of the propulsion system also influences its design. The propulsion system can involve turbojet, turbofan, and ramjet engines.
- ***Accelerator Mission***. This mission involves an aircraft expected to have a conventional take off from a runway, but then performs continuous acceleration to a certain hypersonic speed (e.g., Mach 6+) at which point the aircraft releases a payload or cruises. The aircraft then performs a deceleration and conventional landing onto a runway. The design of the propulsion system involves considerable adaptability and may involve variable geometry and combined-cycle systems that include turbojet or turbofan engines combined with ramjet or scramjet engines.

1.1.2 Engines

A list of possible engine types was presented above. The choice of the type of engine to use for the propulsion system depends mainly on the desired speed of the aircraft and requirements for thrust over the mission. The general complexity and high cost of the development of an engine usually means that the engine and its characteristics are specified as part of the inlet design and analysis problem.

The interface between the end of the inlet and the start of the engine is the ***engine face***, which is typically defined on a plane. The ***engine face shape*** and ***engine face dimensions*** are provided from the dimensions of the specified engine. Further details on the engine face shapes and dimensions will be provided in Subsection 4.13. The ***engine face flow rate*** is the rate of airflow through the engine face and is specified at points within the aircraft mission by the level of thrust required to be generated by the propulsion system. Within an aircraft, the thrust is controlled by the pilot or control system moving the throttle. The location of the engine within the aircraft is based on such considerations as aircraft weight distribution, engine size, and the direction of the thrust. Thus, the ***engine face location*** is also specified as part of the inlet design and analysis problem. Thus, the engine face shape, dimensions, location, and flow rate form the ***downstream boundary conditions*** for the inlet design and analysis problem.

The types of engines and their general characteristics are summarized as:

- ***Turbojet Engine***. A turbojet engine features a centrifugal or axial compressor, combustor, and turbines. The compressor performs the mechanical compression for the propulsion cycle. The combustor burns fuel at low subsonic and high-pressure airflow conditions. The turbines extract energy to drive the compressor while performing some expansion. The outflow of the turbines is delivered to the nozzle. A turbojet has found application for aircraft approaching Mach 3, but its efficiency drops considerably as it reaches this speed. Further, temperatures become high and reach limits for the materials of the compressor. The engine face is at the plane of the start of the compressor and has a circular shape.
- ***Turbofan Engine***. A turbofan engine has an axial compressor, combustor, and turbines at its core, but the turbines also drive a fan that accelerates airflow that bypasses the core engine. The bypass ratio indicates the ratio of flow through the fans to that flowing through the core engine. The use of the fan increases propulsive efficiency. The turbofan may continue operation up to speeds approaching Mach 3, but the efficiency and limits are similar to that of the turbojet. The engine face is at the plane of the start of the fan and has a circular shape.
- ***Ramjet Engine***. A ramjet engine uses the momentum of the approaching airflow to perform kinetic compression to the subsonic conditions required for the combustor. Thus, the ramjet engine does not require mechanical compression, and so, does not need turbines. The subsonic outflow of the combustor is delivered directly to the nozzle. While the ram effect is possible at high-subsonic conditions, it is less efficient than the turbojet and turbofan. The ramjet finds it best operation between Mach 3 and 6. The ramjet engine offers simplicity but requires some other means to get the engine to the take-over conditions for the starting of the ramjet engine. The engine face is at the start of the combustor. While a combustor with a circular cross-section provides structural benefits, the engine face could also be elliptical, rectangular, or a more general cross-section.
- ***Scramjet Engine***. A scramjet (i.e., supersonic combustion ramjet) engine is much like the ramjet; however, the compression does not decelerate the flow to subsonic conditions and the combustion is performed within the combustor at supersonic conditions. The outflow of the combustor remains at supersonic conditions for delivery to the nozzle. As with the ramjet engine, the engine face can take of variety of cross-sectional shapes.

- ***Rocket Engine***. A rocket engine involves the combustion of an oxidizer carried by the aircraft, and therefore no inlet is required. Its mention here is to provide completeness for a later discussion of air-breathing propulsion systems that include a rocket engine.

A ***combined-cycle engine*** combines types of engines into an overall air-breathing propulsion system. Some types of combined-cycle engines include:

- ***Turbo-Ramjet Engine***. A turbo-ramjet combines a turbojet or turbofan engine with a ramjet engine. The turbine operates at subsonic and low supersonic Mach numbers but is then augmented by a ramjet flowpath upon reaching a higher supersonic Mach numbers, such as Mach 2.5. In ramjet mode, flow bypasses the core of the turbine engine to be dumped into an augmenter or ramjet combustion chamber.
- ***Dual-Mode Ramjet / Scramjet (DMRJ) Engine***. A DMRJ engine can start operation as a ramjet engine, but then as flight speeds increase, the engine operates as a scramjet.
- ***Turbine-Based Combined-Cycle (TBCC) Engine***. A TBCC engine features separate flowpaths: one providing airflow to a turbojet or turbofan engine and one providing airflow to a DMRJ engine. Common arrangements involve one flowpath over the other or side-by-side.
- ***Rocket-Based Combined-Cycle (RBCC) Engine***. A RBCC engine involves a rocket engine providing a propulsive jet within the engine flowpath. The propulsive jet provides thrust to supersonic speeds at which the air-breathing flowpath can then operate as a DMRJ engine. The engine face of an inlet for a RBCC can take a variety of shapes since a mechanical compressor is not involved. A likely engine face shape could be annular with the rocket motor placed at the inner diameter of the cross-section.

The turbojet and turbofan engines use a mechanical compressor powered by a shaft driven by the turbine. When the throttle of a turbojet or turbofan engine is increased, more fuel is delivered to the combustor and the compressor turns more rapidly. This creates a greater flowrate through the compressor that lowers the pressure at the engine face. The opposite occurs if the throttle is reduced. That is the engine face flowrate decreases and the static pressure at the engine face increases.

The ramjet and scramjet engines don't use a mechanical compressor, and so, the engine face interfaces the start of the combustor. When the throttle of a ramjet or scramjet engine is increased, more fuel is injected into the combustor and there is greater combustion. This increases the pressure within the combustor, and so, increases the pressure at the engine face. As the throttle is reduced, less fuel is injected and the pressures in the combustor are reduced. This behavior is opposite than that for the turbojet or turbofan.

References 4 and 5 provide further information on the design and analysis of engines.

1.2 Summary of the Inlet Design and Analysis Problem

The inlet design and analysis problem can be summarized as the design and analysis an inlet for the upstream boundary conditions consisting of the approach flow conditions and location of the start of the inlet and the downstream boundary conditions consisting of the engine face shape, dimensions, location, and flow rate. For the upstream and downstream boundary conditions, an inlet should provide high-quality flow at the design points and acceptable flow at ***off-design conditions***. At all operating points along the aircraft mission profile, the inlet should operate in a stable manner to provide the necessary flow to the engine. The inlet should be designed to be as simple as necessary to provide for robust operation. The inlet size should be minimized to reduce weight of the inlet and aircraft. The considerations of inlet drag should be balanced with the improvements of internal aerodynamic performance. The remainder of the document will provide further details on the inlet performance metrics. References 6 and 7 provide further information on inlet design and analysis.

1.3 Subsonic Pitot Inlets

The development of early jet aircraft during the late 1930's and 1940's addressed military needs for higher subsonic speeds in fighter, attack, and bomber aircraft. In the 1930's the turbojet engine was developed in the United Kingdom and Germany and provided thrust for such aircraft as the Gloster Meteor in the United Kingdom and the Messerschmitt Me 262 in Germany, which is shown in the left image of Figure 1.1. The Me 262 used two turbojet engines with each engine mounted beneath each wing. The inlets and nozzles were in-line with the axes of each engine. The inlet protruded ahead of the leading edge of the wing and the nozzle extended past the trailing edge of the wing. The Gloster Meteor similarly used two engines, but the engines were mounted within the wing. This type of installation of the propulsion system provided airflow to the engine that was largely undisturbed by the forward fuselage of the aircraft. The inlets of both aircraft had a nearly circular ***aperture*** or ***capture cross-section*** that was approximately perpendicular to the incoming airflow. Such an inlet is referred to as a ***pitot inlet*** because it operates much like pitot probes traditionally used to measure air speed. The trace of the perimeter of the inlet aperture is called the ***inlet highlight*** (Ref. 6). The area bounded by the inlet highlight is the ***inlet capture area*** referring to the main task of the inlet, which is to capture airflow and deliver it to the engine. The inlets for both aircraft had a short diffusing duct leading to the interface between the inlet and the engine, which is the ***engine face***. The turbojet engine of the Me 262 was an axial compressor and the engine face consisted of the first row of compressor blades about a central hub or ***spinner***, which formed an annular engine face. The turbojet engine of the Gloster Meteor used a centrifugal compressor that took in air within the inlet duct.

An early jet aircraft in the United States was the Lockheed P-80 shown in the right image of Figure 1.1. The P-80 featured two inlets mounted on each side of the fuselage that fed a common duct leading to a single turbojet engine. The engine was based on the design from the United Kingdom and had a centrifugal compressor at the engine face. The inlet was a subsonic, ***conformal pitot inlet*** in which the inlet aperture conforms to the shape of the fuselage. The intent of the conformal inlet was to reduce drag.

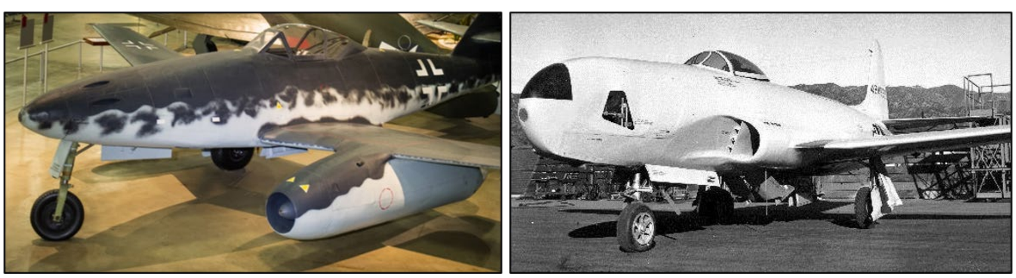

Figure 1.1.—Examples of early subsonic, turbojet-powered aircraft with pitot inlets: Messerschmitt Me 262 (left) and Lockheed P-80 (right). (Photographs are courtesy of the USAF and are in the public domain).

Forward of the inlet, the fuselage was shaped to improve flow into the inlet. The inlet also featured a ***boundary layer diverter***, which removed low-momentum flow of the fuselage boundary layer rather than allowing it to be ingested into the inlet and engine. Another unique example of a subsonic, conformal pitot inlet was the inlet of the Avro Vulcan, in which the inlet was integrated with the leading edge of the wing near the root. The engines were also integrated into the wing. As with the conformal inlet, the intent was to reduce drag. References 8 and 9 provide good references discussing various inlets and their integration with aircraft.

The most common integration approach of a subsonic pitot inlet has been to mount the engines onto pylons that extend beneath the wings or at the sides of the fuselage (Ref. 9). The inlet and nozzle are in-line with the engine axis and a ***nacelle*** encloses the inlet/engine/nozzle combination. Almost all the subsonic commercial jet aircraft, such as the Boeing 737, 777, and 787, have the engines mounted on pylons beneath the wings. Such commercial aircraft use ***turbofan engines*** in which the engine drives a fan that creates most of the jet exhaust. The turbofan engines are more fuel efficient and quieter than earlier turbojet engines. The fan with its spinner forms an annular interface with the inlet at the engine face. The fan can reach a diameter of over 10 ft, which makes it difficult to integrate the propulsion system with the fuselage or wing and results in the preference of mounting on a pylon. The Boeing B-47 Stratojet and Boeing B-52 Stratofortress aircraft featured the engines mounted in pairs on pylons attached beneath the wings. Many business-class aircraft with two engines, such as Gulfstream G650, mount the engines onto short pylons attached to the sides of the fuselage near the tail. When an aircraft has three engines, such as the McDonnell-Douglas DC-10, it is common to mount an engine on the top of the fuselage and integrate it with the tail of the aircraft. A single-engine aircraft may find it advantageous to mount the engine on the top of the fuselage, such as with the Northrop Grumman Global Hawk.

In considering the flow of air through a subsonic pitot inlet, one can envision an ***inlet streamtube*** that originates in the freestream ahead of the aircraft, enters the inlet at the inlet aperture, and extends through the internal ducting of the inlet to the engine face. The streamtube may encounter and be affected by the forward portions of the aircraft prior to entry into the inlet, such as was the case with the P-80 aircraft discussed previously. At the inlet aperture, the cross-section of the inlet streamtube matches the capture cross-section. Within the inlet, the streamtube surface is coincident with the surface of the internal ducting of the inlet. At the engine face, the cross-section of the streamtube matches the cross-section of the engine face.

An analysis of the flow through the inlet can be facilitated using the assumption of ***quasi-one-dimensional flow***, which is a common approximation for the entire propulsion system (Refs. 2 and 3). A streamwise spatial coordinate can be established by defining a streamline passing through the center of the cross-sections of the streamtube from the freestream to the engine face. At each point along the streamline, the cross-sectional area of the streamtube can be defined. The flow properties are represented by the Mach number, total pressure, and total temperature. A later section will show that the continuity of the flow rate through the streamtube provides a relationship between the streamtube area and the flow properties. The flow within an inlet is likely adiabatic, and so, the total temperature along the streamline can be assumed constant at the freestream condition. For subsonic flow, the total pressure may decrease from its freestream value along the streamtube due to viscous dissipation as the streamtube scrubs against the fuselage and inlet surfaces. The Mach number will increase as the cross-sectional area of the streamtube decreases and decrease when the area increases. The subsonic nature of the airflow through the streamtube allows pressure waves to propagate upstream and downstream and facilitates the variation of the Mach number with cross-sectional area.

The rate of airflow through the streamtube is established by the flowrate required for the engine. Throughout the mission of the aircraft, the engine flowrate varies based on the thrust required for that segment of the mission. At take-off, the engine operates at near full throttle. In the later stages of climb and during cruise, the engine is throttled back. The throttle setting effectively changes the Mach number at the engine face (Ref. 2). At full throttle, the engine-face Mach number for turbojet and turbofan engines likely varies from Mach 0.3 to 0.6. At take-off, when the freestream Mach number is lower than the engine-face Mach number, the streamtube approaching the inlet aperture contracts and the Mach number increases as the airflow approaches the inlet aperture. The air is essentially being sucked into the inlet by the engine. As the aircraft speed increases and the engine throttle is decreased, the difference between the freestream and engine-face Mach numbers reduces and the variation of the cross-sectional areas of the streamtube reduces. At low throttle settings during flight, the cross-sectional area of the streamtube at the freestream may be smaller than the inlet capture area, and so, the flow in the streamtube ahead of the inlet aperture decelerates and diffusion of the flow occurs.

A primary task of the design of the subsonic pitot inlet is to establish the cross-sectional areas through the inlet to assure that subsonic flow is maintained within the inlet for all flight conditions. One or more points in the flight are selected as the design points with the cruise condition being a typical design point, especially for commercial transport aircraft.

The inlet aperture or capture area is one of the key properties to be established for the inlet. The ***sizing of the inlet*** concerns establishing the proper cross-sectional area for the inlet aperture. The subsonic character of the flow near the aperture allows the local flow to sense changes in shape of the nearby surfaces. This allows some flexibility in the shape of the inlet aperture, as observed from the examples of the above aircraft. It is of interest to size the capture area to be as small as possible since the capture area scales the overall size, and therefore, the weight, of the inlet. A larger capture area can also directly correlate to a larger inlet drag. Reducing the capture area will increase the Mach number of the flow through the aperture for a specified inlet flow rate. The inlet aperture is commonly sized to be as small as possible such that the local Mach numbers are just below sonic conditions. An additional margin in area is needed because near the sonic flow condition, even a small area change results in sizable changes in the Mach number.

The design of subsonic pitot inlets must also limit gradients in the subsonic diffusion by providing for a gradual turning of the flow. At the inlet aperture, the leading edge or ***cowl lip*** of the inlet usually has a blunt profile, such an elliptical profile. The inlets of the aircraft of Figure 1.1 show examples of blunt cowl lips at the front of the inlets. At the low-speed operation of the aircraft with high inlet flow rate, the bluntness allows gradual turning of the flow past the cowl lip. Excessive turning may result in boundary layer separation, which would incur total pressure losses. There is a trade-off since blunter cowl lips result in higher drag when flow ahead of the inlet is directed toward the inlet axis, such as would be the case at cruise conditions (Ref. 5).

The interior ducting of the subsonic pitot inlet has the primary task of delivering the captured airflow to the engine with the minimum losses in total pressure. For subsonic flow, there is flexibility in shape of the internal cross-sections as the duct transitions from the location and shape of the capture cross-section to the location and shape of the engine face. The locations of the engine face and engine within the aircraft are usually specified based on weight distribution, overall packaging of the aircraft systems, drag considerations, and the direction of thrust for the aircraft. Thus, the internal ducting may involve curving and bends to direct the inlet flowpath. At the design condition, the inlet likely performs some deceleration and diffusion of the subsonic flow as accomplished with a gradual increase in cross-sectional area through the duct. The turning and diffusion of the flow should be accomplished while reducing excesses in gradients that may result in boundary layer separation.

At low aircraft speeds with high engine flow, such as at take-off, climb, and approach to landing, the inlet may require ***auxiliary intakes*** to provide other routes other than the inlet aperture for the increased amounts of airflow (Ref. 9). For example, an inlet capture area may be sized for the cruise condition, but at take-off, the inlet may require a greater amount of airflow. Without the auxiliary intakes, the flow within the inlet could encounter boundary layer separation and choking that would limit the actual flow rate into the inlet. Auxiliary intakes are applicable for all inlets that operate at low-speed conditions during some point of the aircraft mission.

1.4 Supersonic Pitot Inlets

As the power of early turbojet engines increased, the thrust became available to propel fighter aircraft to overcome the large increase in transonic drag to achieve supersonic flight. The first fighter aircraft to reach supersonic speeds in level flight was the North American F-100 Super Sabre in 1953, which is shown in Figure 1.2(a). The F-100 had a pitot inlet at the nose of the aircraft with an oval capture cross-section (Ref. 8). The internal ducting extending along the length of the aircraft to the engine located in the aft portion of the fuselage. The nozzle exhausts out the end of the fuselage.

Supersonic speeds require shock waves to decelerate supersonic flow to subsonic speeds for ingestion into a turbojet or turbofan engine. The F-100 accomplished this through a normal shock wave that extended over the inlet aperture and spilled over the cowl lip. One can see in Figure 1.2(a) that the leading edge of the F-100 inlet had a very small level of bluntness compared to the subsonic pitot inlets of Figure 1.1. The small bluntness of the leading-edge reduced losses and entropy gradients within the shock wave as it spilled over the leading edge. However, the thin leading edges limited the ability of airflow to flow past the leading edge when the aircraft was at incidence to the freestream flow. If the flow has difficulty turning into the inlet, the flow can decelerate and create high gradients which can lead to boundary layer separation within the internal ducting of the inlet. The separated flow can increase the flow ***distortion*** at the engine face with an increased risk of compressor stall.

Figure 1.2.—North American F-100 and Lockheed-Martin F-16.
(Photographs are courtesy of the USAF and are in the public domain).

A current fighter aircraft that uses a pitot inlet for supersonic flight is the Lockheed-Martin F-16 as shown in Figure 1.2(b) (Ref. 11). The maximum speed of the F-16 is Mach 2 at an altitude of 50000 ft. The conformal pitot inlet of the F-16 is positioned below the fuselage and takes advantage of some fuselage shielding at angle-of-attack. The total pressure ratio across a normal shock wave at Mach 2 is about 0.72. Thus, supersonic speeds are limited to brief periods for which high speed is critical. Such limitations on the duration of the supersonic flight of fighter aircraft is common since maneuverability of the aircraft is a more important quality of the aircraft than efficiency.

The steady, inviscid solution of the flow through a normal shock wave is well known from compressible flow theory (Ref. 10). The total or stagnation pressure of the airflow is a measure of the capacity of the airflow to pressurize in response to decelerating Mach numbers. Thus, the ***total pressure losses*** have become a measure of performance of inlets. At Mach 1.3, the total pressure ratio through a normal shock wave is 0.979 with a Mach number downstream of the shock wave of Mach 0.786. This was likely very acceptable to aircraft designers of early supersonic aircraft, especially, since the normal shock wave provided a very easily understood and stable shock wave system for the inlet. For pitot inlets not at the nose and mounted next to the fuselage, there was the possibility of adverse interactions of the normal shock wave with the aircraft boundary layer. Such interactions could lead to boundary layer separation and increased drag. Above Mach 1.3, the losses through a normal shock wave increase dramatically. At Mach 1.6, the ratio of total pressure ratio across the normal shock wave is 0.895 with a downstream subsonic Mach number of 0.668. As mentioned above, for Mach 2.0, the total pressure ratio through the shock wave reduces to 0.721 with a downstream Mach number of Mach 0.557.

At supersonic speeds, the streamtube arrives at the nose of the aircraft undisturbed since acoustic waves cannot travel upstream in supersonic flow. For a nose-mounted pitot inlet, the streamtube passes through the normal shock wave at the inlet aperture and becomes subsonic within the internal ducting. At the design conditions, the normal shock wave sits at the leading edge. This condition represents the maximum flow that the inlet can capture. The area of the aperture is the ***design or reference capture area*** of the inlet, and the flow rate is the ***design or reference capture flow rate***. The reference capture flow rate is used as a reference for flow rates throughout the inlet system. A critical aspect of the design of the inlet is to size this capture area to provide the desired amount of airflow to the engine throughout the flight conditions of the aircraft. Downstream of the inlet aperture, the subsonic flow is diffused in the same manner as with the subsonic pitot inlet.

1.5 Supersonic External-Compression Inlets

The excessive losses in total pressure through a normal shock wave at speeds above Mach 1.3 can be reduced using conical and oblique shock waves and Mach waves for supersonic compression prior to the entrance of the flow into the inlet at the inlet aperture. The analytical solution of planar oblique shock and Mach waves is well-known from compressible flow theory (Ref. 10). In the 1930s both Taylor and Maccoll (Ref. 12) and Busemann (Ref. 13) developed computational methods for the solution of conical shock waves. This has led to the design of external planar ramps and conical spikes for ***supersonic external-compression inlets*** (Ref. 6).

The effect of using ramps and conical bodies for external supersonic compression can be illustrated with several examples of total pressure losses at Mach 1.6 and 2.0. For Mach 1.6 flow through a normal shock wave, the total pressure ratio is 0.895. For a single planar ramp of 8.5 degrees at Mach 1.6 followed by a normal shock wave at Mach 1.3, the ratio of total pressures through the shock wave system is 0.972. For a conical spike with a half-angle of 21.6 degrees at Mach 1.6 followed by a normal shock wave produces a total pressure ratio of 0.974. At Mach 2, a normal shock wave results in a total pressure ratio of 0.721. A single oblique shock wave from a ramp of 18.26 degrees at Mach 2 followed by a normal shock wave produces a total pressure ratio of 0.899. A conical spike of 30.76 degrees at Mach 2 and normal shock wave results in a total pressure ratio of 0.906.

The use of external compression provides for less total pressure losses across the shock wave system; however, it also involves turning of the flow, which has consequences for cowl wave drag and requires the flow to be eventually turned back toward the engine axis.

External supersonic compression was initially used during the 1940's in Germany for an artillery projectile attributed to Trommsdorff that incorporated a ramjet engine to provide greater range (Ref. 14). The projectile used an axisymmetric, conical spike at its front to create a conical, oblique shock wave that performed the external supersonic compression. A shock wave system at the entrance of the internal ducting or cowl lip decelerated the flow to subsonic speeds for combustion within the ramjet. Trommsdorff also consulted with Busemann (Ref. 13) and Oswatitsch (Ref. 15) within Germany on multi-shock wave conical spikes to further reduce total pressure losses for the external supersonic compression.

The work on axisymmetric inlets for ramjet missiles continued within the United States during the latter half of the 1940s and into the 1950s. The NACA Technical Report 1104 by Ferri and Nucci, which was published by NACA in 1952 (Ref. 16) from a classified 1946 report, presented the fundamentals of axisymmetric spike inlets with external supersonic compression. Figure 1.3 shows a schematic presented in the report by Ferri and Nucci. The schematic shows a single conical shock wave created by the spike-nose of the centerbody that projects well-forward of the cowl lip of the inlet aperture. The external, supersonic compression occurs over the forward surface of the centerbody and ends at a normal shock wave as indicated in Figure 1.3. The normal shock wave is referred to as a ***terminal shock wave*** in that it ends the supersonic compression and creates subsonic flow into the internal ducting of the inlet. The external surface extending upstream of the inlet aperture that creates the external shock wave structure is referred to within this document as the ***external supersonic diffuser***. The terminal shock wave structure may consist of a single normal shock wave but may also consist of a ***shock wave train*** consisting of a

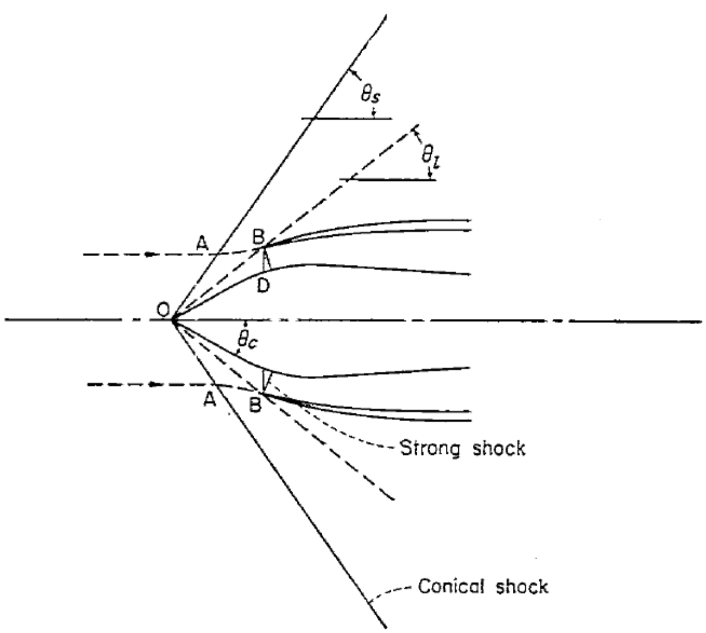

Figure 1.3.—Schematic of the shock structure for an axisymmetric, external-compression inlet (Ferri and Nucci, NACA Technical Report 1104, 1946. Ref. (16)).

series of oblique shock waves that may extend into the forward part of the internal ducting of the inlet (Ref. 17). The shock wave train eventually contains a normal shock wave that performs the final deceleration to subsonic conditions. A shock wave train usually forms when the Mach number ahead of the terminal shock wave is well above Mach 1.3 such that the increase in pressure across the terminal shock wave causes boundary layer separation. The oblique shock waves form at the upstream side of the separation bubble. A key feature of an external-compression inlet is that the terminal shock structure forms about the cowl lip and allows the subsonic flow within the inlet to spill past the cowl lip. This provides a natural mechanism to match the inlet captured flowrate with the required engine flowrate. This capability for subsonic spillage allows the terminal shock system to have inherent stability. The details and design of external supersonic compression and ***subsonic spillage*** will be discussed in a later section. Thus, external compression inlets are a preferred choice above Mach 1.3 to reduce total pressure losses within the inlet and when simplicity and stability of the shock system is desired. Above Mach 2, the turning required for external compression inlets results in considerable wave drag at the cowl exterior and the use of some internal supersonic compression is desired. This will be discussed in the next subsection on mixed-compression inlets. A general statement is that external compression inlets are considered the preferred choice for flight Mach numbers in the range of Mach 1.4 to 2.2.

Axisymmetric external-compression inlets have been used extensively for supersonic aircraft since the 1950s. The Talos missile of the late 1950's through the 1970's represented a typical application for a ramjet missile capable of flight at Mach 2.5. As turbojet engines increased in thrust, fighter and bomber aircraft with axisymmetric external supersonic diffusers were developed. The Convair B-58 aircraft represented an application of an axisymmetric, external-compression inlet with speeds up to Mach 2. The Lockheed F-104 used two semi-span, conical spikes with one on each side of the aircraft to establish an external compression flowfield for flight up to Mach 2 (Ref. 8). Figure 1.4 shows images of the B-58 and F-104 aircraft. The General Dynamics F-111 aircraft featured a quarter-conical spike positioned in the "armpit" of top-mounted wing and fuselage, as shown in Figure 1.5. The aircraft was designed to achieve Mach 2.5 and featured one of the earliest uses of a turbofan engine for a supersonic aircraft. Thus, the engine face denoted the start of the fan stage or fan face. During the development and testing of the F-111, issues with regard to unsteady total pressure distortion at the fan face and subsequent engine instabilities. These challenges led to extensive research of dynamic distortion and methods for characterization and description of total pressure distortion, which will be discussed in later sections. The development of the F-111 involved the integration of boundary-layer diverters and vortex generators within the inlet.

Figure 1.4.—Convair B-58 (left) and Lockheed F-104 (right). (Photographs are courtesy of the USAF and are in the public domain).

Figure 1.5.—General Dynamics F-111. (Photograph is courtesy of the USAF and is in the public domain).

Figure 1.6.—Convair F-102 (left) and F-106 (right). (Photographs are courtesy of the USAF and are in the public domain).

External-compression inlets have also been created by using planar ramps to form oblique shock and Mach waves for which the analytic solution for the flow properties can be readily obtained. Reference 18 presents an early investigation of two-dimensional external-compression inlets. The Convair F-102 and F-106 aircraft illustrated the change from a pitot to two-dimensional ramp inlet (Ref. 8). Figure 1.6 shows the forward portion of both aircraft. Both aircraft were developed in the 1950's to intercept bombers and share many design features. The F-102 was the earlier aircraft intended for low supersonic flight, while the F-106 included a more powerful engine with the intent of reaching speeds of Mach 2. The F-102 had a semi-elliptical pitot inlet with a boundary layer diverter plate for keeping the aircraft boundary layer from being ingested into the inlet. The plate also isolated the normal terminal shock from the aircraft boundary layer ahead of the inlet. The F-106 had a D-shaped inlet with a ramp along the side of the inlet adjacent to the aircraft body. The leading edge of the ramp was offset from the aircraft to avoid the ingestion of the aircraft boundary layer. The ramp could be rotated to change the angle of the ramp to adjust the oblique shock angle to keep the oblique shock out of the inlet aperture. The oblique shock off the leading edge performed the external compression and lowered the Mach number of the flow entering the inlet. The terminal shock was located at the aperture at the design conditions.

Another example of the application of a two-dimensional, external-compression inlet was the Concorde aircraft design for flight speeds of Mach 2.0 (Ref. 19). Figure 1.7 shows the Concorde aircraft with the inlets clearly shown. The inlets were mounted in pairs beneath each of the wings to feed two turbojet engines. The inlets are classified as external-compression inlets; however, the shock structure featured a strong, nearly oblique shock wave that interacted with the wide bleed slot to produce characteristics commonly found with internal supersonic compression (Ref. 19).

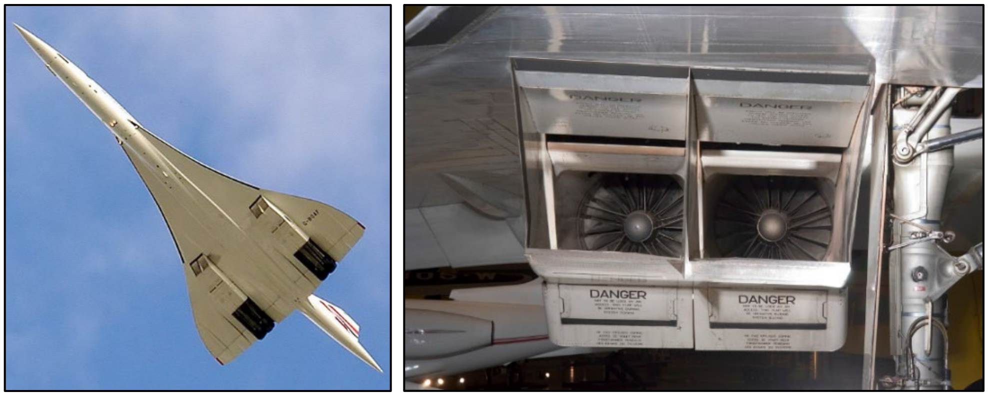

Figure 1.7.—Concorde aircraft (left, public domain) and starboard inlets with bypass doors open (right, courtesy of the National Air and Space Museum, public domain).

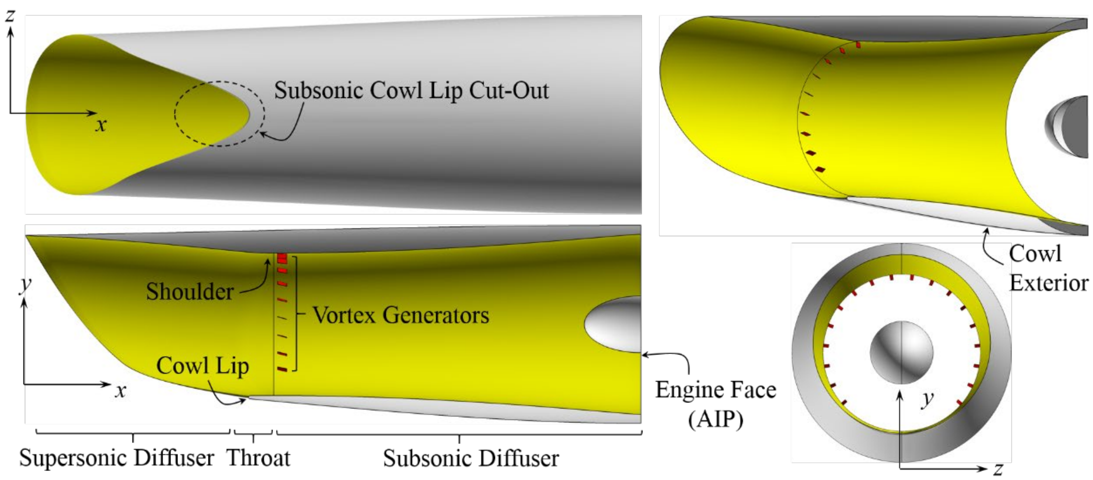

Figure 1.8.—Streamline-Traced External-Compression (STEX) inlet for Mach 1.664. (Ref. 21).

It is certainly possible to perform supersonic compression using three-dimensional surfaces and this is the approach used in streamline tracing methods; however, the methodology is more complex than two-dimensional and conical (axisymmetric spike) methods and relies on computational methods. One approach for establishing a three-dimensional compression surface involves defining a compressive flowfield and tracing streamlines through that flowfield. One such compressive flowfield is the axisymmetric Busemann flowfield (Ref. 13). NASA has performed extensive computational studies of the use of streamline-tracing to design external-compression inlets (Refs. 21 and 22). Images of the NASA inlet for Mach 1.66 is shown in Figure 1.8.

1.6 Supersonic Mixed-Compression Inlets

As ramjet, turbojet, and turbofan engines developed greater thrust, flight speeds exceeding Mach 2 with an airbreathing propulsion system became possible by the early 1960s. The use of fully external supersonic compression incurred greater total pressure losses and drag while increasing the turning of the flow away from the engine axis. The use of ***internal supersonic compression*** was introduced to reduce total pressure losses and inlet wave drag. With internal supersonic compression, the forward portion of the internal diffuser becomes the ***internal supersonic diffuser*** and is shaped to create an internal shock wave system that decelerates, compresses, and turns the supersonic flow toward the engine face. The internal shock waves system consists of conical or oblique and Mach waves. The design of the internal shock wave system requires consideration of shock wave / boundary layer interactions and the possibility of boundary layer separation due to pressure increases across the shock waves. The internal supersonic diffuser may require ***bleed systems*** or other ***flow control systems*** to reduce the occurrence of such adverse conditions. Bleed systems remove a small amount of the core inlet flow to improve the boundary layer to better withstand adverse pressure gradients and other disturbances within the inlet flow. Bleed can be used throughout the inlet, such as on the external supersonic diffuser, but does require pressure differentials to direct the flow from the core inlet flow to other parts of the propulsion system or overboard. Bleed systems within inlets will be discussed further in Section 11.0.

The deceleration to subsonic conditions is facilitated through a terminal shock wave structure located within the ***throat section*** of the internal diffuser. As with the previous discussion, the terminal shock wave structure may consist of a single normal shock wave, a strong oblique shock, or a shock wave train featuring a series of oblique shock waves. The ***subsonic diffuser*** is downstream of the throat section and ends at the engine face.

The combination of external and internal supersonic compression results in these types of inlets being referred to as ***mixed-compression inlets***. Section 9.0 will provide greater details on the design and analysis of internal supersonic compression within the internal diffuser.

The mixed-compression inlet is also used with scramjet engines. In this case, the throat section does not decelerate the flow to subsonic conditions, but rather keeps the flow at supersonic conditions. For this case, the throat section is referred to as an ***isolator*** in that it establishes a shock wave train that isolates the internal supersonic diffuser from the conditions of the combustor, which connects to the end of the isolator.

The Lockheed SR-71 aircraft represented an application of axisymmetric, mixed-compression inlets. The North American XB-70 represented an application of two-dimensional, mixed-compression inlets. Figure 1.9 shows images of these aircraft, which achieved speeds greater than Mach 3. Both aircraft featured bleed systems to control adverse shock wave / boundary layer interactions. The establishment of the internal supersonic compression required ***variable geometry*** within the inlet. The inlets of the SR-71 featured a translating spike, while the inlets of the XB-70 featured ramps that could rotate about a hinge. The intent of the variable geometry was to open the area within the throat section to allow the proper amount of airflow into the inlets at transonic and low-supersonic speeds without choking the flow in the throat section. As the supersonic speed of the aircraft increased, the variable geometry could be actuated to reduce the throat area to form the internal supersonic flow with the internal shock wave system. The

Figure 1.9.—The Lockheed SR-71 (left, NASA photograph) and North American XB-70 (right, USAF photograph, public domain).

establishment of the internal supersonic compression is referred to as ***inlet starting***. The mixed-compression inlet approach results in fully supersonic flow entering the inlet at the cowl lip plane, and so, does not allow subsonic flow within the throat section to be spilled past the cowl lip. The mixed-compression inlet requires ***bleed*** and ***bypass stability systems*** to handle mismatches between the captured inlet flowrate and the required engine flowrate at all supersonic operating conditions of the aircraft. Failure to provide such stability can cause the internal shock wave structure to be expelled in the upstream direction out the inlet aperture in an event referred to as ***inlet unstart***. Such inlet unstarts result in reduced thrust and increased drag. Inlet unstart has been known to have caused the destruction of at least one SR-71 aircraft. The stability of the internal shock wave structure remains a challenge for the design of mixed-compression inlets.

Streamline-tracing methods have also been applied to generate three-dimensional compression surfaces for use with mixed-compression inlets (Refs. 23 and 25). These inlets commonly perform streamline tracing through axisymmetric Busemann flowfields and the shapes of the inlets can vary wildly based on the strategies for performing the streamline tracing. Much of the applications are for hypersonic aircraft. References 5 and 27 provide useful references on hypersonic flow and propulsions systems for hypersonic aircraft. The design methods outlined in this document are limited to supersonic speeds in which high-temperature effects are not significant.

1.7 Overview of SUPIN

The NASA supersonic inlet design and analysis (SUPIN) tool provides a computational approach for the geometric modeling, design, and aerodynamic analysis of both subsonic and supersonic inlets (Ref. 26). The ***geometric modeling*** aspect involves creating the curves and surfaces of an inlet using a set of geometric parameters or ***input factors*** describing the inlet. The ***design*** aspect involves using specified geometric and aerodynamic input factors to establish the dimensions of the curves and surfaces for the inlet. The ***aerodynamic analysis*** aspect involves establishing the aerodynamic performance of the inlet, as represented by the flow rates, total pressure recovery, and drag for the inlet.

To simplify the design and analysis methods within SUPIN, the types of inlets available for modeling are limited to the axisymmetric pitot, three-dimensional pitot, axisymmetric spike, two-dimensional single-duct, two-dimensional bifurcated-duct, and streamline-traced inlets. A common characteristic of this set of inlet types is that much of the geometry of the inlet surfaces can be constructed using simple planar geometry constructs, such as lines and curves that are extruded or formed into surfaces. Such simple geometry constructs can greatly simplify the modeling of the geometry and aerodynamics of the inlet.

SUPIN is written using Fortran 95 and uses analytic, empirical, and computational methods for the modeling, design, and analysis of the inlets. SUPIN reads in a text-based input data file that provides the values of a set of the geometric and aerodynamic factors describing the inlet design and analysis problem. The execution of SUPIN occurs in batch or background mode and requires several seconds to one minute to complete an execution for an inlet.

SUPIN was developed with the intent of providing inlet geometry for use with methods of computational fluid dynamics (CFD) to perform aerodynamic analysis of the inlet flow to obtain a more refined evaluation of the inlet performance. SUPIN creates surface grids for the surfaces of the inlet. These surface grids allow for the visualization of the inlet, as well as provide database geometry for CFD grid generation. In addition, SUPIN can generate multi-block, structured volume grids for use with a CFD flow solver.

SUPIN is available for download through the NASA Software Catalog (software.nasa.gov). On the website, the SUPIN page can be found by inputting "SUPIN" in the search box. SUPIN is only available to US persons and the website provides a process for the verification of those credentials. Once a person is verified, they can download a compressed folder containing the documentation, executable applications, Fortran source code, and sample input and output files for various demonstration inlets. Questions regarding the use of SUPIN can be directed to John Slater at the email address John.W.Slater@nasa.gov. Comments or corrections to this document are also welcomed through an email to the same address.

1.8 Roadmap

This document serves to provide an understanding on using the SUPIN tool for inlet design and analysis. The presentation of the background material and discussion of the geometry modeling, design, and aerodynamic analysis methods also provide useful information for the general topic of the design and analysis of inlets.

Section 2.0 describes the inlet flowpath that extends from freestream flow conditions ahead of the aircraft to the engine face and includes the external flow past the external cowling of the inlet. The modeling of the inlet flowpath is facilitated by dividing the inlet flowpath into components, of which each can be modeled and then assembled to form the complete inlet. Each component is modeled using a set of design or input factors that are related to geometric and aerodynamic properties of the component. The input factors allow the inlet geometry to be constructed in a parametric manner that can facilitate design studies. The range of values for the factors creates the design space for the inlet. Section 2.0 also discusses key stations within the inlet flowpath at which the geometric and aerodynamic properties are defined to characterize the inlet geometry and aerodynamic performance. Section 2.0 then continues with the formulation of the flow rates for the inlet and the continuity and balance of the flow through the inlet.

Section 3.0 discusses inlet performance metrics. The performance of the inlet is mainly characterized by the inlet flow rates, total pressure recovery, and drag. The analysis of the flow rates is concerned with providing adequate flow to the engine while ensuring the proper size and efficient operation of the inlet for the critical operating points. The total pressure recovery measures the aerodynamic efficiency of the flow through the inlet that affects the level of thrust that the engine can generate. The drag measures the creation of forces about the inlet that act against the thrust.

Section 4.0 discusses some basics of SUPIN and starts with a discussion of the input data file that contains the values of the input factors that specify the inlet geometry and flow conditions, and which control the design and analysis process. The input factors are grouped into input data blocks within the input data file that are mainly associated with the components of the flowpath from the freestream to the engine face. Some of the general input factors associated with each block defining the components are presented.

Sections 5.0 and 6.0 discuss axisymmetric and three-dimensional pitot inlets, respectively, and mainly focuses on subsonic flow. The aerodynamic analysis of the pitot inlets for supersonic flow is discussed in Section 5.0. Section 6.0 generalizes the pitot inlet to model variation in the shape of the inlet aperture and subsonic diffuser. The discussion of the pitot inlets introduces the methods for the geometric and aerodynamic modeling of the cowl lip and subsonic diffuser.

Section 7.0 discusses external supersonic compression and involves the solution of flow through conical and planar Mach and shock waves. The Mach and shock wave structures are used to form two-dimensional and axisymmetric external supersonic diffusers.

Section 8.0 discusses axisymmetric spike and two-dimensional, external-compression inlets. The section includes the discussion of the throat section, subsonic diffuser, and modeling of support struts for axisymmetric spike inlets.

Section 9.0 discusses axisymmetric spike and two-dimensional, mixed-compression inlets with discussions of the modeling of the internal supersonic diffuser using the method-of-characteristics, throat section, and subsonic diffusers.

Section 10.0 discusses streamline-traced supersonic inlets. This inlet allows for a rather general shape for the capture cross-section using a set of tracing curves located at the throat section. The flexibility of the shape of the capture cross-section may allow improved integration of the inlet with an aircraft. The discussion of streamline-traced inlets includes the capability for both external-compression and mixed-compression inlets.

Section 11.0 discusses bleed and bypass modeling. Included is a discussion of the modeling of shoulder bleed slots.

Section 12.0 discusses inlet drag and includes topics of additive, wave, and bleed drag.

Section 13.0 discusses the inputs and methods for the generation of curve, surface, and volume grids for visualization of the inlet and CFD analysis.

Section 14.0 discusses additional topics regarding SUPIN and include the writing of a summary table, scheduling of input factors, entity geometric transformation, and entity variable geometry.

Appendices provide further details on planar geometry entities and the method-of-characteristics. Appendix C to Appendix H discuss a collection of sample cases that are released with SUPIN to demonstrate the usage and capabilities of SUPIN.

References

1. Oates, G. C., Aerothermodynamics of Gas Turbine and Rocket Propulsion, AIAA Education Series, New York, 1988.
2. Oates, G. C., editor, Aircraft Propulsion Systems Technology and Design, AIAA Education Series, New York, 1989.
3. Raymer, D. P., Aircraft Design: A Conceptual Approach, AIAA Education Series, New York, 1999.
4. Mattingly, J. D., Heiser, W. H., and Daley, D. H., Aircraft Engine Design, AIAA Education Series, New York, 2002.
5. Heiser, W. H. and Pratt, D. T., Hypersonic Airbreathing Propulsion, AIAA Education Series, New York, 1994.
6. Seddon, J. and Goldsmith, E. L., Intake Aerodynamics, AIAA Education Series, New York, 1999.
7. Seddon, J. and Goldsmith, E. L., editors, Practical Intake Aerodynamic Design, AIAA Education Series, New York, 1993.
8. Surber, L. E., and Robinson, C. P., "Survey of Inlet Development for Supersonic Tactical Aircraft," AIAA Paper 1983-1164, June 1983.
9. Sobester, A., "Tradeoffs in Jet Inlet Design: A Historical Perspective," AIAA Journal of Aircraft, Vol. 44, No. 3, pp. 705-717, May-June 2007.
10. Anderson, J. D., Jr., Modern Compressible Flow, McGraw-Hill Book Company, New York, 1982.
11. Hawkins, J. E., "YF-16 Inlet Design and Performance," AIAA Journal of Aircraft, Vol. 3, No. 6, pp. 436-441, June 1976.
12. Taylor, G. I. and Maccoll, J. W., "The Air Pressure on a Cone Moving at High Speeds," Proceedings of the Royal Society (London), Ser. A, Vol. 139, pp. 278-311, 1933.

13. Busemann, A., "Die achsensymmetrische kegelige Uberschallströmung," Luftfrahrtforschung 19, 137-144 (1942).
14. Cain, T., "Design and Evaluation of High Speed Intakes," NATO EN-AVT-195-03, September 2011.
15. Oswatitsch, K., "Pressure Recovery for Missiles with Reaction Propulsion at High Supersonic Speeds (The Efficiency of Shock Diffusers)," NACA TM 1140, June 1947 (Translation of 1944 German report).
16. Ferri, A. and Nucci, L. M., "Preliminary Investigation of a New Type of Supersonic Inlet," NACA Technical Report 1104, 1952.
17. Mahoney, J. J., Inlets for Supersonic Missiles, AIAA Education Series, Washington, DC, 1990.
18. Conners, J. F. and Wollett, R. R., "Experimental Investigation of a Two-Dimensional Split-Wing Ram-Jet Inlet at Mach Number of 3.85," NACA RM E52F04, August 1952.
19. Candel, S., "Concorde and the Future of Supersonic Transport," AIAA Journal of Propulsion and Power, Vol. 20, No. 1, January-February 2004, pp. 59-68.
20. Slater, J. W., "A Study of the Internal Aerodynamics of the Concorde Inlet," AIAA Paper 2020-3770, August 2020.
21. Otto, S. E, Trefny, C. J. and Slater, J. W., "Inward-Turning Streamline-Traced Inlet Design Method for Low-Boom, Low-Drag Applications," AIAA Journal of Propulsion and Power, Vol. 32, No. 5, 2016, pp. 1178-1189.
22. Slater, J. W., "Refinement of Vortex Generators in a Streamline-Traced, External-Compression Supersonic Inlet," AIAA Paper 2019-4423, August 2019.
23. Mölder, S. and Szpiro, E. J., "Busemann Inlet for Hypersonic Speeds," AIAA Journal of Spacecraft and Rockets, Vol. 3, No. 8, pp. 1303-1304, August 1966.
24. Van Wie, D. and Mölder, S., "Applications of Busemann Inlet Designs for Flight at Hypersonic Speeds," AIAA Paper 1992-1210, February 1992.
25. Billig, F. S., Baurle, R. A., Tam, C.-J., and Wornom, S. F., "Design and Analysis of Streamline Traced Hypersonic Inlets," AIAA Paper 1999-4974, November 1999.
26. Slater, J. W., "SUPIN: A Computational Tool for Supersonic Inlet Design," AIAA Paper 2016-0532, January 2016.
27. Anderson, J. D., Jr., Hypersonic and High Temperature Gas Dynamics, McGraw-Hill, New York, 1989.
28. Tjonneland, E., "The Design, Development, and Testing of a Supersonic Transport Intake System," AGARD-CP-91-71, September 1971.
29. Van Wie, D. M., D'Alessio, S. M., and White, M. E., "Hypersonic Airbreathing Propulsion," Johns Hopkins APL Technical Digest, Volume 26, Number 4, 2005.

2.0 Inlet Flowpath and Flow Rates

A primary function of the inlet is to take in or capture airflow and deliver it to the engine for the generation of the thrust needed for the aircraft. This section discusses the inlet flowpath in terms of an inlet streamtube that extends from the freestream to the engine face. A quasi-one-dimensional assumption is used to establish the flow properties at cross-sections or stations through the flowpath. The flowpath is segmented into components to allow the eventual application of specific design and analysis methods for each component. A key aspect of the design and analysis of inlets is the accounting and conservation of the various flow rates of the inlet flowpath, such as spillage, bleed, bypass, and engine flow rates.

2.1 Inlet Flowpath

The ***inlet flowpath*** can be envisioned as a ***streamtube*** of airflow extending from the ***freestream*** ahead of the aircraft to the end of the inlet at the ***engine face***. An inlet flowpath is illustrated in Figure 2.1 and includes portions external to the inlet and within the internal ducting of the inlet. Between the freestream and the inlet, the streamtube may interact with the forward portions of the aircraft and be affected by shock waves, Mach waves, and boundary layers as the flow approaches the inlet. This segment of the flowpath is referred to as the ***approach flow***. The flow conditions within the flowpath just upstream of the start of the inlet are referred to as the ***local flow*** conditions. Along the flowpath the streamtube can divide, such as when some of the flow is spilled past the inlet entrance to flow past the cowl exterior rather than entering the internal ducting of the inlet. Further, flow may be removed from the flowpath within the inlet, such as when flow is removed through porous bleed holes or slots on the inlet surfaces. The inlet flowpath terminates at the engine face and performs the major objective of providing airflow to the engine.

The inlet streamtube constitutes a control volume for the aerodynamic analysis. Along the flowpath, the cross-sectional area of the streamtube and the aerodynamic properties of the airflow will vary according to the conservation principles of mass, momentum, energy, and entropy production. If the flow is steady, then the streamtube and control volume are fixed in space and time. The flow through the inlet flowpath is affected by shock waves, Mach waves, and boundary layers. The illustration of Figure 2.1 does not show these flow features, but later discussions will provide greater details on the flow processes along the inlet flowpath.

2.2 Frame of Reference

The ***frame of reference*** for the aerodynamic description of the inlet flowpath is a ***Cartesian*** coordinate system fixed to the inlet. Figure 2.2 illustrates the Cartesian coordinate system for a two-dimensional single-duct inlet. The x-axis is directed through the inlet toward the engine face roughly in line with the flow through the inlet. The y-axis is directed upward. The z-axis completes the right-hand

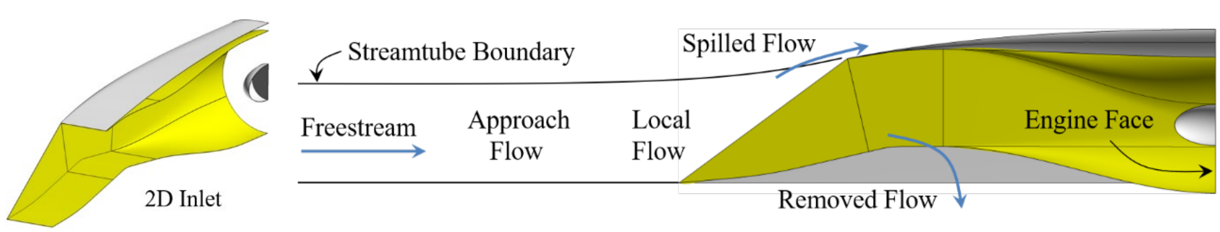

Figure 2.1.—Example of a streamtube for an inlet flowpath.

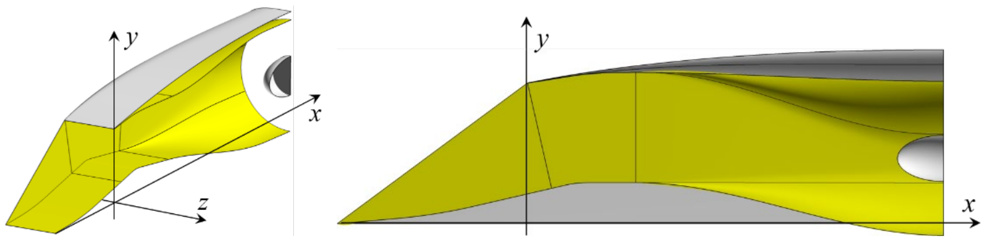

Figure 2.2.—Cartesian frame-of-reference for a two-dimensional inlet.

coordinate system, which is directed to the port side of the inlet from a point-of-view looking upstream in the negative-x direction. For symmetric parts of the inlet, the ***plane-of-symmetry*** is placed on the x-y plane. This frame of reference is an ***Eulerian description*** of the flow in which the coordinate system is fixed to the inlet and the flow approaches the aircraft and inlet. In subsequent discussions of the design of the various inlets, an ***inlet axis*** will be defined for each inlet type. The inlet axis will be parallel with the x-axis, and in some cases, the inlet axis will be coincident with the x-axis.

2.3 Air Models and Properties

An air-breathing propulsion system implies that air is the working fluid of propulsion cycle. The air provides the oxygen, that when mixed with fuel injected into the engine, produces combustion to increase the energy of the flow through the propulsion system. The kinematic and thermodynamic properties of the air include those describing the velocity and thermodynamic state of the airflow (Ref. 1). The mission of the aircraft specifies the altitude, attitude, and speed of the aircraft for the points of interest for the inlet design that define the freestream flow conditions. The flow along the inlet flowpath is part of the compression portion of the Brayton propulsion cycle and the air constitutes the working fluid of cycle.

The freestream air properties are obtained using the US Standard Atmosphere model (Ref. 2). The model can account for standard, cold, and hot days. With the specification of altitude, the thermodynamic properties of static pressure and static temperature at that altitude can be established from the use of curve fits of the model. With the specification of speed (i.e., Mach number) and attitude (i.e., angle-of-attack and angle-of-sideslip), the freestream velocity components can be established.

The flow along the inlet flowpath will change in accordance with interactions with the aircraft and inlet surfaces and the conservation principles as suggested in Subsection 2.1. In consideration that flight speeds would be up to Mach 6 and the deceleration of the flow within the inlet may be as low as Mach 0.15, an estimate of the temperatures of the air can be approximated to help understand the models needed to describe the thermodynamic state of the airflow through the inlet. Figure 2.3 provides a plot of those estimated temperatures, which approach temperatures of 3500 °R at freestream Mach numbers of Mach 6. The temperatures of Figure 2.3 were calculated for freestream Mach numbers from Mach 0.5 to 6.0 assuming freestream dynamic pressures (q) ranging from q = 300 to 2000 psf.

The airflow through the inlet behaves as a perfect gas, which is a gas for which intermolecular forces are negligible. Air consists mostly of nitrogen and oxygen, which are diatomic molecules. For temperatures below 1800 °R, the air molecules exhibit only translational and rotational molecular motion, and the air is considered a calorically perfect gas (Ref. 1). For temperatures above 1800 °R, the vibrational molecular motion of the air molecules increases, and air is considered a thermally perfect gas. The perfect gas equation of state relating the thermodynamic properties of static pressure (p), density (ρ), and temperature (T) is expressed as

$$p = \rho\, R\, T \quad \text{or} \quad pv = R\, T \tag{2-1}$$

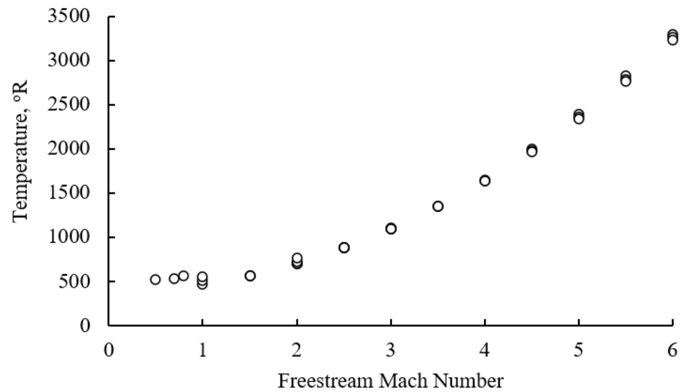

Figure 2.3.—Estimated temperatures within inlets over the range of freestream Mach numbers from Mach 0.5 to 6.0.

The v is the specific volume defined as $v = 1/\rho$. The R is the gas constant, which for both calorically and thermally perfect air is R = 1716.235 ft-lbf / slug °R. The speed of the airflow is characterized by the Mach number defined as

$$M = \frac{V}{a} \tag{2-2}$$

where M is the Mach number, V is the magnitude of the airflow velocity, and a is the acoustic speed of sound defined as

$$a = \sqrt{\gamma R\, T} \tag{2-3}$$

where γ is the ratio of specific heats.

The dynamic pressure (q) is defined as

$$q = \frac{1}{2}\rho V^2 = \frac{1}{2}\gamma p M^2 \tag{2-4}$$

For the data points of Figure 2.3, the freestream Mach number and dynamic pressure were specified. Equation (2-1) was then solved for the static pressure (p) with an assumption of calorically perfect freestream air in which $\gamma = 1.4$. The standard-day atmosphere model could then be used to establish the corresponding altitude (h) and static temperature (T). The freestream total or stagnation temperature (T_t) was then calculated using,

$$T_t = T\left(1 + \frac{\gamma - 1}{2} M^2\right) \tag{2-5}$$

where again calorically perfect air was assumed for the freestream conditions and $\gamma = 1.4$. The freestream total or stagnation pressure is calculated using,

$$p_t = p\left(1 + \frac{\gamma - 1}{2} M^2\right)^{\gamma/(\gamma-1)} \tag{2-6}$$

which assumes an isentropic (i.e., adiabatic, and reversible) process.

An estimate of the temperatures through the inlet flowpath can be obtain by assuming adiabatic conditions through the inlet flowpath, which means the total temperature would be constant. Static temperatures can be obtained using Equation (2-5) and an assumed Mach number within the inlet. For the data of Figure 2.3, Mach numbers at the engine face were assumed that ranged from Mach 0.5 to 0.15 for freestream Mach numbers ranging from Mach 2 to 6, respectively. Another estimate of the maximum temperatures within the inlet is to simply use the value of the freestream total temperature. This assumes that the flow is adiabatically decelerated to static conditions ($M = 0$). This approach likely results in higher than actual temperatures; however, the analysis showed that the difference in temperatures between the approaches were only about 30 to 50 degrees at the higher freestream Mach numbers. Regardless, the data of Equation (2-3) is only intended to provide a rough estimate of the temperatures within inlets.

The data of Figure 2.3 for each freestream Mach number, shows a few data points for different values of dynamic pressure. For Mach 2 to 6, the dynamic pressures used were 1000, 1500, and 2000 psf. The differences in temperatures were very small, as indicated by the closeness of the data points at each Mach number. From this, it is suggested that the temperatures in the inlet at a specific freestream Mach number are not strongly dependent on the value of the dynamic pressure.

With an understanding of the temperatures expected for the inlets across the freestream Mach range up to Mach 6, the appropriate air models can be selected. For temperatures below about 1800 °R (1000 K), air can be considered calorically perfect (Ref. 1). Above 1800 °R, the vibrational motions of the O_2 and N_2 molecules within air become active and contribute to the internal energy and the air can be considered thermally perfect. Dissociation of the O_2 molecules starts at about 4500 °R (2500 K), which is greater than the temperatures expected for inlets for Mach 6 flight. Thus, only calorically and thermally perfect air models will be considered in the discussions of this document.

For both calorically and thermally perfect gases, the relationships between the gas constant (R), specific heat at constant pressure (c_p), specific heat at constant volume (c_v), and ratio of specific heats (γ) are,

$$R = c_p - c_v \quad c_p = \left(\frac{\partial h}{\partial T}\right)_p = \frac{\gamma R}{\gamma - 1} \quad c_v = \left(\frac{\partial e}{\partial T}\right)_v = \frac{R}{\gamma - 1} \quad \gamma \equiv \frac{c_p}{c_v} \tag{2-7}$$

The h and e are the specific enthalpy and specific internal energy, respectively. For both calorically and thermally perfect gases,

$$h = e + pv = e + RT \tag{2-8}$$

The ***calorically perfect air model*** assumes constant specific heats with values of c_p = 6006.823 lbf-ft / slug °R and c_v = 4290.588 lbf-ft / slug °R. The ratio of specific heats becomes $\gamma = 1.4$. Thus, the specific internal energy and specific enthalpy can be computed as

$$h = c_p\, T \quad \text{and} \quad e = c_v\, T \tag{2-9}$$

where it is assumed that $h = e = 0$ at $T = 0$ °R. The specific heats and ratio of specific heats will be designated using the nomenclature, $c_{p\text{-}CP}$, $c_{v\text{-}CP}$, and γ_{CP}. These nomenclatures are not standard but used for convenience for this document.

The change in specific entropy between two states 1 and 2 for constant specific heats, takes the form of

$$s_2 - s_1 = c_p \ln\left(\frac{T_2}{T_1}\right) - R \ln\left(\frac{p_2}{p_1}\right) \tag{2-10}$$

The ***thermally perfect air model*** considers the specific heats as functions of temperature only with $c_p(T)$ and $c_v(T)$. The calculation of the specific enthalpy and specific internal energy now require integration with respect to temperature, as indicated by the differential expressions,

$$dh = c_p(T)\, dT \quad \text{and} \quad de = c_v(T)\, dT \tag{2-11}$$

A model for thermally perfect air can be found in Reference 3. The specific heats for thermally perfect air are designated as $c_{p\text{-}TP}$ and $c_{v\text{-}TP}$ and are modeled with the equations,

$$c_{p-TP} = c_{p-CP} \left\{1 + \frac{\gamma_{CP} - 1}{\gamma_{CP}} \left[\left(\frac{\Theta}{T}\right)^2 \frac{e^{\Theta/T}}{(e^{\Theta/T} - 1)^2}\right]\right\} \tag{2-12}$$

and

$$c_{v-TP} = c_{v-CP} \left\{1 + (\gamma_{CP} - 1) \left[\left(\frac{\Theta}{T}\right)^2 \frac{e^{\Theta/T}}{(e^{\Theta/T} - 1)^2}\right]\right\} \tag{2-13}$$

The Θ is the molecular vibrational energy constant and has a value of Θ = 5500 °R. The specific heat at constant volume could also be computed using the $c_v = c_p - R$. An alternative to using Equation (2-12) to compute $c_{p\text{-}TP}$ is to use established polynomial models. The ratio of specific heats for thermally perfect air is designated and defined as

$$\gamma_{TP} \equiv \frac{c_{p-TP}}{c_{v-TP}} \tag{2-14}$$

The variation of the ratio of specific heats for the thermally perfect air model is shown in Figure 2.4 and indicate that the specific heat decreases with increase in temperature. The plot indicates that the decrease of the ratio of specific heats from the calorically perfect value of γ = 1.4 starts at about 600 °R. The plot on the right correlates the Mach number range of Figure 2.3 with the temperatures and the variation in the ratio of specific heats.

The kinematic and thermodynamic properties of the flow through the inlet flowpath will be established using the principles of conservation of mass, momentum, and energy. These principles will be applied to establish the static density (ρ), velocity components ($\vec{V}$), and specific internal energy (e) within the flowpath. The above air models provide the relationship for the static temperature, $T = T(\rho,e)$. For calorically perfect air, Equation (2-9) allows direct computation of the static temperature (T) from the internal specific energy (e). For thermally perfect air, Equation (2-11) for the specific internal energy differential requires integration to establish the static temperature. With temperature known, the equation of state (Eq. (2-1)) can be applied to obtain the static pressure (p). The specific enthalpy (h) can be established using Equation (2-8).

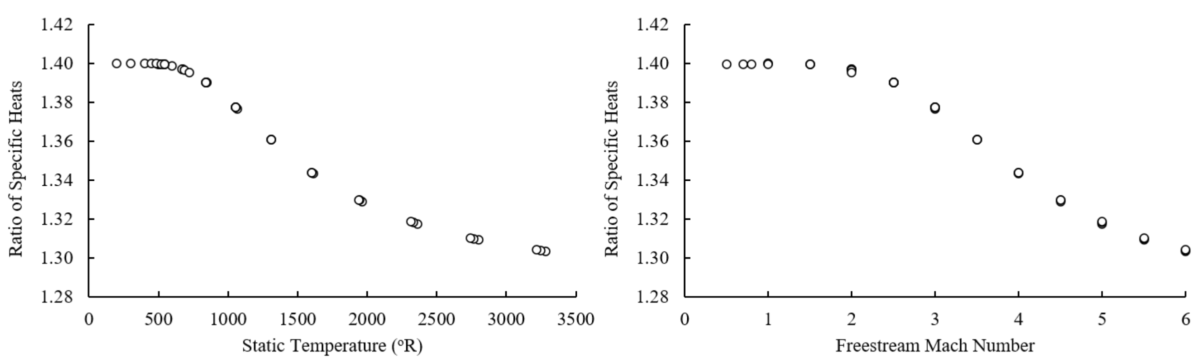

Figure 2.4.—Variation of the ratio of specific heats for the thermally perfect air model over a range of temperatures (left) and freestream Mach numbers (right).

For conceptual inlet and propulsion system design at high temperatures, one approach for considering thermally perfect air models is to use average values of the specific heats over the range of temperatures expected through the compression process (Ref. 5). The average values of the specific heats would be denoted as c_{pc} and c_{vc} with their ratio denoted as γ_c. The thermodynamic analyses would then use the equations for calorically perfect airflow but use the averaged values (c_{pc}, c_{vc}, and γ_c) within the equation. For an inlet design problem, one can consider the range of expected temperatures from Figure 2.4 and establish the average value for the ratio of specific heats ($\bar{\gamma}$) and then use the equations of Equation (2-7) to get the corresponding values of the specific heats.

2.4 Quasi-One-Dimensional Representation

A common practice for propulsion system analysis is the use of the quasi-one-dimensional representation of the flowpath (Ref. 6), which simplifies the aerodynamic analysis of the flow. At locations along the flowpath, the flow is assumed to be uniform such that the flow properties can be represented by averaged values of the properties across the cross-section. For an inlet flowpath, there may be segments for which the flow is not uniform across the cross-section, such as on the external supersonic diffuser or within the internal supersonic diffuser where oblique shock waves may extend across the cross-section. The use of the quasi-one-dimensional representation just assumes that at select stations, average values represent the flow at that location. The next subsection will discuss the segmentation of the inlet flowpath into components and the specification of locations or stations along the inlet flowpath for which the quasi-one-dimensional representation can be used.

2.5 Inlet Flowpath Components and Stations

The design and analysis of the inlet flowpath is facilitated by the segmentation of the inlet flowpath into ***components*** and applying specific design and analysis methods for each component. The primary components of the inlet flowpath are the ***approach flow***, ***external supersonic diffuser***, and ***internal diffuser***, as shown in Figure 2.5. The quasi-one-dimensional averaging is assumed to be applicable at the start and end of the components and these locations are designated as ***stations*** along the flowpath. Each station is associated with coordinates in the Cartesian frame of reference. The primary stations for an inlet for a turbine engine are shown in Figure 2.5 and are designated with numbers as described in the Society of Automotive Engineers (SAE) Aerospace Standard (AS) 755 (Ref. 7). Station 0 is the ***freestream station*** which denotes the atmospheric flow conditions ahead of the aircraft and inlet. The speed of the freestream flow is equal to the speed of the aircraft. With the frame of reference fixed to the aircraft, the direction of the flow is considered toward the aircraft. ***Station 1*** is at the start of the internal ducting of the inlet and is commonly referred to as the ***cowl lip station***. ***Station 2*** is at the ***engine face station*** and marks the end of the inlet and the start of the engine.

The stations illustrated in Figure 2.5 also include ***station L*** to indicate the ***local flow station***, which is immediately upstream of the start of the inlet. The designation of station L is not described within SAE AS 755; however, its use is common to account for changes to the inlet flowpath ahead of the start of the inlet.

Stations 0, L, 1, and 2 indicate cross-sections along the flowpath for which the quasi-one-dimensional representation can be applied. The shapes of the cross-sections at the stations through an inlet depend on the type of inlet, which will be discussed in later sections. The example of Figure 2.5 illustrates an engine face modeled as a turbojet or turbofan engine with annular engine face with a spinner. Such an engine face would mark the interface between the inlet and the inlet guide vanes, compressor (turbojet engine), or fan (turbofan engine) of the turbine engine.

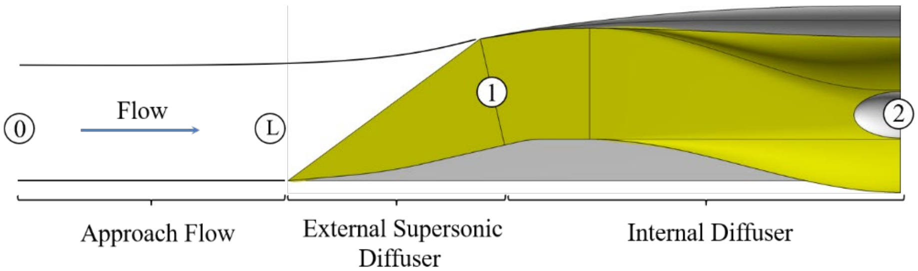

Figure 2.5.—Primary components and stations for an inlet for a turbine engine.

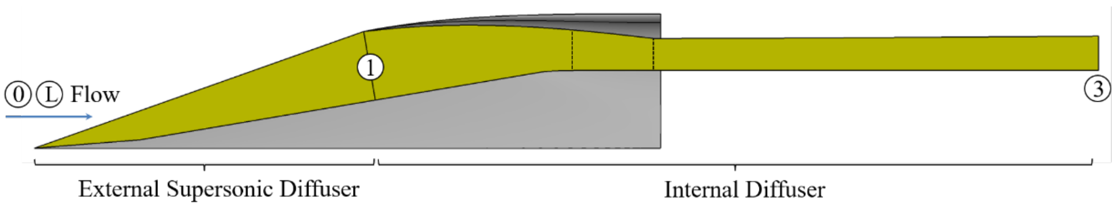

Figure 2.6.—Primary components and stations for an inlet for a ramjet or scramjet engine.

For the case of an inlet for a ramjet or scramjet engine, mechanical compression through turbomachinery is not performed. Rather, the end of the kinetic compression is indicated within SAE AS 755 as station 3, which also indicates the start of the combustor. An example of an inlet for a ramjet or scramjet engine is illustrated in Figure 2.6. Station 2 is not included within the official standard; however, sometimes station 2 is assigned to the end of the internal supersonic diffuser, which will be discussed in a later section. The quasi-one-dimensional representation can be applied at station 3.

The ***approach flow*** is the segment of the inlet flowpath extending between the freestream station 0 and the local flow station L. The approach flow accounts for interactions of the inlet streamtube with the aircraft forward of the inlet. Examples include the interaction of the streamtube with viscous boundary layers formed on the aircraft and the flow of the streamtube through shock waves created by the forward portions of the aircraft. The flow properties of the streamtube may change during these interactions; however, through the interactions, the streamtube maintains flow continuity.

The ***external supersonic diffuser*** is the inlet component that contains forward external surfaces of the inlet that perform external supersonic compression. Examples are the conical centerbody of an axisymmetric spike inlet or the external ramps of a two-dimensional inlet. The external supersonic diffuser starts at station L and ends at the inlet entrance/cowl lip station 1. Further discussion of external supersonic diffusers will be provided in discussions of specific types of inlets.

The ***internal diffuser*** represents the internal ducting of the inlet. The internal diffuser extends from station 1 to station 2 for an inlet for a turbine engine. For an inlet for a ramjet or scramjet engine, the internal diffuser extends from station 1 to station 3. The internal diffuser consists of one or more other components depending on the type of inlet and engine. The possible components of the internal diffuser include the internal supersonic diffuser, throat section, subsonic diffuser, and isolator.

The following subsections will discuss several types of inlets to illustrate the various components and stations for the respective inlet. The various components of the internal diffuser will be discussed. The discussion will account for the various types of engines available for the inlets.

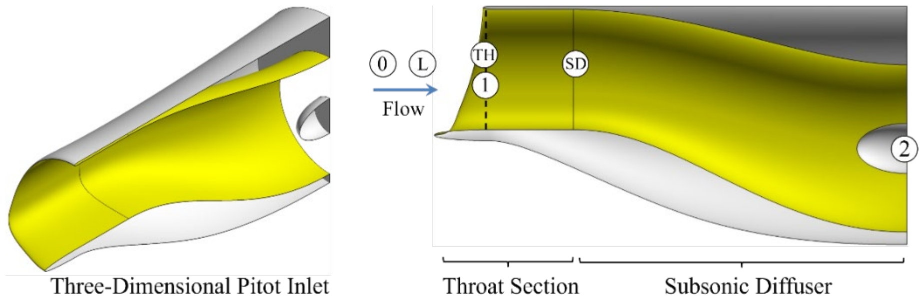

Figure 2.7.—Components and stations for a pitot inlet for a turbine engine.

2.5.1 Components and Stations for Pitot Inlets for a Turbine Engine

Pitot inlets do not contain an external supersonic diffuser, but rather present the leading edge or highlight of the inlet to the local flow. The simplest inlet is perhaps the ***axisymmetric pitot inlet*** in which the inlet surfaces are symmetric about an axis-of-symmetry. For an axisymmetric pitot inlet, the inlet entrance (station 1) and engine face (station 2) are both on planes perpendicular to the inlet axis-of-symmetry. The ***three-dimensional pitot inlet*** features a possible non-planar entrance to the inlet with a general cross-sectional shape. Further, the engine face may involve a vertical offset from the inlet axis. An example of a three-dimensional pitot inlet is illustrated in Figure 2.7.

For supersonic local conditions, a normal shock wave exists across or slightly upstream of the inlet leading edges to decelerate the supersonic freestream flow to subsonic conditions for entry into the inlet. The internal diffuser is divided into the ***throat section*** and ***subsonic diffuser***. The ***stations TH*** and ***SD*** are introduced to indicate the locations of the ***geometric throat*** and the start of the subsonic diffuser, respectively. The geometric throat is the location along the flowpath with the smallest cross-sectional area. Stations TH and SD are not part of the SAE AS 755 standards but are introduced here to facilitate the inlet design and analysis. The quasi-one-dimensional representation is expected to be applicable at stations TH and SD. The intent of the throat section is to provide ducting for subsonic flow to enter the inlet. In the example of Figure 2.7, the intent of the throat section is to provide a straight and nearly constant-area duct to settle the flow prior to the start of the subsonic diffuser at station SD. Since flow in the throat section and subsonic diffuser are expected to be subsonic, the placement of station SD is rather arbitrary and placed for convenience. Station SD could have been placed coincident with station TH to incorporate the throat section within the subsonic diffuser. Likewise, the throat section of Figure 2.7 could have been eliminated entirely and the area increase and turning of the inlet surfaces could have started with the placement of station SD coincident with stations 1 and TH. Such differences constitute design choices that could affect the intended performance of the inlet.

2.5.2 Components and Stations for External-Compression Inlets for a Turbine Engine

The components and stations for two-dimensional and axisymmetric spike, external-compression inlets for a turbine engine are shown in Figure 2.8 and Figure 2.9, respectively. The external supersonic diffuser extends between stations L and 1 and performs supersonic compression external to the internal ducting of the inlet. For the two-dimensional inlet of Figure 2.8, a sidewall is included to contain the externally compressed flow. A later section will provide further details on the configuration and design of the external supersonic diffuser and sidewall.

An external-compression inlet uses a terminal shock wave system about station 1 to decelerate supersonic flow to subsonic conditions. The structure of the terminal shock wave will be discussed in later sections; however, for an external-compression inlet, it is assumed that most of the flow downstream of station 1 is subsonic. The internal diffuser consists of a throat section and subsonic diffuser. The throat

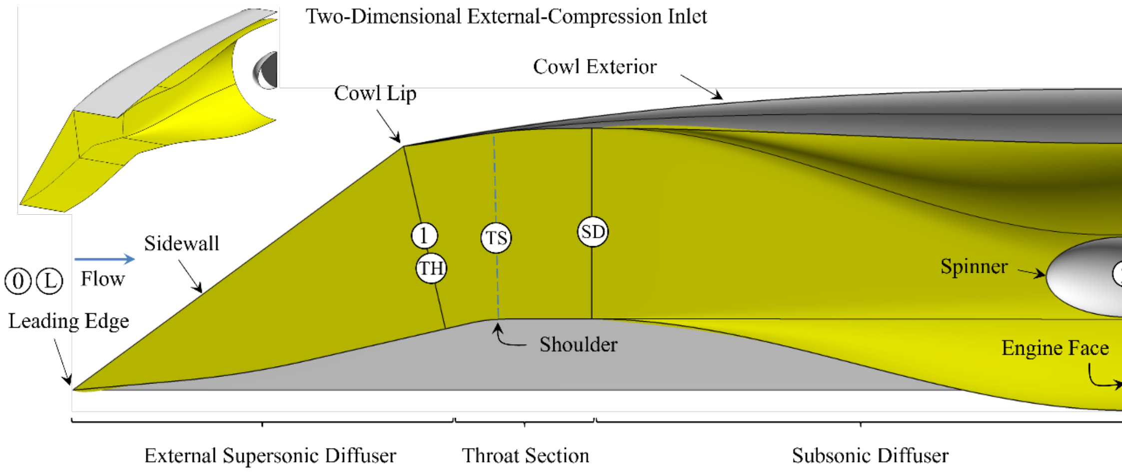

Figure 2.8.—Components and stations for a two-dimensional, external-compression inlet for a turbine engine.

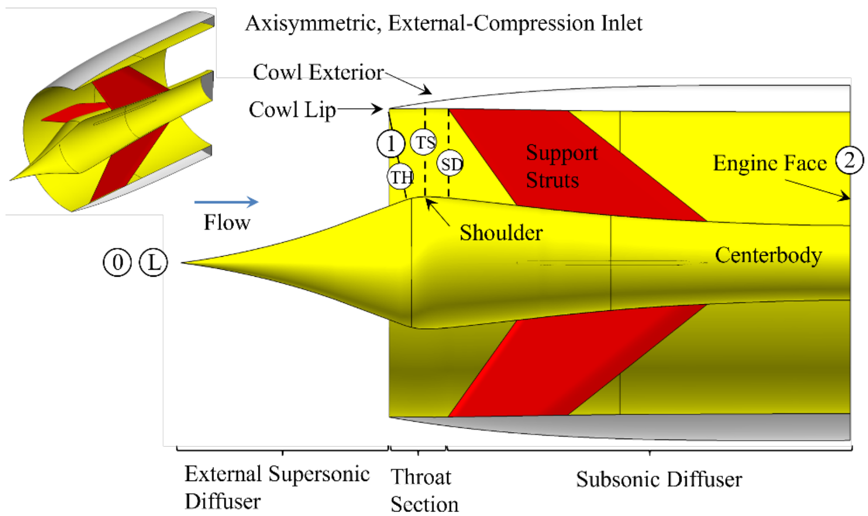

Figure 2.9.—Components and stations for an axisymmetric, external-compression inlet for a turbine engine.

section extends between stations 1 and SD and the geometric throat station TH is considered coincident or slightly downstream of station 1, as with the pitot inlet. The purpose of the throat section is to complete the deceleration of any remaining supersonic flow to subsonic conditions and turn the flow into the start of the subsonic diffuser at station SD and toward the engine face. The ***station TS*** indicates the location of the ***shoulder*** of the inlet. The shoulder is the location on the surface of the inlet in which the slope is along the inlet axis. For the inlet shown in Figure 2.8, the shoulder point is located on the bottom surface, as indicated, where the local slope is zero. The shoulder also marks the location in which the flow changes from being directed away from inlet axis to being directed toward the inlet axis and toward the engine face. The station TS is illustrated by the dashed vertical line. Station TS is a geometric station that is established to provide additional information. The quasi-one-dimensional flow properties may not necessarily be defined. The subsonic diffuser extends between stations SD and 2.

Figure 2.8 also indicates the ***cowl lip***, ***cowl exterior***, and ***spinner***. The cowl lip indicates start of the internal ducting of the inlet. The cowl exterior provides an outer surface for the inlet. Both the cowl lip and cowl exterior are components that exist for all inlets. The components and stations discussed for

Figure 2.8 applies to other types of external-compression inlets for turbine engines, including the axisymmetric spike and streamline-traced inlets.

The axisymmetric spike, external-compression inlet as illustrated in Figure 2.9, has the same components and stations as the two-dimensional, external-compression inlet. Struts are necessary to support the centerbody to the cowl and Figure 2.9 shows an inlet with four support struts positioned at 90-degree intervals about the circumference of the inlet. The centerbody extends to the engine face and covers the hub of the engine in place of the spinner.

The deceleration from supersonic to subsonic flow across the terminal shock wave of an external-compression inlet is facilitated by additional stations within SUPIN. ***Station EX*** represents the state of the flow at the end of the external supersonic diffuser on the upstream side of the terminal shock wave. ***Station NS*** represents the conditions just downstream of the terminal shock wave system, which within SUPIN is modeled as a normal shock wave. Since the normal terminal shock wave is regarded as infinitesimally thin, stations EX and NS are collocated. Stations EX and NS will be further discussed and illustrated in Sections 7.0 and 8.0.

The terminal shock wave structure could form a ***shock wave train*** consisting of a series of oblique shock waves rather than a normal shock wave. This may be the case for inlets for freestream conditions greater than $M_0 = 3$. The shock wave train could extend into the throat section as the flow is decelerated to subsonic conditions through the shock wave train. The modeling of throat sections for such inlets will be discussed in Section 8.0. While supersonic flow exists within the throat section containing the shock wave train, these inlets are still considered external-compression inlets.

2.5.3 Components and Stations for External-Compression Inlets for Ramjet Engines

The description and discussion of the previous subsection on the components and stations of external-compression inlets for a turbine engine also apply to external-compression inlets for a ramjet engine. The only change is that station 2 is replaced with station 3. The ramjet engine does not have any mechanical compression, and so, the subsonic diffuser provides the flow conditions at the interface with the combustor at station 3. Figure 2.10 provides an example of an axisymmetric spike, external-compression inlet for Mach 3 with the components and stations illustrated.

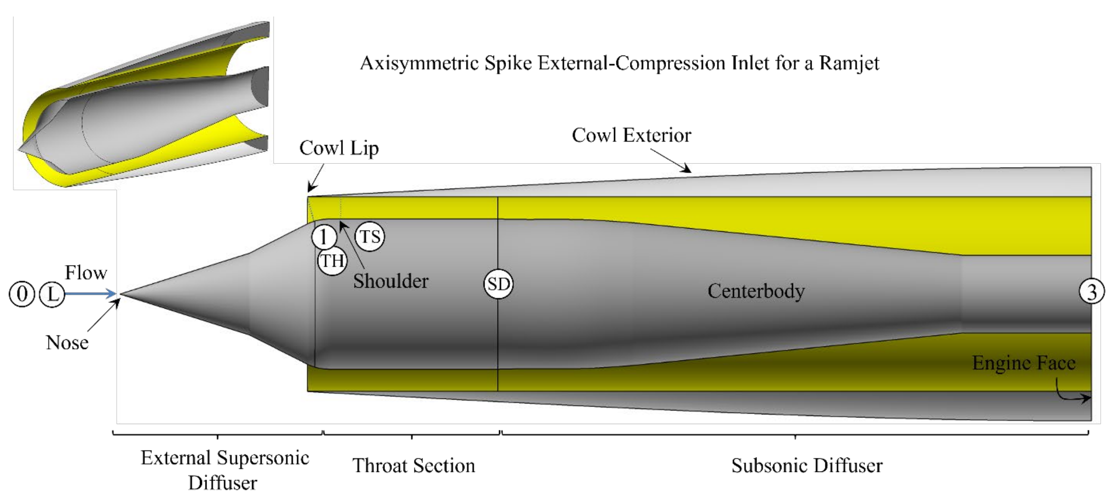

Figure 2.10.—Components and stations for an axisymmetric, external-compression inlet for a ramjet engine.

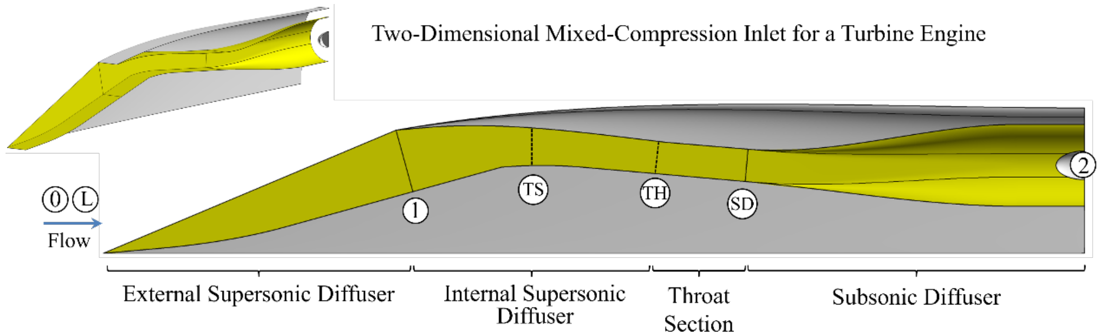

Figure 2.11.—Components and stations for a two-dimensional, mixed-compression inlet for a turbine engine.

2.5.4 Components and Stations for a Mixed-Compression Inlet for a Turbine or Ramjet Engine

The internal diffuser for a mixed-compression inlet for a turbine or ramjet engine consists of the internal supersonic diffuser, throat section, and subsonic diffuser, as illustrated for the two-dimensional inlet of Figure 2.11. The internal supersonic diffuser involves an area contraction, and so, the geometric throat station TH moves to the end of the internal supersonic diffuser, which extends between stations 1 and TH. Within the SAE AS 755 document the geometric throat is identified as station "1_*"; however, within SUPIN, the nomenclature of "TH" is used to designate the geometric throat station. The shoulder station TS may be identified within the internal supersonic diffuser. The throat section extends between stations TH and SD and has the purpose of containing the terminal shock wave system that decelerates the internal supersonic flow to subsonic conditions. ***Station IN*** represents the state of the flow at the end of the internal supersonic diffuser upstream of the terminal shock wave system. As with the external-compression inlet previously discussed, ***station NS*** represents the state of the flow downstream of the terminal shock wave system. If the terminal shock wave is a normal shock wave, then stations IN and NS are located at coincident points. If the terminal shock wave structure is a shock wave train, then stations IN and NS may be located over a segment of the throat section. The length of the throat section is usually designed to contain the terminal shock wave system. Over the operation of an inlet, the terminal shock wave system may move along the length of the throat section in response to inlet conditions, and so, the length of the throat section should account for this range of motion.

The subsonic diffuser extends between stations SD and 2 for the turbine engine. For a ramjet engine, station 3 would be identified in place of station 2 and the spinner shown in Figure 2.11 would not be present. The components and stations discussed for Figure 2.11 apply to other types of mixed-compression inlets for turbine and ramjet engines, such as the axisymmetric spike and streamline-traced inlets.

2.5.5 Components and Stations for Inlets for a Dual-Mode Ramjet (DMRJ) or Scramjet Engine

Inlets for a dual-mode ramjet (DMRJ) and scramjet engines are mixed-compression inlets, and so include an internal supersonic diffuser. Figure 2.12 illustrates the components and stations for a two-dimensional inlet for a DMRJ or scramjet. As with the mixed-compression inlet of the previous section, the internal supersonic diffuser extends between station 1 and the geometric throat station TH with station TS identifying the shoulder station. The internal diffuser also contains an isolator that extends between stations TH and 3, the start of the combustor. The isolator is a near constant-area duct that decelerates and compresses supersonic flow through an oblique shock wave train system. The deceleration could be result in subsonic conditions at station 3 for a ramjet engine. One purpose of the isolator is to "isolate" the flow upstream of station TH from possible unsteadiness within the combustor.

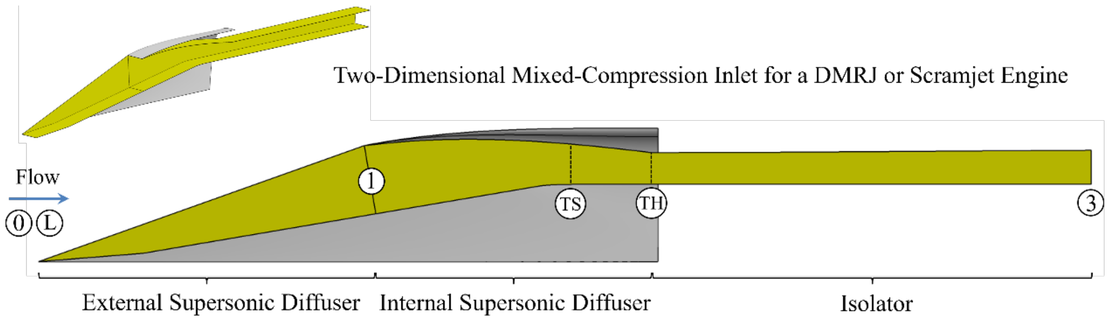

Figure 2.12.—Components and stations for a two-dimensional, mixed-compression inlet for a dual-mode ramjet (DMRJ) or scramjet engine.

TABLE 2.1.—FLOW STATIONS WITHIN AN INLET

Station	Description
0	Freestream
L	Local flow immediately upstream of the inlet
EX	End of the external supersonic compression
NS	Downstream of the external or internal terminal shock system
1	Entrance to interior duct at the cowl lip
TS	Shoulder station
TH	Geometric throat
IN	End of the internal supersonic compression
SD	Start of the subsonic diffuser
2	Engine face for a turbine engine
3	End of compression and start of the combustor

2.5.6 Summary of Components and Stations

The stations of the inlet flowpath defined so far in the previous subsections are summarized in the list of Table 2.1. The numbered stations are those as specified in the SAE AS 755 document (Ref. 7). The alphabetical stations are additional stations defined within SUPIN to facilitate the modeling of the flow through the inlet flowpath. The inlets of the previous subsections did not include any internal-compression inlets; however, internal-compression inlets are similarly described with the listed stations with consideration that the external supersonic diffuser is not included.

2.6 Flow Rates

A primary function of the inlet is to capture the airflow required by the engine during the aircraft mission. This subsection establishes the basic equations of the flow rate and begins the discussion of the accounting of the flow rates through the inlet flowpath, which adhere to the principle of the conservation of the mass, or with consideration of airflow, the conservation of flow rates. In this discussion, it is assumed that the ratio of specific heats (γ) is constant and the flow processes are adiabatic along the inlet flowpath.

The rate of flow (W) through a cross-sectional area (A) can be expressed using static or total properties as

$$W = \rho A V = p\, A\, M \sqrt{\frac{\gamma}{R\, T}} = \frac{p_t\, A}{\sqrt{T_t}}\, \phi \tag{2-15}$$

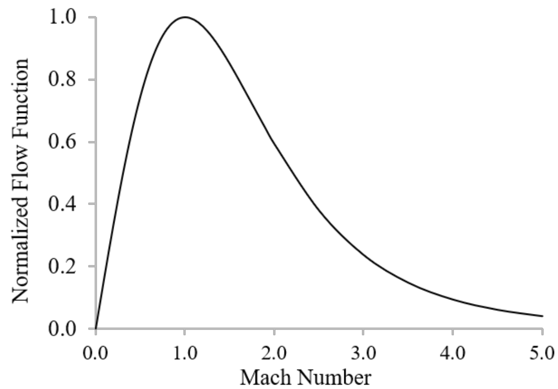

Figure 2.13.—The flow function normalized by its maximum value, which occurs at Mach 1.

The flow rate represents the "mass flow rate" or a "weight flow rate" depending on the units. Within SUPIN, units of slug/s or lbm/s are used. The ϕ is the ***flow function*** or ***mass flow parameter*** (MFP) expressed as

$$\text{Flow Function} = \phi = M\sqrt{\frac{\gamma}{R}}\left(1+\frac{\gamma-1}{2}M^2\right)^{-(\gamma+1)/2\,(\gamma-1)} \tag{2-16}$$

The flow function is a function only of the ratio of specific heats (γ), gas constant (R), and Mach number (M). Figure 2.13 shows the variation of the flow function normalized by its maximum value, which occurs at $M = 1.0$.

Equation (2-15) is a fundamental equation in the design and analysis of inlets. It relates the total pressure, cross-sectional area, and Mach number at stations along the inlet flowpath. The assumption of adiabatic flow through the inlet flowpath results in the total temperature remaining constant and equal to the freestream value through the flowpath. Thus, the inlet design and analysis methods use flow continuity through the inlet flowpath along with an estimate of the total pressure losses and specification of Mach numbers to establish the cross-sectional areas throughout the flowpath. Alternatively, with cross-sectional areas specified, the Mach numbers could be determined.

2.7 Reference Capture Flow Rate

The flow rates through the inlet can be normalized by a ***reference capture flow rate***. The reference capture flow rate is defined using local flow conditions for Equation (2-15) in the manner of

$$W_{cap} = A_{cap}\frac{p_{tL}}{\sqrt{T_{tL}}}\phi_L \tag{2-17}$$

The area A_{cap} is a reference area called the ***reference capture area*** and is defined as the forward projection along the x-axis of the area bounded by the trace of the inlet highlight. Another equivalent definition is that the reference capture area is the cross-sectional area of a streamtube that reaches the highlight of the inlet undisturbed. In other words, the streamlines on the capture streamtube surface are straight until they stagnate at points on the inlet highlight. An example of the capture area for a two-dimensional inlet is shown in Figure 2.14. The image on the left-hand-side shows the projection of the ***capture cross-section*** (shown with the blue shaded parallelogram) for the starboard half of the inlet as viewed in the upstream direction. The image on the right-hand-side shows the capture cross-section in a

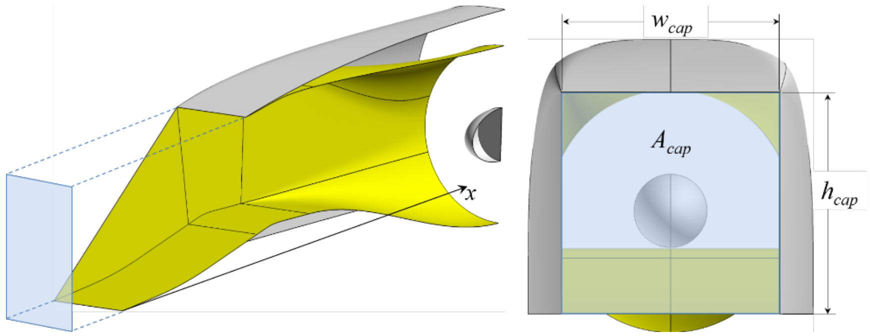

Figure 2.14.—Example of the capture area for a two-dimensional inlet.

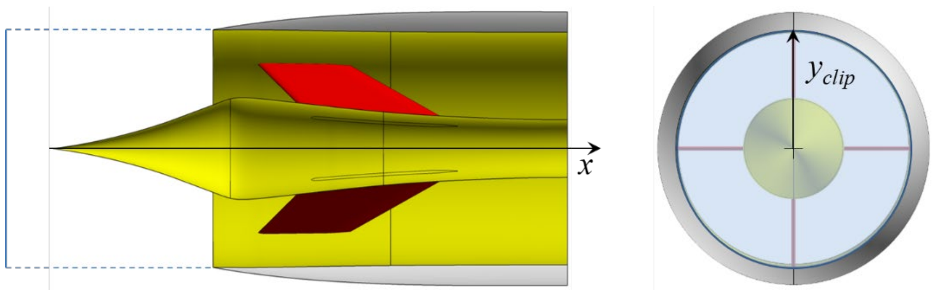

Figure 2.15.—Example of the capture area for an axisymmetric spike inlet.

front view as a rectangle imposed on the highlight of the inlet. The capture area for the two-dimensional inlet is calculated as $A_{cap} = w_{cap}\, h_{cap}$, where w_{cap} and h_{cap} are the width and height of the capture cross-section.

Another example of the capture cross section is the case of an axisymmetric spike inlet as shown in Figure 2.15. The image on the left-hand-side shows a side view with the projection of the inlet leading edge (highlight) in the upstream direction along the x-axis. The image on the right-hand-side shows a front view which shows the capture cross-section as circular. The capture area is calculated as $A_{cap} = \pi y_{clip}^2$, where y_{clip} is the planar coordinate along the y-axis and the radius of the circular capture cross-section. Further definitions of the capture areas for other inlets will be discussed during the sections discussing the respective inlet types.

2.8 Engine Flow Rates

The central purpose of an inlet is to provide the required amount of airflow to the engine at the flow conditions desired by the engine. This is the “matching” requirement for proper operation of the inlet and the propulsion system. As previously stated, the type of engines for consideration include turbojet, turbofan, ramjet, dual-mode ramjet (DMRJ), and scramjet engines. For the design and analysis of an inlet, it is expected that the geometry and flow characteristics of the engine face are established as part of the downstream boundary condition. The aircraft mission specifies the engine throttle setting and the corresponding engine flow rate at the points along the mission.

For turbojet and turbofan engines, the engine face is at station 2 and the cross-sectional shape is circular due to the circular nature of axial flow compressors and fans. If a spinner is included with the engine face, the cross-section is annular. The engine-face area A_2 is the area through which the airflow enters the engine. The rate of flow entering the engine is W_2.

For ramjet, DMRJ, and scramjet engines, the engine face is at station 3 and the cross-sectional shape can range from circular to rectangular according to the cross-sectional shape of the start of the combustor. The flow area and flow rate are A_3 and W_3, respectively.

One approach for specifying the engine flow rate, especially for turbine engines, is to specify the ***altitude corrected engine flow rate*** or ***corrected engine flow rate***, which denoted as W_{C2}. The use of the corrected engine flow rate is due to the practice of indicating engine flow rates based on sea level conditions as the Reference 5.

The relationship between the corrected engine flow rate (W_{C2}) and the actual engine flow rate (W_2) is,

$$W_{C2} = W_2 \frac{\sqrt{\theta_2}}{\delta_2} = \frac{p_{t_{ref}} A_2}{\sqrt{T_{t_{ref}}}} \phi_2 \qquad (2\text{-}18)$$

where

$$\theta_2 = \frac{T_{t2}}{T_{t_{ref}}} \quad and \quad \delta_2 = \frac{p_{t2}}{p_{t_{ref}}} \qquad (2\text{-}19)$$

The reference values are based on standard sea level values and are $T_{t_{ref}} = T_{SSL} = 518.69$ °R, and $p_{t_{ref}} = p_{SSL} = 2116.2$ psf = 14.696 psi. One observation is that the corrected engine flow rate varies only with respect to Mach number for a specified A_2 and constant ratio of specific heats (γ) and gas constant (R). Thus, specifying the engine-face Mach number (M_2) becomes equivalent to specifying W_{C2} for the same engine face area (A_2).

The ***engine flow ratio*** expresses the engine flow rate (W_2) normalized by the reference capture flow rate (W_{cap})

$$\text{Engine Flow Ratio} = \frac{W_2}{W_{cap}} \qquad (2\text{-}20)$$

2.9 Inlet Flow Rates and Ratios

A key aspect of the inlet design and analysis is accounting for the various flow rates about and through the inlet while maintaining the conservation of the rates of flow. This subsection discusses several flow rates associated with the inlet, most of which are illustrated in Figure 2.16. The dashed line illustrates the reference capture streamline representing the boundary of a streamtube that starts upstream of the inlet within the local flow conditions and contains a flow rate equal to the reference capture flow rate (W_{cap}).

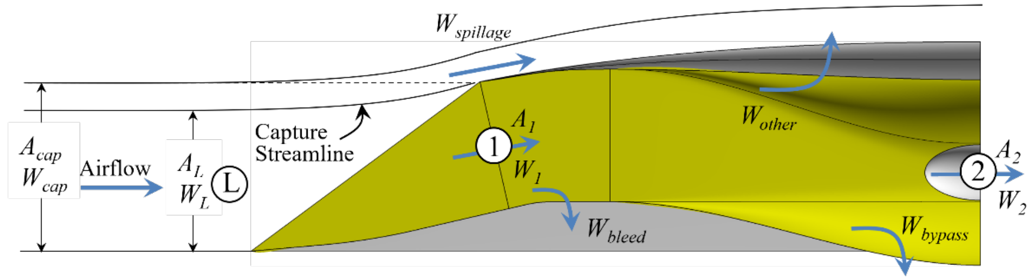

Figure 2.16.—Example of an inlet streamtube and flow rates for an inlet.

The rate of flow that is processed by the inlet is the ***inlet capture flow rate*** (W_L). The inlet is considered to have "captured" this rate of flow. The inlet capture streamtube can be established by tracing streamlines originating at station 1 in the upstream direction to station L. The curve indicated as the "capture streamline" in Figure 2.16 extends from station L to the cowl lip to represent the dividing streamline on the plane of symmetry that separates the flow that enters the inlet and the flow that passes over the external surfaces of the inlet. The inlet capture flow rate (W_L) is shown in Figure 2.16 at station L and is associated with a cross-sectional area (A_L). The inlet capture flow rate (W_L) is defined using Equation (2-15) and the local flow conditions, which is expressed as

$$W_L = A_L \frac{p_{tL}}{\sqrt{T_{tL}}} \phi_L \tag{2-21}$$

Typically, the flow rate (W_L) is determined and then the cross-sectional area (A_L) is computed using Equation (2-21).

The ***inlet capture flow ratio*** is the inlet capture flow rate (W_L) normalized by the reference capture flow rate (W_{cap}). The inlet flow ratio has also been called the ***inlet capture area ratio*** or the ***inlet mass flow ratio***. The inlet capture flow ratio can be expressed as

$$\text{Inlet Capture Flow Ratio} = \frac{W_L}{W_{cap}} = \frac{A_L}{A_{cap}} \tag{2-22}$$

The last ratio of Equation (2-22) represents the inlet capture flow ratio as a ratio of the streamtube cross-section at station L (A_L) and the reference capture area (A_{cap}). It is a common practice for inlet aerodynamics to express the various flow ratios of the inlet in terms of such area ratios. The area ratio (A_L/A_{cap}) is obtained by substituting Equation (2-17) for W_{cap} and Equation (2-21) for W_L in Equation (2-22).

An inlet capture flow ratio of unity indicates that the streamtube enters the inlet undisturbed and the inlet is referred to as operating at ***full flow*** and $A_L = A_{cap}$ or $W_L = W_{cap}$. For subsonic flow at station L, the inlet flow capture ratio can be less or greater than unity. For supersonic flow, the inlet capture flow ratio can only be equal to or less than unity.

If the inlet capture flow ratio is less than unity, then part of the flow that could have entered the inlet under ideal conditions is being "spilled" past the inlet. The spilled flow is called ***spillage*** and has the flow rate $W_{spillage}$. The rate of spillage can be computed as

$$W_{spillage} = W_{cap} - W_L \quad \text{(When } W_L/W_{cap} \leq 1.0\text{)} \tag{2-23}$$

The spillage described above is referred to as ***fore-spillage*** by Seddon and Goldsmith (Ref. 8) in that it occurs forward of the cowl lip. It has a complement called ***aft spillage*** which occurs aft of the cowl lip and is called ***bypass flow*** in this document. The terms fore-spillage and aft spillage are not used further in this document.

The spillage is considered ***subsonic spillage*** when the spilled flow past the cowl lip is subsonic. Subsonic spillage is the result of internal effects, such as reduced engine flow rate, that result in the inlet being unable to accept the all the flow that the capture area can provide. Subsonic spillage occurs for subsonic freestream conditions and for supersonic freestream conditions when the terminal shock wave is located ahead of the cowl lip for an external-compression inlet or during inlet unstart for an internal or mixed-compression inlet.

The spillage is considered ***supersonic spillage*** when the flow past the cowl lip is primarily supersonic. Supersonic spillage requires the terminal shock wave to be located at or downstream of the cowl lip for external-compression inlets or within the throat section, as with internal or mixed-compression inlets. Supersonic spillage also requires the external shock wave system deflect some of the streamlines past the cowl lip. With this deflection of streamlines, the inlet capture flow ratio is less than one and supersonic spillage occurs.

When spillage occurs, it means that the inlet is capturing less flow than theoretically it can accept. This lesser flow rate decreases the thrust that the engine can produce. While a lower thrust may not be desirable, it is not uncommon for an inlet, especially a supersonic inlet, to be designed to allow a small level of supersonic spillage. It has been demonstrated that allowing a small level of spillage can provide a supersonic inlet with some margin against adverse flow effects due to the variations of angle-of-attack and Mach number due to maneuvering or atmospheric variations. One objective of good inlet design is to provide good flow matching in which the flow ratio remains near unity throughout the aircraft mission.

The ***bleed flow*** (W_{bleed}) is extracted from the inlet through porous surfaces, slots, or scoops. One objective of bleed is to remove lower-momentum portions of the boundary layer to increase the overall momentum of the boundary layer to better withstand shock wave/boundary layer interactions and other adverse pressure gradients. Another possible objective of bleed is to remove excess flow within the inlet that is not required by the engine. This objective is similar to the bypass flow that will be discussed later; however, one point of distinction is that the use of bleed systems to remove excess inlet flow involves a lower rate of flow than possible through a bypass system.

A positive value of W_{bleed} indicates flow is extracted from the inlet flowpath. The schematic of Figure 2.16 shows the bleed flow extracted downstream of station 1 and on the centerbody. However, bleed flow can be extracted at locations throughout the inlet from the nose to the engine face and through the various internal surfaces of the inlet.

The accounting of the bleed flows considers several components of the total bleed. For the quasi-one-dimensional representation of the flow through the inlet, each bleed component accounts for the bleed flow extracted between an interval between flow stations of the various inlets. The bleed components considered by SUPIN include:

- W_{bL1} is the bleed flow extracted on the external supersonic diffuser between stations L and 1.
- W_{b1SD} is the bleed flow extracted within the throat section for an external-compression inlet between stations 1 and SD.
- W_{b1TS} is the bleed flow extracted on the sidewall within the internal supersonic diffuser of a two-dimensional, mixed compression inlet between stations 1 and TS.
- W_{b1TH} is the bleed flow extracted within the internal supersonic diffuser of a mixed compression inlet between stations 1 and TH.
- W_{bTHSD} is the bleed flow extracted within the throat section of a mixed-compression inlet between stations TH and SD.
- W_{bSD2} is the bleed flow extracted within the subsonic diffuser between stations SD and 2.
- W_{bTH3} is the bleed flow extracted within the isolator between stations TH and 3.

The subscript "*b*" indicates it's a bleed flow while the remaining numbers and letters indicate the interval between the respective stations. The total bleed flow rate for the inlet is the sum of the respective bleed flow rates for each interval. For an external-compression inlet, the total bleed flow is,

$$W_{bleed} = W_{bL1} + W_{b1SD} + W_{bSD2} \tag{2-24}$$

Equation (2-24) also applies for pitot inlets, but with $W_{bL1} = 0$ since pitot inlets don't have an external supersonic diffuser. For a mixed-compression inlet with a subsonic diffuser,

$$W_{bleed} = W_{bL1} + W_{b1TH} + W_{b1TS} + W_{bTHSD} + W_{bSD2} \tag{2-25}$$

For a mixed-compression inlet with an isolator,

$$W_{bleed} = W_{bL1} + W_{b1TH} + W_{b1TS} + W_{bTH3} \tag{2-26}$$

In consideration of the above discussion of bleed flows, the simple depiction of the bleed flow can be illustrated with the separate contributions through the images of the various inlets within Figure 2.17.

The ***bypass flow*** (W_{bypass}) for inlets is extracted within the subsonic diffuser or isolator forward of the engine face through sets of bypass doors. The objective of bypass flow is to provide a mechanism to match the flow that the inlet supplies to what the engine demands. This is the matching problem for inlet/engine integration. If the flow approaching the engine is greater than what the engine demands, then the bypass offers a means of extracting the excess flow while keeping the upstream flow undisturbed. A positive value of W_{bypass} indicates flow is extracted from the inlet. The assumption is made that any bypass flow is extracted between stations SD and 2.

The bypass function can be performed elsewhere within the inlet, such as the throat section. To keep things simpler within SUPIN, any such bypass outside of the subsonic diffuser or isolator can be accounted through the bleed components discussed in the previous paragraphs.

The ***other flow*** (W_{other}) accounts for any other possible extractions or injections of flow. This includes injection through flow control or cooling jets, airflow from auxiliary inlets for high engine airflow demands, extraction of inlet flow for cooling of the engine or cabin, and leakage of inlet flow through gaps and seals. A positive value of W_{other} indicates flow is extracted from the inlet flow. Alternatively, a negative value of W_{other} indicates flow is injected into the inlet. For simplicity, the assumption is made that W_{other} is extracted or injected between stations SD and 2 for inlets with a subsonic diffuser and between stations TH and 3 for inlets with an isolator. As with the accounting for the bypass, if other types of flows, such as leakage, occur elsewhere within the inlet, they can be accounted for using the bleed components discussed in the previous paragraphs.

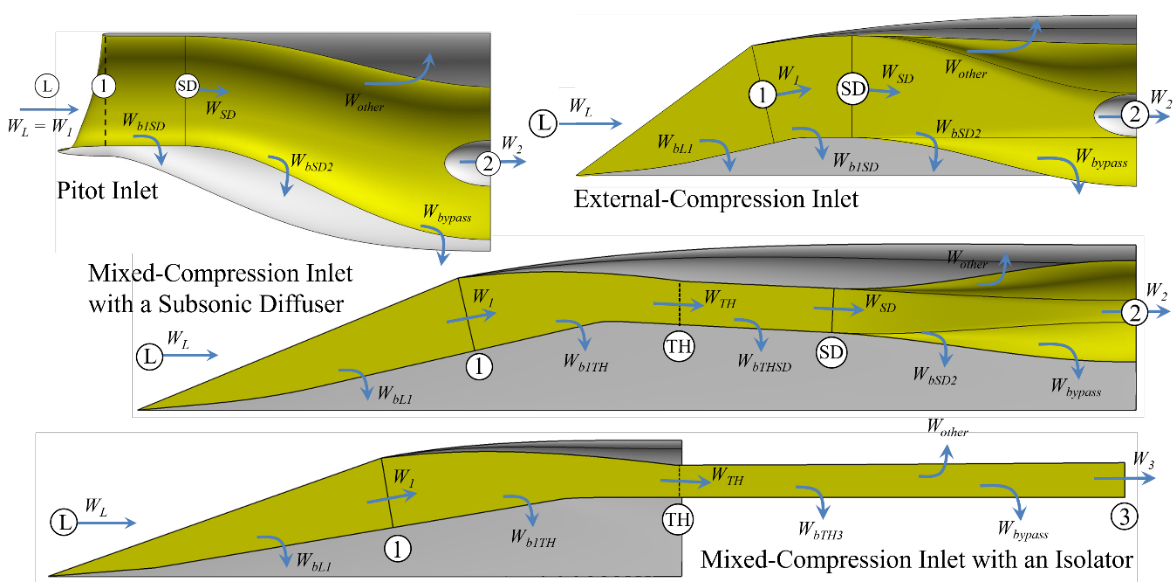

Figure 2.17.—Various types of inlets illustrating the contributions to the total bleed within the inlets.

2.10 Inlet Flow Balance and Streamtube Continuity

The conservation principle for the flow rates through the inlet streamtube are discussed in this subsection. A normalized inlet flow continuity or balance can be expressed by dividing Equation (2-23) by the reference capture flow rate (W_{cap}) and rearranging the terms,

$$\frac{W_L}{W_{cap}} + \frac{W_{spillage}}{W_{cap}} = 1 \tag{2-27}$$

Between station L and the engine face station 2, the flow balance can be expressed as,

$$W_2 = W_L - W_{bleed} - W_{bypass} - W_{other} \tag{2-28}$$

Equation (2-28) can be inserted into Equation (2-27) to yield the inlet flow balance equation,

$$\frac{W_2}{W_{cap}} = 1 - \frac{W_{spillage}}{W_{cap}} - \frac{W_{bleed}}{W_{cap}} - \frac{W_{bypass}}{W_{cap}} - \frac{W_{other}}{W_{cap}} \tag{2-29}$$

Equation (2-29) is especially useful for sizing the capture area of the inlet from a known engine flow rate (W_2) along with specified flow ratios for the spillage, bleed, bypass, and other flows on the right-hand-side of Equation (2-29). One can solve the left-hand-side for W_{cap}, from which A_{cap} can be computed. A later section will discuss inlet sizing in further detail. Equation (2-29) can also be used to estimate the spillage if W_2, W_{bleed}, W_{bypass}, and W_{other} are known.

Much of the inlet flow analysis makes use of Equation (2-15) along with the accounting of the flow continuity. As an illustration, consider the continuity along the inlet streamtube (e.g., between stations 1 and 2) in the absence of flow injection or extraction expressed as $W_2 = W_1$ or

$$\frac{p_{t2}\, A_2}{\sqrt{T_{t2}}}\phi_2 = \frac{p_{t1}\, A_1}{\sqrt{T_{t1}}}\phi_1 \tag{2-30}$$

If one assumes adiabatic flow between stations 1 and 2, then the total temperature remains constant and can be cancelled from the above equation. One can then write,

$$\phi_2 = \left(\frac{p_{t1}}{p_{t2}}\right)\frac{A_1}{A_2}\phi_1 \tag{2-31a}$$

$$A_2 = \left(\frac{p_{t1}}{p_{t2}}\right)\frac{\phi_1}{\phi_2}A_1 \tag{2-31b}$$

$$\frac{p_{t2}}{p_{t1}} = \frac{A_1}{A_2}\frac{\phi_1}{\phi_2} \tag{2-31c}$$

Thus, knowing the Mach number at station 1, areas at stations 1 and 2, and the ratio of total pressures between stations 1 and 2, the right-hand side of Equation (2-31a) can be calculated, and the left-hand side can be iterated to find M_2. Conversely, if M_2 is known, then the equation can be iterated to find M_1. Equation (2-31b) can be solved for an unknown area if the total pressure ratio, Mach numbers, and the other area are known. Equation (2-31c) can be solved for the total pressure ratio if the areas and Mach numbers are known. Thus Equation (2-31) encapsulates the basic relationships between Mach number, area, and total pressure that are central to inlet design and analysis.

Similar flow continuity can be applied for bleed flow extracted between two stations. Possible relations between flow stations are,

$$W_1 = W_L - W_{bL1} \tag{2-32a}$$

$$W_{SD} = W_1 - W_{b1SD} \tag{2-32b}$$

$$W_{TH} = W_1 - W_{b1TS} - W_{b1TH} \tag{2-32c}$$

$$W_{SD} = W_{TH} - W_{bTHSD} \tag{2-32d}$$

2.11 Inlet Operation

The nominal operation of the inlet at its design point involves the inlet capturing enough flow to provide the flow rate required by the engine. The engine operates at a certain corrected flow rate as set by the throttle setting as specified by the aircraft mission. The actual flow rate is related to the corrected flow rate by Equation (2-18) and is dependent on the total pressure at the engine face. When the inlet provides the desired corrected flow rate of the engine, the inlet is operating at its ***critical operating condition***. A well-designed inlet would have the inlet capture flow rate nearly equal to the reference capture flow rate. Such a condition would ensure the inlet is not too large, which adds weight to the propulsion system. The inlet would be operating at full flow with very little or no spillage. For a supersonic, external-compression inlet, this would mean the terminal shock wave would be located at the cowl lip. Figure 2.18 shows Mach number contours from computational fluid dynamics (CFD) simulations of an external-compression inlet operating with $M_L = 1.6$. The middle image of Figure 2.18 shows an inlet operating at the critical operating condition.

When the engine is operated at corrected flow rates below the design point for the inlet, the actual flow rate required by the inlet is lower, and so, flow is spilled at subsonic conditions past the cowl lip rather than being taken into the inlet and engine. In this case, the inlet is operating at a ***subcritical operating condition***. The left image of Figure 2.18 shows the Mach contours of the inlet operating at the subcritical operating condition.

When the engine is operated at corrected flow rates greater than the design point, the inlet is operating at a ***supercritical operating condition***. For the supersonic inlet of Figure 2.18, the maximum inlet capture flow rate (W_1) was achieved at the critical operating condition. The right-hand-side image of Figure 2.18 shows a simulation at the supercritical operating condition. The terminal shock wave was sucked into the inlet, and so, no more flow could be captured. The relation of Equation (2-30) is satisfied by establishing the corresponding lower value of the total pressure at station 2 (p_{t2}). This operating condition results in greater total pressure losses through the inlet.

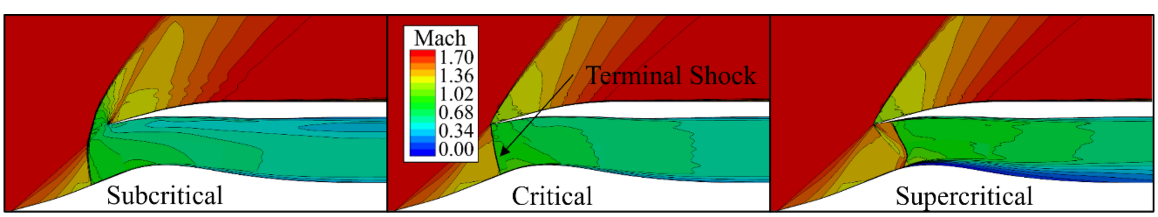

Figure 2.18.—An external-compression inlet operating at subcritical (left), critical (middle), and supercritical (right) conditions.

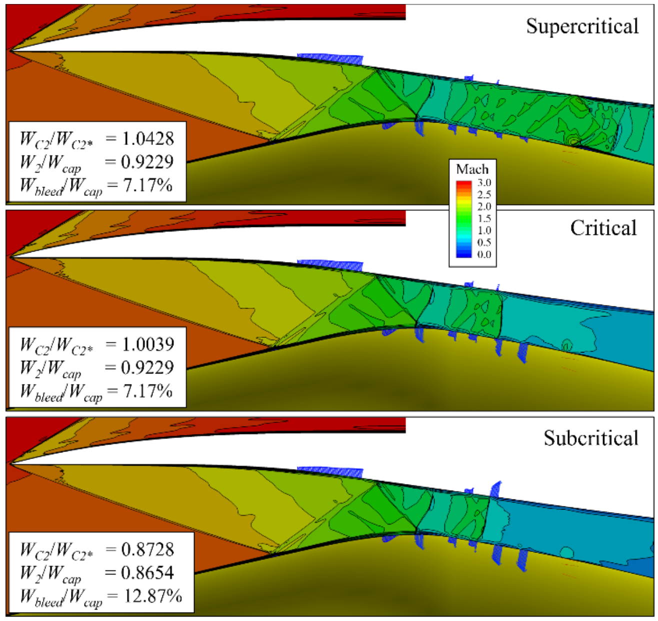

Figure 2.19.—A mixed-compression inlet operating at supercritical (top), critical (middle), and subcritical (bottom) conditions.

For a mixed-compression inlet, the description of the subcritical, critical, and supercritical operating points presented above with respect to the engine corrected flow rates remains the same. However, the terminal shock wave is now positioned within the throat section between stations TH and SD. Figure 2.19 shows the Mach number contours from CFD simulations within the internal supersonic diffuser and throat section of a Mach 3 mixed-compression inlet.

The supercritical operating condition as shown in the bottom image of Figure 2.19 involves the terminal shock wave located downstream within the throat section and the inlet operating with an engine-face corrected flow rate higher than the design corrected flow rate. The critical operating condition has the terminal shock wave located within the throat section as shown in the middle image of Figure 2.19. The subcritical operating condition involves the terminal shock wave moving upstream within the throat section such that the engine-face corrected flow rate is lower than the design corrected flow rate. This is shown in the top image of Figure 2.19. The blue arrows of Figure 2.19 depict bleed flow rates through the various bleed regions. If the flow becomes too subcritical, then the terminal shock wave could be forced upstream of station TH, which would result in the unstart of the inlet.

References

1. Anderson, J. D., Jr., *Modern Compressible Flow*, McGraw-Hill Book Company, New York, 1982.
2. Mattingly, J. D., Heiser, W. H., and Daley, D. H., *Aircraft Engine Design*, AIAA Education Series, New York, 2002.
3. Eggers, A. J., Jr., "One-Dimensional Flows of an Imperfect Diatomic Gas," NACA Report 959, December 1948.
4. Ames Research Staff, "Equations, Tables, and Charts for Compressible Flow," NACA Report 1135, 1953.
5. Heiser, W. H. and Pratt, D. T., *Hypersonic Airbreathing Propulsion*, AIAA Education Series, New York, 1994.

6. Oates, G. C., *Aerothermodynamics of Gas Turbine and Rocket Propulsion*, AIAA Education Series, New York, 1988.
7. Society of Automotive Engineers (SAE), "Aircraft Propulsion System Performance Station Designation and Nomenclature," Aerospace Standard (AS) 755, December 1997.
8. Seddon, J. and Goldsmith, E. L., *Intake Aerodynamics*, AIAA Education Series, New York, 1999.

3.0 Inlet Performance

An assessment of inlet performance within SUPIN involves the evaluation of the inlet flow rates, inlet drag, and efficiency of the compression process as primarily characterized by the total pressure recovery. The previous section discussed the inlet flow rates and a later section will discuss inlet drag. This section discusses the measures of inlet performance that evaluate the compression process for which the inlet functions as part of the thermodynamic cycle in the creation of the thrust created by the propulsion system.

3.1 Inlet Total Pressure Recovery

The inlet provides compression as part of the propulsion cycle. The decrease in total pressure through the inlet results in a decrease of the compression possible at the engine face. The total pressure losses are due to shock waves and viscous dissipation within the viscous boundary and shear layers. Thus, an objective of an inlet design is to minimize any losses in total pressure between the local inflow station L and then engine face, which is either station 2 or 3, depending on the type of flowpath as described in the previous section.

The inlet performance metric that accounts for the loss of total pressure is the inlet total pressure recovery, which is defined as the ratio of the mass-averaged total pressure at the engine face (p_{t2}) to the local total pressure ahead of the inlet (p_{tL}),

$$\text{Inlet Total Pressure Recovery} = \frac{p_{t2}}{p_{tL}} \tag{3-1}$$

Here p_{t2} is used to represent the total pressure at the engine face. For ramjet, DMRJ, and scramjet engines, the inlet total pressure recovery is p_{t3}/p_{tL}.

The inlet total pressure recovery can be modeled as a product of the total pressure ratios across the individual components of the inlet flowpath between the local station L and engine-face. For an external-compression inlet, such as the inlets illustrated in Figure 2.8 and Figure 2.9, and in which a terminal shock wave is located about station 1, the inlet total pressure recovery is calculated using the product,

$$\frac{p_{t2}}{p_{tL}} = \frac{p_{tEX}}{p_{tL}} \frac{p_{tNS}}{p_{tEX}} \frac{p_{t1}}{p_{tNS}} \frac{p_{tSD}}{p_{t1}} \frac{p_{t2}}{p_{tSD}} \tag{3-2}$$

For a mixed-compression inlet represented, such as the inlet illustrated in Figure 2.11, and in which a terminal shock wave system is in the throat section between stations TH and SD, the inlet total pressure recovery is calculated as the product,

$$\frac{p_{t2}}{p_{tL}} = \frac{p_{tEX}}{p_{tL}} \frac{p_{t1}}{p_{tEX}} \frac{p_{tTH}}{p_{t1}} \frac{p_{tIN}}{p_{tTH}} \frac{p_{tNS}}{p_{tIN}} \frac{p_{tSD}}{p_{tNS}} \frac{p_{t2}}{p_{tSD}} \tag{3-3}$$

Similar products can be formulated for other inlet configurations and depending on whether the freestream flow is subsonic, or shock waves exist within the inlet streamtube. Thus, the calculation of the inlet total pressure recovery for an inlet involves the modeling of each total pressure ratio across the respective components. The discussions of several later sections will describe the appropriate models for computing those total pressure ratios.

3.2 Inlet Total Pressure Characteristic Curve

The inlet total pressure recovery (p_{t2}/p_{tL}) can be characterized by its variation with an inlet flow ratio and the resulting curve is known as the ***inlet characteristic curve***. As discussed in a Subsection 2.11, the inlet operation varies between subcritical and supercritical operation with a critical operating point designating the critical operation at which the inlet flow rate matches the design flow rate. An example of a characteristic curve for the total pressure recovery with respect to the engine flow ratio (W_2/W_{cap}) is shown in Figure 3.1. The inlet capture flow ratio (W_1/W_{cap}) can also be used if variations in the bleed, bypass, and other flows are to be excluded from the characteristic curve.

The inlet total pressure characteristic curve shown on the left-hand-side of Figure 3.1 is from the analysis of an external-compression inlet with no bleed or bypass. Thus, the engine flow ratio is equal to the inlet capture flow ratio. With no bleed or bypass within the inlet, the supercritical leg of the curve is the vertical segment that indicates choked flow with a constant inlet flow rate. The inlet total pressure recovery varies for the supercritical leg due to larger total pressure losses as the terminal shock wave is drawn further into the inlet, as illustrated in Figure 2.18. The ***critical point*** of the curve is at the top of the supercritical leg where the total pressure recovery is at its maximum while the inlet flow ratio remains at its maximum. For the external-compression inlet, this corresponds to the terminal shock wave being positioned at the cowl lip and the inlet flow rate at its design condition, which is illustrated in Figure 2.18. The subcritical leg is that portion of the curve that indicates an almost constant total pressure recovery and the inlet flow ratio decreases. The reduction of the inlet flow ratio is accompanied by an equal increase in the subsonic spillage. The inlet total pressure characteristic curve is also known as a "***cane curve***" due to its frequent similarity to the shape of a walking or candy cane. The critical point is also known as the "***knee***" of the cane curve.

For the external-compression inlet represented by the characteristic curve of Figure 3.1, the subcritical operation of the inlet involves the terminal shock wave being located on the external supersonic diffuser and forward of the cowl lip, as illustrated in left-hand-side image of Figure 2.18. The position of the terminal shock wave is dependent on the amount of subsonic spillage resulting from the decrease in the engine flow. A greater amount of subsonic spillage pushes the terminal shock wave further upstream, which can move the shock wave into regions of higher Mach number flow. This can increase the likelihood of shock wave / boundary-layer interactions that result in boundary-layer separation. At some point, the interactions may become severe enough to cause unsteady terminal shock wave behavior known as ***inlet buzz***. Further details of inlet buzz are not discussed here other than to mention that the characteristic curve sometimes shows the limit on the reduced inlet flow ratio for which inlet buzz becomes severe, as illustrated in Figure 3.1.

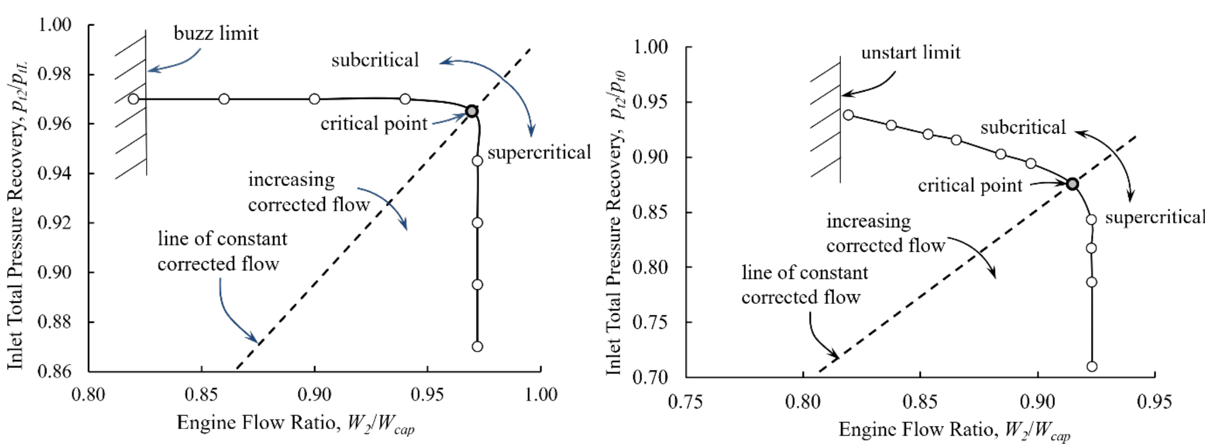

Figure 3.1.—Examples of characteristic curves for the inlet total pressure recovery for an external-compression inlet (left) and a mixed-compression inlet (right).

Each point on the characteristic curve is also associated with an engine-face corrected flow rate (W_{C2}). Understanding the variation of the total pressure characteristic curve with the engine-face corrected flow rate can be useful for understanding the behavior of both the total pressure recovery and actual engine flow rate with changes in the engine operation. Equation (2-18) for the relationship between the corrected and actual flow rates can be rewritten into the form,

$$\frac{p_{t2}}{p_{tL}} = \left(\frac{p_{tref}}{p_{tL}} W_{cap}\sqrt{\theta_2}\right)\left(\frac{1}{W_{C2}}\right)\frac{W_2}{W_{cap}} \tag{3-4}$$

The terms in the first group of terms in parenthesis on the right-hand-side of Equation (3-4) are all fixed in value over the variation of the characteristic curve. Thus, Equation (3-4) represents the equation of a line that passes through the origin of the characteristic curve and has a slope that is dependent on the inverse of the engine-face corrected flow rate. The dashed lines of Figure 3.1 shows an example of the line passing through the critical point. An increase in the engine-face corrected flow rate will result in a lower slope of the line and the inlet operation becomes more supercritical.

The total pressure characteristic curve for an internal- or mixed-compression inlet has much of the same features as discussed and shown above; however, the reduction in the engine flow rate for the internal- or mixed-compression inlets is due to internal bleed rather than subsonic spillage past the cowl lip. Examples of sub-critical, critical, and super-critical inlet flows for a mixed-compression inlet were shown in Figure 2.19. The characteristic curve on the right-hand-side of Figure 3.1 is from the simulations of a mixed-compression inlet. The total pressure characteristic curve for an internal- and mixed-compression inlet established as the internal terminal shock wave system moves upstream through the throat section of the inlet and the inlet flow changes from supercritical to critical to subcritical operation. As the inlet operation becomes more subcritical, a limit is reached in which the terminal shock wave structure reaches the geometric throat of the inlet (station TH), and the inlet unstarts. With inlet unstart, the terminal shock wave moves rapidly upstream through the internal supersonic diffuser and upstream of the cowl lip plane (station 1). Once the terminal shock wave is onto the external supersonic diffuser, the shock wave may exhibit buzz as it interacts with the external shock wave system and the boundary layer of the external supersonic diffuser.

3.3 Military Standard Total Pressure Recovery

An estimate of the expected inlet total pressure recovery is provided by military specification MIL-E-5007E, and Equation (3-5) lists the equations for the total pressure recovery per that standard (Ref. 1). For subsonic Mach numbers, the total pressure losses are assumed to be the result of viscous losses through the inlet boundary layers; however, the standard assumes no losses for subsonic flow. Figure 3.2 presents a plot and list of the variation of the total pressure recoveries as computed using MIL-E-5007E for a range of Mach numbers up to Mach 6.

$$\begin{aligned} \frac{p_{t2}}{p_{tL}} &= 1.0 \qquad\qquad for\ M_L \le 1 \\ \frac{p_{t2}}{p_{tL}} &= [1 - 0.075(M_L - 1)^{1.35}]\ for\ 1 < M_L \le 5 \\ \frac{p_{t2}}{p_{tL}} &= \left[\frac{800}{M_L^4 + 935}\right] \qquad for\ M_L > 5 \end{aligned} \tag{3-5}$$

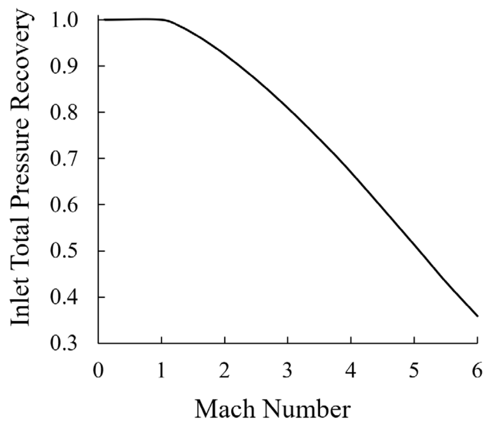

Mach	p_{t2}/p_{tL}
0.1	1.000
1.0	1.000
1.3	0.985
1.5	0.971
1.6	0.962
1.7	0.954
2.0	0.925
2.5	0.870
3.0	0.809
3.5	0.742
4.0	0.669
5.0	0.513
5.5	0.432
6.0	0.359

Figure 3.2.—MIL-E-5007E estimates of total pressure recovery.

3.4 Inlet Total Pressure Distortion

The variation of the total pressure at the engine face is expressed in terms of the ***total pressure distortion***. The ideal condition would be for the total pressure and other flow properties to be uniform at the engine face and the flow directed into the engine face. However, non-uniformities arise from gradients introduced from turbulent boundary layers, shock wave/boundary layer interactions, separated boundary layers, vortex sheets, and other disturbances ingested by the inlet or originating within the inlet. In general, higher levels of distortion result in lower performance of the engine. High levels of distortion can cause excessive vibration of fan and compressor blades which result in accelerated fatigue and possible failure. Excessive levels of distortion may also cause the flow over the fan or compressor blades of a turbine engine to stall, which leads to drastically reduced flow rates and possibly engine and inlet instabilities (i.e., compressor surge). Non-uniform conditions at the entrance to the combustor for all types of engines could lead to combustor blow-out. The assessment as to whether an inlet provides an acceptable total pressure distribution at the engine face is an aspect of the assessment of the ***inlet/engine compatibility***.

The inlet performance metrics for total pressure distortion attempt to represent the ***intensity*** and ***spatial distribution*** of the total pressure distortion. A simple and common method for representing the intensity of the total pressure distortion is,

$$\text{Min-Max Distortion} = \frac{p_{t2-max} - p_{t2-min}}{p_{t2}} \tag{3-6}$$

where $p_{t2\text{-}min}$ and $p_{t2\text{-}max}$ are the minimum and maximum measured total pressures at the engine face. This implies some way to measure or obtain the total pressures at the engine face. The metric of Equation (3-6) only assesses the intensity and provides no indication of the distribution of the total pressure at the engine face.

One approach for characterizing both the intensity and distribution of the total pressure distortion at an engine face is provided by the Society of Automotive Engineers (SAE) Aerospace Recommended Practices (ARP) 1420 document (Ref. 2). The total pressure values are obtained on a rake array at the engine face. The rake array consists of an array of total pressure probes to measure the total pressure at points at the engine face. The rake array approach is applicable for wind-tunnel and flight tests, as well as computational fluid dynamics (CFD) flowfield simulations. A rake array suggested by the SAE ARP 1420 document is the 40-probe rake array consisting of eight radial rakes with each rake containing five total pressure probes. In the circumferential direction the eight probes are located at a constant radius and form a ring about the circumference of the engine face. Each ring is placed radially at the centroid of equal-area sectors. The SAE ARP 1420 document results in circumferential and radial distortion indices for each ring, which are represented as $(DPC/P)_k$ and $(DPR/P)_k$, respectively, where the index "k" represents a ring. Also, for each ring, the procedures provide a "multiple-per-rev" index that indicates how much of the total pressure variation along the circumference of a ring was below the average for the ring. This index suggests the extent of the low-total-pressure regions at the engine face. The radial and circumferential indices for each ring can be assessed to determine if the distortion is greater at the hub or tip. A greater $(DPR/P)_k$ distortion index at the hub of the engine face is characterized as ***hub distortion*** and the overall radial distortion index (DPR/P) is set to the value of the radial distortion index at the hub or first ring, $DPR/P = (DPR/P)_1$. A greater $(DPR/P)_k$ distortion index at the tip of the engine face is characterized as ***tip distortion*** and the overall radial distortion index is set to the value of the radial distortion index at the tip or last ring, $DPR/P = (DPR/P)_5$. The overall circumferential distortion (DPC/P) is computed as the average of the two rings nearest the hub or tip depending on whether the radial distortion is hub or tip distortion. Several examples of distortion calculations are provided in the SAE AIR 1419 document (Ref. 3).

Another approach for characterizing the total pressure at the engine face are the General Electric IDC and IDR circumferential and radial distortion indices (Ref. 4). The IDR index is computed in the same manner as the SAE ARP 1420 DPR/P index. The IDC index is different than the DPC/P index and provides higher values than DPC/P.

Another approach for characterizing the total pressure at the engine face is the DC(60) distortion index computed as

$$\text{DC(60) Distortion} = \frac{p_{t2} - p_{t2(60)}}{p_{t2}} \tag{3-7}$$

where $p_{t2(60)}$ is the average total pressure over the 60-degree sector of the engine face with the lowest average total pressure. This requires some procedure for identifying the 60-degree sector and then performing the averaging over the sector.

Evaluating the severity of the values of the circumferential and radial distortion indices requires understanding the requirements of the engines as far as their tolerance to total pressure distortion. For a specific engine, tests can be conducted to assess how the engine responds to different levels of distortion and limits on the distortion indices can be stated. A general rule of thumb seems to be that $DPC/P < 0.1$ and $DPR/P < 0.1$ are baseline levels of distortion. Further, for the GE distortion indices, $IDC < 0.2$ and $IDR < 0.1$. A goal of the inlet designer is ensured that over the mission and different inlet flow conditions, the distortion indices remain well below the limits to ensure a safety margin against excessive total pressure distortion at the engine face.

3.5 Static Pressure Ratio

The static pressure ratio is the ratio of the average static pressure at the engine face to the static pressure of the local flow ahead of the inlet,

$$\text{Static Pressure Ratio} = \frac{p_2}{p_L} \tag{3-8}$$

The static pressure ratio reflects the ability of the inlet to accomplish its purpose, which is to convert kinetic energy into increased static pressure.

3.6 Static Temperatures

The discussions of Subsection 2.3 provided some understanding the effect of static temperature on the properties of the airflow through the inlet. Figure 2.3 provided one indication of temperatures within the inlet with respect to freestream Mach number with the observation that the temperatures increase as the Mach number increases. The static temperatures within the inlet are of concern with regards to inlet design and analysis when considering material limits, thermal management, and the performance of the propulsion system. The materials within the inlet have a temperature limit (T_{max}) which is not to be exceeded during normal operations. Understanding the temperatures within the inlet aids in ensuring the limits are not exceeded and that conditions within the propulsion system remain acceptable for normal operation of the engine. The ***static temperature ratio*** (ψ) is defined as the average static temperature at the engine face (T_2 or T_3) divided by the temperature of the local flow entering the inlet (T_L)

$$\psi = \frac{T_3}{T_L} \tag{3-9}$$

The static temperature at station (T_3) is used in Equation (3-9) since temperatures are of greater concern at the higher Mach numbers of inlets for ramjet and scramjet engines.

For turbojet and turbfan engines, the static temperature ratio would use the average static temperature at station 2 (T_2). A mechanical compressor further compresses the flow to station 3 with a static temperature of T_3. The maximum allowable compression temperature is usually limited by the ability of the compressor and combustor materials to withstand the higher temperatures, the desired temperature at which to inject the fuel, and the limit to the static temperature at the end of the combustion as the flow enters the turbines, T_{4max}. Under normal operating conditions, the engine can usually adapt to the normal variations of the freestream flow into the inlet. There may be instances of concern when higher temperature flow is ingested into the inlet. This may occur for helicopters or VSTOL aircraft in hover when high-temperature nozzle or exhaust flow gets ingested in the inlet.

For ramjet or scramjet inlets, the inlet compresses the flow to station 3 with a static temperature of T_3. Thus, the inlet design must not exceed the maximum allowable temperature. The limit is imposed due to limits of the combustor. Further, the limit is imposed to avoid dissociation of the flow. This unequilibrated dissociation represents a loss of energy in the flow. This is of real concern for hypersonic systems. The exit static temperature depends on the flight altitude and Mach number, inlet losses, and engine cycle design. A typical limit is T_{3max} = 2800 °R (1560 K) (Ref. 5).

3.7 Engine-Face Mach Number

The Mach number at the exit of the inlet is of importance because the engine is usually designed to accept a certain range and limit of Mach numbers. A gas turbine engine requires a subsonic Mach number at station 2, which usually ranges approximately $0.3 < M_2 < 0.6$. This compressor face Mach number can be directly related to the corrected mass flow, as discussed in Subsection 2.8. Ramjet engines require a subsonic entry flow at station 3 (M_3) while scramjet engines require a supersonic entry flow ($M_3 > 1$). The limit on the maximum allowable temperature leads directly to the limit on the entry Mach number for scramjet engines. The result is that the flow must remain supersonic. The frequently used rule of thumb (Ref. 5) is,

$$\frac{M_3}{M_0} = \sqrt{\frac{T_0}{T_3}} \cong \sqrt{\frac{400}{2800}} \cong 0.38 \tag{3-10}$$

It has been further determined from combustion studies that supersonic combustion is possible starting at approximately $M_3 \approx 6.4$. This result enforces the belief that hypersonic flight requires scramjet propulsion (Ref. 5).

3.8 Contraction Ratio

A contraction ratio involves a ratio of cross-sectional areas between two stations within the inlet. Several contraction ratios can be defined, and their use is mainly of interest for supersonic compression, in which the cross-sectional area of the inlet streamtube contracts as the Mach number is decreased. Thus, a contraction ratio provides a measure of the level of the supersonic compression. Some of the contraction ratios of interest are,

$$\text{Geometric Contraction Ratio}, CR_g = \frac{A_{cap}}{A_{TH}} \tag{3-11}$$

$$\text{Effective Contraction Ratio}, CR_{eff} = \frac{A_L}{A_{TH}} \tag{3-12}$$

$$\text{Internal Contraction Ratio}, CR_{int} = \frac{A_1}{A_{TH}} \tag{3-13}$$

Figure 3.3 shows the stations and areas used for defining the contraction and compression ratios for a mixed-compression inlet. For an external-compression inlet, the supersonic compression only occurs to station 1, and so, the Equations (3-11) and (3-12) would use A_1 rather than A_{TH} for the geometric and effective contraction ratios, respectively. For the mixed-compression inlet of Figure 3.3, station TH marks the end of the supersonic compression and A_{TH} is the smallest area along the supersonic portion of the inlet streamtube.

For a mixed-compression inlet, the contraction ratios provide a measure of the split between external and internal supersonic compression that can be used to characterize mixed-compression inlets (Ref. 6). The split is defined as compression ratios using the differences in areas at the respective stations. The external and internal compression ratios are calculated as,

$$\text{External Compression Ratio} = \frac{A_L - A_1}{A_L - A_{TH}} \tag{3-14}$$

$$\text{Internal Compression Ratio} = \frac{A_1 - A_{TH}}{A_L - A_{TH}} \tag{3-15}$$

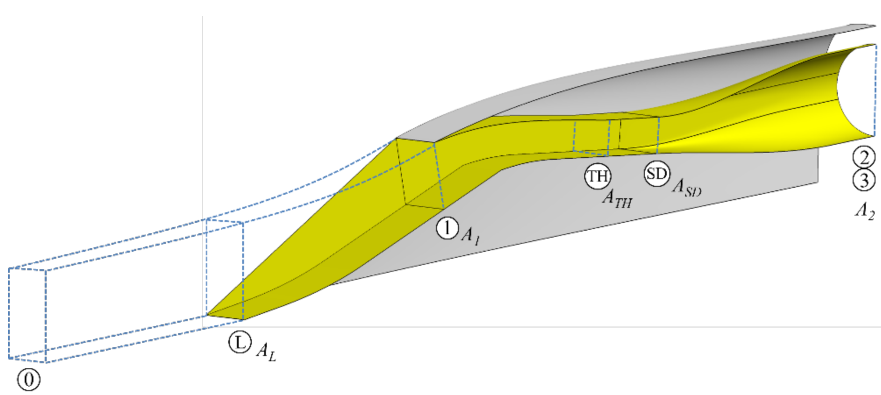

Figure 3.3.—Inlet stations and areas used for determining contraction and compression ratios for a mixed-compression inlet.

A common approach for expressing the split between external and internal compression is using percentages of each compression. For example, an inlet for which the external and internal compression ratios are 0.55 and 0.45, respectively, would be referred to as having a supersonic compression split of 55% external compression and 45% internal compression. Informally, the inlet would be considered a "55-45" inlet (Ref. 6).

3.9 Adiabatic Compression Efficiency

The ***adiabatic compression efficiency*** (η_C) is the basic thermodynamic efficiency for a compression process that relates the actual compression to an ideal compression. It is defined as

$$\eta_C = \frac{h_3 - h_x}{h_3 - h_L} \tag{3-16}$$

In Equation (3-16), station 3 is used as the end of the compression process, but station 2 could be used depending on the type of inlet and compression process. Likewise, the subscript L can be replaced by the freestream station subscript 0 if conditions don't change across the approach flow segment. The specific enthalpy h_X is the specific enthalpy at end of the compression (station 2 or 3) if it were isentropically expanded to local static pressure (p_L). The compression process is represented on the enthalpy-entropy diagram of Figure 3.4 showing the conditions of Equation (3-16). The curves of constant pressure are shown within Figure 3.4.

It is assumed that the air behaves as calorically perfect air during the compression process with average values for the specific heat at constant pressure (C_{pc}) and ratio of specific heats (γ_C). Thus,

$$h = C_{pc}\, T \tag{3-17}$$

The adiabatic compression efficiency can then be expressed in terms of the static temperature ratio (ψ) as

$$\eta_C = \frac{\psi - \frac{T_x}{T_L}}{\psi - 1} \tag{3-18}$$

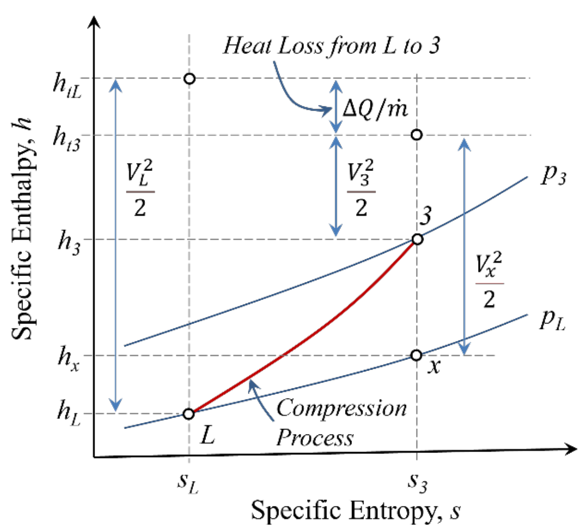

Figure 3.4.—Compression process on the enthalpy-entropy diagram.

Where T_x is the temperature associated with h_x as computed using Equation (3-17). The temperature T_x can also be calculated from Equation (2-10) using the assumption of isentropic conditions, constant specific heats, and known values of p_L, p_3, and T_3.

3.10 Kinetic Energy Efficiency

The ***kinetic energy efficiency*** (η_{KE}) measures the ability of the inlet to maintain kinetic energy during the compression process and is defined as

$$\eta_{KE} = \frac{h_{t3} - h_X}{h_{tL} - h_L} \tag{3-19}$$

The conditions of Equation (3-19) are illustrated in the enthalpy-entropy diagram of Figure 3.4. With the definition of specific total enthalpy of $h_t = h + V^2/2$, Equation (3-19) can be expressed as.

$$\eta_{KE} = \frac{V_x^2}{V_L^2} \tag{3-20}$$

where V_x^2 is the velocity that the inlet exit flow would achieve if it were isentropically expanded to freestream static pressure and can be calculated as

$$V_x^2 = V_L^2 - 2C_{pc}(T_L - T_x) \tag{3-21}$$

The kinetic energy efficiency can be expressed in terms of the adiabatic compression efficiency and the static temperature ratio as

$$\eta_{KE} = 1 - \frac{2(\psi - 1)(1 - \eta_C)}{(\gamma_c - 1)M_L^2} \tag{3-22}$$

In terms of total pressure, the kinetic energy efficiency can be computed as

$$\eta_{KE} = 1 - \frac{2}{(\gamma_c - 1)M_L^2}\left\{\left(\frac{p_{tL}}{p_{t2}}\right)^{(\gamma_c-1)/\gamma_c} - 1\right\} \tag{3-23}$$

The kinetic energy efficiency is commonly used in hypersonics because it is referenced to the freestream conditions, rather than the stagnation conditions, which are used to define the total pressure recovery and may be difficult to properly define when high-temperature effects are significant. Further, the kinetic energy efficiency is directly related to the kinetic energy, which is the most important for producing thrust in ramjet and scramjet propulsion (Ref. 5).

The compression process may involve heat transfer due to absorption by the inlet structure of the heat generated by the viscous dissipation or by cooling of the inlet surface. The amount of heat transfer ($\Delta Q/\dot{m}$) is illustrated in Figure 3.4 and can be expressed as

$$\frac{\Delta Q}{\dot{m}} = h_{tL} - h_{t3} \tag{3-24}$$

For adiabatic compression, there is no heat transfer and the total enthalpy remains unchanged between stations L and 3 (i.e., $h_{t3} = h_{tL}$). The adiabatic kinetic energy efficiency can then be expressed as

$$\eta_{KE,ad} = \frac{h_{tL} - h_X}{h_{tL} - h_L} \tag{3-25}$$

3.11 Incompressible Flow Ratio

The ***incompressible flow ratio*** (η_{σ_i}) uses the differences between the total and local static pressures (p_L) to define the ratio and provides a better measure for subsonic conditions. The incompressible flow ratio is defined by the formula,

$$\eta_{\sigma_i} = \frac{p_{t_f} - p_L}{p_{t_L} - p_L} \tag{3-26}$$

References

1. MIL-E-5007E, “Engines, Aircraft, Turbo-Jet, and Turbofan, General Specifications For,” September 1983.
2. Society of Automotive Engineering (SAE), “Gas Turbine Engine Inlet Flow Distortion Guidelines,” Aerospace Recommended Practice (ARP) 1420, Revision C, April 2017.
3. Society of Automotive Engineering (SAE), “Inlet Total-Pressure-Distortion Considerations for Gas Turbine Engines,” Aerospace Information Report (AIR) 1419, Revision C, November 2017.
4. Moore, M. T. “Distortion Data Analysis,” Report AFATPL-TR-72-111, February 1973.
5. Heiser, W. H. and Pratt, D. T., *Hypersonic Airbreathing Propulsion*, AIAA Education Series, New York, 1994.
6. Bowditch, D. N., “Some Design Considerations for Supersonic Cruise Mixed Compression Inlets,” NASA TM X-71460, November 1973.

4.0 SUPIN

The Supersonic Inlet Design and Analysis Tool (SUPIN) is a computer program developed by the Inlets and Nozzles Branch of the NASA John H. Glenn Research Center to provide a fundamental capability for the design and analysis of inlets. This section provides an overview of the key aspects of SUPIN and its input and output files. Later sections will provide additional information on the design and analysis methods within SUPIN as they relate to specific types of inlets, as well as the inputs required for the specification of those inlets.

4.1 Overview of SUPIN

The primary objective of the development of SUPIN has been to develop a self-contained computational tool capable of running on Windows, Unix/Linux, and Macintosh systems that uses mostly analytical methods to generate inlet geometry and perform aerodynamic design and analysis of inlets. The geometry modeling uses mostly planar geometry constructs with some three-dimensional geometry modeling. SUPIN performs aerodynamic analysis using analytic, empirical, and computational methods. Many of the methods assume quasi-one-dimensional flow; however, some methods, such as for oblique shock waves and method-of-characteristics, use planar geometry assumptions. The SUPIN code is written in Fortran 95. SUPIN does not require external software licenses, such as for geometry generation or aerodynamic analysis. SUPIN is executed in batch or background mode in which an ***input data file*** named SUPIN.in is read in and an ***output data file*** named SUPIN.Out.txt is written out. The input and output data files are both standard ASCII text files. During execution, SUPIN will write some lines to the screen to indicate progress, as well as a couple lines of summary results. SUPIN generally executes in a matter of seconds when just performing geometry generation and design and analysis. SUPIN may write some other output files, such as for plotting the quasi-one-dimensional properties through the inlet or coordinates for the planar geometry. SUPIN can automatically generate a ***surface grid*** for visualizing the inlet surfaces, as well as provide surface definition for grid generation for computational fluid dynamics (CFD) analysis. The surface grid is output to the Plot3D-formatted file named SUPIN.xyz. For some inlets, SUPIN can generate complete three-dimensional, multi-block, structured grids ready for CFD analysis. For the generation of grid files of about 30 million grid points, the execution of SUPIN may require a couple of minutes. Section 13.0 will provide further details on the surface and CFD grid generation.

4.2 SUPIN Input Data File

The SUPIN ***input data file*** named ***SUPIN.in*** is an ASCII text file that is read in at the start of the execution of SUPIN and should completely define the inlet design and analysis problem and provide all instructions to SUPIN. The first three lines of the input data file are lines of text that can be used to describe or document the input data file. These three lines are referred to as the ***title block*** for the input data file and are read in as character streams and can be any text that describes the input data file.

The remainder of the input data file consists of a series of ***input data blocks*** that contain input factors that direct the operations that SUPIN is to perform and define the inlet design and analysis problem. Each block is identified by its ***data block identification number*** (***DataID***). The DataID number indicates to SUPIN how to read the data within the respective input data block. Table 4.1 lists the input data blocks available within SUPIN and their corresponding DataID number. The input data blocks shown in red italics are not yet fully developed or implemented but are included as placeholders. An important input data block is one which provides the main control of SUPIN (DataID = 0). This data block and its input

TABLE 4.1.—INPUT DATA BLOCKS AND ID NUMBERS FOR THE INPUT DATA FILE
[*The items listed in red italics are not yet fully functional.*]

DataID	Description	DataID	Description
0	Main Control of SUPIN	16	Components and Entities
1	Freestream Conditions	17	Geometry Transformations
2	Approach Flow	18	Variable Geometry
3	*Capture Cross-Section*	19	Schedules
4	External Supersonic Diffuser	20	*Not assigned*
5	Uniform Cowl Lip	21	*Inlet surface grid input*
6	Cowl Exterior	22	*Vortex generators*
7	Three-Dimensional Cowl Lip	23	Unit Problem Calculations
8	Throat Section	24	Reference Dimension
9	Support Struts	25	Forebody Step Diverter
10	Subsonic Diffuser	26	Forebody Geometry Model
11	Engine Face	27	*Sidewall Geometry*
12	Bleed and Bypass	28	*Auxiliary Intake*
13	Flow Domain and Grid Spacing	29	Global Geometry Transformations
14	Variations	30	Output Summary Table
15	Shoulder Bleed Slot	31	*3D Engine Face*

factors are described in Subsections 4.3, 4.4, and 4.5. Subsections 4.6 through 4.13 discuss the common inputs for the components and stations of the inlet flowpath, which include the freestream, approach flow, external supersonic diffuser, cowl lip, cowl exterior, throat section, internal supersonic diffuser, subsonic diffuser, and engine face. Subsection 4.15 discusses the specification of geometric entities that can be used to form the components of the inlet.

The input data blocks can be listed in any order within the input data file. Further, the input data file does not have to include certain input data blocks that don't apply to the specific inlet design and analysis problem. Some analyses may not require a certain part to be specified or SUPIN can use default values of inputs. For example, SUPIN can design just the external supersonic diffuser without having to design the throat or subsonic diffuser, and so, the blocks for the throat and subsonic diffuser do not need to be in the input data file.

Within each input data block, the lines of input provide values for the various input factors that specify the geometric and aerodynamic characteristics of the respective component described by the input data block. The lines of input within the input data block consists of header lines and data input lines. The header lines contain text to describe the block or input factors. Most of the header lines are then followed by a data line that specifies integer and real number inputs for the input factors listed in the header file. Most of the input factors involving lengths require input values that have been normalized by a reference dimension, which is nominally the diameter of the engine face. Some inputs for lengths and area are required to be dimensional and use units of feet or square feet. Input factors involving angles require the inputs to be in units of degrees. Further details on the structure and the input factors contained within each block will be presented in later sections of this document for a specific inlet type and component. Examples of these input lines will be provided below.

All the input data blocks must start with a standard header of 4 lines: 1) a blank spacer line, 2) a separator line consisting of a string of dashes or other character, 3) a header for the DataID input, and then 4) a line containing an integer corresponding to the input data ID. Table 4.2 shows an example input data block for DataID = 0, which provides some of the main inputs for SUPIN. The DataID number, as well as other inputs, do not need to be in a certain column, but the number and type of inputs needs to be as specified. The DataID number signals to the input data file reader which block is being read and how to interpret the rest of the lines of input in that input data block.

TABLE 4.2.—EXAMPLE INPUT BLOCK FOR THE MAIN CONTROL OF SUPIN (DataID = 0)

```
(blank spacer line)
-----------------------------------------------------------
DataID.  Main Control for SUPIN
  0
Kmode   Ktyp   Kcomp   Ksurf   KgCFD
  2       3      1       1       0
KWinp     FWinp     KWunit     FAcap     Fwclip
  3     0.520000       0     6.005044    1.0000
WRspill   WRbleed   WRbypass   WRother
0.02000   0.04000    0.00000   0.00000
```

The remaining inputs for the input data block consist of a series of header and input data lines. In the example of Table 4.2, the header line that starts with "Kmode" is followed by an input data line containing values for the input factors. The input data consists of integer flags and real number values. Later sections will describe these factors for the various blocks which are listed in Table 4.1. Each line of each block will not be described here, but the tables and example input data files should provide a good starting point for understanding the input data file. The general format is to have a header line listing the sequence of input data followed by a line containing the values of the input data. The inputs are not required to be in specific columns, but spaces are needed between values to distinguish between the input data. Some inputs need several lines of input, such as inputs for several stages of the external supersonic diffuser. The input data file reader will continue to read the input data file until all the input data blocks have been read and the end of the file has been reached.

The structure of the input data file and the values of the input factors are written to the start of the ***output data file*** named ***SUPIN.Out.txt***. This "echo" of the input data file provides a record of what SUPIN read. Once SUPIN has completed its execution, it writes a new input data file (***SUPIN.new.in***) with updated values of some of the inlet factors listed in the input data file (e.g., the calculated lengths and angles will be written to the new input data file). One can then use the new input data file as the input data file for SUPIN by copying it over to SUPIN.in.

4.3 Main Control of SUPIN

The input factors that provide the main control of the execution of SUPIN are found in the input data block with DataID = 0. Table 4.2 provides an example of this input data block. The input factors discussed in this subsection include $\boldsymbol{K_{mode}}$, $\boldsymbol{K_{typ}}$, and $\boldsymbol{K_{comp}}$. Such input factors that at begin with "*K*" indicate flags that select between specific options, and so, within Fortran are read and written as integers. The factors that begin with "*F*" provide inputs and within Fortran are read and written as real floating-point numbers. The reading of the input data file requires the input factors in each line be listed in the order shown and the lines be read in order shown. Along each line, the factors and values are not required to be in specific columns; however, there must be at least one space between each input value.

The input factor $\boldsymbol{K_{mode}}$ establishes the design and analysis mode for SUPIN and there are four options:

- K_{mode} = 0. *Unit Problem Mode*. This mode is used to perform certain aerodynamic calculations apart from the design or analysis of an inlet. Examples of such calculations include computation of the flow about a cone or through a normal shock wave. Sample SUPIN input files are provided and described in the Appendices for these types of computations.
- K_{mode} = 1. *Inlet Geometry Mode*. For the Inlet Geometry Mode, the input factors should explicitly define the geometry of the inlet. SUPIN constructs the profiles and surfaces of the inlet geometry and reports on the area distributions through the inlet. The aerodynamic performance of the inlet

is not calculated. This mode can only be used for the pitot, axisymmetric spike, and two-dimensional inlets and not the streamline-traced inlet.

- K_{mode} = 2. *Inlet Design Mode*. For the Inlet Design Mode, the inlet is sized and designed according to a design point associated with freestream and engine-face conditions, flow rates, and design objectives specified within the input data file. The profiles, area distributions, and surfaces of the inlet are determined. The aerodynamic performance of the inlet is also calculated.
- K_{mode} = 3. *Inlet Analysis Mode*. For the Inlet Analysis Mode, the inlet geometry is specified, and the aerodynamic performance of the inlet is calculated. This mode is used to evaluate the performance of an inlet for off-design freestream conditions and flow rates. *At this time, this mode is still being developed and is not fully functional.*
- K_{mode} = 4. *Inlet Flowpath Analysis Mode*. This mode allows an analysis of the quasi-one-dimensional flow through the inlet streamtube with consideration of just the cross-section area, total pressure, and Mach number at the stations of the flowpath.

The input factor $\boldsymbol{K_{typ}}$ specifies the type of inlet. SUPIN uses a set of six inlet types to facilitate the inlet design and analysis. Those inlet types are listed in Table 4.3. Example images of the inlet types are presented in Figure 4.1. The set encompasses traditional inlet shapes (e.g., pitot, two-dimensional, and axisymmetric spike inlets) while allowing some flexibility for the design and analysis of more advanced inlet concepts (e.g., streamline-traced inlets). This set of inlet types can be used to establish baseline inlet properties and performance data for inlet concepts and design conditions. Further, these inlet types can provide inlet geometry from which detailed inlet design can be performed with other software packages. The specification of the type of inlet simplifies the geometry modeling and design methodology since the general topology of an inlet is established with the selection of the inlet type.

Each inlet type is associated with a set of input factors that defines and parameterizes the geometry and flow conditions for the inlet. Thus, a variety of inlet shapes can be generated within each inlet type. Each inlet is defined in an inlet-fixed Cartesian coordinate (x,y,z) system. Much of the geometry of the inlets can be constructed from planar geometry constructs, such as lines, conics, and curves that are then extruded about an axis or curve. This reduces the complexity of the geometry modeling and eliminates the need for complex geometry software. Each inlet type is discussed in greater detail in later subsections.

The input factor $\boldsymbol{K_{comp}}$ specifies the manner of supersonic compression for the inlet. Table 4.4 lists the options for K_{comp}. The option of K_{comp} = 0 indicates a subsonic inlet with no supersonic compression. The option of K_{comp} = 1 indicates that only external supersonic compression is expected for the inlet, and so, the inlet is regarded as an external-compression inlet. The supersonic compression occurs on the external supersonic diffuser and the terminal shock wave is in the region of station 1, which is the start of the internal ducting and cowl lip of the inlet. External supersonic compression allows subsonic flow to spill past the cowl lip to allow for matching of the inlet flow to the engine. For the design mode (K_{mode} = 2), it is assumed that the external-compression inlet is operating at its critical operating point with a specified level of supersonic spillage.

TABLE 4.3.—INPUT FACTOR FOR THE INLET TYPE

K_{typ}	Type of Inlet
0	Generic Quasi-1D Inlet for Flowpath Analysis
1	Axisymmetric Pitot Inlet
2	Two-Dimensional Inlet
3	Axisymmetric Spike Inlet
4	Two-Dimensional, Bifurcated-Duct Inlet
5	Streamline-Traced Inlet
6	Three-Dimensional Pitot Inlet

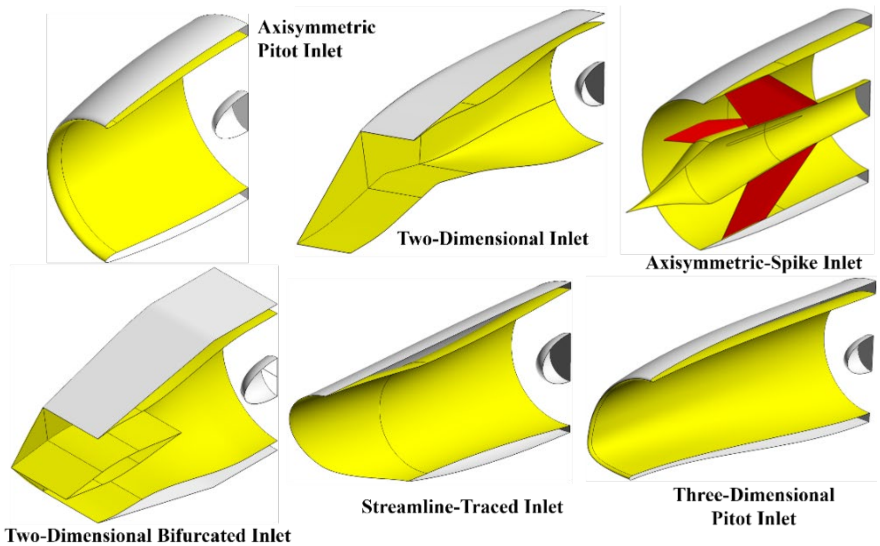

Figure 4.1.—Images of examples of the types of inlets available within SUPIN.

TABLE 4.4.—INPUT FACTOR FOR THE FORM OF THE SUPERSONIC COMPRESSION

K_{comp}	Type of Supersonic Compression
0	Subsonic inlet
1	External-compression inlet
2	Mixed-compression inlet with subsonic outflow
3	Mixed-compression inlet with supersonic outflow

The option of K_{comp} = 2 indicates that both external and internal supersonic compression is expected for the inlet, and so the inlet is regarded as a mixed-compression inlet. As with the external-compression inlet, supersonic compression occurs on the external supersonic diffuser. The flow at the end of the external supersonic diffuser at station EX is supersonic and coincides with station 1. The internal supersonic diffuser extends between stations 1 and the geometric throat station TH. SUPIN offers several methods for the design of the internal supersonic diffuser. For the design mode (K_{mode} = 2), it is assumed that the terminal shock wave is placed between stations TH and SD within the throat section. The inlet contains a subsonic diffuser, and so, is of use for turbine and ramjet engines.

The option of K_{comp} = 3 also indicates a mixed-compression inlet, however, the internal supersonic diffuser is followed by an isolator. This compression option is used for dual-mode ramjet (DMRJ) and scramjet engines. The outflow of the isolator can be subsonic or supersonic. In scramjet mode of the DMRJ or for the scramjet engine, the outflow is supersonic.

4.4 Inlet Flow Rates and Ratios

The inlet operates to capture airflow and provide the airflow to the engine. The design (K_{mode} = 2) and analysis (K_{mode} = 3) modes of SUPIN require some specification of the capture or engine face flow rate. SUPIN offers several options for these flow rates. The various input factors that specify the inlet flow rates are presented in Table 4.5. The input factor $\boldsymbol{K_{Winp}}$ indicates how the inlet flow rate is specified. The value listed in the square brackets (e.g., “[0]”) at the end of the description text indicates the default value for the input factor K_{Winp}. The input factor $\boldsymbol{F_{Winp}}$ is the input value corresponding to K_{Winp}. The input factor $\boldsymbol{K_{Wunit}}$ indicates the units for F_{Winp}.

TABLE 4.5.—INPUT FACTORS FOR THE INLET FLOW RATE AND FLOW RATIOS

Factor	Input	Description
K_{Winp}	`KWinp`	Flag indicating nature of the flow rate input [0] = 0 no flow rate information specified = 1 specify actual engine flow rate W_2 (F_{Winp} is W_2) = 2 specify corrected engine flow rate W_{C2} (F_{Winp} is W_{C2}) = 3 specify average engine face Mach M_2 (F_{Winp} is M_2) = 4 specify capture flow rate W_{cap} (F_{Winp} is W_{cap}) = 5 specify capture area A_{cap} then compute W_{cap} (F_{Acap} is A_{cap})
F_{Winp}	`FWinp`	Input for flow rate (see K_{Winp})
K_{Wunit}	`KWunit`	Flag indicated the units of the flow rate [0] = 0 non-dimensional. = 1 slug/s. = 2 lbm/s.
F_{Acap}	`FAcap`	Input for reference capture area (ft^2)
F_{wclip}	`Fwclip`	Width or circumferential extent of the capture cross-section For K_{typ} = 1, 5, and 6, F_{wclip} = 1.0 for the full extent of the circumference For K_{typ} = 2 and 4, F_{wclip} is the cross-stream width normalized by D_{ref} For K_{typ} = 2 and 4, $F_{wclip} < 0$, $\lvert F_{wclip} \rvert$ is the capture aspect ratio (w_{cap}/h_{cap}) For K_{typ} = 3, F_{wclip} indicates the extent of the circumference
$W_{spillage}/W_{cap}$	`WRspill`	Flow ratio for the spillage [0.0]
W_{bleed}/W_{cap}	`WRbleed`	Flow ratio for the bleed flow [0.0]
W_{bypass}/W_{cap}	`WRbypass`	Flow ratio for the bypass flow [0.0]
W_{other}/W_{cap}	`WRother`	Flow ratio for other flows (leakage, cooling) [0.0]

For option K_{Winp} = 1, the actual engine-face flow rate (W_2) is explicitly specified through the input F_{Winp}. For option K_{Winp} = 2, the engine-face corrected flow rate (W_{C2}) is explicitly specified through the input F_{Winp}. For option K_{Winp} = 3, the mass-averaged Mach number at the engine face (M_2) is specified through the input F_{Winp} and Equation (2-18) is used to calculate the corresponding corrected engine flow rate W_{C2}. For option K_{Winp} = 4, the reference capture flow rate (W_{cap}) is specified through the input F_{Winp}. For option K_{Winp} = 5, the reference capture area (A_{cap}) as specified by $\boldsymbol{F_{Acap}}$ is used along with the freestream conditions to establish the reference capture flow rate, W_{cap}. The units for $\boldsymbol{F_{Acap}}$ are in square feet.

For the geometry mode (K_{mode} = 1) and the analysis mode (K_{mode} = 3), it is assumed the inlet geometry is completely specified. In some cases, the capture area (A_{cap}) is required to be specified to complete the generation of the inlet geometry. The input factor $\boldsymbol{F_{Acap}}$ provides the means of specifying the reference capture area for the inlet. The units for $\boldsymbol{F_{Acap}}$ are in square feet.

The input factor $\boldsymbol{F_{wclip}}$ specifies the extent of the capture cross-section and external supersonic diffuser. For the two-dimensional inlets (K_{typ} = 2 or 4), the factor F_{wclip} is the width in the cross-stream direction normalized by the reference dimension D_{ref}. The reference dimension is discussed in further detail below in Subsection 4.14, but nominally is the diameter of a circular engine face. If F_{wclip} is specified as a negative value, then its absolute value is ($|F_{wclip}|$) the desired aspect ratio of the capture cross-section (w_{cap}/h_{cap}). For an axisymmetric spike inlet (K_{typ} = 3), the factor F_{wclip} is the fraction of the full circumferential extent for the external supersonic diffuser. An axisymmetric spike inlet with a full 360-degree aperture would have F_{wclip} = 1.0, while a half-circumference axisymmetric spike inlet would have F_{wclip} = 0.5. For the pitot (K_{typ} = 1 or 6) and streamline-traced inlets (K_{typ} = 5), F_{wclip} = 1.0. This use of this input factor will be discussed further in the later sections on the specific inlets.

The flow balance of Equation (2-29) relates the normalized actual engine flow (W_2/W_{cap}) to other flow rates in the inlet. The sizing procedure requires estimates of the normalized flow rates listed on the right-hand side of Equation (2-29). The input data file allows inputs for these flow ratios for spillage ($W_{spillage}/W_{cap}$), bleed (W_{bleed}/W_{cap}), bypass (W_{bypass}/W_{cap}), and other (W_{other}/W_{cap}) flows and the input factors for these flow ratios are listed in Table 4.5. The defaults for all these input factors are values of zero flow ratios. For supersonic freestream flow with an external supersonic diffuser, the input factor for

$W_{spillage}/W_{cap}$ specifies the desired value of supersonic spillage. Section 7.0 discussing external supersonic compression will provide further details on how this input factor for supersonic spillage is used to establish the geometric dimensions of the external supersonic diffuser. The input factor for the bleed flow ratio W_{bleed}/W_{cap} specifies the total bleed of the of inlet and the bleed flow is assumed to be taken within the throat section. Section 11.0 will discuss further details concerning bleed flows. Included within Section 11.0 are input factors for specifying bleed throughout the inlet in a more detailed manner.

The estimates for the spillage, bleed, bypass, and other flow ratios affect the sizing of the inlet. Using the estimates for the flow ratios, Equation (2-29) can be solved for the normalized engine flow rate (W_2/W_{cap}). Equation (2-18) can then be used to calculate the actual engine flow rate (W_2) from the corrected flow rate (W_{C2}) if the total pressure (p_{t2}) and total temperature (T_{t2}) at the engine face are known or estimated. The total temperature at the engine face is determined by assuming adiabatic flow through the inlet, $T_{t2} = T_{tL}$. The total pressure recovery (p_{t2}/p_{tL}) for the inlet is obtained through an iteration procedure as part of the inlet sizing. Within SUPIN, an initial estimate of the total pressure recovery is obtained using the military specification MIL-E-5007E as discussed in Subsection 3.3. SUPIN then performs a fixed-point iteration to converge on a value of the total pressure recovery and inlet flow rate. This involves performing the aerodynamic analysis of each part of the inlet. If SUPIN is performing an inlet design ($K_{mode} = 2$), then the actual flow rate can be used to determine the required reference capture flow rate (W_{cap}) and the reference capture area (A_{cap}). An iterative process is involved as part of the design process to converge to the proper reference capture area for the inlet. If the reference capture area is specified through $K_{Winp} = 5$ and the value of F_{Acap}, then the specified value of A_{cap} is imposed and the iteration process converges on the inlet total pressure ratio (p_{t2}/p_{tL}).

4.5 Surface and CFD Grid Files

SUPIN can generate surface and volume grids for use with methods of computational fluid dynamics (CFD). The generation of surface grids provides a means of visualizing the inlet geometry, as well as, providing geometry for the generation of computational grids for CFD. The input factor $\boldsymbol{K_{surf}}$ indicates whether the inlet surface grids are to be generated and in which format they are to be written. Table 4.6 lists the options for K_{surf}. For $K_{surf} = 1$, SUPIN generates structured, quadrilateral surface grids for the inlet surfaces and writes out a file named SUPIN.xyz that is a three-dimensional, unformatted, multi-block, structured Plot3D file (Ref. 1). For $K_{surf} = 2$, SUPIN generates triangles from the quadrilaterals and writes the surface grids as a formatted stereolithography (STL) file named SUPIN.stl. For $K_{surf} = 3$, SUPIN generates and writes both the Plot3D and stereolithography files.

SUPIN can generate planar and three-dimensional multi-block, structured grids for use with a CFD solver to perform simulations of the inlet flowfield. The input factor $\boldsymbol{K_{gCFD}}$ indicates whether planar or three-dimensional CFD grids are to be generated. Table 4.6 lists the options for K_{gCFD}. Planar CFD grids are generated on the plane of symmetry of the inlet when $K_{gCFD} = 2$. Planar CFD grids can only be generated for the axisymmetric inlets ($K_{typ} = 1$ or 3) and for the two-dimensional inlet ($K_{typ} = 2$) in which the subsonic diffuser has a rectangular cross-section. It is not possible to generate a planar CFD grid for a two-dimensional inlet in which the subsonic diffuser transitions from a rectangle to circular cross-section. The three-dimensional CFD grids are generated when $K_{gCFD} = 3$.

If K_{surf} and K_{gCFD} are not one of the values listed in Table 4.6, then the flags are set to zero and the surfaces or CFD grids are not generated. If $K_{surf} = 0$ and $K_{gCFD} = 2$ or 3, then K_{surf} is reset to $K_{surf} = 1$, by default, so that the surface grids can be generated for the CFD grids. Section 13.0 will discuss further details on the generation of the surface and CFD grids and the input factors that provide inputs for grid spacings and flow domain boundaries.

TABLE 4.6.—INPUT FACTORS FOR THE SURFACE AND CFD GRID GENERATION

Factor	Input	Description
K_{surf}	`Ksurf`	Flag indicating whether the inlet surface grids are generated [0] = 0 do not generate the inlet surface grids = 1 generate the inlet surface grids and output grids in Plot3D format = 2 generate the inlet surface grids and output grids in STL format = 3 generate the inlet surface grids and output grids in Plot3D and STL formats
K_{gCFD}	`KgCFD`	Flag indicating whether the CFD grids are to be generated [0] = 0 do not generate CFD grids = 2 generate the two-dimensional CFD grids = 3 generate the three-dimensional CFD grids

4.6 Freestream

The ***freestream*** represents the flow conditions approaching the aircraft or an isolated inlet. The freestream is designated as station 0, as discussed in Section 2.0. The freestream flow conditions are established based on a reference point from the aircraft mission, wind tunnel test section flow conditions, or explicitly specified flow conditions for a given analysis. Within SUPIN, the freestream flow conditions are assumed to be uniform and steady. The speed of the flow is indicated by the freestream Mach number (M_0). The attitude of the inlet with respect to the freestream flow is specified by the angle-of-attack (α_0) and angle-of-sideslip (β_0). The freestream angle-of-attack (α_0) is the angle-of-incidence of the aircraft with respect to the freestream flow direction in the x-y plane with a positive value indicating an upward deflection of the nose of the aircraft. The freestream angle-of-sideslip (β_0) is the angle-of-incidence of the aircraft with respect to the freestream flow direction in the x-z plane with a positive value indicating a deflection to the left side of the aircraft. *At this time, SUPIN does not yet have models implemented which account for angle-of-attack and angle-of-sideslip. Thus, SUPIN, by default, sets both angles to zero ($\alpha_0 = \beta_0 = 0$).* The final two properties required to define the freestream flow conditions are two thermodynamic properties, such as the static pressure (p_0) and static temperature (T_0).

The input factors for specifying the freestream flow conditions within SUPIN are listed in Table 4.7. The input factor $\boldsymbol{K_{fs}}$ indicates the options for specifying the two thermodynamic properties. For $K_{fs} = 1$, atmospheric models are used to obtain the two thermodynamic properties as a function of the altitude (h_0) in feet. The input factor $\boldsymbol{K_{atm}}$ indicates the atmospheric model used and has options for standard, cold day, hot day, and tropical day atmospheric models. References 2 and 3 discuss the 1976 US Standard Atmosphere. The description of the cold, hot, and tropical days are discussed in Reference 3. For $K_{fs} = 2$, the static pressure (p_0) and static temperature (T_0) are specified. Pressures are input in units of pounds-force per square foot (psf). Temperatures are input in units of degrees Rankine (°R). For $K_{fs} = 3$, the total pressure (p_{t0}) and total temperature (T_{t0}) are specified. For $K_{fs} = 4$, the dynamic pressure (q_0) is specified in units of pounds-force per square foot (psf). With the freestream Mach number (M_0) specified, the static pressure (p_0) can be computed using Equation (2-4). The respective atmospheric model (K_{atm}) is used to establish the altitude (h_0) and the static temperature (T_0). This option is useful when the freestream conditions are constrained to a dynamic pressure along the aircraft flightpath. The option for $K_{fs} = 5$ is similar to $K_{fs} = 4$; however, the total pressure (p_{t0}) is specified for the pressure input. The option for $K_{fs} = 6$ computes the freestream thermodynamic conditions based on the specified Reynolds number per foot (Re/ft) and static temperature (T_0). Table 4.8 provides multiple example freestream input data blocks for the different options of K_{fs}. The DataID = 1 indicates that the input data block is specifying the freestream conditions.

TABLE 4.7.—INPUT FACTORS FOR THE FREESTREAM CONDITIONS

Factor	Input	Description
K_{fs}	`Kfs`	Flag indicating the manner of specification of p and T [1] = 1 specify altitude (h_0) and use atmospheric models = 2 specify static pressure (p_0) and static temperature (T_0) = 3 specify total pressure (p_{t0}) and total temperature (T_{t0}) = 4 specify dynamic pressure (q_0) and calculate altitude (h_0) = 5 specify total pressure (p_{t0}) and calculate altitude (h_0) = 6 specify Reynolds number (/ft) and static temperature (T_0)
K_{atm}	`Katm`	Flag indicating the atmospheric model [0] = 0 standard model = 2 hot day model = 1 cold day model = 3 tropical day model
h_0	`fsalt`	Altitude (ft) [0 ft]
M_0	`fsmach`	Freestream Mach number [0.6]
Re/ft	`fsreyn`	Reynolds number (/ft)
α_0	`fsalph`	Angle-of-attack (deg) [0 deg]
β_0	`fsbeta`	Angle-of-sideslip (deg) [0 deg]
p_0	`fspres`	Freestream static pressure (psf)
p_{t0}	`fsptot`	Freestream total pressure (psf)
q_0	`fsqdyn`	Freestream dynamic pressure (psf)
T_0	`fstemp`	Freestream static temperature (°R)
T_{t0}	`fsttot`	Freestream total temperature (°R)

TABLE 4.8.—EXAMPLE INPUT DATA BLOCKS FOR THE FREESTREAM CONDITIONS

```
DataID.  Freestream
  1
Kfs   Katm   fsmach   fsalph   fsbeta
 1       0     0.6000   0.000    0.000
  fsalt
 30000.0
```

```
Kfs   Katm   fsmach   fsalph   fsbeta
 2       0     0.6000   0.000    0.000
 fspres     fstemp
 420.000    379.20
```

```
Kfs   Katm   fsmach   fsalph   fsbeta
 3       0     0.6000   0.000    0.000
 fsptot     fsttot
 650.000    469.80
```

```
Kfs   Katm   fsmach   fsalph   fsbeta
 4       0     0.6000   0.000    0.000
 fsqdyn
 810.000
```

```
Kfs   Katm   fsmach   fsalph   fsbeta
 5       0    0.6000    0.000    0.000
 fsptot
 650.000
```

```
Kfs   Katm   fsmach   fsalph   fsbeta
 6       0    0.6000    0.000    0.000
 fsreyn     fstemp
 2.5E+06     390.0
```

4.7 Approach Flow

The ***approach flow*** represents the segment of the inlet streamtube from the freestream station 0 to a point just upstream of the start of the inlet at the local inlet station L, as shown in Figure 2.5. The change in flow properties through the approach flow can be attributed to interactions of the streamtube with the forward portions of an aircraft which could include Mach and shock waves and boundary layers. As such, the approach flow can be used to account for integration of the inlet onto an aircraft. The modeling assumes a quasi-one-dimensional approximation to the flow through the approach flow segment, and it is assumed that the flow at station L is uniform and steady.

The approach flow model modifies the Mach number, incidence, and thermodynamic properties of the flow between stations 0 and L. Table 4.9 lists the input factors that establish the modification of the flow properties of the approach flow. The input factor $\boldsymbol{K_{app}}$ is a flag that indicates how the approach flow is to be evaluated. For K_{app} = 0, no approach flow effects are modeled and the flow properties at station L are set to those of the freestream.

For K_{app} = 1, the approach flow is modeled as N_{sapp} stages through which the flow is modified in terms of a turning of the flow within a plane through an angle $\Delta\theta_{sapp}$ through each stage. Compression of the flow is indicated by a positive angle change ($\Delta\theta_{sapp} > 0$) while expansion is indicated by a negative angle change ($\Delta\theta_{sapp} < 0$). The model does not consider the spatial locations of the stages, only the flow deflection. Each stage is modeled as a planar oblique shock wave compression or Prandtl-Meyer expansion (K_{sapp} = 1), conical shock wave compression (K_{sapp} = 2), or an isentropic compression or expansion (K_{sapp} = 3). Each stage can change the total pressure, Mach number, and streamtube area. All these processes assume adiabatic flow. As an example, Figure 4.2 provides a schematic of an approach flow involving three stages. The first two stages generate oblique shock wave compression while the third stage generates a Prandtl-Meyer expansion. This approach flow model only changes the Mach number (M_L) and thermodynamic properties (p_L,T_L) of the flow, but not the flow angles (α_L,β_L).

For K_{app} = 2, the flow conditions at station L are explicitly defined by the input factors of the Mach number at station L (M_L), the ratio of total pressures at stations L and 0 (p_{tL}/p_{t0}), and the flow angles α_L and β_L. It is also assumed that the flow between stations 0 and L is adiabatic. From this information, the complete state of the flow is known.

For K_{app} = 3, the approach flow is modeled using the subroutine *ApproachFlowCode*. This allows the user to program a specific model of their choice. The version of the subroutine *ApproachFlowCode* provided with SUPIN simply sets the conditions at station L the same as the freestream conditions at station 0. To implement a new model, the user would need to modify the code in the subroutine and compile the SUPIN source code.

For K_{app} = 4, the model assumes that no approach flow effects occur and the flow properties at station L are the same as the freestream at station 0.

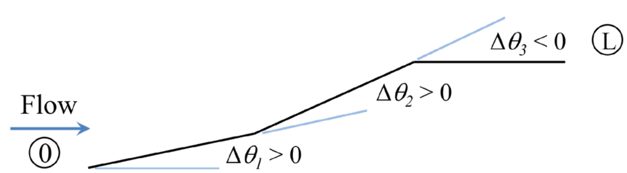

Figure 4.2.—Example of flow turning for the approach flow.

TABLE 4.9.—INPUT FACTORS FOR THE APPROACH FLOW

Factor	Input	Description
K_{app}	`Kapp`	Flag for the approach flow [0] = 0 no approach flow conditions are to be set = 1 approach flow is defined by N_{sapp} flow segments = 2 specify the Mach number, total pressure ratio, and angles at station L = 3 use code defined in subroutine `FlowApproachCode` = 4 use freestream conditions for station L
α_{inlet}	`alphIn`	Angle-of-incidence of the inlet [0 deg]
β_{inlet}	`betaIn`	Angle of inlet axis with respect to the aircraft symmetry plane [0.0 deg]
M_L	`FmachL`	Mach number at station L
p_{tL}/p_{t0}	`FptLpt0`	Total pressure recovery between stations 0 and L
α_L	`FalphL`	Angle-of-incidence of the flow at station L [0.0 deg]
β_L	`FbetaL`	Angle-of-sideslip of the flow at station L [0.0 deg]
N_{sapp}	`Nsapp`	Number of stages for the approach flow [0.0]
K_{sapp}	`Ksapp`	Flag for the type of flow process for each stage [0] = 1 2D oblique shock wave compression or isentropic expansion = 2 conical shock wave compression = 3 isentropic compression or expansion
$\Delta\theta_{sapp}$	`Dthapp`	Change in angle of the approach flow through the stage [0.0 deg]

The input factor α_{inlet} is the angle-of-incidence of the inlet with respect to an axis running along the length of the aircraft. It is assumed here that the only change of the flow direction in the vertical plane is due to the incidence of the aircraft with respect to the freestream flow and the incidence of the inlet with respect to the aircraft, or

$$\alpha_L = \alpha_0 + \alpha_{inlet} \tag{4-1}$$

The input factor β_{inlet} is the angle-of-incidence of the inlet with respect to the vertical plane of symmetry of the aircraft. At this time, SUPIN has no model that considers non-zero values of β_{inlet}, thus the β_{inlet} input is ignored and reset to $\beta_{inlet} = 0$.

Table 4.10 shows several examples of the input data blocks for the approach flow. The input flag DataID = 2 indicates that the input block is specifying the input for the approach flow. The first, fourth, and fifth example input data blocks for which K_{app} = 0, 3, and 4, respectively, require no additional lines of input within the input data block. The first and fifth example input data blocks are also equivalent to not including the approach flow input data block within the input data file. For the second example with K_{app} = 1, the model consists of two planar ramps with oblique shock waves. The first ramp deflects the flow 10.0 degrees, and the second ramp deflects the flow 8.0 degrees. The flow conditions at station L would be the flow conditions downstream of the second oblique shock wave. For the third example with K_{app} = 2, the model imposes the Mach number of M_L = 1.7, a total pressure ratio of p_{tL}/p_{t0} = 0.98, and no change in flow incidence ($\alpha_L = \beta_L = 0$ degrees) for the approach flow.

TABLE 4.10.—EXAMPLE INPUT DATA BLOCKS FOR THE APPROACH FLOW

```
DataID.  Approach Flow
  2
Kapp   FalphIn   FbetaIN
  0     0.000     0.000
```

```
DataID.  Approach Flow
  2
Kapp   FalphIn   FbetaIN
  1     0.000     0.000
Nsapp
  2
Ksapp      Dthapp
  1        10.000
  1         8.000
```

```
DataID.  Approach Flow
  2
Kapp   FalphIn   FbetaIN
  2     0.000     0.000
FmachL    FptLpt0    FalphL    FbetaL
1.7000    0.98000     0.000     0.000
```

```
DataID.  Approach Flow
  2
Kapp   FalphIn   FbetaIN
  3     0.000     0.000
```

```
DataID.  Approach Flow
  2
Kapp   FalphIn   FbetaIN
  4     0.000     0.000
```

4.8 External Supersonic Diffuser

The ***external supersonic diffuser*** of an inlet compresses and decelerates supersonic flow through shock wave and Mach waves on surfaces of the inlet that are upstream and external to the internal ducting of the inlet, which starts at station 1. The external supersonic diffusers for an axisymmetric spike (K_{typ} = 3) or two-dimensional (K_{typ} = 2 and 4) inlet have a planar character. In other words, the shape of the diffuser can be established by a profile or curves defined on a planar or two-dimensional space. The external supersonic diffuser for a streamline-traced inlet (K_{typ} = 5) has a three-dimensional character defined by streamlines through a parent flowfield. The pitot inlets (K_{typ} = 1 and 6) do not have an external supersonic diffuser.

The SUPIN input factors for the external supersonic diffuser will vary depending on the type of inlet and are specified through the input data block with DataID = 4. Table 4.11 shows the general form of the input data block. The first four lines shown in the input data block are required and common for all types of external supersonic diffusers for all types of inlets. Any additional lines of inputs for the data block depend on the value of the input factor $\boldsymbol{K_{exd}}$. The example of Table 4.11 indicates a value of K_{exd} = 2. The options for the values of K_{exd} are listed in Table 4.12. The value of K_{exd} = 0 indicates that the inlet has no external supersonic diffuser, which is the default for SUPIN and would be the case for the pitot inlets. For the case of K_{exd} = 0, the external supersonic diffuser input data block does not even need to be included in the input data file.

TABLE 4.11.—EXAMPLE THE INPUT DATA BLOCK FOR THE EXTERNAL SUPERSONIC DIFFUSER SHOWING THE FIRST FOUR LINES COMMON TO ALL INPUT DATA BLOCKS FOR DataID = 4

```
DataID.  External Supersonic Diffuser
  4
Kexd    FptEXptL    Fpt1ptEX
  2      -0.9950     -0.9850
        :
  Additional input lines defined according to Kexd
        :
```

TABLE 4.12.—THE COMMON INPUT FACTORS FOR THE EXTERNAL SUPERSONIC DIFFUSER

Factor	Input	Description
K_{exd}	Kexd	Flag indicating how the external supersonic diffuser geometry is created [0] = 0 no external supersonic diffuser is specified = 1 quasi-one-dimensional external supersonic diffuser model = 2 single stage ramp or single cone (K_{typ} = 2, 3, or 4) = 3 two-stage ramp or bi-cone (K_{typ} = 2, 3, or 4) = 4 three-stage ramp or triple-cone (K_{typ} = 2, 3, or 4) = 5 three-stage ramp or triple-cone with isentropic second stage (K_{typ} = 2, 3, or 4) = 6 streamline-traced external supersonic diffusers (K_{typ} = 5) = 7 simplified design inputs for planar inlets (K_{typ} = 2, 3, or 4, and K_{mode} = 2) = 8 external supersonic diffuser geometry is specified using entities
p_{tEX}/p_{tL}	FptEXptL	Total pressure ratio between stations L and EX
p_{t1}/p_{tEX}	Fpt1ptEX	Total pressure ratio between stations EX and 1

The value of K_{exd} = 1 indicates that the external supersonic diffuser is modeled in a quasi-one-dimensional manner between stations L, EX, and 1 for a flowpath analysis, which will be discussed in Subsection 4.16. The values of K_{exd} = 2 to 7 indicate that the external supersonic diffuser is created using a specific geometry model that may involve flow condition input factors (i.e., Mach numbers) as part of the design of the external supersonic diffuser geometry for the respective inlets. Table 4.12 lists the options for K_{exd} and the geometry models for axisymmetric spike, two-dimensional, and streamline-traced inlets. A value of K_{exd} = 8 indicates that the geometry of the external supersonic diffuser is specified using geometric entities, such as lines, cubic splines, and non-rational B-spline (NURBS) curve, as will be described in Subsection 4.15. The use of entities provides a much more general manner for specifying the geometry of the external supersonic diffuser.

Table 4.11 and Table 4.12 also list the input factors FptEXptL and Fpt1ptEX for the ratio of total pressures across the respective stations between stations L and 1. The external supersonic diffuser models within SUPIN will compute these total pressure ratios as part of the design and analysis modes (K_{mode} = 2 and 3) when FptEXptL < 0 and Fpt1ptEX < 0. However, when the input factors are specified such that 0.0 < FptEXptL ≤ 1.0 or 0.0 < Fpt1ptEX ≤ 1.0, those values are used to directly specify the total pressure ratios. One may wish to specify these ratios if the values computed by SUPIN don't seem correct or if the user wishes to override the model and specify values of these ratios.

4.9 Cowl Lip

The ***cowl lip*** forms part or all the leading edge and surfaces of the inlet at the start of the internal ducting of the inlet, which is station 1. Thus, the cowl lip contributes to the definition of the capture cross-section of the inlet, which is integral to the inlet performing its primary function of capturing airflow for the engine.

The geometric details of the cowl lip vary with the type of inlet; however, the general aspects of the cowl lip geometry model can be illustrated by the example of the cowl lip for a subsonic, axisymmetric pitot inlet (K_{typ} = 1) shown in Figure 4.3. Since the inlet is axisymmetric, the leading edge of the inlet is a circle about the axis-of-symmetry, which is collinear with the x-axis with $y = z = 0$. The leading edge is also referred to as the ***highlight*** of the inlet. For an axisymmetric inlet, the highlight is on a constant-x plane perpendicular to the inlet axis-of-symmetry, The area enclosed by the highlight is the reference capture area, as discussed in Section 2.7.

Downstream of the leading edge, the cowl lip consists of the ***cowl lip interior*** and ***cowl lip exterior*** surfaces. The highlight is the common edge between the cowl lip interior and exterior surfaces. The cowl lip interior and exterior surfaces guide the flow into the interior ducting of the inlet and about the exterior of the inlet, respectively. For the case of the subsonic, axisymmetric pitot inlet shown in the left-hand-side of Figure 4.3, the cowl lip has a blunt character to provide a more gradual turning of the subsonic flow past the cowl lip.

The axisymmetric character of the cowl lip allows its geometry to be modeled using planar profiles as shown in the image in the middle of Figure 4.3. The planar profiles both start at the ***cowl lip point*** $(x,y)_{clip}$ that defines the axial and radial location of the highlight in the plane. The profile for the cowl lip interior ends at point $(x,y)_{clin}$ that also denotes the start of the planar profile for the cowl interior. Likewise, the profile for the cowl lip exterior ends at point $(x,y)_{clex}$ that also denotes the start of the planar profile for the cowl exterior.

SUPIN uses elliptical curves to define the planar profiles of the cowl lip interior and exterior. The blue and green shaded regions denote a section of ellipses that are used to define the profiles. The cowl lip interior and the cowl lip exterior profiles are defined with separate input factors to allow for different profiles for the cowl lip interior and exterior. For an ellipse, the input factors include the lengths of the semi-minor (b) and semi-major (a) axes. The a_{clin} and b_{clin} are the lengths of the semi-major and semi-minor axes, respectively, of the profile for the cowl lip interior. Similarly, the a_{clex} and b_{clex} are the lengths of the semi-major and semi-minor axes, respectively, of the profile for the cowl lip exterior. The aspect ratios of the cowl lip profiles are defined as $AR_{clin} = a_{clin}/b_{clin}$ and $AR_{clex} = a_{clex}/b_{clex}$. Circular profiles for the cowl lip can be formed by setting the respective aspect ratios equal to unity (e.g., AR_{clin} = 1). The cowl lip interior terminates at point $(x,y)_{clin}$. This point is established as the point along the elliptic profile such

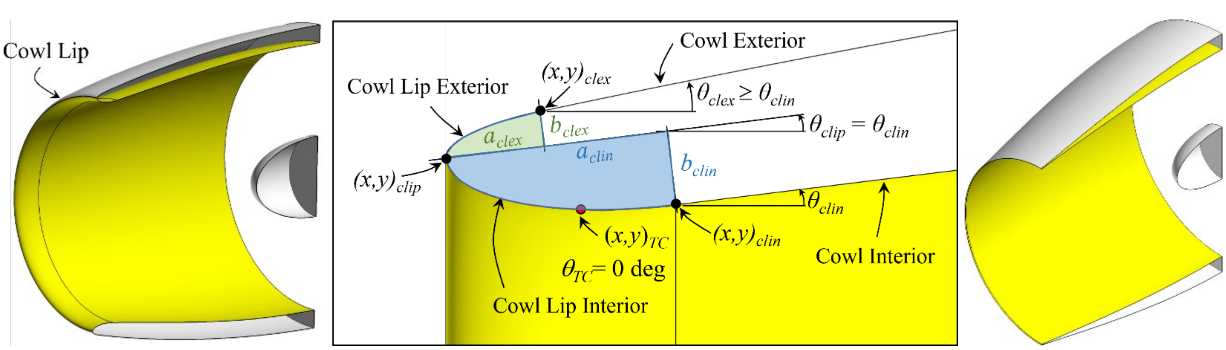

Figure 4.3.—Geometry model for the elliptical profiles for the cowl lip.

that the slope at point $(x,y)_{clin}$ is θ_{clin}, which is set equal to the angle θ_{clip} (i.e., $\theta_{clin} = \theta_{clip}$). Thus, the cowl lip interior is a full quarter-section of an ellipse. It is assumed that $\theta_{clin} = \theta_{clip} \geq 0$ degrees for all inlets.

The cowl lip exterior terminates at point $(x,y)_{clex}$ with the slope at point $(x,y)_{clex}$ of θ_{clex}. The value of θ_{clex} is typically set to a value greater than θ_{clin} by at least 3 to 5 degrees to ensure the structural integrity of the cowl lip if the dimensions of b_{clin} and b_{clex} are small dimensions. The value of θ_{clex} is also set to provide a cowl exterior that covers the inlet while also reducing drag on the cowl exterior. The thickness of the cowl lip is computed as the sum of b_{clin} and b_{clex}. Since it is likely that $\theta_{clex} > \theta_{clin}$, the profile for the cowl lip exterior is typically less than a quarter-segment of an ellipse.

The cowl lip for supersonic inlets, such as the axisymmetric spike inlet ($K_{typ} = 3$), prefer cowl lips with very little bluntness or essentially sharp cowl lips. Such sharpness can be achieved by using very small values of the lengths of the semi-minor axes (e.g., $b_{clin} \approx 0.0001$ ft). The image on the right-hand-side of Figure 4.3 shows an axisymmetric pitot inlet designed with a very small dimensions for the cowl lip.

The cowl lip interior and exterior surfaces for axisymmetric inlets ($K_{typ} = 1$ or $K_{typ} = 3$) are obtained by extruding the respective planar profiles about the axis-of-symmetry of the inlet. For the case of a two-dimensional inlet ($K_{typ} = 2$), as illustrated in Figure 4.4, the cowl lip forms the top portion of the leading rectangular edge of the inlet. The remainder of the leading edge of the inlet is formed by the leading edges of the sidewalls and the external supersonic diffuser. The cowl lip interior and exterior surfaces for the two-dimensional inlets ($K_{typ} = 2$ and 4) are formed using a linear extrusion in the z-coordinate over the width of the capture cross-section of the inlet.

For the streamline-traced inlet ($K_{typ} = 5$), the elliptic profiles as defined above are still used; however, the cowl lip can be divided into a supersonic segment for most of the circumference and a subsonic segment with a blending of the cowl lip profiles over the subsonic cowl lip. The details discussing the three-dimensional pitot inlet will be presented in Subsection 6.2.

For the three-dimensional pitot inlet ($K_{typ} = 6$), the elliptic profiles are still used; however, the dimensions of the profiles can vary over the circumference of the cowl lip. The details will be presented in a Subsection 6.2 discussing the three-dimensional pitot inlet.

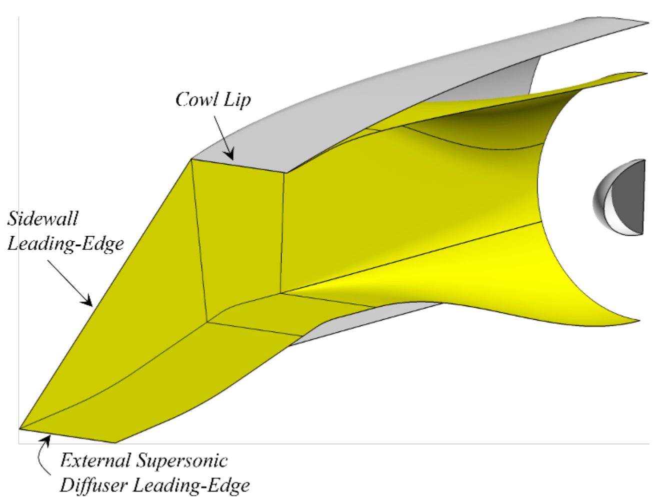

Figure 4.4.—Cowl lip for a two-dimensional inlet.

TABLE 4.13.—EXAMPLE INPUT DATA BLOCK FOR THE ELLIPTICAL COWL LIP PROFILES

```
DataID.  Cowl Lip Profile
  5
ARclin   Fbclin   Fthclin    ARclex   Fbclex   Fthclex
 2.000   0.00200   10.000     2.000   0.00200   15.000
```

TABLE 4.14.—INPUT FACTORS FOR THE ELLIPTICAL COWL LIP PROFILES

Factor	Input	Description
AR_{clin}	ARclin	Aspect ratio (a/b) for the cowl lip interior
b_{clin}	Fbclin	Length of semi-minor axis for cowl lip interior (ft) (M_{TC} if Fbclin < 0)
θ_{clin}	Fthclin	Angle of the cowl lip interior (deg)
AR_{clex}	ARclex	Aspect ratio (a/b) for the cowl lip exterior
b_{clex}	Fbclex	Length of semi-minor axis for cowl lip exterior (ft)
θ_{clex}	Fthclex	Angle of the cowl lip exterior (deg)

The point $(x,y)_{TC}$ is illustrated in Figure 4.3 and indicates the point on the cowl lip interior at which the slope $\theta_{TC} = 0$ degrees. If $\theta_{clin} = 0.0$ degrees, the $(x,y)_{TC} = (x,y)_{clin}$. For subsonic inlets and supersonic, external-compression inlets the point TC may define the geometric throat station TH for the inlet. This condition will be discussed in further detail in the sections describing those inlet types. For the subsonic axisymmetric pitot inlet ($K_{typ} = 1$, $K_{comp} = 0$, and $M_L < 1$), the point $(x,y)_{TC}$ can be established based on the specification of the desired subsonic quasi-one-dimensional Mach number (M_{TH}) at the geometric throat, which is located at the point $(x,y)_{TC}$. With $(x,y)_{TC}$ established, the geometric factor a_{clin} and the rest of the factors defining the cowl lip interior can be established. This design approach will be discussed in full detail in Section 5.2.

An example input data block for the cowl lip profiles is shown in Table 4.13. The DataID = 5 indicates that the input data block is specifying the input factors for the cowl lip. Those input factors are listed in Table 4.14. The units for the lengths of the semi-minor axes b_{clin} and b_{clex} are in feet. The units for the angles θ_{clin} and θ_{clex} are degrees.

4.10 Cowl Exterior

The ***cowl exterior*** is the exterior surface of the inlet that encloses the inlet and provides an exterior aerodynamic surface. The geometric shaping of the cowl exterior is ultimately dependent on the way the inlet and the rest of the propulsion system are integrated with the aircraft. In some cases, the cowl exterior can also be considered as part of the ***nacelle*** that encloses not only the inlet, but also the engine and nozzle. In the accounting for forces on the nacelle, a divide is needed to establish which portion of the nacelle and its forces are associated with the inlet and which are associated with the nozzle.

SUPIN has only a limited capability to model the cowl exterior. Since SUPIN only considers isolated inlets and not the geometry of the aircraft, this capability creates a representative cowl exterior to allow the calculation of cowl drag. While this representative cowl exterior and its associated forces do not provide information about the inlet / aircraft integration, the representative cowl exterior can be used to compare levels of drag between different inlets designed within SUPIN.

The modeling of the cowl exterior is illustrated with the example of a cowl exterior for an axisymmetric pitot ($K_{typ} = 1$) inlet as shown in Figure 4.5. The cowl exterior surface is formed by defining a planar curve and then extruding that curve about the axis-of-symmetry. The planar curve starts at the end of the cowl lip exterior surface at the point $(x,y)_{clex}$ and extends downstream to an endpoint at $(x,y)_{cwex}$. The cowl exterior may cover the entire axial length of the inlet or only a portion of the inlet depending on

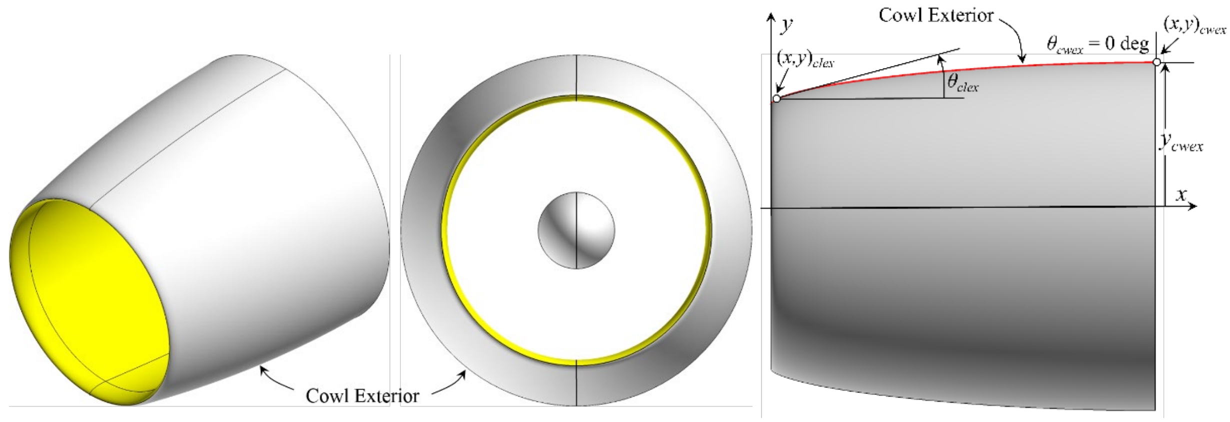

Figure 4.5.—Cowl exterior for an axisymmetric pitot inlet.

where the divide is between the inlet and the assumed nozzle or aircraft. The end of the cowl exterior is specified to have a zero slope with θ_{cwex} = 0 degrees to effectively end any forward-facing portions of the cowl exterior that may contribute to wave drag.

The extrusion of a planar curve about the axis-of-symmetry is also used to define the cowl exterior for an axisymmetric spike (K_{typ} = 3) inlet. For the two-dimensional (K_{typ} = 2 or 4) inlets, the cowl exterior extends downstream of the sidewalls, as well as the cowl lip exterior. This requires defining three-dimensional curves that form the cowl exterior surface. These curves are formed by defining a planar curve and then transforming the curve to three-dimensional space. Similarly, three-dimensional curves are used to define the cowl exterior for the streamline-traced (K_{typ} = 5) and three-dimensional pitot (K_{typ} = 6) inlets. Later sections will provide further details and examples of the cowl exterior for these inlets.

The input factors for the geometry model of the cowl exterior are listed in the example of the input data block for the cowl exterior shown in Table 4.15. The DataID = 6 indicates that the input block is specifying the input factors for the cowl exterior. Table 4.16 lists and describes the input factors for the geometry model of the cowl exterior.

The input factor $\boldsymbol{K_{cwex}}$ indicates the type of planar curve used for generating the cowl exterior surface. A value of K_{cwex} = 0 indicates no cowl exterior is to be modeled.

For K_{cwex} = 1, the planar curve consists of a single four-point-NURBS curve from the cowl lip exterior point $(x,y)_{clex}$ with a slope of θ_{clex} to the endpoint of the cowl exterior, which has the coordinates $(x,y)_{cwex}$ and slope θ_{cwex} = 0 degrees. Figure 4.5 shows an example of the planar curve created from the four-point-NURBS curve for the axisymmetric pitot inlet. Further information on the four-point-NURBS curve is provided in Appendix A.

The point $(x,y)_{cwex}$ is defined using the input factors F_{xcwex} and F_{rcwex}. If $F_{xcwex} > 0$, then $x_{cwex} = F_{xcwex}$. If $F_{xcwex} < 0$, then $x_{cwex} = x_{EF}$, which is the case of the example shown in Figure 4.5. The y-coordinate or radial coordinate of the end of the cowl exterior (y_{cwex}) is determined as a ratio (F_{rcwex}) of the radius of the engine face (r_{EF}).

$$y_{cwex} = y_{EF} + F_{rcwex}\, r_{EF} \tag{4-2}$$

If the value of y_{cwex} computed by Equation (4-2) is less than y_{clex}, then y_{cwex} computed as

$$y_{cwex} = y_{inlet} + F_{rcwex}\,(\, y_{clex} - y_{inlet}\,) \tag{4-3}$$

This helps ensure that the cowl exterior curve avoids having a negative slope. If the generated profile does have a negative slope, then that suggests the value of F_{rcwex} could be increased.

TABLE 4.15.—EXAMPLE INPUT DATA BLOCK FOR THE COWL EXTERIOR

```
DataID.  Cowl Exterior
  6
Kcwex    Frcwex    Fxcwex    thswex
  1      1.1500    -2.000     5.000
```

TABLE 4.16.—INPUT FACTORS FOR THE COWL EXTERIOR

Factor	Input	Description
K_{cwex}	`Kcwex`	Method for constructing the cowl exterior geometry [0] = 0 No cowl exterior is modeled = 1 Create cowl exterior curves using planar NURBS curves = 2 Create cowl exterior curves using planar ogive curves = 3 Create cowl exterior curves using the NACA-1 profile = 4 Use entities to define the cowl exterior (K_{comt} = 18)
F_{xcwex}	`Fxcwex`	Factor for axial placement of the end of the cowl exterior
F_{rcwex}	`Frcwex`	Factor for radial placement of the cowl exterior
θ_{swex}	`thswex`	Angle of the sidewall (deg) (For K_{typ} = 2 and 4 only)

For K_{cwex} = 2, the planar curve for the cowl exterior is formed as a planar ogive curve. Information on the construction of the ogive curve is provided in Appendix A. The curve starts at the cowl lip exterior point $(x,y)_{clex}$ with a slope of θ_{clex}. The other piece of information needed to construct the ogive curve is the value of y_{cwex} as computed using the input factor F_{rcwex}. Using the equations of the planar ogive, the value of x_{cwex} is computed. Thus, the cowl exterior may not cover the entire inlet.

For K_{cwex} = 3, the planar curve for the cowl exterior is formed using the NACA-1 airfoil, which is discussed in Appendix A. The NACA airfoil curve starts at the cowl lip point $(x,y)_{clip}$ rather than the cowl lip exterior point $(x,y)_{cwex}$ and ends at the endpoint of the cowl exterior, $(x,y)_{cwex}$. Thus, for K_{cwex} = 3, the cowl lip exterior surface is included in the cowl exterior surface rather than defined by the cowl lip input factors. The horizontal and vertical distances between $(x,y)_{clip}$ and $(x,y)_{cwex}$ define the scale of the NACA-1 profile and the coordinate points of the NACA-1 profile as listed in Table A-7 are fitted with a cubic spline.

A value of K_{cwex} = 4 indicates that the curve is defined as a collection of entities specified using the component and entity input data block (DataID = 16) that will be discussed in Subsection 4.15.
The input factor θ_{swex} specifies the slope for the start of the portion of the cowl exterior covering the sidewalls of a two-dimensional inlet. Further details and an example for the cowl exterior for two-dimensional inlets is provided in a Subsection 8.8.

4.11 Throat Section, Internal Supersonic Diffuser, and Isolator

The internal diffuser of the inlet was discussed in Subsection 2.5 as starting at station 1 and ending at either station 2 or 3 depending on the type of engine for which the inlet is intended. The possible components contained within the internal diffuser are the throat section, internal supersonic diffuser, subsonic diffuser, and isolator. The choice of components used within an inlet is determined by the type of inlet, type of internal supersonic compression, and the type of engine. This section introduces some input factors for the geometry modeling of the throat section, internal supersonic diffuser, and isolator. The details of most of the input factors for these components are left to Sections 5.0 through 10.0 that discuss specific inlet types and their variations. The introduction of the input factors for the subsonic diffuser is provided in the next section.

TABLE 4.17.—EXAMPLE OF THE INPUT DATA BLOCK FOR THE THROAT SECTION SHOWING THE FIRST FOUR LINES COMMON TO ALL INPUT DATA BLOCKS FOR DataID = 8

```
DataID.  Throat Section.
  8
Kthrt    FptsegA     FptsegB     FptsegC
  5     -0.99000     0.99500    -1.00000
        :
  Additional input lines defined according to Kthrt
        :
```

TABLE 4.18.—THE COMMON INPUT FACTORS FOR THE THROAT SECTION, INTERNAL SUPERSONIC DIFFUSER, AND ISOLATOR

Factor	Input	Description
K_{thrt}	Kthrt	Flag indicating the geometry model [0] = 0 no model = 1 quasi-one-dimensional Mach-area flowpath analysis = 2 model for axisymmetric pitot inlets (K_{typ} = 1) = 3 model for three-dimensional pitot inlets (K_{typ} = 6) = 4 model for 2D and axisymmetric spike Mahoney inlet (K_{typ} = 2, 3) = 5 model for 2D and axisymmetric spike mixed-compression inlets (K_{typ} = 2, 3, 4) = 6 model for 2D and axisymmetric spike mixed-compression inlets using MOC = 7 model for streamline-traced inlets (K_{typ} = 5) = 8 model using specified components and entities = 9 model for external-compression 2D and axi-spike inlets (K_{typ} = 2, 3, 4)
p_{tsegA}	FptsegA	Ratio of total pressures for segment A
p_{tsegB}	FptsegB	Ratio of total pressures for segment B
p_{tsegC}	FptsegC	Ratio of total pressures for segment C

The input factors for the throat section, internal supersonic diffuser, and isolator are specified through an input data block with DataID = 8 in the general form shown in Table 4.17. The first four lines shown in the input data block are required and common for this input data block for all inlet types. The input factor $\boldsymbol{K_{thrt}}$ indicates which geometry model is to be used. Any additional lines of inputs for the data block depend on the value of K_{thrt}. The options for the K_{thrt} are listed in Table 4.18. For K_{thrt} = 0, no geometry model is applied, and this input data block is not required. The geometry models for the rest of the choices of K_{thrt} are discussed in Sections 5.0 through 10.0 for specific inlet types. For K_{thrt} = 8, the geometry is defined as a collection of entities specified using the component and entity input data block (DataID = 16) as will be discussed in Subsection 4.15.

SUPIN has aerodynamic models that compute the total pressure ratios between the stations within the throat section and internal supersonic diffuser. However, the input data block does allow specification of those total pressure ratios. This might be the case if the user feels the models don't estimate the correct total pressure ratio. The input data block shown in Table 4.17 has input factors for total pressure ratios FptsegA, FptsegB, and FptsegC across segments A, B, and C correspond to sequential segments of the throat section, internal supersonic diffuser, and isolator depending on which components are included.

For example, an external-compression inlet with just a throat section would relate segment A to be between stations 1 and the shoulder station TH and segment B would be between stations TH and SD. Segment C would be undefined. Thus, the total pressure ratios would be set as p_{tTH}/p_{t1} = FptsegA and p_{tSD}/p_{tTH} = FptsegB if the values specified for FptsegA and FptsegB are positive values. A negative value would indicate that the respective aerodynamic model within SUPIN should be used to compute the total pressure ratios. In the example of Table 4.17, the value of FptsegB = 0.995 was specified indicating a total pressure ratio of p_{tSD}/p_{tTH} = 0.995. Further details on these input factors will be discussed in Sections 5.0 through 10.0.

4.12 Subsonic Diffuser

Inlets for turbojet and turbofan engine use a ***subsonic diffuser*** to decelerate and compress subsonic flow for entrance to the engine. A ramjet engine may use either a subsonic diffuser or an isolator. The subsonic diffuser for a turbojet or turbofan is the aft portion of the interior diffuser of the inlet extending from station SD to the engine face station 2, as was shown in the inlets of Figure 2.7 to Figure 2.11. The subsonic diffuser may involve a transition of the cross-sectional geometry along its path from station SD to the engine face station 2. Such is the case for subsonic diffusers of two-dimensional inlets for a turbofan engine, where the cross-section transitions from a rectangular shape at station SD to a circular shape at the engine face, as was shown in Figure 2.8. The subsonic diffuser for a ramjet engine is similarly formed, but with the diffuser extending between stations SD and 3, as was shown for Figure 2.10.

The input factors for the subsonic diffuser establish the length and shape of the surfaces between the established cross-sections at station SD and the engine face. The input factors for the subsonic diffuser are specified through an input data block with DataID = 10. The specific form of the input data block depends on the type of inlet (K_{typ}). However, the form of the first four lines of the input data block is the same for all inlet types. Table 4.19 shows an example of the input data block for those four lines. The input factor $\boldsymbol{K_{subd}}$ indicates the geometry model to be used for creating the subsonic diffuser and its value depends on the type of inlet. The options for K_{subd} are listed in Table 4.20. For K_{subd} = 0, the inlet has no subsonic diffuser. In this case, the input data block for the subsonic diffuser does not need to be in the SUPIN input data file (SUPIN.in). For K_{subd} = 1, the subsonic diffuser is modeled as a quasi-one-dimensional duct between stations SD and 2 for a flowpath analysis as discussed below in Subsection 4.16. For K_{subd} = 2 to 8, the subsonic diffuser is created using the various geometry models. The input factors for those models are specified in the remaining lines of the input data block. Later sections will discuss those inputs with respect to the individual inlet types. For K_{subd} = 15, the geometry of the subsonic diffuser is defined as a collection of entities specified using the component and entity input data block (DataID = 16) as will be discussed in Subsection 4.15.

TABLE 4.19.—EXAMPLE OF THE INPUT DATA BLOCK FOR THE SUBSONIC DIFFUSER SHOWING THE FIRST FOUR LINES COMMON TO ALL INPUT DATA BLOCKS FOR DataID = 10

```
DataID.  Subsonic Diffuser
 10
Ksubd    KLsubd    FLsubd    theqsd    Fpt2ptSD
  2         1     4.50000     3.000    -0.97500
         :
Additional lines of input based on the value of Ksubd
```

TABLE 4.20.—THE COMMON INPUT FACTORS FOR THE SUBSONIC DIFFUSER

Factor	Input	Description
K_{subd}	`Ksubd`	Flag for the model of the subsonic diffuser [0] = 0 undefined. Subsonic diffuser is not modeled = 1 simple quasi-one-dimensional subsonic diffuser model (All inlets) = 2 subsonic diffuser for axisymmetric pitot inlets (K_{typ} = 1) = 3 subsonic diffuser for an axisymmetric spike inlet (K_{typ} = 3) = 4 subsonic diffuser for a two-dimensional inlet (K_{typ} = 2) = 5 subsonic diffuser for a two-dimensional, bifurcated-duct inlet (K_{typ} = 4) = 6 subsonic diffuser as a sequence of super-elliptical cross-sections = 7 subsonic diffuser as a network of NURBS curves (K_{typ} = 5 and 6) = 8 subsonic diffuser for a rectangular engine face (K_{typ} = 2, K_{thrt} = 8) = 15 entities for centerbody and cowl interior components (K_{comt} = 16 and 17)
K_{Lsubd}	`KLsubd`	Flag indicating how the length of the subsonic diffuser is computed = 1 $F_{Lsubd} = L_{subd}$ (ft) = 2 $F_{Lsubd} = L_{subd} / D_{ref}$ = 3 L_{subd} is computed as the distance between x_{SD} and the specified value of x_{EF} = 4 L_{inlet} is specified (F_{Lsubd}) and L_{subd} is remaining distance between x_{SD} to x_{EF} = 5 L_{subd} is computed based on cross-sectional areas and conical angle θ_{eqsd}
F_{Lsubd}	`FLsubd`	Input defining the length of the subsonic diffuser (value based on K_{Lsubd})
θ_{eqsd}	`theqsd`	Equivalent conical angle of the subsonic diffuser (deg)
p_{t2}/p_{tSD}	`Fpt2ptSD`	Factor specifying the total pressure ratio within the subsonic diffuser

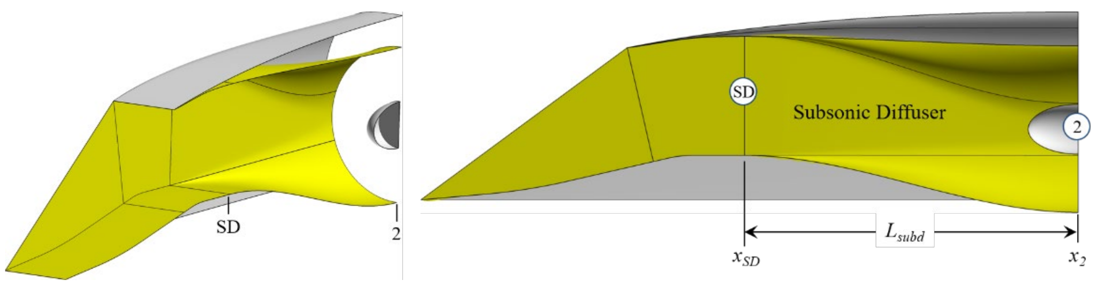

Figure 4.6.—Subsonic diffuser stations and length.

The input factors associated with the length of the subsonic diffuser are also common for all inlet types using a subsonic diffuser and for all options of K_{subd}. The length of the subsonic diffuser L_{subd} is defined as the axial distance between station SD and the engine face station 2.

$$L_{subd} = x_2 - x_{SD} \tag{4-4}$$

Figure 4.6 shows images of a two-dimensional inlet, which illustrates how the subsonic diffuser length L_{subd} is defined. The subsonic diffuser of Figure 4.6 is an example of the transition from a rectangular cross-section at station SD to an annular cross-section at the engine face station 2.

The input factor K_{Lsubd} indicates how the length of the subsonic diffuser is computed. Table 4.20 lists the options for K_{Lsubd}. The input factors F_{Lsubd} and θ_{eqSD} provide additional inputs for computing the length based on K_{Lsubd}. For K_{Lsubd} = 1, the length is explicitly specified with the value provided by F_{Lsubd} in units of feet. For K_{Lsubd} = 2, the length is specified as a factor of the reference dimension D_{ref}, which in some cases is the diameter of the engine face ($D_{ref} = D_{EF}$). For K_{Lsubd} = 3, the subsonic diffuser length is calculated using Equation (4-4) using the value of x_{SD} computed from the throat section modeling and the value of x_{EF} as specified by the input factor F_{xEF} from the engine face input data block, which is discussed in the next subsection.

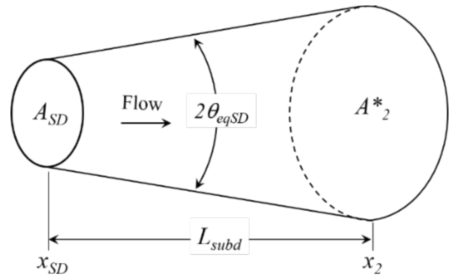

Figure 4.7.—Representation of the subsonic diffuser as a conical diffuser.

For K_{Lsubd} = 4, the length of the subsonic diffuser is calculated as the length remaining of the desired total length of the inlet (L_{inlet}) as specified by F_{Lsubd}. The inlet is constructed up to station SD and the length of the inlet from the nose to station SD is subtracted from the specified total length of the inlet. The remaining length is the length of the subsonic diffuser. Using this length, the axial position of the engine face (x_{EF}) is established.

For K_{Lsubd} = 5, the length of the subsonic diffuser is calculated to yield a specified equivalent conical diffuser angle, $2\theta_{eqSD}$. The equivalent conical diffuser angle is the wall-to-wall included angle of a conical diffuser. Figure 4.7 shows an illustration of a conical diffuser representing the subsonic diffuser with the conical diffuser angle defined.

The length of the subsonic diffuser is calculated as,

$$L_{subd} = \frac{\sqrt{A_2^*} - \sqrt{A_{SD}}}{\sqrt{\pi}\ \tan\theta_{eqSD}} \tag{4-5}$$

The A_2^* is used to denote the area of the engine face without the spinner hub, or in other words, for a circular engine face, A_2^* is the area of the circle with a radius equal to the radius of the engine face (r_{EF}) rather than the annular area. The shapes of the engine face cross-sections available in SUPIN are discussed in the next section. The calculation of Equation (4-5) may result in a very short subsonic diffuser if A_{SD} and A_2^* are comparable areas. For such a case, it may be better to directly specify the length of the subsonic diffuser to ensure an acceptable length for the subsonic diffuser.

SUPIN has an aerodynamic model for calculating the total pressure ratio for the subsonic diffuser, p_{t2}/p_{tSD}. In addition, there is the option to directly specify the total pressure ratio through the input factor Fpt2ptSD, if the user feels the total pressure ratio computed by the model is not correct. When 0 < Fpt2ptSD ≤ 1, then the total pressure ratio is set to the value of the input factor, p_{t2}/p_{tSD} = Fpt2ptSD. If Fpt2ptSD < 0, the subsonic diffuser loss model as discussed later in Section 6.5 is used to calculate p_{t2}/p_{tSD}.

SUPIN can specify the distribution of cross-sectional area through the subsonic diffuser for some of the inlets based on a desired area, Mach number, or static pressure distribution. The input factors for selecting the desired distribution are $\boldsymbol{K_{sdprp}}$ and $\boldsymbol{K_{sdvar}}$. These two input factors are specified in input lines associated with each type of subsonic diffuser as indicated by K_{subd} and are discussed in later sections with respect to the specific inlet types. Table 4.21 lists the possible values of K_{sdprp} and K_{sdvar}. The value of K_{sdprp} indicates whether the area distribution is calculated based on a specified variation of cross-sectional area, Mach number, or static pressure from station SD to station 2. The value of K_{sdvar} indicates the type of variation of the property specified by K_{sdprp}. The options for K_{sdvar} include a linear, cosine-sine-squared, or four-point NURBS variation. Each of these types of variations are discussed in Appendix A. The effects of these two input factors on the shape and area distribution of the subsonic diffuser will be illustrated in upcoming sections discussing the subsonic diffuser associated with each of the inlet types. The only inlet types that these input factors can't be used yet are the two-dimensional inlets with K_{typ} = 2 or 4.

TABLE 4.21.—INPUT FACTORS FOR THE AREA DISTRIBUTION THROUGH A SUBSONIC DIFFUSER

Factor	Input	Description
K_{sdprp}	`Ksdprp`	Property establishing the area distribution [0] = 0 no area distribution is used = 1 specify the axial distribution of the cross-sectional area = 2 specify the axial distribution of Mach number = 3 specify the axial distribution of static pressure
K_{sdvar}	`Ksdvar`	Type of variation [0] = 0 no area distribution is used = 1 linear variation = 2 cosine-sine-squared variation = 3 four-point NURBS variation with 1/3rd weighting

4.13 Engine Face

The ***engine face*** is the interface between the inlet and engine and marks the end of the inlet. An inlet is typically designed for a specified engine for which the dimensions and flow rates are specified. The engine flow rate was discussed in Subsection 2.8 and the formats for the SUPIN inputs for the flow rates were discussed in Subsection 4.4. In this subsection, the shape, dimensions, and location of the engine face as modeled by SUPIN are discussed.

The engine face is assumed to be defined on a plane that is oriented in the (x,y,z) coordinate system. The axis of the engine face plane is coincident with the axis of the engine. The engine face plane is placed within the global coordinate system of the inlet such that the center of the engine face is located at point $(x,y,z)_{EF}$. SUPIN currently assumes that the inlet and engine face are symmetric about the (x,y) plane, and so, SUPIN sets $z_{EF} = 0$. The angle θ_{EF} specifies the orientation of the engine axis with respect to the x-axis on the plane of symmetry. Currently, SUPIN assumes that the engine face plane is perpendicular to the x-axis, and so, SUPIN sets $\theta_{EF} = 0$. The coordinates for the engine face for the various inlets are illustrated in Figure 4.8.

The input factors defining the location of the engine face are listed in Table 4.22. The input factor $\boldsymbol{K_{xEF}}$ indicates the axial placement of the center of the engine face, x_{EF}. For $K_{xEF} = 1$, the axial position is explicitly specified through the input factor $\boldsymbol{F_{xEF}}$ and the units are feet. For $K_{xEF} = 2$, the axial position is set at the end of the subsonic diffuser once the dimensions of the subsonic diffuser have been established. The input factor $\boldsymbol{K_{yEF}}$ indicates the vertical placement of the center of the engine face, y_{EF}. This input factor is only used for the two-dimensional ($K_{typ} = 2$), streamline traced ($K_{typ} = 5$), and the three-dimensional pitot ($K_{typ} = 6$) inlets. For the other inlet types, the engine axis is placed by default as collinear with the inlet axis. For the axisymmetric inlets ($K_{typ} = 1$ and 3), $y_{EF} = 0$. For $K_{yEF} = 1$, the vertical position is explicitly specified through the input factor $\boldsymbol{F_{yEF}}$ and the units are feet. For $K_{yEF} = 2$, the vertical position is offset from the inlet axis by an increment as specified by F_{yEF} in units of feet. For $K_{yEF} = 3$, the vertical position is set equal to the vertical position of the inlet axis, y_{inlet}. The option of $K_{yEF} = 4$ is only valid for the two-dimensional inlet ($K_{typ} = 2$) and the vertical position is calculated such that the forward-facing area of the cowl exterior is minimized. The option of $K_{yEF} = 5$ is also only valid for the two-dimensional inlet ($K_{typ} = 2$) and the engine face is positioned so that the top of the engine face has the same y-coordinate as the y-coordinate of the top of the cross-section at station SD. The option of $K_{yEF} = 6$ places the engine axis in line with the y-coordinate of station SD (e.g., $y_{EF} = y_{SD}$). The option of $K_{yEF} = 7$ places the engine axis at on offset from the y-coordinate at station SD, y_{SD}, with the offset indicated by F_{yEF}, which is the offset scaled by the length of the subsonic diffuser (e.g., $F_{yEF} = \Delta y/L_{subd}$).

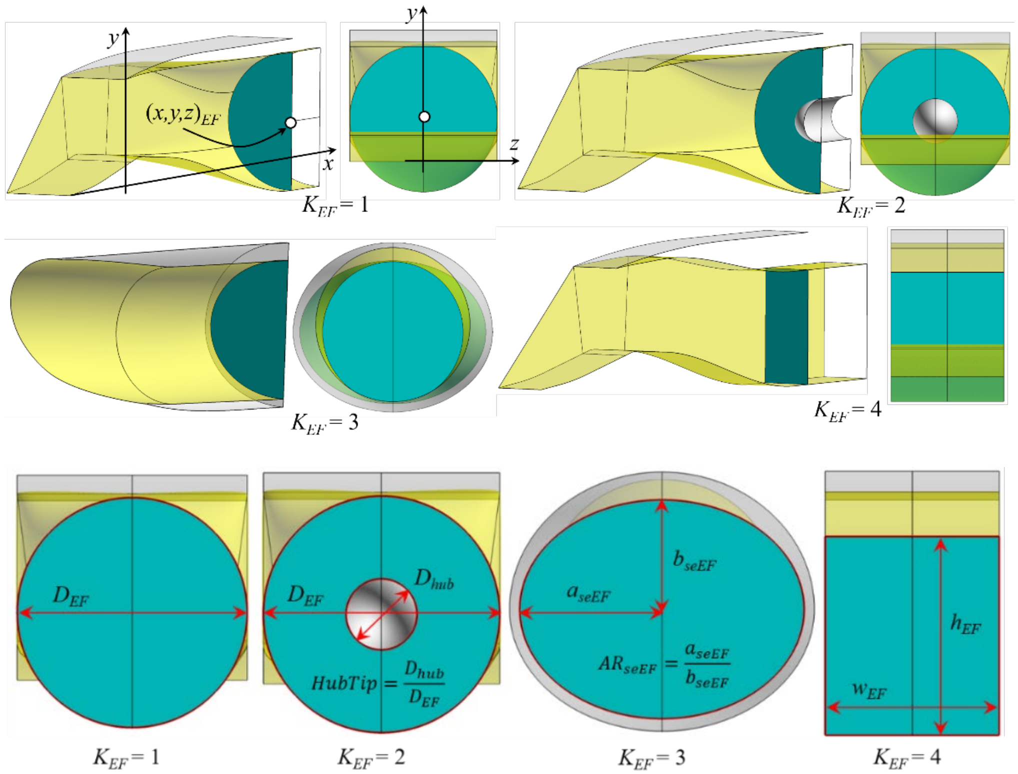

Figure 4.8.—The coordinates, cross-sectional shapes, and dimensions for the engine faces: 1) circular, 2) annular, 3) super-elliptical, and 4) rectangular.

TABLE 4.22.—INPUT FACTORS FOR THE ENGINE-FACE PLACEMENT AND ORIENTATION

Factor	Input	Description
K_{xEF}	KxEF	Flag for determining x_{EF} [2] = 1 x_{EF} is an input through F_{xEF} (ft) = 2 x_{EF} is placed at the end of the subsonic diffuser
F_{xEF}	FxEF	Input for the axial position of the center of the engine face (ft)
K_{yEF}	KyEF	Flag for determining y_{EF} [3] = 1 y_{EF} is specified by F_{yEF} (ft) = 2 y_{EF} is the offset from y_{inlet} by the value of F_{yEF} (normalized by D_{ref}) = 3 $y_{EF} = y_{inlet}$ = 4 y_{EF} is computed to reduce cowl drag ($K_{typ} = 2$) = 5 y_{EF} is placed to make flat top for subsonic diffuser ($K_{typ} = 2$) = 6 $y_{EF} = y_{SD}$, center of station SD ($K_{typ} = 2, 5, 6$) = 7 $y_{EF} = y_{SD} + F_{yEF} L_{subd}$. So, $F_{yEF} = \Delta y_{EF} / L_{subd}$. ($K_{typ} = 2, 5, 6$)
F_{yEF}	FyEF	Input for the vertical position of the center of the engine face
θ_{EF}	thetEF	Angle of the engine face within the (x,y) plane about the z-axis (deg)

The possible shapes of the engine-face cross-section are circular, annular, super-elliptic, and rectangular. Figure 4.8 illustrates those shapes and shows the dimensions associated with each engine-face shape. All the engine face cross-sections are symmetric about vertical and horizontal axes through the center of the engine face. Further, the plane of symmetry is assumed to be on the $z = 0$ plane. The input factor K_{EF} indicates the choice of engine-face cross-sectional shape. Table 4.23 lists the options for K_{EF} along with other input factors that define the dimensions of the engine face. The option of $K_{EF} = 1$ indicates a circular shape with no spinner or centerbody. The only other input factor that is needed to establish the dimensions is the diameter of the engine face, D_{EF}.

TABLE 4.23.—INPUT FACTORS FOR THE SHAPE OF THE ENGINE-FACE

Factor	Input	Description
K_{EF}	KEF	Flag for the cross-sectional, planar shape of the engine face [1] = 1 circular engine face = 2 circular engine face with a spinner or centerbody (co-annular) = 3 super-elliptical engine face = 4 rectangular engine face
D_{EF}	diamEF	Diameter of a circular or co-annular engine face (ft) [1.0]
r_{hub} / r_{EF}	HubTip	Ratio of the radii of the hub to the tip of a co-annular circular engine face
a_{seEF}	aseEF	Length of semi-major axis of super-elliptical engine face (ft)
AR_{seEF}	ARseEF	Aspect ratio of a super-elliptical engine face ($AR_{seEF} = a_{seEF} / b_{seEF}$)
p_{seEF}	pseEF	Parameter for super-elliptical engine face
h_{EF}	hEF	Height of a rectangular engine face (ft)
w_{EF}	wEF	Width of a rectangular engine face (ft)

The option of $K_{EF} = 2$ indicates an annular shape. Turbojet and turbofan engines have a spinner about the hub of the compressor or fan face, respectively, which results in the annular engine-face shape, where the hub diameter is equal to the diameter of the spinner at the engine face. The axisymmetric spike inlet has a centerbody that covers the hub of the engine face to form an annular shape. The input factors needed to establish the dimensions of the annular shape are the diameter of the engine face, D_{EF}, and the ratio of the hub radius to the tip radius, r_{hub} / r_{EF}. The radius of the hub is the radius of the spinner or centerbody at the engine face and is calculated as

$$r_{hub} = \left(\frac{r_{hub}}{r_{EF}}\right) \frac{D_{EF}}{2} \tag{4-6}$$

The option of $K_{EF} = 3$ indicates a super-elliptical shape for the engine face. The super-ellipse is symmetric about its minor and major axes. The super-ellipse allows the engine face to have a circular or elliptical shape, as well as a cross-section that approaches rectangular engine face. The input factors include the length of the semi-major axis of the super-ellipse (a_{seEF}), the aspect ratio of the super-ellipse (AR_{seEF}), and the super-ellipse parameter (p_{seEF}). The length of the semi-minor axis is computed as $b_{seEF} = a_{seEF} / AR_{seEF}$. The super-ellipse parameter has a value of $p_{seEF} = 2$ for a circle and ellipse. As $p_{seEF} > 2$, the cross-section approaches a rectangular shape. Appendix A.6 provides further details on the properties of a super-ellipse. The super-elliptical shape is currently only to be used for the streamline traced ($K_{typ} = 5$) and three-dimensional pitot ($K_{typ} = 6$) inlets.

The option of $K_{EF} = 4$ indicates a rectangular shape for the engine face. The input factors are the height (h_{EF}) and width (w_{EF}) of the engine face in units of feet. The rectangular engine face is currently only able to be used for the two-dimensional ($K_{typ} = 2$) inlet with a rectangular subsonic diffuser ($K_{subd} = 8$).

The spinner is axisymmetric about the axis of the engine and projects forward of the engine face. The possible shapes for the spinner that are modeled within SUPIN include conical, circular, elliptical, and conical with a circular nose. Figure 4.9 illustrates these shapes for the spinner. The surface of the spinner is formed by defining a profile and then sweeping the profile about the engine/spinner axis. The input factors associated with the spinner profile are listed and described in Table 4.24. The input factor $\boldsymbol{K_{spin}}$ indicates the shape for the spinner. For all the spinner shapes, the radius of the spinner at the engine-face plane is defined as r_{hub} as calculated by Equation (4-6).

For $K_{spin} = 1$, the spinner is conical. The half-angle of the conical spinner ($\boldsymbol{\theta_{spin}}$) is an input factor and the units are degrees. The length of the spinner is determined as $L_{spin} = r_{hub} / \tan \theta_{spin}$.

For $K_{spin} = 2$, the spinner is a semi-spheroid, and no input factors are needed. The radius of the semi-spheroid is set to the radius of the hub and $L_{spin} = r_{hub}$.

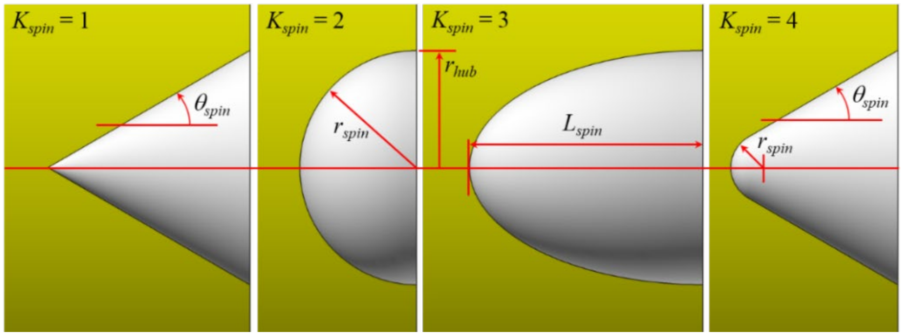

Figure 4.9.—Spinner shapes and dimensions.

TABLE 4.24.—INPUT FACTORS FOR THE SPINNER GEOMETRY

Factor	Input	Description
K_{spin}	`Kspin`	Flag for the shape of the nose of an axisymmetric spinner [3] =0 no spinner =1 conical spinner (specify θ_{spin}) =2 circular spinner ($r_{spin} = r_{hub}$) =3 elliptical ($b_{spin} = r_{hub}$, specify AR_{spin}) =4 conical spinner with circular nose (specify r_{spin} and θ_{spin})
θ_{spin}	`thspin`	Half-angle of the conical spinner (deg) (K_{spin} = 1 and 4)
Fr_{spin}	`Frspin`	Fraction for the nose radius of a conical spinner, $Fr_{spin} = r_{spin} / r_{hub}$ (K_{spin} = 4)
AR_{spin}	`ARspin`	Aspect ratio of the spinner ($AR_{spin} = L_{spin} / b_{spin}$) [2.0] (K_{spin} = 3)

For K_{spin} = 3, the spinner is a semi-ellipsoid. The length of the semi-minor axis of the ellipsoid is equal to the radius of the hub, $b_{spin} = r_{spin}$. The aspect ratio of the ellipse ($\boldsymbol{AR_{spin}} = a_{spin}/b_{spin}$) is needed to be specified as an input factor. The length of the semi-major axis (a_{spin}) is equal to the length of the spinner, which is computed from the aspect ratio as $L_{spin} = AR_{spin}\, r_{hub}$.

For K_{spin} = 4, the spinner is conical with a circular nose. The input factors include the fraction for the radius of the circular nose ($\boldsymbol{Fr_{spin}}$) and the half-angle of the conical shape (θ_{spin}). The radius of the circular nose is specified as a fraction of the radius of the hub, $r_{spin} = Fr_{spin}\, r_{hub}$. The length is established from r_{hub}, r_{spin}, and θ_{spin}.

Table 4.25, Table 4.26, Table 4.28, and Table 4.29 lists example input data blocks for the four shapes of an engine face. The DataID = 11 indicates that the input block is specifying the inputs for the engine face. Table 4.27 lists examples of segments of the input blocks that show the four options for the shape of the spinner.

TABLE 4.25.—EXAMPLE INPUT DATA BLOCK FOR A CIRCULAR ENGINE FACE (K_{ef} = 1)

```
DataID.  Engine Face
 11
KxEF     FxEF     KyEF     FyEF     thetEF
  2    6.00000      1    1.00000     0.000
KEF
 1
 diamEF
 3.00000
```

TABLE 4.26.—EXAMPLE INPUT DATA BLOCK FOR A CO-ANNULAR ENGINE FACE ($K_{ef} = 2$)

```
DataID.  Engine Face
 11
KxEF     FxEF     KyEF     FyEF     thetEF
  2    6.00000      1    1.00000     0.000
KEF
 2
 diamEF     HubTip
 3.00000    0.3000
Kspin
  3
ARspin
2.0000
```

TABLE 4.27.—EXAMPLE INPUT DATA BLOCK LINES FOR THE SHAPE OF THE PROFILE OF THE SPINNER

```
Kspin
  1
thspin
30.000
```

```
Kspin
  2
```

```
Kspin
  3
ARspin
2.0000
```

```
Kspin
  4
Frspin    thspin
0.3000    30.000
```

TABLE 4.28.—EXAMPLE INPUT DATA BLOCK FOR A SUPER-ELLIPTICAL ENGINE FACE ($K_{ef} = 3$)

```
DataID.  Engine Face
 11
KxEF     FxEF     KyEF     FyEF     thetEF
  2    6.00000      1    1.00000     0.000
KEF
 3
  aseEF     ARseEF     pseEF
 1.50000    1.0000     2.000
```

TABLE 4.29.—EXAMPLE INPUT DATA BLOCK FOR A RECTANGULAR ENGINE FACE ($K_{ef} = 4$)

```
DataID.  Engine Face
 11
KxEF     FxEF     KyEF     FyEF     thetEF
  2    6.00000      1    1.00000     0.000
KEF
 4
  FhEF       FwEF
3.44000    3.00000
```

4.14 Reference Dimension

A ***reference dimension***, $\boldsymbol{D_{ref}}$, is used within SUPIN to normalize many of the input factors describing lengths. For example, the input factors F_{wclip} and F_{Lsubd} described previously are lengths that are normalized by the reference dimension. Within SUPIN, the expected reference dimension is the diameter of the engine face, $D_{ref} = D_{EF}$, for a circular engine face. Using this approach, if the size of the engine face changes, then most of the dimensions of the inlet scale in a similar manner. In the case of a rectangular engine face, the width of the rectangular engine face is used as the reference dimension, $D_{ref} = w_{EF}$. For a super-elliptic engine face, the width of the super ellipse is used as the reference dimension, $D_{ref} = 2\ a_{seEF}$. These selections of the reference dimension assume that the input data file includes the input data block for the engine face with DataID = 11.

TABLE 4.30.—EXAMPLE INPUT DATA BLOCK FOR THE SPECIFICATION OF THE REFERENCE DIMENSION, D_{ref}

```
DataID.  Reference Dimension
  24
 FDref
4.00000
```

The reference dimension can also be directly specified within the input data file using the input data block with DataID = 24. This input data block is used when one wishes to use a different reference dimension than one based on the engine face, or in the case that the engine face is not specified within the input data file. An example of the input data block for DataID = 24 is shown in Table 4.30. For the case that the input data file does not contain input data blocks for the reference dimension (DataID = 24) or the engine face (DataID = 11), then the default value of the reference dimension is set to $D_{ref} = 1.0$.

4.15 Components and Entities

The previous subsections discussed some of the input factors and geometry models that are used for defining the geometry of the various inlet components, such as the external supersonic diffuser, throat section, and subsonic diffuser. Further inputs for these components are discussed in later sections with respect to the specific inlet types. In those sections, one or more geometry models will be discussed that allow the dimensions and surfaces of the components to be created based on the values of the input factors. For example, one geometry model for the external supersonic diffuser creates a diffuser with three stages in which the first stage creates an oblique shock wave and the second stage uses a sequence of Mach waves focused on the cowl lip. Another example is a geometry model that forms a subsonic diffuser that transitions from a rectangular cross-section to a circular cross-section using a collection of curves. The geometry models for the components were created to represent some common shapes for the components. However, the geometry models are limited by the assumptions and constraints of the respective geometry model.

Greater flexibility in creating the geometry of the inlet components is provided through the specification of ***geometric entities***, such as lines, cubic-spline curves, fitted curves, and conic sections that define the component. This subsection discusses the specification of the input factors for the entities that define a component. Table 4.31 lists the components for which entities can be specified as part of the input approach of this subsection. Each component corresponds to a value of the input factor $\boldsymbol{K_{comt}}$. The components listed in red italics are not available at this time.

Each component consists of one or more entities that define the geometric shape of the component. Much of the focus in SUPIN is on planar entities. One of the guiding ideas of SUPIN is the recognition that many traditional inlets have a planar character (e.g., two-dimensional and axisymmetric inlets) such that the three-dimensional surface can be constructed using planar entities. Table 4.32 lists the entities that are available for use in a component. These entities are described in further detail in Appendix A.

Each entity is associated with a set of input factors and control points. Appendix A provides details and the input factors and control points that define each type of entity. In most cases, an entity is defined with respect to a local planar coordinate system (X,Y) that may or may not align with the global Cartesian (x,y,z) coordinate system. A ***geometric transformation*** can be associated with each entity to scale, translate, rotate, and assemble the entity within the component and within the global coordinate system. Subsection 14.3 describes the specification of the geometric transformations. A ***variable-geometry schedule*** can be associated with an entity to translate and rotate the entity within the component with respect to time. An example of an entity with a variable-geometry schedule could be a line entity

TABLE 4.31.—LIST OF COMPONENTS

K_{comt}	Component	K_{comt}	Component
1	External Supersonic Diffuser	12	Subsonic Diffuser Cowl Interior
2	*External Diffuser Sidewall*	13	*Subsonic Diffuser Sidewall*
3	*Capture Cross-Section*	14	*Engine Face*
4	*Cowl Lip Interior*	15	*Spinner*
5	*Cowl Lip Exterior*	16	Centerbody
6	*Throat Section Duct*	17	Cowl Interior
7	Throat Section Centerbody	18	Cowl Exterior
8	Throat Section Cowl Interior	19	*Bleed Slot and Plenum*
9	*Throat Section Sidewall*	20	*Support Struts*
10	*Subsonic Diffuser Duct*	21	*Outflow Nozzle*
11	Subsonic Diffuser Centerbody	22	Planar Forebody

TABLE 4.32.—LIST OF ENTITIES

K_{ent}	Entity Type	K_{ent}	Entity Type
0	Point	10	NURBS Curve
1	Line	11	Four-Point NURBS Curve
2	Circular Curve	12	*Fitted NURBS Curve*
3	Ogive Curve	13	Cosine-Sine Curve
4	Elliptical Curve	14	Cosine-Sine-Squared Curve
5	Super-Elliptical Curve	15	Annular Cross-Section
6	NACA-1 Series Curve	16	Super-Elliptical / Rectangular Cross-Section
7	Polynomial Curve	17	NURBS Cross-Section
8	Piecewise Linear Curve	18	*Transfinite Interpolation (TFI) Surface*
9	Fitted Cubic Spline Curve	19	*NURBS Surface*

representing a ramp of a planar external supersonic diffuser. The variable-geometry schedule could specify the rotation of the ramp with respect to time. Such capability could be used to model the variable-geometry of an inlet. Subsection 14.4 describes the specification of the variable-geometry schedules.

A component and its entities are specified using an input data block in which DataID = 16. An example of such an input data block is shown in Table 4.33. The essential format of this input data block is to indicate a component and then list the entities and its inputs that define the geometry of the component. An input data block can only contain one component and a single data block should contain all the entities for that component. The specification of multiple components requires multiple instances of this input data block format. For example, the sample test case SUPIN.K3.M166.LBSS contains specification of the centerbody (K_{comt} = 16) and cowl interior (K_{comt} = 17) components, and so, uses two instances of an input data block with DataID = 16. The instances of the input data blocks can be listed in any order within the input data file. As with any input data file, the entire set of input data blocks and their respective input factors should provide a complete description so that the inlet can be constructed.

The input data block starts with the same two lines as shown by lines 3 and 4 in Table 4.33. The main input factors for the specification of components and entities are listed in Table 4.34. The input factor $\boldsymbol{K_{comt}}$ indicates the type of component and corresponds to one of the components listed in Table 4.31. The input factor $\boldsymbol{N_{ents}}$ indicates the number of entities contained within the component. The input factor $\boldsymbol{K_{part}}$ is an input factor that provides a means of specifying an integer flag that can be used to further define the component and its meaning depends on the value of K_{comt}. For example, if the component was part of the throat section, the K_{part} may be used to further define how the component is to be modeled, such as defining the value of the input factor K_{thrt}. This will be further explained in the subsections describing each type of inlet.

The remainder of the input data block contains a listing of input lines for each of the N_{ents} entities of the component. It is assumed that the entities connect end-to-end to form a contiguous sequence to define the component. The example of Table 4.33 contains two entities. The first entity is a line, and the second entity is a NURBS curve. For each entity, the input lines start with a blank line to separate the input lines of each entity. A header line that starts with "Kent" provides the basic data for the entity that includes the input factors K_{ent}, K_{trf}, K_{vgm}, and N_{cps}. The input factor $\boldsymbol{K_{ent}}$ identifies the type of entity as listed in Table 4.32. The $\boldsymbol{K_{trf}}$ is a pointer to a set of information defining any geometric transformations that are to be applied to the entity. The $\boldsymbol{K_{vgm}}$ is a pointer to a set of information defining a variable geometry schedule for the entity. Section 14.0 will discuss the transformation and variable-geometry input factors.

The $\boldsymbol{N_{cps}}$ is in most cases the number of control points for the entity. For some entities, such as the cubic spline curve (K_{ent} = 9), the value of N_{cps} indicates the number of control points through which the cubic spline must be fitted. Thus, the number of (X,Y) coordinate points listed for that entity must match the value of N_{cps}. In other words, the value of N_{cps} indicates how may lines of (X,Y) coordinates that SUPIN must read. In the example of Table 4.33, the second entity is a NURBS curve that has four control points. For the polynomial curve entity (K_{ent} = 7) the value of N_{cps} is the order of the polynomial. For some entities, such as the line or circle entity, the specified value of N_{cps} is not used since the number of control points depends on the entity type, and so, the proper value of N_{cps} is assumed.

TABLE 4.33.—EXAMPLE OF AN INPUT DATA BLOCK FOR COMPONENTS AND ENTITIES

```
DataID.  Geometry Component
 16
Kcomt  Nents  Kpart
  1      2      5

Kent  Ktrf  Kvgm  Ncps           !..Line
  1     1     3     4
Kline    Xbeg      Ybeg      Xend      Yend    Thline   Lline
  1    0.00000   0.00000   8.31200   1.84250   12.500  8.51376

Kent    Ktrf    Kvgm    Ncps     !..NURBS Curve.
 10       0       0       4
         Xcp         Ycp
      0.7500      0.3930
      1.1653      0.3820
      1.5645      0.3755
      1.9641      0.3755
```

TABLE 4.34.—MAIN INPUT FACTORS FOR THE SPECIFICATION OF COMPONENTS AND ENTITIES

Factor	Input	Description
K_{comt}	`Kcomt`	Type of component (see Table 4.33)
N_{ents}	`Nents`	Number of entities in the component
K_{part}	`Kpart`	Flag for further defining the component
K_{ent}	`Kent`	Type of entity (see Table 4.34)
K_{trf}	`Ktrf`	Pointer to the geometric transformation information for an entity (=0, none)
K_{vgm}	`Kvgm`	Pointer to the variable geometry schedule for an entity (=0, entity is static)
N_{cps}	`Ncps`	Number of control points for the entity

The remaining lines of input for the entity specify input factors that define how to explicitly construct the geometry of that entity. Appendix A provides greater details on the forms and input factors appropriate for each entity, as well as examples of the lines of input. The specification of the entities within a component, along with values of other input factors specified in the input data file, help construct the topology to assemble the components for the inlet.

Subsections 4.8, 4.10, 4.11, and 4.12 above indicated options of K_{exd} = 8, K_{cwex} = 4, K_{thrt}, = 8, and K_{subd} = 15 for the external supersonic diffuser, cowl exterior, throat section / internal supersonic diffuser, and subsonic diffuser, respectively, to specify that the component was defined by entities. These options require that the input data file should also contains an input data block with DataID = 16 to specify the entities associated with the respective component.

Internally, SUPIN represents each component in terms of the entities defined in Table 4.32. At the end of the execution of SUPIN, an updated input data file is written that is given the name SUPIN.new.in. This file lists the input data blocks for the inlet with the actual dimensions listed for the values of the input factors. At the end of SUPIN.new.in, the input data blocks for each component with the entities is written for reference.

4.16 Quasi-One-Dimensional Flowpath Analysis

The basis of the aerodynamic analysis with SUPIN is the assumption of quasi-one-dimensional flow through the inlet. SUPIN provides a capability to perform a simple quasi-one-dimensional analysis of the inlet flowpath. Such an analysis only involves the variation of the Mach number, cross-sectional area, and total pressure at the flow stations within the inlet while considering the balance of the flow rates for the inlet. The flowpath analysis does not consider the spatial dimensions of the flowpath, just the change in the flow properties between the stations. The flowpath analysis allows a simple examination of the interactions between Mach number, total pressure, and cross-sectional area prior to a more detailed inlet design.

This capability uses the SUPIN Inlet Flowpath Analysis Mode with K_{mode} = 4. The primary equation involved is Equation (2-15) applied at the inlet stations as identified in the figures of Subsection 2.5 and listed in Table 2.1. The analysis also considers the continuity of the flow rate between the stations while accounting for extractions of the flow rate due to spillage, bleed, bypass, and other flows, as described in Subsection 2.9. The flowpath analysis requires input data blocks for the main control of SUPIN (DataID = 0), freestream (DataID = 1), external supersonic diffuser (DataID = 4), throat section / internal supersonic diffuser (DataID = 8), subsonic diffuser (DataID = 10), and the engine face (DataID = 11). Input data blocks can be included for an approach flow (DataID = 2) and specification of bleed and bypass flows (DataID = 12). The inputs require specification of total pressure ratios between stations as described in the subsections above for each component and Mach numbers at certain stations.

Examples of the lines of input needed for the external supersonic diffuser, throat section, and subsonic diffuser for the flowpath analysis of an external-compression inlet are listed in Table 4.35. For the external supersonic diffuser, input flag K_{exd} = 1 and the inputs are the total pressure ratios p_{tEX}/p_{tL} and p_{t1}/p_{tEX} and either the Mach number (M_{EX}) or cross-sectional area (A_{EX}) at the end of the external supersonic diffuser. If FmachEX > 0, then that M_{EX} = FmachEX is used, and the area is calculated using the appropriate continuity equations of Equations (2-31) and (2-32). Alternatively, if FmachEX < 0.0 and FareaEX > 0.0, the A_{EX} = FareaEX and the corresponding Mach number (M_{EX}) is computed. For an external-compression inlet (K_{comp} = 1), a normal terminal shock wave is placed between stations EX and 1 and the total pressure ratio p_{tNS}/p_{tEX} is computed along with the Mach number (M_{NS}) downstream of the terminal shock wave. The input Fpt1ptEX specifies any losses between station NS and 1.

TABLE 4.35.—EXAMPLE OF LINES OF INPUT THE INPUT DATA BLOCKS FOR THE EXTERNAL SUPERSONIC DIFFUSER (TOP), THROAT SECTION (MIDDLE), AND SUBSONIC DIFFUSER (BOTTOM) FOR THE FLOWPATH ANALYSIS OF AN EXTERNAL-COMPRESSION INLET

```
DataID.  External Supersonic Diffuser
  4
Kexd    FptEXptL    Fpt1ptEX
  1      0.99500     1.00000
FmachEX    FareaEX
 1.3000    -1.0000
```

```
DataID.  Throat Section
  8
Kthrt      FptSDs1     FptsegB    FptsegC
  1        0.98500    -0.99500   -1.00000
FmachTS  FmachTH  FmachSD
 -0.70    -0.70     0.65
```

```
DataID.  Subsonic Diffuser
 10
Ksubd    KLsubd    FLsubd    theqsd    Fpt2ptSD
  1         2      1.0000     3.000     0.98500
```

The flowpath analysis for the throat section is indicated by K_{thrt} = 1. The throat section of the external-compression inlet uses inputs for FptsegA = FptSDpt1 for the total pressure ratio between station 1 and SD, which is considered to involve subsonic flow. The input factors FmachTS, FmachTH, and FmachSD are provided to input Mach numbers for stations TS, TH, and SD; however, for an external-compression inlet, only FmachSD is used, and a positive value provides the Mach number at station SD.

These same inputs are used for the flowpath analysis of a subsonic inlet (K_{comp} = 0). For the internal supersonic diffuser and throat section of a mixed-compression inlet (K_{comp} = 2 or 3), the input factors are the total pressure ratios p_{tTH}/p_{t1} and p_{tSD}/p_{tTH} and the Mach numbers M_{TH} and M_{SD}. A normal shock wave is assumed at station TH.

The flowpath analysis for the subsonic diffuser is indicated by K_{subd} = 1. The only input needed is Fpt2ptSD for the total pressure ratio between stations SD and 2. The other inputs for the length of the subsonic diffuser are neglected for the flowpath analysis.

4.17 Output Data File

As SUPIN is executed, it writes an output data file named SUPIN.Out.txt. The file is an ASCII text file formatted to provide a readable description of the inlet geometry and aerodynamic performance. At the start of SUPIN, a header is written to the output data file. Once SUPIN has read the input data file, the contents of that file are written at the beginning of the output data file as an “echo” of the input to provide the user with a record of what was input into SUPIN. While SUPIN is performing the design and analysis of the inlet, it writes information on the iterations being performed for the sizing or analysis of the inlet. Once the inlet has been constructed, designed, or analyzed, SUPIN writes out information on the inlet, which includes geometry information and the flow conditions at each station, aerodynamic properties, and inlet performance results if K_{mode} = 2 or 3. Toward the end of the output data file, a summary is provided on the performance and characteristics of the inlet. If a surface or CFD grid is generated, the output data file lists properties and statistics of the grids. If SUPIN encounters problems, a message may be written to the output data file and may be useful in understanding why and where the failure occurred.

4.18 Other Files Written by SUPIN

In addition to the output data file (SUPIN.Out.txt), the surface grid (SUPIN.xyz), and any CFD grid files, SUPIN also writes other files that provide further information and data on the inlets. The files include:

- ***SUPIN.new.in.*** This ASCII text file that has the same form as the input data file (SUPIN.in) but with values of some of the input factors that reflect the final inlet. This file could be used as input to recreate the inlet using the SUPIN geometry mode (K_{mode} = 1). This file also writes out the components and entities for the planar profiles for the axisymmetric and two-dimensional inlets (K_{typ} = 1, 2, 3, and 4).
- ***SUPIN.Geom.txt.*** This ASCII text file is like the SUPIN.new.in input data file but writes the input data file using the entity description and entity format for the inlet components. Thus, this file provides the control points that can be used to define the planar geometry of the axisymmetric and two-dimensional inlets.
- ***SUPIN.Table.txt***. This ASCII text file provides a summary table of select inlet input factors, inlet geometric properties, and inlet performance metrics. The format of the summary table lists the values in a column followed by a description. This format makes it convenient for reading into a computational spreadsheet application, such as Microsoft Excel®. The writing of the output summary table file is specified through the input data block with DataID = 30, which is discussed in Section 14.0.
- ***SUPIN.PlotData.txt.*** This ASCII text file contains inlet profile geometry and quasi-one-dimensional coordinates and flowfield data. The profile geometry are lists of planar (x,y) coordinates and slopes defining the profiles of the inlet components, such as the external supersonic diffuser, cowl interior, and cowl exterior. The quasi-one-dimensional data also include lists of coordinates, areas, and flow properties of the quasi-one-dimensional representation of the inlet. While the file is readable as text, the form of the file is intended to facilitate the plotting of the coordinates, areas, and flow properties by some other application. The data could also be read into a spreadsheet program (e.g., Microsoft Excel®) for tabulations and plotting. The file is also intended to be read by a still-do-be-developed Python application that will allow convenient plotting of the data to allow a visualization of the inlet characteristics. The file consists of a standard header describing the inlet followed by data sets for the specific information. For example, one data set could contain the list of coordinates for the cowl interior profile. Table 4.36 lists the data sets that could be included in the file. Each data set is identified by its ID number and the data is listed in a specific format.
- ***SUPIN.ComponentPoints.txt***. This text file lists the coordinates of the entities for the components of the inlet as identified in Subsection 4.15. The format of the lists is the same as the input structure for the components and entities as discussed in Subsection 4.15 for the input data block with DataID = 16.

TABLE 4.36.—DATA SETS WITHIN THE SUPIN.PLOTDATA.TXT FILE

Data Set ID	Description
1	Coordinates for the Nose Profile
2	Coordinates for the External Supersonic Diffuser
3	Coordinates for the Throat Section Centerbody
4	Coordinates for the Subsonic Diffuser Centerbody
5	Coordinates for the Centerbody Profile
6	Coordinates for the Cowl Lip Interior Profile
7	Coordinates for the Throat Section Cowl Interior
8	Coordinates for the Subsonic Diffuser Cowl Interior
9	Coordinates for the Cowl Interior Profile
10	Coordinates for the Cowl Lip Exterior Profile
11	Coordinates for the Cowl Exterior Profile
12	Cowl Exterior Wave Drag
13	Coordinates for the Spinner Profile
14	Quasi-1D Upper and Lower Coordinates
15	Quasi-1D Coordinates and Areas
16	Diverging portion of the Internal Diffuser
17	Subsonic Diffuser Super-Ellipse Data
18	Flow Properties along the Quasi-1D Flowpath
19	Coordinates for the Planar Capture Streamline
20	Information on ICFA solution
21	Information on axisymmetric Busemann solution
22	Coordinates for streamline-traced profile at top of diffuser

- ***SUPIN.mocA.xyz***, ***SUPIN.mocA.q***, ***SUPIN.mocB.xyz***, ***SUPIN.mocB.q***, ***SUPIN.mocC.txt***, ***SUPIN.mocC.xyz***, ***SUPIN.mocC.q***, ***SUPIN.mocD.txt***, ***SUPIN.mocD.xyz***, and ***SUPIN.mocD.q***. These files are written when the method-of-characteristics (MOC) is used (K_{thrt} = 6) for the design of two-dimensional and axisymmetric spike inlets, which will be discussed in Section 9.0. The files *.xyz contain the coordinates in Plot3D format of the characteristic net for each of the MOC regions. The files *.q contain the flow solution in Plot3D format, but the only useful information is the Mach numbers and flow angles at each point of the characteristic net. The mocC.txt and mocD.txt files contain the flow properties along the centerbody and cowl interior for regions C and D, respectively.
- ***SUPIN.gman.txt***. This text file lists the boundary conditions associated with the assembled CFD grids for the inlet. The file is in the format for use with the gman pre-processing tool for the Wind-US CFD solver.
- ***SUPIN.cfsplit.txt***. This text file is intended for use with the cfsplit pre-processing tool for the Wind-US CFD solver. The purpose is to indicate how to split the blocks of the CFD grid to reduce the grid size of the larger blocks for multi-processing operations.

References

1. Walatka, P. P., Buning, P. G., Pierce, L., and Elson, P. A., “PLOT3D User’s Manual,” NASA-TM-101067, March 1990.
2. Anderson, J. D., Jr., *Introduction to Flight*, McGraw-Hill Book Company, New York, 1978.
3. Mattingly, J. D., Heiser, W. H., and Daley, D. H., *Aircraft Engine Design*, AIAA Education Series, New York, 2002.

5.0 Axisymmetric Pitot Inlets

The types of inlets modeled within SUPIN were listed in Table 4.3 and illustrated in Figure 4.1. The next several sections will discuss these inlet types. This section discusses the ***axisymmetric pitot inlet*** (K_{typ} = 1), which is perhaps the simplest inlet and can be used for subsonic and supersonic flight. This discussion of the axisymmetric pitot inlet also serves to illustrate some fundamental features and design methods using a relatively simple inlet.

5.1 Axisymmetric Pitot Inlet Geometry

Figure 5.1 shows some images and nomenclature for an axisymmetric pitot inlet. The inlet is defined with respect to an ***inlet axis***, which can be considered a reference axis used to define the inlet. For the axisymmetric pitot inlet, the inlet axis is coincident with the axis-of-symmetry.

The ***engine face*** for the axisymmetric pitot inlet is circular with a diameter of D_{EF}. Figure 5.1 shows an axisymmetric spinner with an elliptical profile. The hub-to-tip ratio is defined as D_{hub} / D_{EF} and is zero for the case that no spinner exists. The ***engine axis*** runs through the center of the engine face and is coincident with the inlet axis and axis-of-symmetry. The inlet coordinate system (x,y,z) is positioned such that y = 0 and z = 0 are on the inlet axis, and so, $y_{inlet} = y_{EF} = 0$ and $z_{inlet} = z_{EF} = 0$. The engine face is on a perpendicular plane to the inlet axis (θ_{EF} = 0.0 deg).

The ***cowl lip*** is the forward-most part of the inlet and defines the location of station 1. For an axisymmetric pitot inlet, the cowl lip point is positioned at a radius of y_{clip} from the inlet axis. The y-coordinate is used here as the measure of radius to keep this dimension consistent between the various types of inlets. The axial position of the cowl lip is placed at x_{clip} = 0, but this specification is arbitrary and can be translated for convenience.

The trace of the cowl lip radius about the inlet axis creates a circular curve that is the ***highlight*** curve of the inlet. The highlight bounds the circular ***capture cross-section***, which is the aperture through which the airflow enters the internal ducting of the inlet. The area of the capture cross-section defines the ***reference capture area***, A_{cap}. The axisymmetric nature results in the capture cross-section being circular with a reference capture area of

$$A_{cap} = \pi y_{clip}^2 = \frac{\pi}{4} D_{clip}^2 \tag{5-1}$$

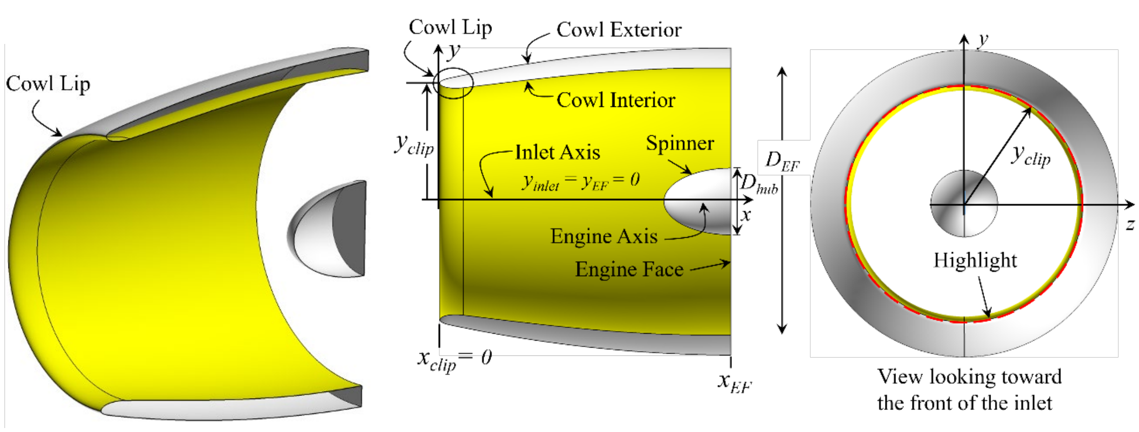

Figure 5.1.—An axisymmetric pitot inlet.

The surfaces of the inlet consist of the ***cowl interior*** and ***cowl exterior*** surfaces. Both surfaces are formed by defining planar profiles and then extruding the profiles about the inlet axis-of-symmetry. The profile for the cowl interior starts at the cowl lip point and includes profiles that define the cowl lip interior, throat section, and subsonic diffuser. The cowl interior ends at the engine face. The profile for the cowl exterior also starts at the cowl lip point and includes profiles for the cowl lip exterior and cowl exterior. The cowl exterior ends at point $(x,y)_{cwex}$, as discussed in Section 4.10. The next four subsections will discuss further details of the cowl lip, throat section, subsonic diffuser, and cowl exterior for the axisymmetric pitot inlet.

5.2 Cowl Lip

The cowl lip consists of the cowl lip interior and cowl lip exterior surfaces, as was previously discussed in Section 4.9. The highlight is the common edge of those surfaces and forms the leading edge of the axisymmetric pitot inlet. The input factors defining the elliptical profiles of the cowl lip and the extrusion of those profiles to generate the cow lip surfaces were also discussed in Section 4.9. An axisymmetric pitot inlet intended for subsonic flight tends to have a rather blunt cowl lip defined by dimensions (i.e., b_{clin} and b_{clex}) that can be a few percentages of the cowl lip radius, y_{clip}. The blunt nature of the cowl lip allows the subsonic flow to turn into the inlet without causing boundary layer separation. For supersonic flight, a blunt cowl lip will result in a detached bow shock wave about the cowl lip, which results in increased cowl lip drag. Thus, the cowl lip for supersonic flight has smaller dimensions (i.e., b_{clin} and b_{clex}) for the elliptic profiles, as discussed in Section 4.9, that approximate a sharp cowl lip. In Figure 4.3, the inlet on the left-hand-side represents a subsonic axisymmetric pitot inlet with a blunt cowl lip. The inlet on the right-hand-side of Figure 4.3 represents a supersonic axisymmetric spike inlet with a cowl lip with very small dimensions.

For a subsonic inlet with a blunt cowl lip interior, the cross-sectional area of the inlet streamtube will decrease in the axial direction about the cowl lip and a minimal cross-sectional area for the inlet will occur due to this geometric definition. This minimal axial cross-sectional area becomes the geometric throat for the inlet and the cross-sectional area is designated A_{TH} located at planar point $(x,y)_{TH} = (x,y)_{TC}$, as illustrated in Figure 4.3. For subsonic flow, the axial quasi-one-dimensional Mach number will increase from the Mach number at station 1 (M_1) to a Mach number at the geometric throat at point TH designated as M_{TH}. A common design constraint for subsonic inlets is to specify a desired Mach number for M_{TH} and then compute the corresponding dimensions a_{clin} and b_{clin} for the cowl lip interior. This design method involves computing the corresponding cross-sectional area A_{TH} that results in M_{TH} with the assumption of isentropic, quasi-one-dimensional flow between stations 1 and TH and the continuity of Equation (2-31). Thus, the equation for A_{TH} becomes,

$$A_{TH} = A_1 \frac{\phi_1}{\phi_{TH}} \tag{5-2}$$

The coordinate y_{TH} can be computed from A_{TH} and the equation of an ellipse can be used to establish the required values of a_{clin} and b_{clin}. Within SUPIN, the use of this design method for an axisymmetric pitot inlet is activated when the input factor for M_{TH} is specified as $0.0 < M_{TH} =$ FmachTH < 1.0. This method is only applied for the axisymmetric pitot inlet ($K_{typ} = 1$) using the inlet design mode ($K_{mode} = 2$) and $K_{thrt} = 2$.

5.3 Throat Section

The throat section starts at the end of the cowl lip interior at point $(x,y)_{\mathrm{clin}}$ and ends at the start of the subsonic diffuser at station SD at point $(x,y)_{cwSD}$ to form the forward portion of the internal diffuser of the inlet. The throat section model described in this subsection can be used for both subsonic and supersonic axisymmetric pitot inlets. For subsonic freestream conditions, the flow into the inlet is expected to remain subsonic through the geometric throat unless the area ratio of A_{TH}/A_L is low enough to choke the flow and reach sonic conditions at station TH. In that case, a shock wave may form to decelerate the flow to subsonic conditions. At supersonic freestream conditions, it is expected that a normal shock wave would form about station 1 to decelerate the flow to subsonic conditions. Thus, a purpose of the throat section for the axisymmetric pitot inlet is to ensure that subsonic flow is established for entry to the subsonic diffuser.

The throat section geometry model for the axisymmetric pitot inlet is illustrated in Figure 5.2. The model creates a profile for the portion of the cowl interior between points $(x,y)_{clin}$ and $(x,y)_{cwSD}$ and then creates the surface by extruding the profile about the inlet axis-of-symmetry. For an axisymmetric pitot inlet, the y-coordinate is the radial coordinate for the inlet. The profile is formed using a four-point NURBS curve using the endpoints $(x,y)_{clin}$ and $(x,y)_{cwSD}$ and end-slopes θ_{clin} and θ_{cwSD}. The four-point NURBS curve segments are computed using the factor $K_S = 2$, which places the interior control points one-third the distance between the points, as discussed in Appendix A. The coordinates for the point $(x,y)_{cwSD}$ are established by specifying the length L_{cwSD} from station 1 to station SD and the area ratio A_{SD}/A_1. The radial coordinates at station SD (y_{cwSD}) are established with the calculation of the cross-sectional area A_{SD}, and the recognition that the shape of the cross-sectional area is a circle for an axisymmetric spike inlet.

For subsonic, quasi-one-dimensional flow through the throat section, the area ratio A_{SD}/A_1 can be calculated for a specified value of M_{SD}. With consideration that flow could be extracted from the inlet between stations 1 and SD through a bleed region (W_{b1SD}), the flowrate at station SD (W_{SD}) can be computed the using the continuity statement of Equation (2-32b). The cross-sectional area at station SD (A_{SD}) can then be computed using Equation (2-15) for the specified Mach number (M_{SD}). Adiabatic flow between stations 1 and SD is assumed ($T_{tSD} = T_{t1}$) and the total pressure ratio (p_{tSD}/ p_{tS1}) is estimated using the subsonic duct total pressure loss model discussed below in Subsection 5.7.

This geometry model for the axisymmetric pitot inlet is imposed when $K_{thrt} = 2$ is specified within the throat section input data block (DataID = 8). Table 5.1 lists the SUPIN input factors for this model and Table 5.2 lists an example input data block. The input factor FmachTH specifies the Mach number at station TH and is imposed when FmachTH > 0.0. In that case, M_{TH} = FmachTH and M_{TH} is used to calculate the cowl interior dimensions (a_{clin}, b_{clin}) as described in Subsection 5.2. The input factor FLcwSD specifies the length L_{cwSD} in the axial direction from station 1 to station SD, as indicated in Figure 5.2. The input factor FLcwSD is normalized by the reference dimension D_{ref}, which for an axisymmetric pitot inlet is by default the diameter of the engine face, $D_{ref} = D_2 = D_{EF}$. The input factor FaSDa1 specifies the area ratio A_{SD}/A_1, from which the area A_{SD} can be calculates from the known value of the area A_1. The input factor thcwSD specifies the slope of the cowl interior at station SD (θ_{cwSD}). The input factor FmachSD specify the desired Mach number M_{SD} at station SD. The hierarchy of the input factors is such that if FmachSD > 0.0, then M_{SD} = FmachSD and the input factor FaSDa1is ignored. The area at station SD (A_{SD}) is then calculated as described earlier in this subsection.

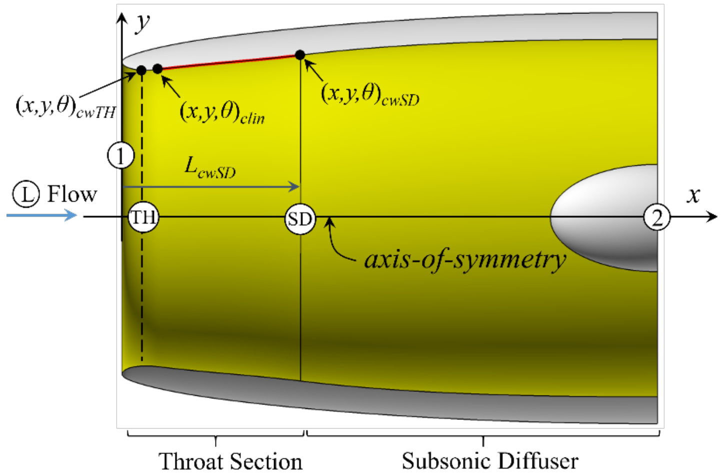

Figure 5.2.—Subsonic axisymmetric pitot inlet with station SD within the internal diffuser.

TABLE 5.1.—INPUT FACTORS FOR THE THROAT SECTION OF AN AXISYMMETRIC-PITOT INLET (K_{thrt} = 2)

Factor	Input	Description
M_{TH}	FmachTH	Mach number at the station TH
L_{cwSD}	FLcwSD	Axial distance from station 1 to station SD (normalized by D_{ref})
A_{SD}/A_1	FaSDa1	Ratio of cross-sectional area at station SD to area at station 1
θ_{cwSD}	thcwSD	Slope of the cowl at station SD (deg)
M_{SD}	FmachSD	Mach number at the station SD

TABLE 5.2.—EXAMPLE INPUT DATA BLOCK FOR THE THROAT SECTION FOR AN AXISYMMETRIC PITOT INLET (K_{thrt} = 2)

```
DataID.  Throat Section.
  8
Kthrt    FptTHpt1    FptSDptTH     FptsegC
  2      -0.99000     -0.99500    -1.00000
 FmachTH     FLcwSD      FaSDa1    thcwSD      FmachSD
-0.75000    1.00000     1.04000     5.000     -0.60000
```

The above geometry model does allow the start of the subsonic diffuser at station SD $(x,y)_{cwSD}$ to be coincident with the cowl lip interior point $(x,y)_{clin}$. This is done by specifying FLcwSD ≤ 0.0. This then sets $L_{cwSD} = x_{cwSD} - x_1$. An example of such a configuration is shown in Figure 5.3. The throat section then includes just the cowl lip region. Such a configuration considers most of the internal diffuser as part of the subsonic diffuser, which is a reasonable approach for an axisymmetric pitot inlet. The same effect can be realized by eliminating the input data block for the throat section or specifying K_{thrt} = 0 in the input data block with no additional lines of input for the block.

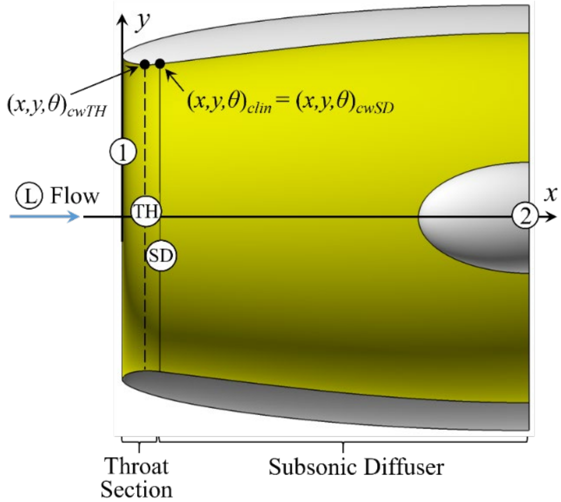

Figure 5.3.—Subsonic, axisymmetric pitot inlet with FLcwSD = 0 to place station SD at the end of the cowl lip interior.

5.4 Subsonic Diffuser

The subsonic diffuser connects the end of the throat section at station SD to the engine face at station 2 as shown in Figure 5.4. The flow at station SD is assumed to be subsonic. The subsonic diffuser nominally incorporates an increasing cross-sectional area to diffuse the flow to a lower subsonic Mach number between station SD and station 2. The cross-sectional shape at stations SD and 2 are both circular since the inlet is axisymmetric.

The surface of the subsonic diffuser for an axisymmetric pitot inlet is formed by extruding a planar profile of the subsonic diffuser cowl interior about the inlet axis-of-symmetry. The planar profile extends between the planar coordinates $(x,y)_{cwSD}$ of the subsonic diffuser and $(x,y)_{TEF}$, the top of the engine face. As with the throat section, the y-coordinate is used to denote the radial coordinate for the axisymmetric surface. Figure 5.4 shows an axisymmetric pitot inlet, where the profile of the subsonic diffuser is shown as a curve that consists of two segments. The first segment is a four-point NURBS curve that forms the diffusing characteristic of the subsonic diffuser. The second segment is a line that forms a constant-area section ahead of the engine face. The use of the line segment and constant-area section is optional and is implemented by setting the length L_{cwX}, as described in the next paragraph. The overall axial length of the subsonic diffuser is L_{subd}.

Table 5.3 lists a sample input data block for the subsonic diffuser of an axisymmetric pitot inlet with DataID = 10. The input factor $K_{subd} = 2$ indicates that the form of the inputs is for an axisymmetric pitot inlet. Most of the input factors were discussed in Subsection 4.12 Table 5.4 lists the input factors specifically for the subsonic diffuser of an axisymmetric pitot inlet. The axial length of the constant-area section ahead of the engine face is specified by the input factor F_{LcwX}, which is normalized by the reference dimension, D_{ref}. Thus, $L_{cwX} = F_{LcwX}\, D_{ref}$. The line defining the constant-area section extends from coordinate $(x,y)_{cwX}$ to $(x,y)_{TEF}$. The line is oriented at an angle $\theta_{EF} = 0$ degrees so that it is parallel to the engine axis. The NURBS curve starts at coordinate $(x,y)_{cwSD}$ and ends at coordinate $(x,y)_{cwX}$. If the input factor $F_{LcwX} < 0$, then there is no constant-area section and $(x,y)_{cwX} = (x,y)_{TEF}$. The NURBS curve has a slope of θ_{cwSD} at the start and a slope of $\theta_{EF} = 0$ degrees at the end. The interior control points for the four-point-NURBS curve are placed according to the input factors F_{NcwSD} and F_{NcwX}, which are fractions of the distance of a line from $(x,y)_{cwSD}$ to $(x,y)_{cwX}$. For example, values of $F_{NcwSD} = 0.33$ and $F_{NcwX} = 0.33$ place the interior control points approximately one-third the distance and are reasonable default values. Increasing or decreasing the values of the factors for the interior control point increases or decreases, respectively, the influence of the slope and provides a mechanism to adjust the area variation and slope of the cowl interior surface through the diffuser.

The input data block of Table 5.3 contains the input factors K_{sdprp} and K_{sdvar} as discussed previously in Section 4.12. The values of these inputs can be specified to obtain the desired distribution of the cross-sectional area of the subsonic diffuser for the axisymmetric pitot inlet. The area distribution is imposed by starting with the profile of the cowl interior for the subsonic diffuser as created by the geometry model described above and illustrated in Figure 5.4. Using the area distribution as calculated based on the values of K_{sdprp} and K_{sdvar}, the profile of the cowl interior is modified so the axial distribution of the radii results in the desired area distribution. The area distribution does not account for the cross-sectional area of the spinner.

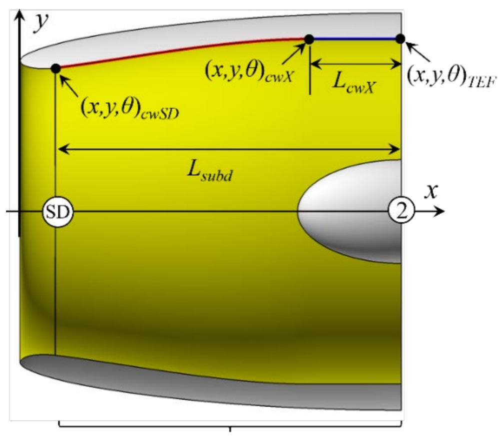

Figure 5.4.—Planar profiles used to define the subsonic diffuser of an axisymmetric pitot inlet.

TABLE 5.3.—SAMPLE INPUT BLOCK FOR THE SUBSONIC DIFFUSER FOR AN AXISYMMETRIC PITOT INLET

```
DataID.   Subsonic Diffuser
 10
Ksubd     KLsubd     FLsubd     theqsd      Fpt2ptSD
  2          1      4.50000      3.000      -0.97500
FNcwSD     FNcwX      FLcwX     Ksdprp       Ksdvar
0.3333    0.3333     0.2000        2             1
```

TABLE 5.4.—INPUT FACTORS FOR THE SUBSONIC DIFFUSER OF AN AXISYMMETRIC PITOT INLET

Factor	Inputs	Description
F_{NcwSD}	FNcwSD	Factor for NURBS interior control point at station SD
F_{NcwX}	FNcwX	Factor for NURBS interior control point at point cwX
F_{LcwX}	FLcwX	Length of constant-area section normalized by D_{ref}

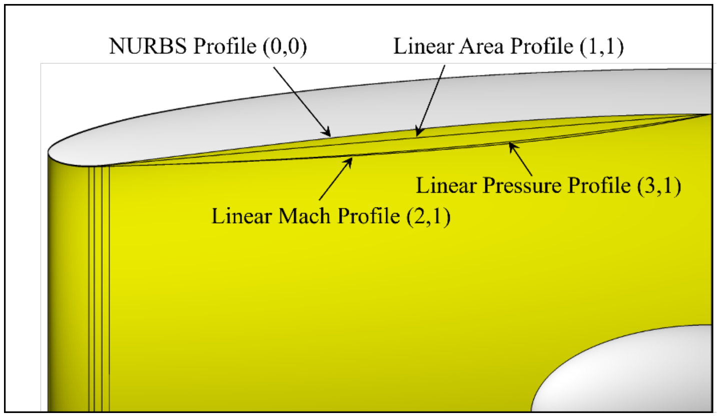

Figure 5.5.—Variation of the profiles of the subsonic diffuser for a subsonic axisymmetric pitot inlet with selection of K_{sdprp} and K_{sdvar}, whose respective values are indicated within the parentheses.

Figure 5.5 shows an example of variations of the cross-sectional area within the subsonic diffuser by applying various values of K_{sdprp} and K_{sdvar}. The inlet image shown as shaded surfaces is the same the inlet shown in Figure 5.3. The profile of the subsonic diffuser was generated using a NURBS curve as described above, which occurs when $K_{sdprp} = 0$ and $K_{sdvar} = 0$. The respective values of K_{sdprp} and K_{sdvar} used for the images of Figure 5.5 are listed within the parentheses of the labels of the curves within Figure 5.5 with the form (K_{sdprp}, K_{sdvar}). The slope at the start of the curve was specified to be $\theta_{clin} = \theta_{cwSD} = 7$ degrees. A linear distribution of the cross-sectional area within the subsonic diffuser was achieved with $K_{sdprp} = 1$ and $K_{sdvar} = 1$. and the profile of that inlet is shown as a black outline indicated within Figure 5.5. For an axisymmetric inlet, this profile is a straight line. The value of θ_{clin} was reduced to match the slope of the subsonic diffuser profile with $\theta_{clin} = \theta_{cwSD} = 4.8$ degrees. A linear variation of Mach number through the subsonic diffuser was specified with $K_{sdprp} = 2$ and $K_{sdvar} = 1$. The linear Mach profile started with a very small rate of area diffusion, and so the cowl lip interior angle was specified to be $\theta_{clin} = \theta_{cwSD} = 0.0$ degrees. A linear variation of the static pressure was specified with $K_{sdprp} = 3$ and $K_{sdvar} = 1$. The linear pressure profile is similar to the linear Mach profile, but θ_{clin} was specified to be $\theta_{clin} = \theta_{cwSD} = 2.2$ degrees. The sample cases for these inlet configurations are available within the series K1.M065 described in Appendix C. For these cases, CFD simulations were performed to verify that the area variations did result in linear distributions of Mach number or static pressure, as the case specified. These results will be further discussed in Appendix C.

5.5 Cowl Exterior

The cowl exterior for an axisymmetric pitot inlet forms an exterior surface that encloses the inlet and can be considered the forward portion of a nacelle. The cowl exterior geometry model within SUPIN has the purpose of creating a surface about the inlet for which the cowl drag can be computed. The input factors for the SUPIN geometry model for the cowl exterior were discussed earlier in Subsection 4.10 and listed in Table 4.16.

5.6 Axisymmetric Pitot Inlet Flowfield

The flowfield about and through an axisymmetric pitot inlet can be approximated with a quasi-one-dimensional representation. The flowfield can be characterized through consideration of the relative values of the Mach numbers M_0, M_1, and M_2. For turbojet, turbofan, and ramjet engines, a reasonable range for M_2 is $0.35 < M_2 < 0.65$.

For subsonic freestream conditions ($M_0 \leq 1$) in which $M_2 > M_0$, the flow of the inlet streamtube is accelerated as it approaches and enters the inlet. This would be the case during low-speed flight or take-off / landing conditions of an aircraft. For this case, $M_2 > M_1 > M_0$. The inlet streamtube ahead of the cowl lip plane at station 1 is contracting and the inlet flow ratio is greater than unity ($A_L/A_{cap} > 1$).

If the flow within the inlet duct remains subsonic, then the acceleration of the flow is mostly isentropic except for some viscous dissipation within the boundary layers, which would form under a positive and favorable pressure gradient. Subsection 5.7 below presents a model for the losses in total pressure for subsonic flow through the subsonic diffuser.

The flow entering the inlet turns past the cowl lip interior toward an axial direction. If the dimensions of the cowl lip interior are small relative to the cowl lip radius (e.g., $b_{clin} << y_{clip}$), such as for the supersonic pitot inlet illustrated on the right-hand-side of Figure 4.3, the flow may have difficulty negotiating the turning and separate. Subsection 5.8 provides a model to estimate the losses in total pressure for this condition.

A critical condition would occur if the flow within the inlet approaches sonic conditions and chokes within the throat section. At this critical condition, the flow rate through the engine face (W_2) would reach a maximum. Shock waves would likely form within the inlet to form the subsonic flow for the engine face while creating the necessary total pressure losses to match the specified corrected flow rate for the engine face. The flow balance equations of Equation (2-32) and the definition of the flow rate (Eq. (2-15)) can be applied to estimate the total pressure ratio p_{t2}/p_{t1} through the inlet.

For the case of $M_0 \leq 1$ and $M_2 < M_0$, the flow within the inlet streamtube is decelerated and remains subsonic as it approaches and flows into the inlet. This could be the case of a subsonic aircraft at cruise conditions. The inlet streamtube ahead of the cowl lip plane at station 1 is the same cross-sectional area or expanding as it approaches station 1 and the inlet flow ratio is equal or less than unity ($A_L/A_{cap} \leq 1$). The flow process is mostly isentropic, except with viscous dissipation within the boundary layers. For the inlet flow ratio less than unity ($A_L/A_{cap} < 1$) additive drag would be created upon the expanding streamtube ahead of station 1.

For supersonic freestream conditions ($M_0 > 1$) and subsonic engine face conditions ($M_2 < 1$), a normal shock wave occurs to create the subsonic conditions within the inlet. The location of the normal shock wave depends on the balance of flow rates through the inlet. At the critical operating condition, the normal shock wave is expected to be located coincident with station 1 at the cowl lip plane. Subsection 5.9 discusses the normal shock wave and the change in total pressure and other flow properties across the normal shock wave.

5.7 Total Pressure Loss Model for Subsonic Diffusion

The model for total pressure loss through a subsonic diffuser was ported from the IPAC code (Ref. 1) and is based on the empirical data presented by Henry, Wood, and Wilbur (Ref. 2). The model expresses the total pressure ratio through the subsonic diffuser as

$$\left(\frac{p_{t2}}{p_{tSD}}\right)_{sub} = 1 - \left[K_D\left(1-\frac{A_{SD}}{A_2}\right)^2 + K_O + K_F\right]K_M\left[1-\left(1+\frac{\gamma-1}{2}M_{SD}^2\right)^{-\frac{\gamma}{\gamma-1}}\right] \tag{5-3}$$

With the coefficients defined by the relations and constants defined by

$$\boldsymbol{K_D = f(2\theta_{eqsd}) \quad K_O \cong 1.2\left(\frac{|y_{SD}-y_2|}{L_{subd}}\right) \quad K_F = 4\,f_D\left(\frac{L_{subd}}{D_2}\right) \quad K_M = f(M_{SD})} \tag{5-4}$$

The K_D coefficient is a function of the duct divergence angle (θ_{eqsd}) and the left plot of Figure 5.6 shows the variation of K_D. The coefficient K_O accounts for the offset of the engine face to the entrance of the subsonic diffuser at station SD. The coefficient K_F accounts for viscosity due to the length of the subsonic diffuser. The viscosity constant is approximated to be $f_D \approx 0.0025$. The K_M coefficient is a function of the Mach number at station SD (M_{SD}) and its variation is shown in the right plot of Figure 5.6. The functional variation of the coefficients K_D and K_M are modeled as fifth and sixth-order polynomials, respectively.

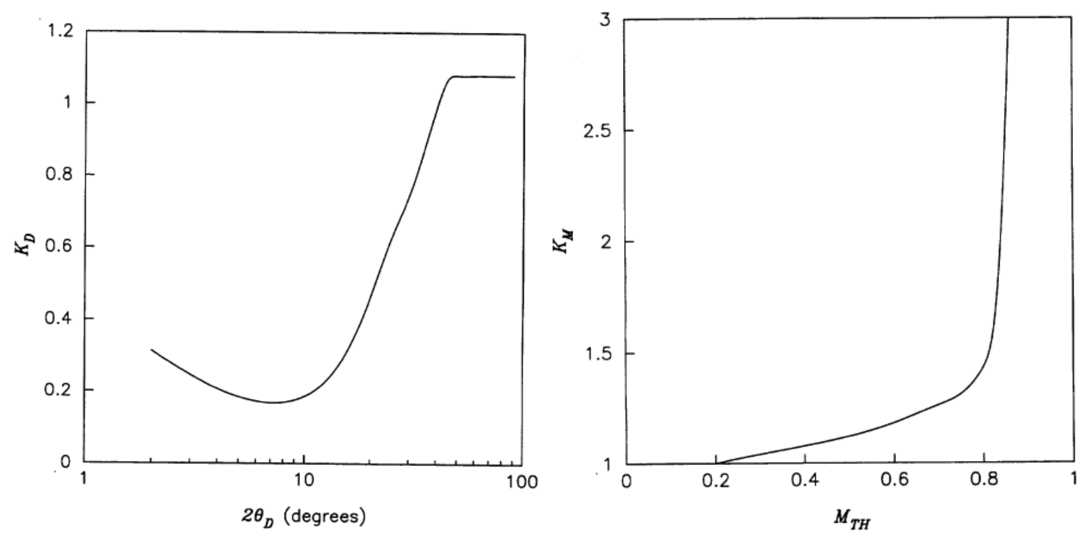

Figure 5.6.—Subsonic diffuser total pressure loss factors K_D and K_M. These plots are from Reference 2.

5.8 Total Pressure Losses over a Sharp Cowl Lip

The acceleration and turning of flow into the inlet and past the cowl lip interior, especially for cowl lips with very small dimensions (i.e., sharp cowl lip), could cause boundary layer separation. This produces a dissipative loss and drop in total pressure through the interaction. Such could be the case for inlets operating at low speeds and high engine flow, such as at take-off or climb. A model for the decrease in total pressure about a sharp cowl lip was developed by Fradenburgh and Wyatt (Ref. 3) and implemented into SUPIN and Equation (5-5) computes the loss in the total pressure ratio $(p_{t1}/p_{tL})_{sl}$ as produced by a sharp lip.

$$\left[\frac{p_{t1}}{p_{tL}}\right]_{sl} = \frac{\left[\dfrac{1+\dfrac{\gamma-1}{2}M_1^2}{1+\dfrac{\gamma-1}{2}M_L^2}\right]^{\frac{\gamma+1}{2(\gamma-1)}}}{(1+\gamma\, M_1^2)\left[\dfrac{1+\dfrac{\gamma-1}{2}M_1^2}{1+\dfrac{\gamma-1}{2}M_L^2}\right]^{-\frac{1}{2}} - \gamma\, M_1 M_L} \tag{5-5}$$

The Mach number at the cowl lip (M_1), can be determined from continuity in the form of Equation (5-6). Equation (5-6) is solved iteratively to find M_1 as a function of the inlet throat Mach number (M_{TH}) and the contraction area ratio from the inlet lip to the inlet throat $\left(\frac{A_{TH}}{A_1}\right)$.

$$\frac{A_1}{A^*}(M_1) = \frac{\dfrac{A_{TH}}{A^*}(M_{TH})}{\dfrac{A_{TH}}{A_1}} \tag{5-6}$$

For cowl lips which are not sharp, but have some degree of bluntness, Equation (5-7) was developed by Barnhart (Ref. 2) to account for the effects of a non-zero cowl lip radius on the total pressure ratio given by Equation (5-5). Wind-tunnel data (Ref. 4) was used to determine the exponential damping constant used in Equation (5-7),

$$\frac{p_{t1}}{p_{tL}} = \frac{1}{1+\exp^{-1}\left[4.66\left(\frac{r_C}{Y_C}\right)\right]\left[\left(\left[\frac{p_{t1}}{p_{tL}}\right]_{sl}\right)^{-1} - 1\right]} \tag{5-7}$$

5.9 Normal Shock Waves

The normal shock wave is the mechanism through which supersonic flow decelerates to subsonic flow and can exist external or internal to the inlet (Ref. 5). A normal shock wave forms when there is sufficient static pressure in the downstream direction such that the only way flow continuity can be preserved is through a discontinuity in the form of the normal shock wave. The normal shock wave involves an infinitesimal interaction in which the flow changes from supersonic to subsonic in a one-dimensional, adiabatic process. For upstream supersonic conditions at state 0 of $M_0 > 1$, the properties across a normal shock wave to conditions at state 1 are,

$$M_1^2 = \frac{(\gamma-1)M_0^2 + 2}{2\gamma M_0^2 - (\gamma-1)} \tag{5-8}$$

$$\frac{p_1}{p_0} = 1 + \frac{2\gamma}{\gamma + 1}(M_0^2 - 1) \tag{5-9}$$

$$\frac{\rho_1}{\rho_0} = \frac{(\gamma + 1)M_0^2}{(\gamma - 1)M_0^2 + 2} \tag{5-10}$$

$$\frac{T_1}{T_0} = \frac{[2\gamma M_0^2 - (\gamma - 1)][(\gamma - 1)M_0^2 + 2]}{(\gamma + 1)^2\, M_0^2} \tag{5-11}$$

$$\frac{p_{t1}}{p_{t0}} = \left[\frac{(\gamma + 1)\, M_0^2}{(\gamma - 1)M_0^2 + 2}\right]^{\frac{\gamma}{(\gamma-1)}} \left[\frac{\gamma + 1}{2\gamma M_0^2 - (\gamma - 1)}\right]^{\frac{1}{(\gamma-1)}} \tag{5-12}$$

$$M_0^2 = \frac{(\gamma - 1)M_1^2 + 2}{2\gamma M_1^2 - (\gamma - 1)} \tag{5-13}$$

The axisymmetric pitot inlets can be used for supersonic flight and the normal shock wave is the mechanism through which the supersonic flow decelerates to subsonic flow. The left image of Figure 5.7 shows an example of an axisymmetric pitot inlet designed for Mach 1.4 freestream. The cowl lip profiles have very small dimensions to make the cowl lip essentially sharp to reduce drag. The right image of Figure 5.7 shows the Mach number contours from a CFD simulation of the inlet flow with the freestream at $M_0 = 1.4$. At the design conditions, a normal shock wave forms across the cowl lip plane and subsonic flow forms downstream of the shock wave and within the inlet. For $M_0 = 1.4$, the total pressure ratio across the normal shock wave is $p_{t1}/p_{t0} = 0.958$.

The total pressure ratios across the normal shock wave according to Equation (5-11) for $M_0 = 1.3$, 1.5, and 2.0 are $p_{t1}/p_{t0} = 0.979$, 0.930 and 0.721, respectively. Thus, the total pressure losses increase rapidly above $M_0 = 1.3$ and the use of an external supersonic diffuser capable of creating oblique Mach and shock waves becomes attractive.

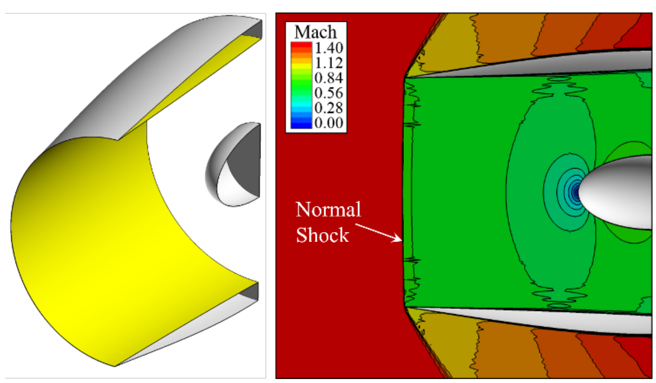

Figure 5.7.—A Mach 1.4 axisymmetric pitot inlet with a computational flow solution illustrating a normal shock wave.

References

1. Henry, J. R., Wood, C. C., and Wilbur, S. W., "Summary of Subsonic-Diffuser Data," NACA RM L56F05, October 1956.
2. Barnhart, P. J., "IPAC – Inlet Performance Analysis Code," NASA CR-204130, July 1997.
3. Fradenburgh, E. A. and Wyatt, D. D., "Theoretical Performance Characteristics of Sharp-Lip Inlets at Subsonic Speeds," NACA Report 1193, January 1954.
4. Blackaby, J. R. and Watson, E. C., "An Experimental Investigation at Low Speeds of the Effects of Lip Shape on the Drag and Pressure Recovery of a Nose Inlet in a Body of Revolution," NACA TN 3170, April 1954.
5. Anderson, J. D., Jr., *Modern Compressible Flow*, McGraw-Hill Book Company, New York, 1982.

6.0 Three-Dimensional Pitot Inlets

The three-dimensional pitot inlet allows a greater geometric flexibility than available with the axisymmetric pitot inlet in that a) the shape of the capture cross-section can take on a more general shape, b) the cowl highlight can be non-planar, and c) the engine face can be offset from the inlet axis within the plane of symmetry. Figure 6.1 shows an example of a three-dimensional pitot inlet. The capture cross section has a circular shape for the top portion, but a flattened shape on the bottom to create a “D” shaped capture cross-section. The leading edge of the inlet is projected more forward on the bottom than on the top. The engine axis is below the inlet axis by about half of the engine face diameter. The following subsections discuss the geometry models for the three-dimensional pitot inlet, which involves defining the geometry of the capture cross-section, cowl lip, throat section, subsonic diffuser, and cowl exterior.

6.1 Capture Cross-Section

The capture cross-section of a three-dimensional pitot inlet is bounded by the highlight curve. The left-hand-side image of Figure 6.2 shows a view of the front of the inlet in Figure 6.1, looking along the x-axis with the capture cross-section shaded in pink. The right-hand-side image of Figure 6.2 shows the two highlight curve segments with the y- and z-axes shown. The highlight curve consists of a “bottom” segment colored in red and a “top” segment colored in blue. Within SUPIN, these highlight curve segments are modeled as super-ellipse curves in the (y,z) plane. The cross-section is symmetric with respect to the y-axis. The top and bottom curves are split at the $y = 0$ plane and the inlet axis is defined by $y = 0$ and $z = 0$. The top curve segment has $y \geq 0$ and the bottom curve segment has $y \leq 0$. The top super-ellipse curve segment is defined by the length of its semi-major axis (a_{cap}), length of its semi-minor axis (b_{topcap}), and the super-ellipse parameter (p_{topcap}). The top curve segment shown colored in blue in Figure 6.2 has the characteristics that $a_{cap} = b_{topcap}$ and $p_{topcap} = 2$, which results in a semi-circular curve segment. The bottom super-ellipse curve segment shares the same value of the semi-major axis length as the top segment but has its unique values of the semi-minor axis (b_{botcap}) and super-ellipse parameter (p_{botcap}). The bottom curve segment shown in red in Figure 6.2 has the characteristics that $a_{cap} = 2\, b_{botcap}$ and $p_{botcap} = 4$, which results in a flattened curve. The higher value of the super-ellipse parameter for the bottom curve (p_{botcap}) creates a smaller radius of curvature for the “corners” of the super-ellipse curve. The effect of the super-ellipse parameter can be better understood by considering Figure A-6 in Appendix A. The ratio of the semi-minor axis and semi-major axis lengths is the aspect ratio of the super-ellipse segment. Thus, for the inlet of Figure 6.1 and Figure 6.2, $AR_{topcap} = b_{topcap} / a_{cap} = 1.0$ and $AR_{botcap} = b_{botcap} / a_{cap} = 0.5$.

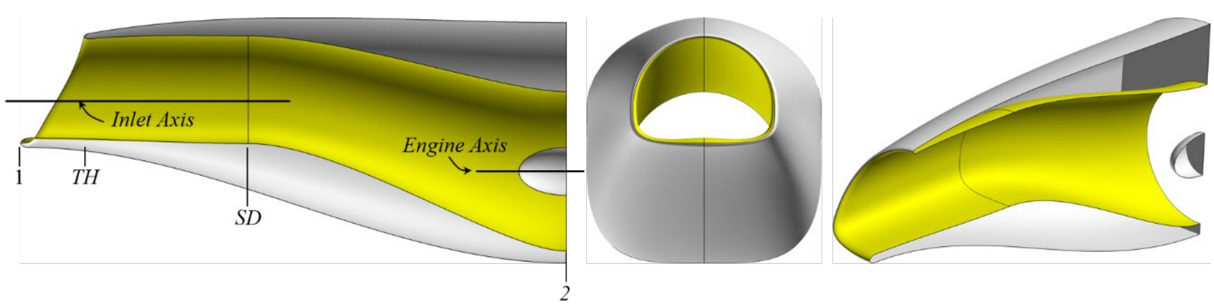

Figure 6.1.—Example of a three-dimensional pitot inlet.

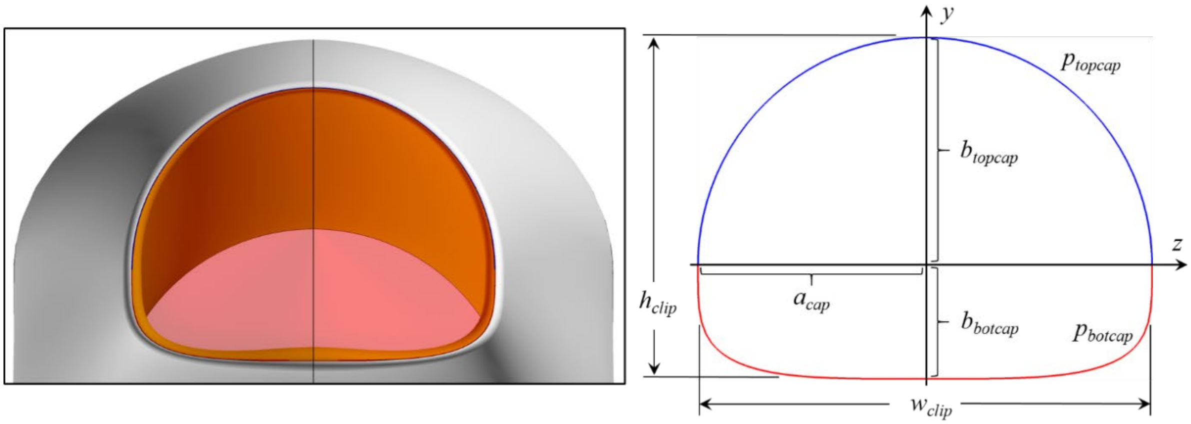

Figure 6.2.—Capture cross-section and highlight curve for the three-dimensional pitot inlet.

TABLE 6.1.—INPUT FACTORS FOR THE CAPTURE CROSS-SECTION OF THE THREE-DIMENSIONAL PITOT INLET

Factor	Input	Description
AR_{topcap}	`ARtopcap`	Aspect ratio (a/b) of the super-ellipse for the top of the capture cross-section
p_{topcap}	`ptopcap`	Parameter of the super-ellipse for the top of the capture cross-section
AR_{botcap}	`ARbotcap`	Aspect ratio (a/b) of the super-ellipse for the bottom of the capture cross-section
p_{botcap}	`pbotcap`	Parameter of the super-ellipse for the bottom of the capture cross-section
$F_{dxcaptop}$	`Fdxcaptop`	Axial displacement of the top of the highlight normalized by D_{ref}
$F_{dxcapbot}$	`Fdxcapbot`	Axial displacement of the bottom of the highlight normalized by D_{ref}

The planar area of the capture cross-section is equal to the reference capture area (A_{cap}) for the inlet and is computed from the properties of the top and bottom super-ellipses as

$$A_{cap} = \frac{1}{2}\left(A_{cap-bot} + A_{cap-top}\right) \qquad (6\text{-}1)$$

The dimensions of the super-ellipses can be calculated once the reference capture area of the inlet is known. For a specified inlet geometry (K_{mode} = 1 or 3), the inlet capture area is known. For an inlet design (K_{mode} = 2), the capture area is established as part of the inlet sizing. With a value for the inlet capture area and specified values for the aspect ratios and parameter of the super-ellipses, an iteration can be performed on the length of the semi-major axis (a_{cap}) until Equation (6-1) is satisfied. The width of the capture cross-section is $w_{clip} = 2\ a_{cap}$. The height of the capture cross section is $h_{clip} = b_{topcap} + b_{botcap}$. The SUPIN input factors for the capture cross-section are listed in Table 6.1 and consist of the aspect ratios and super-ellipse parameters for the top and bottom curve segments.

6.2 Three-Dimensional Cowl Lip

Three-dimensionality of the cowl lip is obtained by allowing axial displacement of the highlight curve and the variation of the cowl lip thickness and incidence angle about the circumference of the capture cross-section. Within SUPIN, axial displacement and cowl lip profile properties are specified at the top and bottom locations on the capture cross-section plane of symmetry. The variation of the axial displacement and the cowl lip profile properties about the circumference is then realized using a variation in the form of a four-point NURBS curve. Figure 6.3 illustrates the axial displacement of the highlight curve used for the inlet of Figure 6.1.

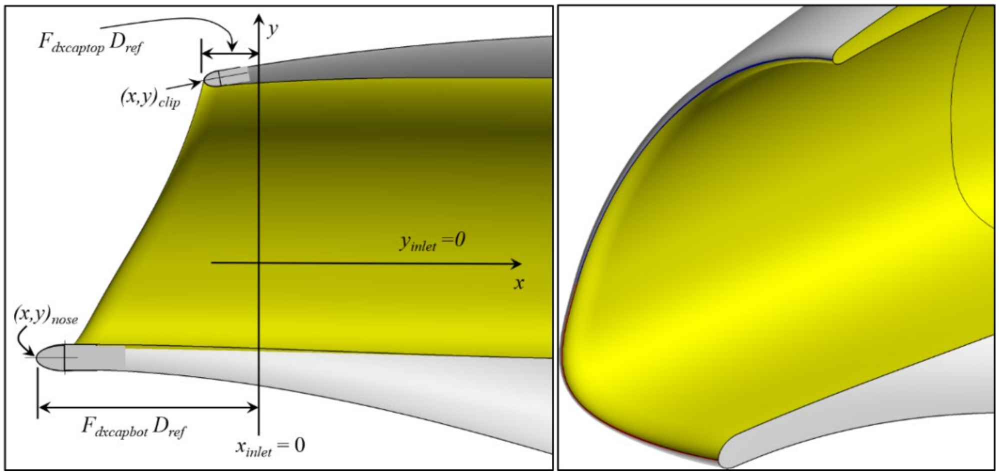

Figure 6.3.—Specification of the axial displacement of the highlight curve.

The input factor $F_{dxcapbot}$ indicates the distance for the axial displacement at the bottom of the highlight curve at the plane-of-symmetry normalized by the reference dimension (D_{ref}). Likewise, the input factor $F_{dxcaptop}$ indicates the normalized distance for the axial displacement at the top of the highlight curve at the plane-of-symmetry. The axial displacement is with respect to the x_{inlet} = 0 station. The nose point $(x,y)_{nose}$ is located at the forward-most point of the leading edge on the symmetry plane. The cowl lip point $(x,y)_{clip}$ is located at the rearward point of the leading edge on the symmetry plane. The nose and cowl lip points will always be on the symmetry plane and can switch places between top and bottom depending on whether the forward-most point is at the top of bottom of the highlight.

The cowl lip profile is modelled as an ellipse in the same manner as described in Subsection 4.9 and Table 4.14 listed and described the input factors for the elliptical profiles for the cowl lip interior and exterior. The thickness, angle, and aspect ratio of the elliptical profile can vary about the circumference of the highlight in much the same manner as the axial displacement. The angle and elliptical properties of the profile are specified at the "bottom" and "top" of the leading edge on symmetry plane. The input factors for b_{clin}, b_{clex}, AR_{clin}, AR_{clex}, θ_{clin}, and θ_{clex} have the same character as for the axisymmetric pitot inlet as discussed in Subsection 4.9. The circumferential variation of the cowl lip allows the variation of the factors defining the cowl lip profile, which involves the thickness of the cowl lip interior and cowl lip exterior (b_{clin} and b_{clex}, i.e., lengths of the ellipse semi-minor axes), the aspect ratio of the elliptical curves (AR_{clin} and AR_{clex}), and angles at the ends of the cowl lip interior and cowl lip exterior (θ_{clin} and θ_{clex}). These factors are specified at the "bottom" and "top" of the highlight. A four-point NURBS curve is then used to provide a smooth variation of these properties about the circumference.

Table 6.2 contains a sample input data block for the specification of the capture cross-section of a three-dimensional pitot inlet. The DataID = 7 is used to indicate the type of input data block data. The last two lines of the input data block provide the values for the input factors for the bottom and top profiles, respectively. The values in the table correspond to the inlet of Figure 6.1 and Figure 6.2.

TABLE 6.2.—SAMPLE INPUT DATA BLOCK FOR THE CAPTURE CROSS-SECTION
OF THE THREE-DIMENSIONAL PITOT INLET

```
DataID.  Cowl Lip
  7
ARtopcap   ptopcap   ARbotcap   pbotcap
 1.0000     2.000     0.5000     4.000
 Fdxcap   bclin   ARclin   thclin   bclex   ARclex   thclex
-0.4000  0.10000   2.000    0.000  0.08000   2.000    0.000
 0.0000  0.05000   2.000    5.000  0.05000   2.000   10.000
```

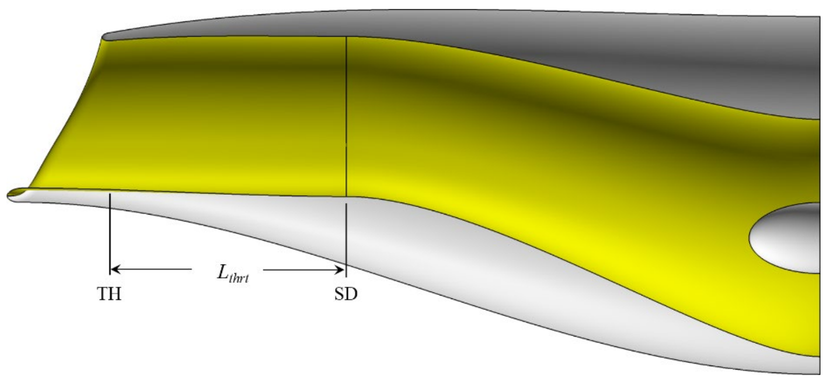

Figure 6.4.—Throat section for a three-dimensional pitot inlet.

6.3 Throat Section

The throat section model for a three-dimensional pitot inlet simply incorporates an axial length and an area ratio between stations 1 and SD. Station TH is defined at the *x*-coordinate at the end of the aft-most cowl lip interior point on the plane-of-symmetry. The *x*-coordinate of station SD is then an axial distance of L_{thrt} downstream of station TH. Figure 6.4 illustrates the positions of stations TH and SD for the inlet shown if Figure 6.1. The cross-sectional area of station SD is computed as a ratio A_{SD}/A_1 of the cross-sectional area at station 1, which is the reference capture area for the inlet ($A_1 = A_{cap}$). The cross-section at station SD is modeled with super-ellipses in the same manner as the capture cross-section and the values of aspect ratios and super-ellipse parameters used at station SD are equal to those of the capture cross-section. Station SD is also located about the inlet axis. The throat section cowl interior surface is formed by establishing a network of four-point NURBS curves between points at the cowl lip interior to respective points at station SD. A value of $L_{thrt} = 0$ is possible, which would place station SD at station TH.

Table 6.3 lists the input factors for the throat section. The input factor F_{Lthrt} specifies L_{thrt} and is normalized by the reference dimension of the inlet (D_{ref}), which is commonly the engine-face diameter. A value of $F_{Lthrt} \leq 0$ should be used to specify a value of $L_{thrt} = 0$, which would place station SD at TH and no throat section would be created. The input factor FaSDa1 is the area ratio between stations 1 and SD. Table 6.4 contains an example input data block for the specification of the throat section of a three-dimensional pitot inlet. The DataID = 8 is used to indicate that the throat section input factors are for the throat section. The input factor $K_{thrt} = 3$ indicates that the input factors are for the throat section of a three-dimensional pitot inlet.

TABLE 6.3.—INPUT FACTORS FOR THE THROAT SECTION OF THE THREE-DIMENSIONAL PITOT INLET

Factor	Input	Description
L_{thrt}	FLthrt	Axial length of the throat (normalized by D_{ref})
A_{SD}/A_1	FaSDa1	Ratio of cross-sectional area at station SD to area at station 1

TABLE 6.4.—EXAMPLE INPUT DATA BLOCK FOR THE THROAT SECTION OF THE THREE-DIMENSIONAL PITOT INLET

```
DataID.  Single-surface throat
  8
Kthrt   FptTHpt1   FptTXptTH   FptSDptTX
  3     -0.99000    -0.99500    -1.00000
 FLthrt      FaSDa1
1.00000     1.02000
```

6.4 Subsonic Diffuser

The subsonic diffuser for a three-dimensional pitot inlet involves a transition over its length from the cross-section at station SD defined by super-ellipse curve segments to the cross-section at the engine face, which is defined according to the input factors discussed in Subsection 4.13. The options and input factors for establishing the length of the subsonic diffuser were discussed in Subsection 4.12. Also discussed in Subsection 4.12 was the input factor (Fpt2ptSD) for the specification of the total pressure ratio (p_{t2}/p_{tSD}) through the subsonic diffuser. In this section, two methods are described for establishing the shape of the cowl interior surfaces of the subsonic diffuser.

The first method for establishing the cowl interior surfaces of the subsonic diffuser involves generating cross-sections along a guiding curve extending from station SD to the engine face station 2. Each cross-section is defined using super-ellipse segments in a manner similar to the capture cross-section shown on the right-hand-side of Figure 6.2. The super-elliptic cross-sections at stations SD and 2 and their related factors form the upstream and downstream boundary conditions, respectively, for the distribution of cross-sections through the subsonic diffuser. The method involves generation of a smooth guiding curve from the point of station SD, $(x,y)_{SD}$, to the engine face point, $(x,y)_{EF}$. A four-point-NURBS curve is used to define this guiding curve. The local origin of each super-elliptic cross-section of the subsonic diffuser is placed along this guiding curve. Along the guiding curve, the planar cross-sections are defined by two super-ellipse segments for the top and bottom of the cross-section in a similar manner as shown for the capture cross-section in Figure 6.2. The top and bottom super-ellipse segments have the cross-width or semi-major length (a_{wid}) but can differ by the values of the height or semi-minor length (b_{bot} and b_{top}) and the super-ellipse parameters (p_{bot} and p_{top}). The variations of these properties (a_{wid}, b_{bot}, b_{top}, p_{bot}, and p_{top}) establish the shape of the subsonic diffuser between stations SD and 2. The method uses the four-point NURBS curve to establish smooth variations of the super-ellipse parameters (p_{bot} and p_{top}) and the aspect ratios (b_{bot}/a_{wid} and b_{top}/a_{wid}) between stations SD and 2. At each cross-section, an iteration is performed to find the width of the cross-section (a_{wid}) that along with the other factors for the cross-section, match the desired cross-sectional area. The left-hand-side image of Figure 6.5 illustrates the super-elliptical curves defining the cross-sections through the subsonic diffuser using this method.

The variation of the cross-sectional area is established in the same manner as described in Subsection 4.12 for the general input factors for the subsonic diffuser and Subsection 5.4 in the case of the axisymmetric pitot inlet. Table 6.5 lists an example input data block for subsonic diffuser using this method, which is implemented when K_{subd} = 6. The input factors work in much the same manner as the input factors listed in Table 5.3 for the axisymmetric pitot inlet. However, for the three-dimensional pitot

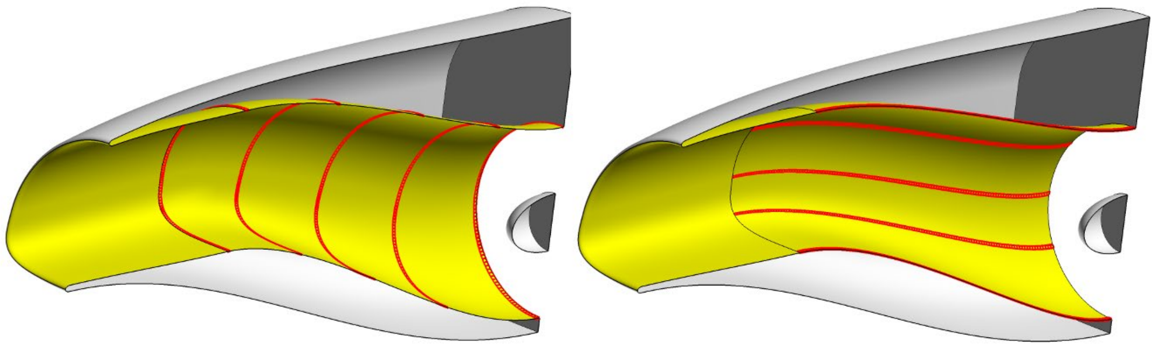

Figure 6.5.—Examples of subsonic diffusers for the three-dimensional pitot inlets created through the generation of super-elliptical cross-sections (K_{subd} = 6, left) and through the generation of streamwise NURBS curves (K_{subd} = 7, right).

TABLE 6.5.—EXAMPLE INPUT BLOCK FOR THE SUBSONIC DIFFUSER FOR A THREE-DIMENSIONAL PITOT INLET (K_{TYP} = 6)

```
DataID.  Subsonic Diffuser
 10
Ksubd     KLsubd    FLsubd     theqsd    Fpt2ptSD
  6          1     4.50000     3.000     -0.97500
FNcwSD    FNcwX      FLcwX     Ksdprp     Ksdvar
0.3333    0.3333    0.2000       2           1
```

inlet, the input factors F_{NcwSD} and F_{NcwX} influence the location of the interior control points for the four-point NURBS curve describing the variation of the cross-sectional area through the subsonic diffuser. The length of the constant-area section ahead of the engine face is specified by the input factor F_{LcwX}, which is normalized by the reference dimension, D_{ref}. The input factors K_{sdprp} and K_{sdvar} control the additional options for distributing the cross-sectional area, as described in Subsections 4.12 and 5.4.

The second method for establishing the surface of the cowl interior for the subsonic diffuser involves forming a network of four-point-NURBS curves extending in the streamwise direction between stations SD and 2 about the circumference of the subsonic diffuser. This method is used when K_{subd} = 7 within the input data block of Table 6.5. The input factors F_{NcwSD} and F_{NcwX} influence the location of the interior control points for each of the four-point NURBS curves of the network. A straight section ahead of the engine face is implemented when $F_{LcwX} > 0$ in the same manner as discussed previously. Each NURBS curve is created in a planar manner using the axial coordinate and the radius of the grid point from the inlet axis. The NURBS curve is then transformed to the surface using a linear variation of the circumferential angle. This approach allows the slope of the surface at the start to match that of station SD and the slope at the surface at the end to match that of station 2. This method is based entirely on specified geometry rather than flow properties, and so, the method can be used for all values of K_{mode}. While the method creates a smooth surface for the subsonic diffuser, it does not allow control over the area distribution. Thus, the input factors K_{sdprp} and K_{sdvar} are neglected when specified within the input data block. The right-hand-side image of Figure 6.5 illustrates the streamwise NURBS curves that form the surface of the subsonic diffuser using this method.

An illustration of the options available for the variation of the cross-sectional area of the subsonic diffuser is provided in Figure 6.6. Shown is a representative three-dimensional pitot inlet that is axisymmetric with the line at the bottom showing the axis-of-symmetry. The throat section is a straight duct of length equal to the diameter of the engine face, which does not have a spinner. The subsonic diffuser has a length twice the diameter of the engine face. Four different shapes are shown for the profile

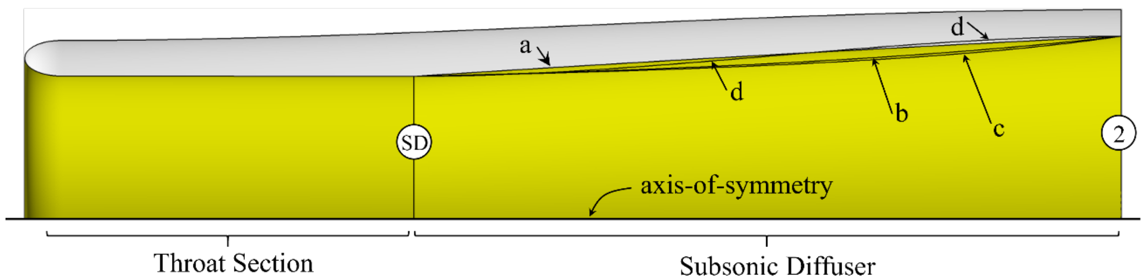

a) Ksubd = 6, Ksdprp = 1, Ksdvar = 1. Linear variation of area.
b) Ksubd = 6, Ksdprp = 2, Ksdvar = 1. Linear variation of Mach number.
c) Ksubd = 6, Ksdprp = 3, Ksdvar = 1. Linear variation of static pressure.
d) Ksubd = 7, FNcwSD = 0.33, FNcwX = 0.33. Smooth NURBS curve for surface.

Figure 6.6.—Example of the options for the design of the shape of the subsonic diffuser for the three-dimensional pitot inlet.

of the subsonic diffuser from station SD to the engine face that correspond to different values of K_{subd}, K_{sdprp}, and K_{sdvar}. The letters in the figure point to the profiles for each of the subsonic diffuser shapes. The shaded surfaces for the subsonic diffuser are for the profile “d”.

The profile indicated by “a” was generated using a linear variation of the cross-sectional area between stations SD and 2 and results in a straight line for its profile. The shaded inlet surfaces of Figure 6.6 are those of this inlet. This inlet was generated using $K_{subd} = 6$, $K_{sdprp} = 1$, and $K_{sdvar} = 1$.

The profile indicated by “b” was generated using a linear variation of the Mach number between stations SD and 2. This inlet was generated using $K_{subd} = 6$, $K_{sdprp} = 2$, and $K_{sdvar} = 1$. The subsonic diffuser involves a diffusion from a Mach number at station SD of $M_{SD} = 0.72$ to an engine face Mach number of $M_2 = 0.35$. The Mach number are the result of the inlet sizing and engine face conditions and are not affected by the choice of the shape of the subsonic diffuser. This profile “b” involves a lesser rate of area growth at the start of the diffuser than at the end, which is considered beneficial in that most of the area increase occurs at a lower Mach number.

The profile indicated by “c” was generated using a linear variation of the static pressure between stations SD and 2. This inlet was generated using $K_{subd} = 6$, $K_{sdprp} = 3$, and $K_{sdvar} = 1$. The static pressure ratio over the subsonic diffuser is $p_2/p_{SD} = 1.28$. The profiles of “c” shows a slightly slower rate of area growth than the profile of “b” and an increased rate of growth right before the engine face. The similarity of profile “b” with “c” suggest that the linear Mach number variation also provides a nearly linear pressure gradient for the subsonic diffuser. A linear Mach number or static pressure gradient are reasonable design choices for the subsonic diffuser.

The profile indicated by “d” was generated using a four-point NURBS curve that has zero slopes at both stations SD and 2. This inlet profile was generated using $K_{subd} = 7$. The weightings for the curve place the interior control points at distances of one-third of the length. The profile is below the straight line of shape “a” for the first half of the length and above the line for the second half.

6.5 Cowl Exterior

The cowl exterior for a three-dimensional pitot inlet is specified using the input data block as described in Section 4.10, but only $K_{cwex} = 1$ can be used for the three-dimensional pitot inlet. With this method, four-point-NURBS curves are formed between points distributed about the circumferences of the inlet at the start and end of the cowl exterior. The surface is formed from the network of these streamwise curves. Figure 6.7 shows an example cowl exterior surface generated for the three-dimensional pitot inlet.

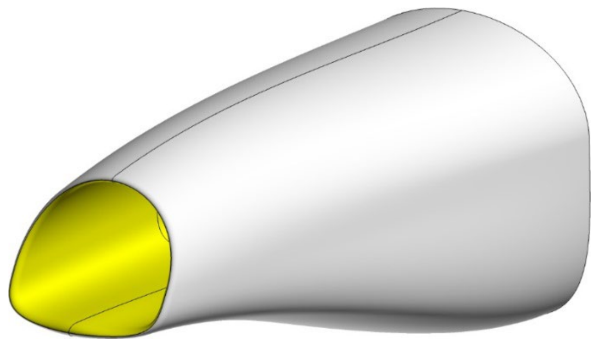

Figure 6.7.—Example of the cowl exterior surface for a three-dimensional pitot inlet.

7.0 External Supersonic Compression

The nature of supersonic flow enables deceleration and compression of supersonic flow through the turning of the inlet streamtube. This has led to the use of ramps and conical forebodies extending ahead of the internal ducting of the inlet to create oblique shock and Mach waves that turn portions of the inlet flowfield. The total pressure losses through oblique shock waves are lower than for a normal shock wave, and so above Mach 1.4, external compression is used within inlets to reduce the total pressure losses and achieve a higher total pressure recovery for the inlets. This section starts with a discussion of planar oblique shock waves, Mach waves, and conical shock waves, which are all used as mechanisms for external supersonic compression. The analytical and computational solution methods for shock and Mach waves are well known (Refs. 1 to 4). The discussion will then focus on axisymmetric and two-dimensional, external supersonic diffusers which use the oblique and conical waves for supersonic compression for the two-dimensional (K_{typ} = 2 and 4) and axisymmetric spike (K_{typ} = 3) inlets.

7.1 Oblique Shock Waves

An oblique shock wave has a two-dimensional or planar character. Analytic, algebraic relations define the change in Mach number and other flow properties across the shock wave. Figure 7.1 shows a schematic of a planar oblique shock wave created by a deflection angle (δ) and with a shock wave angle (β). The flow upstream and downstream of the shock wave is uniform. Downstream of the shock wave, the flow angle equals the deflection angle. The changes in properties across an oblique shock wave are computed with respect to the value of the Mach number normal to the shock wave. This normal Mach number is used in the normal shock wave relations (Eqs. (5-8) to (5-12)) to determine the properties across the oblique shock wave. The tangential component of the velocity does not change across the shock wave. The Mach number reduces across the shock wave and the static pressure and temperature increase. Thus, compared to a normal shock wave, an oblique shock wave produces a more efficient compression with lower total pressure loss. The deflection angle (δ), the shock wave angle (β), and the inflow Mach number (M_0) are related using the δ-β-M relation [4, p. 91] expressed as,

$$\tan\delta = 2\,\cot\beta\left[\frac{M_0^2\sin^2\beta - 1}{M_0^2(\gamma + \cos 2\beta) + 2}\right] \tag{7-1}$$

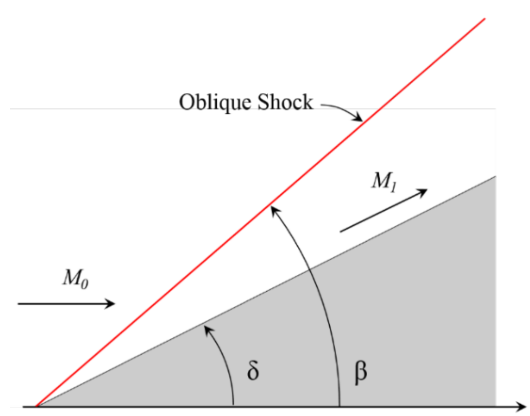

Figure 7.1.—Schematic of a planar oblique shock wave.

For a given inflow Mach number (M_0), there exists a maximum deflection (δ_{max}) for which an oblique shock wave can remain attached to the start of the deflection. For the case of $\delta < \delta_{max}$, there exists two solutions for the shock wave angle (β). The lower value of the shock wave angle is associated with the weak oblique shock wave solution and results in supersonic flow conditions downstream of the oblique shock wave. The higher value of the shock wave angle is associated with the strong oblique shock wave solution and results in subsonic flow downstream of the oblique shock wave and higher pressures than the weak oblique shock wave solution.

An algebraic approximation for the solution of Equation (7-1) with respect to the shock wave angle (β) for an attached, weak oblique shock wave is a 6th-order polynomial of the form,

$$\sin^6 \beta + b\ \sin^4 \beta + c\ \sin^2 \beta + d = 0 \tag{7-2}$$

where the following expressions provide the values of the coefficients,

$$b = -\frac{M_0^2 + 2}{M_0^2} - \gamma \sin^2 \delta \quad c = \frac{2\ M_0^2 + 1}{M_0^4} + \left[\frac{(\gamma + 1)^2}{4} + \frac{\gamma - 1}{M_0^2}\right] \sin^2 \delta \quad d = -\frac{\cos^2 \delta}{M_0^4} \tag{7-3}$$

The direct solution of Equation (7-2) is obtained by a generalized solution of a third-order polynomial substitution (note that Eq. (7-2) has only even powers) to yield the expression,

$$\sin^2 \beta = -\frac{b}{3} + \frac{2}{3}\sqrt{b^2 - 3c} \cos\left(\frac{\varphi + 4\pi}{3}\right) \tag{7-4}$$

where

$$\cos \varphi = \frac{9bc - 2b^3 - 27d}{2\sqrt{(b^2 - 3c)^3}} \tag{7-5}$$

Once the shock wave angle β is determined, the normal component of the inflow Mach number can be computed as

$$M_{N_0} = M_0 \sin \beta \tag{7-6}$$

The normal component of the Mach number downstream of the shock wave (M_{N_2}) can be computed using Equation (5-8) for a normal shock wave. The downstream Mach number can then be determined through trigonometry as

$$M_1 = \frac{M_{N_1}}{\sin(\beta - \delta)} \tag{7-7}$$

This assumes that the tangential component of the velocity remains unchanged through the oblique shock wave. The change in flow properties across the oblique shock wave are expressed by Equations (5-9) to (5-12) using the upstream and downstream normal Mach numbers. Compared to normal shock waves, the oblique shock wave results in lower changes in the static pressure, static temperature, and total pressure.

7.2 Conical Shock Waves and Flow

The external supersonic diffuser for an axisymmetric spike inlet (K_{typ} = 3) has a conical nose section. Figure 7.2 illustrates a schematic of the supersonic flow about a cone. The primary coordinate is the conical angle θ measured from the axis-of-symmetry of the cone. The equations of motion for inviscid, adiabatic conical flow over a sharp cone can be simplified to form the Taylor-Maccoll equation (Ref. 5)

$$\frac{\gamma-1}{2}\left[V_{max}^2 - V_r^2 - \left(\frac{dV_r}{d\theta}\right)^2\right]\left[2V_r + \frac{dV_r}{d\theta}\cot\theta + \frac{d^2V_r}{d\theta^2}\right] - \frac{dV_r}{d\theta}\left[V_r\frac{dV_r}{d\theta} + \frac{dV_r}{d\theta}\left(\frac{d^2V_r}{d\theta^2}\right)\right] = 0 \tag{7-8}$$

with the condition that

$$V_\theta = \frac{dV_r}{d\theta} \tag{7-9}$$

The Taylor-Maccoll equation assumes the flow is axisymmetric and that flow properties are constant along a ray from the vertex of the cone. Thus, the equation becomes an ordinary differential equation with respect to the angle of the ray (θ) with respect to the axial coordinate (x). The independent variable is V_r. The reference by Anderson (Ref. 4) provides a derivation of the Taylor-Maccoll equation. There is no closed-form solution to Equation (7-8) and numerical methods are required to solve it (Ref. 4). To simplify the numerical solution, a non-dimensional velocity is defined as

$$V' \equiv \frac{V}{V_{max}} \tag{7-10}$$

It can be shown that the non-dimensional velocity is a function of Mach number,

$$V' = \frac{1}{\sqrt{\frac{2}{(\gamma-1)M^2} + 1}} \tag{7-11}$$

The Taylor-Maccoll equation in the form of the non-dimensional velocity becomes,

$$\frac{\gamma-1}{2}\left[1 - V_r'^2 - \left(\frac{dV_r'}{d\theta}\right)^2\right]\left[2V_r' + \frac{dV_r'}{d\theta}\cot\theta + \frac{d^2V_r'}{d\theta^2}\right] - \frac{dV_r'}{d\theta}\left[V_r'\frac{dV_r'}{d\theta} + \frac{dV_r'}{d\theta}\left(\frac{d^2V_r'}{d\theta^2}\right)\right] = 0 \tag{7-12}$$

where

$$V' = \sqrt{V_r'^2 + V_\theta'^2} \tag{7-13}$$

and

$$V_\theta' = \frac{dV_r'}{d\theta} \tag{7-14}$$

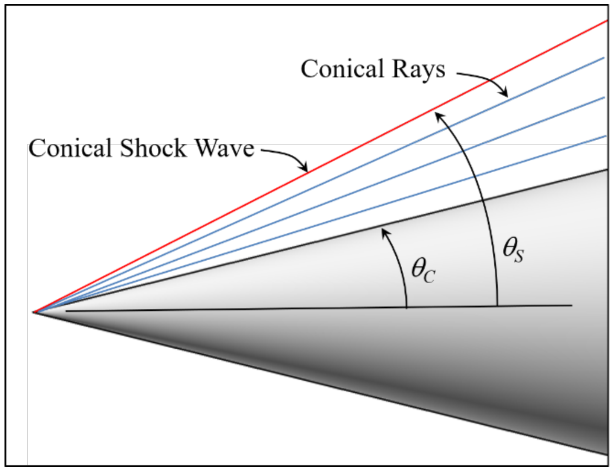

Figure 7.2.—Schematic of supersonic flow about a cone.

The Mach number and flow properties are constant along rays emanating from the apex. Thus, the flow properties will change along a streamline. Figure 7.2 illustrates the conical shock wave (red line) and the constant-Mach number rays (blue lines). The Mach number is lowest and the pressure the greatest at the ray along the surface of the cone. Thus, a streamline will move through the shock wave and approach the cone surface while compressing isentropically downstream of the conical shock wave.

The Taylor-Maccoll solution is an inverse numerical solution that starts with a guess to the shock wave angle θ_S and then Equation (7-12) is integrated using a fourth-order Runge-Kutta method in increments of $\Delta\theta$ toward the surface of the cone. The objective is to arrive at the cone surface while satisfying the flow tangency boundary condition of

$$V_\theta' = \left.\frac{dV_r'}{d\theta}\right|_{\theta=\theta_C} = 0 \tag{7-15}$$

$$\tan(\theta - \delta) = \frac{V_\theta'}{V_r'} \tag{7-16}$$

$$\left.\frac{V_\theta'}{V_r'}\right|_{\theta=\theta_S} = \tan\theta_S \frac{(\gamma-1)M_1^2 \sin^2\theta_S + 2}{(\gamma+1)M_1^2 \sin^2\theta_S} \tag{7-17}$$

Within the routine for the Taylor-Maccoll solver, arrays contain the Mach number (M), flow deflection angle (δ), and ray angle (θ). The index (k) of the arrays has $k = 1$ at the shock wave and $k = N_{rays}$ at the cone surface, where N_{rays} is the number of rays used for the solution.

7.3 Mach Waves and Prandtl-Meyer Flow

A Mach wave is an infinitesimal, isentropic change in supersonic flow properties due to an infinitesimal deflection of the surface ($\Delta\delta$), as illustrated in Figure 7.3. Both compression and expansion are possible through Mach waves depending on whether $\Delta\delta > 0$ or $\Delta\delta < 0$, respectively. A contour for generating Mach waves can be constructed by smoothly changing the slope of the contour. A focal point can be specified and the change in slope controlled to create Mach waves that pass through the focal point.

The change in Mach number with isentropic turning is related through the Prandtl-Meyer function defined as

$$\nu(M) = \sqrt{\frac{\gamma+1}{\gamma-1}}\tan^{-1}\sqrt{\frac{\gamma-1}{\gamma+1}(M^2-1)} - \tan^{-1}\sqrt{M^2-1} \tag{7-18}$$

The Prandtl-Meyer function has units of radians and is a function of the Mach number for perfect gases. At $M = 1$, the Prandtl-Meyer function has a value of $\nu = 0$. The Prandtl-Meyer function is related to the turning angle $\Delta\delta$ through the expression,

$$\nu(M_1) = \nu(M_0) - \Delta\delta \tag{7-19}$$

The turning angle is negative ($\Delta\delta < 0$) for an expansion and positive ($\Delta\delta > 0$) for a compression. Figure 7.3 shows a positive deflection. The Mach number after the turning can be determined from the solution of Equation (7-18) for a specified value of ν. The angle of a Mach wave is related to the Mach number ahead of the wave in the form of

$$\sin\mu_0 = \frac{1}{M_0} \tag{7-20}$$

At $M = 1$, the angle of the Mach wave is $\mu = 90°$. The angle decreases as the Mach number increases.

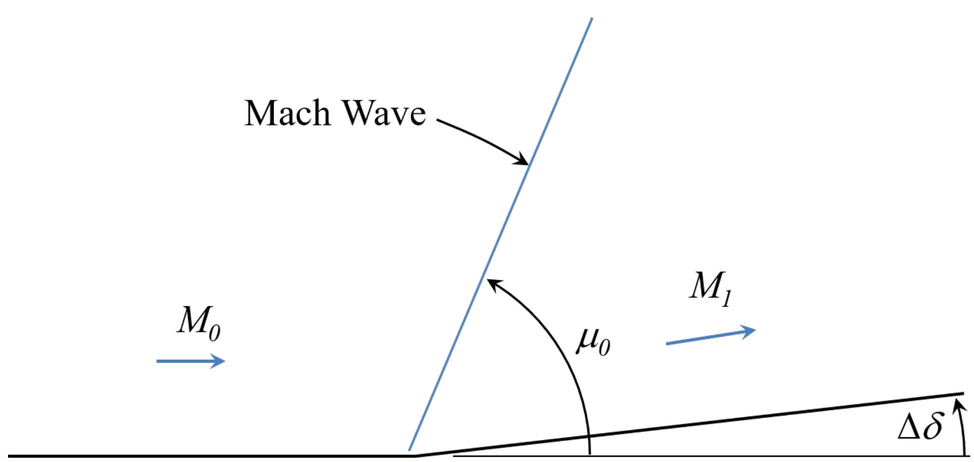

Figure 7.3.—Schematic of a Mach wave in Prandtl-Meyer supersonic flow.

7.4 Axisymmetric and Two-Dimensional External Supersonic Diffusers

The purpose of the ***external supersonic diffuser*** is to decelerate and compress the supersonic flow approaching the inlet prior to the flow entering the internal ducting of the inlet. In general terms, the external supersonic diffuser decelerates supersonic flow from a local Mach number (M_L) to a lower Mach number approaching station 1 ($M_{EX} < M_L$). The deceleration and compression are performed using two-dimensional oblique shock waves, conical shock waves, and Mach waves depending on the shape of the external supersonic diffuser. The previous three subsections provided methods for computation the change of flow properties across these fluid dynamic processes. The ***method-of-characteristics (MOC)*** provides another approach for solving the flow properties of supersonic flow over the external supersonic diffuser (Refs. 4, 6, and 7). The MOC approach is discussed briefly below, but Appendix B provides greater details on the MOC approach for the external supersonic diffuser.

It was recognized during the 1940's that for supersonic flow, an axisymmetric conical centerbody extending ahead of the entrance of an inlet created a conical shock wave through which the total pressure loss was less than that of a normal shock wave (Ref. 8). The concept was eventually extended to an inlet with a forebody that used two-dimensional ramps that created planar oblique shock waves (Ref. 9). Such axisymmetric and two-dimensional forebodies formed ***axisymmetric spike*** and ***two-dimensional external supersonic diffusers***, respectively, since their shape could be represented by a planar profile that is extruded about an axis-of-symmetry or through a linear cross-stream direction, respectively. Examples of such external supersonic diffusers and inlets are shown in Figure 7.4. The planar profiles that create the surface for the external supersonic diffuser are colored in red. For the case of the two-dimensional inlets (K_{typ} = 2 and 4), the planar profile is extruded into the z-coordinate direction to create a system of planar ramps and surfaces. For the case of the axisymmetric spike inlet (K_{typ} = 3), the planar profile is extruded about the inlet axis-of-symmetry.

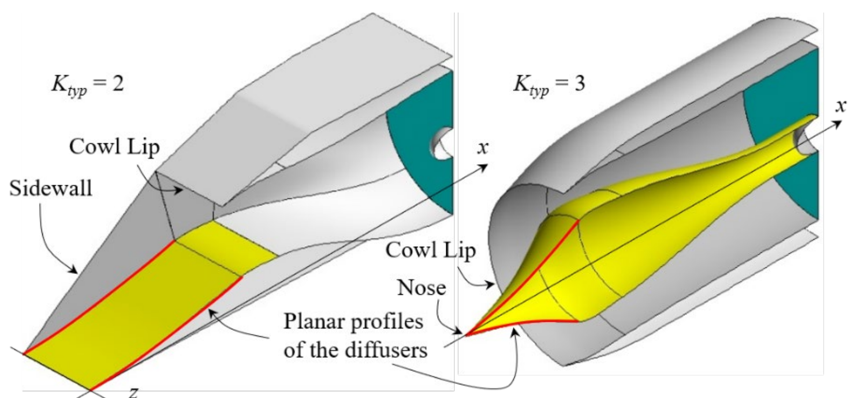

Figure 7.4.—Planar profiles of the external supersonic diffusers of two-dimensional and axisymmetric spike inlets.

The use of such two-dimensional and axisymmetric spike shapes took advantage of the ability to solve two-dimensional oblique and conical shock waves and Mach waves analytically or computationally, as described above. This subsection discusses axisymmetric spike and two-dimensional external supersonic diffusers and their modeling within SUPIN. External supersonic diffusers can also be formed using streamline-tracing through compressive parent flowfields and those diffusers will be discussed in Section 10.0 which discusses streamline-traced inlets (K_{typ} = 5).

The modeling of the external supersonic diffusers within SUPIN is illustrated in Figure 7.5. The external supersonic diffuser extends between the local station L and the cowl lip / inlet entrance station 1. The external supersonic diffuser consists of a number of stages (N_{stgs}) in which each stage turns the flow outward away from the inlet axis and into itself with the creation of shock or Mach waves. This turning of the flow decelerates and compresses the supersonic flow and causes a reduction in the cross-sectional area of the streamtube. SUPIN assumes external supersonic diffusers with either N_{stgs} = 1, 2, or 3. For the two-dimensional and axisymmetric spike inlets, one or more lines or curves is used to define the planar profile for each stage. For N_{stgs} = 1 or 2, only lines are possible for defining the profile of the stages, which correspond to ramps for a two-dimensional inlet and conical sections for an axisymmetric spike inlet. Each stage is characterized by its slope ($\theta_{stg\#}$) and the (x,y)-coordinates of the endpoint ($x_{stg\#}$, $y_{stg\#}$), where the "#" indicates the stage number. For diffusers with three stages (N_{stgs} =3), an option exists to form the second stage with a curve that generates Mach waves. Figure 7.5 shows examples of one, two-, and three-stage external supersonic diffusers. The bottom-right image shows Mach waves created by the second stage that focus on the cowl lip. The end of the last stage and end of the external supersonic diffuser are defined as the point on the last stage that intersects a line that passes through the cowl lip coordinate $(x,y)_{clip}$ and is perpendicular to the last stage. This definition of the end of the external supersonic diffuser ensures that the supersonic flow of the final stage continues to the station 1 plane, which is the considered the start of the internal ducting.

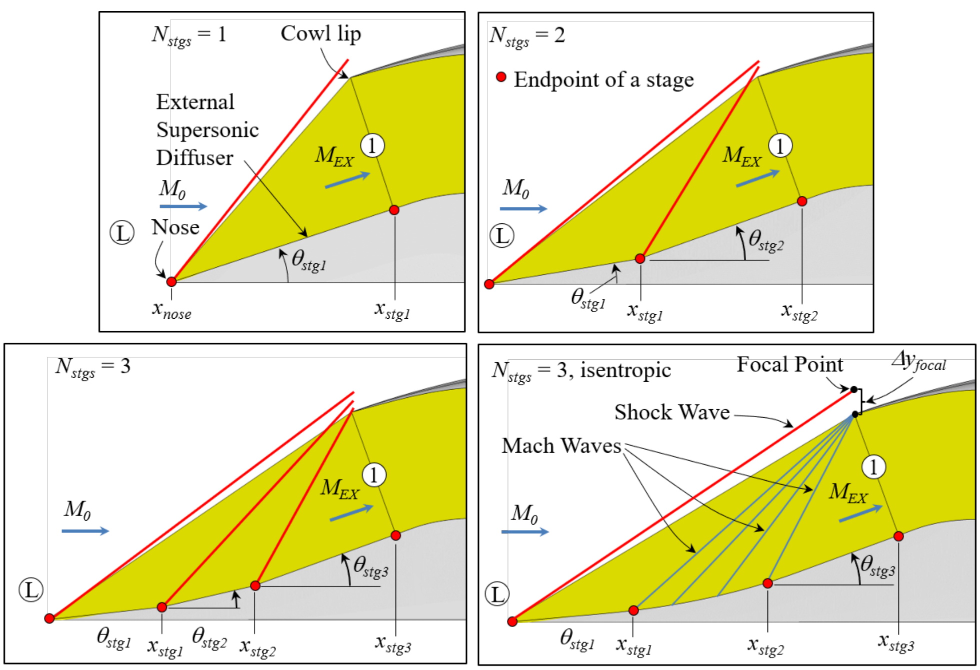

Figure 7.5.—Examples of planar external supersonic diffusers.

The shock and Mach waves generated by the stages of the external supersonic diffuser have ***focal points*** associated with each wave. Each wave passes through its associated focal point. Figure 7.6 illustrates the focal points. Within SUPIN, the focal points are assumed to be placed along a vertical line defined by $x = x_{clip}$ with a specified planar y-coordinate of the focal point defined as

$$y_{focal} = y_{clip} + \Delta y_{focal} \tag{7-21}$$

The planar character of the wave system allows diagraming the waves and focal points on a plane. Figure 7.6 shows two external supersonic diffusers with the waves and focal points indicated. The image on the left-hand-side shows an axisymmetric diffuser with two conical stages that create shock waves. Both shock waves pass through the same focal point that is located above the cowl lip coordinate by an offset of Δy_{focal}. The image on the right-hand-side of Figure 7.6 shows a three-stage axisymmetric diffuser with the second stage creating Mach waves. For this diffuser, the focal points are coincident with the cowl lip coordinate, which is known as the "***shock-on-lip***" condition. This yields the shortest planar external supersonic diffuser with the maximum supersonic flow capture. The shock-on-lip condition results in zero spillage of the supersonic flow of the external supersonic diffuser. Thus, the rate of flow entering station 1 is equal to the reference capture flow rate, $W_1 = W_{cap}$ and $W_{spillage} = 0$.

If a focal point is placed above y_{clip}, then there will be some level of supersonic spillage due to the deflection of the flow past the waves. Specifying a level of supersonic spillage is an option for the design of the external supersonic diffuser. Including a small percentage of supersonic spillage may be beneficial as a means of avoiding the ingestion of the waves into the inlet when the inlet is at an angle-of-attack or sideslip, or the approach flow conditions vary in Mach number or flow angle due to atmospheric disturbances.

The spatial dimensions of the external supersonic diffuser are established from trigonometry using the slopes and focal point coordinates of each stage. The nose coordinates are first defined followed by the (x,y)-coordinates of the endpoints $(x,y)_{stg\#}$ of the stages. The nose coordinate is characterized by $(x,y)_{nwav}$ as illustrated in Figure 7.7 and computed using simple trigonometry as

$$y_{nwav} = y_{inlet} \tag{7-22}$$

$$x_{nwav} = x_{foc1} - \left(y_{foc1} - y_{nwav}\right)/\tan\beta_{stg1} \tag{7-23}$$

where $(x,y)_{foc1}$ are the coordinates of the focal point associated with the leading shock wave of the external supersonic diffuser.

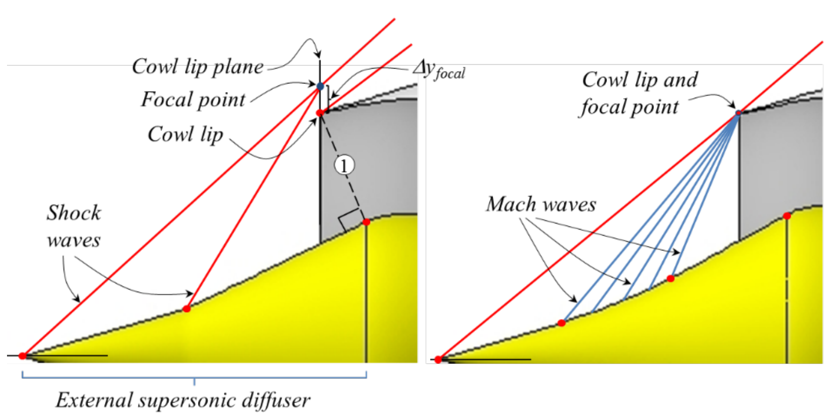

Figure 7.6.—External supersonic diffusers with examples of wave systems and focal points.

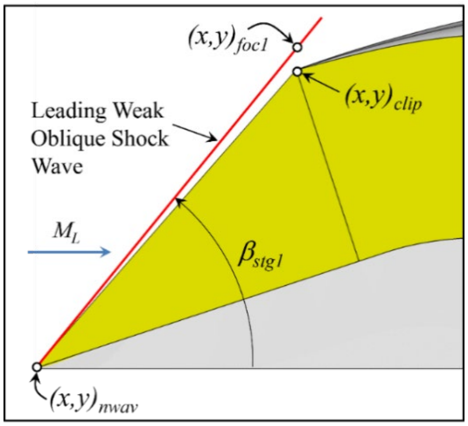

Figure 7.7.—Establishing the nose coordinate for a planar external supersonic diffuser.

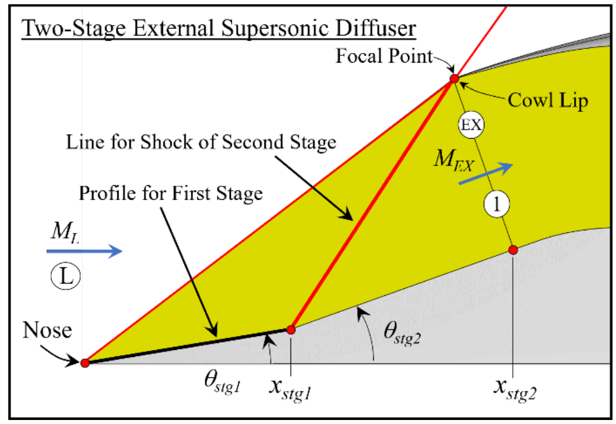

Figure 7.8.—Intersection of linear stage profile and linear wave angle for the calculation of the endpoint of the stage.

For second and third stages with linear profile segments, the coordinates of the endpoints $(x,y)_{stg\#}$ are computed by finding the planar intersection of the line for the stage profile and line for the wave at the end of the stage which also passes through the focal point for the next stage. An example is provided in Figure 7.8 in which the endpoint of the first stage $(x,y)_{stg1}$ is calculated as the point of intersection of line representing the profile of the first stage (shown by the bold black line) and the oblique shock wave generated by the start of the second stage (shown by the bold red line). The coordinates for the start of the first stage at the nose are known, as well as the coordinates for the focal point of the oblique shock wave. Further, the slope of the first stage and the angle of the oblique shock wave are also known. Thus, the only unknowns are the coordinates of the end of the first stage at $(x,y)_{stg1}$. The solution involves a system of two algebraic equations obtained from the point-slope formula for a line.

The shape of the profile for a curved isentropic second stage that generates Mach waves, such as illustrated in the lower-right image of Figure 7.5 and the right-hand-side image of Figure 7.6, is established using MOC methods. The design process starts with solution of the flow about the first stage using either the oblique or conical shock wave solution discussed previously and depending on whether the diffuser is two-dimensional or an axisymmetric spike, respectively. This solution serves as a starting upstream solution for the MOC method to solve through the second stage. Within the MOC methods, the second stage is referred to as MOC flow region A. It is assumed for the second stage that the Mach waves are focused upon the cowl lip, as illustrated in Figure 7.6 and that a linear Mach number deceleration is applied at the focal point through the Mach waves. With the upstream solution and the Mach number distribution known, the algebraic relations of the MOC methods can be solved upon a characteristic net through the second stage. A flow continuity relation is used through each Mach wave of the characteristic net to calculate the (x,y)-coordinates of the curved profile of the second stage until the trailing downstream Mach wave is reached. Further details of the MOC methods for an isentropic second stage are discussed in Appendix B.

The ***nose*** of the inlet is the start of the external supersonic diffuser and has the coordinate $(x,y)_{nose}$. The nose can be modeled as sharp or circular. For a sharp nose, the nose is a point, and the first stage starts at $(x,y)_{nose} = (x,y)_{nwav}$, as defined by Equations (7-22) and (7-23). For a circular nose, a circular arc with a radius of r_{nose} is used for the profile of the nose. The circular arc starts at point $(x,y)_{nose}$ and ends at $(x,y)_{nexd}$ with a slope of θ_{stg1}, which connects to the start of the first stage at $(x,y)_{nexd}$. Figure 7.9 shows examples of sharp and circular noses and the corresponding points.

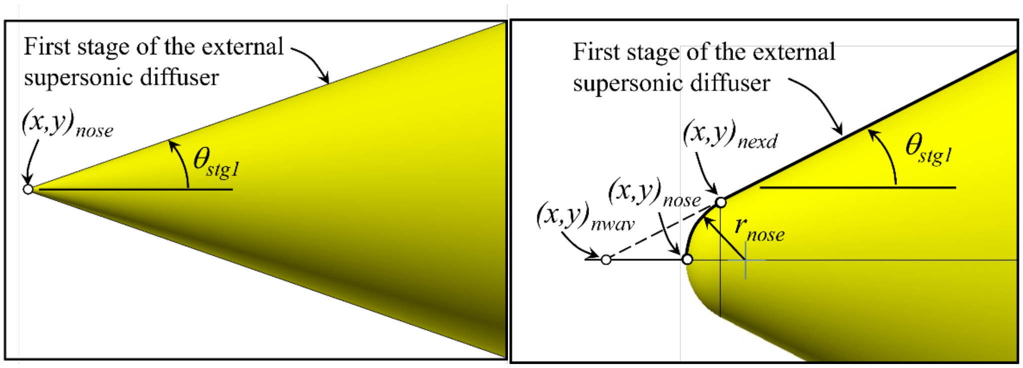

Figure 7.9.—Examples of sharp (left) and circular (right) noses for a planar external supersonic diffuser.

The coordinates $(x,y)_{nexd}$ and $(x,y)_{nose}$ for a circular nose can be calculated using the expressions,

$$y_{nexd} = y_{nwav} + r_{nose} \cos \theta_{stg1} \tag{7-24}$$

$$x_{nexd} = x_{nwav} + (y_{nexd} - y_{nwav}) / \tan \theta_{stg1} \tag{7-25}$$

$$x_{nose} = x_{nexd} - r_{nose} (1 - \sin \theta_{stg1}) \tag{7-26}$$

$$y_{nose} = y_{nwav} \tag{7-27}$$

For supersonic flow, the nose is typically sharp to create an attached oblique shock wave at the nose rather than a detached, blunt-body shock wave. A sharp nose can be modeled using a circular nose with a very small radius.

7.5 Input Data Block for Axisymmetric Spike and Two-Dimensional External Supersonic Diffusers

This section discusses the input factors of the input data file (SUPIN.in) that specify the external supersonic diffusers for two-dimensional and axisymmetric spike inlets. Table 7.1 shows an example input data block specifying a multi-stage, external supersonic diffuser. Table 7.2 lists and describes each of the input factors.

The character and number of stages of the external supersonic diffuser are indicated by the input factor $\boldsymbol{K_{exd}}$ and Table 4.12 lists the options available for K_{exd}. The options K_{exd} = 2, 3, 4, 5, 7, and 8 are used to create external supersonic diffusers for the two-dimensional inlets (K_{typ} = 2 and 4) and the axisymmetric spike inlet (K_{typ} = 3). These options create external supersonic diffusers with one, two, or three stages using ramps for the two-dimensional inlets and conical sections for the axisymmetric spike inlet. The option K_{exd} = 7 is a simplified input data block for the design of the external supersonic diffusers using the design mode (K_{mode} = 2) for the axisymmetric spike and two-dimensional inlets. Table 7.3 shows an example of a simplified input block for K_{exd} = 7, which is described below. The option K_{exd} = 8 is used to indicate that the external supersonic diffuser is defined by entities specified using the input data block with DataID = 16.

TABLE 7.1.—EXAMPLE INPUT DATA BLOCK FOR A PLANAR EXTERNAL SUPERSONIC DIFFUSER

```
DataID.  External Supersonic Diffuser
  4
Kexd    FptEXptL    Fpt1ptEX
  5      -0.9950     -0.9850
Kmtexd    Fmtexd    Kfocal
  1      1.30000       1
Knose     Fxnose     Frnose
  1      0.00000    0.05000
Stage      thstg      xstg       dyfocal
  1       8.0000    1.00000     0.00000
  2      12.0000    2.00000     0.00000
  3      15.0000    3.00000     0.00000
```

TABLE 7.2.—INPUT FACTORS FOR THE EXTERNAL SUPERSONIC DIFFUSER

Factor	Input	Description
K_{mtexd}	`Kmtexd`	Flag indicating the flow condition to match at the supersonic outflow [0] = 0 do not match a flow property, use stage angles explicitly = 1 F_{mtexd} is the outflow Mach number = 2 F_{mtexd} is the static pressure ratio, p_{EX} / p_L = 3 F_{mtexd} is the flow angle at station EX, θ_{EX} (degrees)
F_{mtexd}	`Fmtexd`	Flow condition value at diffuser outflow to be matched
K_{focal}	`Kfocal`	Flag indicating how focal points are used [0] = 1 use shock-on-lip condition for all focal points (Δy_{focal} = 0 ft) = 2 use the first-stage offset (Δy_{focal}) for all focal points = 3 use specified offsets (Δy_{focal}) for each stage = 4 focal points are linearly interpolated between first and last stage points = 5 the offsets (Δy_{focal}) are specified as a factor of y_{clip} = 6 a single focal point is placed to provide for specified supersonic spillage
K_{nose}	`Knose`	Flag for the shape of the nose [1] = 1 sharp = 2 circular
Fr_{nose}	`Frnose`	Radius of a circular nose (ft)
Fx_{nose}	`Fxnose`	x-coordinates for the start of the nose (ft)
θ_{stexd}	`thstexd`	Angle at the end of the stage (deg)
x_{stexd}	`xstexd`	Axial x-coordinate at the end of a stage (ft)
Δy_{focal}	`dyfocal`	Offset in y-direction from y_{clip} for focal point for a stage [0.0 ft]

Further details on the input factors for K_{exd} = 2, 3, 4, 5, and 7 are now discussed. The input factor of K_{exd} also implies the number of stages of the external supersonic diffuser. The option of K_{exd} = 2 creates a single-stage diffuser (N_{stgs} = 1) consisting of a single ramp for the two-dimensional inlet or a single cone for the axisymmetric spike inlet. The option of K_{exd} = 3 creates a two-stage diffuser (N_{stgs} = 2) consisting of two ramps for the two-dimensional inlet and a bi-cone for the axisymmetric spike inlet. The option of K_{exd} = 4 creates a three-stage diffuser (N_{stgs} = 3) consisting of three ramps for the two-dimensional inlet and a triple-segmented cone for the axisymmetric spike inlet. The option of K_{exd} = 5 also creates a three-stage diffuser; however, the second stage is a smooth contour such as to create Mach waves rather than shock waves.

The fifth line of the input block starting with the label "Kmtexd" starts the inputs that define the condition that the external supersonic diffuser must match at its end at station EX. The input factor $\boldsymbol{K_{mtexd}}$ indicates what condition is matched. Table 7.2 lists the options for K_{mtexd}. The input factor $\boldsymbol{F_{mtexd}}$ provides the desired value to be matched. The input factors K_{mtexd} and F_{mtexd} are only used for mode $K_{mode} = 2$ for which the external supersonic diffuser is being designed. A value of $K_{mtexd} = 0$ indicates that no matching is specified, and the deflection angles of the stages are specified in the inputs. A value of $K_{mtexd} = 1$ indicates that Mach number ($M_{EX} = F_{mtexd}$) is to be matched. A value of $K_{mtexd} = 2$ indicates that the static pressure ratio ($p_{EX}/p_L = F_{mtexd}$) is to be matched. A value of $K_{mtexd} = 3$ indicates that the angle of the flow in degrees is to be match ($\theta_{EX} = F_{mtexd}$). For the two-dimensional inlets ($K_{typ} = 2$ or 4), the Mach number, static pressure ratio, and the flow angle are all uniform at station EX at the outflow plane of the external supersonic diffuser. For the axisymmetric spike inlet ($K_{typ} = 3$), the flow properties vary at station EX from the diffuser surface to the cowl lip. In this case, the inlet design methods match the mass-averaged value of the property specified by K_{mtexd} and F_{mtexd}. Through the external supersonic diffuser, the outflow Mach number (M_{EX}) is decreased and the static pressure ratio (p_{EX}/p_L) and deflection angle of the external supersonic diffuser (θ_{EX}) increases.

The seventh line of the input block starting with the label "Knose" starts the inputs that define the shape of the nose of the planar external supersonic diffuser. The options are either a sharp nose ($K_{nose} =1$) or a circular nose ($K_{nose} = 2$). Figure 7.9 showed the planar profile of a circular nose, which is characterized by the radius of the nose, r_{nose}. The x-coordinate of the start of the nose (x_{nose}) is listed as an input factor; however, it is used only when the geometry of the external supersonic diffuser is specified explicitly ($K_{mode} = 1$ or 3). When the external supersonic diffuser is being designed ($K_{mode} =2$), the value of x_{nose} is calculated based on the leading oblique shock wave angle and its associated focal point, as discussed previously.

The ninth line of the inlet block starting with the label "Stage" starts the inputs that define the information for each stage. Below the ninth line, the input data block requires an input line for each stage. The lines contain the angle of the stage (θ_{stg}) in units of degrees, the x-coordinate of the endpoint of the stage (x_{stg}) in units of feet, and the vertical offset of the focal point ($\boldsymbol{\Delta y_{focal}}$).

SUPIN offers several options for placing the focal points. The input factor $\boldsymbol{K_{focal}}$ indicates how the vertical offsets of the focal points (Δy_{focal}) are calculated and Table 7.2 lists the options. A value of $\boldsymbol{K_{focal} = 1}$ indicates that all the focal points are located at the cowl lip, which is the "shock-on-lip" condition for the entire wave structure. The vertical offsets are set to zero values, $\Delta y_{focal} = 0$. A value of $\boldsymbol{K_{focal} = 2}$ indicates that all the focal points are defined by the vertical offset specified for the first stage. Thus, all the waves of the stages are focused to a single focal point defined for the first stage. The vertical offset is specified in units of feet. The x-coordinate of all the focal points is $x_{focal} = x_{clip} = 0$. The y-coordinate is calculated as $y_{focal} = y_{clip} + \Delta y_{focal}$. A value of $\boldsymbol{K_{focal} = 3}$ indicates that the focal points are independently defined for each stage through their respective vertical offset values. The offset applies to the first wave of the stage. A value of $\boldsymbol{K_{focal} = 4}$ distributes the focal points through a linear interpolation of the vertical offsets specified for the first and last stages. This has the effect of spreading out the compression system. A value of $\boldsymbol{K_{focal} = 5}$ indicates that the vertical offset for each stage is specified as a factor of the cowl lip height rather than units of feet. Thus, $y_{focal} = y_{clip} (1 + \Delta y_{focal})$. This allows the focal points location to be scaled with respect to the cowl lip dimension, y_{clip}. A value of $\boldsymbol{K_{focal} = 6}$ indicates that all stages have the same focal point, and the value of the vertical offset is computed to provide the amount of supersonic spillage, $W_{spillage}$, as specified by the input factor WRspill which is $W_{spillage}/W_{cap}$. The WRspill input factor was described in Section 4.4 and Table 4.5. When WRspill > 0.0, then K_{focal} is set to $K_{focal} = 6$ internally within SUPIN and any other values of K_{focal} specified in the input data file are ignored.

When $K_{exd} = 7$, the focal points are assumed to be located at the cowl lip and K_{focal} is imposed to be $K_{focal} = 1$, unless WRspill > 0, whereas $K_{focal} = 6$ is imposed and the focal point is computed as described above.

TABLE 7.3.—SIMPLIFIED INPUT DATA BLOCK FOR THE DESIGN OF AN EXTERNAL SUPERSONIC DIFFUSER FOR TWO-DIMENSIONAL AND AXISYMMETRIC SPIKE INLETS

```
DataID.  External Supersonic Diffuser
  4
Kexd    FptEXptL    Fpt1ptEX
  7      -0.9950     -0.9850
Nstgs    thstg1     Isenstg2    Kmtexd    Fmtexd
  3      10.000        1           1      1.3000
Knose    Frnose
  1     0.05000
```

When the inlet is being designed (e.g., K_{mode} = 2), the geometry of the diffuser is calculated based on both geometric and aerodynamic input factors. For the geometry (K_{mode} = 1) and analysis (K_{mode} = 3) modes, the geometry of the diffuser should be explicitly defined and specified so that a physically realistic external supersonic diffuser can be constructed.

The external supersonic diffuser specified by the input block of Table 7.1 has a shape like the right-hand-side image of Figure 7.6. The diffuser has a sharp nose and three stages with the second stage being a smooth curve generating Mach waves. The oblique shock wave from the nose and the Mach lines has their focal points at the cowl lip. The flow condition at the end of the diffuser is specified to be a Mach number of M_{EX} = 1.3.

Table 7.3 shows an example of a simplified input data block for the external supersonic diffuser for the case of the inlet design mode (K_{mode} = 2). This form of the input block is used when $\boldsymbol{K_{exd}}$ **= 7**. The input factor N_{stgs} indicates the number of stages. When N_{stgs} = 3, the input factor Isenstg2 indicates whether the second stage should be designed for isentropic compression (**Isenstg2** = 1).

7.6 Oswatitsch Condition for Two-Dimensional Multiple-Ramp Diffusers

Oswatitsch (Ref. 8) calculated that for an axisymmetric spike external supersonic diffuser involving two or more stages, the total pressure ratio through the stages (p_{tEX}/p_{tL}) could be maximized if the total pressure ratio across each stage were equal. The same holds for a two-dimensional external supersonic diffuser. SUPIN can compute the deflections of the stages ($\theta_{stg\#}$) that satisfies this ***Oswatitsch condition*** for two-dimensional inlets (K_{typ} = 2 or 4) with two or three stages (N_{stgs} = 2 or 3) for its external supersonic diffuser. This requires K_{mode}= 2 and K_{exd} = 3 (two ramps) or K_{exd} = 4 (three ramps). The Oswatitsch condition is imposed when a non-zero value of K_{mtexd} is specified. SUPIN uses a carpet search algorithm to find the optimum set of ramp deflections. When K_{mtexd} = 0, the ramp deflections as specified in the input lines of the form of Table 7.1 are used and the Oswatitsch condition is not imposed. The Oswatitsch condition is also imposed for two-dimensional diffusers when the input format for K_{exd} = 7 is used and N_{stgs} = 2 or 3.

7.7 Three-Stage Diffuser with an Isentropic Second Stage (K_{exd} = 5)

For planar external supersonic diffusers with three stages (N_{stgs} = 3), the second stage can be designed to be an ***isentropic compression surface*** that forms a series of Mach waves rather than a shock wave. The bottom-right image of Figure 7.5 and the right-hand-side image of Figure 7.6 illustrate such external supersonic diffusers. This design method is applied when K_{mode} = 2 and K_{exd} = 5 or K_{exd} = 7 for both two-dimensional and axisymmetric spike external supersonic diffusers. For K_{exd} = 7, the input factor Isenstg2 = 1 is also needed.

The profile of the first stage is a ramp (K_{typ} = 2 or 4) or a cone (K_{typ} = 3) in which the angle of the first stage (θ_{stg1}) is explicitly specified. A first-stage angle of θ_{stg1} = 5 degrees for a two-dimensional ramp and θ_{stg1} = 10 degrees for a cone are reasonable minimum values for these angles. The flow over the first stage is computed using numerical methods for oblique shock wave theory (K_{typ} = 2 or 4) described in Subsection 7.1 or conical shock wave theory (K_{typ} = 3) described in Subsection 7.2.

The profile of the second stage is created using the MOC design methods to form a focused isentropic contour in which all the Mach waves are focused on a single focal point located at the cowl lip point $(x,y)_{clip}$. The design method matches the diffuser outflow Mach number (M_{EX}) as specified by the input F_{mtexd} when K_{mtexd} = 1. The method involves an iteration of the change of Mach number through the Mach waves at the focal point until the desired values of M_{EX} is obtained. Appendix B discusses further details on the method of characteristics. Figure B-5 illustrates the characteristic net for the isentropic second stage, which is referred to as MOC flow region A.

The profile of the third stage is a ramp or cone surface. Its angle matches that at the end of the second stage. The flow about the third stage is also computed using the MOC methods. Figure B-6 of Appendix B illustrates the characteristic net through the third stage, which is referred to as MOC flow region B.

With the second stage being isentropic and the third stage not forming any waves and being isentropic, the total pressure losses of the external supersonic diffuser are due only to the shock wave of the first stage and viscous dissipation of the boundary layers on the external supersonic diffuser.

7.8 Sidewall Surfaces

Sidewalls are created to contain the compression on the external supersonic diffuser for the two-dimensional inlets (K_{typ} = 2 and 4). The sidewalls are modeled as flat surfaces that are parallel to the *x*-*y* plane and extend from the nose of the external supersonic diffuser to the cowl lip station 1. The leading edge of the sidewall is modeled as a line extending from the nose to the cowl lip point. The surface for a sidewall is formed by defining planar curves for the boundaries and then performing a transfinite interpolation between the bounding curves. An example of a sidewall is indicated in Figure 7.4.

7.9 Total Pressure Loss through the External Supersonic Diffuser

Within SUPIN, the total pressure losses for the external supersonic diffuser are computed as the sum of the total pressure losses through each oblique or conical shock wave. The total pressure ratio for the external supersonic diffuser is the product of the total pressure ratios through each stage,

$$\frac{p_{tEX}}{p_{tL}} = \frac{p_{t_{(1)}}}{p_{tL}} \prod_{n=2}^{N_{stg}} \frac{p_{t_{(n)}}}{p_{t_{(n-1)}}} \tag{7-28}$$

The total pressure ratio across an oblique shock wave is calculated using Equation (5-12) for the normal shock wave relations; however, the Mach number used in Equation (5-12) is the component of the Mach number normal to the oblique shock wave as computed by Equation (7-6).

Another source of total pressure loss through the external supersonic diffuser is the viscous dissipation occurring within the boundary layers about the stages and sidewall. These losses are not modeled within SUPIN for the external supersonic diffuser.

References

1. Ames Research Staff, “Equations, Tables, and Charts for Compressible Flow,” NACA Report 1135, 1953.
2. Liepmann, H. W. and Roshko, A., *Elements of Gasdynamics*, John Wiley & Sons, 1957.
3. Zucrow, M. J. and Hoffman, J. D., *Gas Dynamics: Volume 1*, John Wiley & Sons, New York, 1976.
4. Anderson, J. D., Jr., *Modern Compressible Flow*, McGraw-Hill Book Company, New York, 1982.
5. Taylor, G. I. and Maccoll, J. W., “The Air Pressure on a Cone Moving at High Speeds,” *Proceedings of the Royal Society* (London), Ser. A, Vol. 139, pp. 278-311, 1933.
6. Anderson, B. H., “Design of Supersonic Inlets by a Computer Program Incorporating the Method of Characteristics,” NASA TN D-4960, January 1969.
7. Sorensen, V. L., “Computer Program for Calculating Flowfields in Supersonic Inlets,” NASA TN D-2897, July 1965.
8. Oswatitsch, K., “Pressure Recovery for Missiles with Reaction Propulsion at High Supersonic Speeds (The Efficiency of Shock Diffusers),” NACA TM 1140, June 1947. (Translation of 1944 report in German).
9. Conners, J. F. and Woollett, R. R., “Experimental Investigation of a Two-Dimensional Split-Wing Ram-Jet Inlet at Mach Number of 3.85,” NACA RM E52F04, August 1952.

8.0 External-Compression, Axisymmetric Spike and Two-Dimensional Inlets

This section and the next section discuss the modeling of axisymmetric spike (K_{typ} = 3) and two-dimensional inlets (K_{typ} = 2 or 4) within SUPIN. The discussion of two-dimensional inlets will include those with a single duct (K_{typ} = 2) or bifurcated duct (K_{typ} = 4) leading to the engine-face. The general characteristics and application of axisymmetric spike and two-dimensional inlets were discussed in the historical overview of Section 1.0. Their components and reference stations were identified in Section 2.5 and their SUPIN models were introduced in the discussion of inlet types in Section 4.3. This section discusses external-compression, axisymmetric spike and two-dimensional inlets while the next section discusses mixed-compression, axisymmetric spike and two-dimensional inlets. Subsection 8.1 starts with a presentation of some more general features of the SUPIN geometric models for the external-compression, axisymmetric spike, two-dimensional single-duct, and two-dimensional bifurcated-duct inlets. Subsection 8.2 provides a summary of the cowl lip for the inlets.

The previous section provided details on the design and flow analysis for the external supersonic diffusers that created the external shock wave systems for axisymmetric spike and two-dimensional inlets. For an external-compression inlet, the ***terminal shock wave system*** is expected to form in the region of station 1 with portions of the shock wave system wrapping about the cowl lip. Such a terminal shock wave system allows for ***subsonic spillage*** past the cowl lip, which serves as a mechanism for the ***matching*** of the inlet and engine flowrates and the ***stabilization*** of the terminal shock wave system. Subsection 8.3 will provide a further discussion of the terminal shock wave structure. As discussed in Section 2.5, the ***internal diffuser*** for an external-compression inlet contains a ***throat section*** and ***subsonic diffuser*** and is expected to contain mostly subsonic flow. Subsection 8.4 discusses a geometry model for the throat section that assumes primarily subsonic flow within the throat section but may allow a strong oblique terminal shock wave system rather than a normal terminal shock wave. Subsection 8.5 discusses a throat section model described by Mahoney (Ref. 1) that allows for supersonic flow and a terminal shock wave train structure to exist within the throat section yet allow subsonic spillage past the cowl lip. Subsection 8.6 discusses the geometric modeling of the subsonic diffusers for the inlets. Subsection 8.7 discusses the use of entities to explicitly specify the geometry of the inlet components. Subsection 8.8 discusses the geometric modeling of the cowl exteriors for the inlets. Subsection 8.9 discusses the geometric modeling of support struts for axisymmetric spike inlets.

8.1 Descriptions of External-Compression, Axisymmetric Spike and Two-Dimensional Inlets

This subsection discusses the features of the geometric models of the axisymmetric spike (K_{typ} = 3), two-dimensional (K_{typ} = 2), and two-dimensional bifurcated-duct (K_{typ} = 4) inlets.

8.1.1 External-Compression, Axisymmetric Spike Inlet

The axisymmetric spike inlet (K_{typ} = 3) was introduced in various previous sections and illustrated in Figure 2.9 and Figure 4.1. The axisymmetric spike inlet features an axisymmetric centerbody with a conical nose referred to as the spike. The axisymmetric spike inlet compresses supersonic flow by turning the flow away from the axis-of-symmetry through a series of axisymmetric stages using shock or Mach waves, as described in Section 7.0. The internal diffuser of the external-compression, axisymmetric spike inlet includes a throat section and subsonic diffuser, as illustrated in Figure 2.9. Due to the axisymmetric nature of the inlet, the geometry model involves defining the planar profiles of the external supersonic diffuser, cowl lip, cowl exterior, throat section, and subsonic diffuser. These profiles are then extruded

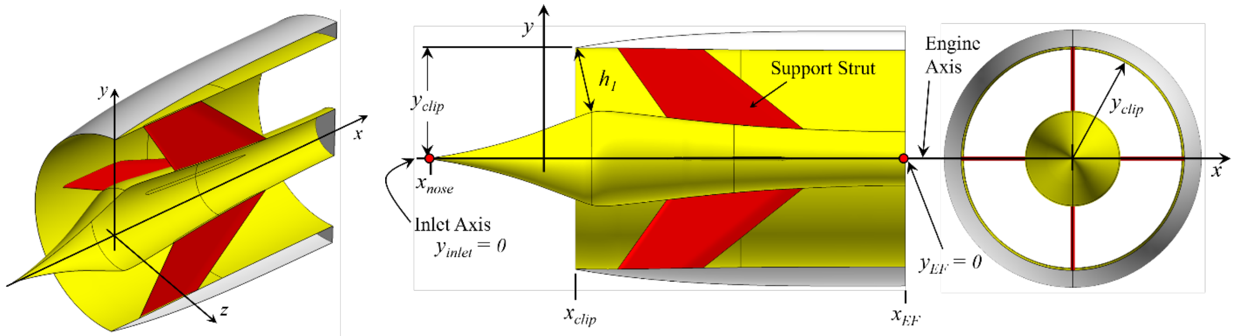

Figure 8.1.—An example of an external-compression, axisymmetric spike inlet.

about the axis-of-symmetry to form the respective surfaces of the inlet. The cross-sections through the inlet duct are co-annular as formed by the centerbody and cowl interior. The inlet also requires support struts to support the centerbody through the cowl structure. For the SUPIN geometry model, the centerbody covers the hub of the engine, and so, a spinner is not needed. An alternative model could be defined in which the centerbody ends upstream of the engine face; however, such a model is not yet available within SUPIN.

Figure 8.1 shows views of an external-compression, axisymmetric spike inlet showing the axes and geometric properties. The inlet and engine axes are coincident with the $y_{inlet} = y_{EF} = y = 0$ axis. The cowl lip is placed at the origin of the global coordinate system, $x_{clip} = 0$. The coordinate y_{clip} is the radial dimension to the cowl lip point. The capture cross-section is circular with a reference capture area of $A_{cap} = \pi\, y_{clip}^2$. The height of station 1 is designated as h_1. The angle of the engine face is set to zero, $\theta_{EF} = 0$. The axisymmetric spike inlet requires support struts to provide support between the centerbody and cowling. Figure 8.1 shows an axisymmetric spike inlet with four support struts about its circumference.

8.1.2 External-Compression, Two-Dimensional Single-Duct Inlet

The two-dimensional single-duct inlet ($K_{typ} = 2$) was introduced in previous sections and illustrated in Figure 2.8 and Figure 4.1. The inlet features an external supersonic diffuser consisting of one or more stages of planar ramps that create two-dimensional shock and Mach wave systems, as discussed in Section 7.0. The surfaces of the external supersonic diffuser are formed through the extrusion of planar profiles in the cross-stream direction (z-direction). A sidewall contains the compression on the external supersonic diffuser. The two-dimensional inlet has a rectangular capture cross-section. The top of the capture cross-section is a linear edge defined by the cowl lip. The bottom of the capture cross-section is a line defined by the leading edge or nose of the external supersonic diffuser. The sides of the capture cross-section are lines defined by the leading edges of the sidewalls. Figure 8.2 shows views of a two-dimensional single-duct inlet showing the axes and geometric properties. The inlet axis is coincident with the $y_{inlet} = 0$. The cowl lip is placed at the origin of the global coordinate system, $x_{clip} = 0$. The dimensions for the rectangular capture cross-section are the height (h_{cap}) and the width (w_{cap}) with a reference capture area of $A_{cap} = w_{cap}\, h_{cap}$. The aspect ratio of the capture cross-section is w_{cap}/h_{cap}. The height of station 1 is designated as h_1. The angle of the engine face is set to zero, $\theta_{EF} = 0$.

The internal diffuser of the external-compression, two-dimensional single-duct inlet includes a throat section and subsonic diffuser, as illustrated in Figure 2.8 and Figure 8.2. The throat section retains the rectangular cross-section of the capture plane through the length of the throat section. For an external-compression inlet, the terminal shock wave structure is located about the inlet entrance station 1 and subsonic flow is expected within the throat section. The planar shape of the throat section, as well as, the external supersonic diffuser, simplifies the manufacturing of the inlet and the incorporation of variable geometry. The subsonic diffuser contains a transition from the rectangular cross-section at station SD to an annular cross-section at the engine face (station 2), as illustrated in Figure 8.2. The two-dimensional single-duct inlet does allow the vertical location of the engine face (y_{EF}) to be offset from the inlet axis. This offset can be used to provide some flexibility in the relative positions of the capture cross-section and engine face to provide for improved inlet/airframe integration.

8.1.3 External-Compression, Two-Dimensional, Bifurcated-Duct Inlet

The two-dimensional, bifurcated-duct inlet (K_{typ} = 4) essentially consists of two two-dimensional, single-duct inlets previously described mounted back-to-back to feed a single engine face. The inlet contains two separate external supersonic diffusers and throat sections. The forward portions of the subsonic diffuser are separate, but then merge to form a trailing edge at some point through the subsonic diffuser to form a common mixing duct leading to the engine face. Figure 8.3 shows an example of a two-dimensional bifurcated-duct inlet for an annular engine face.

The two-dimensional, bifurcated-duct inlet has a rectangular capture cross-section that includes the upper and lower apertures of the mirrored two-dimensional inlet components. The top and bottom of the capture cross-section are lines defined by the cowl lips of the upper and lower two-dimensional inlet components. The sides of the capture cross-section are lines defined by the leading edges of the sidewalls. Figure 8.3 shows views of the two-dimensional, bifurcated inlet showing the axes and geometric factors. The inlet and engine axes are coincident with the $y_{inlet} = y_{EF} = 0$ axis. The cowl lip is placed at the origin of the global coordinate system, $x_{clip} = 0$. The angle of the engine face is set to zero, $\theta_{EF} = 0$. The geometric factors for the rectangular capture cross-section are the height (h_{cap}) and the width (w_{cap}) of the capture cross-section with a reference capture area of $A_{cap} = w_{cap}\, h_{cap}$. The aspect ratio of the capture cross-section is w_{cap}/h_{cap}. The height of station 1 is designated as h_1. The cowl lip coordinate is related to the height of the capture area as $y_{clip} = 0.5\ h_{cap}$.

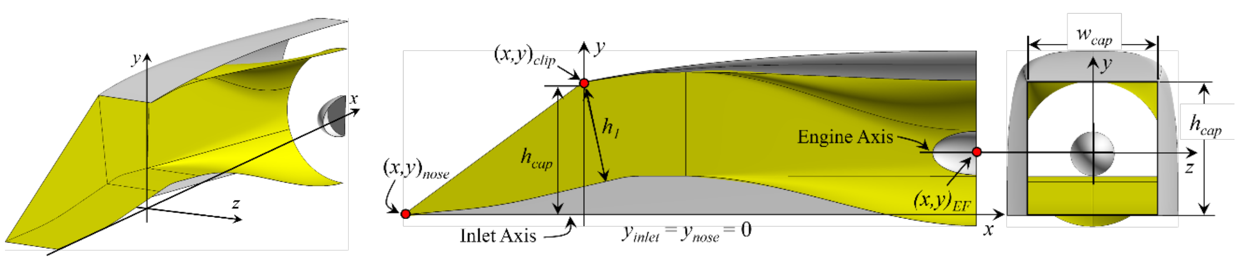

Figure 8.2.—An example of an external-compression, two-dimensional single-duct inlet.

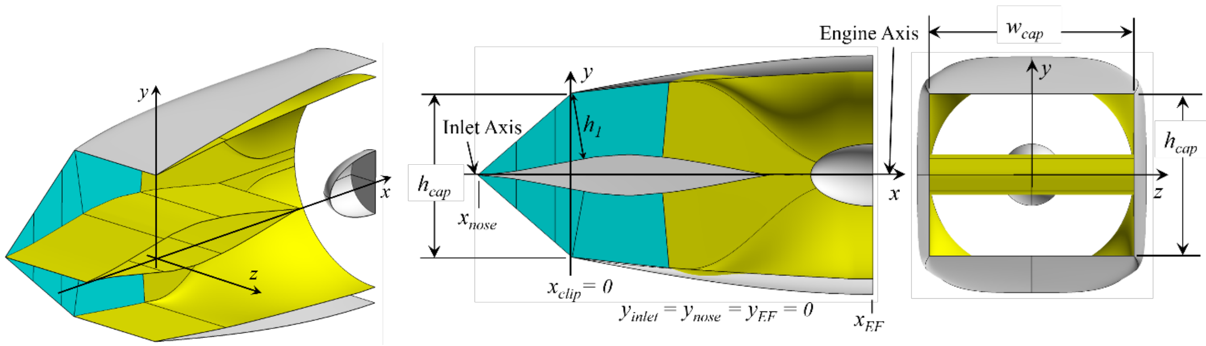

Figure 8.3.—An example of an external-compression, two-dimensional bifurcated-duct inlet.

8.2 Cowl Lip

The cowl lip surfaces for the axisymmetric spike (K_{typ} = 3) and two-dimensional (K_{typ} = 2 and 4) inlets are formed in the same manner as described in Subsection 4.9. The cowl lip surfaces are created using the elliptic profiles with the input factors specified as described in Subsection 4.9 and listed in Table 4.13 and Table 4.14. As mentioned with Subsection 4.9, the dimensions (a_{clin}, b_{clin}, a_{clex}, b_{clex}) for supersonic inlets are very small compared to the capture or engine face dimensions of the inlet. Such small dimensions create an essentially sharp cowl lip suitable for supersonic flow and shock waves. For a cowl lip with an elliptical leading edge, a shock wave would stand off from the leading edge; however, for small dimensions and essentially sharp cowl lip leading edge, the stand-off distance would be very small and within SUPIN such a stand-off distance is not considered.

SUPIN does offer some options not described previously for establishing the cowl lip interior and exterior angles θ_{clin} and θ_{clex} in the SUPIN design mode (K_{mode} = 2) for the axisymmetric spike and two-dimensional inlets. When the cowl lip interior angle, θ_{clin}, is specified such that $\theta_{clin} < -10.0$, the angle is set to the angle of the flow at the cowl lip, $\theta_{clin} = \theta_{clflow}$. SUPIN calculates the angle of the flow at the cowl lip, θ_{clflow}, as part of the solution of the flow of the external supersonic diffuser. When $-10.0 < \theta_{clin} < 0.0$, the angle of the cowl lip interior is computed as $\theta_{clin} = \theta_{clflow} + \theta_{clin}$. When the input factor θ_{clex} is specified as a negative number, then the cowl lip exterior angle is computed as $\theta_{clex} = \theta_{clin} + |\theta_{clex}|$.

Once the properties of the elliptic profiles for the cowl lip interior and exterior are established, the surfaces are created through an extrusion. For the axisymmetric spike inlet (K_{typ} = 3), the elliptic profiles are extruded about the axis-of-symmetry. For the two-dimensional inlets (K_{typ} = 2 or 4), the extrusion is across the width of the capture cross-section and in the z-direction. Examples of the cowl lips for these inlets are illustrated in Figure 8.1, Figure 8.2, and Figure 8.3.

8.3 External Terminal Shock Wave Structure

This subsection discusses some details on possible external terminal shock wave structures and their implications with regard to the design of the external supersonic diffuser and throat section for external-compression, axisymmetric spike and two-dimensional inlets. An external-compression inlet involves a terminal shock wave structure that allows for subsonic spillage of flow past the cowl lip. This specifically implies that at subcritical flow conditions, the terminal shock wave structure has a portion of the shock wave that wraps about the cowl lip in a blunt-body, detached shock wave form such that subsonic flow can pass from the inlet core flow to the exterior flow through a gap between the downstream side of the shock wave and the cowl lip. Here we consider three types of terminal shock wave systems for an external-compression inlet: 1) a normal shock wave, 2) a strong oblique shock wave, and 3) a shock wave train. The form of the terminal shock wave system mainly depends on the Mach number at the end of the external supersonic diffuser and just upstream of the shock wave system (M_{EX}), the differences between the direction of the flow at the cowl lip and the cowl lip interior angle (θ_{clin}), the level of pressurization within the inlet, and presence of any bleed systems on the inlet surfaces about the inlet entrance station 1.

A ***normal terminal shock wave system*** is formed when $M_{EX} \approx 1.3$, the cowl lip interior angle is aligned with the local flow at the cowl lip, and the inlet is operating near its critical condition. For the design of an external compression, axisymmetric spike or two-dimensional inlet, SUPIN assumes that the normal shock wave is positioned across station 1. At subcritical operating conditions, the normal shock wave will be pushed upstream of station 1, and subsonic flow will spill past the cowl lip to balance the captured flow with the engine flow demand. At supercritical operating conditions, the normal shock wave will be sucked into the inlet such that the total pressure losses increase to impose flow continuity within

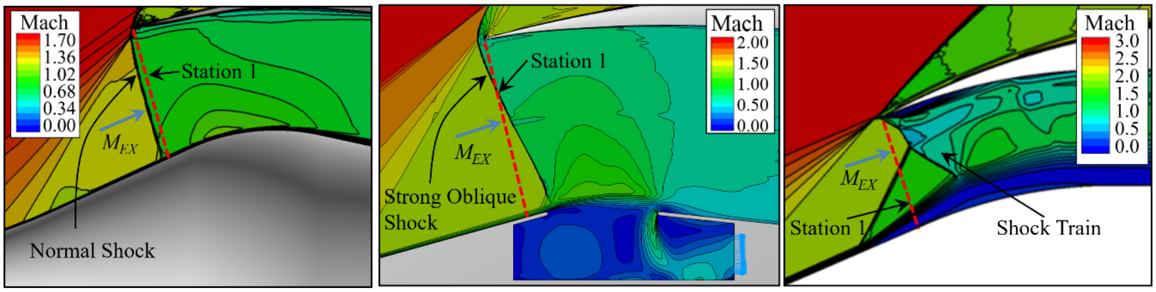

Figure 8.4.—Examples of terminal shock wave structures with a normal shock wave (left), a strong oblique shock wave (middle), and shock wave train (right).

the internal diffuser of the inlet. With the terminal shock wave within the inlet, the subsonic spillage approaches zero. The image on the left-hand-side of Figure 8.4 shows Mach number contours from a CFD simulations of a Mach 1.7 axisymmetric spike inlet with a normal terminal shock wave slightly upstream of station 1. The station 1 cross-section is illustrated by the red-dashed line in the image.

A ***strong oblique terminal shock wave system*** is formed when $M_{EX} > 1.3$ and the cowl lip interior angle is mis-aligned with the local flow at the cowl lip such as to cause a deflection that forms the oblique shock wave that propagates into the throat section. Further, the pressurization within the inlet is great enough such that the strong oblique shock wave is established rather than the weak oblique shock wave. As it was discussed in Section 1.4, the two-dimensional inlets for the Concorde aircraft used a strong oblique terminal shock wave system. In that application, the inlet involved $M_{EX} = 1.38$, a mismatched cowl lip, and a wide bleed slot to help create and stabilize the shock wave. The middle image of Figure 8.4 shows Mach number contours from a CFD simulations of a Mach 2.0 two-dimensional inlet with a strong oblique terminal shock wave. The inlet flow is slightly sub-critical with the terminal shock wave wrapped about the cowl lip but with a significant stand-off to allow for subsonic spillage. However, most of the shock wave is downstream of station 1. The terminal shock wave interacts with a wide bleed slot at the shoulder of the inlet. The slot bleed helps to stabilize the terminal shock wave structure by allowing the bleed rate to adjust to the change of local conditions due to variations in the engine flowrate.

The design of the external supersonic diffuser and the entrance of the throat section should consider the interaction of the terminal shock wave system with the boundary layer generated on the external supersonic diffuser with the goal of preventing or minimizing ***boundary layer separation***. Nussdorfer (Ref. 1) provided one of the earliest assessments of incipient boundary layer separation with terminal shock wave waves of external-compression inlets. Nussdorfer examined data from wind-tunnel experiments involving axisymmetric spike and two-dimensional inlets up to Mach 3 and categorized the terminal shock waves as either ***normal***, ***curved***, or ***branched***. A normal shock wave would form if there was no boundary layer separation at the external diffuser surface. A curved shock wave would form if a small region of separated flow existed. The start of the separated flow region would cause the shock wave to curve near the surface, but then take a normal form away from the surface. The separated flow would eventually reattach in a short distance downstream of the shock wave. The branched terminal shock wave would be the result of a large-scale separation region on the external diffuser with the branching of the shock wave occurring about the start of the separation region. The reattachment of the boundary layer would not occur for a branched shock wave. Nussdorfer established an empirical criterion that to avoid boundary layer separation with a normal terminal shock wave, the Mach number preceding the shock wave should not be greater than Mach 1.33 (i.e., $M_{EX} \leq 1.33$). For an axisymmetric spike inlet, the Mach number varies across the station 1 location, and so, this Mach number criterion is applied to the Mach number at the centerbody, which is lower than the Mach number at the cowl lip across station 1. The Mach number criterion corresponds to a pressure rise across the shock wave as $p_1/p_{EX} = 1.89$. Nussdorfer suggested using this criterion for inlets operating up to $M_0 = 2$. Above Mach 2, it is expected that the terminal shock wave would cause boundary layer separation. Nussdorfer reported that this boundary layer separation criterion was similarly observed for flows involving blunt-body shock waves and airfoils.

Kuehn (Ref. 2) also examined pressure ratios for incipient boundary-layer separation and examined flows about corners, curved surfaces, and flat plates with an incident shock wave. The Kuehn data supported the conclusions of Nussdorfer. Kuehn considered Mach numbers from Mach 1.6 to 4.2 and Reynolds number of 1.5×10^4 to 7.5×10^4 based on the boundary layer thickness. Kuehn also examined unsteadiness in the separation using shadowgraphs. One observation was that a small region of boundary layer separation may be acceptable if it quickly reattaches to the inlet surface. A small separation region is defined as having a length less than 10 to 15 boundary layer heights (Ref. 2). Concern about separation exists when the separation becomes unstable or becomes sizable as to significantly decrease the boundary layer momentum or create excessive total pressure losses.

As a summary of the previous two paragraphs in application to the design of external-compression inlets with normal terminal shock waves, a suggested guideline is to achieve $M_{EX} \leq 1.3$ to keep the pressure ratio $p_1/p_{EX} < 1.89$. The value of M_{EX} for axisymmetric spike inlets could be slightly greater because the Mach number at the centerbody surface at the end of the external supersonic diffuser is lower than at the cowl lip. As indicated above, if a small separation region is created, it may be acceptable if it quickly reattaches, is steady, and doesn't introduce excessive total pressure losses within the inlet. With such small separation region, the terminal shock wave has a curve near the separation region, which Nussdorfer termed a "curved shock wave". The strong oblique terminal shock wave system involves $M_{EX} > 1.3$, and so, this type of terminal shock wave system likely requires bleed slots or porous bleed regions to prevent boundary layer separation. The use of bleed systems will be discussed in a later section.

The guideline of $M_{EX} \leq 1.3$ for a normal terminal shock wave to avoid boundary layer separation has been found to be achievable for external-compression inlets operating up to $M_0 \approx 2$. For $M_0 > 2.0$, it has been found that the flow turning required to achieve $M_{EX} \leq 1.3$ results in cowl lip exterior angles that result in excessive cowl exterior wave drag or possible detachment of the cowl exterior shock wave. One approach for inlets for $M_0 > 2.0$, is to accept $M_{EX} > 1.3$ along with the separated boundary layer. This approach seems to have been used for the earliest inlets for missiles using ramjet engines in the 1940s through 1960s. The boundary-layer separation region is large enough to create a branched terminal shock wave structure as noted by Nussdorfer (Ref. 1). Such a branched terminal shock wave structure can be seen in the right-hand-side image of Figure 8.4 showing the Mach number contours from a CFD simulation of an external-compression, two-dimensional inlet for $M_0 = 3.0$. For this inlet, $M_{EX} = 1.99$. The separation regions show as the blue regions and a large separation region is shown on the centerbody. The branching of the terminal shock wave extends about two-thirds across station 1. A small separation region is also indicated downstream of the cowl lip interior with a much smaller branching of the terminal shock wave. A short normal segment of the terminal shock wave is indicated with subsonic flow downstream of this shock wave segment. In other parts of the flow downstream of the terminal shock wave, the flow remains or accelerates to supersonic conditions with the separation region extending into the throat section. This terminal shock wave system is an example of the ***shock wave train terminal shock wave system***. This flow has considerable total pressure losses caused by the shock waves and separated flow. While such flow doesn't seem very good, it has been considered acceptable for a ramjet-powered missile application in which high speed, yet simplicity is important. A concern of this flow are the levels of unsteadiness. However, if the inlet can provide the performance and operability to allow the missile to accomplish its intended mission, then the inlet could be acceptable.

8.4 Subsonic Throat Section Model

The subsonic throat section geometry model assumes that the terminal shock wave structure is either a single normal or a strong oblique terminal shock wave system positioned at or about station 1 and for which subsonic flow is created downstream of the terminal shock wave system. For a normal shock wave, the geometry model assumes that the terminal shock wave is positioned across station 1 and is normal to the ramp or centerbody surface at the point that marks the end of the external supersonic diffuser. For a strong oblique shock wave, the terminal shock wave will have a shock wave angle that results in the shock wave bending downstream of station 1 as the shock wave approaches the ramp or centerbody.

The subsonic throat section geometry model assumes that the geometric throat of the inlet is located just downstream of station 1 at the minimum cross-sectional area created by the cowl lip interior. As discussed in a previous subsection, the cowl lip interior is a modeled with an elliptical profile. The minimum cross-sectional area occurs across the plane at the point on the cowl lip interior that is closest to the centerbody. Since the dimensions of the cowl lip interior for a supersonic inlet are likely very small (i.e, $b_{clin} << 1.0$), the geometric throat is essentially located at station 1 and with a slightly smaller cross-sectional area (e.g., $A_{TH} \approx A_1$).

One task of the throat section is to turn the flow toward the engine face. The external supersonic diffuser of the axisymmetric spike and two-dimensional inlets turn the flow away from the inlet axis. The start of the throat section accepts the flow from the external supersonic diffuser and then turns the flow through the curving of the surfaces of the centerbody and cowl interior. The discussion of the throat section uses the term "centerbody" which originated from consideration of an axisymmetric spike inlets in which the axisymmetric spike and interior surfaces created a body of revolution about the axis-of-symmetry. While this still applies to the axisymmetric spike inlets modeled within SUPIN, the term "centerbody" is also used for the modeling of the throat section of the two-dimensional inlets to maintain commonality with the modeling of the axisymmetric spike inlet. For two-dimensional inlets, the "centerbody" is technically a system of planar ramps which may be flat or curved. For the two-dimensional bifurcated-duct inlet, the mirroring of the ramp system could be considered as a centerbody. The term "cowl interior" is applicable to both axisymmetric spike and two-dimensional inlets.

A schematic of the subsonic throat section geometry model is shown in Figure 8.5. This geometry model is used when the input factor $K_{thrt} = 9$ is specified. In previous versions of SUPIN, the geometry model invoked with $K_{thrt} = 5$, which will be discussed in Subsection 9.1, was used to create the throat section for external-compression inlets. However, that model locates the geometric throat station TH downstream of shoulder of the centerbody. For an external-compression inlet, the correct location for the geometric throat is about the cowl lip interior. Thus, the geometry model with $K_{thrt} = 9$ was created to specifically model the throat section for external-compression, axisymmetric spike and two-dimensional inlets. While the geometry model with $K_{thrt} = 5$ could still be used, it is strongly recommended that the geometry model discussed in this section with $K_{thrt} = 9$ be used for external-compression inlets.

The geometry model involves explicitly specifying the lengths, angles, and area ratios that define the planar profiles for the centerbody and the cowl interior. These planar profiles are then extruded about the axis-of-symmetry for the axisymmetric spike inlet or in the z-direction over the span of the capture width (w_{cap}) for the two-dimensional inlets to form the surfaces of the centerbody and cowl interior. The profile for the centerbody starts at point $(x,y)_{cb1}$ and ends at point $(x,y)_{cbSD}$. The profile for the cowl interior starts at point $(x,y)_{clin}$ and ends at point $(x,y)_{cwSD}$. The abbreviations "cb" and "cw" in the subscripts indicate the centerbody and cowl interior, respectively.

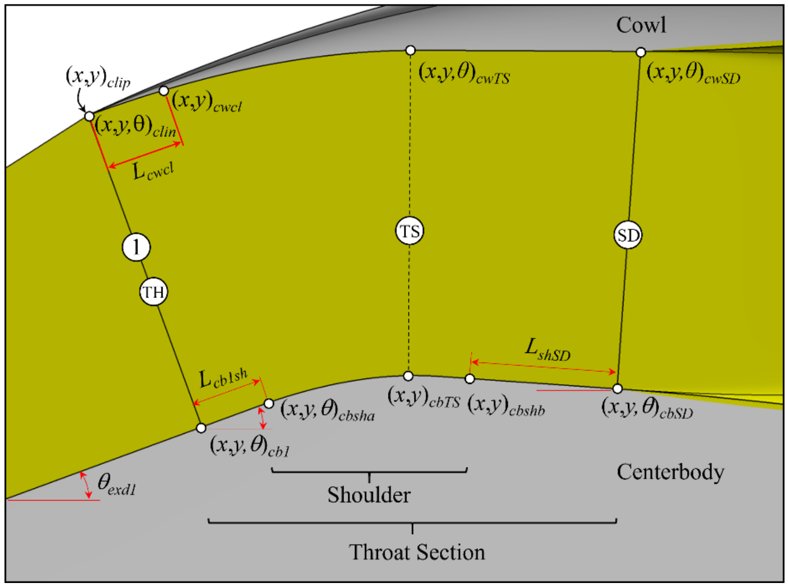

Figure 8.5.—Geometry model for the subsonic throat section for external-compression, axisymmetric spike, and two-dimensional inlets.

For this geometry model, the width of the throat section for the two-dimensional inlets is uniform and equal to the capture width (w_{cap}). The shape of the centerbody and cowl profiles establish the variation of the cross-sectional area through the throat section. With the geometry throat just downstream of station 1, the throat section may or may not provide significant levels of subsonic diffusion. At the least, the cross-sectional area should not decrease through the throat section and the use of a constant-area throat section is one approach. In this case, the throat section works to turn the flow. However, another valid approach is to increase the cross-sectional area through the throat section to provide some accounting for boundary-layer growth or some subsonic diffusion.

The geometry model first defines the planar profile of the centerbody, which can consist of up to three segments. The first segment is a line which starts at the point $(x,y)_{cb1}$ and ends at the point at the start of the centerbody shoulder $(x,y)_{cbsha}$. The slope of the line is established as

$$\theta_{cb1} = \theta_{exd1} + \Delta\theta_{cb1} \tag{8-1}$$

Where θ_{exd1} is the slope of the centerbody at the end of the external supersonic diffuser and $\Delta\theta_{cb1}$ is a specified change in slope of the centerbody profile at station 1. The length of the first segment of the centerbody is the length L_{cb1sh}. The coordinates for the start of the shoulder are calculated as

$$\begin{aligned} x_{cbsha} &= x_{cb1} + L_{cb1sh}\cos\theta_{cb1} \\ y_{cbsha} &= y_{cb1} + L_{cb1sh}\sin\theta_{cb1} \end{aligned} \tag{8-2}$$

A value for $L_{cb1sh} = 0$ is allowed in this geometry model, which would place $(x,y)_{cbsha} = (x,y)_{cb1}$.

The second segment of the centerbody profile defines the shoulder of the centerbody. The shoulder is modeled as a smooth curve using a four-point NURBS curve. The slope at the start of the shoulder is θ_{cbsha}. The input $\Delta\theta_{cbsha}$ is the change in the slope of the centerbody at the start of the shoulder. The slope of the profile at the start of the shoulder is calculated as

$$\theta_{cbsha} = \theta_{cb1} + \Delta\theta_{cbsha} \tag{8-3}$$

The shoulder is modeled as a four-point NURBS curve with the interior control points evenly spaced between the end control points. The endpoint of the shoulder is the coordinate $(x,y)_{cbshb}$ calculated as

$$x_{cbshb} = x_{cbsha} + \Delta x_{cbsh}$$
$$y_{cbshb} = y_{cbsha} + \Delta y_{cbsh} \tag{8-4}$$

where the incremental coordinate distances are Δx_{cbsh} and Δy_{cbsh} and are input factors. One requirement of the geometry model is that $\Delta x_{cbsh} > 0$ so that a shoulder can be properly defined. The slope at the end of the shoulder at point $(x,y)_{cbshb}$ is specified as θ_{cbSD}, which also defines the slope of the line defining the third segments of the centerbody extending between points $(x,y)_{cbshb}$ and $(x,y)_{cbSD}$. A condition is specified such that $\theta_{cbSD} \leq 0$.

The point $(x,y)_{cbTS}$ is defined as the point along the centerbody at which the slope of the centerbody profile is zero. Since $\theta_{cbsha} > 0$ and $\theta_{cbSD} \leq 0$, the point $(x,y)_{cbTS}$ is located within the shoulder profile. If $\theta_{cbSD} = 0$, then the shoulder point $(x,y)_{cbTS}$ is placed at the end of the shoulder. A bisection search method is used within SUPIN to find the point $(x,y)_{cbTS}$ along the four-point NURBS curve.

The change in slope of the centerbody shoulder segment helps turn the flow within the throat section. If the change in slope of the shoulder occurs too rapidly, the boundary layers on the shoulder could degrade and approach separation. One possible approach for defining acceptable values for $(\Delta x,\Delta y)_{cbsh}$ involves approximating the NURBS curve as a circular arc in which the radius of curvature of the arc is four times the height of the cross-section at station 1 ($r = 4\ h_1$). SUPIN performs this calculation and writes the corresponding values of $(\Delta x,\Delta y)_{cbsh}$ within the output data for the throat section in the output data file (SUPIN.Out.txt).

The third segment of the centerbody profile is a line that extends from the end of the shoulder to station SD and has a slope of $\theta_{cbSD} <= 0$. The distance of the line segment is L_{shSD} and the model does allow $L_{shSD} = 0$. The coordinates of the point $(x,y)_{cbSD}$ defining the location of station SD on the centerbody are calculated as

$$x_{cbSD} = x_{cbshb} + L_{shSD} \cos\theta_{cbSD}$$
$$y_{cbSD} = y_{cbshb} + L_{shSD} \sin\theta_{cbSD} \tag{8-5}$$

The input factors for the centerbody of the throat section are listed in Table 8.1. The angular input factors $\Delta\theta_{cb1}$, $\Delta\theta_{cbsha}$, and θ_{cbSD} are specified with units of degrees. The input factors for the lengths L_{cb1sh}, Δx_{cbsh}, Δy_{cbsh}, and L_{shSD} are specified as normalized by the reference dimension D_{ref}.

The profile of the cowl interior consists of up to two segments. The first segment is a line that starts at the cowl lip interior point $(x,y)_{clin}$ and has an initial slope specified by θ_{clin}. The length of the line is L_{cwcl} and can be of zero length (e.g., $L_{cwcl} = 0$). The coordinates of the point at the end of this first segment are calculated as

$$x_{cwcl} = x_{clin} + L_{cwcl} \cos\theta_{clin}$$
$$y_{cwcl} = y_{clin} + L_{cwcl} \sin\theta_{clin} \tag{8-6}$$

TABLE 8.1.—INPUT FACTORS FOR THE CENTERBODY FOR THE SUBSONIC THROAT SECTION MODEL

Factor	Inputs	Description
$\Delta\theta_{cb1}$	`dthcb1`	Change in the slope of centerbody at station 1 (deg)
L_{cb1sh}	`FLcb1sh`	Length along the centerbody from station 1 to start of shoulder (normalized by D_{ref})
$\Delta\theta_{cbsha}$	`dthsha`	Change in slope at the start of the centerbody shoulder (deg)
Δx_{cbsh}	`Fdxcbsh`	Axial distance between start and end of the shoulder (normalized by D_{ref})
Δy_{cbsh}	`Fdycbsh`	Vertical distance between start and end of the shoulder (normalized by D_{ref})
θ_{cbSD}	`thcbSD`	Slope of the centerbody at the end of the shoulder and station SD (deg)
L_{shSD}	`FLshSD`	Length from the end of the shoulder to station SD (normalized by D_{ref})

TABLE 8.2.—INPUT FACTORS FOR THE COWL INTERIOR PROFILE OF THE SUBSONIC THROAT SECTION MODEL

Factor	Inputs	Description
L_{cwcl}	`FLcwcl`	Length of straight segment after the cowl lip interior (normalized by D_{ref})
θ_{cwSD}	`thcwSD`	Slope of the cowl interior at station SD (deg)
A_{SD}/A_1	`FaSDa1`	Ratio of the cross-sectional area at station SD to area at station 1
M_{SD}	`FmachSD`	Mach number for station SD
F_{cwds}	`Fcwds`	Vertical displacement of the cowl at station SD to account for boundary layer (ft)

The second segment of the cowl interior profile is modeled as a four-point NURBS curve with an initial slope of θ_{clin} and an end-slope of θ_{cwSD} at the point $(x,y)_{cwSD}$. The point $(x,y)_{cwSD}$ is established along a line passing through and normal to point $(x,y)_{cbSD}$ with a height of h_{SD}. The value of the height at station SD (h_{SD}) is computed from the computed cross-sectional area at station SD, A_{SD}. For an axisymmetric spike inlet, the cross-section at station SD is annular. For the two-dimensional inlets, the cross-section is rectangular. Two approaches are possible for computing the area A_{SD}. The first uses the specified area ratio A_{SD}/A_1. An alternative to specifying the area ratio A_{SD}/A_1 is to specify the mass-averaged Mach number M_{SD} and then use flow continuity (Eq. (2-32b)) to compute the cross-sectional area A_{SD}. The calculation requires calculating or assuming a value of the total pressure p_{tSD}. The flow continuity must also account for bleed flow being extracted between stations 1 and SD (W_{b1SD}).

The choice of the value for A_{SD} or M_{SD} in the design of the throat section is driven by how one wishes to have the internal diffuser diffuse the subsonic flow. One may wish to have a constant-area or nearly constant-area throat section, and so, M_{SD} would not decrease much from M_1. One may wish the throat section to perform some diffusion to a certain Mach number $M_{SD} < M_1$. For example, one may wish a linear variation from M_1 through M_{SD} and M_2 along the length of the internal diffuser.

The input factors for the cowl interior of the throat section are listed in Table 8.2. The input factor for the length L_{cwcl} is specified as normalized by the reference dimension, D_{ref}. The slope θ_{cwSD} is specified in units of degrees. The use of the area ratio A_{SD}/A_{TH} or the Mach number M_{SD} is determined by the sign of the input factor FmachSD for the Mach number M_{SD}. For example, if the input factor FmachSD < 0, then the input factor A_{SD}/A_1 is used to establish the area A_{SD}. However, if FmachSD > 0, then M_{SD} = FmachSD, and Equation (2-32b) is solved to establish A_{SD}.

An example of the input data block for the subsonic throat section geometry model is presented in Table 8.3. The format of this input data block is associated with $K_{thrt} = 9$. The input factor FptSDpt1 provides a means of specifying the total pressure ratio across the throat section. If FptSDpt1 > 0, then p_{tSD}/ p_{t1} = FptSDpt1.

TABLE 8.3.—EXAMPLE INPUT DATA BLOCK FOR THE SUBSONIC THROAT SECTION MODEL FOR EXTERNAL-COMPRESSION, AXISYMMETRIC SPIKE AND TWO-DIMENSIONAL INLETS

```
DataID.   Subsonic Throat Section
  8
Kthrt       FptSDs1      FptsegB    FptsegC
  9        -0.99000     -0.99500   -1.00000
 dthcb1      dthsha       thcbSD
  0.000       0.000       -5.000
FLcb1sh     Fdxcbsh      Fdycbsh     FLshSD
 0.2000      0.5000       0.0000     0.5000
 FLcwcl      thcwSD       FaSDa1     FmachSD
 0.1000      -5.000       1.0300    -1.3000
  Fcwds
 0.0500
```

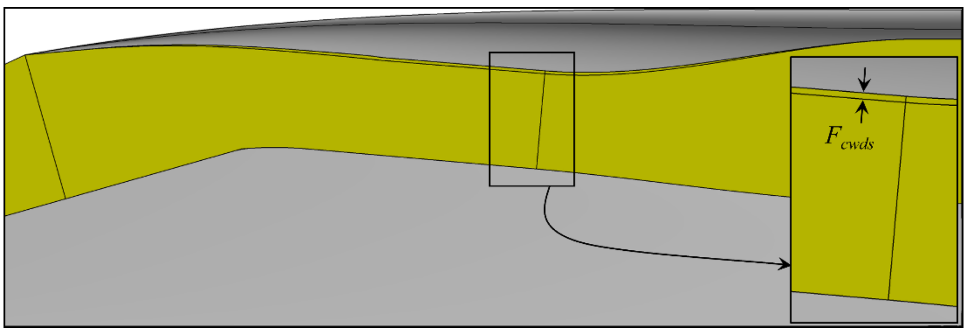

Figure 8.6.—Modifications of the cowl profile using F_{cwds}.

The input factor $\boldsymbol{F_{cwds}}$ provide a means for adjusting the cowl profiles to account for the displacement thickness of the boundary layers through the throat section. The value of F_{cwds} is specified in units of feet and controls the distance that the cowl interior profile at station SD is moved outward. This distance should be on the order of the displacement thickness of the boundary layers and can be obtained from preliminary viscous CFD simulations or from other boundary layer estimation methods. Thus, accounting for the growth of the boundary layers may involve some iterations within the design process. Between the cowl lip interior point and station SD, the outward displacement of the throat section cowl interior profile is linearly interpolated. Likewise, the displacement of the cowl interior profile of the subsonic diffuser is linearly interpolated between station SD and the engine face. This modification essentially increases the cross-sectional areas at station SD. The images of Figure 8.6 illustrate the effect of this modification.

8.5 Mahoney Throat Section Model

This throat section geometry model implements an approach for designing the throat section as documented in the book "*Inlets for Supersonic Missiles*" by Mahoney (Ref. 3). The book discussed inlets intended for ramjet missiles operating at freestream Mach numbers up to $M_0 = 5$. For such inlets, simplicity of the inlets and stability of the inlet flow were of high interest, rather than high efficiency. Thus, the inlets were designed to operate as external-compression inlets with a terminal shock wave system that allowed subsonic spillage. As discussed above, the Mach number at the end of the external supersonic diffuser (M_{EX}) influences the character of the terminal shock wave and its interaction with the boundary layers formed on the surfaces of the external supersonic diffuser. As the freestream Mach number exceeds Mach 2.0 and approaches $M_0 = 5.0$, the turning of the external supersonic diffuser increases as the difference between M_0 and M_{EX} increases. The greater turning of the flow means that the angle of the flow approaching the cowl lip from the external supersonic diffuser also increases. A feature of the Mahoney model is that the angle of the cowl lip interior (θ_{clin}) is matched to the angle of the flow approaching the cowl lip from the external supersonic diffuser. The increase in the cowl lip interior angle results in the increase of the cowl lip exterior angle (θ_{clex}), which results in increased cowl exterior wave drag. The approach taken within the Mahoney model is to select the Mach number M_{EX} to keep the increase of the cowl exterior wave drag within reason as the freestream Mach number (M_0) increases. Within Reference 3, example inlets for $M_0 = 2$, 3, and 4 use values of $M_{EX} = 1.47$, 1.99, and 2.47, respectively. However, these values of M_{EX} exceed the limit of $M_{EX} = 1.3$ for boundary-layer separation, as discussed in Subsection 8.3. Thus, the approach of the Mahoney model is to accept the boundary-layer separation as a compromise to reduce cowl wave drag. The boundary-layer separation becomes considerable and likely does not reattach. Thus, the terminal shock wave structure is characterized as a shock wave train terminal shock wave system as described in Subsection 8.3 and illustrated in the right-hand-side image of Figure 8.4. The shock wave train is expected to extend into and be contained within the throat section. While the shock wave train includes supersonic flow and performs supersonic compression within the throat section, the inlet is still considered an external-compression inlet due to the ability of the terminal shock wave system to spill subsonic flow past the cowl lip through the separated boundary layers on the cowl interior within the shock wave train and a likely detached shock wave about the cowl lip. The subsonic spillage acts to balance the captured flow within the inlet with the engine flow demands. Downstream of the terminal shock wave train, subsonic conditions are formed near the end of the throat section due to a final normal shock wave. Thus, subsonic flow is delivered to the subsonic diffuser and engine.

The shock wave train terminal shock wave system described in the previous paragraph does include considerable losses in total pressure recovery. The example inlets of Reference 3 for $M_0 = 2$, 3, and 4 result in values of inlet total pressure recovery as low as $p_{t2}/p_{t0} = 0.88$, 0.69, and 0.47, respectively. However, such values of recovery may be considered acceptable for a missile application in which simplicity of the inlet system and stability of an external-compression inlet is desired. An alternative is to incorporate some bleed systems to reduce boundary-layer separation and perhaps change the shock wave train terminal shock wave to a strong oblique terminal shock wave. A more complicated alternative would be to incorporate internal supersonic compression as will be described in Section 9.0. This alternative would likely involve bleed systems and variable geometry.

The stations and dimensions of the Mahoney model are illustrated in Figure 8.7. The throat section starts at station 1 with its inflow from the external supersonic diffuser. The planar profile of the centerbody starts at point $(x,y)_{cb1}$ with a slope of θ_{cb1}. Station 1 extends between point $(x,y)_{cb1}$ and $(x,y)_{clip}$ and is also the station TH of the geometric throat of the inlet. The one-dimensional Mach number at station 1 is set to the Mach number at the end of the external supersonic diffuser, or $M_1 = M_{EX}$. The throat section accomplishes the turning of the flow over its length through the curving of the centerbody and cowl surfaces. The curving of the centerbody surface is modeled as a planar profile consisting of a circular arc or ogive that curves the centerbody from the slope at the end of the external supersonic diffuser (θ_{cb1}) at station 1 to an axial slope of $\theta_{cbTS} = 0$ degrees at station TS. The radius of the ogive segment (r_{circ}) is calculated as

$$r_{circ} = Fr_{circ}\, h_1 \tag{8-7}$$

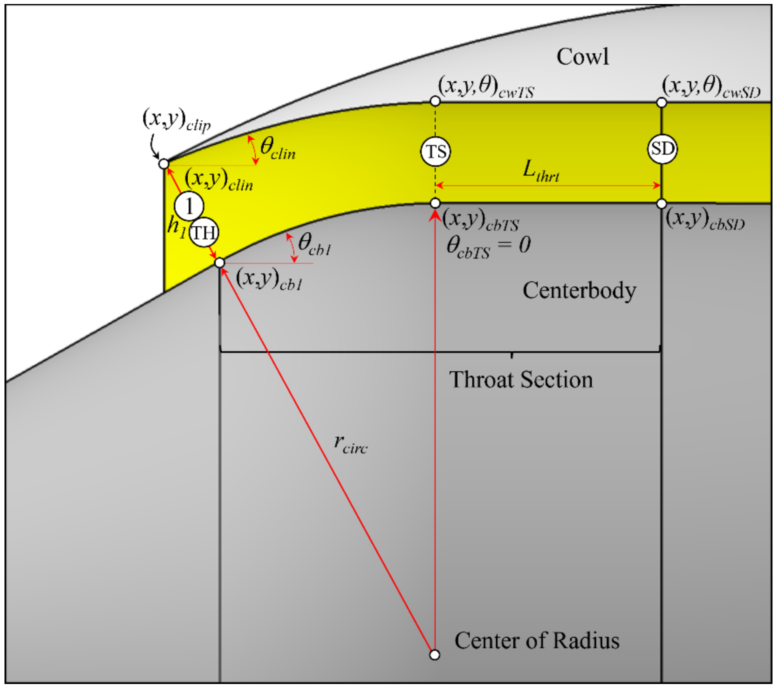

Figure 8.7.—Modeling of the Mahoney throat section model (K_{thrt} = 4).

Where Fr_{circ} is a factor of the height of the inlet flowpath at station 1, which is h_1. Reference 3 suggests a value of $Fr_{circ} = 4$ as a reasonable choice for gradual turning. The radius of the circular ogive (r_{circ}) and the slopes θ_{cb1} and $\theta_{cbTS} = 0$ degrees determine the coordinates $(x,y)_{cbTS}$ defining the location of the centerbody shoulder.

The point $(x,y)_{cwTS}$ on the cowl interior is established with $x_{cwTS} = x_{cbTS}$ and y_{cwTS} determined by the area ratio A_{TS}/A_1. As specified with the input factor FA_{TS}/A_1. The cross-sectional area at station TS is computed as

$$A_{TS} = (FA_{TS}/A_1)\, A_1 \tag{8-8}$$

The shape of the cross-section is used to establish the height h_{TS} and y_{cwTS} is computed as

$$y_{cwTS} = y_{cbTS} + h_{TS} \tag{8-9}$$

Reference 3 suggests a constant area between stations 1 and TS, which implies $A_{TS}/A_1 = 1.0$; however, it may be desirable to specify $A_{TS}/A_1 > 1.0$ to allow area expansion to account for boundary-layer growth between stations 1 and TS. For two-dimensional inlets the cross-sections through the throat section are rectangular with the width equal to the capture width of the external supersonic diffuser. For axisymmetric spike inlets, the cross-sections are annular.

The planar profile of the cowl interior starts at point $(x,y)_{clin}$ with a slope of θ_{clin} and ends at point $(x,y)_{cwTS}$. The slope of the cowl interior at station TS is set to $\theta_{cwTS} = 0$ degrees to match the slope at the centerbody. The model sets the cowl lip interior angle equal to the local flow angle at the cowl lip. This is specified in the input data file by setting the input factor for the cowl lip interior angle (θ_{clin}) to a negative number such that $\theta_{clin} < -10.0$ as described in Subsection 8.2. For a two-dimensional, external supersonic diffuser, the cowl lip interior angle is equal to the angle at the end of the external supersonic diffuser, $\theta_{clin} = \theta_{cb1}$. For an axisymmetric spike inlet, the local flow angle and slope at the cowl lip is lower than the slope of the centerbody at station 1, $\theta_{clin} < \theta_{cb1}$. The curved planar profile of the cowl interior is modeled as a four-point NURBS curve as described in Appendix A. The inputs are the coordinates and slopes of the start and end points, $(x,y,\theta)_{clin}$ and $(x,y,\theta)_{cwTS}$, respectively. It is possible to specify the cowl lip interior angle to be mis-aligned with the local flow at the cowl lip by specifying the desired angle for θ_{clin}. A value of θ_{clin} less than the local flow angle will result in a deflection of the flow at the cowl lip and the creation of an oblique shock wave. If the conditions are right, then a strong oblique terminal shock wave may be created; however, bleed systems may be needed to control shock wave/boundary layer interactions and reduce separation to establish the oblique terminal shock wave.

The streamwise distance between stations 1 and TS establishes the minimum length for the throat section. An aft segment of the throat section continues from station TS to the start of the subsonic diffuser at station SD. This aft segment has a zero slope on the centerbody and has a length L_{thrt} specified by the input factor F_{Lthrt}, which is normalized by h_1. Thus,

$$L_{thrt} = F_{Lthrt}\, h_1 \tag{8-10}$$

For the example inlets of Reference 3, the suggested values of F_{Lthrt} for freestream Mach numbers of M_0 = 2.0, 3.0, and 4.0 are F_{Lthrt} = 0.0, 4.0, and 8.0, respectively. As mentioned above, the value of F_{Lthrt} does not include the length from station 1 to TS. Thus, a value of FL_{thrt} = 0.0 will result in a throat section in which stations TS and SD are coincident. The length of the throat section is determined by the desire to fully contain the length of the shock wave train. As the inflow Mach number (M_1) increases, the length of the terminal shock wave train system will increase, which is reflected in the values for FL_{thrt} suggested by Reference 3.

A line segment defines the shape of the planar profile of the centerbody between stations TS and SD. The cross-sectional area at station SD (A_{SD}) is specified by the input factor FA_{SD}/A_{TS}, such that,

$$A_{TS} = (FA_{SD}/A_{TS})\, A_{TS} \tag{8-11}$$

The factor $FA_{SD}/A_{TS} \geq 1.0$ is chosen to set a constant area to diffusive duct based on the desires of an increase in the cross-sectional area between stations TS and SD.

Mahoney suggested setting the cowl exterior angle (θ_{clex}) to be a 5-degree increment of the cowl lip interior angle (θ_{clin}). Within SUPIN, this can be specified by setting the input factor for the cowl lip exterior angle to θ_{clex} = -5.0, as discussed in Subsection 8.2. If other values of the cowl lip interior and exterior angles are desired, they can be set by directly specifying them with the cowl lip interior and exterior angle input factors as described in Subsection 4.9.

Table 8.4 lists the input factors for the Mahoney throat section model. Table 8.5 provides a sample input data block. The Mahoney throat section model is chosen within SUPIN through specification of K_{thrt} = 4.

TABLE 8.4.—INPUT FACTORS FOR THE GEOMETRY OF THE MAHONEY THROAT SECTION MODEL

Factor	Input	Description
FL_{thrt}	`FLthrt`	Length of throat section normalized by the height of station 1, h_1
Fr_{circ}	`Frcirc`	Radius of circular arc of centerbody and cowl normalized by h_1
FA_{TS}/A_1	`FaTSa1`	Ratio of cross-sectional area at station TS to area at station 1
FA_{SD}/A_{TS}	`FaSDaTS`	Ratio of cross-sectional area at station SD to area at station TS

TABLE 8.5.—SAMPLE INPUT BLOCK FOR THE MAHONEY THROAT SECTION MODEL

```
DataID.  Mahoney Throat Section
  8
Kthrt   FptTSpt1   FptSDptTS     FptsegC
  4     -0.99000    -0.99500    -1.00000
 FLthrt      Frcirc    FaTSa1      FaSDaTS
8.00000    4.00000    1.0000       1.0000
```

8.6 Subsonic Diffusers

The subsonic diffuser decelerates and compresses the subsonic flow between stations SD and 2. The design and modeling of the throat section establishes the area A_{SD} and Mach number M_{SD} at station SD. The engine-face geometric properties establish the shape and dimensions of the engine face, and the engine flow conditions establish the Mach number M_2 at the engine face. Establishing the length of the subsonic diffuser was discussed in Section 4.12. The following subsections discuss geometry models for establishing the shapes of the surfaces of the subsonic diffuser for the axisymmetric spike, two-dimensional single-duct, and two-dimensional bifurcated-duct inlets.

8.6.1 Subsonic Diffuser for the Axisymmetric Spike Inlet

The geometry model for the subsonic diffuser for the axisymmetric spike inlet defines the planar profiles for the centerbody and cowl interior for the subsonic diffuser. The surfaces of the centerbody and cowl interior for the subsonic diffuser are formed by extruding these profiles about the inlet axis-of-symmetry. The geometry model is illustrated in Figure 8.8. The input factors defining the length of the subsonic diffuser (L_{subd}) were discussed in Subsection 4.12.

The planar profile for the cowl interior for the subsonic diffuser is created in the same manner as described in Subsection 5.4 for the axisymmetric pitot inlet. The profile for the cowl interior starts with a four-point NURBS curve that starts at the point $(x,y)_{cwSD}$ with the slope θ_{cwSD} and ends at point $(x,y)_{cwX}$ with a slope of $\theta_{cwX.}$ The optional second segment of the profile of the cowl interior is a line between points $(x,y)_{cwX}$ and $(x,y)_{TEF}$, which is the top of the engine face. The slope of the line equals the angle of the engine face axis, where $\theta_{cwX} = \theta_{TEF} = \theta_{EF} = 0$ degrees. The length of the line is L_{cwX} and a value of $L_{cwX} = 0$ is allowed, which would make point $(x,y)_{cwX}$ coincident with point $(x,y)_{TEF}$. The input factors for the cowl interior profile are F_{NcwSD}, F_{NcwX}, and F_{LcwX} and are listed in Table 5.3. A value of $F_{LcwX} \leq 0$ is used to indicate that $L_{cwX} = 0$.

The planar profile of the centerbody for the subsonic diffuser is created using a combination of a four-point NURBS curve and a line in much the same manner as the cowl interior. The NURBS curve starts at point $(x,y)_{cbSD}$ with the slope θ_{cbSD} and ends at point $(x,y)_{cbX}$ with a slope θ_{cbX}. The optional second segment of the profile of the centerbody is a line between points $(x,y)_{cbX}$ and $(x,y)_{HEF}$, which is at the hub of the engine face. The slope of the line segment equals the angle of the engine face axis, $\theta_{HEF} = \theta_{EF} = 0$ degrees. The length of the line is L_{cbX} and a value of $L_{cbX} = 0$ is allowed, which would make point $(x,y)_{cbX}$ coincident with point $(x,y)_{HEF}$. The slope θ_{cbX} only applies to the end NURBS curve and does not have to match the slope of the second linear segment. This allows a discontinuity in the slope of the centerbody profile at point $(x,y)_{cbX}$. In the example inlet shown in Figure 8.8, $\theta_{cbX} = -10.0$ degrees. Such a discontinuity of the slope at point $(x,y)_{cbX}$ has been used in past inlets in which the forward segment of the centerbody translated about a cylindrical, constant-radius aft segment of the centerbody, which would be the segment of between point $(x,y)_{cbX}$ and the engine face point $(x,y)_{HEF}$. Such translation of the centerbody was used to adjust the cross-section area distribution of the inlet for off-design operation.

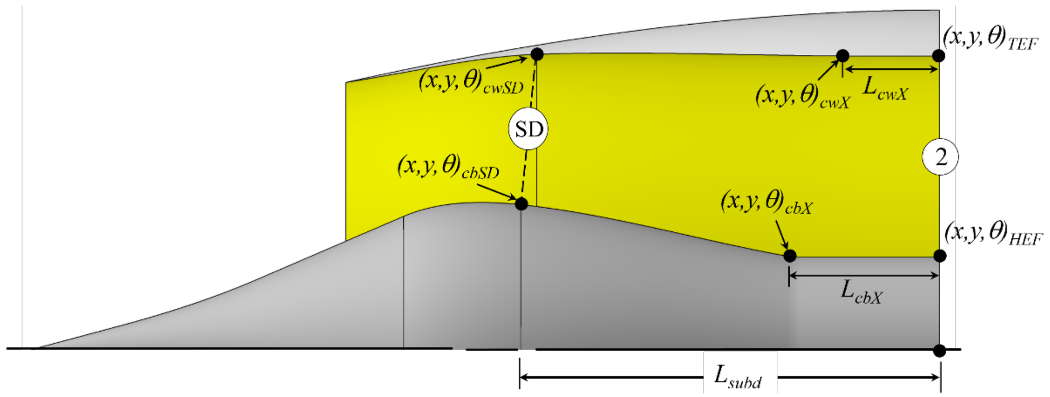

Figure 8.8.—Geometry model for the subsonic diffuser for an axisymmetric spike inlet (K_{typ} = 3).

TABLE 8.6.—INPUT FACTORS FOR THE PROFILE OF THE CENTERBODY OF THE SUBSONIC DIFFUSER FOR AN AXISYMMETRIC SPIKE INLET

Factor	Inputs	Description
θ_{cbX}	`thcbX`	Slope of the centerbody at point cbX (deg)
F_{NcbSD}	`FNcbSD`	Factor for NURBS interior control point at station SD
F_{NcbX}	`FNcbX`	Factor for NURBS interior control point at point cbX
F_{LcbX}	`FLcbX`	Length of straight-line segment on centerbody normalized by D_{ref}

TABLE 8.7.—EXAMPLE INPUT DATA BLOCK FOR THE SUBSONIC DIFFUSER OF AN AXISYMMETRIC SPIKE INLET

```
DataID.  Subsonic Diffuser
 10
Ksubd     KLsubd    FLsubd    theqsd    Fpt2ptSD
  3         2      1.50000     3.000    -0.97500
FNcbSD     FNcbX     thcbX     FLcbX
0.3333    0.3333    10.000    0.2500
FNcwSD     FNcwX     FLcwX    Ksdprp    Ksdvar
0.3333    0.3333    0.1200      2          1
```

The input factors for the centerbody profile are F_{NcbSD}, F_{NcbX}, θ_{cbX}, and F_{LcbX} and are listed in Table 8.6. The interior control points for the four-point-NURBS curve for the first segment of the subsonic diffuser are placed according to the input factors F_{NcbSD} and F_{NcbX}, which are fractions of the distance of a line from $(x,y)_{cbSD}$ to $(x,y)_{cbX}$. For example, the values of $F_{NcbSD} = 0.33$ and $F_{NcbX} = 0.33$ place the interior control points approximately one-third the distance and are reasonable default values. The unit for θ_{cbX} is degrees. The input value for F_{LcbX} indicates the distance L_{cbX} as normalized by the reference length D_{ref}. A value of $F_{LcbX} \leq 0$ is used to indicate that $L_{cbX} = 0$.

Table 8.7 lists an example input data block for the subsonic diffuser. The input factor $K_{subd} = 3$ indicates that the block specifies the inputs for the subsonic diffuser for an axisymmetric spike inlet. The input factors K_{sdprp} and K_{sdvar} provide a means to specify an area distribution through the subsonic diffuser. These input factors were introduced in Subsection 4.12, and Table 4.21 lists the options for these input factors. For the axisymmetric spike inlet, the area distribution is imposed by adjusting the cowl interior profile through the subsonic diffuser while keeping the centerbody profile fixed. The area distribution is applied between points $(x,y)_{cwSD}$ and $(x,y)_{cwX}$ while maintaining the coordinates of the line.

8.6.2 Subsonic Diffuser for the Two-Dimensional, Single-Duct Inlet

The subsonic diffuser for the two-dimensional, single-duct inlet involves a transition in the cross-section from a rectangle at station SD to the shape of the cross-section at the engine face station 2. The possible shapes of the cross-section at the engine face were discussed in Subsection 4.13 and can include circular, annular, rectangular, or elliptical. For the two-dimensional inlet, the engine axis can be offset within the symmetry plane from the inlet axis and has the coordinate y_{EF}, as illustrated in Figure 8.2. The placement of the engine face influences the shape of the cowl exterior and the resulting cowl wave drag, which then affects the integration of the inlet with the aircraft.

The images of Figure 8.2 show an inlet in which the subsonic diffuser transitions in cross-sectional shape from a rectangular cross-section at station SD to an annular cross-section at the engine face. The subsonic diffuser duct consists of three surfaces joined at their edges. The three surfaces originate from the flat segments that form the bottom, side, and top of the throat at station SD. The three surfaces transition in shape from a flat cross-profile to a segment of a circular arc at the engine face.

An example of the input data block for the subsonic diffuser for the two-dimensional inlet is shown in Table 8.8. The input factor $K_{subd} = 4$ indicates that the block specifies the inputs for the subsonic diffuser of a two-dimensional, single-duct inlet. The factors define the cowl interior surfaces of the subsonic diffuser. The subsonic diffuser may have a straight section just before the engine face with the length specified by the input factor F_{LcwX}, which is normalized by the reference dimension, D_{ref}. An input of $F_{LcwX} \leq 0$ indicates that $L_{cwX} = 0$. The input factors F_{NcwSD} and F_{NcwX} influence the location of the interior control points for four-point NURBS curves defining the edges of the three surfaces between station SD and the start of the straight section. Each of the three surfaces is formed by performing three-dimensional transfinite interpolations of grid coordinates distributed along the four edges of each of the three surfaces. The input factors K_{sdprp} and K_{sdvar} for setting the area distribution through the subsonic diffuser are not yet functional for this subsonic diffuser.

A two-dimensional, single-duct inlet may also have a rectangular engine face, such might be the case for an inlet for a ramjet engine. Figure 8.9 shows an example of such an inlet. The subsonic diffuser is formed with a centerbody (bottom), sidewall, and cowl interior (top) surfaces similar to the form of the throat section. The bottom and top surfaces are generated from planar profiles that are extruded in the cross-stream (z-direction). Table 8.9 provides an example input data block for the rectangular subsonic diffuser. The input factor $K_{subd} = 8$ indicates that the block specifies the inputs for the subsonic diffuser of a two-dimensional inlet with a rectangular subsonic diffuser. The other input factors influence the shape of the four-point NURBS curve and straight sections that define the profile of the bottom and top surfaces. The input factors K_{sdprp} and K_{sdvar}, as described previously, are functional for the rectangular subsonic diffuser.

TABLE 8.8.—EXAMPLE INPUT DATA BLOCK FOR THE SUBSONIC DIFFUSER FOR A TWO-DIMENSIONAL, SINGLE-DUCT INLET

```
DataID.  Subsonic Diffuser
 10
Ksubd    KLsubd    FLsubd    theqsd    Fpt2ptSD
  4         5      4.0000     3.000    -0.97500
FNcwSD    FNcwX     FLcwX    Ksdprp      Ksdvar
0.3333   0.3333    0.2000       0           0
```

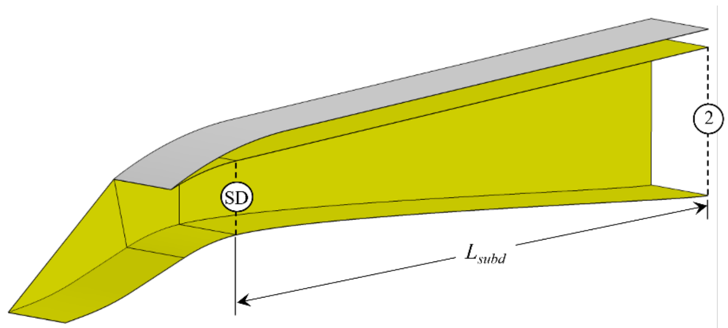

Figure 8.9.—A two-dimensional, single-duct inlet with a rectangular subsonic diffuser and engine face.

TABLE 8.9.—EXAMPLE INPUT DATA BLOCK FOR THE SUBSONIC DIFFUSER FOR A RECTANGULAR ENGINE FACE (K_{typ} = 2 AND K_{subd} = 8)

```
DataID.  Subsonic Diffuser
 10
Ksubd    KLsubd    FLsubd    theqsd    Fpt2ptSD
  8        1      4.50000     3.000    -0.97500
FNcbSD    FNcbX     FLcbX
0.3333   0.3333    0.2000
FNcwSD    FNcwX     FLcwX    Ksdprp     Ksdvar
0.3333   0.3333    0.2000       0          0
```

8.6.3 Subsonic Diffuser for the Two-Dimensional Bifurcated-Duct

The geometry model for the subsonic diffuser of a two-dimensional, bifurcated-duct inlet forms a three-dimensional duct that transitions from a rectangular cross-section at station SD to a semi-circular cross-section of the engine face at station 2. The semi-circular cross-section conforms to half of an annular engine-face consistent with a turbine engine with a spinner. The subsonic diffuser duct consists of three surfaces joined at their streamwise edges. The bottom surface retains a planar character and is generated by linear extrusion of a planar profile. This surface ends ahead of the spinner to create an open area for the two inlet bifurcations to mix ahead of the engine face. The side and top surfaces continue the sidewall and cowl interior between station SD and the engine face. The surfaces of the subsonic diffuser are illustrated in Figure 8.3 and Figure 8.10.

The centerbody surface is formed by defining a planar profile in the (x,y) plane between points $(x,y)_{cbSD}$ and $(x,y)_{cbX}$ and then extruding the profile in the z-direction through the width of the throat section. This planar profile is created using a four-point NURBS curve in the same manner as described previously. The input factors F_{NcbSD} and F_{NcbX}, along with the slope θ_{cbX} at the end of the profile act to establish the shape of the profile. The input factor F_{LcbX} sets the length L_{cbX} to place the point $(x,y)_{cbX}$ on the inlet axis upstream of the engine face point. The input factor F_{LcbX} is normalized by the reference dimension, D_{ref}. The length L_{cbX} provides the open region for the flow from the two bifurcated ducts to mix upstream of the engine face. The spinner extends into the mixing region. The input factor F_{LcbX} should be specified such that the length L_{cbX} is greater than the length of the spinner (L_{spin}) to provide clearance between the end of the centerbody and start of the spinner, as well as length for sufficient mixing of the flow from the two bifurcated ducts.

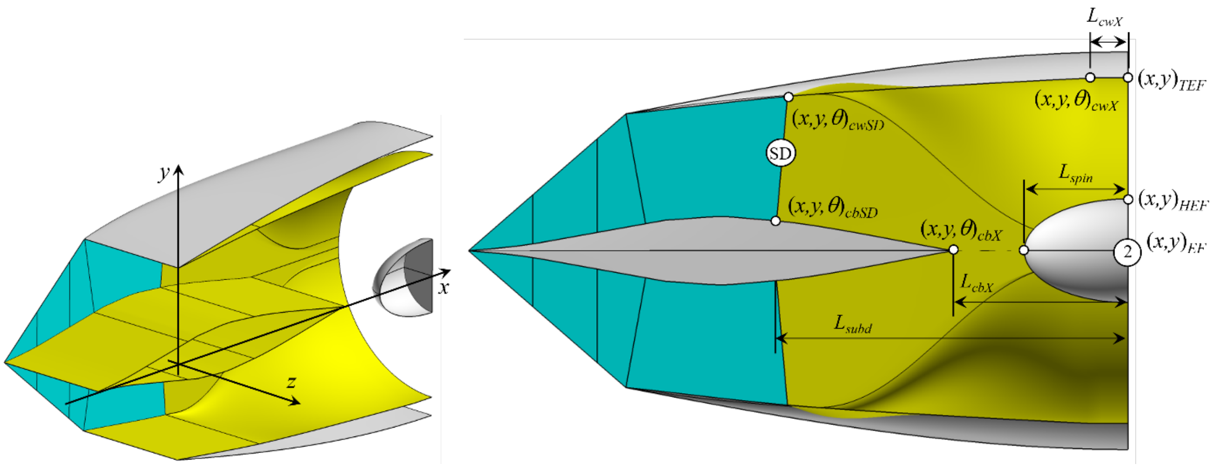

Figure 8.10.—Geometry model for the subsonic diffuser of a two-dimensional bifurcated-duct inlet (K_{typ} = 4 and K_{subd} = 5).

TABLE 8.10.—EXAMPLE INPUT DATA BLOCK FOR THE SUBSONIC DIFFUSER FOR A TWO-DIMENSIONAL BIFURCATED-DUCT INLET (K_{typ} = 4 AND K_{subd} = 5)

```
DataID.  Subsonic Diffuser
 10
Ksubd    KLsubd    FLsubd    theqsd    Fpt2ptSD
  5        1      4.50000     3.000    -0.97500
FNcbSD    FNcbX     thcbX     FLcbX
0.3333   0.3333    -5.000    0.2000
FNcwSD    FNcwX     FLcwX    Ksdprp     Ksdvar
0.3333   0.3333    0.2000      0           0
```

The planar profile at the symmetry plane at the top of the subsonic diffuser is generated using a four-point-NURBS curve and a line. The line is used to create a straight section ahead of the engine face. The curve is defined in much the same manner as for the previous subsonic diffusers. The length of the straight section just before the engine face is specified by the input factor F_{LcwX}, which is normalized by the reference dimension, D_{ref}. The input factors F_{NcwSD} and F_{NcwX} influence the location of the interior control points, as discussed in previously.

The side and top surfaces of the subsonic diffuser are constructed by performing three-dimensional transfinite interpolations of grid coordinates distributed along the four edges of each of the surfaces. Table 8.10 lists an example input data block for the subsonic diffuser of the two-dimensional bifurcated inlet, which specifies K_{subd} = 5. The input factors K_{sdprp} and K_{sdvar} for setting the area distribution through the subsonic diffuser are not yet functional for this subsonic diffuser.

8.7 Component and Entity Specifications

The profiles that define the geometry of the external supersonic diffuser, throat section, and subsonic diffuser components of the axisymmetric spike and two-dimensional inlets can be specified using the component and entity input factor option as introduced in Subsection 4.15. This approach for specifying geometry provides flexibility in defining geometry of the inlet components that can't be created using the models described in the previous subsections.

Such an approach is useful in the case that the geometry of the centerbody and cowl interior profiles are specified as list of (*x*,*y*) coordinates. For example, the inlet of Reference 4 provided geometry data for the Gulfstream/NASA Low-Boom Single-Stream (LBSS) axisymmetric spike inlet as a list of axial and radial coordinates for the planar profile of the axisymmetric centerbody and cowl interior. Figure 8.11 shows the curves for the profiles of the axisymmetric centerbody and cowl interior. The points in the image of Figure 8.11 indicate the coordinates that were provided. The coordinate points define linear and curved segments of the centerbody and cowl interior. The curved segments are modeled with cubic spline entities. The shaded image shows the resulting inlet. From these profiles, the external supersonic diffuser, throat section, and subsonic diffuser components and the related geometric properties are established. The following paragraphs discuss the methods used to establish the external supersonic diffuser, throat section, and subsonic diffuser.

For the external supersonic diffuser, the geometric information for the entities, such as the coordinate points discussed above, is provided through the input data block with DataID = 16. Within the input data block with DataID = 4 for the external supersonic diffuser, the use of the component and entity option is indicated by specifying the input factor K_{exd} = 8 as indicated in Table 4.12. Additional inputs of K_{exdop} and F_{exdop1} are needed to provide specific instructions on using the entities, as described in Table 8.11. For K_{exdop} = 0, the entities are defined using K_{comt} = 1, which indicates the geometry information defines just the external supersonic diffuser. Each entity is assumed to be a separate stage of the external supersonic diffuser. The endpoint of the last entity is assumed to be at station 1 defining the end of the external supersonic diffuser. For K_{exdop} = 1, the entity geometry information is used to define the centerbody component that starts at the nose of the centerbody and extends to the engine face. Thus, the centerbody component (K_{comt} = 16) defines the entities for centerbody profiles through the external supersonic diffuser, throat section, and subsonic diffuser. A search is performed to find the point on the centerbody component that is closest to the cowl lip point. That point on the centerbody is set as the end of the

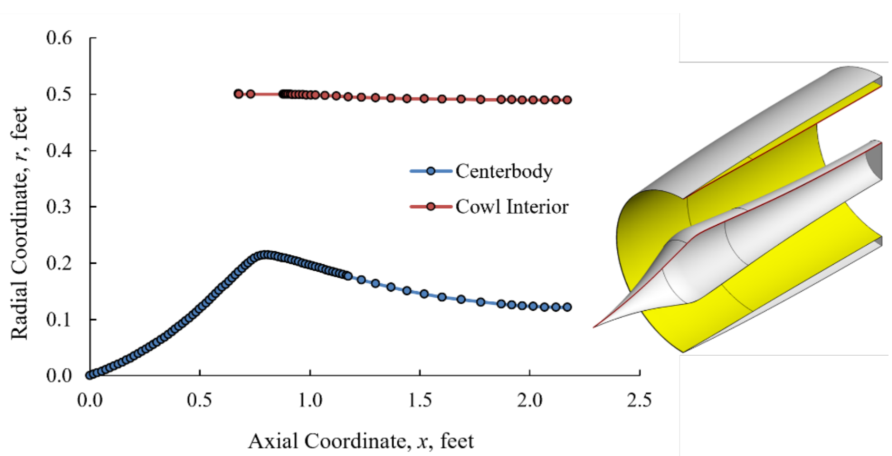

Figure 8.11.—Planar curves used to define the profiles of the centerbody and cowl interior of the Mach 1.7 Gulfstream/NASA Low-Boom Single-Stream (LBSS) axisymmetric spike inlet (Ref. 4).

TABLE 8.11.—THE INPUT FACTORS FOR SPECIFYING THE INFORMATION FOR AN EXTERNAL SUPERSONIC DIFFUSER DEFINED USING COMPONENTS AND ENTITIES

Factor	Input	Description
K_{exdop}	`Kexdop`	Flag indicating how to use entities listed in input data block DataID = 16 = 0 Use entities of the external supersonic diffuser defined with K_{comt} = 1 = 1 Use entities of the centerbody specified with K_{comt} = 16
F_{exdop1}	`Fexdop1`	Input to be used according to K_{exdop} (currently not used)

TABLE 8.12.—EXAMPLE INPUT DATA BLOCK FOR THE EXTERNAL SUPERSONIC DIFFUSER FOR K_{exd} = 8 IN WHICH THE EXTERNAL SUPERSONIC DIFFUSER IS DEFINED USING ENTITIES

```
DataID.  External Supersonic Diffuser
  4
Kexd    FptEXptL    Fpt1ptEX
  8      -0.9950     -0.9850
Kexdop   Fexdop1
  1          0.0
```

external supersonic diffuser and assigned the coordinates $(x,y)_{cb1}$. Each entity of the centerbody leading up to the end of the external supersonic diffuser is assumed to be a stage of the external supersonic diffuser. The input factor F_{exdop1} allows the input of additional information for constructing the external supersonic diffuser based on the value of K_{exdop}. Currently, the input F_{exdop1} is not being used and a dummy value (F_{exdop1} = 0.0) should be specified. Table 8.12 provides an example of the input data block for the external supersonic diffuser with K_{exd} = 8.

For the throat section, the use of components and entities is indicated by specifying the input factor K_{thrt} = 8 within the input data block for DataID = 8 as indicated in Table 4.18. Additional inputs of K_{thop}, F_{xcwTH}, and F_{xcwSD} are available to provide specific instructions on establishing the coordinates for the throat section using the entities. Table 8.13 list the options. For K_{thop} = 0, the entities are defined using K_{comt} = 7 for the throat section centerbody and K_{comt} = 8 for the throat section cowl interior and the coordinates for station SD are established using endpoints of entities. This assumes that the respective endpoints of the entities match to the desired locations for the respective stations. For K_{thop} = 1, the entities are defined using K_{comt} = 16 for the centerbody and K_{comt} = 17 for the cowl interior. The coordinate x_{cwSD} is specified using the input factor F_{xcwSD}. The entities of the cowl interior are searched to find the coordinate y_{cwSD}. The coordinates $(x,y)_{cbSD}$ on the centerbody for station SD are found from a search of the centerbody entities for the closest point on the centerbody to point $(x,y)_{cwSD}$. The option of K_{thop} = 2 is discussed in Subsection 9.5 in relation to mixed-compression inlets. Table 8.14 lists an example input data file for the case of K_{thrt} = 8.

For the subsonic diffuser, the use of components and entities is indicated by specifying the input factor K_{subd} = 15 within the input data block for DataID = 10 as indicated in Table 4.20. No additional input factors are required. Table 8.15 lists an example input data file for the case of K_{subd} = 15. The input factors KLsubd, FLsubd, and theqsd are ignored when establishing the geometry of the subsonic diffuser with K_{subd} = 15. The use of Fpt2ptSD for the total pressure ratio for the subsonic diffuser is the same as previously discussed.

TABLE 8.13.—THE INPUT FACTORS FOR SPECIFYING THE INFORMATION FOR A THROAT SECTION DEFINED USING COMPONENTS AND ENTITIES

Factor	Input	Description
K_{thop}	`Kthop`	Flag indicating how to use entities listed in input data block DataID = 16 = 0 Use endpoints of entities for the coordinates of the throat section = 1 Use FxcwSD to establish station SD = 2 Use FxcwTH and FxcwSD to establish stations TH and SD
F_{xcwTH}	`FxcwTH`	x-coordinate for point x_{cwTH} on the cowl interior (ft)
F_{xcwSD}	`FxcwSD`	x-coordinate for point x_{cwSD} on the cowl interior (ft)

TABLE 8.14.—EXAMPLE INPUT DATA BLOCK FOR THE THROAT SECTION WITH K_{thrt} = 8 IN WHICH THE THROAT SECTION IS DEFINED USING ENTITIES

```
DataID.  Throat Section
  4
Kthrt    FptSDs1     FptsegB     FptsegC
  8     -0.99000    -0.99500    -1.00000
Kthop    FxcwTH    FxcwSD
  2      1.0000    1.2000
```

TABLE 8.15.—EXAMPLE INPUT DATA BLOCK FOR THE THROAT SECTION WITH K_{subd} = 15 IN WHICH THE SUBSONIC DIFFUSER IS DEFINED USING ENTITIES

```
DataID.  Subsonic Diffuser
 10
Ksubd    KLsubd    FLsubd    theqsd    Fpt2ptSD
 15         3     0.76115     3.000    -0.98000
```

8.8 Cowl Exterior

A geometry model for creating a planar profile for a cowl exterior was described in Subsection 4.10 and illustrated in Figure 4.5. An example of the input data block was provided in Table 4.16 and is applicable for the axisymmetric spike and two-dimensional inlets. The input factors were listed and described in Table 4.17. The cowl exterior for the axisymmetric spike inlet is formed by extruding the planar profile about the axis-of-symmetry in the same manner as for the axisymmetric pitot inlet. An image of an external-compression, axisymmetric spike inlet showing the cowl exterior is shown in Figure 8.12.

The cowl exterior surfaces for the two-dimensional single-duct and bifurcated-duct inlets are formed as a network of three-dimensional curves about the circumference of the inlet. Each three-dimensional curve extends from an upstream point connected to the cowl lip or leading edge of the sidewall to a downstream point with an axial coordinate of x_{cwex}. The three-dimensional curve is formed by starting with the planar curve of the model described in Section 4.10, but then transforming the planar curve along its length as it is matched to the upstream and downstream points of the three-dimensional cowl exterior. The creation of the curves originating from the sidewall use the input factor θ_{swex} described in Subsection 4.10 for the slope of the cowl exterior external to the sidewall. Figure 8.13 shows images of the cowl exterior for a two-dimensional inlet.

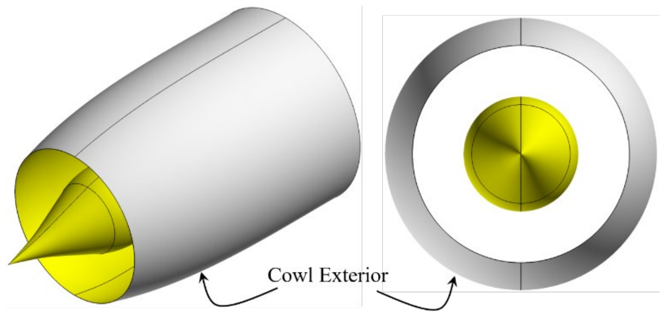

Figure 8.12.—Cowl exterior of an axisymmetric spike inlet.

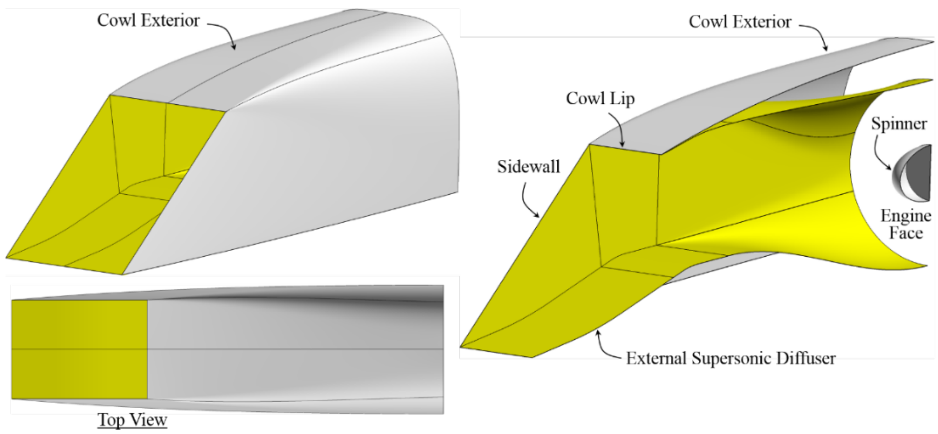

Figure 8.13.—Images of a two-dimensional inlet showing the cowl exterior.

8.9 Support Struts for Axisymmetric Spike Inlets

Axisymmetric spike inlets require the use of struts to support the centerbody by connecting the centerbody to the cowl. An example of an axisymmetric-spike inlet with support struts was shown in Figure 2.9. The struts exist within the internal subsonic flow of the inlets, and so, are aerodynamic surfaces within the subsonic diffuser. For an external-compression inlet, the strut may also extend into the subsonic flow of the throat section. Support struts have also been used to duct bleed flow extracted from the bleed regions on the centerbody. For this case, the interior of the struts to be hollowed to provide a duct for the bleed flow to move from the centerbody toward the cowl. The bleed flow would then be ducted within the cowling to be used elsewhere within the propulsion system or dumped overboard to the external flow. The number and dimensions of the struts is determined by the needs for structural integrity of the inlet and ducting of centerbody bleed flow.

SUPIN provides for the modeling of three or four support struts. The support struts are equally distributed about the circumference of the inlet. The struts can be positioned circumferentially with a strut at the top-center location or clocked so that the top-most strut is located by half of the circumferential span between the struts. Figure 8.14 shows the variation in number and position of the struts.

All the struts have the same shape and are defined by a planform and cross-section, as shown in Figure 8.15 and Figure 8.16. The leading (upstream) edge of a support strut is specified by its coordinate at the centerbody (x_{ssle}) and its angle with respect to the horizontal (θ_{ssle}). The trailing (downstream) edge of a support strut is specified by its coordinate at the centerbody (x_{sste}) and its angle with respect to the horizontal (θ_{sste}). With a definition of the planar profile of the centerbody, the radial coordinates of the points for the leading and trailing edges on the centerbody (r_{ssle} and r_{sste}, respectively) is obtained. With

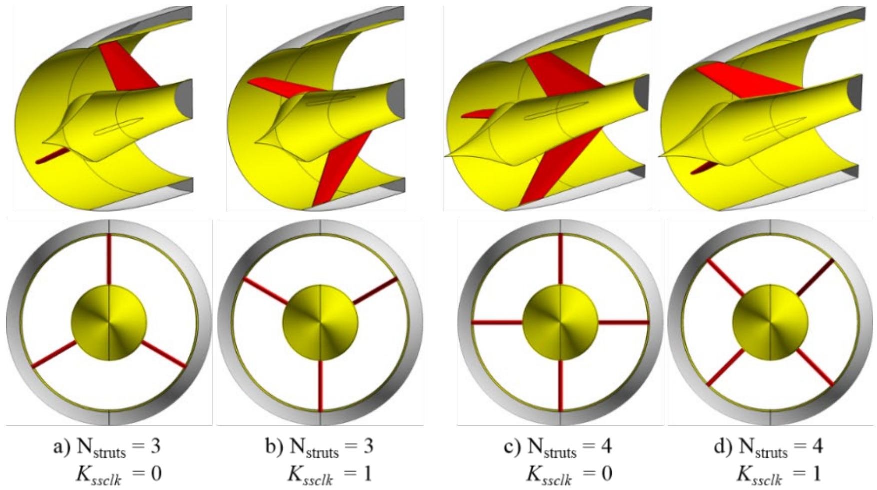

Figure 8.14.—Variations of the layout for the support struts.

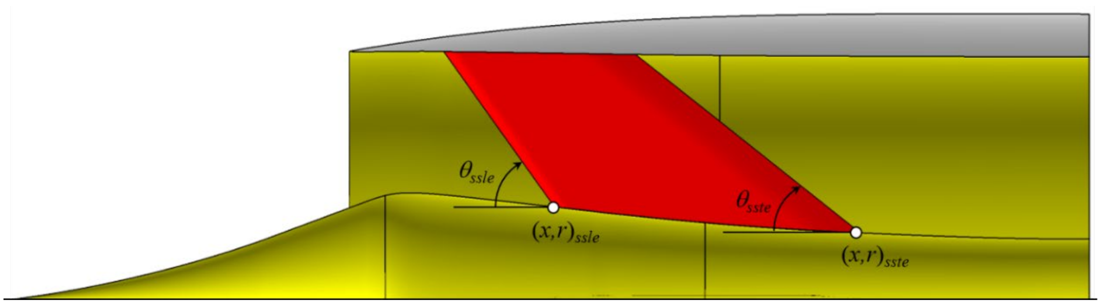

Figure 8.15.—Planform for the support struts.

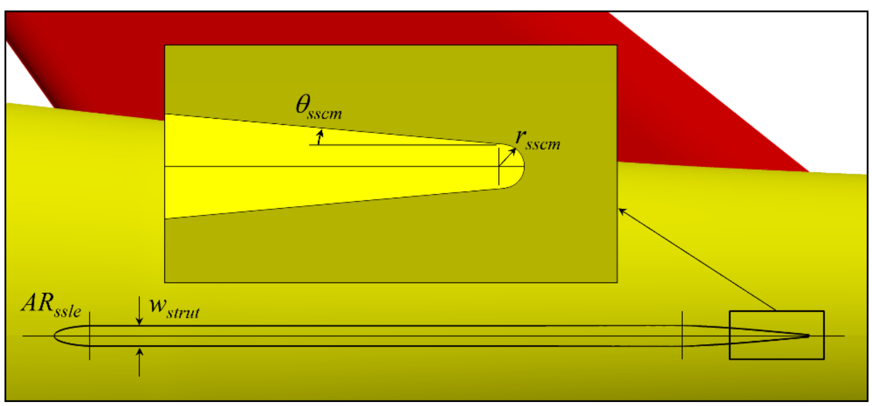

Figure 8.16.—Cross-section for the support struts.

the definition of the planar profile for the cowl interior, the axial and radial coordinates of the points for the leading and trailing edge on the cowl interior is obtained with the assumption of straight leading and trailing edges.

The cross-section of the struts has an elliptical leading edge, flat sides, and a wedge-like trailing edge that ends with a circular profile as shown in Figure 8.16. The width of the strut (w_{strut}) is an input factor that also sets the length of the minor axis of the elliptical leading edge (b_{ssle}) with $b_{ssle} = w_{strut} / 2$. The length of the semi-major axis of the elliptical leading edge (a_{ssle}) is defined using the aspect ratio of the elliptical leading edge (AR_{ssle}), which is an input factor. Thus, $a_{ssle} = AR_{ssle}\, b_{ssle}$. Further information on

TABLE 8.16.—FACTORS DEFINING THE SUPPORT STRUTS FOR AN AXISYMMETRIC SPIKE INLET

Factor	Inputs	Description
N_{struts}	`Nstruts`	Number of support struts for the inlet
x_{ssle}	`xssle`	x-coordinate of the strut leading edge at the centerbody (ft)
θ_{ssle}	`thssle`	Angle of the leading edge from horizontal (deg)
x_{sste}	`xsste`	x-coordinate of the strut trailing edge at the centerbody (ft)
θ_{sste}	`thsste`	Angle of the trailing edge from horizontal (deg)
AR_{ssle}	`ARssle`	Aspect ratio of the elliptical profile of the strut leading edge
w_{strut}	`wstrut`	Width of the struts (ft)
θ_{sscm}	`thsscm`	Slope of the strut cross-section at the trailing edge (deg)
r_{sscm}	`rsscm`	Radius of the circular profile of the strut trailing edge (ft)
K_{ssclk}	`Kssclk`	Flag indicating if struts are clocked (=0 no, =1 yes)

TABLE 8.17.—EXAMPLE INPUT DATA BLOCK FOR THE SUPPORT STRUTS FOR AN AXISYMMETRIC SPIKE INLET

```
DataID.  Support Struts
  9
Nstruts    xssle     thssle     xsste     thsste
  4       1.0900      54.52    1.7077      38.46
ARssle    wstrut     thsscm     rsscm     Kssclk
 4.00     0.0167       5.00     0.002         0
```

elliptical profiles can be found in Subsection A.4 of Appendix A. The trailing edge of the strut has a wedge-like cross-section with a slope of θ_{sscm} that ends with a circular profile with a radius of r_{sscm} as illustrated in Figure 8.16. Both θ_{sscm} and r_{sscm} are input factors. The profile for the wedge-like trailing edge involves a smooth change in slope at the start of the trailing edge from the flat sidewalls of the strut to the specified slope θ_{sscm}. The circular profile of the trailing edge is matched to the slope θ_{sscm}.

Table 8.16 lists and describes the input factors that define the shape and position of the struts. The input factors include the number of struts, which should be N_{struts} = 3 or 4, and a flag indicating whether the struts are clocked (K_{ssclk}) about the axis-of-symmetry. For K_{ssclk} = 0, a strut is placed at the top center of the inlet. For K_{ssclk} = 1, the struts are "clocked" about the axis-of-symmetry by a circumferential angle equal to half of the angular spacing between the struts. Table 8.17 presents an example input data block for specification of the inputs for the support struts.

References

1. Nussdorfer, T. J., "Some Observations of Shock-Induced Turbulent Separation on Supersonic Diffusers," NACA RM E51L26, May 1954.
2. Kuehn, D. M., "Experimental Investigation of the Pressure Rise Required for the Incipient Separation of Turbulent Boundary Layers in Two-Dimensional Supersonic Flow," NASA RM 1-21-59A, February 1959.
3. Mahoney, J. J., *Inlets for Supersonic Missiles*, AIAA Education Series, Washington, DC, 1990.
4. Hirt, S. M., Chima, R. V., Vyas, M. A., Conners, T. R., Wayman, T. R., and Reger, R. W., "Experimental Investigation of a Large-Scale Low-Boom Inlet Concept," AIAA-2011-3796, June 2011.

9.0 Mixed-Compression, Axisymmetric Spike and Two-Dimensional Inlets

The mixed-compression, axisymmetric spike and two-dimensional inlets have an internal supersonic diffuser for the internal compression of supersonic flow. The internal supersonic diffuser starts at station 1 and ends at the geometric throat station TH. A throat section extends between stations TH and SD with the task of decelerating the supersonic flow from the internal supersonic diffuser at station TH to subsonic conditions for subsonic diffuser at station SD. Subsection 9.1 discusses a basic geometry model for the internal supersonic diffuser and throat section based mostly on geometric constructs such as lengths and angles. Subsection 9.2 discusses the use of method-of-characteristics (MOC) methods to establish many of the lengths and angles of the internal supersonic diffuser discussed in the geometry model of Section 9.1. Subsection 9.3 discusses the use of entities to define the geometry of the internal supersonic diffuser and throat section. Subsection 9.4 discusses the terminal shock wave structures for mixed-compression inlets. Subsection 9.5 discusses subsonic diffusers for mixed-compression inlets. Subsection 9.6 discusses a model for total pressure losses through supersonic diffusion.

9.1 Geometry Model for the Internal Supersonic Diffuser and Throat Section for Mixed-Compression Inlets

This subsection presents a geometry model for the construction of the internal supersonic diffuser and throat section for mixed-compression, axisymmetric spike and two-dimensional inlets. The model is mostly based on geometric factors rather than any flow conditions; however, there are options to specify the Mach numbers at station TH and SD to calculate areas at those stations. The geometric factors define the planar profiles for the centerbody and cowl interior between stations 1 and SD. The surfaces of the centerbody and cowl interior are then formed through extrusion of these profiles. For an axisymmetric spike inlet, the extrusion is about the axis-of-symmetry and the cross-sections are annular. For a two-dimensional inlet, the extrusion is in cross-stream (z) coordinate with the width equal to the capture width (w_{cap}). Thus, for the two-dimensional inlets, the internal supersonic diffuser and throat section maintain a constant width equal to the capture width (w_{cap}) and the cross-sections are rectangular.

A schematic of the geometry model is presented in Figure 9.1 showing the input factors, dimensions, and flow stations. The internal supersonic diffuser extends between stations 1 and TH and serves to decelerate the supersonic flow through shock and Mach waves as the cross-sectional area is decreased. Station TH is the geometric throat of the inlet at which the cross-sectional area is at a minimum. The throat section extends between stations TH and SD and has the task of decelerating the supersonic flow to subsonic conditions through a terminal shock wave system, which could be a single normal shock wave or an oblique shock wave train system.

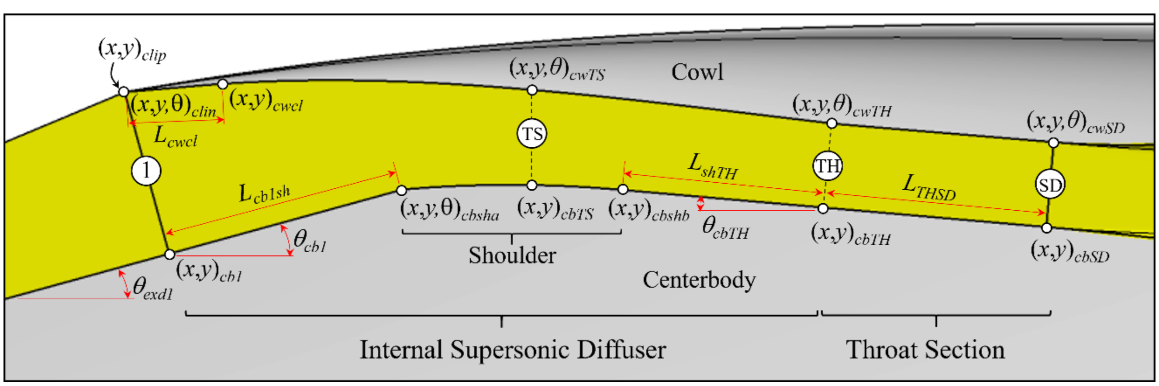

Figure 9.1.—Geometry model for the internal supersonic diffuser and throat section for two-dimensional and axisymmetric spike inlets.

The geometry model first defines the planar profile of the centerbody, which can consist of up to four segments. The first segment is a line which starts at the point $(x,y)_{cb1}$ and ends at the point at the start of the centerbody shoulder $(x,y)_{cbsha}$. The slope of the line is established as

$$\theta_{cb1} = \theta_{exd1} + \Delta\theta_{cb1} \tag{9-1}$$

where θ_{exd1} is the slope of the centerbody at the end of the external supersonic diffuser and $\Delta\theta_{cb1}$ is an input factor that specifies an optional change in slope of the centerbody profile at station 1. The length of the first segment of the centerbody is the length L_{cb1sh}, which is an input factor. A zero value for L_{cb1sh} is allowed in the model. The coordinates for the start of the shoulder are calculated as

$$\begin{aligned} x_{cbsha} &= x_{cb1} + L_{cb1sh}\cos\theta_{cb1} \\ y_{cbsha} &= y_{cb1} + L_{cb1sh}\sin\theta_{cb1} \end{aligned} \tag{9-2}$$

The second segment of the centerbody profile defines the shoulder of the centerbody. The shoulder performs most of the turning of the centerbody profile and is modeled as a smooth curve using a four-point NURBS curve, which is described in Subsection A.12 of Appendix A. The slope at the start of the shoulder is θ_{cbsha}. The input factor $\Delta\theta_{cbsha}$ is the change in the slope of the centerbody at the start of the shoulder. The slope of the profile at the start of the shoulder is calculated as

$$\theta_{cbsha} = \theta_{cb1} + \Delta\theta_{cbsha} \tag{9-3}$$

The shoulder is modeled as a four-point NURBS curve with the interior control points evenly spaced between the end control points. The endpoint of the shoulder is the coordinate $(x,y)_{cbshb}$ calculated as

$$\begin{aligned} x_{cbshb} &= x_{cbsha} + \Delta x_{cbsh} \\ y_{cbshb} &= y_{cbsha} + \Delta y_{cbsh} \end{aligned} \tag{9-4}$$

where the incremental coordinate distances are Δx_{cbsh} and Δy_{cbsh} and are input factors. One requirement of the geometry model is that $\Delta x_{cbsh} > 0$ so that a shoulder can be properly defined. The slope at the end of the shoulder at point $(x,y)_{cbshb}$ is specified with the input factor θ_{cbTH}, which also defines the slope of the third and fourth segments of the centerbody.

The point $(x,y)_{cbTS}$ is defined as the point on the shoulder at which the slope of the centerbody profile is zero. In most cases, $\theta_{cbsha} > 0$ and $\theta_{cbTH} < 0$, and so, the point $(x,y)_{cbTS}$ is located within the shoulder profile. A bisection search method is used within SUPIN to find the point $(x,y)_{cbTS}$ along the four-point NURBS curve at which $\theta_{cbTS} = 0$. The point $(x,y)_{cbTS}$ is referred to as the shoulder point. In the case that $\theta_{cbTH} = 0$, the shoulder point is set to end of the shoulder segment, which results in $(x,y)_{cbTS} = (x,y)_{cbshb}$.

The third segment of the centerbody profile is a line with a slope of θ_{cbTH} that extends from the end of the shoulder segment at point $(x,y)_{cbshb}$ to station TH at point $(x,y)_{cbTH}$. The slope θ_{cbTH} is an input factor. The distance of the line segment is specified through an input factor as L_{shTH} and the model requires $L_{shTH} > 0$. The coordinates of the point $(x,y)_{cbTH}$ defining the location of station TH on the centerbody are calculated as

$$\begin{aligned} x_{cbTH} &= x_{cbshb} + L_{shTH}\cos\theta_{cbTH} \\ y_{cbTH} &= y_{cbshb} + L_{shTH}\sin\theta_{cbTH} \end{aligned} \tag{9-5}$$

The fourth segment of the centerbody profile is a line with a slope of θ_{cbTH} that extends from station TH to station SD, which is the start of the subsonic diffuser. The length of this line segment is L_{THSD}. A value of $L_{THSD} = 0$ is possible, which would place station SD at station TH. The coordinates of the point $(x,y)_{cbSD}$ defining the location of station SD on the centerbody are calculated as

$$\begin{aligned} x_{cbSD} &= x_{cbTH} + L_{THSD} \cos\theta_{cbTH} \\ y_{cbSD} &= y_{cbTH} + L_{THSD} \sin\theta_{cbTH} \end{aligned} \tag{9-6}$$

The input factors for the profile of the centerbody of the internal supersonic diffuser and throat section are listed in Table 9.1. The angular input factors $\Delta\theta_{cb1}$, $\Delta\theta_{cbsha}$, and θ_{cbTH} are specified with units of degrees. The input factors for the lengths L_{cb1sh}, Δx_{cbsh}, Δy_{cbsh}, L_{shTH}, and L_{THSD} are specified as lengths normalized by the reference dimension D_{ref}.

The profile of the cowl interior can consist of up to four segments and is formed using a set of input factors described below. Some of the input factors compute coordinates in reference to the centerbody. The shape of the centerbody and cowl profiles establish the variation of the cross-sectional area through the throat section.

The first segment of the cowl interior profile is a line that starts at the cowl lip interior point $(x,y)_{clin}$ and has a slope specified by θ_{clin}. The length of the line is L_{cwcl} and can be of zero length. The coordinates of the point at the end of this first segment are calculated as

$$\begin{aligned} x_{cwcl} &= x_{clin} + L_{cwcl} \cos\theta_{clin} \\ y_{cwcl} &= y_{clin} + L_{cwcl} \sin\theta_{clin} \end{aligned} \tag{9-7}$$

The second segment of the cowl interior profile is modeled as a four-point NURBS curve that starts at the point $(x,y)_{cwcl}$ with a slope of θ_{clin} and ends at the point $(x,y)_{cwTS}$ with a slope of θ_{cwTS}. The point $(x,y)_{cwTS}$ is established along a vertical line ($x_{cwTS} = x_{cbTS}$) with the height computed to establish the area A_{TS} as computed from the specified area ratio A_{TS}/A_1. Thus, for the two-dimensional inlet, $h_{TS} = A_{TS} / w_{cap}$. For the axisymmetric spike inlet, h_{TS} is computed using the radius of the centerbody and A_{TS} for an annular cross-section.

The third segment of the cowl interior profile is modeled as a four-point NURBS curve that starts at the point $(x,y)_{cwTS}$ with a slope of θ_{cwTS} and ends at the point $(x,y)_{cwTH}$ with a slope of θ_{cwTH}. The point $(x,y)_{cwTH}$ is established along a line passing through and normal to point $(x,y)_{cbTH}$. The height at station TH, h_{TH}, is computed to establish the area A_{TH} using the specified ratio A_{TH}/A_1.

The fourth segment of the cowl interior profile is modeled as a four-point NURBS curve that starts at the point $(x,y)_{cwTH}$ with a slope of θ_{cwTH} and ends the point $(x,y)_{cwSD}$ with a slope of θ_{cwSD}. The point $(x,y)_{cwSD}$ is established along a line passing through and normal to point $(x,y)_{cbSD}$. The height at station SD, h_{SD}, is computed to establish the area A_{SD} using the specified ratio A_{SD}/A_{TH}.

TABLE 9.1.—INPUT FACTORS FOR THE CENTERBODY OF MIXED-COMPRESSION, AXISYMETRIC SPIKE AND TWO-DIMENSIONAL INLETS

Factor	Inputs	Description
$\Delta\theta_{cb1}$	`dthcb1`	Change in the slope of centerbody at station 1 (deg)
L_{cb1sh}	`FLcb1sh`	Length along the centerbody from station 1 to start of shoulder (normalized by D_{ref})
$\Delta\theta_{cbsha}$	`dthsha`	Change in slope at the start of the centerbody shoulder (deg)
Δx_{cbsh}	`Fdxcbsh`	Axial distance between start and end of the shoulder (normalized by D_{ref})
Δy_{cbsh}	`Fdycbsh`	Vertical distance between start and end of the shoulder (normalized by D_{ref})
θ_{cbTH}	`thcbTH`	Slope of the centerbody at the end of the shoulder and stations TH and SD (deg)
L_{shTH}	`FLshTH`	Length from end of shoulder to station TH (normalized by D_{ref})
L_{THSD}	`FLTHSD`	Length between stations TH and SD (normalized by D_{ref})

TABLE 9.2.—INPUT FACTORS FOR THE COWL INTERIOR OF MIXED-COMPRESSION, AXISYMMETRIC SPIKE AND TWO-DIMENSIONAL INLETS

Factor	Inputs	Description
L_{cwcl}	FLcwcl	Length of straight segment after the cowl lip interior (normalized by D_{ref})
θ_{cwTS}	thcwTS	Slope of the cowl interior at station TS (deg)
θ_{cwTH}	thcwTH	Slope of the cowl interior at station TH (deg)
θ_{cwSD}	thcwSD	Slope of the cowl interior at station SD (deg)
A_{TS}/A_1	FaTSa1	Ratio of the cross-sectional area at station TS to area at station 1
A_{TH}/A_1	FaTHa1	Ratio of the cross-sectional area at station TH to area at station 1
A_{SD}/A_{TH}	FaSDaTH	Ratio of the cross-sectional area at station SD to area at station TH
M_{TS}	FmachTS	Mach number for station TS
M_{TH}	FmachTH	Mach number for station TH
M_{SD}	FmachSD	Mach number for station SD

An alternative to specifying the area ratios A_{TS}/A_1, A_{TH}/A_1, and A_{SD}/A_{TH} at the respective stations TS, TH, and SD is to specify the Mach numbers M_{TS}, M_{TH}, and M_{SD} at those stations and then use flow continuity (Eqs. (2-31) and (2-32)) to compute the corresponding cross-sectional area. This alternative requires SUPIN to be used in the design mode (K_{mode} = 2). The total pressures for the continuity relations can be either computed or specified using the appropriate input factors.

The input factors for the profile of the cowl interior of the throat section are listed in Table 9.2. The input factor for the length L_{cwcl} is specified as normalized by the reference dimension, D_{ref}. The slopes θ_{cwTS}, θ_{cwTH}, and θ_{cwSD} are specified in units of degrees. The use of the area ratios or the Mach numbers is determined by the sign of the input factors for the Mach numbers. For example, if the input factor FmachTH < 0, then the input factor A_{TH}/A_1 is used to establish the area A_{TH}. However, if FmachTH > 0, then M_{TH} = FmachTH, and Equation (2-31) is solved to establish A_{TH}. If bleed is extracted between stations TS and TH, then the change in the flow rate through the segment needs to be accounted for within the continuity calculations. The same logic applies for the input factors for the pair M_{TS} and A_{TS}/A_1 and the pair M_{SD} and A_{SD}/A_{TH}.

An example of the input data block for this geometry model is presented in Table 9.3. The format of this input data block is associated with K_{thrt} = 5. The input factor $\boldsymbol{K_{th234}}$ indicates the design methods used to create the internal supersonic diffuser and throat section using the input factors. The options for K_{th234} are listed in Table 9.4. For K_{th234} = 0, the input factors discussed above and listed in Table 9.1 and Table 9.2 explicitly define the geometry of the throat section. For K_{th234} = 2, the method-of-characteristics is used to compute the values of some of the factors. Subsection 9.2 will discuss the method-of-characteristics for designing the internal supersonic diffuser. The options for K_{th234} = 1 and 3 are not fully developed at this time and should not be used.

The input factors $\boldsymbol{F_{cbds}}$ and $\boldsymbol{F_{cwds}}$ are provided to adjust the centerbody and cowl profiles. The input factor F_{cbds} specifies the extent of smoothing of any discontinuous slope on the centerbody at the start of the shoulder due to the change in angle $\Delta\theta_{cbsha}$. The input factor F_{cbds} controls the distance along the centerbody over which the smoothing occurs and is specified as a fraction of the reference length of the inlet, D_{ref}. The image at the lower left of Figure 9.2 shows the original and modified profiles of the centerbody shoulder. The surfaces shaded in yellow are for the modified inlet.

The input factor F_{cwds} accounts for the displacement thicknesses of the boundary layer on both the centerbody and the cowl. The value of F_{cwds} is specified in units of feet and controls the distance that the cowl interior profile at station SD is moved outward. This distance should be on the order of the displacement thickness of the boundary layers and can be obtained from preliminary viscous CFD simulations or from other boundary layer estimation methods. Thus, accounting for the growth of the

TABLE 9.3.—EXAMPLE INPUT DATA BLOCK FOR THE GEOMETRIC MODEL OF THE INTERNAL SUPERSONIC DIFFUSER AND THROAT SECTION OF MIXED-COMPRESSION, AXISYMMETRIC SPIKE AND TWO-DIMENSIONAL INLETS

```
DataID.  Throat for 2D and axisymmetric spike inlets
  8
Kthrt    FptTSpt1    FptTHptTS    FptSDptTH
  5      -0.99000     -0.99500     -1.00000
Kth234
  0
dthcb1       dthsha       thcbTH
 0.000        0.000       -5.000
FLcb1sh     Fdxcbsh      Fdycbsh      FLshTH      FLTHSD
 0.2000      0.5000       0.0000      0.5000      0.5000
 FLcwcl      thcwTS       thcwTH      thcwSD
 0.1000       0.000       -5.000      -5.000
 FaTSa1      FaTHa1      FaSDaTH
 1.0100      1.0300       1.0500
FmachTS     FmachTH      FmachSD
-1.2500      1.3000      -1.3500
 Fcwds        Fcbds
0.0000       0.0500
```

TABLE 9.4.—INPUT FACTORS FOR THE GEOMETRIC MODEL AND PROFILE MODIFICATIONS

Factor	Inputs	Description
K_{th234}	Kth234	Flag indicating option for geometric model for K_{typ} = 2, 3, and 4 = 0 Geometry is explicitly defined *= 1 Shock-free flow through throat section (currently not available)* = 2 Internal supersonic compression with MOC and cowl shock cancellation *= 3 Cowl shock with reflected shock waves downstream (currently not available)*
F_{cwds}	Fcwds	Vertical displacement of the cowl at station SD to account for boundary layer (ft)
F_{cbds}	Fcbds	Factor for the rounding of the start of the shoulder

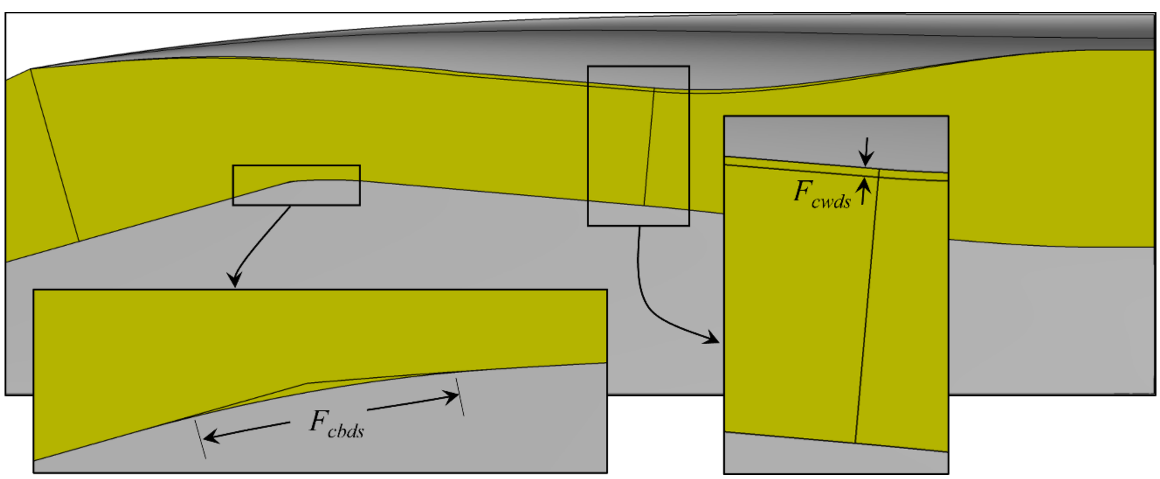

Figure 9.2.—Modifications to the inlet throat section centerbody shoulder and cowl profile.

boundary layers may involve some iterations within the design process. Between the cowl lip interior point and station SD, the outward displacement of the throat section cowl interior profile is linearly interpolated. Likewise, the displacement of the cowl interior profile of the subsonic diffuser is linearly interpolated between station SD and the engine face. This modification essentially increases the cross-sectional areas at stations TH and SD. The images of Figure 9.2 illustrate the effect of this modification.

9.2 Method-of-Characteristics (MOC) Model for the Internal Supersonic Diffuser

This geometry model uses the method-of-characteristics (MOC) to define the profile of the cowl interior for the internal supersonic diffuser based on a specified profile for the centerbody and some additional aerodynamic specifications. The MOC method solves for the inviscid supersonic flowfield through the internal supersonic diffuser with the formation of a cowl shock wave that is cancelled at the start of the shoulder. Downstream of the cowl shock wave, the supersonic compression is isentropic using Mach waves. The MOC methods are based on those presented by Anderson (Ref. 1).

The geometric model of the previous subsection as shown in Figure 9.1 is used as a basis for the MOC model. The MOC methods are used to establish values for several of the input factors for the geometric model rather than direct specification of those input factors. The methods for designing the throat section using the MOC model are presented below. Additional details on the MOC methods are provided in Appendix B.

The external supersonic diffuser provides the supersonic flow at station 1 as the inflow to the internal supersonic diffuser. The MOC methods applied for the design of the external supersonic diffuser provide the flowfield across the span of station 1. A central feature of the supersonic flow in the internal supersonic diffuser is the formation of an internal cowl shock wave created by the deflection of the flow coming into station 1 due to a cowl lip internal angle (θ_{clin}) that introduces a deflection in the flow at the cowl lip. This cowl shock wave is illustrated in Figure 9.3. The MOC methods are used to solve the flowfield between station 1 and the cowl shock wave, which is designated as Region C in Figure 9.3. The MOC model imposes that $\Delta\theta_{cb1} = 0$ so that additional waves are not introduced into Region C from the centerbody. The MOC model place the start point of the shoulder of the centerbody $(x,y)_{cbsha}$ at the point of intersection of the cowl shock wave with the centerbody. This establishes the length L_{cb1sh}.

The MOC model imposes the cancellation of the cowl shock wave at point $(x,y)_{cbsha}$ such that no shock wave is reflected. This involves computing the deflection $\Delta\theta_{cbsha}$ at the start of the shoulder such that the slope at the start of the shoulder is aligned with the local flow angle downstream of the cowl shock wave at the intersection point. Thus, at the start of the shoulder, a finite value of the change in slope $\Delta\theta_{cbsha}$ is calculated as part of the MOC model. Thus, the MOC model introduces a discontinuity in the slope of the centerbody at the start of the shoulder that creates a “sharp” corner. The input factor F_{cbds} described in the previous section provides a means of smoothing out this discontinuity, if desired.

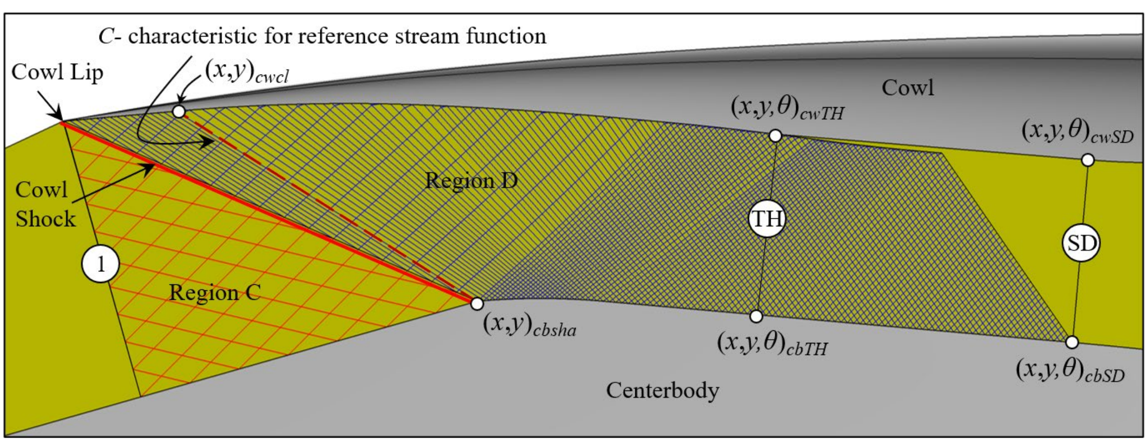

Figure 9.3.—MOC regions C and D for the MOC throat section model.

The remainder of the profile of the shoulder and rest of the centerbody of the throat section is explicitly defined through specification of Δx_{cbsh}, Δy_{cbsh}, θ_{cbTH}, L_{shTH}, and L_{THSD} using the respective input factors. The geometry of the centerbody downstream of the start of the shoulder is explicitly defined in the manner as described in the previous subsection. The specification of the lengths L_{shTH} and L_{THSD} for the centerbody may involve manual iteration of values within the throat design to ensure enough length for the internal supersonic compression. Both L_{shTH} and L_{THSD} should be specified as finite lengths, and so, zero values are not allowed.

The MOC methods compute the inviscid flowfield downstream of the cowl shock wave and through station TH, which is designated as Region D in Figure 9.3. The design methods establish the profile for the cowl interior through station TH to obtain the desired level of internal supersonic compression. The level of internal supersonic compression is set by the mass-averaged Mach number at station TH (M_{TH}), as specified using the input factor FmachTh with M_{TH} = FmachTH. The MOC method uses a flow boundary condition in which the Mach number is specified on the centerbody from x_{cbsha} to x_{cbSD}. The Mach number at x_{cbsha} is the Mach number just downstream of the cowl shock wave at the centerbody. The Mach number at x_{cbSD} is set to M_{TH}. A linear variation is used to compute the Mach number along the centerbody between x_{cbsha} and x_{cbSD}. Appendix D discusses further details of the MOC methods for Region D downstream of the cowl shock wave.

The first segment of the cowl interior profile maintains the cowl lip interior angle (θ_{clin}) over the length L_{cwcl}. The length L_{cwcl} is established as the length from the cowl lip interior point $(x,y)_{clin}$ to the point on the cowl that the first *C*- characteristic completely extends from the centerbody to the cowl. This *C*- characteristic is also known as the reference C_- characteristic and is illustrated in Figure 9.3.

The cowl profile from point $(x,y)_{cwcl}$ to $(x,y)_{cwTH}$ is calculated as part of the MOC methods. As the MOC characteristic net is solved downstream of the reference *C*- characteristic, the cowl profile is developed as the collection of points along downstream *C*- characteristics at which the stream function value equals the reference stream function value. The point $(x,y)_{cwTH}$ is computed as the point on the cowl interior at which the Mach number equals the specified value of M_{TH}. The point $(x,y)_{cbTH}$ is determined as the point on the centerbody along a normal to the centerbody that passes through point $(x,y)_{cwTH}$. This establishes station TH and its cross-sectional area, A_{TH}.

The profiles for the centerbody and cowl interior of the throat section between stations TH and SD are formed in the same manner as described in the previous subsection. The centerbody profile is linear with the slope equal to $\theta_{cbTH} = \theta_{cbSD}$ and length equal to L_{THSD} as specified by the input factor FLTHSD. The input factor FaSDaTH is used to compute the cross-sectional area at station SD (A_{SD}). A four-point NURBS curve is used to model the segment of the cowl interior profile from point $(x,y)_{cwTH}$ to point $(x,y)_{cwSD}$.

The sample input data block shown in Table 9.3 for $K_{thrt} = 5$ can be used to apply the MOC methods by using $K_{th234} = 2$ and using appropriate values of the respective input factors. A simplified version of the input data block for the MOC model is presented in Table 9.5. The factor $K_{thrt} = 6$ indicates this simplified input data block. This input block includes only those input factors needed by the MOC model and is the recommended form of the input data block for use of the MOC model.

As described above, the MOC method computes the shape of the cowl interior profile from point $(x,y)_{cwcl}$ to $(x,y)_{cwTH}$. To ensure that this profile is a smooth curve, SUPIN forms a four-point NURBS curve to approximate the profile curve created by the MOC method. However, differences may arise between the NURBS curve and the intended shape from the MOC methods. The intended shape can be observed by viewing the mocD.xyz file containing the characteristic net for the MOC region D. The profile of the cowl interior may need to be adjusted to tailor the internal supersonic compression. SUPIN provides some input factors to adjust the four-point NURBS curve defining the cowl interior profile

TABLE 9.5.—EXAMPLE INPUT DATA BLOCK FOR THE MOC GEOMETRY MODEL FOR THE INTERNAL SUPERSONIC DIFFUSER AND THROAT SECTION

```
DataID.  MOC model for internal supersonic diffuser
  8
Kthrt   FptTSpt1   FptTHptTS   FptSDptTH
  6     -0.99000    -0.99500    -1.00000
Fdxcbsh  Fdycbsh     FLshTH     FLTHSD
 0.5000   0.0000     0.5000     0.5000
thcbTH   FmachTH    FaSDaTH      Fcwds      Fcbds
-5.000    1.3000      1.050     0.0000     0.0500
dthcbeg   FNcbeg     FNcend     dthcend
 0.000    0.3000     0.3000      0.000
```

between points $(x,y)_{cwcl}$ and $(x,y)_{cwTH}$. The slope at the start of the NURBS curve at point $(x,y)_{cwcl}$ is set to match the cowl lip interior angle (θ_{clin}). The input factor dthcbeg allows specification of an incremental adjustment of this slope at the beginning of the curve ($\Delta\theta_{cbeg}$) either to increase or decrease the slope. The slope is adjusted as

$$\theta_{cbeg} = \theta_{clin} + \Delta\theta_{cbeg} \tag{9-8}$$

Similarly the slope of the end of the curve at point $(x,y)_{cwTH}$ can be adjusted by a similar increment ($\Delta\theta_{cend}$) specified by the input factor dthcend,

$$\theta_{cend} = \theta_{cwTH} + \Delta\theta_{cend} \tag{9-9}$$

Both dthcbeg and dthcend are specified in units of degrees. The input factors FNcbeg and FNcend are the weightings for the interior control points of the four-point NURBS curves. SUPIN assumes values of FNcbeg = FNcend = 0.333 for these weightings to place the interior control points one-third of the distance between the two endpoints. The input factors provide a means to change these weightings to adjust the shape of the curve. The process for making these adjustments involves viewing the inlet geometry along with the intended MOC characteristic net and then adjusting the curve to achieve the desired shape. This may involve CFD simulations to assess the aerodynamics of the internal supersonic compression process.

9.3 Internal Terminal Shock Wave Structure

For a mixed-compression inlet (K_{comp} = 2), an internal terminal shock wave structure is needed to perform the deceleration of the internal supersonic flow to subsonic conditions. One approach is to establish conditions within the throat section so that a normal terminal shock wave can exist. These conditions include limiting the extent of the boundary layer on the surfaces within the throat section compared to the cross-section at station TH and establishing the Mach number across station TH as $M_{TH} \approx 1.3$, as discussed in Subsection 8.3 in connection with establishing an external normal terminal shock wave. In the case of a mixed-compression inlet (K_{comp} = 2), SUPIN assumes that a normal shock wave is placed at station TH for the calculation of the Mach numbers and total pressure losses due to the terminal shock wave system.

It is also possible for a shock wave train terminal shock wave system to form within the throat section. This occurs when $M_{TH} > 1.3$ and boundary layer separation occurs. The shock wave train consists of a series of oblique shock waves that interact with the separated flow to compress the flow. Typically, the length of the throat section is set such that the length of the shock wave train would be contained within the throat section in a similar manner as the Mahoney throat section described in Subsection 8.5.

The shock wave train may or may not result in fully subsonic flow depending on the level of back-pressure at the end of the throat section. The throat section containing a shock wave train may be considered an isolator depending on the level of back-pressure. Currently, SUPIN does not model a shock wave train in its estimation of the Mach numbers and total pressure losses through the throat section. SUPIN does allow consideration of supersonic flow through the throat section (K_{comp} = 3). In this case, the Mach number through the throat section is determined using flow continuity using Equations (2-31) and (2-32).

The establishment of the internal supersonic compression and terminal shock wave structure for mixed-compression inlets has involved the use of bleed systems to control the growth of boundary layers and the adverse effects of shock wave / boundary layer interactions. Likely bleed regions will be needed within the internal supersonic diffuser and throat section. The discussion of bleed systems is deferred to Section 11.0.

9.4 Subsonic Diffusers for Mixed-Compression Inlets

The subsonic diffusers for the mixed-compression axisymmetric spike and two-dimensional inlets take the same form and use the same models as for the external-compression inlets as described in Subsection 8.6. One feature of subsonic diffusers for mixed-compression inlets that may not be used for external-compression inlets are engine bypass systems. The internal shock wave structure of mixed-compression inlets does not allow spillage of excess inlet flow past the cowl lip as with external-compression inlets. Thus, the excess flow not taken by the engine must be extracted using bleed systems or bypass systems located within the subsonic diffuser so as to not disturb the internal shock wave structure. Bypass systems are typically located on the cowl interior of the subsonic diffuser just upstream of the engine face. The bypass system may dump excess flow overboard or direct the excess flow past the engine to be exhausted through the nozzle. Section 11.0 will discuss some further issues related to bypass systems.

9.5 Component and Entity Specification

An alternative to using the geometry model of Subsection 9.1 or the MOC model of Subsection 9.2, is to specify entities and components that define the profiles of the inlets, as discussed in Subsection 8.7. The specification and use of entities for the external supersonic diffusers and subsonic diffusers of mixed-compression inlets follows the same procedures as for external-compression inlets. For mixed-compression inlets, the inclusion of the internal supersonic diffuser involves defining station TH, as well as station SD as done for external-compression inlets. For Kthop = 0 the coordinates $(x,y)_{cwTH}$ and $(x,y)_{cwSD}$ are established at the end-points of entities defined using K_{comt} = 7 for the throat section centerbody and K_{comt} = 8 for the throat section cowl interior. For K_{thop} = 2, the entities are defined using K_{comt} = 16 for the centerbody and K_{comt} = 17 for the cowl interior. When K_{thop} = 2, the input factors F_{xcwTH} and F_{xcwSD} are used to specify the x-coordinates on the cowl interior for stations TH and SD. A search is performed of the cowl interior entities to find the respective y-coordinates, y_{cwTH} and y_{cwSD}. The points $(x,y)_{cbTH}$ and $(x,y)_{cbSD}$ on the centerbody for stations TH and SD, respectively, are found from a search of the points on the centerbody entities closest to points $(x,y)_{cwTH}$ and $(x,y)_{cwSD}$, respectively.

9.6 Total Pressure Loss for the Internal Supersonic Diffuser

The supersonic flow through the internal supersonic diffuser creates total pressure losses through viscous diffusion within the boundary layer in addition to those losses through any shock waves. A model for the total pressure losses between stations 1 and TH due to viscous diffusion is provided by Reference 2. The total pressure loss can be calculated as

$$\left(\frac{p_{tTH}}{p_{t1}}\right)_{sup} = 1 - \left[K_D\left(1 - \frac{A_1}{A_{TH}}\right)^2 + K_O + K_F\right] K_M \left[1 - \left(1 + \frac{(\gamma-1)^2 M_1^2 + 2(\gamma-1)}{4\gamma M_1^2 - 2(\gamma-1)}\right)^{-\frac{\gamma}{\gamma-1}}\right] \tag{9-10}$$

where,

$$K_M = f\left(\sqrt{\frac{(\gamma-1)\, M_1^2 + 2}{2\gamma M_1^2 - (\gamma-1)}}\right) \tag{9-11}$$

The values of K_D, K_O, and K_F are computed in the same manner as discussed in Subsection 5.7.

The total pressure losses through the throat section are mainly due to the total pressure loss through a normal shock wave positioned at station TH, which can be computed using Equation (5-12). The total pressure losses for subsonic flow within the throat section between stations TH and SD can be computed using the model of Subsection 5.7.

The total pressure ratio for the entire internal supersonic diffuser (p_{tSD}/p_{t1}) can be calculated as the product of the total pressure ratios through the cowl shock wave, the ratio of Equation (9-10), ratio through the normal shock wave, and ratio due to subsonic viscous diffusion through the throat section.

References

1. Anderson, B. H., “Design of Supersonic Inlets by a Computer Program Incorporating the Method of Characteristics,” NASA TN D-4960, January 1969.
2. Henry, J. R., Wood, C. C., and Wilbur, S. W., “Summary of Subsonic-Diffuser Data,” NACA RM L56F05, October 1956.

10.0 Streamline-Traced Inlets

Streamline-traced inlets have supersonic compression surfaces formed from the ***tracing*** of the ***streamlines*** through a compressive, supersonic ***parent flowfield***. The streamline tracing approach is flexible in that it allows a wide variety of parent flowfields and cross-sections upon which the streamline tracing is based. Thus, a wide variety of inlet shapes and capture cross-sections are possible that may be beneficial for conforming to aircraft and propulsion system configurations. Further, the three-dimensional nature of the compression could allow a greater rate of flow compression compared to axisymmetric or two-dimensional supersonic compression.

Subsection 10.1 provides schematics showing the features of streamline-traced inlets. Subsections 10.2, 10.3, and 10.4, discuss the axisymmetric Busemann, ICFA-Otto-Busemann, and two-dimensional wedge parent flowfields, respectively, available within SUPIN. Subsection 10.5 discusses other possible parent flowfields. Subsection 10.6 discusses the tracing curves for streamline tracing. Subsection 10.7 discusses some traditional axisymmetric streamline-traced inlets. Subsection 10.8 discusses the SUPIN input factors that specify the supersonic streamline tracing capabilities. Subsections 10.9, 10.10, and 10.11 discuss the modeling of the throat section, subsonic diffuser, and cowl exterior for streamline-traced inlets.

10.1 Features of Streamline-Traced Inlets

This subsection discusses the main features of external and mixed-compression streamline-traced inlets. An example of a streamline-traced, external-compression inlet for $M_0 = 1.7$ is shown in Figure 10.1. It was generated using the axisymmetric Busemann parent flowfield with subsonic outflow and circular tracing curves offset from the axis of the parent flowfield to create a scarfed leading edge. The features, stations, and dimensions are shown. The nose point is the forward-most point of the leading edge while the cowl lip is the aft-most point on the leading edge. The shoulder is defined at the end of the external supersonic diffuser at which the inlet surface has a zero slope. The throat section is designed to contain a strong oblique terminal shock wave structure. The subsonic diffuser allows the offset of the engine face from the inlet axis.

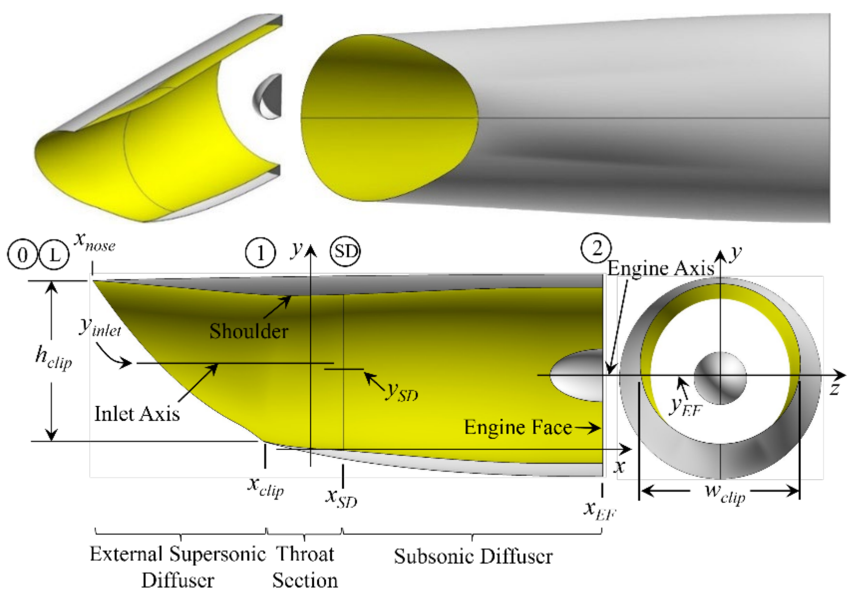

Figure 10.1.—An example of a streamline-traced, external-compression inlet.

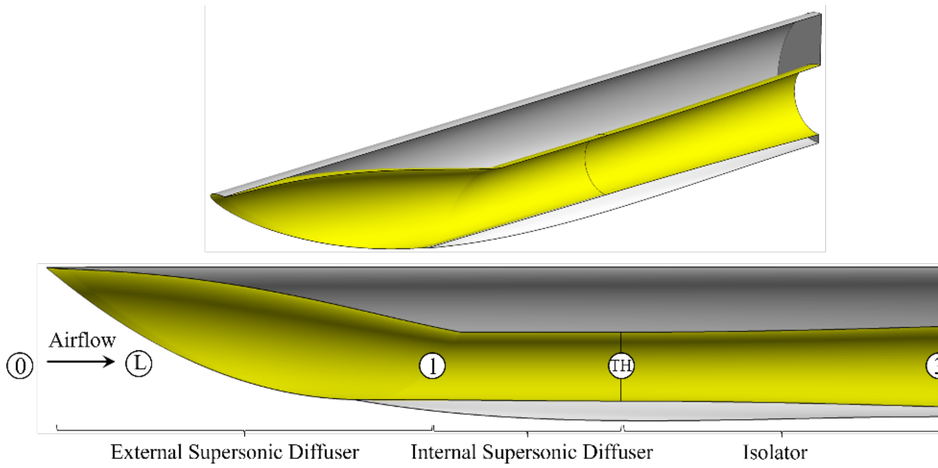

Figure 10.2.—An example of a streamline-traced, mixed-compression inlet.

An example of a streamline-traced, mixed-compression inlet for $M_0 = 4.0$ is shown in Figure 10.2. It was generated using the ICFA-Otto-Busemann parent flowfield with supersonic outflow and circular tracing curves. The inlet is intended for a ramjet or scramjet application. The internal supersonic diffuser consists of a nearly constant-area duct ending at the geometric throat station TH. The isolator would likely contain a shock wave train terminal shock wave system ending at station 3 which is the start of the combustor.

10.2 Axisymmetric Busemann Parent Flowfield

The ***axisymmetric Busemann flowfield*** is a conical flowfield that compresses an axial supersonic inflow through a series of isentropic waves and a freestanding conical shock wave at the outflow, which is also directed axially (Refs. 1 and 2). The axial character of the inflow and outflow makes this compressive flowfield attractive for inlets since the axial flow integrates well with an engine axis that is also aligned with the inlet axis. In addition, the flowfield involves inward turning of the flow, which may result in lower external cowl angles which lowers cowl wave drag. Figure 10.3 shows a schematic of the axisymmetric Busemann flowfield.

The vertex of the axisymmetric Busemann flowfield is placed at the origin of the global coordinate system, $(x,y,z) = (0,0,0)$. The flowfield is completely defined by the specification of the inflow and outflow Mach numbers. The inflow Mach number is the local Mach number at station L (M_L) and should be supersonic. The outflow Mach number (M_{stex}) can be either supersonic for the case of a weak conical shock wave or subsonic for the case of a strong conical shock wave. The bounds of M_{stex} should be consistent with the inflow Mach number (M_L) and the intent for the design. A lower value of M_{stex} will create a more compressive flowfield.

The flowfield is determined through the numerical solution of the Taylor-Maccoll equations for the axisymmetric conical flowfield about the vertex (Refs. 3 and 4). Figure 10.3 shows the conical rays upon which the flow properties are constant. The numerical solution involves a marching algorithm that starts at the outflow conditions. For the specified outflow Mach number (M_{stex}) an initial guess is made for the angle of the conical shock wave (β_{stex}). The conditions ahead of the conical shock wave can then be computed. The Taylor-Maccoll equations can then then marched upstream using a fourth-order

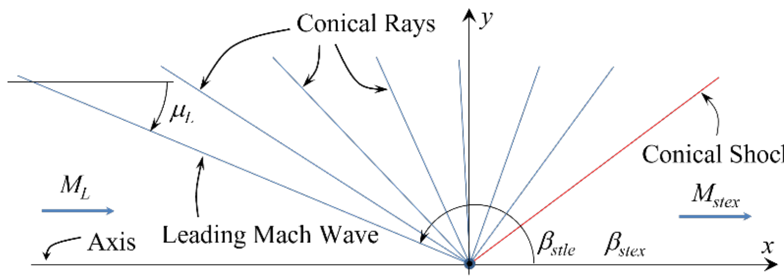

Figure 10.3.—Axisymmetric Busemann flowfield.

Runge-Kutta method until reaching the leading Mach wave at the angle β_{stle}. For a specified inflow Mach number (M_L), the angle of the leading Mach wave can be computed as

$$\beta_{stle} = \pi - \mu_L \tag{10-1}$$

In which μ_L is the angle of the Mach wave for M_L as computed as

$$\mu_L = \sin^{-1}\left({}^{1}/_{M_L}\right) \tag{10-2}$$

A further condition of the parent flowfield is that the angle of the inflow should also be axial. Thus, an iteration on the value of the conical shock wave angle (β_{stex}) is used to ensure that when the leading Mach wave is reached, the inflow will be axial and corresponding to the inflow Mach number (M_L).

The axisymmetric Busemann flowfield has a disadvantage in that the forward portion involves very little compression over a relatively long length. It may be desirable to shorten the flowfield by truncating the forward portion. This would create a deflection angle at the start of the internal cowl, which would form an oblique shock wave at the start of the external supersonic diffuser. The approach for truncating the axisymmetric Busemann flowfield within SUPIN is to truncate the upstream marching of the streamline tracing. The angle of the upstream wave (β_{stle}) is reduced by an input factor F_{strunc} through the equation,

$$\beta_{stle} = F_{strunc}\,(\pi - \mu_L) \tag{10-3}$$

The reasonable bounds of the truncation input factor are shown by Equation (10-4), with additional SUPIN code specific bounds discussed in Subsection 10.8,

$$0.8 \le F_{strunc} \le 1.0 \tag{10-4}$$

10.3 Axisymmetric ICFA-Otto-Busemann Parent Flowfield

The truncation of the axisymmetric Busemann flowfield described above will create a leading-edge oblique shock wave, but the shock wave is a product of the truncation, and the result may not provide the desired conditions downstream of the shock wave. An alternative is to establish a parent flowfield in which the desired leading-edge shock wave is a part of the flowfield. The ***axisymmetric ICFA-Otto-Busemann flowfield*** provides an approach for introducing a leading-edge shock wave (Ref. 5). The leading-edge shock wave is formed by a deflection angle, θ_{stle}, for the leading edge of the inlet. The deflection creates a local flowfield called the internal conical flowfield A or ICFA (Ref. 6). The image on the left-hand-side of Figure 10.4 shows a schematic of the ICFA flowfield. The equations can only be integrated a short distance before a singularity develops; however, the short distance is enough to establish the leading-edge shock wave and the start of a compressive flowfield. The ICFA flowfield ends with a Mach number and flow angle of M_a and θ_a, respectively.

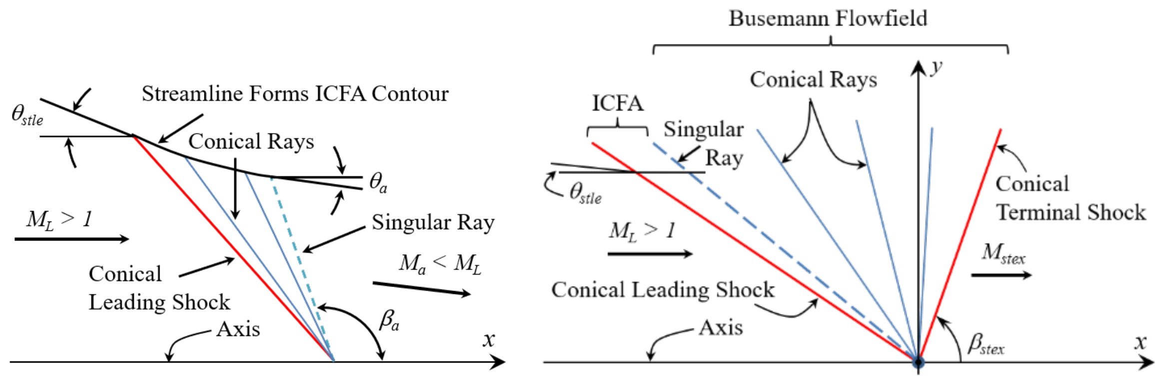

Figure 10.4.—The Internal Conical Flowfield A (ICFA, left) and the axisymmetric ICFA-Otto-Busemann parent flowfield (right).

Downstream of the ICFA flowfield, an axisymmetric Busemann flowfield is established in the same manner as discussed in the previous subsection with integration in the upstream direction starting from the outflow conditions. The difficulty comes about at the interface of the ICFA flowfield with the Busemann flowfield at the singular ray. A schematic of the axisymmetric ICFA-Otto-Busemann flowfield are shown in the image on the right-hand-side of Figure 10.4. Both the Mach number and flow angle (M_a and θ_a) need to be consistent at the interface to combine these two flowfields. Otto developed a methodology to use a Prandtl-Meyer expansion of the ICFA to match the Mach number of the forward wave of the Busemann flowfield (Ref. 5). A computational iteration procedure solves the ICFA, Prandtl-Meyer, and Busemann flowfields in sequence until the conditions at the interface are matched. The resulting external supersonic diffuser has a discontinuity in the slope at the interface of the ICFA and Busemann profiles, which adds a slight expansion; however, any detrimental effects are minimal.

The additional information required for the ICFA-Otto-Busemann parent flowfield is the angle of the leading-edge, θ_{stle}, which is specified by the input factor F_{stle}. To be consistent with an inward turning slope, the value of F_{stle} should be less than zero and is expressed in units of degrees.

10.4 Oblique Shock Wave Parent Flowfield

The oblique shock wave flow over a two-dimensional wedge or ramp can be used as a parent flowfield. Figure 10.5 shows a schematic of this flowfield. The ***oblique shock wave flowfield*** is completely described by the inflow Mach number (M_L) and the Mach number downstream of the oblique shock wave, which is specified by the input factor M_{stex} where $M_{stex} > 1$ is required to obtain a weak oblique shock wave solution. The steady-state, inviscid solution for the flowfield can be found from the oblique shock wave relations as described in Subsection 7.1. The oblique shock wave solution establishes the deflection angle θ_{stle} and shock wave angle β_{stle}. An oblique shock wave is formed at the leading edge and the flow downstream of the oblique shock wave is aligned with the wedge angle and is uniform (Ref. 4). This flowfield is not inward turning and the outflow is not axial, but rather has a flow angle equal to θ_{stle}. The use of this flowfield for an external or mixed-compression inlet would require the throat section to turn the flow toward the engine axis and decelerate the flow to subsonic conditions.

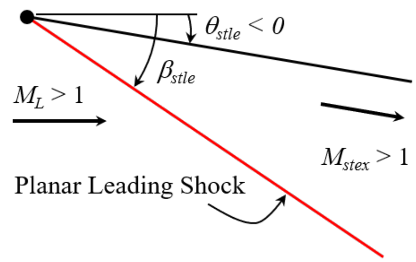

Figure 10.5.—The two-dimensional wedge parent flowfield.

10.5 Other Parent Flowfields

An attractive characteristic of streamline-traced inlets is that there is flexibility in the choice of the parent flowfield. For an inlet, the parent flowfield should be compressive and desired direction of the flow. Further, the flowfield should not contain excessive losses in total pressure. It is possible to form a numerically generated parent flowfield, such as a flowfield from a CFD simulation.

10.6 Streamline Tracing Curves

The surface of the external supersonic diffuser is formed by tracing streamlines through a parent flowfield. It is possible to perform the tracing in either the upstream or downstream direction. For SUPIN, the streamlines are traced in the upstream direction starting at points distributed along tracing curves placed in the downstream outflow of the parent flowfield. The ***tracing curves*** are defined as a closed circuit defined on a plane perpendicular to the parent flowfield axis. Here, we consider tracing curves consisting of two curve segments – one curve segment forms the top of the closed circuit, and the other curve segment forms the bottom of the closed circuit (Ref. 7). Figure 10.6 illustrates the placement of the tracing curves (shown from a side-view) within the outflow and the creation of streamlines within an axisymmetric Busemann flowfield. Figure 10.7 shows two examples of tracing curves from the viewpoint along the axis of the flowfield looking in the downstream direction. In Figure 10.6 and Figure 10.7, the top tracing curve is shown in red, while the bottom tracing curve is shown in blue.

Each tracing curve is described using a super-ellipse (Ref. 8). The super-ellipse is characterized by the lengths of the semi-major (a) and semi-minor axes (b) and a super-ellipse parameter (p). A parameter value of $p = 2$ creates an ellipse. As the parameter p increases greater than $p = 2$, the super-ellipse approaches a rectangle. Appendix A provides further details on the super-ellipse and Figure A-6 shows an example of curves for increasing values of p. Both tracing curves share the same semi-major axis length (a_{st}) but can have different values of the semi-minor axis lengths (b_{sttop}, b_{stbot}) and parameters (p_{sttop}, p_{stbot}). This provides flexibility in the shape of the tracing curves. The tracing curves on the left of Figure 10.7 consist of super ellipses that form circular arcs for the top and bottom ($b_{sttop} = b_{stbot} = a_{st}$ and $p_{sttop} = p_{stbot} = 2$). The tracing curves on the right of Figure 10.7 consist of super ellipses that form a circular arc for the bottom section ($b_{stbot} = a_{st}$ and $p_{stbot} = 2$) and a more rectangular shape for the top ($b_{sttop} = a_{st}$ and $p_{sttop} = 10$). The tracing curves are defined in a local coordinate system in which the center is on the $z = 0$ plane but can be translated in the y-direction by a value y_{stex}. The center of the tracing curves establishes the inlet axis such that $y_{inlet} = y_{stex}$.

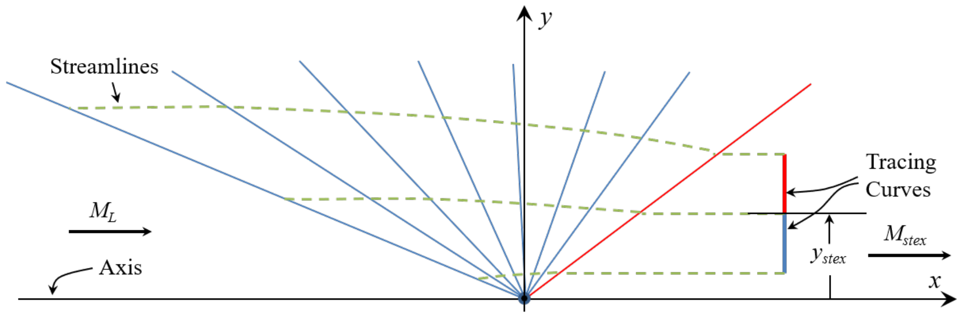

Figure 10.6.—An example of the tracing of streamlines through the axisymmetric Busemann flowfield with streamlines originating from the tracing curves.

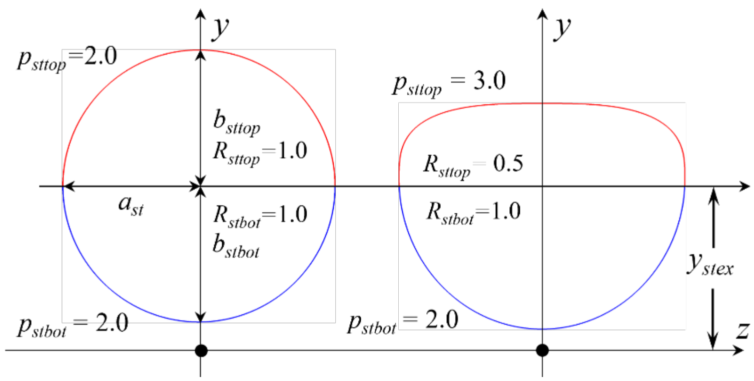

Figure 10.7.—Tracing curves used for the two streamline-traced inlets of Figure 10.8 (view is looking downstream).

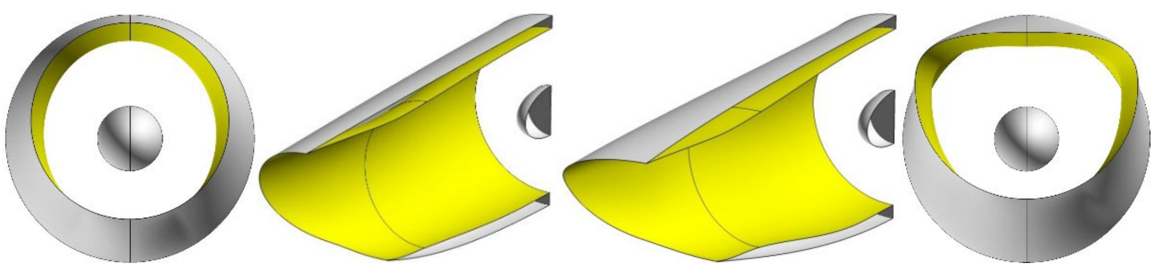

Figure 10.8.—Examples of streamline-traced inlets with the tracing curves of Figure 10.7.

The flexibility in defining the shape of the tracing curves and the ability to offset the inlet axis from the axis-of-symmetry of the Busemann flowfield allows for the creation of a wide variety of shapes for the external supersonic diffuser. Figure 10.6 shows three examples of streamlines indicated by green dashed lines originating from points on the bottom, middle, and top of the tracing curves placed above the axis-of-symmetry of the Busemann flowfield. The value of y_{stex} was chosen so that the tracing curve does not contain the focal point of the Busemann flowfield. A larger offset of y_{stex} will result in a longer and scarfed external supersonic diffuser surface. Each point on the tracing curve is associated with a circumferential angle of the axisymmetric flow. Thus, the integration of each streamline is a planar integration problem. The streamline originating from the top of the tracing curve forms a longer curve through the flowfield than the streamline originating from the bottom of the tracing curve. This creates a leading edge for the surface that is scarfed with the bottom of the leading edge downstream of the top of the leading edge. Such a configuration may allow spillage at the downstream portion of the leading edge. Figure 10.8 shows two examples of streamline-traced inlets created from the tracing curves of Figure 10.7.

During the inlet sizing, the capture area (A_{cap}) is determined. For the streamline-traced inlets, the capture area cross-section is a product of the streamline-tracing. Thus, an iterative approach is used to establish the desired capture area. The factor a_{st} is initialized with the value of the radius of the engine face. The iteration adjusts the size of a_{st} to match the capture area required for flow continuity consistent with the inlet aerodynamics. The values of b_{stbot}, b_{sttop}, and y_{stex} are adjusted as the value of a_{st} is adjusted as part of the iteration.

The design of an external-compression inlet based on streamline tracing requires further modifications to the external supersonic diffuser to work with an external terminal shock wave and subsonic throat. These modifications will be discussed in a later subsection for which the throat geometry is discussed.

10.7 Axisymmetric Streamline-Traced Inlets

The streamline tracing is demonstrated through the generation of a classic "axisymmetric Busemann" inlet and its comparison with an axisymmetric inlet generated from the ICFA-Otto-Busemann parent flowfield. The inlets were generated using M_L = 4 and M_{stex} = 1.5. The tracing curves were circular and centered on the axis-of-symmetry (y_{stex} = 0), which resulted in their axisymmetric character. Both inlets were generated using the same reference capture area (A_{cap}) so that they both had the same inlet flow rate. The streamline-traced supersonic diffuser is fully internal for the axisymmetric streamline-traced inlets. Thus, the resulting inlets involved fully internal supersonic compression. Images of the inlets are shown in Figure 10.9. These inlets contrast with those of Figure 10.1 and Figure 10.2 that show a scarfed leading edge due to $y_{stex} > 0$ and designation of an external supersonic diffuser.

A comparison of the side views of the inlets is shown in Figure 10.10 where the axisymmetric Busemann inlet is shown in an outline while the axisymmetric ICFA-Otto-Busemann inlet is shown as the shaded image. The ICFA-Otto-Busemann inlet used a cowl interior angle of θ_{stle} = - 5.0 degrees which introduced the internal oblique cowl shock wave at the leading edge as part of the ICFA flowfield. The effect of this cowl shock wave is to create an 18% shorter inlet than the Busemann inlet, which required θ_{stle} = 0 degrees to form Mach waves at the leading edge. The smaller size of the ICFA-Otto-Busemann inlet would likely results into lower weight. The choice of θ_{stle} impacts the shape of the cowl exterior. If the cowl lip exterior angle is specified to be 5 degrees greater than the cowl lip interior angle (i.e., $\theta_{clex} = \theta_{stle}$ + 5 degrees), then this results in θ_{clex} = 5 degrees for the Busemann inlet, but θ_{clex} = 0 degrees for the ICFA-Otto-Busemann inlet. The result of this can be seen in the images of Figure 10.9 and Figure 10.10. This will also result in the ICFA-Otto-Busemann inlet having lower cowl wave drag than the Busemann inlet, which is quantified through the sample cases for these inlets discussed in Appendix G. The throat sections for these inlets were constant-area circular ducts intended to maintain the Mach 1.5 outflow.

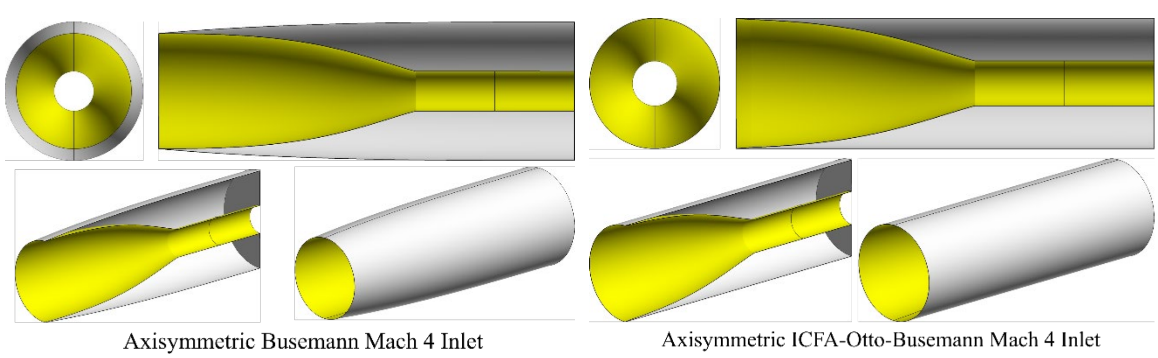

Figure 10.9.—Axisymmetric streamline-traced inlets for Mach 4.

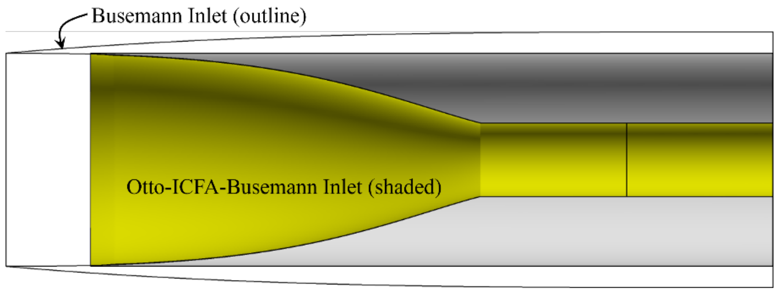

Figure 10.10.—Comparison of the axisymmetric ICFA-Otto-Busemann (shaded) and the axisymmetric Busemann (outline) streamline-traced inlets for Mach 4.

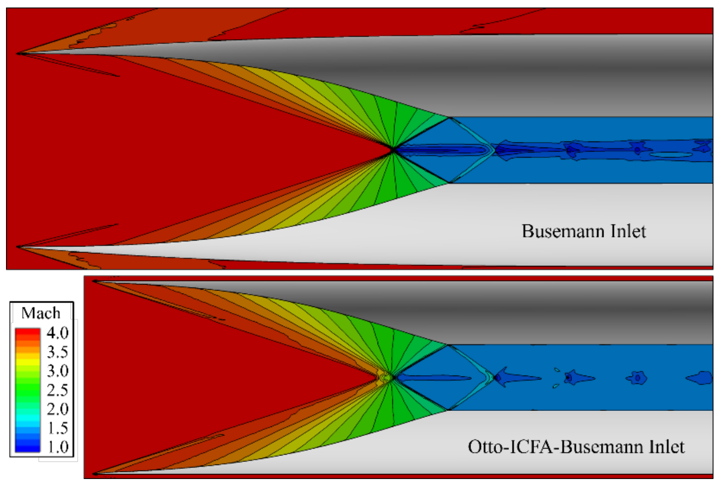

Figure 10.11.—Mach number contours from inviscid CFD simulations of the axisymmetric Busemann (top) and ICFA-Otto-Busemann (bottom) streamline-traced inlets for Mach 4.

Inviscid CFD simulations were performed of the two inlets to verify that the compressive flowfields were generated. Mach number contour images on the symmetry plane of the inlets are shown in Figure 10.11. The focusing of the Mach waves at $x = 0$ and the outflow conical shock wave are visible. The cowl shock wave of the ICFA-Otto-Busemann inlet is also visible in the bottom image. The cowl lip exterior of the Busemann inlet creates an exterior cowl shock wave and expansion waves downstream along the cowl exterior. For both simulations, the outflow conical shock wave seems properly placed with their intersections at the sharp shoulder points. Slight reflections of the outflow conical shock wave are visible. Downstream of the outflow conical shock wave, both images show approximately Mach 1.5 flow, but some variation in Mach number is noticeable within the contours. The results of the CFD simulations will be discussed in greater detail in the sample cases of Appendix G.

10.8 SUPIN Input Factors for the Streamline-Traced Supersonic Diffuser

The creation of the streamline-traced supersonic diffuser within SUPIN uses several design factors for the parent flowfield and tracing curves that are discussed in this subsection. Table 10.1 summarizes the input factors for the parent flowfields. The choice of the parent flowfield is specified by the input factor K_{stex}. The three choices are the axisymmetric Busemann flowfield ($K_{stex} = 0$), the axisymmetric ICFA-Otto-Busemann flowfield ($K_{stex} = 1$), and the two-dimensional wedge flowfield ($K_{stex} = 2$). Each of these parent flowfields were discussed in previous subsections. All three parent flowfields act to decelerate and compress the supersonic inflow to a lower Mach number outflow. The axisymmetric Busemann and the axisymmetric ICFA-Otto-Busemann flowfields contain a conical shock wave at the end of the external supersonic diffuser. For both flowfields, the outflow is axial and may be supersonic or subsonic depending on the whether the conical shock wave is a weak or strong oblique shock wave, respectively. The desired outflow Mach number is specified through the input factor M_{stex}. The input factor F_{stle} specifies the deflection at the leading edge (θ_{stle}) for the axisymmetric ICFA-Otto-Busemann flowfield. The units for F_{stle} are degrees and a negative value ($F_{stle} < 0$) is needed to indicate a deflection for the leading-edge shock wave.

The input factor F_{strunc} indicates the amount of truncation of the axisymmetric Busemann flowfield as discussed in the subsection above. Equation (10-1) calculates its use in the truncation. A value of $F_{strunc} = 1.0$ specifies no truncation. Values of $F_{strunc} < 1$ produce a truncation of the axisymmetric Busemann flowfield with greater truncation as F_{strunc} is reduced. The truncation of the wave angle using F_{strunc} can be very sensitive as the freestream Mach number increases. For example, for a Mach 6 Busemann flowfield, values of $0.97 \le F_{strunc} \le 0.995$ are likely a reasonable range for F_{strunc}. The use of the ICFA-Otto-Busemann parent flowfield does not require a truncation compared to the axisymmetric Busemann flowfield and includes the leading-edge conical shock wave as a natural part of the flowfield. Thus, the use of the ICFA-Otto-Busemann flowfield may be a better choice than the axisymmetric Busemann flowfield if an initial oblique shock is needed for a parent flowfield featuring an axisymmetric Busemann flowfield.

The two-dimensional wedge flowfield establishes a uniform supersonic flowfield at the end of the external supersonic diffuser and the input factor M_{stex} is used to specify the Mach number of the flow downstream of the oblique shock wave and flowing over the wedge. The oblique shock solution establishes the wedge flow angle θ_{stle}. The wedge flowfield would require turning within an internal supersonic diffuser.

The input factors for the tracing curves are listed in Table 10.2. The lengths of the semi-minor axes b_{stbot} and b_{sttop} are specified using the aspect ratios $(b/a)_{stbot}$ and $(b/a)_{sttop}$. The input factors p_{stbot} and p_{sttop} specify the super-ellipse parameters for the bottom and top tracing curves. The factor y_{stex} specifies the vertical translation of the tracing curves and is specified as a value normalized by a_{st}. Thus, the value of y_{stex} in units of feet is obtained by multiplying the value in the input data file by the value of a_{st}. The axisymmetric inlets of the previous subsection were created with $y_{stex} = 0$. The inlets of Figure 10.1 and Figure 10.2 were created with $y_{stex} = 1.0005$.

Table 10.3 shows an example input data block for the streamline-traced external supersonic diffuser. The streamline-traced supersonic diffuser is specified using the input factor $K_{exd} = 6$ for the input data block for external supersonic diffusers.

TABLE 10.1.—INPUT FACTORS FOR THE PARENT FLOWFIELD

Factor	Input	Description
K_{stex}	`Kstex`	Type of parent flowfield used for streamline tracing = 0 Axisymmetric Busemann flowfield = 1 Axisymmetric ICFA-Busemann flowfield = 2 Two-dimensional wedge flowfield
M_{stex}	`Mstex`	Mach number at the outflow of the parent flowfield
F_{stle}	`Fstle`	Slope at the leading edge of the streamline-traced surface (deg)
F_{strunc}	`Fstrunc`	Factor for the truncation of the axisymmetric Busemann flowfield

TABLE 10.2.—INPUT FACTORS FOR THE TRACING CURVES

Factor	Input	Description
$(b/a)_{stbot}$	strbot	Ratio of (b/a) for semi-minor axis for the bottom tracing cross-section
$(b/a)_{sttop}$	strtop	Ratio of (b/a) for semi-minor axis for the top tracing cross-section
p_{stbot}	stpbot	Super-ellipse parameter for the bottom tracing cross-section, $p_{stbot} \geq 2$
p_{sttop}	stptop	Super-ellipse parameter for the top tracing cross-section, $p_{sttop} \geq 2$
y_{stex}	stdyax	Vertical translation of tracing cross-section (normalized by a_{st})

TABLE 10.3.—EXAMPLE INPUT DATA BLOCK FOR THE
STREAMLINE-TRACED EXTERNAL SUPERSONIC DIFFUSER

```
DataID.  External Supersonic Diffuser
  4
Kexd     FptEXptL     Fpt1ptEX
  6       -0.9950      -0.9850
Kstex       Mstex    Fstrunc      Fstle
  1         0.900      1.000     -5.000
strbot     strtop     stpbot     stptop     stdyax
1.0000     1.0000      2.000      2.000     1.0005
```

10.9 Internal Supersonic Diffuser and Throat Section

Downstream of the streamline-traced supersonic diffuser, the formation of the internal ducting depends on whether the outflow of the parent flowfield is subsonic ($M_{stex} < 1$) or supersonic ($M_{stex} > 1$). While station 1 is identified in Figure 10.1 and Figure 10.2, it is not well-defined in the flowfield and may not be of importance. Of greater importance is the state of the flow downstream of the outflow conical shock wave from the parent flowfield. The Mach number M_1 is the mass-averaged Mach number downstream of the terminal shock wave (i.e., $M_1 = M_{stex}$). If the outflow is subsonic ($M_{stex} < 1$), the outflow conical shock wave becomes a strong oblique terminal shock wave, and the internal ducting takes the form of a throat section that processes the subsonic flow for the start of the subsonic diffuser at station SD. If the flow is supersonic ($M_{stex} > 1$), then the internal ducting becomes an internal supersonic diffuser leading to a geometric throat station TH. Likely, the internal supersonic diffuser is a nearly constant-area duct with very little supersonic diffusion occurring. At station TH, the supersonic flow would enter an isolator that would contain a shock wave train terminal shock wave system prior to the combustor at station 3.

The geometry model within SUPIN for the subsonic throat section can also be used for the internal supersonic diffuser. The input factors for that model are discussed in the next several paragraphs. The length of the throat section or internal supersonic diffuser is established through specification of the input factor for ΔxSD, which is the length from the downstream end of the external supersonic diffuser to station SD and is normalized by the reference dimension, D_{ref}. The input factor ΔySD allows a vertical adjustment to the center point of the cross-section at station SD and is also normalized by the reference dimension.

Station SD is specified to be at a constant-x plane with a cross-section defined by the upper and lower super ellipse curves in much the same manner as the tracing curves. The cross-section has geometric factors that include a_{SD}, b_{topSD}, b_{botSD}, p_{topSD}, and p_{botSD}. The quantities a_{SD}, b_{topSD}, and b_{botSD} are determined through specification of the input factor A_{SD}/A_1, which is the area ratio of the cross-section at station SD to the area of the cross-section at station 1. If the input factor $A_{SD}/A_1 < 0$, then the cross-sectional area at station SD is set to the same value as calculated for the cross-sectional area of the throat station TH. The quantities p_{topSD} and p_{botSD} are specified as input factors. The input factors θ_{botSD} and θ_{topSD} specify the streamwise slope of the throat surface at the bottom and top of the throat surface at station SD, respectively. Table 10.4 summarizes the input factors for the length of the throat and properties of the cross-section at station SD.

The streamline-traced external supersonic diffuser surface generates a surface that has an inward slope at the end of the diffuser. The outflow conical shock wave turns the flow parallel to the axis. This creates a sharp corner at the end of the surface that may not be favorable for all operating conditions of the inlet. Thus, a modification is permitted in the surface which involves the rounding of the sharp corner using a circular arc. The input factor Fx_{stsh} specifies the extent of this rounding. A value of $Fx_{stsh} = 1.0$ indicates no rounding, while $Fx_{stsh} < 1.0$ indicates the fraction of the length from the leading edge to the trailing edge at which the rounding starts. A value of $Fx_{stsh} = 0.95$ is a reasonable value to apply some rounding. A circular arc is fitted to impose the rounding.

The streamline-traced supersonic diffuser can be modified to adjust for the growth of the boundary layer. The input factor Fr_{stsh} is the desired amount of vertical displacement at the end of the diffuser. The unit for the input factor Fr_{stsh} is feet. This value is expected to be approximately equal to the value of the boundary layer displacement thickness for the longest streamwise length from the leading edge to the trailing edge along the diffuser. For the inlets of Figure 10.1 and Figure 10.2, this length would be at the top-center of the external supersonic diffuser. The outward displacement of the diffuser profile would be applied linearly from the leading edge of the diffuser where the displacement would be zero to the end of the diffuser where the displacement would be the value specified by Fr_{stsh}. Circumferentially, the displacement would decrease as the length along the supersonic diffuser decreases. These modifications are similar to those discussed in Subsection 9.1 and illustrated in Figure 9.2. Table 10.5 summarizes the input factors that smooth the corner at the shoulder and adjust for the boundary layer at the end of the streamline-traced supersonic diffuser.

For the streamline-traced external-compression inlet, the strong oblique terminal shock wave sits near the entrance of the interior ducting of the inlet. The terminal shock wave is mostly bounded by the surface of the streamline-traced supersonic diffuser; however, there is a region at the bottom over which the terminal shock wave spills past the leading edge of the inlet. The result is that subsonic flow downstream of the terminal shock wave is allowed to be spilled past the leading edge, which is a feature of external-compression inlets to provide a means of matching the inlet and engine-face flowrates. An illustration of this spillage of the terminal shock wave is shown in Figure 10.12. The expected circumferential extent of the spilled shock wave is denoted as $\Delta\phi_{stcl}$ and is illustrated in Figure 10.12. The value of $\Delta\phi_{stcl}$ is an input factor and will be discussed below.

TABLE 10.4.—INPUT FACTORS DEFINING THE LENGTH OF THE THROAT AND PROPERTIES OF STATION SD

Factor	Inputs	Description
A_{SD}/A_1	`FaSDa1`	Ratio of the cross-sectional area at station SD to area at station 1
Δx_{SD}	`FdxSD`	Displacement for specification of the x-coordinate of station SD (normalized by D_{EF})
Δy_{SD}	`FdySD`	Displacement for specification of the y-coordinate of station SD (normalized by D_{EF})
p_{botSD}	`pbotSD`	Super-ellipse parameter for bottom curve of the cross-section at station SD
p_{topSD}	`ptopSD`	Super-ellipse parameter for top curve of the cross-section at station SD
θ_{botSD}	`thbotSD`	Slope of bottom of the cowl interior on the symmetry plane at station SD (deg)
θ_{topSD}	`thtopSD`	Slope of top of the cowl interior on the symmetry plane at station SD (deg)

TABLE 10.5.—INPUT FACTORS FOR MODIFICATION TO THE STREAMLINE-TRACED DIFFUSER

Factor	Input	Description
Fx_{stsh}	`Fxstsh`	Axial extent of the “rounding” of the sharp corner
Fr_{stsh}	`Frstsh`	Radial displacement of the end of the streamline-traced external supersonic diffuser (ft)

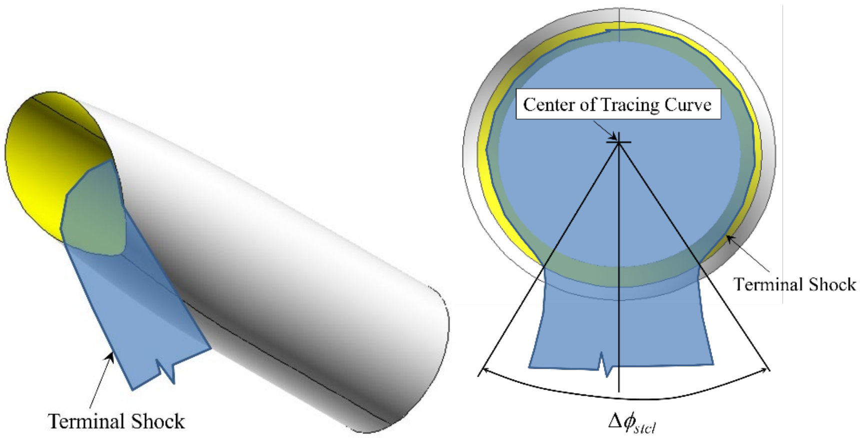

Figure 10.12.—Schematic of the placement of the strong oblique terminal shock for a streamline-traced, external-compression inlet.

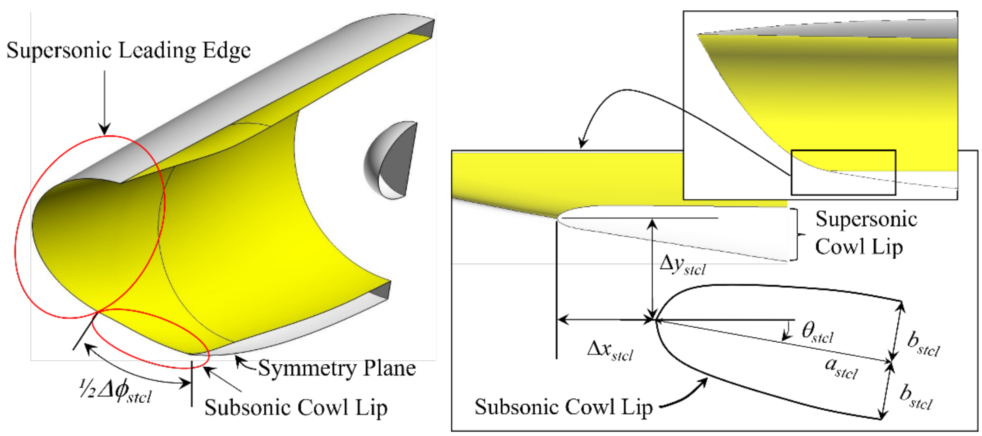

Figure 10.13.—Division of the inlet leading edge into a supersonic leading edge and a subsonic cowl lip (left). Profile on the symmetry plane of the subsonic cowl lip (right) along with input factors for its specification.

The subsonic flow spilled past the leading edge can be facilitated by dividing the leading edge of the streamline-traced inlet into a supersonic leading edge and a subsonic cowl lip, as shown in Figure 10.13. The supersonic leading-edge encounters supersonic flow and the profile is modeled as an ellipse with a very small thickness in the same manner as described for the axisymmetric spike and two-dimensional inlets in Subsection 8.2. The subsonic cowl lip is intended to encounter the subsonic flow of the subsonic spillage downstream of the terminal shock wave. For such subsonic spillage, a thicker and more blunt cowl lip may be desired to reduce the possibility of boundary layer separation of the subsonic flow past the cowl lip. Also, the local subsonic flow angles may be different than that of the supersonic flow. Input factors are provided to modify the leading edge of the inlet to impose a subsonic cowl lip to provide for a thicker cowl lip and angles aligned to the subsonic flow. The circumferential extent of the subsonic cowl lip is coincident with the expected circumferential extent of the spillage of the terminal shock wave ($\Delta\phi_{stcl}$) as shown in Figure 10.12 and Figure 10.13.

The shape of the subsonic cowl lip surface is established by specifying the profile of the subsonic cowl lip at the symmetry plane and then blending this shape with the profile of the supersonic leading edge over the semi-circumference of the subsonic cowl lip ($\Delta\phi_{stcl}/2$) to form a three-dimensional surface. A schematic showing the profiles of the supersonic and subsonic cowl lips and the input factors that

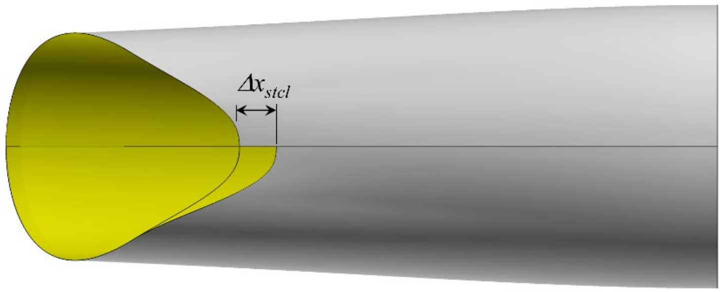

Figure 10.14.—Input factor Δx_{stcl} defining the length of the cut-back of the subsonic cowl lip at the symmetry plane.

create the subsonic cowl lip profile is shown in image of the right-hand-side of Figure 10.13. The profile of the subsonic cowl lip is established on the inlet symmetry plane as an ellipse with a semi-major axis length of a_{stcl} and a semi-minor axis length of b_{stcl}. The ellipse is oriented at an angle θ_{stcl} to the inlet axis. The leading edge of the profile can be offset from the leading edge of the supersonic leading edge by increments Δx_{stcl} and Δy_{stcl}. In the image of Figure 10.13, the subsonic cowl lip has been positioned below and downstream of the original location of the supersonic leading edge at the symmetry plane. The impact of the input factor Δx_{stcl} is also illustrated in Figure 10.14 showing the bottom view of two inlets with their halfs cut and mirrored about the x-y plane of symmetry. The inlet at the top of the image was created with $\Delta x_{stcl} = 0$ for no cut-back of the subsonic cowl lip. The inlet at the bottom was created with $\Delta x_{stcl} = 0.265$ to create a cut-back. The value for Δx_{stcl} is normalized by the inlet reference dimension (D_{ref}).

The cut-back provides an opening for the subsonic spillage to occur. The limiting of the subsonic spillage over the circumferential segment $\Delta\phi_{stcl}$ of the leading edge could be used as an advantage for the integration of the inlet with an aircraft. For example, the inlet could be mounted on the top of the fuselage with the subsonic cowl lip oriented away from the fuselage to limit interference of the spillage flow and shock wave with the fuselage.

With the definition of the elliptic profile of the subsonic cowl lip at the symmetry plane, the surface of the subsonic cowl lip can be established by blending the elliptic profile over the circumference of the subsonic cowl lip ($\Delta\phi_{stcl}$). The dimensions (a,b), incidence angle (θ), and leading edge displacement (Δx,Δy) of the elliptical profiles through the circumference are varied using a variation based on the four-point NURBS curve. The variation also accounts for specification of the angle of the leading edge or highlight curve at the symmetry plane (ξ_{stcl}). The angle ξ_{stcl} is illustrated in Figure 10.15 showing the bottom of a streamline-traced inlet. The blending of the subsonic cowl profile also incorporates the blending of this angle over the circumference of the subsonic cowl lip.

Table 10.6 lists the factors for the subsonic cowl lip and lists the factors within SUPIN that allow the specification of the value of these factors. The input factors Δx_{stcl} and Δy_{stcl} specify the horizontal and vertical displacement of the profile of the subsonic cowl lip as normalized by the reference dimension (D_{ref}). The length of the semi-minor axis of the subsonic cowl lip is specified by the input factor b_{stcl} and its units are feet. The length of the semi-major axis is defined as the aspect ratio ($AR_{stcl} = a_{stcl}/b_{stcl}$) of the elliptical segment defining the profile. The input factor θ_{stcl} specifies the angle-of-incidence of the subsonic cowl lip in units of degrees. The input factor ξ_{stcl} specifies the angle of the highlight of the subsonic cowl lip at the plane-of-symmetry in units of degrees. Table 10.7 provides an example input data block for the throat of the streamline-traced inlet.

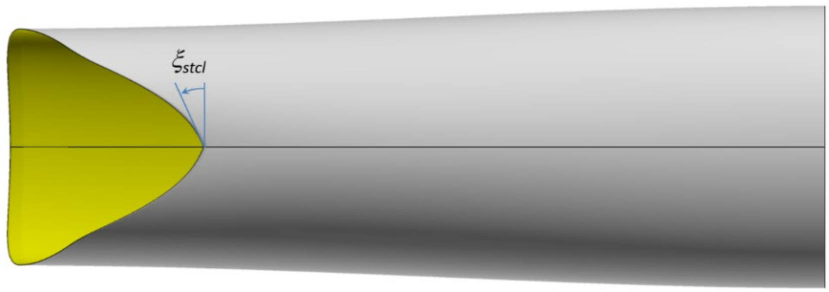

Figure 10.15.—Input factor ξ_{stcl} defining the slope of the subsonic cowl lip at the symmetry plane.

TABLE 10.6.—FACTORS FOR THE SUBSONIC COWL LIP OF A STREAMLINE-TRACED EXTERNAL-COMPRESSION INLET

Factor	Input	Description
$\Delta\phi_{stcl}$	`stclphi`	Circumferential extent of subsonic cowl lip (<=0 for no subsonic cowl lip) (deg)
Δx_{stcl}	`Fstcldx`	Axial displacement of the subsonic cowl lip at the symmetry plane (normalized by D_{ref})
Δy_{stcl}	`Fstcldy`	Vertical displacement of the subsonic cowl lip at the symmetry plane (normalized by D_{ref})
ξ_{stcl}	`stclxi`	Transverse angle of the subsonic cowl lip at the symmetry plane (deg)
θ_{stcl}	`stclth`	Angle of incidence of the subsonic cowl lip at the symmetry plane (deg)
b_{stcl}	`Fstclb`	Thickness of the semi-minor axis for the elliptical profile of the subsonic cowl lip (ft)
AR_{stcl}	`stclar`	Aspect ratio of the elliptical profile of the subsonic cowl lip (a_{stcl}/b_{stcl})

TABLE 10.7.—EXAMPLE INPUT DATA BLOCK FOR A SUBSONIC THROAT SECTION FOR A STREAMLINE-TRACED INLET

```
DataID.  Throat Section
  8
Kthrt   FptTSpt1   FptTHptTS   FptSDptTH
  7     -0.99000    -0.99500    -1.00000
 Fxstsh    Frstsh    stclxi    thSDK1    thSDKM
0.95000   0.00500     0.000     0.000     0.000
stclphi   Fstcldx   Fstcldy    stclth    Fstclb    stclar
120.000   0.26500   0.00000     0.000   0.00010     4.000
 FaSDa1     FdxSD     FdySD    pbotSD    ptopSD
1.03000   0.10000   0.00000     2.000     2.000
```

10.10 Subsonic Diffuser and Isolator

The subsonic diffuser exists downstream of the subsonic throat section as illustrated in Figure 10.1 between stations SD and 2. An isolator exists downstream of the internal supersonic diffuser as illustrated in Figure 10.2 between stations TH and 3. Both the subsonic diffuser and isolator are internal ducts in which the cross-sections at their start and end are established by the throat section/internal supersonic diffuser and engine face, respectively. The design and input factors for these ducts use the same methods as described in Subsection 6.4 for the three-dimensional pitot inlet with K_{subd} = 6 or K_{subd} = 7. While a subsonic diffuser may feature an offset engine face and significant cross-sectional area variation, an isolator typically is a nearly straight, constant-area duct. Both can be modeled using the same input factors listed in Table 6.5 for K_{subd} = 6. These same input factors and form of the input data block apply for K_{subd} = 7.

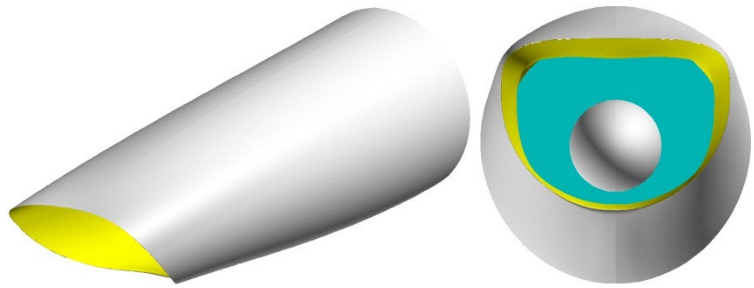

Figure 10.16.—An example of a cowl exterior for a streamline-traced inlet.

10.11 Cowl Exterior

The cowl exterior for the streamline-traced inlet is formed as a collection of NURBS curves extending from a cowl lip exterior point to the endpoint of the cowl exterior at x_{cwex} about the circumference of the inlet. This type of cowl exterior was described in Subsection 4.10 and the input factors for the cowl exterior were listed in Table 4.16. Figure 10.16 shows an example of a cowl exterior for a streamline-traced inlet along with the frontal projection.

References

1. Busemann, A., "Die achsensymmetrische kegelige Uberschallströmung," Luftfrahrtforschung 19, 137-144 (1942).
2. Mölder, S. and Szpiro, E. J., "Busemann Inlet for Hypersonic Speeds," *AIAA Journal of Spacecraft and Rockets*, Vol. 3, No. 8, pp. 1303-1304, August 1966.
3. Taylor, G. I. and Maccoll, J. W., "The Air Pressure on a Cone Moving at High Speeds," *Proceedings of the Royal Society (London)*, Ser. A, Vol. 139, pp. 278-311, 1933.
4. Anderson, J. D., Jr., *Modern Compressible Flow*, McGraw-Hill Book Company, New York, 1982.
5. Otto, S. E, Trefny, C. J. and Slater, J. W., "Inward-Turning Streamline-Traced Inlet Design Method for Low-Boom, Low-Drag Applications," *AIAA Journal of Propulsion and Power*, Vol. 32, No. 5, pp. 1178-1189, September-October 2016.
6. Mölder, S., "Internal, Axisymmetric, Conical Flow," *AIAA Journal*, Vol. 5, No. 7, pp. 1252-1255, July 1967.
7. Slater, J. W., "Methodology for the Design of Streamline-Traced External-Compression Supersonic Inlets," AIAA Paper 2014-3593, July 2014.
8. Koncsek, J. L., "An Approach to Conformal Inlet Diffuser Design for Integrated Propulsion Systems," AIAA Paper 1981-1395, July 1981.

11.0 Inlet Bleed and Bypass

This section discusses the specification and modeling of ***bleed*** and ***bypass*** within SUPIN. Subsection 11.1 provides an overview of the types and role of bleed within supersonic inlets. Subsection 11.2 discusses the modeling of porous bleed regions with the use of the Slater bleed model (Refs. 1 and 2). Subsection 11.3 discusses the input factors for describing porous bleed within SUPIN. Subsection 11.4 discusses the geometric modeling of bleed slots.

11.1 Role of Bleed and Bypass within a Supersonic Inlet

Supersonic inlets involve shock waves for compression and these shock waves will interact with viscous boundary layers. The inlet flowfield by nature involves an adverse pressure gradient. The interactions cause localized adverse pressure gradients that may cause excessive thickening or separation of the boundary layer from the inlet surface. Boundary layer separation leads to recirculated flow and total pressure losses through mixing and viscous dissipation. Even without adverse interactions of shock waves, the thickening of boundary layers over the inlet surfaces may cause excessive blockage of the flow within the inlet. One approach for alleviating the adverse effects of these interactions and blockage has been to use ***bleed systems*** that extract a portion of the boundary layer. The central idea is that by removing a portion of the lower momentum flow of the boundary layer, the remaining flow has higher total momentum to withstand further adverse conditions within the inlet. The placement of bleed regions within the inlet, especially within the throat section where shock wave interactions are mostly likely to occur, and the tailoring of bleed flow rates are effective means of improving inlet performance.

Bleed also provides a mechanism for small adjustments of the inlet flow rate to better match the demands of the engine flow rate. This can provide a stabilizing effect on both external and internal terminal shock wave systems. The required engine flow rate varies throughout the aircraft mission as throttle settings are changed and as the engine encounters transients. Atmospheric disturbances can cause variations in the inlet conditions which introduce pressure waves and change the inlet flow rate. The bleed regions provide a passage for excess inlet flow to be removed. For an external-compression inlet, the bleed regions within the throat section can provide this balancing of flow rates while avoiding changes to the external terminal shock wave system. For a mixed-compression inlet, bleed regions within the throat section can limit the forward motion of the internal terminal shock wave system by removing excess flow downstream of the terminal shock wave.

The previous two paragraphs highlight the two primary roles of bleed: 1) to improve inlet performance and 2) stabilize the terminal shock wave structure. This leads to the characterization of bleed regions as either ***performance bleed regions*** or ***stability bleed regions***, respectively.

The possible openings within bleed regions include slots, scoops, and holes as illustrated in Figure 11.1. A ***slot*** involves a streamwise opening in the inlet surface that spans the width or circumference of the inlet surface. The length of the slot opening can be considerable in relation to the local boundary layer height or height of the inlet. A ***scoop*** is similar to the slot, but the opening is in the perpendicular direction to the surface. A porous bleed region containing ***holes*** and typically involves a large number of holes placed in a pattern with their openings flush with the surface. The diameters, shapes, and inclination of the holes are factors in establishing the bleed flow.

With any of these types of bleed regions, a small fraction of the captured inlet flow (on the order of a few percent) is extracted through the bleed region and directed into a ***bleed plenum***. The bleed flow is drawn into the plenum due to the lower static pressure within the plenum. The bleed flow is then evacuated from the plenum through ducting that can either expel the bleed flow directly to the exterior of the inlet or duct the bleed flow to be used by other parts of the propulsion system. Such uses include

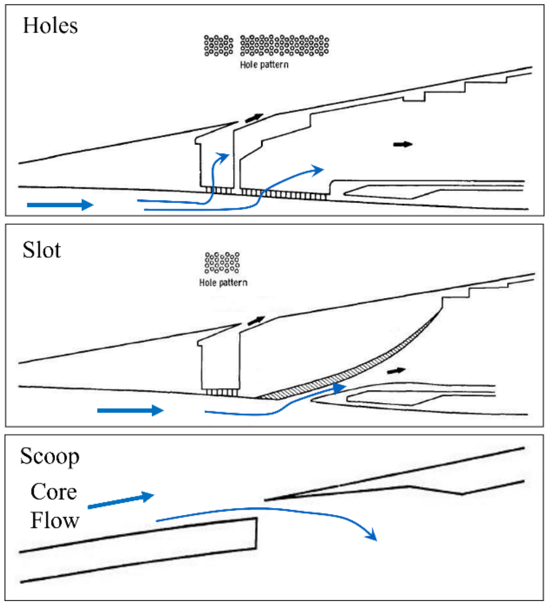

Figure 11.1.—Examples of bleed holes (top), slot (middle), and scoop (bottom).

engine cooling or nozzle flow augmentation. It is a lower static pressure of the exterior or nozzle flow that draws the bleed flow from the bleed plenum.

A couple disadvantages to the use of bleed is that less airflow is delivered to the engine to produce thrust and the expelled bleed flow can generate drag. Further, the use of bleed will result in an inlet with a larger reference capture area since more flow needs to be captured to account for the bleed flow in addition to the flow required by the engine. The larger capture area may have implications with respect to inlet total pressure recovery, drag, and weight.

Bypass systems within an inlet act to draw off excess inlet flow not accepted by the engine at the engine face. Bypass systems are typically located within the subsonic diffuser just ahead of the engine face. Compared to bleed systems, bypass systems are expected to be capable of extracting a much higher percentage of the inlet flow than bleed systems – the bypass flow could be 20-30% of the inlet capture flow at extreme conditions such as during engine shutdown or failure.

11.2 Porous Bleed Model

A ***porous bleed model*** is available within SUPIN for locating and estimating properties of the bleed regions. An assumption is that a porous bleed region contains many bleed holes such that the effect of the bleed is an almost continuous extraction of the bleed flow over the surface rather than discrete extractions through individual bleed holes. The left-hand-side image of Figure 11.2 shows a streamline-traced inlet with such a porous bleed region illustrated by the blue meshed region.

The right-hand-side image of Figure 11.2 shows a schematic used for the porous bleed model (Refs. 1 and 2). The schematic shows a porous bleed region with the inlet flow at the bottom of the schematic. A boundary layer forms on the inlet surface with a thickness (δ) and Mach number (M_δ), total pressure ($p_{t\delta}$), and total temperature ($T_{t\delta}$) at the edge of the boundary layer as it flows over the bleed region. The schematic shows a normal shock wave, such as a normal terminal shock wave, interacting with the boundary layer. The porous bleed region is shown as an array of bleed holes oriented 90-degrees to the inlet surface and connected to the bleed plenum. The bleed region is assumed to cover a surface area of

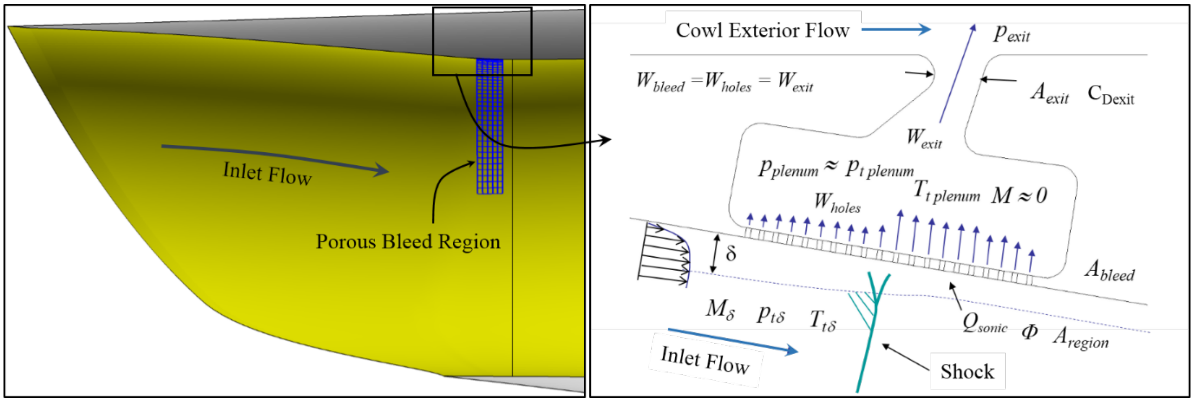

Figure 11.2.—Illustration of a porous bleed region for an inlet (left) and the schematic of the bleed region and plenum within the cowl of the inlet for the bleed model (right).

A_{region} of the throat section surface with x-coordinates for the start and end of the bleed region. The bleed holes are distributed within this bleed region. The bleed model does not identify each individual bleed hole, but rather, the combined area of the openings of the holes (A_{holes}) is characterized by a porosity,

$$\Phi = \frac{A_{holes}}{A_{region}} \tag{11-1}$$

The rate of bleed flow (W_{bleed}) equals the rate of bleed flow through the holes (W_{holes}) and is modeled using an empirically based relation for the bleed sonic coefficient (Q_{sonic}) that is of the form,

$$W_{bleed} = W_{holes} = Q_{sonic}\, W_{sonic} \tag{11-2}$$

The W_{sonic} is a reference flow rate defined using Equation (2-15) with the use of the area of the bleed region, bleed hole porosity, total conditions at the edge of the boundary layer, and the assumption of sonic flow ($M = 1$) within the bleed holes. The resulting expression is,

$$W_{sonic} = \Phi\, A_{region}\, p_{t\delta} \sqrt{\frac{\gamma}{R\, T_{t\delta}}} \left(\frac{\gamma+1}{2}\right)^{-(\gamma+1)/2\,(\gamma-1)} \tag{11-3}$$

The bleed sonic coefficient (Q_{sonic}) is based on experimental data and can depend on such quantities as the boundary layer edge Mach number (M_δ), the geometry of the bleed holes, the orientation of the bleed holes, and the bleed plenum pressure ratio ($p_{plenum}/p_{t\delta}$). The p_{plenum} is the static pressure in the plenum. It is assumed that the plenum is of large enough volume such that the bleed flow nearly stagnates within the plenum and the static and total pressures in the plenum are approximately the same. With the assumption of adiabatic flow through the bleed holes, the total temperature within the plenum is the same as the total temperature of the inlet flow.

Reference 2 introduced a modified form of Equation (11-2) that simplified the bleed model for 90-degree bleed holes. The bleed flow rate was expressed as

$$W_{bleed} = Q_{sonic-B}\, W_{sonic-B} \tag{11-4}$$

The $W_{sonic\text{-}B}$ is a reference flow rate defined using Equation (11-3) in which the total pressure and temperature at the edge of the boundary layer is replaced by the static pressure (p_B) and temperature (T_B) at the inlet surface,

$$W_{sonic-B} = \Phi_{bleed}\, A_{region}\, p_B \sqrt{\frac{\gamma}{R\, T_B}} \left(\frac{\gamma+1}{2}\right)^{-(\gamma+1)/2\,(\gamma-1)} \tag{11-5}$$

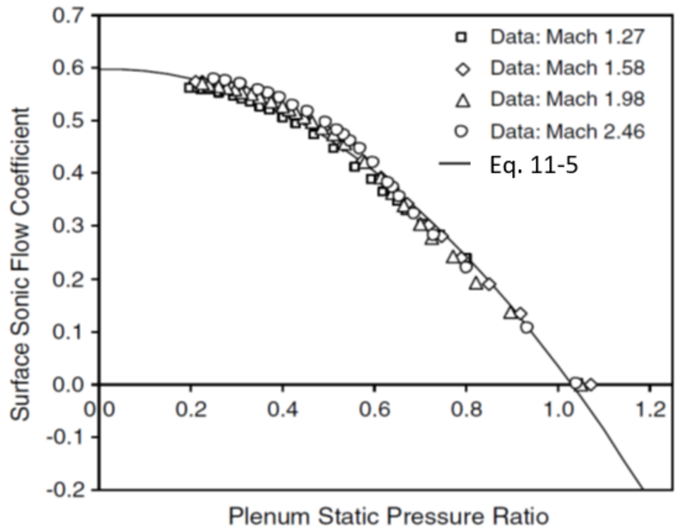

Figure 11.3.—Variation of $Q_{sonic\text{-}B}$ with the plenum pressure ratio p_{plenum}/p_B (Ref. 2).

This form is useful for CFD simulations since the static pressure and temperature at the inlet surface are more easily determined than the conditions at the edge of the boundary layer. This form also facilitated the scaling of the sonic bleed coefficient data with respect to Mach number such that a curve fit was developed for 90-degree bleed holes of the form,

$$Q_{sonic-B} = -\,0.57\left(^{p_{plenum}}/_{p_B}\right)^2 + 0.6 \tag{11-6}$$

Figure 11.3 shows the form of Equation (11-6) along with the plots of data points used to create Equation (11-6). The behavior of Equation (11-6) indicates that as the plenum pressure is reduced, the bleed coefficient, and therefore, the bleed rate increases. At a plenum pressure ratio of about $p_{plenum}/p_B \approx 0.2$, the curve levels off. This reflects that the flow in the bleed holes is becoming choked and no more bleed flow can pass through the holes into the plenum. Reference 2 provides details on the sonic bleed coefficient scaling and the derivation of Equations (11-5) and (11-6).

As seen above, the plenum static pressure is a key property of the bleed plenum that controls the bleed flow rate. The plenum pressure depends on the way the bleed flow exits the bleed plenum. The schematic of Figure 11.1 shows the bleed flow exiting the plenum through an exit that passes through a duct with a cross-sectional area of A_{exit}. The rate of flow exiting the bleed plenum is W_{exit}. The exit flow is shown to leave the plenum and mixes with the exterior flow about the cowl exterior. The static pressure at the bleed flow exit is p_{exit}. It is the lower value of p_{exit} that draws the bleed flow from the plenum and through the bleed region. An alternative to the flow being dumped to the external flow is for the exit flow to be ducted further down the propulsion system to be used for engine cooling and then mixed with the engine nozzle flow. Such a process still depends on a lower static pressure downstream of the bleed plenum.

Reference 1 discussed a model for the exit flow (W_{exit}) as illustrated in the schematic. The exit flow can be expressed as

$$W_{exit} = C_{Dexit}\, W_{ideal} \tag{11-7}$$

The W_{ideal} is a reference flow rate defined using Equation (2-15) with the total pressure and temperature being that of the bleed plenum, the area being that of the bleed plenum exit cross-section (A_{exit}), and the Mach number (M_{exit}) being the Mach number of the flow at A_{exit}. The resulting equation is,

$$W_{ideal} = p_{plenum}\, A_{exit}\, M_{exit} \sqrt{\frac{\gamma}{R\, T_{t\, plenum}}} \left(1 + \frac{\gamma - 1}{2} M_{exit}^2\right)^{-(\gamma+1)/2(\gamma-1)} \tag{11-8}$$

The discharge coefficient of the flow through the exit (C_{Dexit}) represents the reduction of flow rate through the exit due to boundary layer blockage and viscous losses. For a bleed system shown in the schematic of Figure 11.2, a reasonable value for the coefficient is $0.9 \leq C_{Dexit} < 1.0$. Equation (11-8) reflects the assumption that the plenum static pressure and the plenum total pressure are equal for stagnant flow in the plenum. The Mach number of the exit flow (M_{exit}) depends on the size of the exit area (A_{exit}). It is assumed within the model that the exit flow is choked ($M_{exit} = 1.0$) at the exit area. This choked condition ensures that the exterior flow cannot enter or influence the flow within the bleed plenum. A balance of the flow through the plenum requires that $W_{exit} = W_{bleed}$.

Equations (11-4) through (11-8) form a system of equations to be used for the design and analysis of the bleed region, plenum, and plenum exit of the bleed system. The way the equations are solved depends on whether the inlet is being designed and sized (design mode) or whether an existing inlet is being analyzed (analysis mode). For the inlet design mode, the bleed flow rate (W_{bleed}) is specified as part of the inlet sizing and bleed system properties of A_{region}, p_{plenum}, and A_{exit} are to be determined. For the inlet analysis mode, the properties of A_{region} and A_{exit} are known and the W_{bleed} and p_{plenum} are to be determined.

For both the inlet design mode and analysis mode, it is assumed that the porosity of the bleed region (Φ_{bleed}) and the discharge coefficient of the bleed plenum exit (C_{Dexit}) are specified. The conditions within the inlet flow at the bleed region (p_B, T_B, $T_{t\, plenum} = T_{t0}$) are obtained from the solution of the inlet flowfield. SUPIN uses a one-dimensional representation of the flow, and so, the spatial design of the bleed region is limited to specification of the x-coordinates within the throat section for the start and end of the bleed region (x_{Bbeg}, x_{Bend}). There is no distinction as to whether the bleed region is on the cowl or a centerbody.

There are a couple approaches for establishing the bleed plenum static pressure (p_{plenum}) within the bleed system of an inlet for both the inlet design mode and inlet analysis mode. The first approach is the ***constant-pressure approach*** in which the plenum pressure is maintained at a constant value. The inlet bleed system for a constant-pressure approach would require a control system to sense and adjust the plenum pressure as the inlet flow conditions change. Typically, this involves adjusting the bleed plenum exit area (A_{exit}). With the plenum pressure (p_{plenum}) determined, then Equations (11-4) to (11-6) can be used to compute the area of the bleed region (A_{region}) in the design mode or the bleed flow rate (W_{bleed}) in the analysis mode. Equations (11-7) and (11-8) are then used to compute the area of the bleed plenum exit (A_{exit}).

The second approach for establishing the bleed plenum station pressure is the ***fixed-exit approach*** in which the bleed plenum exit area (A_{exit}) is fixed. The fixed-exit bleed system would be used if mechanical simplicity is desired for the bleed system. The bleed plenum pressure would vary in response to the varying inlet flow conditions over the bleed region. In the inlet design mode, the bleed flow rate (W_{bleed}) is known and the plenum pressure (p_{plenum}) at the design conditions would be specified. The above equations are then solved for the area of the bleed region (A_{region}) and the area of the bleed plenum exit (A_{exit}). In the inlet analysis mode, the area of the bleed region (A_{region}) and the area of the bleed plenum exit (A_{exit}) are specified. The bleed flow rate (W_{bleed}) and the plenum pressure (p_{plenum}) are computed using an iteration of Equations (11-4) to (11-8).

11.3 Specification of Bleed and Bypass Regions within SUPIN

The specification of the number, location, size, and other properties of bleed and bypass regions within SUPIN is facilitated through the input data block with DataID = 12. SUPIN offers two formats for specifying this information based on the input factor $\boldsymbol{K_{bleed}}$.

A value of K_{bleed} = 0 indicates that no bleed/bypass regions are specified for the inlet. This option is the default within SUPIN and is imposed when the input data file (SUPIN.in) does not include an input data block for DataID = 12. However, bleed and bypass flow rates can still be specified and accounted for within the balance of flow rates within the inlet using the input factors WR_{bleed} and WR_{bypass}, respectively, within the input data block for DataID = 0. The location within the inlet that the bleed is extracted depends on the value of K_{comp} defining the type of supersonic compression. For subsonic inlets (K_{comp} = 0) and external-compression inlets (K_{comp} = 1), the bleed flow is extracted between stations 1 and SD. For mixed-compression inlets with a subsonic diffuser (K_{comp} = 2), the bleed flow is extracted between stations TH and SD. For mixed-compression inlets with an isolator (K_{comp} = 3), the bleed flow is extracted between stations 1 and TH.

The option of K_{bleed} = 1 provides a simple format to specify the general location and flowrate of bleed/bypass regions and restricts each bleed/bypass region to one segment. The option of K_{bleed} = 2 provides a more detailed format to specifically locate bleed/bypass regions which may contain multiple segments. Further, this option includes more input factors to model the bleed/bypass flowrates. The option of K_{bleed} = 3 provides a format for specifying bleed rates for certain segments of the inlet flowpath. Table 11.1, Table 11.2, and Table 11.3 present example input data blocks for the bleed/bypass regions using K_{bleed} = 1, 2, and 3, respectively. The third line of both input data block formats is a header line for the input factors K_{bleed}, N_{breg}, and N_{bseg}. The fourth line is where the values are specified.

The input factor $\boldsymbol{N_{breg}}$ specifies the number of bleed/bypass regions within the inlet. Each bleed/bypass region can have one or more segments distributed over the bleed region. For example, the NASA 1507 inlet (Ref. 3) shown in Figure 11.4 has four bleed regions (N_{breg} = 4). Each bleed region is a band of bleed holes that extends over the circumference of the axisymmetric centerbody and cowl interior. Bleed regions 1 and 2 each have one segment. Bleed region 3 contains two segments and bleed region 4 contains four bleed segments, as indicated in Figure 11.4. Figure 11.4 also includes some Mach number contours from a CFD simulation which shows the variation of the Mach number at several axial stations in the subsonic diffuser. The blue arrows within the bleed segments and on the plane of symmetry indicate the momentum vectors of the bleed flow. The longer arrows indicate a greater amount of bleed flow.

TABLE 11.1.—EXAMPLE INPUT DATA BLOCK FOR THE BLEED/BYPASS REGIONS USING K_{bleed} = 1

```
DataID.  Bleed Modeling
  12
Kbleed   Nbreg   Nbseg
   1       3       3
Mbreg Kbtyp Kbloc Kbplen  Fbplen
  1     1     32     1     0.020
  2     1     35     1     0.010
  3     4     35     1     0.040
```

TABLE 11.2.—EXAMPLE INPUT DATA BLOCK FOR THE BLEED/BYPASS REGIONS USING K_{bleed} = 2

```
DataID.  Bleed Modeling
 12
Kbleed   Nbreg    Nbseg
  2        4        8
Mbreg Kbtyp Kbplen    Fbplen   CDexit   Fbexit   Mbexit
  1     1      1      0.0100   0.9500   45.00    1.000
  2     1      1      0.0100   0.9500   45.00    1.000
  3     1      1      0.0100   0.9500   45.00    1.000
  4     1      1      0.0100   0.9500   45.00    1.000
Mbreg Mbseg Kbloc   xbbeg   xbend   Fbext   Fbpor   Fbang
  1     1     33    2.748   2.919   1.000   0.415   90.00
  2     1     23    2.945   3.047   1.000   0.415   90.00
  3     1     34    3.195   3.215   1.000   0.415   90.00
  3     2     34    3.263   3.284   1.000   0.415   90.00
  4     1     24    3.115   3.136   1.000   0.415   90.00
  4     2     24    3.170   3.190   1.000   0.415   90.00
  4     3     24    3.237   3.258   1.000   0.415   90.00
  4     4     24    3.305   3.326   1.000   0.415   90.00
```

TABLE 11.3.—EXAMPLE INPUT DATA BLOCK FOR THE BLEED/BYPASS REGIONS USING K_{bleed} = 3

```
DataID.  Bleed Modeling
 12
Kbleed   Nbreg    Nbseg
  3        1        1
  WrbL1    Wrb1SD    Wrb1TS    Wrb1TH
 0.0000    0.0200    0.0000    0.0000
WrbTHSD    WrbSD2    WrbTH3
 0.0000    0.0000    0.0000
```

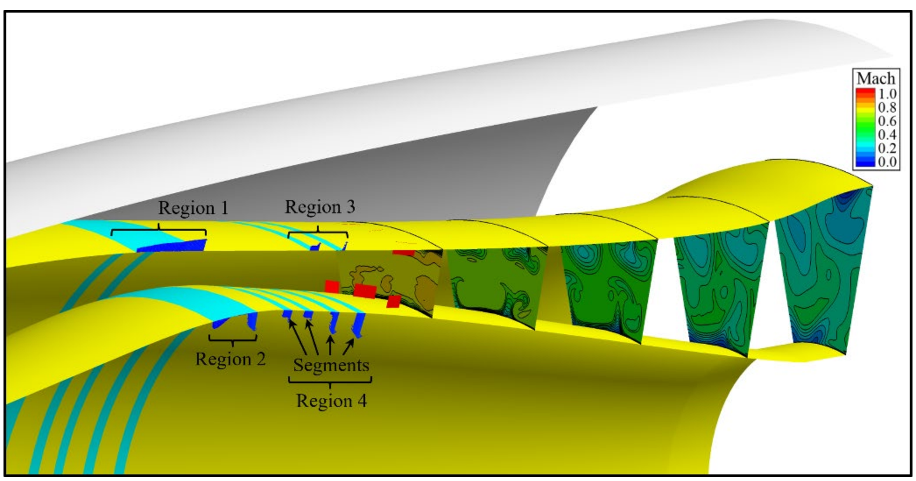

Figure 11.4.—Example of multiple bleed regions and segments within the Mach 3 NASA 1507 axisymmetric spike inlet (Ref. 3).

TABLE 11.4.—INPUT FACTORS FOR THE SPECIFICATION OF BLEED/BYPASS REGIONS

Factor	Input	Description
K_{bleed}	`Kbleed`	Flag indicating format for specification of input factors [0] = 0 bleed and bypass specified by Wrbleed and Wrbypass = 1 bleed/bypass regions with a single segment and simplified input = 2 bleed/bypass regions with multiple segments and more inputs = 3 directly specify bleed rates for each span of the stations
N_{breg}	`Nbreg`	Number of bleed regions within the inlet
N_{bseg}	`Nbseg`	Total number of segments from all the bleed/bypass regions
M_{breg}	`Mbreg`	Integer label for a bleed/bypass region
M_{bseg}	`Mbseg`	Integer label for a segment within a bleed/bypass region
K_{btyp}	`Kbtyp`	Type of bleed/bypass region = 1 porous bleed, = 2 bleed slot, = 3 bleed scoop, = 4 bypass
K_{bloc}	`Kbloc`	Flag for location of bleed/bypass region (see Table 11.4)
x_{bbeg}	`xbbeg`	x-coordinate of the beginning of the bleed/bypass region (ft)
x_{bend}	`xbend`	x-coordinate of the end of the bleed/bypass region (ft)
F_{bext}	`Fbext`	Extent of bleed/bypass region as fraction of the cross-stream span
Φ_{bleed}	`Fbpor`	Porosity of a bleed/bypass region or segment
θ_{bang}	`Fbang`	Incidence angle for bleed/bypass holes or slots within a segment (deg)
K_{bplen}	`Kbplen`	Flag for the bleed plenum conditions and meaning of F_{bplen} = 0 bleed and bypass rates for inlet are set by WR_{bleed} and WR_{bypass} = 1 constant flow rate: F_{bplen} is fraction of capture flow = 2 constant flow rate: F_{bplen} is actual flow rate (lbm/sec) = 3 constant flow rate: F_{bplen} is actual flow rate (slug/sec) = 4 constant plenum static pressure: F_{bplen} is fraction of p_L = 5 constant plenum static pressure: F_{bplen} is pressure (psi) = 6 constant plenum static pressure: F_{bplen} is pressure (psf) = 7 choked fixed-exit: F_{bplen} is the exit throat area (frac of A_{cap}) = 8 choked fixed-exit: F_{bplen} is the exit throat area (in^2) = 9 choked fixed-exit: F_{bplen} is the exit throat area (ft^2)
F_{bplen}	`Fbplen`	Input for the bleed/bypass plenum condition based on value of K_{bplen}
M_{bexit}	`Mbexit`	Mach number of plenum exit
C_{Dexit}	`CDexit`	Discharge coefficient for the bleed plenum exit
θ_{bexit}	`Fbexit`	Incidence angle of the bleed plenum exit (deg)

All the segments of a bleed region share a common bleed plenum, so the distance over which the individual segments are located is expected to be small relative to the length of the inlet. The separate segments within a bleed region allow the bleed region to extend over a longer streamwise distance while limiting the amount of bleed openings. Further, the properties of the bleed segments, such as hole porosity and angle can be varied for each segment. The input factor $\boldsymbol{N_{bseg}}$ specifies the total number of bleed and bypass segments within the inlet. For the example of Figure 11.4, $N_{bseg} = 1 + 1 + 2 + 4 = 8$. The option of $K_{bleed} = 1$ limits the specification of the bleed/bypass regions to one segment per region and SUPIN imposes that $N_{breg} = N_{bseg}$. If one wishes to specify multiple segments for a region, the option $K_{bleed} = 2$ should be used. The example of Table 11.2 uses input for a case for the Mach 3 NASA 1507 inlet with the four bleed regions and a total of eight segments.

The format of the subsequent input lines starting with line 5 depends on the value of K_{bleed} and include various input factors that are listed in Table 11.4. The input factor $\boldsymbol{M_{breg}}$ listed in Table 11.1 and Table 11.2 is an integer label indicating the bleed/bypass region and should start with $M_{breg} = 1$ and increment by a value of one until N_{breg} lines are specified. For $K_{bleed} = 2$, the input factor $\boldsymbol{M_{bseg}}$ is a label that identifies a segment within a bleed or bypass region. Within each region, the segments are labeled with numbers starting with 1 and ending with the number of segments of that region.

The option of $\boldsymbol{K_{bleed}}$ **= 1** provides for the specification of the input factors M_{breg}, K_{btyp}, K_{bloc}, K_{bplen}, and F_{bplen}. The header line for these inputs is the fifth line of the input data block. The remaining lines should be N_{breg} in number and list the input factors for each bleed/bypass region.

The input factor $\boldsymbol{K_{btyp}}$ specifies the type of bleed/bypass region, and the options are $K_{btyp} = 1$ for a porous bleed region, $K_{btyp} = 2$ for a bleed slot, and $K_{btyp} = 3$ for a bleed scoop, and $K_{btyp} = 4$ for a bypass region. Bleed regions should be specified with values of $K_{btyp} = 1$, 2, or 3 while a bypass region should only be specified with $K_{btyp} = 4$.

The input factor $\boldsymbol{K_{bloc}}$ indicates the location of each bleed/bypass region. The factor is a two-digit integer of the form $K_{bloc} = nm$. The first digit (n) indicates the inlet surface on which the bleed/bypass region is located. The second digit (m) indicates the interval between two respective stations for which the bleed/bypass region is located. The options for the digits n and m are listed in Table 11.5. As an example of K_{bloc}, a bleed region located on the cowl interior and within the throat section of a mixed-compression inlet would be specified with $K_{bloc} = 34$. The digit "3" indicates the region is on the cowl interior and the digit "4" indicates that the region is located between stations TH and SD.

The specification of K_{bloc} should be consistent with the type of bleed/bypass region (K_{btyp}), type of inlet (K_{typ}), and the type of supersonic compression (K_{comp}). Bleed regions can be specified to be located on all the surfaces listed for the first digit (e.g., $n = 1$, 2, 3, or 4) and all the intervals (e.g., $m = 1$, 2, 3, 4, 5, 6, or 7). However, the pitot inlets ($K_{typ} = 1$ and 6) don't contain an external supersonic diffuser, and so bleed regions with values of K_{bloc} with $n = 1$ are not valid. Bleed regions for axisymmetric spike ($K_{typ} = 3$) and streamline-traced inlets ($K_{typ} = 5$) do not contain sidewalls, and so values K_{bloc} with $n = 4$ are not valid. Bleed regions for pitot inlets ($K_{typ} = 1$) should use values of K_{bloc} with $m = 2$ or 5. Bleed regions for external-compression inlets ($K_{comp} = 1$) should use values of K_{bloc} with $m = 1$, 2, and 5. Bleed regions for mixed-compression inlets with subsonic outflow ($K_{comp} = 2$) should use values of K_{bloc} with $m = 1$, 3, 4, and 5. Bleed regions for mixed-compression inlets with supersonic outflow ($K_{comp} = 3$) should use values of K_{bloc} with $m = 1$, 3, and 6. These choices for m reflect that the internal supersonic diffuser exists between stations 1 and TH, but downstream of station TH the station intervals differ depending on the existence of the throat section and subsonic diffuser or an isolator. Table 11.6 presents a summary of the possible values of n and m for the various inlets and types of supersonic compression.

The values of K_{bloc} with $m = 7$ are used only for mixed-compression, two-dimensional inlets ($K_{typ} = 2$ and $K_{comp} = 2$ or 3) to indicate a bleed region located on the sidewall ($n = 4$) between station 1 and the shoulder station TS. The choice of $m = 7$ further specifies that the bleed region is to be aligned with the cowl shock wave that extends from the cowl lip and intersects the centerbody at the start of the shoulder, as discussed in Subsection 9.2. Such a bleed region can be useful for controlling the adverse effects of the interaction of the cowl shock wave with the boundary layer on the sidewall. Figure 11.5 shows an example of a mixed-compression, two-dimensional bifurcated duct inlet for Mach 2.7 (Ref. 4) with porous bleed regions on the sidewall and aligned with the expected locations of the cowl shock wave interactions with the sidewall.

TABLE 11.5.—OPTIONS FOR THE INTEGERS (n,m) USED TO DEFINE K_{bloc}

n	Inlet Surface		m	Station Interval
1	External Supersonic Diffuser		1	L to 1
2	Centerbody		2	1 to SD
3	Cowl Interior		3	1 to TH
4	Sidewall		4	TH to SD
			5	SD to 2
			6	TH to 3
			7	1 to TS (cowl shock wave)

TABLE 11.6.—DESCRIPTION OF THE INTEGERS (n,m) USED TO DEFINE K_{bloc}

K_{typ}	K_{comp}	K_{btyp}	n	m	Comment
1	0	1,2,3	3	2	Subsonic or supersonic axi-pitot inlets
2,4	1	1,2,3	1,2,3,4	1,2,5	External compression 2D inlets
2,4	2	1,2,3	1,2,3,4	1,3,4,5	Mixed compression 2D inlets with subsonic outflow
2,4	3	1,2,3	1,2,3,4	1,3,6	Mixed compression 2D inlets with supersonic outflow
2,4	2,3	1,2,3	4	7	Mixed compression 2D inlet with bleed region aligned to cowl shock
3	1	1,2,3	1,2,3	1,2,5	External compression axi-spike inlets
3	2	1,2,3	1,2,3	1,3,4,5	Mixed compression axi-spike inlets with subsonic outflow
3	3	1,2,3	1,2,3	1,3,6	Mixed compression axi-spike inlets with supersonic outflow
5	1	1,2,3	1,3	1,2,5	External compression streamline-traced inlets
5	2	1,2,3	1,3	1,3,4,5	Mixed compression streamline-traced inlets with subsonic outflow
5	3	1,2,3	1,3	1,3,6	Mixed compression streamline-traced inlets with supersonic outflow
1 to 6	0,1,2	4	2,3,4	5	Bypass region for all inlets with subsonic diffusers

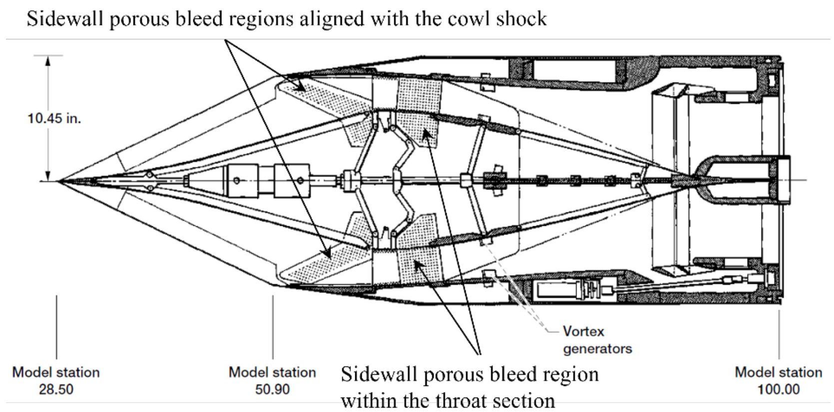

Figure 11.5.—Example of sidewall porous bleed regions for a Mach 2.7 mixed-compression, two-dimensional, bifurcated duct inlet [4] with bleed regions aligned with the cowl shock (NASA).

Bypass regions (K_{btyp} = 4) are expected to be located within the subsonic diffuser, which is between stations SD and 2. Thus, values for K_{bloc} for bypass regions need to specify that m = 5. Further, the value for K_{bloc} needs to specify that n = 2, 3, or 4, since n = 1 indicating the external supersonic diffuser is not valid. These conditions result in the only valid values for bypass regions are K_{bloc} = 25, 35, and 45.

The input factor $\boldsymbol{K_{bplen}}$ is a flag indicating the manner for establishing the flowrate for the bleed/bypass region. The possibilities can be grouped as either directly specifying the bleed/bypass flowrates, the plenum static pressures, or conditions for a fixed plenum exit. The value of K_{bplen} also indicates which input factors are used to establish the flowrates. The input factor $\boldsymbol{F_{bplen}}$ provides a means of specifying additional data and its meaning is based on the value of K_{bplen}.

A value of $\boldsymbol{K_{bplen}}$ **= 0** indicates that the bleed and bypass flow ratios are specified by the input factors WR_{bleed} and WR_{bypass}, respectively. Since only one value of WR_{bleed} and one value of WR_{bypass} can be specified, only one bleed region and one bypass region can be specified with K_{bplen} = 0, respectively. Also, each region with K_{bplen} = 0 can only contain one segment. Either input format K_{bleed} = 1 or 2 can be used. Other bleed/bypass regions can be specified, but only one bleed region and one bypass region with K_{bplen} = 0 can be specified. When K_{bplen} = 0 is specified for a region, any specified values of the input factors F_{bplen}, C_{Dexit}, F_{bexit}, M_{bexit}, F_{bpor}, and F_{bang} for that region are ignored.

For values of $\boldsymbol{K_{bplen}}$ **= 1, 2, or 3**, the bleed/bypass flowrate for the region is directly specified. For K_{bplen} = 1, the flowrate is specified as a fraction F_{bplen} of the reference capture flow rate (W_{cap}). For example, to specify a 1% bleed rate for a bleed region, F_{bplen} = 0.01. For K_{bplen} = 2, the flowrate is directly specified by the value of F_{bplen} in units of lbm/sec. For K_{bplen} = 3, the flowrate is directly specified by the value of F_{bplen} in units of slug/sec.

For values of $\boldsymbol{K_{bplen}}$ **= 4, 5, or 6**, the bleed/bypass flowrate for the region is computed using the model of Subsection 11.3 with the value of the input factor F_{bplen} being the plenum static pressure (p_{plenum}). For K_{bplen} = 4, the plenum static pressure is specified as a fraction F_{bplen} of the approach static pressure, p_L. For K_{bplen} = 5, the plenum static pressure is directly specified by the value of F_{bplen} in units of pounds-force per square inch (psi). For K_{bplen} = 6, the plenum static pressure is directly specified by the value of F_{bplen} in units of pounds-force per square foot (psf). This approach requires that the area of the bleed/bypass region (A_{region}), porosity (Φ_{region}), and static pressure and temperature (p_B,T_B) at the boundary be established to compute the flowrate using Equations (11-4) to (11-6). The A_{region} can be calculated for the region using the input factors x_{bbeg}, x_{bend}, and F_{bwid} along with the inlet surface geometry, which could be the inlet surface grid. The porosity is specified by the input factor F_{bpor}, which will be further discussed below. The values for p_B and T_B could be obtained from an estimate of the quasi-one-dimensional solution of the flow through the inlet. The use of this approach with K_{bplen} = 4, 5, or 6 requires that the input data block format for K_{bleed} = 2 be used to provide all the necessary input factors.

For values of $\boldsymbol{K_{bplen}}$ **= 7, 8, or 9**, the bleed/bypass flowrate for the region is computed using the model of Subsection 11.3 with inclusion of a fixed plenum exit. The value of the input factor F_{bplen} specifies the cross-sectional area of the throat (minimum area) of the plenum exit (A_{exit}). For K_{bplen} = 7, the exit area A_{exit} is specified as a fraction F_{bplen} of the reference capture area, A_{cap}. For K_{bplen} = 8, the exit area A_{exit} is directly specified by the value of F_{bplen} in units of square inches (in^2). For K_{bplen} = 9, the exit area A_{exit} is directly specified by the value of F_{bplen} in units of square feet (ft^2). An additional input factor required by the fixed-exit approach is the discharge coefficient for the flow through the plenum exit (C_{Dexit}). This approach for calculating the bleed/bypass flowrate uses Equations (11-7) and (11-8) with the assumption that the throat of the plenum exit is choked and M_{exit} = 1.0 within Equation (11-8). The total temperature of flow within the plenum ($T_{tplenum}$) in Equation (11-8) is assumed to be equal to the approach flow total temperature (T_{tL}) with the assumption of adiabatic flow through the inlet. As described in Subsection 11.3, the fixed-exit approach involves an iteration on the plenum static pressure (p_{plenum}) until the flowrate into the plenum as calculated by Equation (11-4) equals the flowrate out of the plenum exit as calculated by Equation (11-7). The use of this approach with K_{bplen} = 7, 8, or 9 requires that the input data block format for K_{bleed} = 2 be used to provide all the necessary input factors.

The input data block for $\boldsymbol{K_{bleed}}$ **= 2** has a group of input lines specifying input factors for the bleed/bypass regions and a second group specifying input factors for individual segments. The first group consists of a series of lines that provide inputs for K_{bplen}, F_{bplen}, C_{Dexit}, F_{bexit}, and M_{bexit} to provide information for each bleed/bypass region and it associated bleed plenum. The second group consists of a series of lines that provide inputs for M_{bseg}, K_{bloc}, x_{bbeg}, x_{bend}, F_{bwid}, F_{bpor}, and F_{bang} to provide information for each bleed/bypass segment. The following paragraphs provide further details on these input factors.

The use of bleed and bypass in which the bleed/bypass flow is ejected out of the inlet and into the external flow results in bleed/bypass drag. The methods used to compute this drag term will be discussed in Subsections 12.7 and 12.8. The information needed for the calculation of the bleed/bypass drag includes the speed and orientation of the ejected flow. This information is specified for each bleed region using the input factors M_{bexit} and F_{bexit}. The input factor $\boldsymbol{M_{bexit}}$ specifies the Mach number of the flow ejected from the bleed plenum exit. The Mach number M_{bexit} is not necessarily the same as the Mach number at the geometric throat of the bleed/bypass plenum exit (M_{exit}). The bleed/bypass modeling assumes that the throat of the bleed plenum exit is choked (M_{exit} = 1) in Equation (11-7). It is possible that a diverging nozzle exists downstream of the exit throat such that $M_{bexit} > M_{exit} = 1$. The input factor $\boldsymbol{F_{bexit}}$

specifies the incidence angle (θ_{bexit}) of the flow exiting the bleed plenum exit and being injected into the exterior flowfield. This input factor is specified in units of degrees and is measured with respect to a line parallel to the x-axis of the inlet. As will be described in Subsections 12.7 and 12.8, the bleed/bypass drag is related to the change in momentum in the bleed/bypass flow between its intake by the inlet and ejection from the bleed plenum exit. Thus, if $\boldsymbol{F_{bexit}}$ could be specified as a low angle, it would be possible to recover the axial momentum of the flow and reduce bleed/bypass drag.

The input factor $\boldsymbol{C_{Dexit}}$ specifies a discharge coefficient for the exit of the bleed plenum and is used in calculating the flow through the bleed plenum exit. If a value for C_{Dexit} is unknown, a choice of C_{Dexit} = 0.95 is reasonable for a conceptual level of inlet design.

The input factors $\boldsymbol{x_{bbeg}}$ and $\boldsymbol{x_{bend}}$ specify the x-coordinates of the beginning and end of the bleed/bypass segment in units of feet. The specification of x_{bbeg} and x_{bend} requires some consistency with the specification of K_{bloc}. For example, if K_{bloc} = 24, then the values of x_{bbeg} and x_{bend} should define a segment on the centerbody within stations TH and SD. If there is an inconsistency, the value of K_{bloc} takes priority in locating the position of the bleed segment. In locating a bypass region, the values of x_{bbeg} and x_{bend} should exist within the subsonic diffuser between stations SD and 2. Since all segments of a region share a common bleed plenum, the x-coordinates should identify locations grouped closely together on an inlet surface so that they can share the same plenum. For example, a bleed region on the centerbody about station TH could consist of three separate segments grouped about station TH. Each segment could be a band of bleed holes each with its own bleed hole size and porosity. However, the three segments all feed into the same bleed plenum.

The input factor $\boldsymbol{F_{bext}}$ specifies the extent of the bleed segments in terms of the width or span in the crossflow direction. For example, a bleed segment on the centerbody of a two-dimensional inlet with a value of F_{bext} = 1.0 would indicate that the bleed segment spans the entire width of the centerbody. A value of F_{bext} = 0.90 would indicate that the bleed segment spans only 90% of the width of the centerbody. Such a choice can be used to limit the bleed segment from extending all the way into the corner region of a centerbody, cowl, or sidewall of a two-dimensional inlet.

The input factors x_{bbeg}, x_{bend}, and F_{bext} are used within SUPIN to establish the surface area of a bleed/bypass segment. The sum of the areas of all the segments of a bleed region can provide the area A_{region} for the bleed/bypass region.

The porosity of the bleed holes of a bleed segment (Φ_{bleed}) is set by the input factor $\boldsymbol{F_{bpor}}$. A porosity of Φ_{bleed} = 0.40 is a reasonable choice if a value of the porosity is not known. For a bleed slot or scoop, a value of Φ_{bleed} = 1.0 indicates the bleed region covers the opening of the bleed slot or scoop.

The input factor $\boldsymbol{F_{bang}}$ specifies the incidence angle (θ_{bang}) of the bleed holes or slot within bleed/bypass segment. This input factor indicates the empirical data to be used for the sonic flow coefficient ($Q_{sonic\text{-}B}$) of Equation (11-4). The empirical curve fit of Equation (11-6) is for bleed holes with a hole incidence angle of $F_{bang} = \theta_{bang}$ = 90 degrees. This is currently the only empirical data for $Q_{sonic\text{-}B}$ available within SUPIN, so therefore the value for the input factor θ_{bang} is ignored. In future versions of SUPIN, similar empirical data for $20 \leq \theta_{bang} < 90$ degrees will hopefully become available.

One use of the bleed/bypass input factors x_{bbeg}, x_{bend}, and F_{bwid} is to locate the bleed segments and regions within the surface grids for the inlet. Once the surface grids are generated for the inlet, SUPIN will identify those surface grid points that fall within the bleed regions. The grid indices identifying the start and end of the bleed/bypass segments and regions are reported within the output data file (SUPIN.Out.txt). Such information can be used to assign boundary conditions to impose bleed for CFD simulations. For two-dimensional inlets (K_{typ} = 2) SUPIN also generates grid blocks for each bleed region to further facilitate setting of boundary conditions for bleed regions. This is discussed in further detail in Section 13.0 discussing CFD grid generation.

Since the specification of bleed changes the rate of flow into the subsonic diffuser, the Mach number at station SD may be less than that of the inlet designed with no bleed. This may change the estimate of the total pressure loss through the subsonic diffuser. However, SUPIN does not model a change in total pressure recovery due to the removal of a portion of the lower-momentum flow of the boundary layer in the throat.

11.4 Geometric Modeling of Bleed Slots

Bleed slots are openings within the inlet surface that feature a larger transverse dimension than a streamwise dimension. An example of a bleed slot for a two-dimensional, Mach 1.7 external-compression inlet is shown in Figure 11.6. The bleed slot is formed over the shoulder of the inlet centerbody and spans the width of the throat section. The slot features a plenum to accumulate the bleed flow prior to being ducted elsewhere within the propulsion system or dumped into the freestream, as discussed previously.

The dimensions of the bleed slot can vary in size. Small-sized slots could allow multiple slots within the inlet. The inlet for the SR-71 featured a region on the centerbody with dozens of small-scale slots. The inlet for the Concorde aircraft featured a single bleed slot that spanned the width of the inlet and had a sizable streamwise length, which can be seen in the right-hand-side photograph of the inlets in Figure 1.7. While the slot opening allows bleed flow to be extracted, the slot may also perform a secondary aerodynamic function. For example, the bleed slot for the Concorde created a shear layer that also was used to control the terminal shock wave structure and flowrate within the inlet. Further, the break in the inlet surface due to the slot allowed for variable geometry such as the rotation of ramps and surfaces within the inlet.

The right-hand-side image of Figure 11.6 shows the dimensions for the geometry model of the shoulder bleed slot and plenum. For the two-dimensional inlet, the bleed slot extends over the length of the shoulder from point $(x,y)_{cbsha}$ to $(x,y)_{cbshb}$ as shown in Figure 11.6. An elliptical profile is used to provide bluntness to the leading and trailing edges of the bleed slot opening. The length of the minor axis of the elliptical profiles forms the thickness of the leading and trailing edge surfaces of the slot.

The input factors for the bleed slot are listed in Table 11.7. The input factor F_{tslot} specifies the thickness of the leading and trailing edge surfaces of the slots in units of feet. The input factor F_{arslot} specifies the aspect ratio of the elliptical profile of the leading and trailing edges. The bleed slot plenum

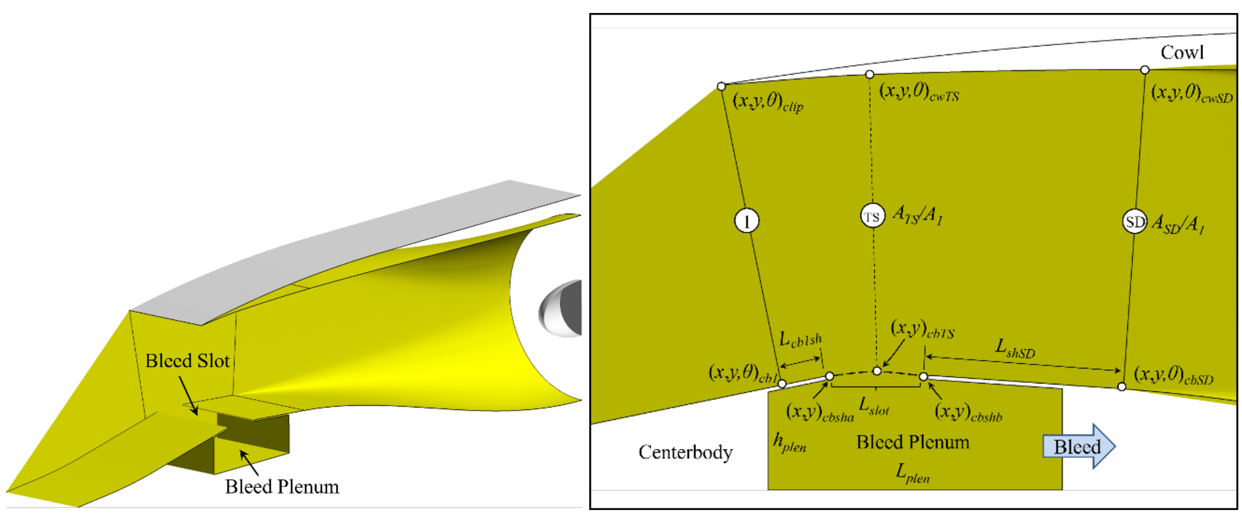

Figure 11.6.—Example of a shoulder bleed slot for a Mach 1.7 external-compression inlet (left) and the dimensions for the geometry model of the bleed slot (right).

TABLE 11.7.—INPUT FACTORS FOR THE SHOULDER BLEED SLOT

Factor	Input	Description
F_{Lslot}	`FLslot`	Factor for the length of the slot (L_{slot}) normalized by D_{ref}
F_{tslot}	`Ftslot`	Thickness of the elliptical profile of the slot edges (ft)
F_{arslot}	`Farslot`	Aspect ratio of the elliptical profile for the slot edges
F_{Lpslot}	`FLpslot`	Length of the bleed slot plenum (L_{pslot}) normalized by D_{ref}
F_{ypslot}	`Fypslot`	Factor for the *y*-coordinate for the bottom of the plenum normalized by D_{ref}

TABLE 11.8.—EXAMPLE INPUT DATA BLOCK FOR THE SHOULDER BLEED SLOT

```
DataID.  Shoulder Bleed Slot
 15
 Lslot   Ftslot   Farslot   FLpslot   Fypslot
 0.950   0.0300    2.000     6.000     2.000
```

has a nearly rectangular shape with dimensions for its length and height of L_{pslot} and h_{pslot}. The input factor for the length of the bleed slot plenum is F_{Lpslot} and specifies the length normalized by D_{ref}. The height of the bleed plenum is set by specifying the *y*-coordinate of lower surface of the plenum through the input factor F_{ypslot}, which is normalized by D_{ref}. Table 11.8 provides an example of the input data block for the bleed slot, which uses DataID = 15 to specify the form of the input data block.

Within SUPIN, the bleed flowrate through the slot can be modeled using the bleed model. The bleed region should be specified to extend over the opening of the bleed slot and the porosity is set to be $\Phi = 1.0$.

SUPIN has the capability to generate CFD grids for the bleed slot and plenum for the two-dimensional inlet ($K_{typ} = 2$), such as the inlet shown in Figure 11.6. One requirement is that L_{shSD} should have specified lengths greater than zero. This is needed to satisfy assumptions on the generation of grid blocks for the slot subdomain.

References

1. Slater, J. W. and Saunders, J. D., “Modeling of Fixed-Exit Porous Bleed Systems for Supersonic Inlets,” *AIAA Journal of Propulsion and Power*, Vol. 26, No. 2, p. 193-202, March-April 2010.
2. Slater, J. W., “Improvement in Modeling 90-degree Bleed Holes for Supersonic Inlets,” *AIAA Journal of Propulsion and Power*, Vol. 28, No. 4, pp. 773-781. July-August 2012.
3. Sorensen, N. E., and Smeltzer, D. B., “Investigation of a Large-Scale Mixed-Compression Axisymmetric Inlet System Capable of High Performance at Mach Numbers 0.6 to 3.0,” NASA TM X-1507, February 1968.
4. Wasserbauer, J. F., Meleason, E. T, and Burstadt, P. L., “Experimental Investigation of the Performance of a Mach-2.7 Two-Dimensional Bifurcated Duct Inlet With 30 Percent Internal Contraction,” NASA TM 106728, May 1996.

12.0 Inlet Drag

Inlet drag is the sum of pressure and viscous forces on the inlet surfaces that act in the opposite direction of thrust (Ref. 1). These forces can vary depending on the flight conditions, engine throttle setting, and/or thrust generated by the propulsion system. The inlet is part of the propulsion system of an aircraft and the interaction of the inlet flow with the rest of the aircraft flow will affect the inlet and aircraft drag. While the integration of the inlet and propulsion system onto the aircraft and their interaction are important topics of study, we consider here the forces acting on an isolated inlet. Thus, the calculation of drag will be limited to forces acting on the approach streamtube, the cowl exterior, and loss of momentum within the bleed and bypass systems. Further, the effect of friction on the external surfaces of the cowl will not be included in this discussion of drag, as it is customary to account for the viscous forces with the aircraft drag rather than with the inlet.

12.1 Drag

The discussion of drag starts with the integral form of the steady-state momentum equation applied for a control volume fixed in shape and space (Ref. 2),

$$\oint_S \rho\,(\vec{v}\cdot\hat{n})\,\vec{v}\,dA = -\oint_S (p - p_L)\,\hat{n}\,dA + \int_S \boldsymbol{\tau}\cdot\hat{n}\,dA \tag{12-1}$$

Where $\hat{n}$ is the unit normal for the incremental surface dA and is oriented such that it points out of the control volume. The $\boldsymbol{\tau}$ is the stress tensor. The first integral on the right-hand-side of Equation (12-1) (including the minus sign) is the drag due to pressure forces acting on the inlet. The second integral on the right-hand-side of Equation (12-1) is the drag due to the viscous forces acting on the inlet. Equation (12-1) can be expressed as

$$D = D_{pressure} + D_{viscous} \tag{12-2}$$

The drag coefficient is referenced with respect to the dynamic pressure at station L with the reference area equal to the reference capture area,

$$C_D = \frac{D}{q_L\,A_{cap}} \tag{12-3}$$

and

$$C_{Dpressure} = \frac{D_{pressure}}{q_L\,A_{cap}} \tag{12-4}$$

where the dynamic pressure is calculated as

$$q_L = \frac{1}{2}\,\rho_L\,V_L^2 = \frac{1}{2}\,\gamma\,p_L M_L^2 \tag{12-5}$$

Substituting Equation (12-5) into Equation (12-4) and the pressure integral on the right-hand-side of Equation (12-1) yields

$$C_{Dpressure} = -\frac{1}{q_L\,A_{cap}}\int (p - p_L)\,dA_x \tag{12-6}$$

The pressure coefficient is defined as

$$C_p = \frac{p - p_L}{q_L} \tag{12-7}$$

Substituting Equation (12-7) into Equation (12-6) results in the alternative form

$$C_{Dpressure} = -\int C_p \frac{dA_x}{A_{cap}} \tag{12-8}$$

12.2 Inlet Drag Components

The inlet drag coefficient (C_{Dinlet}) is calculated as the sum of several drag components and is expressed in the form of

$$C_{Dinlet} = C_{Dspillage} + C_{Dcowl} + C_{Dbleed} + C_{Dbypass} + C_{Dother} \tag{12-9}$$

The spillage drag ($C_{Dspillage}$) is only present when the inlet capture flow ratio is less than one (W_1/W_{cap} < 1) which indicates that there is some combination of subsonic and supersonic spillage past the cowl lip. The primary component of the spillage drag is the additive drag (C_{Dadd}), which is due to the pressure forces acting on the inlet streamtube ahead of the cowl lip. When there is subsonic spillage for which the inlet is in subcritical operation, there is a correction for cowl lip suction (C_{LS}) as the subsonic flow spills over the cowl lip. Thus, the spillage drag coefficient is expressed as

$$C_{Dspillage} = C_{Dadd} - C_{LS} \tag{12-10}$$

The cowl drag coefficient (C_{Dcowl}) accounts for the pressure drag acting on the cowl lip and cowl exterior and is the sum of the cowl lip drag (C_{Dlip}) and the wave drag (C_{Dwave}) coefficients,

$$C_{Dcowl} = C_{Dlip} + C_{Dwave} \tag{12-11}$$

The following subsections will discuss each of these drag components.

12.3 Additive Drag, C_{Dadd}

The additive drag is a pressure drag and it is due to the pressure forces applied by the local flow on the surface of the inlet streamtube between stations L and 1. Additive drag occurs when the inlet flow ratio is less than one or W_1/W_{cap} < 1. The cross-sectional area of the inlet streamtube increases between stations L and 1 and presents a forward-faces surface upon which a pressure acts to create the drag. The additive drag is also known as the pre-entry drag (Ref. 1) to indicate that it is due to axial pressure forces acting on the streamtube ahead of the cowl lip.

One approach for calculating the additive drag is to establish the shape of the streamtube and the pressures along the streamtube, and then perform the integration of Equation (12-6). For the two-dimensional and axisymmetric inlets in supersonic flow, this is possible.

For pitot inlets in either subsonic or supersonic flow, the additive drag coefficient (C_{Dadd}) is calculated (Ref. 3) as

$$C_{Dadd} = \frac{2}{\gamma M_L^2}\left[\left(\frac{p_1}{p_L}\right)(1 + \gamma M_1^2) - 1\right] - 2\left(\frac{A_L}{A_{cap}}\right) \tag{12-12}$$

The last term in Equation (12-12) is the inlet flow ratio. The Mach number at the cowl lip station 1 (M_1) can be determined from continuity using Equation (2-30). The static pressure ratio (p_1/p_L) can be determined from the total pressures with use of the isentropic flow relation, Equation (2-6).

12.4 Cowl Lip Suction, C_{LS}

The cowl lip suction is a thrust term resulting from a low-pressure region formed on the forward-facing surface of the exterior cowl lip (Ref. 1). As a result of subcritical airflow spillage around the inlet cowl lip, the static pressure over the cowl leading edge is decreased, thus reducing the effective cowl pressure drag. This effect, known as cowl lip suction, can be viewed as a correction to the additive drag calculation as presented previously. The net combination of the additive drag and cowl lip suction is the total inlet spillage drag as shown in Equation (12-10). Equation (12-13) shows the definition of the cowl lip suction coefficient. This model for the cowl lip suction coefficient (C_{LS}) is based entirely on empirical relations (Ref. 4),

$$C_{LS} = (1 - K_\alpha)C_{Dadd} - (K_\beta - K_\alpha)C_{D2} \tag{12-13}$$

Equations (12-14) through (12-20) provides details on the empirical terms used in Equation (12-13). The first cowl lip suction factor (K_α) is described functionally in Equation (12-14) and shown graphically in the top-left plot of Figure 12.1. The effective cowl lip angle correction factor (σ) is defined in

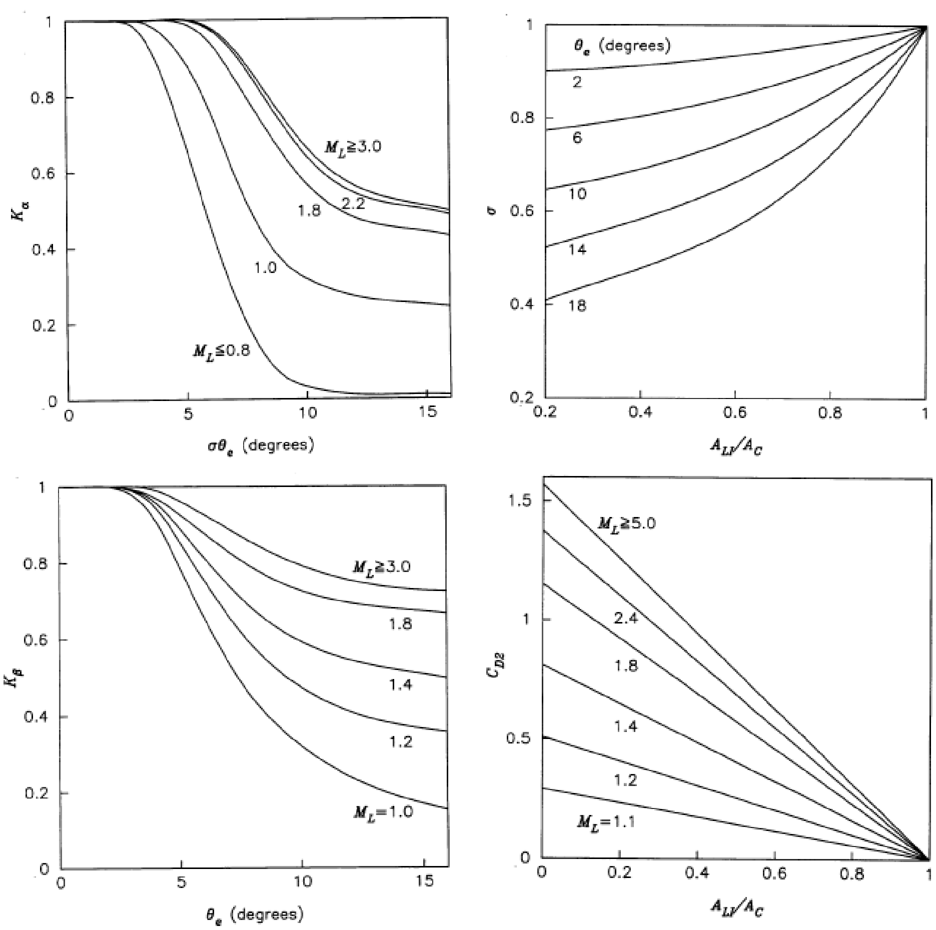

Figure 12.1.—Empirical relations for coefficients in the calculation of the cowl lip suction coefficient C_{LS} (images are from the IPAC manual, (Ref. 5)).

Equation (12-15) and shown graphically in the top-right plot of Figure 12.1. The procedure for computing the effective cowl lip angle (θ_e) is given in Equation (12-16) through (12-18). Equation (12-16) is an approximation for the effective cowl lip angle, in degrees, and is determined from the integral parameter (Ω), which is defined by Equation (12-17). This integral parameter evaluates the cowl surface curvature from the cowl lip leading edge to the maximum of the cowl forward projected area location. In Equation (12-17) and (12-18), the cowl profile is defined by coordinates (X,Y) and the cowl lip leading edge is located at (X_C,Y_C). The second cowl lip suction factor (K_β), is defined in Equation (12-19) and is shown graphically in the bottom-left plot of Figure 12.1. The final empirical cowl lip suction factor (C_{D2}) is defined in Equation (12-20) and is shown graphically in the bottom-right plot of Figure 12.1.

$$K_\alpha = f(\sigma\theta_e, M_L) \tag{12-14}$$

$$\sigma = \begin{cases} 1, M_L > 0.8 \\ f\left(\frac{A_{LI}}{A_{cap}}, \theta_e\right), M_L \leq 0.8 \end{cases} \tag{12-15}$$

$$\theta_e \approx \sqrt{2}\,\Omega \tag{12-16}$$

$$\Omega = \int_1^{\max} \frac{\left(\frac{\mathrm{Y}}{\mathrm{Y_C}}\right) \cos\overline{\Psi}}{1 + 2\pi\left(\frac{\mathrm{X} - \mathrm{X_C}}{\mathrm{Y_C}}\right)^2}\, \mathrm{d}\left(\frac{\mathrm{Y}}{\mathrm{Y_C}}\right) \tag{12-17}$$

$$\overline{\Psi} = \tan^{-1}\left(\frac{\mathrm{Y} - \mathrm{Y_C}}{\mathrm{X} - \mathrm{X_C}}\right) \tag{12-18}$$

$$K_\beta = \begin{cases} f(\theta_e, M_L), M_L \geq 1 \\ 0, M_L < 1 \end{cases} \tag{12-19}$$

$$C_{D2} = \begin{cases} f\left(\frac{A_{LI}}{A_{cap}}, M_L\right), M_L > 1 \\ 0, M_L \leq 1 \end{cases} \tag{12-20}$$

12.5 Cowl Lip Drag, C_{Dlip}

The cowl lip drag coefficient (C_{Dlip}) is due to the increased pressure behind a detached shock wave ahead of a blunt cowl lip. This drag component is only significant when the inlet is operating at full flow. If the cowl lip is sharp, then the cowl lip drag would be negligible. An estimate of the pressure acting on the blunt cowl lip is obtained as a simple arithmetic mean of the stagnation and static pressures behind a normal shock wave,

$$C_{Dlip} = \frac{2}{\gamma M_L^2}\left(\frac{\bar{p}}{p_L} - 1\right)\frac{A_{xlip}}{A_{cap}} \tag{12-21}$$

The static pressure on the blunt cowl lip is approximated as the average of the total pressure behind a normal shock wave and the static pressure behind a normal shock wave. This is expressed as

$$\frac{\bar{p}}{p_L} \approx \frac{1}{2}\left(\frac{p_{tNS}}{p_{tL}}\frac{p_{tL}}{p_L} + \frac{p_{NS}}{p_L}\right) \tag{12-22}$$

Inserting Equations (5-9) and (5-12) for flow through a normal shock wave and the isentropic relation Equation (2-6), yield the following equation for the cowl lip drag coefficient.

$$C_{Dlip} = \frac{1}{\gamma M_L^2}\left\{\left[\frac{(\gamma+1)M_L^2}{2}\right]^{\frac{\gamma}{\gamma-1}}\left[\frac{\gamma+1}{2\gamma M_L^2-(\gamma-1)}\right]^{\frac{1}{\gamma-1}} + \left[\frac{2\gamma M_L^2-(\gamma-1)}{\gamma+1}\right] - 2\right\}\frac{A_{xlip}}{A_{cap}} \tag{12-23}$$

The forward projection of the blunt cowl lip area is denoted as A_{xlip} in Equation (12-23). The forward projection of the blunt cowl lip area A_{xlip} for a two-dimensional inlet is,

$$A_{xlip} = (\, y_{clex} - y_{clin}\,)\, w_z \tag{12-24}$$

and for an axisymmetric inlet is

$$A_{xlip} = \pi\left(y_{clex}^2 - y_{clin}^2\right) \tag{12-25}$$

12.6 Wave Drag, C_{Dwave}

The wave drag is due to pressures acting on the cowl exterior at supersonic conditions. The wave drag coefficient (C_{Dwave}) is computed using Equation (12-26) whereas the integration is performed over the cowl exterior surface and A_x is the forward projection of the cowl exterior surface.

$$C_{Dwave} = \frac{2}{\gamma A_{cap} M_L^2}\int\left(\frac{p}{p_L} - 1\right) dA_x \tag{12-26}$$

The integration is performed by dividing the cowl exterior into segments and estimating the static pressure acting on that segment. The wave drag can then be expressed as

$$C_{Dwave} = \frac{2}{\gamma M_L^2}\sum_{i=1}^{N}\left(\frac{p_i}{p_L} - 1\right)\frac{A_{xi}}{A_{cap}} \tag{12-27}$$

or in terms of the pressure coefficient

$$C_{Dwave} = \sum_{i=1}^{N} C_p \frac{A_{xi}}{A_{cap}} \tag{12-28}$$

Here we consider two-dimensional and axisymmetric cowl exteriors consisting of segments that can be straight or curved. The profile of the cowl exterior can be described by (x, r) coordinates. The geometry modeling creates a grid for this profile with grid points (x_i, r_i). For two-dimensional cowl exteriors, the static pressures can be estimated for each segment using oblique shock wave or Prandtl-Meyer expansions depending on whether the segment involves positive or negative turning.

For axisymmetric cowl exteriors, the static pressures are estimated using linearized, supersonic slender body theory (Ref. 6). The pressure coefficient is evaluated as

$$C_p = -2\frac{\partial \emptyset}{\partial x} \tag{12-29}$$

The perturbation velocity potential $\emptyset$ is governed by the partial differential equation for the linearized, supersonic potential flow for an axisymmetric coordinate system,

$$(1 - M_L^2)\frac{\partial^2 \emptyset}{\partial x^2} + \frac{\partial^2 \emptyset}{\partial r^2} + \frac{1}{r}\frac{\partial \emptyset}{\partial r} = 0 \tag{12-30}$$

The generalized solution of Equation (12-30) is discussed in Reference 7. The velocity potential can be expressed as

$$\emptyset(x,r) = \int_0^{x-\lambda r} \frac{f(\xi)\, d\xi}{\sqrt{(x-\xi)^2 - \lambda^2 r^2}} \tag{12-31}$$

The pressure coefficient requires the first derivative of the velocity potential with respect to x, which is also the axial velocity component, and is expressed as

$$\frac{\partial \emptyset}{\partial x} = u(x,r) = \int_0^{x-\lambda r} \frac{f'(\xi)\, d\xi}{\sqrt{(x-\xi)^2 - \lambda^2 r^2}} \tag{12-32}$$

Similarly, the radial velocity component is expressed as

$$v(x,r) = -\frac{1}{r}\int_0^{x-\lambda r} \frac{(x-\xi)\, f'(\xi)\, d\xi}{\sqrt{(x-\xi)^2 - \lambda^2 r^2}} \tag{12-33}$$

The $f'(\xi)$ is the singularity distribution along the centerline axis for the perturbation velocity potential where ξ is the integration parameter. The singularity distribution uniquely determines the flowfield on and about the slender body surface. The λ is the Mach number parameter defined as

$$\lambda^2 = M_L^2 - 1 \tag{12-34}$$

A statement that the flow is tangent to the body surface on the body surface can be used as a boundary condition to determine the singularity distribution for that body. A more detailed description of the analyses which follow can be found in Reference 6. If the axisymmetric cowl exterior profile is described by the coordinate pairs (x, r) then the body surface tangent flow boundary condition can be written as

$$r'(x) = \frac{\partial r}{\partial x} = v(x,r) = -\frac{1}{r}\int_0^{x-\lambda r} \frac{(x-\xi) f'(\xi) d\xi}{\sqrt{(x-\xi)^2 - \lambda^2 r^2}} \tag{12-35}$$

Furthermore, if the cowl exterior profile is discretized and the singularity distribution, $f'(\xi)$, can be assumed piece-wise constant over a small interval $[\xi_{i-1}, \xi_i]$, then the discrete elements of the singularity distribution can be moved outside of the integration,

$$-r_n' r_n = \sum_{i=1}^{n} f_i' \int_{\xi_{i-1}}^{\xi_i} \frac{(x-\xi) f'(\xi) d\xi}{\sqrt{(x-\xi)^2 - \lambda^2 r^2}} \tag{12-36}$$

where

$$\xi_i = x_i - \lambda\, r_i \tag{12-37}$$

and the limits of the integration become,

$$\xi_0 = 0 \tag{12-38}$$

and

$$\xi_n = x_n - \lambda\, r_n \tag{12-39}$$

The piece-wise integral is now readily evaluated in closed form, and the solution becomes,

$$-\,r_n'\, r_n = -\sum_{i=1}^{n} f_i' \left(\sqrt{(x_n - \xi_i)^2 - \lambda^2 r_n^2} - \sqrt{(x_n - \xi_{i-1})^2 - \lambda^2 r_n^2} \right) \tag{12-40}$$

A marching scheme can easily be developed to determine the value of a discrete singularity, f_n', corresponding to a location (x_n, r_n) on the cowl surface in terms of a summation of all the upstream singularities. Therefore, the entire singularity distribution can be determined by simply marching down the cowl surface using the equation,

$$f_n' = \frac{-\,r_n'\, r_n + \sum_{i=1}^{n-1} f_i' \left(\sqrt{(x_n - \xi_i)^2 - \lambda^2 r_n^2} - \sqrt{(x_n - \xi_{i-1})^2 - \lambda^2 r_n^2} \right)}{\sqrt{(x_n - \xi_{i-1})^2 - \lambda^2 r_n^2}} \tag{12-41}$$

Once the discrete singularity distribution is known, the pressure coefficient can be determined by an analogous procedure with the pressure coefficient expressed as

$$C_p = -2 \sum_{i=1}^{n} f_i' \int_{\xi_{i-1}}^{\xi_i} \frac{d\xi}{\sqrt{(x_n - \xi)^2 - \lambda^2 r_n^2}} \tag{12-42}$$

Again, the resulting piece-wise integral of the above equation can be evaluated in closed form, yielding the equation

$$C_p = -2 \sum_{i=1}^{n} f_i' \ln \left[\frac{x_n - \xi_{i-1} + \sqrt{(x_n - \xi_{i-1})^2 - \lambda^2 r_n^2}}{x_n - \xi_i + \sqrt{(x_n - \xi_i)^2 - \lambda^2 r_n^2}} \right] \tag{12-43}$$

The above equation calculates the pressure coefficient at discrete points along the cowl surface in terms of the discretized singularity distribution. The axisymmetric wave drag coefficient is then determined by numerical integration of Equation (12-42) using the calculated distribution of the pressure coefficient.

12.7 Bleed Drag, C_{Dbleed}

The bleed drag is the drag due to the change in momentum of the bleed flow that is dumped overboard from the inlet bleed system. The contribution of the bleed drag to the total inlet drag increases when bleed rates increase. The bleed flow passes through the bleed system and encounters losses that reduce the kinetic energy of the flow. The bleed flow is then ejected into the inlet external flow, usually about the cowl exterior. The bleed drag is calculated as a deficit in the momentum of the flow stream in the axial direction as referenced to the local flow. The integral form of the momentum equation of Equation (12-1) can be applied with the result for the bleed drag coefficient (C_{Dbleed}) being,

$$C_{Dbleed} = \frac{D_{bleed}}{q_L\, A_{cap}} = \frac{W_{bleed}(V_L - V_{bexit} \cos\theta_{bexit})}{q_L\, A_{cap}} \tag{12-44}$$

where W_{bleed} is the bleed flow rate. It is assumed that the static pressure at the exit is close to the local value ($p_{bexit} = p_L$). The bleed flow exits the bleed system with a speed of V_{ex} at an angle of θ_{ex} relative to the inlet axis, which is the direction for which the drag is computed.

The bleed flow W_{bleed} can be expressed as

$$W_{bleed} = \rho_L V_L A_{LB} \tag{12-45}$$

where A_{LB} is the area of the portion of the inlet streamtube at station L that contains the amount of flow rate of W_{bleed}. When these are substituted into Equation (12-43), the bleed drag coefficient becomes,

$$C_{Dbleed} = 2\left(\frac{A_{LB}}{A_{cap}}\right)\left[1 - \frac{V_{bexit}}{V_L}\cos\theta_{bexit}\right] \tag{12-46}$$

The flow through the bleed system is assumed adiabatic, and so, the ratio of (V_{bexit}/V_L) can be expressed in terms of Mach number as

$$\frac{V_{bexit}}{V_L} = \frac{M_{bexit}}{M_L}\left[\frac{1 + \frac{\gamma - 1}{2}M_L^2}{1 + \frac{\gamma - 1}{2}M_{bexit}^2}\right]^{\frac{1}{2}} \tag{12-47}$$

Subsection 11.3 discussed the input factors for specifying the properties and conditions of the bleed regions, including input factors for M_{bexit} and θ_{bexit} needed for Equations (12-46) and (12-47). The equations indicate that the bleed drag will decrease as M_{bexit} is closer to the freestream Mach number M_L, which indicates less momentum loss of the bleed flow. A value of $\theta_{bexit} = 0$ degrees indicates the bleed plenum exit flow is directed axially and its momentum reduces the bleed drag. As θ_{bexit} is made larger, the flow is directed away from the axial direction and doesn't work to recover the axial momentum, so therefore the bleed drag increases.

12.8 Bypass Drag, $C_{Dbypass}$

The bypass drag coefficient ($C_{Dbypass}$) is computed in the same manner as the bleed drag, which accounts for the loss of momentum of the bypass flow as it flows through the bypass system. Equations (12-44) to (12-47) can be applied with appropriate modeling of the W_{bypass}, M_{bexit}, and θ_{bexit} for the bypass system.

References

1. Seddon, J. and Goldsmith, E. L., Intake Aerodynamics, AIAA Education Series, New York, 1999.
2. Anderson, J. D., Fundamentals of Aerodynamics, McGraw-Hill, New York, 1984.
3. Sibulkin, M., "Theoretical and Experimental Investigation of Additive Drag," NACA Report 1187, January 1954.
4. Crosthwait, E. L., et al, "Preliminary Design Methodology for Air-Induction Systems," General Dynamics Technical Report SEG-TR-67-1, pp. 222-231, 184-195, 1967.
5. Barnhart, P. J., "IPAC – Inlet Performance Analysis Code," NASA CR-204130, July 1997.
6. Barnhart, P. J., "A Non-Axisymmetric Linearized Supersonic Wave Drag Analysis: Mathematical Theory," NASA CR 198430, May 1996.
7. Liepmann, H. W. and Roshko, A., Elements of Gasdynamics, John Wiley & Sons, 1957.

13.0 Inlet Surface and CFD Grid Generation

The inlet geometry is represented in part by grid point coordinates for profiles and surfaces of the inlet components. These profile and surface grids can be used for the generation of planar and volume grids for use with computational fluid dynamic (CFD) methods to solve for the flowfield for a flow domain about and through the inlet. This section discusses the capability within SUPIN for the generation of profile, surface, and volume grids.

13.1 Grid Generation along Profiles

The inlet geometry created by SUPIN is mostly constructed from planar profiles in which shapes are defined by lines and curves in the planar space. Those planar profiles can be extruded to create surfaces. In some cases, the lines and curves are constructed in three-dimensional space and surfaces are created through transfinite interpolations.

Those profiles can be represented by a set of Cartesian coordinates of grid points distributed along the entities comprising the profile. Figure 13.1 shows an example of a profile with grid points distributed along its length. The coordinate along the entity is the parameter s and is the distance along the entity starting at its beginning at point a with $s = 0$ and ending at point b where $s = s_{max}$. The index i is the counter for the individual grid points. The total number of grid points is N. The spacing between grid points is indicated as Δs.

The generation of the grid along the profile involves specifying the spacing of the grid points at the start and end of the entity (Δs_{beg},Δs_{end}), the maximum grid spacing allowed for the entity (Δs_{max}), and the maximum grid spacing ratio allowed along the profile (R_{gsmax}). The grid spacing ratio (R_{gsi}) at a point i is defined as

$$R_{gsi} = \frac{\max(\Delta s_{i-1}, \Delta s_i)}{\min(\Delta s_{i-1}, \Delta s_i)} \tag{13-1}$$

An automated procedure is applied to compute the number of grid points (N) for the profile that satisfy the above conditions. The procedure requires use of a mathematical relationship for the distribution of the grid points. The options for distributions include evenly spaced grid points, geometric progression, and hyperbolic-tangent methods. The geometric progression starts with the (Δs_{beg}) as the minimum grid spacing and then grows the grid spacing amount by the factor (R_{gsmax}) until the maximum grid spacing (Δs_{max}) is reached. The hyperbolic-tangent method distributes the grid points along the entity in a smooth manner while satisfying the specification of end-point grid spacings (Δs_{beg},Δs_{end},Δs_{max}).

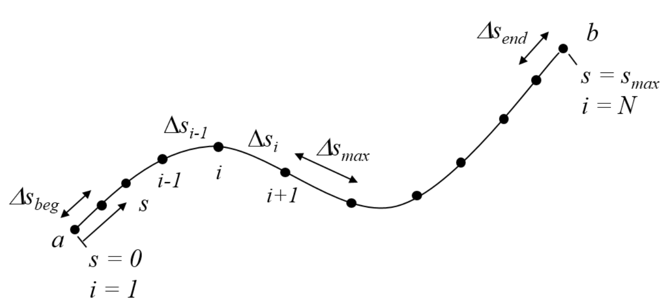

Figure 13.1.—Grid points along a profile.

13.2 Surface Grid Generation

The distributions of grid points along the profiles are then assembled to construct three-dimensional surface grids to represent the surfaces of the components of the inlet. The surface grids provide a means for visualization of the inlet geometry and can also be used to construct volume grids for CFD analysis of the inlet flow. Since some of the inlets have two-dimensional or axisymmetric character, some of the surfaces are formed by extruding the profiles along a cross-stream line or an axis-of-symmetry. Other surfaces are formed through a transfinite interpolation of four bounding edges consisting of an assembly of profiles. Each surface grid is mathematically a quadrilateral with a structured surface grid in (x,y,z) space in which the grid indices are (i,j), (i,k), or (j,k). Figure 13.2 provides an example of surface grids for a streamline-traced inlet (K_{typ} = 5).

The surface grids are generated in an automated manner within SUPIN using knowledge of the type of inlet and key grid spacings through the inlet. These key grid spacings include the streamwise grid spacing in the throat (Δs_{thrt}), the crosswise grid spacing at the symmetry boundaries (Δs_{sym}), the streamwise grid spacing for the cowl exterior (Δs_{cwex}), and the grid spacing of the first grid point in the normal direction off of a wall (Δs_{wall}). These key grid spacings, except for Δs_{wall}, are shown in the surface grid of Figure 13.2. Knowing these key grid spacings, the appropriate number of grid points along the profiles or edges are computed and the grid points are distributed along the profiles or edges and upon the surface. A constraint is also imposed to limit the change in grid spacing between adjacent grid points as specified by the grid spacing ratio (R_{gsmax}). The values of these key grid spacings are specified based on the desired resolution of the geometric shapes and flow features, such as shock waves, boundary layers, and flow gradients.

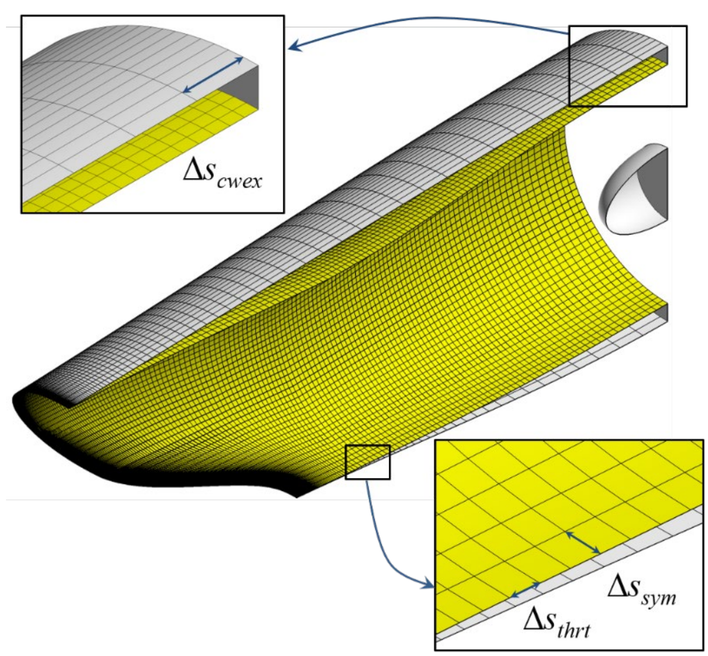

Figure 13.2.—Example of the surface grid for the streamline-traced inlet along with the key grid spacing factors.

The surface grid is output by SUPIN using the Plot3D and stereo-lithography (STL) file formats. A Plot3D file has a filename extension of ".xyz" and is an unformatted file using the three-dimensional, structured, multi-block Plot3D format (Ref. 1). The file **SUPIN.xyz** contains the starboard half (e.g., right-side half of the inlet from a viewpoint of looking upstream) because SUPIN assumes symmetry about the plane defined by $z = 0$. The file **Solid.xyz** contains both the starboard and port or left-hand half of the inlet to form the full inlet. The STL files has a filename extension of ".stl". The STL file contains a listing of triangles that form the surface. Within SUPIN, the triangles are formed by inserting diagonals into the quadrilaterals of the structured surface grid to create two triangles for each quadrilateral. The file named **SUPIN.stl** file is written as a formatted file and contains both the starboard and port halves of the inlet.

The input factor K_{surf}, as discussed in Subsection 4E, specifies within SUPIN whether the surface grid is to be generated and the file format of the output file for the surface grid. A value of $K_{surf} > 0$ indicates that the surface grid is to be generated. A value of $K_{surf} = 1$ indicates that the surface grid file is to be output in the Plot3D format. A value of $K_{surf} = 2$ indicates that the surface grid file is to be output in the STL format. A value of $K_{surf} = 3$ indicates that both Plot3D and STL files are to be created.

13.3 CFD Grid Generation

SUPIN can generate grids for CFD flow analysis. This eases the inlet design and analysis process by automating much of the setup process for the flow analysis of the inlet designs created by SUPIN. SUPIN generates multi-block, structured grids for either planar (two-dimensional or axisymmetric) or three-dimensional CFD analysis. The computational approach requires the specification of the extent of the boundaries of the flow domain about and through the inlet. SUPIN divides this flow domain into sub-domains. A structured, multi-block grid is then generated within each sub-domain. Each block contains a structured, three-dimensional array of grid points. SUPIN does not generate unstructured grids. However, the surfaces grids files described in the previous subsection could be input to a grid generation software package as a definition of the inlet geometry for the generation of an unstructured grid for a CFD solver.

The CFD grid for each sub-domain is output by SUPIN to files in the Plot3D format (unformatted, three-dimensional, multi-block, and structured). The complete CFD grid for the entire flow domain is created by merging the grids of the sub-domains. The sub-domains are listed below along with the name of the Plot3D file.

- ***Cowl Lip Sub-Domain***. Plot3D grid file: **CFD3Dclip.xyz**. This grid consists of eight blocks that wrap about the cowl lip interior and exterior. The elliptical profile of the cowl lip allows two C-type blocks to cluster grid points on the surface of the cowl lip interior and exterior. The outer six blocks transition the grid topology from a C-type to an H-type. The k-index of the grid is along the circumference or span of the inlet. At each k-index, the grid surface is planar. This grid is generated for all inlet types.
- ***Cowl Exterior Sub-Domain***. Plot3D grid file: **CFD3Dcwex.xyz**. This grid consists of one block that wraps about the cowl exterior downstream of the cowl lip exterior grid blocks. The grid is clustered with the intention of providing a high-quality grid to resolve the viscous boundary layer on the cowl exterior surface. This grid is generated for all inlet types.
- ***Farfield Sub-Domain***. Plot3D grid file: **CFD3Dfar.xyz**. This grid consists of four blocks and encompasses the outer region of the flow domain and spans from the inflow and farfield freestream boundaries to the external outflow boundaries. This grid abuts and matches the grid of the cowl lip and cowl exterior sub-domains. This grid is generated for all inlet types.

- ***Cowl Interior Sub-Domain***. Plot3D grid file: **CFD3Dcwin.xyz**. This grid sub-domain has different number of blocks and extents depending upon the type of inlet and whether a planar or three-dimensional volume grid is being generated. The sub-domain extends over some portion of the cowl interior and has grid points clustered against the cowl interior surface with the intention of providing a high-quality grid to resolve the viscous boundary layer on the cowl interior surface. For the axisymmetric pitot (K_{typ} = 1), the streamline-traced (K_{typ} = 5), and the three-dimensional pitot (K_{typ} = 6) inlets, the grid consists of three zones that are placed in series in the streamwise direction downstream of the cowl lip sub-domain. The cowl interior sub-domain extends away from the wall a sufficient distance to full capture the boundary layer and some of the core inlet flow. The rest of the inlet core flow is filled by the inner and spinner sub-domains, which are discussed below. For the two-dimensional (K_{typ} = 2) inlet and a three-dimensional grid (K_{gCFD} = 3), the cowl interior sub-domain consists of a single block that extends along the cowl interior surface of the subsonic diffuser. The subsonic diffuser cowl interior surface transitions from a rectangular cross-section at station SD to a circular cross-section at the engine face. This sub-domain grid accounts for this transition. For the two-dimensional (K_{typ} = 2) inlet with a planar grid (K_{gCFD} = 2), the cowl interior sub-domain is not generated. The cowl interior sub-domain is also not generated for the axisymmetric spike inlet (K_{typ} = 3).
- ***Forebody Sub-Domain***. Plot3D grid file: **CFD3Dfore.xyz**. This grid is only created for two-dimensional (K_{typ} = 2) or axisymmetric (K_{typ} = 3) inlets. The sub-domain consists of three blocks for the axisymmetric spike inlet and four blocks for the two-dimensional inlet. The sub-domain extends the inflow freestream boundary forward of the nose of the inlet. The sub-domain has the external supersonic diffuser as one of its boundaries. The outer or top boundary of this grid is point-matched with the farfield sub-domain. For the two-dimensional inlet, the fourth block is below the nose of the inlet to allow computations at angles-of-attack.
- ***Throat Sub-Domain***. Plot3D grid file: **CFD3Dthrt.xyz**. This grid is created for the two-dimensional (K_{typ} = 2) and axisymmetric (K_{typ} = 3) inlets. This grid consists of one block that fills most of the throat section. The inflow boundary of this block is point-matched with the cowl lip and forebody sub-domains.
- ***Inner Sub-Domain***. Plot3D grid file: **CFD3Dinner.xyz**. This grid fills in the inner portion of the flow domain. For streamline-traced (K_{typ} = 5) and three-dimensional pitot (K_{typ} = 6) inlets, this grid extends from the inflow freestream boundary to either the boundary of the spinner region or the engine face, depending on whether the spinner is included or not, respectively. For two-dimensional (K_{typ} = 2) and axisymmetric (K_{typ} = 3) inlets, this grid extends between the end of the throat section sub-domain to the spinner domain or engine-face. The grids of the inner sub-domain consist of grid blocks that abut against the farfield, cowl lip, cowl interior, throat, and spinner sub-domains as necessary. The grids are likely not point-matched across these interfaces between these sub-domains. This allows flexibility in generating the grids. An example of this non-matched grids is presented below.
- ***Subsonic Diffuser Sub-Domain***. **CFD3Dsubd.xyz**. This grid consists of one block that fills the subsonic diffuser of two-dimensional inlets with rectangular subsonic diffusers (K_{typ} = 2 and K_{subd} = 8) and axisymmetric spike inlets (K_{typ} = 3). The grid for the i = 1 grid surface abuts and matches $i = i_{max}$ grid surface of the throat sub-domain.
- ***Spinner Sub-Domain***. Plot3D grid file: **CFD3Dspin.xyz**. This grid consists of four blocks about the spinner. The first block is a C-grid about the spinner surface. The second block is ahead of the first block and contains a singular axis. The third and fourth blocks are adjacent to the cowl

interior sub-domain. The grid blocks of the spinner sub-domain abut against grid blocks of the cowl interior, inner, and outflow nozzle sub-domains and likely the grids are non-matched across these interfaces.

- ***Bleed Slot Sub-Domain***. Plot3D grid file: **CFD3Dslot.xyz**. This grid consists of twenty blocks and fills the domain of the throat section, bleed slot, and bleed slot plenum for two-dimensional inlets (K_{typ} = 2). This sub-domain is used in place of the throat sub-domain grid when the inlet has a bleed slot.
- ***Struts Sub-Domain***. Plot3D grid file: **CFD3Dstruts.xyz**. This grid consists of twenty-eight blocks formed about the support struts for an axisymmetric spike inlet (K_{typ} = 3). The blocks fill the domain of the throat section and subsonic diffuser for the axisymmetric spike inlet and replaces the grids for those sub-domains.
- ***Outflow Nozzle Sub-Domain***. Plot3D grid file: **CFD3Dnoz.xyz**. This grid consists of four blocks and provides the "cold pipe" and converging-diverging nozzle for the internal outflow boundary. The cross-sectional area of the nozzle throat is determined by the SUPIN input factor Fgnoz. Within a CFD grid, the nozzle throat area can be changed by replacing the grid blocks for the converging and diverging portions of the nozzle.
- ***Bleed Model Sub-Domain***. Plot3D grid file: **CFD3Dbld.xyz**. This grid consists of blocks formed for bleed regions specified through the bleed model input data block (DataID = 12) for the two-dimensional inlet (K_{typ} = 2). These bleed grid blocks are intended to assist in setting bleed boundary conditions. One face of the bleed blocks interface with portions of the inlet surface over which the porous bleed boundary conditions are to be applied. The common interface can be used in identifying surface grid points that should be specified to have the porous bleed boundary conditions applied.
- ***Sidewall Sub-Domain***. Plot3D grid file: **CFD3Dswin.xyz**. This grid consists of blocks formed to identify the sidewall for the two-dimensional inlet (K_{typ} = 2). These grid interface to the sidewall of the external supersonic diffuser and can be used to specify viscous boundary conditions for the sidewall.

13.4 Grid Generation Input Data Block

The grid generation input factors are specified using the input data block with DataID = 13. The input factors specify the extent of the flow domain and the key grid spacings. Table 13.1 lists the input factors for the key grid spacings. The input Δs_{wall} specifies the spacing of the first grid point away from a surface or wall in roughly the normal direction. Such spacing becomes important for resolving viscous boundary layers. The input Δs_{sym} specifies the grid spacing in the cross-stream or circumferential direction at the plane of symmetry. The input Δs_{cwex} specifies the maximum axial grid spacing on the cowl exterior. The input Δs_{thrt} specifies the axial grid spacing within the throat. The values of the input factors for Δs_{sym}, Δs_{cwex}, and Δs_{thrt} are specified as a factor of the reference dimension (D_{ref}) for the inlet. This is typically the engine-face diameter or similar representative dimension of the engine-face. The units for the input factor Δs_{wall} are feet.

The input F_{gds} is a scaling factor that is applied to the values of Δs_{sym}, Δs_{cwex}, and Δs_{thrt}. This factor can be used to adjust the resolution of the grid without having to adjust all three of these values. This can be used coarsen or refine the grid as part of a grid refinement exercise for CFD simulations. Thus, a value of F_{gds} = 0.5 would reduce the grid spacing values by half.

TABLE 13.1.—INPUT FACTORS FOR THE GRID SPACING

Factor	Input	Description
F_{gds}	`Fgds`	Factor to scale the grid spacings
R_{gsmax}	`Rgsmax`	Maximum grid spacing ratio allowed for the grid
Δs_{wall}	`Fdswall`	Grid spacing in the grid normal to an inlet surface (ft)
Δs_{sym}	`Fdssym`	Grid spacing in the grid normal to a symmetry boundary
Δs_{cwex}	`Fdscwex`	Streamwise grid spacing along the cowl exterior
Δs_{thrt}	`Fdsthrt`	Streamwise grid spacing in the throat

TABLE 13.2.—INPUT FACTORS FOR THE FLOW DOMAIN

Factor	Input	Description
d_{dinf}	`ddinf`	Horizontal distance for inflow boundary
d_{dfar}	`ddfar`	Vertical distance to the farfield boundary at inflow boundary
d_{dnoz}	`ddnoz`	Length of the constant-area section of the outflow nozzle
d_{dclp}	`ddclp`	Extent of the cowl lip grid block
θ_{far}	`thfar`	Angle of farfield boundary above cowl lip (deg)
F_{gnoz}	`Fgnoz`	Outflow nozzle throat radius as factor of the engine-face radius

TABLE 13.3.—EXAMPLE INPUT DATA BLOCK FOR THE GRID SPACING AND FLOW DOMAIN

```
DataID.  Grid Spacing
 13
 Fgdds   Rgsmax    Fdswall    Fdssym    Fdscwex    Fdsthrt
 1.000    1.15    0.000020    0.0150     0.0700     0.0130
 ddinf   ddfar       ddnoz     ddclp      thfar      Fgnoz
 0.200   1.000       1.000     0.030     45.000     0.9000
```

The input R_{gsmax} is the maximum grid spacing ratio allowed for the surface grid. The grid spacing ratio (R_{gs}) is defined by Equation (13-1) and is the ratio of the distances between two successive sets of grid points with the smaller distance placed in the denominator, which would result that $R_{gsi} > 1.0$. Thus, $1.0 \leq R_{gsi} \leq R_{gsmax}$.

Table 13.2 lists the input factors specifying the extent of the flow domain for the CFD grid. Table 13.3 lists an example input data block for the block type DataID = 13. The extent of the flow domain is specified by the input factors of d_{dinf}, d_{dfar}, d_{dnoz}, and d_{dclp}. These inputs are normalized by the reference dimension of the inlet (D_{ref}). The input d_{dinf} specifies the distance ahead of the nose of the inlet at which the inflow boundary is located. The nose of the inlet is the forward-most point on the inlet. The input d_{dfar} specifies vertical distance above the nose at which the farfield boundary connects to the inflow boundary. The input θ_{far} specifies the angle of the farfield boundary. These dimensions for the flow domain are illustrated in Figure 13.3 and Figure 13.4. The input d_{dclp} specifies the distance from the cowl lip to the boundary of the grid block that wraps around the cowl lip.

The flow domain includes an outflow nozzle block that is attached downstream of the engine face. The purpose of the nozzle block is to move the internal outflow boundary downstream of the engine face, so that the application of the outflow boundary condition does not affect the engine face. The nozzle block consists of a straight constant-area section followed by a converging-diverging nozzle section. The input d_{dnoz} is used to establish the axial lengths of the constant-area section, the converging section, and the diverging section. The constant-area section is of length equal to 2 d_{dnoz} D_{ref}. The converging and diverging sections are each of length d_{dnoz} D_{ref}. A value of $d_{dnoz} = 1.0$ is a nominal length; however, if the

CFD flow simulation indicates large regions of boundary layer separation within the inlet and outflow nozzle section, then a higher value of d_{dnoz} would be suggested so that the separated flow reattaches prior to the converging section. The objective is to avoid the boundary layer separation regions from approaching the converging-diverging sections of the nozzle and interfering with the ability of the nozzle to create choked flow at the nozzle throat.

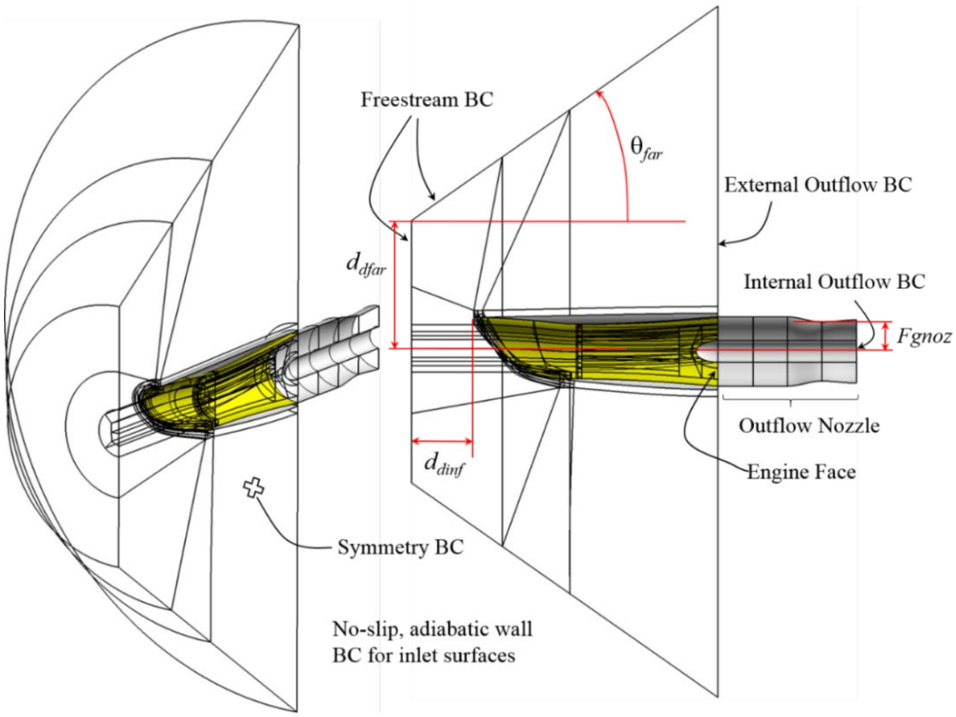

Figure 13.3.—Input factors defining the flow domain for a CFD grid for a streamline-traced inlet.

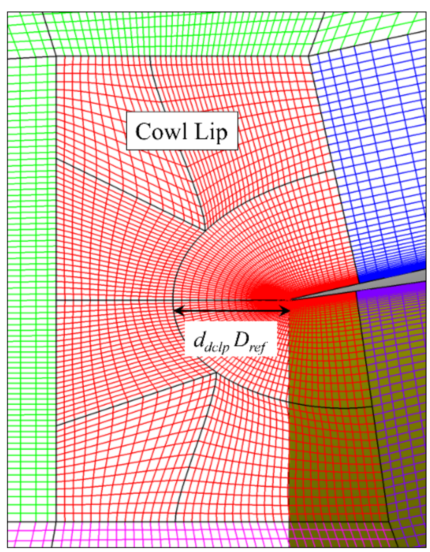

Figure 13.4.—Input factor for the extent of the grid block and grid about the cowl lip.

The input F_{gnoz} specifies the radius (or height) of the throat of the outflow nozzle with respect to the radius (height) of the engine face. A value of $F_{gnoz} < 0.0$, indicates that the outflow nozzle block should not be generated. With choked flow at the nozzle throat, the outflow of the nozzle is supersonic, and so, the outflow boundary condition uses extrapolation of flow variables, and no information is propagated upstream from the boundary. Decreasing the nozzle throat area leads to an increase in the static pressure at the engine face, which is also known as "back-pressuring".

Figure 13.5 shows the flow domain and grid for planar grid for an axisymmetric spike inlet. The labels identify the farfield, forebody, and outflow nozzle sub-domains. Each sub-domain is of a different color. Figure 13.6 shows a closer view of the internal ducting of the axisymmetric spike inlet with labels identifying the sub-domains for the cowl lip, cowl exterior, throat, and subsonic diffuser. Figure 13.7 shows a view of a streamline-traced inlet with some of the flow domain boundaries and grids on the symmetry plane. Shown are the sub-domains for the cowl interior, inner, spinner, and outflow nozzle. The grid for the streamline-traced inlet uses non-matched grids across interfaces of blocks of the cowl interior, inner, and spinner sub-domains. Figure 13.8 shows a closeup of the grid across these interfaces that show an example of non-matched grid points.

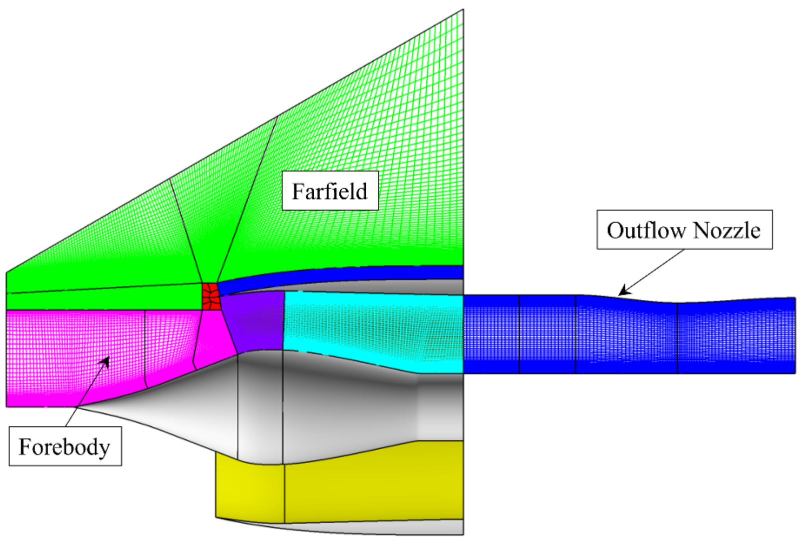

Figure 13.5.——Planar CFD grid for an axisymmetric spike inlet.

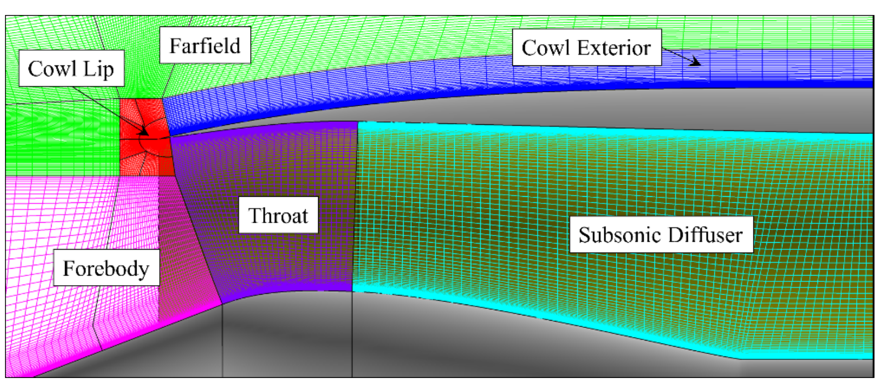

Figure 13.6.—Planar CFD grid through the throat section and subsonic diffuser.

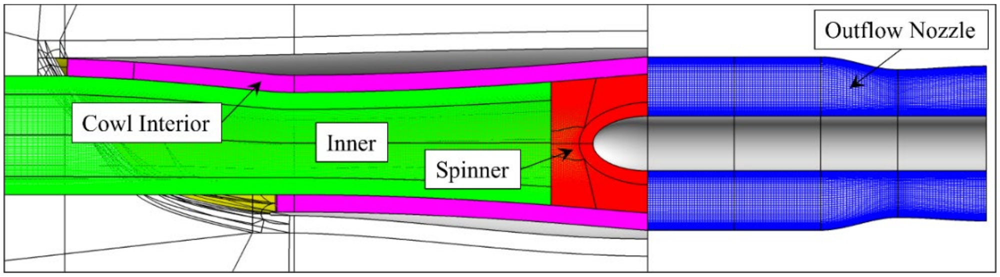

Figure 13.7.—CFD grids on the symmetry plane of a streamline-traced inlet.

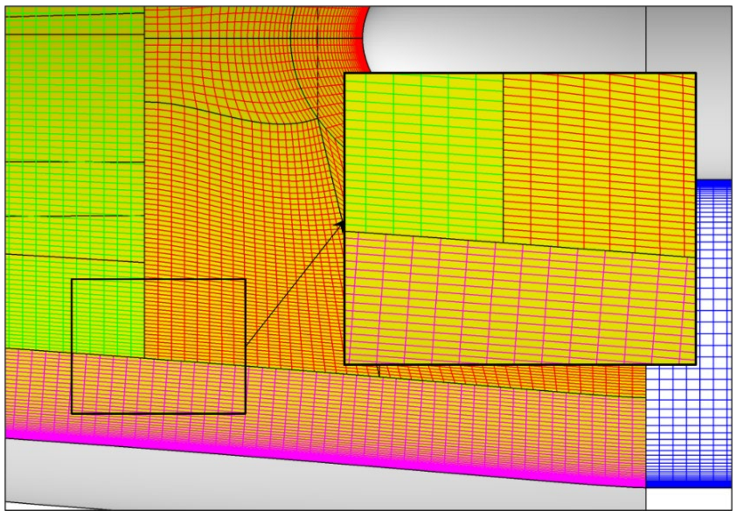

Figure 13.8.—Closeup of the grids on the symmetry plane of a streamline-traced inlet highlighting the non-point-matched grid blocks at the interface of the cowl interior, inner, and spinner sub-domains.

13.5 Outflow Nozzle Sub-Domain

The outflow nozzle sub-domain facilitates the application of the boundary condition for the engine face that establishes the flow through the inlet. The previous two subsections discussed some aspects of the outflow nozzle sub-domain. This subsection provides some further details to describe its generation and use within a flow simulation. Figure 13.9 shows an image of a two-dimensional inlet with an outflow nozzle sub-domain attached downstream of the engine face. The engine face of the image is annular with a spinner. The spinner results in a constant-diameter, axisymmetric centerbody for the outflow nozzle sub-domain in which the diameter is the diameter of the spinner hub (D_{hub}). The same situation occurs for the axisymmetric spike inlet with the diameter equal to the diameter of the inlet centerbody at the hub. If a spinner is not used for the inlets other than the axisymmetric spike inlet, then the outflow nozzle sub-domain does not contain the centerbody.

The effect of the outflow nozzle sub-domain is to place the outflow boundary condition for the internal flow downstream of the engine face, as shown in Figure 13.9. The outflow nozzle sub-domain consists of four blocks. The first two blocks form an axisymmetric constant-area, section. Figure 13.10 indicates that this straight section has a length of L_{nA}. The length of the straight section is specified by the input factor d_{dnoz} and expressed as a factor normalized by the inlet reference dimension (D_{ref}) which for the image of Figure 13.9 is the equal to the diameter of the engine-face, $D_{ref} = D_{EF}$. Thus,

$$L_{nA} = d_{dnoz} \, D_{EF} \tag{13-2}$$

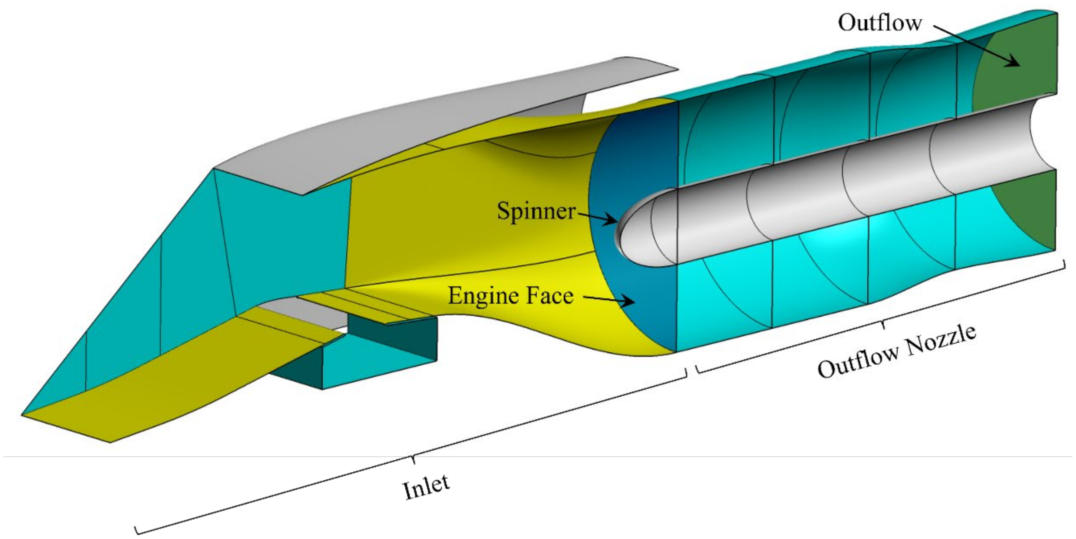

Figure 13.9.—Two-dimensional, single-duct inlet with an outflow nozzle sub-domain attached to downstream of the engine face.

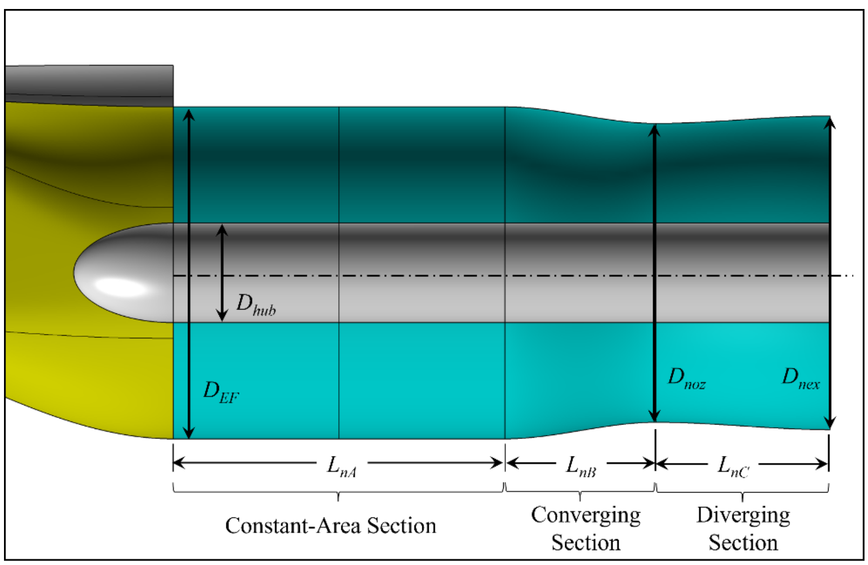

Figure 13.10.—Outflow nozzle sub-domain with dimensions for the nozzle.

A value of d_{dnoz} = 1.0 is a reasonable first choice for establishing the flow domain of the nozzle. The objective is to move the outflow boundary conditions downstream of the engine face to reduce any effects on the engine face of applying the computational outflow boundary condition. The constant-area duct works to settle the flow out of the inlet. If the flow within the subsonic diffuser has separated boundary layers, then there may be a region of separated flow that exists at the engine face. This type of condition is generally a difficult situation for a numerical boundary condition, such as a static pressure or flow rate outflow boundary condition. The constant-area section allows some length for the boundary layer to reattach and get the flow directed in the streamwise direction. If the length of the constant-area section seems too short to contain the separated flow and produce reattachment, then the value of d_{dnoz} can be increased to perhaps d_{dnoz} = 1.5 or 2.0.

The third block is the converging section of the nozzle and has a length of L_{nB}. The fourth block is the diverging section of the nozzle and has a length of L_{nC}. These two lengths are established as

$$L_{nB} = 0.65\ (D_{EF} - D_{hub}) \tag{13-3}$$

and

$$L_{nC} = 0.75\ (D_{EF} - D_{hub}). \tag{13-4}$$

The value of the factors 0.65 and 0.75 have no solid aerodynamic basis other than they were set based on experience with CFD simulations of various inlet.

The diameter of the outflow nozzle throat, D_{noz}, is established by the input factor F_{gnoz} which is expressed as a factor of the engine-face diameter,

$$D_{noz} = F_{gnoz}\, D_{EF} \tag{13-5}$$

As noted in Subsection 13.4 above, a value of $F_{gnoz} < 0$ will cause the outflow nozzle subdomain not to be generated.

The intent of the outflow nozzle is to form a choked throat in which $M_{noz} = 1$ where Mnoz is the average Mach number across the cross-section of the nozzle throat. The flow rate established by the nozzle can be expressed using continuity in the form of

$$W_2 = W_{noz} = \frac{p_{tnoz}\, A_{noz}}{\sqrt{T_{tnoz}}}\, \phi_{noz} \tag{13-6}$$

The choked condition sets $\phi_{noz} = \phi(M_{noz} = 1)$. The adiabatic conditions provide that $T_{tnoz} = T_{t2} = T_{tL}$. The total pressure at the nozzle throat, p_{tnoz}, depends on the total pressure losses through the inlet up to the nozzle throat. Thus, the control for establishing the engine-face flow rate is the area of the nozzle throat, A_{noz}, as set by the diameter of the nozzle throat as computed by Equation (13-5). During the inlet CFD flow simulations, the input factor F_{gnoz} is varied to obtain the desired engine-face flow rate.

The diverging section of the nozzle has the intent of accelerating the nozzle flow to low supersonic conditions such that an extrapolation boundary condition can be applied for the supersonic outflow. The area of the nozzle exit is set to $A_{nex} = 1.047\ A_{noz}$ with the objective of accelerating the flow to $M_{nex} = 1.25$. Based on A_{nex}, the value of D_{nex} can be computed based on the cross-section of the nozzle exit.

SUPIN generates a multi-block, structured CFD grid for the outflow nozzle consisting of four blocks, as shown in Figure 13.9, Figure 13.10, and Figure 13.11. Figure 13.11 shows the inlet and nozzle with several grid planes in each of the four blocks. The I1 face of the first block abuts with the engine face.

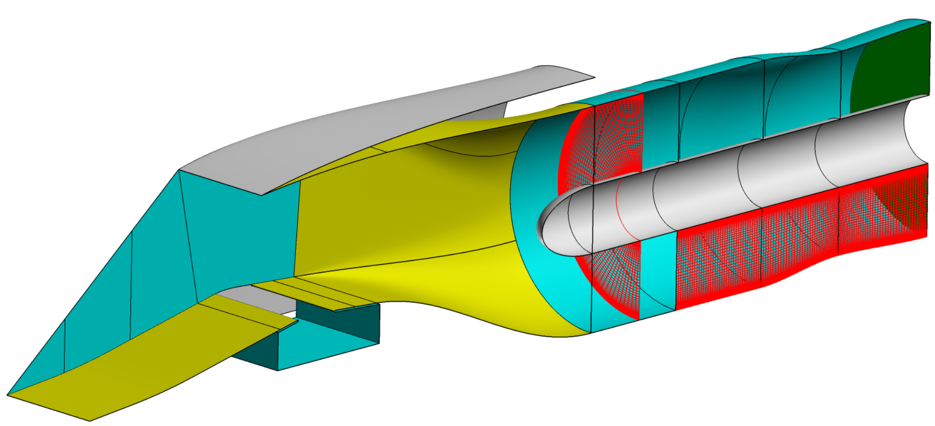

Figure 13.11.—Grid planes within the outflow nozzle sub-domain.

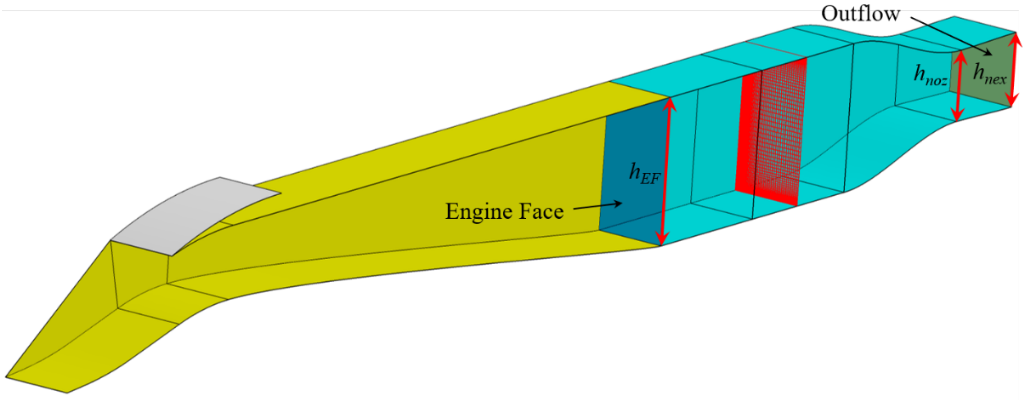

Figure 13.12.—Outflow nozzle for a rectangular engine face.

The IMAX face of the fourth block is the outflow boundary. The JMAX faces of the blocks are coincident with the outer surface of the nozzle. The J1 faces are coincident with the constant diameter centerbody. If the centerbody does not exist, then the J1 faces form a singular axis. The I-planes of the grids are perpendicular to the axis of the nozzle. This facilitates the computation of the engine-face flow rate as the integration of the flow through the grid planes. The flow rates for each of the constant-I grid planes can be computed, and a statistical analysis can be performed of the variations as a measure of the convergence of the engine flow rate for the simulation.

For the case of the rectangular engine face ($K_{EF} = 4$), the outflow nozzle maintains the rectangular cross-section with the width equal to the width of the engine face, w_{EF}. Figure 13.12 illustrates a rectangular outflow nozzle sub-domain. The height of the engine face becomes the reference dimension that is used in establishing the dimensions of the outflow nozzle. The lengths and heights are computed as

$$L_{nA} = d_{dnoz} \, h_{EF} \tag{13-7}$$

$$L_{nB} = 1.2 \, h_{EF} \tag{13-8}$$

$$L_{nC} = 0.6 \, h_{EF} \tag{13-9}$$

and

$$h_{noz} = F_{gnoz} \, h_{EF}. \tag{13-10}$$

The height of the exit boundary uses the same area expansion as the nozzle described above and results in

$$h_{nex} = 1.047 \, h_{noz}. \tag{13-11}$$

The CFD grid planes through the nozzle are rectangular, as shown in Figure 13.12.

13.6 Global Transformation of Surface Grids

Global transformations can be applied to the surface grids generated by SUPIN to rotate, translate, and scale the surface grid coordinates. This can be used to position the inlet relative to an aircraft geometry and scale the grid coordinates to other units from the units of feet for which SUPIN generates the coordinates. The input data block for the global transformation input factors uses DataID = 29. An example input data block is shown in Table 13.4. Table 13.5 lists the descriptions of the input factors. The input factors Kxmir and Kymir indicate if the grid is to mirror in the *x* or *y* directions. Currently the Kxmir input factor is not functional. The value of Kymir = 1 has the effect of mirroring the y-coordinates about the *x*-*z* plane. The input factor Fscale applies the specified scaling factor to the grid points. The rotation of the grid points is specified by the input factors XRot, YRot, and RotAng. The input factors dX, dY, and dZ specify translations in the *x*, *y*, and *z* coordinate directions. Currently, rotations and translations can only be specified in the *x*-*y* plane. The order of the transformations are rotation, translation, scaling, and mirroring.

TABLE 13.4.—EXAMPLE INPUT DATA BLOCK FOR THE GLOBAL TRANSFORMATIONS OF THE SURFACE AND CFD GRIDS

```
DataID.  Global Grid Transformations
 29
Kxmir     Kymir      Fscale
  0         1        12.000
   xRot        yRot       RotAng
  0.00000     0.00000      0.000
    dx          dy          dz
  0.00000     0.00000     0.00000
```

TABLE 13.5.—INPUT FACTORS FOR THE GLOBAL TRANSFORMATION OF SURFACE AND CFD GRIDS

Factor	Input	Description
K_{xmir}	`Kxmir`	Flag for mirroring about *x*-axis (=0 no, =1 yes)
K_{ymir}	`Kxmir`	Flag for mirroring about *y*-axis (=0 no, =1 yes)
F_{scale}	`Fscale`	Scale factor for the for the grid coordinates
X_{rot}	`Xrot`	Center of rotation (*x* coordinate)
Y_{rot}	`Yrot`	Center of rotation (*y* coordinate)
$\Delta\theta_{rot}$	`RotAng`	Angle to rotate grid point (deg)
ΔX_{sg}	`dx`	Distance to translate grid point in *x*-coordinate direction
ΔY_{sg}	`dy`	Distance to translate grid point in *y*-coordinate direction
ΔZ_{sg}	`dz`	Distance to translate grid point in *z*-coordinate direction

References

1. Walatka, P. P., Buning, P. G., Pierce, L., and Elson, P. A., “PLOT3D User’s Manual,” NASA-TM-101067, March 1990.

14.0 Other SUPIN Features and Capabilities

This section discusses several additional features and capabilities of SUPIN.

14.1 Inlet Summary Table

The inlet summary table is written to an ASCII text file named **SUPIN.Table.txt** that was mentioned in Subsection 4.18. The inlet summary table provides a summary of select inlet input factors, inlet geometric properties, and inlet performance metrics. The format of the summary table lists the values in a column followed by a description. The intent of the file is to provide a concise summary of the inlet characteristics and performance. The file has found use when read into a spreadsheet program such as Microsoft Excel® for tabulating and plotting of results from various inlets. The writing of the output summary table file is specified through the input data block with DataID = 30, for which an example is listed in Table 14.1. The input factor Ktabin is a flag that expects an integer input and a value of Ktabin = 1 indicates that a summary table is to be written. The information within the summary table depends on the SUPIN mode of operation (K_{mode}), type of inlet (K_{typ}), and type of supersonic compression (K_{comp}).

14.2 Scheduling of the Input Factors

The scheduling of the input factors allows a series of SUPIN inlet design and analysis operations to be performed using a single input data file by sequencing certain input factors over a range of values. An example could be designing a series of two-dimensional inlets over a range of freestream Mach numbers (fsmach), capture widths (Fwclip), and engine-face Mach numbers (FWinp). The intent of the scheduling is to provide a means to explore a range of values for one or more input factors to produce performance data that can create a trend curve or carpet plot.

The process involves specifying one or more schedules within the input data file (SUPIN.in). A schedule expresses the variation of a single input factor, such as freestream Mach number (fsmach). It is possible to create a schedule for any of the input factors listed in the above sections. A schedule would specify which input factors are to be varied, the manner of the variation, and the values of those input factors.

A schedule can be specified as either a one-factor or two-factor schedule. A ***one-factor schedule*** just has one factor that is varied. For example, one can specify a one-factor schedule with the freestream Mach number as the factor and provide several discrete Mach numbers for the schedule. SUPIN would then sequence through each of freestream Mach numbers and perform the specified design and analysis operations. The other input factors would remain the same. For another example, one can specify a schedule that varies the dimension of the cowl lip interior (bclin) to examine the sensitivity of the inlet performance to cowl lip bluntness. One-factor schedules can be specified as either ***discrete values*** or as a ***range of values*** with a start, end, and increment indicated.

TABLE 14.1.—EXAMPLE INPUT DATA BLOCK FOR INDICATING THAT AN INLET SUMMARY TABLE IS TO BE CREATED

```
DataID.  Summary Table
 30
Ktabin
  1
```

A ***two-factor schedule*** has the first factor as the ***independent factor*** and the second factor as the ***dependent factor***. For example, the dependent factor could be specified as the engine-face corrected flow rate (FWinp) that varies with respect to the freestream Mach number (fsmach). The one-factor and two-factors schedules are intended to work together. In the previous example of the variation of the freestream Mach number, the freestream Mach number would first be established from the one-factor schedule and then that Mach number would be used to establish the corresponding engine-face corrected flow rate from the two-factor schedule. Thus, the two-factor schedule allows specification of dependence of one input factor upon another input factor. The options available for describing the manner of the variation of the dependent variable with respect to the independent factor are a ***stepwise*** or a ***linear variation***. A stepwise variation would hold the value of the dependent factor constant until the value of the independent factor has reached or exceeded the next value of the independent factor listed in the schedule. A linear variation would perform a linear interpolation of the independent factor between two adjacent values within the schedule. The example below will provide another explanation of these variations.

Scheduling is indicated within the input data file through an input data block with DataID = 19. Table 14.2 lists the inputs within the input data block for specifying schedules. The input factor N_{sched} specifies the number of schedules. The input factor K_{sched} indicates the type of schedule and the variation of the schedule. The input N_{ptsch} indicates the number of points used to specify the variation of the schedule. The input F_{1sched} indicates the name of the factor for the one-factor schedule or the name of the independent factor for the two-factor schedule. The input F_{2sched} indicates the name of the dependent factor for the two-factor schedule. The names used for F_{1sched} and F_{2sched} should match exactly the names listed under the "Input" column of the tables describing the input factors presented in the previous sections (e.g., Table 4.8 or Table 7.3). The names should be enclosed with double quotes so SUPIN can read them as character inputs.

Table 14.3 presents an example of an input data block for the scheduling of input factors that includes three schedules (N_{sched} = 3). The remainder of the input data block consists of the listing of each schedule. A blank line is needed preceding each schedule to separate each schedule. The first schedule is a one-factor schedule listing three discrete freestream altitudes (h_0). The choice of freestream altitude assumes that within the input data block for DataID = 1, the input factor K_{fs} = 1 was specified to indicate the freestream thermodynamic factors are evaluated using the atmosphere models which use altitude as the independent factor. The second schedule is a one-factor schedule that varies through a range of freestream Mach numbers (M_0) starting at Mach 0.6 and ending at Mach 1.8 with an increment of Mach 0.2 for a total of seven Mach numbers. The third schedule is a two-factor schedule containing four points that describe the variation of the engine-face corrected flow rate (W_{C2}) with respect to the freestream Mach number (M_0). The input factor FWinp would be interpreted as the engine-face corrected flow rate in units of lbm/s if KWinp = 2 and KWunit = 2 are specified within the input data block for DataID = 0. The input

TABLE 14.2.—INPUTS FOR THE SCHEDULING OF INPUT FACTORS

Factor	Input	Description
N_{sched}	`Nsched`	Number of schedules
K_{sched}	`Ksched`	Type of variation for a schedule = 0 integer step values starting at 1 = 1 one-factor, discrete = 2 one-factor, range (begin, end, increment) = 3 two-factor, step variation = 4 two-factor, linear variation
N_{ptsch}	`Nptsch`	Number of points in a schedule
F_{1sched}	`F1sched`	Name of Factor 1, independent factor
F_{2sched}	`F2sched`	Name of Factor 2 of two-factor schedules, dependent factor

TABLE 14.3.—EXAMPLE INPUT DATA BLOCK FOR THE SCHEDULING OF INPUT FACTORS

```
DataID.  Schedules.
  19
Nsched, Number of schedules
   3

Ksched, Type of schedule
   1
F1sched   Nptsch
“fsalt”     3
F1_val
35000.
40000.
45000.

Ksched, Type of schedule
   2
F1sched   F1_beg    F1_end    F1_inc
“fsmach”    0.6       1.8       0.2

Ksched, Type of schedule
   4
F1sched   F2sched  Nptsch
“fsmach”  “FWinp”     4
F1_val     F2_val
  0.0       400.0
  1.0       400.0
  1.4       386.0
  2.0       360.0
```

factor Ksched = 4 indicates that the list of engine-face corrected flow rates is linearly interpolated. For example, when M_0 = 1.2, the schedule would be interpolated to provide W_{C2} = 393 lbm/s. If Ksched = 3 was specified for a step variation, then W_{C2} = 400 lbm/s would be set until M_0 = 1.4 when the value would step down to W_{C2} = 386 lbm/s until M_0 = 2.0.

In the execution of SUPIN, the list of schedules would be interpreted to create an array of states for the input factors involved in the schedule and the design and analysis process would be performed for each of the states. In the example of Table 14.3, there are three freestream altitudes and seven freestream Mach numbers which would result in 21 states that would need to be processed for each combination of freestream altitudes (h_0) and Mach numbers (M_0). For each value of freestream Mach number, the two-factor schedule would be linearly interpolated to obtain the corresponding engine-face corrected flow rate (W_{C2}) for the state. The values of freestream altitude (h_0), freestream Mach number (M_0), and engine-face corrected flow rate (W_{C2}) of the states would overwrite the other values for these factors listed in the input data blocks for DataID = 0 and 1 of the input data file. Other values of the input factors listed in the input data file would remain fixed during the operation of SUPIN. Some thought is needed to ensure that the range of input factors in the schedules makes sense for the range of inlet design and analysis operations.

The specification of multiple schedules offers the ability to create multi-dimensional arrays of states for the execution of SUPIN. Each state will produce a unique inlet or aerodynamic condition. To output and process the results, the data for each state of the inlet is written within the output data file (SUPIN.Out.txt) in sequential order that the states are created. If surface grids are to be generated, they are written to a series of surface grid files (SUPIN.xyz) with a modifier added to the file to create a sequence of output data files with the grid for each inlet for each state. In the above case with 21 states, SUPIN will write the surface grid file in the form of SUPIN.001.xyz, SUPIN.002.xyz, …, SUPIN.021.xyz. For the input summary table file (SUPIN.Table.txt), the lines of the summary will be repeated for each state with a header separating each state. These files can then be analyzed to obtain data to explore trends in the inlet characteristics with respect to the varied input factors of the schedules.

14.3 Entity Geometric Transformation

The specification of inlet components using entities was introduced in Subsection 4.15 and Appendix A describes the fundamental character each entity and provides the details in specifying the geometry of the entities. This subsection presents a means of applying a geometric transformation to an entity to scale, translate, rotate, and/or mirror the entity to assemble the entity within the global coordinate system of the inlet and fully define a component of the inlet. This can simplify the geometry input process and provide for greater flexibility in specifying the geometry. For example, the entity inputs of Appendix A can specify the control points of a cubic spline curve in a local coordinate system. This was the case of the Gulfstream/NASA inlet described in Subsection 8.6. A geometric transformation can then be applied to scale the entity to the dimensions and units of the inlet and then translate the cubic spline curve to a component, such as the centerbody of the inlet.

It was mentioned in Subsection 4.15 and shown in Table 4.33 and Table 4.34 that each entity is associated with a geometric transformation indicated by the input factor K_{trf}. If an entity is specified with $K_{trf} = 0$, then that entity does not have a geometric transformation associated with it and it is assumed the description of the entity has the proper scale and position for the inlet.

This subsection discusses how to specify geometric transformations within an input data block using a block with DataID = 17. Table 14.4 lists the input factors for specifying a geometric transformation set for an entity. Table 14.5 provides an example input data block with DataID = 17 that specifies the input factors for the geometric transformation. The input data block first involves specifying the number of geometric transformation sets (N_{trf}) be specified. More than one entity can be associated with a specific geometric transformation set. The remainder of the input data block lists the inputs for each geometric transformation set. A blank line is needed between each set of geometric transformation inputs.

Each geometric transformation set includes four lines of which two lines are header lines each followed by a line of numeric inputs. The first header line starts with the "Trf" and specifies an integer that labels the set. It is assumed that the first set specified has Trf = 1, followed by the next set with Trf = 2, and so on. This number is mapped to the value of K_{trf} is specified for the entity. In other words, when specifying an entity, the K_{trf} value indicates which geometric transformation set is to be used for that

TABLE 14.4.—INPUT FACTORS FOR THE GEOMETRIC TRANSFORMATIONS

Factor	Input	Description
N_{trf}	`Ntrf`	Number of sets of transformations
trf	`trf`	Label to identify the set of transformation information
F_{scale}	`Fscale`	Scale factor for the entity geometry coordinates
K_{xmir}	`Kxmir`	Flag for mirroring about x-axis (=0 no, =1 yes)
K_{ymir}	`Kymir`	Flag for mirroring about y-axis (=0 no, =1 yes)
X_{rot}	`Xrot`	Center of rotation (X coordinate) (ft)
Y_{rot}	`Yrot`	Center of rotation (Y coordinate) (ft)
$\Delta\theta_{trf}$	`RotAng`	Angle to rotate entity (deg)
ΔX_{trf}	`dX`	Distance to translate entity in X-coordinate direction (ft)
ΔY_{trf}	`dY`	Distance to translate entity in Y-coordinate direction (ft)

TABLE 14.5.—SAMPLE INPUT BLOCK FOR THE GEOMETRY TRANSFORMATIONS

```
DataID.  Geometry Transformation
 17
Ntrf, Number of Transformation Sets
  2

Trf    Kxmir    Kymir     Fscale    Klink
 1       0        0     1.00000      0
   XRot       YRot      RotAng       dX         dY
  0.00000    0.00000     0.000    0.00000    0.00000

Trf    Kxmir    Kymir     Fscale
 2       0        0     0.02540
   XRot       YRot      RotAng       dX         dY
  0.00000    0.00000     0.000    0.12000    0.00000
```

entity. The values of *trf* should be input and labeled sequentially (e.g. 1, 2, 3…) as SUPIN automatically assumes this regardless of the value of *trf* that is input into the input data block. The values of X_{rot} and Y_{rot} indicate the center of rotation for the rotational transformation angle $\Delta\theta_{trf}$. The sense of the rotation follows the right-hand rule. The values of ΔX_{trf} and ΔY_{trf} indicate the amount of translational transformation of the entity. The value of F_{scale} indicates the amount to scale the specified dimensions. The values of K_{xmir} and K_{ymir} are integer flags that indicate if the entity needs to be mirrored about the *x*- or *y*-axes.

The geometric transformations are applied in the order of rotation, translation, scaling, and then mirroring. The rotation is applied as

$$X_{new} = X_{rot} + (X_{old} - X_{rot})\cos\Delta\theta - (Y_{old} - Y_{rot})\sin\Delta\theta$$
$$Y_{new} = Y_{rot} + (X_{old} - X_{rot})\sin\Delta\theta + (Y_{old} - Y_{rot})\cos\Delta\theta \tag{14-1}$$

The translations are applied as

$$X_{new} = X_{new} + \Delta X_{trf}$$
$$Y_{new} = Y_{new} + \Delta Y_{trf} \tag{14-2}$$

The scaling is applied as

$$X_{new} = F_{scale}\, X_{new}$$
$$Y_{new} = F_{scale}\, Y_{new} \tag{14-3}$$

14.4 Entity Variable Geometry

Within a supersonic inlet, a component may involve parts that translate and rotate at times during the mission of the aircraft. An example is the NASA Mach 2.5 Variable Diameter Centerbody (VDC) mixed-compression inlet (Ref. 1) that is illustrated in Figure 14.1. The forward portion of the centerbody has a set of overlapping leaves that allow that portion to rotate about a hinge located at its upstream end. Likewise, a portion of the centerbody just downstream of the shoulder also has overlapping leaves that all that portion to rotate about a hinge located at its downstream end. A shoulder slot provides a break between the forward set of moving leaves and the aft set of moving leaves. These parts form aft part of the external supersonic diffuser and centerbody of the internal supersonic diffuser and throat section. The effect of the rotation of those parts is to allow the central part of the centerbody about the shoulder to collapse to increase the cross-sectional area of the internal supersonic diffuser and throat section. In

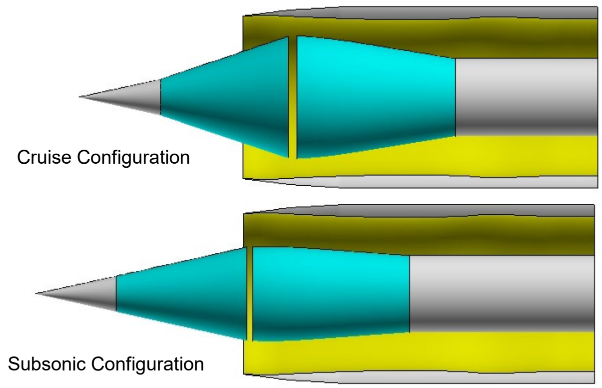

Figure 14.1.—Example of variable geometry for the variable-diameter-centerbody (VDC) inlet.

addition to collapsing the centerbody, the nose section along with the forward and aft centerbody leaves of the VDC can translate forward. Such variable geometry is needed at lower speeds to avoid choking the inlet and for starting or restarting the internal supersonic diffusion during acceleration of the aircraft to cruise conditions or inlet unstart during normal operation. The images of Figure 14.1 illustrate the variable nature of the inlet at cruise and subsonic conditions.

It was mentioned in Subsection 4.15 and shown in Table 4.33 and Table 4.34 that each entity is associated with a variable geometry schedule indicated by the input factor K_{vgm}. A variable geometry schedule dictates how one or more entities rotate or translate in time. If an entity is specified with K_{vgm} = 0, then that entity does not have a variable geometry schedule associated with it and the entity is considered static.

This subsection discusses how to specify variable geometry schedules with an input data block. Table 14.6 lists the input factors for specifying a variable geometry schedule for an entity. Table 14.7 provides an example input data block with DataID = 18 that specifies the input factors for the variable geometry schedules. The input data block first involves specifying the reference time (t_{vgm}) that corresponds to the geometric configuration of the inlet as specified by the input data file. The reference time indicates the time associated with the inlet geometric configuration as described by the various geometry models or entities. The variable geometry schedule then uses this reference time in determining how much the entities have rotated and translated compared to the reference inlet configuration.

The next two lines of the input data file specify the input factor for the number of variable geometry schedules (N_{vgm}). More than one entity can be associated with a specific variable geometry schedule. The remainder of the input data block lists the inputs for each variable geometry schedule. A blank line is needed between each variable geometry schedule.

Each schedule provides information on how the entity rotates and translate with respect to time. The first input factor in a schedule is a label (*isched*) to identify the schedule. This number is mapped to the value of K_{vgm} specified for the entities, as discussed in Subsection 4.15. In other words, when specifying an entity in the input blocks for DataID = 16, the K_{vgm} value indicates which variable geometry schedule is to be applied to that entity. The values of *isched* should be input and labeled sequentially (e.g., 1, 2, 3…) as SUPIN automatically assumes this regardless of the value of *isched* that is input into the data block. The schedule is specified with N_{pvgm} points in time (t_{svgm}) with the values of the rotation ($\Delta\theta_{svgm}$) and translation (ΔX_{vgm}, ΔY_{vgm}) specified at each time point. The time (t_{svgm}) is a real number that has no units, and so can be second or minutes and involve a fraction of the unit of time. It is assumed that the reference time (t_{vgm}) and schedule time (t_{svgm}) have the same units. The value of K_{fvgm} indicates the type of variation of the schedule. The step variation (K_{fvgm} =1) indicates instantaneous change at the corresponding time

TABLE 14.6.—INPUT FACTORS FOR VARIABLE GEOMETRY

Factor	Input	Description
t_{vgm}	`vgmtime`	Time at which to generate the inlet variable geometry
N_{svgm}	`Nsvgm`	Number of variable geometry schedules
isched	`isched`	Label for the variable geometry schedule
K_{fvgm}	`Kfvgm`	Type of variation of translation and rotation = 0 undefined = 1 step = 2 linear
N_{pvgm}	`Npvgm`	Number of points in a variable geometry schedule
X_{rot}	`Xrot`	Center of rotation (X coordinate)
Y_{rot}	`Yrot`	Center of rotation (Y coordinate)
t_{svgm}	`Time`	Time points for a schedule
$\Delta\theta_{svgm}$	`RotAng`	Angle to rotate the entity (deg) for points
ΔX_{svgm}	`dX`	Amount to translate entity in the X-coordinate direction for points
ΔY_{svgm}	`dY`	Amount to translate entity in the Y-coordinate direction for points

TABLE 14.7.—EXAMPLE INPUT DATA BLOCK FOR THE
INPUT FACTORS FOR VARIABLE GEOMETRY

```
DataID.  Variable Geometry Schedules
 18
vgmtime, Time of Geometry Configuration
  0.0
Nsvgm, Number of Variable Geometry Schedules
  2

isched  Npvgm  Kfvgm     Xrot        Yrot
   1      2      2     8.31200     1.84250
 Point   Time       dX          dY         RotAng
   1      0.0      0.0         0.0           0.0
   2      1.0     -4.7         0.0          -6.0

isched  Npvgm  Kfvgm     Xrot        Yrot
   2      2      2    38.51900     3.95520
 Point   Time       dX          dY         RotAng
   1      0.0      0.0         0.0           0.0
   2      1.0     -4.5         0.0          -6.0
```

with the change remaining constant until the next time point. The linear variation (K_{fvgm} =2) indicates a linear interpolation of the translation or rotation between the two bracketed times. The values of X_{rot} and Y_{rot} indicate the center of rotation for the rotational transformation angles $\Delta\theta_{svgm}$ of the schedule. The direction of the rotation follows the right-hand rule.

References

1. Saunders, J. D. and Girvin, R., "VDC Inlet Experimental Results," First NASA/Industry High Speed Research Propulsion/Airframe Integration Workshop, October 1993.

Appendix A.—Geometric Entities

This appendix provides details on the geometric entities used to construct the coordinates, curves, and surfaces for the components that can form the geometry of an inlet. Subsection 4.15 provided an overview of the approach for specifying components and entities and Table 4.32 listed the entities available for use within SUPIN. Table 4.33 listed an example input data block with DataID = 16 that is used to specify the entities within a component. The first set of lines of the input data block after the DataID input lines list the values for the input factors K_{comt}, N_{ents}, and K_{part}, as described in Subsection 4.15. As mentioned, K_{comt} indicated the inlet component as listed in Table 4.31. The N_{ents} is the number of entities listed in the input data block for the component. The input data block lists the entities that are used to construct a single component, such as the external supersonic diffuser (K_{comt} = 1) or cowl interior (K_{comt} = 17).

The remainder of the input data block lists the input factors for each of the N_{ents} entities with a blank line separating each group of input lines for each entity. The input data block can only list the entities associated with the component as indicated by K_{comt}. Further, the list of entities should define entities that connect end-to-end in a mostly upstream to downstream direction. If more than one component needs to be defined for the inlet using the entity specification, multiple instances of input data blocks with DataID = 16 can be used within the input data file (SUPIN.in).

Each group of input lines for an entity start with a header line and data input line that provide the values for the input factors K_{ent}, K_{trf}, K_{vgm}, and N_{cps} for the entity. Each entity is assigned an entity type (K_{ent}), a geometric transformation (K_{trf}), and a variable geometry schedule (K_{vgm}). Table 4.32 listed the possible values of input factor K_{ent} along with the type of entity associated with that input factor. The geometric transformation and variable geometry schedule and the explanation of the input factors K_{trf} and K_{vgm} were discussed in Subsections 4.3 and 4.4, respectively. The N_{cps} is the number of control points that define the entity and Subsection 4.15 discussed how this input factor is used for some of the entities. The subsections below provide details on how N_{cps} is used for each type of entity.

Each entity is defined through the assumption of a local frame of reference or coordinate system and a set of geometric input factors. The geometric input factors for an entity may be coordinates, angles, distances, and other information that describe the entity. The input factors are then used to form a set of control points used to define the entity geometry within SUPIN. Once an entity is constructed in its frame of reference, the geometric transformations and the variable geometry schedules are applied to assemble the entity into the inlet component and overall inlet geometry. The subsections below provide the details for each entity and list the input factors and provide example lines of input used to define the entity within the input data block. The subsections also list the structure of the control points for each entity that is used internally within SUPIN.

A.1 Point (K_{ent} = 0)

This entity defines a point in the (X,Y) plane. This point can be used to help define an adjacent entity. Table A-1 lists the input factors and shows an example of the input lines needed to define the point entity for the component input data block (DataID = 16). There is only one control point possible, and so, the value of N_{cps} is set to $N_{cps} = 1$. Table A-1 also lists the control point structure used within SUPIN.

TABLE A-1.—INPUT FACTORS, EXAMPLE LINES OF INPUT, AND CONTROL POINT STRUCTURE FOR A POINT ENTITY

Factor	Input	Description
X_{pt}	`Xpt`	X-coordinate of the point (ft)
Y_{pt}	`Ypt`	Y-coordinate of the point (ft)

```
Kent Ktrf Kvgm Ncps
  0    0    0    1
   Xpt      Ypt
 0.00000 0.00000
```

CP	X_{CP}	Y_{CP}
1	X_{pt}	Y_{pt}

A.2 Line (K_{ent} = 1)

This entity defines a line in the (X,Y) plane, as shown in Figure A-1. The equations for the line (Ref. 1) include the following forms:

$$X_{beg} = X_{end} - L\cos\theta \qquad Y_{beg} = Y_{end} - L\sin\theta$$
$$X_{end} = X_{beg} + L\cos\theta \qquad Y_{end} = Y_{beg} + L\sin\theta \tag{A-1}$$

The L is the length of the line and θ is the slope of the line (dY/dX). A line in a plane only requires four quantities of the group (X_{beg}, Y_{beg}, X_{end}, Y_{end}, L, θ). The input factor K_{line} indicates which of these quantities is specified. The remaining quantities are computed using one or more of Equation (A-1).
Table A-2 lists the options for K_{line} along with the other input factors for the line. Values of K_{line} = 5 to 8 provide options for the line to be specified as connecting to the previous entity within the component. These options allow the chaining of line entities and possible simplification of the input for a component consisting of a series of lines. The option of K_{line} = 5 creates a line connecting the previous entity and the next entity listed for a component. These options also allow the line geometry to vary if an adjacent entity has variable geometry. Table A-2 also lists an example of the input lines for the line entity for the component input data block (DataID = 16), as well as the control point structure used within SUPIN.

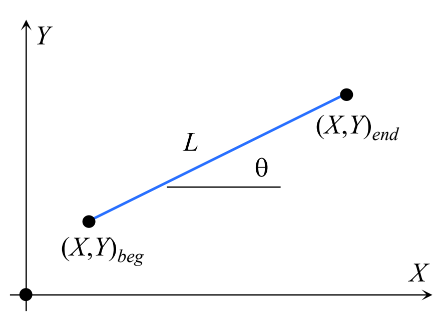

Figure A-1.—Line entity.

TABLE A-2.——INPUT FACTORS, EXAMPLE LINES OF INPUT, AND CONTROL POINT STRUCTURE FOR A LINE ENTITY

Factor	Input	Description
K_{line}	Kline	Flag to indicate the form of inputs defining a line = 1 X_{beg}, Y_{beg}, X_{end}, and Y_{end} = 2 X_{beg}, Y_{beg}, X_{end}, and θ = 3 X_{beg}, Y_{beg}, L, and θ = 4 L, θ, X_{end}, and Y_{end} = 5 Connect previous and next entities = 6 Connect end of previous entity with X_{end} and Y_{end} = 7 Connect end of previous entity with X_{end} and θ = 8 Connect end of previous entity with L and θ
X_{beg}	Xbeg	X-coordinate at the beginning of the line
Y_{beg}	Ybeg	Y-coordinate at the beginning of the line
X_{end}	Xend	X-coordinate at the end of the line
Y_{end}	Yend	Y-coordinate at the end of the line
θ	Thline	Slope of the line (deg)
L	Lline	Length of the line

```
Kent Ktrf Kvgm Ncps
  1    1    3    4
Kline   Xbeg     Ybeg      Xend      Yend    Thline   Lline
  1   0.00000  0.00000  8.31200  1.84250  12.500  8.51376
```

CP	X_{CP}	Y_{CP}
1	K_{line}	-
2	X_{beg}	Y_{beg}
3	X_{end}	Y_{end}
4	θ	L

A.3 Circular Curve (K_{ent} = 2)

This entity defines a circular curve or arc in the (X,Y) plane with its center at $(X,Y) = (0,0)$. Equations (A-2) provide the mathematical representation of the circular curve (Ref. 1). Figure A-2 shows an image of a circular curve. Several options exist for defining the circular curve as indicated by the input factor K_{circ}. Table A-3 lists the available options. The definition of a circular curve needs three input factors to define its radius (r_{circ}), start point (X_{beg}, Y_{beg}, ϕ_{beg}), and angular extent ($\Delta\phi$). Table A-3 also lists an example of the input lines for the circular curve entity for the component input data block (DataID = 16), as well as the control point structure used within SUPIN.

$$X^2 + Y^2 = r^2 \qquad X = r\cos\phi \qquad Y = r\sin\phi \tag{A-2}$$

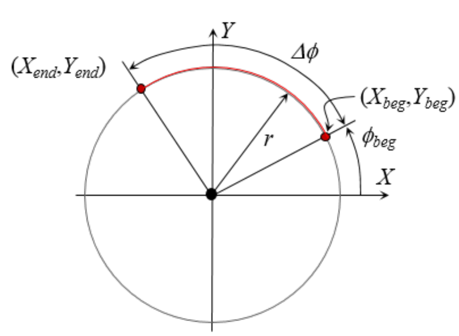

Figure A-2.—Circular curve entity.

TABLE A-3.—INPUT FACTORS, EXAMPLE LINES OF INPUT, AND CONTROL POINT STRUCTURE FOR A CIRCULAR CURVE ENTITY

Factor	Input	Description
K_{circ}	`Kcirc`	Flag to indicate the form of inputs defining a circular curve = 1 r_{circ}, ϕ_{beg}, and $\Delta\phi$ = 2 X_{beg}, Y_{beg}, and θ_{cend} = 3 Y_{beg}, r_{circ}, and θ_{cend}
X_{beg}	`Xbeg`	X-coordinate at the beginning of the circular curve
Y_{beg}	`Ybeg`	Y-coordinate at the beginning of the circular curve
X_{end}	`Xend`	X-coordinate at the end of the circular curve
Y_{end}	`Yend`	Y-coordinate at the end of the circular curve
r_{circ}	`rcirc`	Radius of the circular curve
ϕ_{beg}	`Phibeg`	Angle for start of the circular curve
$\Delta\phi$	`dPhi`	Angular extent for the circular curve
θ_{cend}	`Thcend`	Slope at the end of the circular arc (deg)

```
Kent  Ktrf  Kvgm  Ncps
  2     1     0     5
Kcirc    rcirc  Phibeg   dPhi
  1    1.00000   0.000  80.000
```

```
Kent  Ktrf  Kvgm  Ncps
 2      1     0     5
Kcirc   Xbeg      Ybeg    Thcend
  2   1.00000  0.00000  10.000
```

```
Kent  Ktrf  Kvgm  Ncps
  2     1     0     5
Kcirc   Ybeg     rcirc    Thcend
  3   0.00000  0.00000  10.000
```

CP	X_{CP}	Y_{CP}
1	K_{circ}	-
2	X_{beg}	Y_{beg}
3	X_{end}	Y_{end}
4	r_{circ}	θ_{end}
5	ϕ_{beg}	$\Delta\phi$

A.4 Ogive Curve (K_{ent} = 3)

This entity defines an ogive curve in the (X,Y) plane, as illustrated in Figure A-3. The ogive is a segment of a circular arc with a radius of curvature (r). Uses of the ogive curve include defining a tangent ogive for the nose of a body or the cowl exterior of an inlet. The ogive is defined with the start of the curve at (X_{beg},Y_{beg}) with a slope of $\theta = \theta_{beg}$. The ogive curve ends at a point (X_{end},Y_{end}) with a slope of θ_{end} = 0. The ogive of Figure A-3 as its origin at (X_{beg},Y_{beg}) = (0,0). The length (L) and height (H) of the ogive are illustrated in Figure A-3 and the requirements are that $L > 0$ and $H > 0$. The equations relating the properties of the ogive (Ref. 1) are,

$$L = r \ \sin\theta_{beg} = X_{end} - X_{beg}$$

$$H = r \left(1 - \cos\theta_{beg} \right) = Y_{end} - Y_{beg}$$

$$r = \frac{(L^2 + H^2)}{2\,H} \qquad \text{(A-3)}$$

$$r = H \left(\frac{1 + \sqrt{1 - \sin^2\theta_{beg}}}{\sin^2\theta_{beg}} \right)$$

Table A-4 lists the input factors for the ogive curve entity. The input factor K_{ogive} indicates what data is provided to define the geometry of the ogive. The input factors for the radius (r), length (L), and height (H) of the ogive are specified as values normalized by the reference dimension of the inlet (D_{ref}).
Table A-4 also shows examples of the input lines needed to define the ogive curve entity for each value of K_{ogive}. Table A-4 also lists the control point structure used within SUPIN.

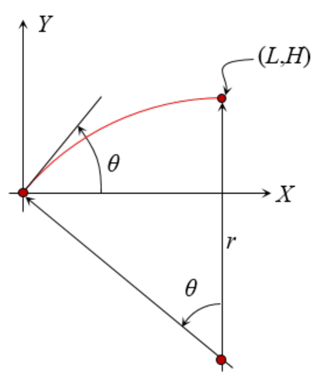

Figure A-3.—Ogive curve entity.

TABLE A-4.—INPUT FACTORS, EXAMPLE LINES OF INPUT, AND CONTROL POINT STRUCTURE FOR AN OGIVE CURVE ENTITY

Factor	Input	Description
K_{ogive}	`Kogive`	Flag indicating form of inputs for the ogive curve = 1 specify X_{beg}, Y_{beg}, L, and H = 2 specify X_{beg}, Y_{beg}, r, and θ_{beg} = 3 specify X_{beg}, Y_{beg}, H, and θ_{beg} = 4 specify X_{beg}, Y_{beg}, L, and θ_{beg} = 5 specify X_{beg}, Y_{beg}, X_{end}, and Y_{end}
θ_{beg}	`Thogive`	Slope of the ogive curve at its beginning (degrees)
r	`Frogive`	Radius of the ogive curve
L	`FLogive`	Length of the ogive curve
H	`FHogive`	Height of the ogive curve

```
Kent  Ktrf  Kvgm  Ncps
  3     1     0     5
Kogive   Xbeg     Ybeg   FLogive  FHogive
   1   1.00000  0.30000  1.50000  0.50000
```

```
Kent  Ktrf  Kvgm  Ncps
  3     1     0     5
Kogive   Xbeg     Ybeg   Frogive  Thogive
   2   1.00000  0.30000  3.00000   15.000
```

```
Kent  Ktrf  Kvgm  Ncps
  3     1     0     5
Kogive   Xbeg     Ybeg   FHogive  Thogive
   3   1.00000  0.30000  0.50000   15.000
```

```
Kent  Ktrf  Kvgm  Ncps
  3     1     0     5
Kogive   Xbeg     Ybeg   FLogive  Thogive
   2   1.00000  0.30000  1.50000   15.000
```

```
Kent  Ktrf  Kvgm  Ncps
  3     1     0     5
Kogive   Xbeg     Ybeg     Xend     Yend
   5   1.00000  1.00000  4.00000  1.30000
```

CP	X_{CP}	Y_{CP}
1	K_{ogive}	-
2	θ_{beg}	r
3	L	H
4	x_{beg}	y_{beg}
5	x_{end}	y_{end}

A.5 Elliptical Curve (K_{ent} = 4)

This entity defines an elliptical curve in the (X,Y) plane. Equation A-4 is the equation for an ellipse (Ref. 1). One use of the elliptical curve is to define a profile for the cowl lip or a spinner. Figure A-4 shows an image of the elliptical curve entity centered at the origin and is defined by the length of the semi-major axis (a) and the length of the semi-minor axis (b). An aspect ratio for the elliptical curve can be defined as $AR = a/b$. The elliptical curve is defined by specifying the start angle ϕ_{beg} and the circumferential extent $\Delta\phi$ of the segment. The direction of the one-dimensional curve parameter for the entity follows the right-hand rule with the normal extending out of the plane. Table A-5 lists the input factors for the elliptical curve entity. Table A-5 also shows an example of the input lines needed to define the elliptical curve entity for the component input data block (DataID = 16), as well as the control point structure used within SUPIN. The second control point imposes that the exponent of Equation (A-4) for an ellipse is $p = 2$. The next subsection will discuss that super-elliptical curve, of which, the ellipse is a special case with $p = 2$.

$$\left(\frac{x}{a}\right)^2 + \left(\frac{y}{b}\right)^2 = 1 \tag{A-4}$$

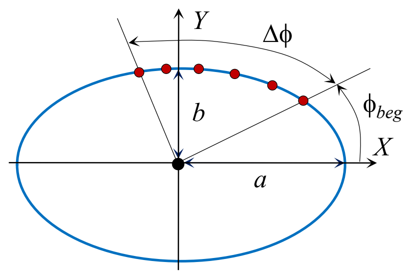

Figure A-4.—Elliptical curve entity.

TABLE A-5.—INPUT FACTORS, EXAMPLE LINES OF INPUT, AND CONTROL POINT STRUCTURE FOR AN ELLIPTICAL CURVE ENTITY

Factor	Input	Description
a	aell	Length of the semi-major axis of the elliptical curve
b	bell	Length of the semi-minor axis of the elliptical curve
ϕ_{beg}	Phibeg	Circumferential angle for start of the elliptical curve
$\Delta\phi$	dPhi	Angular extent for the elliptical curve

```
Kent  Ktrf  Kvgm  Ncps
  4     1     0     3
  aell      bell    Phibeg     dPhi
1.00000  0.50000    0.000    80.000
```

```
Kent  Ktrf  Kvgm  Ncps
  4     0     0     3
 ARclin    bclin    thclin     dPhi
2.00000  0.00500    6.000    84.000
```

```
Kent  Ktrf  Kvgm  Ncps
  4     0     0     3
 ARclex    bclex    thclex     dPhi
2.00000  0.00500   11.000    79.000
```

CP	X_{CP}	Y_{CP}
1	a	b
2	$p = 2$	-
3	ϕ_{beg}	$\Delta\phi$

A.6 Super-Elliptical Curve (K_{ent} = 5)

The super-elliptical curve entity is defined in the local coordinate system (X,Y) by Equation (A-5), where a represents the length of the semi-major axis, b represents the length of the semi-minor axis, and the exponent p is the super-ellipse parameter that influences the shape of the super-ellipse and has the condition that p ≥ 2. Values of p less than 2 are not useful since the curves start to develop "points" where they cross the axes. Reference 2 provides a good reference of super-ellipses as applied to inlet geometries.

$$\left(\frac{x}{a}\right)^p + \left(\frac{y}{b}\right)^p = 1 \qquad \text{(A-5)}$$

The three parameters required to define a super ellipse have immediate geometric significance and are therefore intuitive to the user. When p is equal to 2, the shape is an ellipse. When also $a = b$, the shape is a circle. As the value of p increases, the shape approaches that of a rectangle with $w = a$ and $h = b$. Figure A-5 shows a quadrant of the super-ellipse for various values of the parameter p. The squaring of the corner of the super-ellipse becomes apparent quickly as the value of p increases with a close approximation of a rectangle with $p = 100$.

The area of the super-ellipse is,

$$A = \frac{\left[\Gamma\left(1 + \frac{1}{p}\right)\right]^2}{\Gamma\left(1 + \frac{2}{p}\right)}(4ab) \qquad \text{(A-6)}$$

where Γ is the gamma function, defined as

$$\Gamma(z) = \int_0^\infty t^{z-1} e^{-t} dt \qquad \text{(A-7)}$$

The slope (dy/dx) along a super-elliptical curve entity is established as

$$y = b\left\{1 - \left(\frac{x}{a}\right)^p\right\}^{1/p} \qquad \text{(A-8)}$$

$$\frac{dy}{dx} = -\frac{b}{a}\left(\frac{x}{a}\right)^{(p-1)}\left\{1 - \left(\frac{x}{a}\right)^p\right\}^{\left(\frac{1-p}{p}\right)} \qquad \text{(A-9)}$$

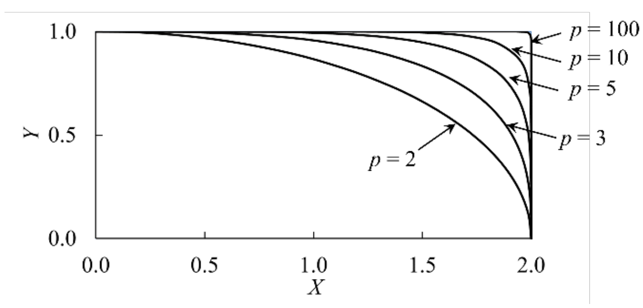

Figure A-5.—Super-elliptical curve entity with variation in the parameter p.

Table A-6 lists the input factors for the super-elliptical curve entity. Table A-6 also shows an example of the input lines needed to define the super-elliptical curve entity for the component input data block (DataID = 16), as well as the control point structure used within SUPIN.

TABLE A-6.—INPUT FACTORS, EXAMPLE LINES OF INPUT, AND CONTROL POINT STRUCTURE FOR A SUPER-ELLIPTICAL CURVE ENTITY

Factor	Input	Description
a	`aell`	Length of the semi-major axis of the super-elliptical curve
b	`bell`	Length of the semi-minor axis of the super-elliptical curve
p	`pell`	Super-ellipse parameter
ϕ_{beg}	`Phibeg`	Circumferential angle for start of the super-elliptical curve
$\Delta\phi$	`dPhi`	Angular extent for the super-elliptical curve

```
Kent  Ktrf  Kvgm  Ncps
  5     1     0     3
   aell     bell    pell  Phibeg   dPhi
 1.00000  0.80000  4.000   0.000  90.000
```

CP	X_{CP}	Y_{CP}
1	a	b
2	p	-
3	ϕ_{beg}	$\Delta\phi$

A.7 NACA 1-Series Curve (K_{ent} = 6)

The NACA 1-Series curve entity defines a curve based on the NACA 1-Series airfoil (Refs. 3 to 5). This curve has traditionally been used for low-drag, subsonic cowl exterior shapes. The shape of the curve is defined by a radius for the leading edge and a set of scaled coordinates downstream of the leading edge, which are listed in Table A-7. The axial coordinate is scaled by the axial length (L_1) of the curve and the transverse coordinate scaled by the height (Y_1) of the curve. The curve is defined as an axisymmetric curve for which the maximum radial dimension from the axis-of-symmetry is D_{max}, which traditionally was the maximum diameter of a cowl exterior. The form of the NACA 1-Series airfoil is NACA-1-N_d-N_{L1}. Where N_d is a two-digit integer for the ratio of the inner diameter of the cowl and D_{max} expressed as a percentage,

$$N_d = \left(\frac{d}{D_{max}}\right) \text{x } 100\% \text{ or } \left(\frac{D_{clip}}{D_{max}}\right) \text{x } 100\% \tag{A-10}$$

The N_{L1} is an integer for the ratio of the length of the curve and D_{max} expressed as a percentage,

$$N_{L1} = \left(\frac{L_1}{D_{max}}\right) \text{x } 100\% \tag{A-11}$$

With specification or knowledge of N_d, N_{L1}, and D_{max}, Equations (A-10) and (A-11) can be solved for d and L_1, respectively.

The Y_1 dimension is the height of the curve from the local X-axis, which passes through the origin of the circle defining the leading edge of the airfoil. For a cowl exterior, this is intended to be coincident with the cowl lip point, y_{clip}. The height Y_1 is computed as

$$Y_1 = \left(\frac{D_{max} - d}{2}\right) - r \tag{A-12}$$

Where r is the radius of the circle defining the leading edge and is defined here as

$$r = C_1\, Y_1 \tag{A-13}$$

A value of C_1 = 0.025 is the default within SUPIN. By substituting Equation (A-13) into Equation (A-12), the value of Y_1 can be calculated. The coordinates of the curve can then be found by using the scaled coordinates of Table A-7. The circular leading edge is blended into the remaining curve coordinates. Figure A-6 shows an example of a NACA 1-Series curve designated as NACA 1-85-100 with D_{max} = 1.0 and C_1 = 0.025. Table A-8 lists the input factors for the NACA 1-Series curve entity. Table A-8 also shows an example of the input lines needed to define the NACA 1-Series curve entity for the component input data block (DataID = 16), as well as the control point structure used within SUPIN.

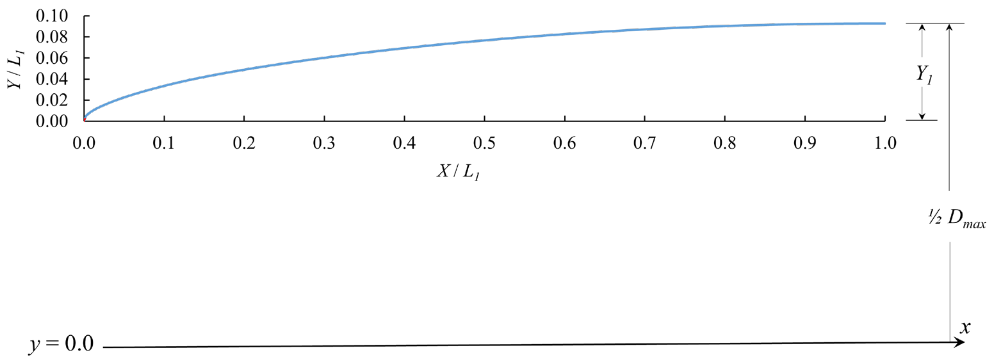

Figure A-6.—NACA 1-85-100 curve entity with D_{max} = 1.0 and C_1 = 0.025.

TABLE A-7.—SCALED COORDINATES OF THE NACA 1-SERIES CURVE

X/L_1	Y/Y_1	X/L_1	Y/Y_1	X/L_1	Y/Y_1	X/L_1	Y/Y_1
0.000	0.0000	0.130	0.4194	0.340	0.6908	0.600	0.8911
0.002	0.0480	0.140	0.4366	0.350	0.7008	0.620	0.9020
0.004	0.0663	0.150	0.4530	0.360	0.7105	0.640	0.9123
0.006	0.0812	0.160	0.4688	0.370	0.7200	0.660	0.9220
0.008	0.0933	0.170	0.4840	0.380	0.7294	0.680	0.9311
0.010	0.1038	0.180	0.4988	0.390	0.7385	0.700	0.9395
0.015	0.1272	0.190	0.5131	0.400	0.7475	0.720	0.9475
0.020	0.1472	0.200	0.5270	0.410	0.7563	0.740	0.9548
0.025	0.1657	0.210	0.5405	0.420	0.7648	0.760	0.9616
0.030	0.1831	0.220	0.5537	0.430	0.7732	0.780	0.9679
0.035	0.1994	0.230	0.5666	0.440	0.7815	0.800	0.9735
0.040	0.2148	0.240	0.5792	0.450	0.7895	0.820	0.9787
0.045	0.2296	0.250	0.5915	0.460	0.7974	0.840	0.9833
0.050	0.2436	0.260	0.6035	0.470	0.8050	0.860	0.9874
0.060	0.2701	0.270	0.6152	0.480	0.8125	0.880	0.9909
0.070	0.2947	0.280	0.6267	0.490	0.8199	0.900	0.9940
0.080	0.3181	0.290	0.6379	0.500	0.8269	0.920	0.9965
0.090	0.3403	0.300	0.6489	0.520	0.8410	0.940	0.9985
0.100	0.3613	0.310	0.6597	0.540	0.8545	0.960	0.9993
0.110	0.3815	0.320	0.6703	0.560	0.8673	0.980	0.9998
0.120	0.4009	0.330	0.6807	0.580	0.8795	1.000	1.0000

TABLE A-8.—INPUT FACTORS, EXAMPLE LINES OF INPUT, AND CONTROL POINT STRUCTURE FOR THE NACA 1-SERIES CURVE ENTITY

Factor	Input	Description
K_{NACA}	`Knaca`	Flag indicating form of inputs for the NACA 1 airfoil profile = 1 use $(x,y)_{cwex}$ to compute N_d, N_{L1} and other properties = 2 use N_d, N_{L1}, and L_1 to compute properties = 3 use N_d, N_{L1}, and D_{max} to compute properties
C_1	`FCnaca`	Coefficient C_1 for cowl lip radius for NACA 1-Series curve (0.025)
N_d	`FNdnaca`	Ratio for inner diameter (d) (%)
N_{L1}	`FNLnaca`	Ratio for length of the NACA 1-Series curve (%)
L_1	`FLnaca`	Axial length for NACA 1-Series curve
D_{max}	`FDnaca`	Axial length for NACA 1-Series curve

```
Kent  Ktrf  Kvgm  Ncps
  6     0     0     3
Knaca  FCnaca  FNdnaca  FNLnaca  FLnaca  FDnaca
  1     0.025    85.0    100.0    1.000   1.000
```

CP	X_{CP}	Y_{CP}
1	K_{NACA}	C_1
2	N_d	N_{L1}
3	L_1	D_{max}

A.8 Polynomial Curve (K_{ent} = 7)

The polynomial curve entity defines a polynomial curve in the (X,Y) plane and has the form of

$$Y = \sum a^n X^n \tag{A-14}$$

The a^n are the coefficients and n are the exponents which vary from $0 \le n \le N$. The N is the order of the polynomial that is specified in place of the N_{cps} input factor described in Table 4.34. The polynomial extends from X_{beg} to X_{end} where X is monotonically increasing. Table A-9 lists the input factors for the polynomial curve entity. Table A-9 also shows an example of the input lines needed to define the polynomial curve entity for the component input data block (DataID = 16), as well as the control point structure used within SUPIN.

TABLE A-9.—INPUT FACTORS, EXAMPLE LINES OF INPUT, AND CONTROL POINT STRUCTURE FOR A POLYNOMIAL CURVE ENTITY

Factor	Input	Description
N	`Order`	Order for the polynomial
a_n	`Coef`	Coefficients for the polynomial, n = 0 to N
X_{beg}	`Xbeg`	X-coordinate at the beginning of the polynomial curve
X_{end}	`Xend`	X-coordinate at the end of the polynomial curve

```
Kent  Ktrf  Kvgm  Order
  7     0     0     3
   Xbeg      Xend
 2.87348  3.43532
Coefficients (Order+1)
  -0.117560
  -0.068680
   0.244820
  -0.045080
```

CP	X_{CP}	Y_{CP}
1	X_{beg}	X_{end}
2	a^0	-
3	a^1	-
:	:	-
N+2	a^N	-

A.9 Piecewise Linear Curve (K_{ent} = 8)

The piecewise linear curve entity constructs a curve consisting of linear segments connecting each of the specified set of control points (X_{CP},Y_{CP}) where N_{cps} is the number of control points. Figure A-7 shows a plot of a piecewise linear curve entity. Table A-10 lists the input factors for the polynomial curve entity. Table A-10 also shows an example of the input lines needed to define the polynomial curve entity for the component input data block (DataID = 16), as well as the control point structure used within SUPIN.

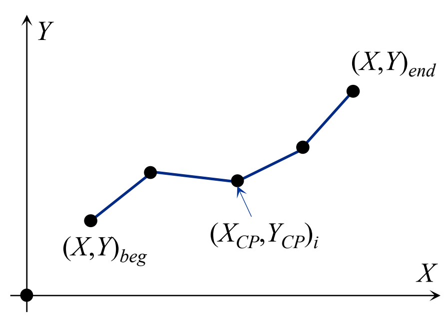

Figure A-7.—Piecewise linear curve entity.

TABLE A-10.—INPUT FACTORS, EXAMPLE LINES OF INPUT, AND CONTROL POINT STRUCTURE FOR A PIECEWISE LINEAR ENTITY

Factor	Input	Description
N_{cps}	`Ncps`	Number of points on the curve
X_{cp}	`Xcp`	X-coordinate of the point on the curve
Y_{cp}	`Ycp`	Y-coordinate of the point on the curve

```
Kent  Ktrf  Kvgm  Ncps
  8     1     0     4
   Xcp       Ycp
 0.00000  1.00000
 1.00000  1.45000
 2.25000  1.83500
 4.50000  2.31750
```

CP	X_{CP}	Y_{CP}
1	X_1	Y_1
2	X_2	Y_2
3	X_3	Y_3
:	:	:
N_{cps}	X_{Ncps}	Y_{Ncps}

A.10 Fitted Cubic Spline Curve (K_{ent} = 9)

The fitted cubic spline curve passes through a set of control points using a cubic spline. Figure A-8 shows a plot of a cubic spline curve through a set of N_{cps} control points (X_{CP},Y_{CP}). The form of the input factors and the lines for the example input data block are the same as for Table A-10 shown above. However, for the fitted cubic spline curve, K_{ent} = 9. The control point structure is also the same as shown in Table A-10.

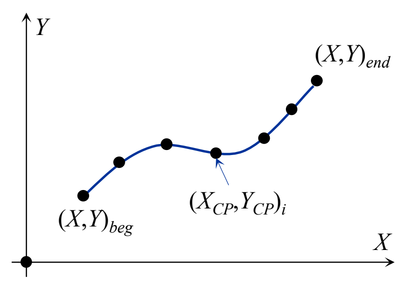

Figure A-8.—Fitted cubic spline curve entity.

A.11 Non-Uniform Rational B-Spline (NURBS) Curve (K_{ent} = 10)

The non-uniform rational B-spline (NURBS) curve entity creates a smooth curve based on a set of control points. Reference 6 provides a detailed discussion of NURBS curves. A B-spline curve, **C**(u), of pth-degree is defined according to Equation (A-15),

$$\mathbf{C}(u) = \sum_{i=0}^{n} N_{i,p}(u)\, \mathrm{P}_i \tag{A-15}$$

where P_i are the control points and $N_{i,p}(u)$ are the pth degree B-spline basis functions defined on the nonperiodic and nonuniform knot vector, U, composed of (m + 1) knots:

$$U = \left\{ \underbrace{a, \ldots, a}_{p+1}, u_{p+1}, \ldots, u_{m-p-1}, \underbrace{b, \ldots, b}_{p+1} \right\} \tag{A-16}$$

The B-spline basis is non-global, as opposed to the Bernstein basis used to produce Bézier curves. This yields an advantageous property of B-spline curves called local support, which states that each $f_i(u)$ is nonzero on a limited number of subintervals; therefore, moving one of the control points, $\mathbf{P}_i$, does not affect the entire curve, but rather only the subinterval where $f_i(u)$ is nonzero. This property results in the intuitive nature of B-spline curves, in that, particular sections of the curve can be manipulated by simply moving the corresponding control point.

Beyond their intuitive nature, a second advantage of B-spline curves is that they can be evaluated in a numerically stable way through De Boor's algorithm, a recursive definition of the basis functions that is well-suited for computational implementation, as illustrated below in Equation (A-17).

$$N_{i,0}(u) = \begin{cases} 1, \text{if } u_i \leq u \ \leq u_{i+1} \\ 0, \text{otherwise} \end{cases}$$

$$N_{i,p}(u) = \frac{u - u_i}{u_{i+p} - u_i} N_{i,p-1}(u) + \frac{u_{i+p+1} - u}{u_{i+p+1} - u_{i+1}} N_{i+1,p-1}(u) \tag{A-17}$$

Figure A-9 shows a plot of a NURBS curve controlled by four control points. The two control points at each end control the angle of the curve at the endpoints. The curve does not go through points 2 and 3 but are influenced by them.

The form of the input factors and the lines for the example input data block are the same as for Table A-10 shown above for the piecewise linear curve. However, now K_{ent} = 10. The control point structure is also the same as shown in Table A-10.

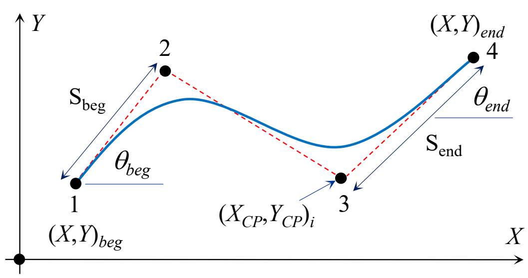

Figure A-9.—NURBS curve entity.

A.12 Four-Point NURBS Curve (K_{ent} = 11)

The four-point NURBS curve is a NURBS curve with only four control points, as depicted in Figure A-9. It is used to create a smoothly varying curve using only information specified at the endpoints. The factors are listed in Table A-11. The factors include the planar coordinates and the tangency conditions at the endpoints. The coordinates of the two interior control points are established based on the flags K_{XY}, K_{Angle}, and K_S and perhaps on the input factor θ and S. Figure A-9 shows how the second control point is positioned based on the values of S_{beg} and θ_{beg} and the third control point is positioned based on the values of S_{end} and θ_{end}. The flag K_{XY} indicates how the coordinates of the respective endpoint are established. The coordinates can be directly specified, or it can be specified that the endpoint connect to the adjacent entity listed for the component. The four-point NURBS curve is useful to connect an entity that has variable geometry. So, by specifying the endpoint to connect to the adjacent entity, the four-point NURBS entity will continue to connect to the adjacent entity as the adjacent entity moves. The flag K_{Angle} indicates the tangency condition for the endpoint. For $K_{Angle} = 1$, the angles are directly specified in by the input factors. For $K_{Angle} = 2$, the angles are set equal to the straight line between the two endpoints. For $K_{Angle} = 3$ to 6, the angles are established with respect to the tangency condition of the adjacent entities in the respective manner as specified by K_{Angle}. The flag K_S indicates the way the spacing of the two interior control points with respect to the endpoints is determined. These inputs allow the shape of NURBS curve to be adjusted. Table A-11 also shows an example of the input lines needed to define the four-point NURBS curve entity for the component input data block (DataID = 16), as well as the control point structure used within SUPIN.

TABLE A-11.—INPUT FACTORS, EXAMPLE LINES OF INPUT, AND CONTROL POINT STRUCTURE FOR THE FOUR-POINT NURBS ENTITY

Factor	Input	Description
X	`X`	X-coordinate of beginning or end of the curve
Y	`Y`	Y-coordinate of beginning or end of the curve
θ	`Angle`	Planar slope angle at the beginning or end of the curve
S	`S`	Distance from an endpoint to the adjacent interior control point
K_{XY}	`Kxy`	Flag for the specifying (X,Y) coordinates of an endpoint = 1 specify (X,Y) = 2 attach to adjacent entity
K_{Angle}	`Kang`	Flag for the specifying the planar slope angle of the curve at an endpoint = 1 specify the angle = 2 angle is set by the line between the endpoints = 3 tangent to the adjacent entity = 4 opposite to the tangent of the adjacent entity = 5 normal to the adjacent entity = 6 opposite to the normal of the adjacent entity
K_S	`KS`	Flag for the specifying the distance to the interior control point =1 specify the distance =2 set distance to 1/3 of the distance between the endpoints =3 specify a fraction of the distance between the endpoints

```
Kent  Ktrf  Kvgm  Ncps
 11     1     0     7
Kxy    X         Y     Kangle  Angle  KS    S
 2  20.00000  6.50000    1   30.000   3  0.20000
 2  22.50000  6.65000    1    0.000   3  0.40000
```

CP	X_{CP}	Y_{CP}
1	X_{beg}	Y_{beg}
2	X_{end}	Y_{end}
3	K_{XYbeg}	K_{XYend}
4	K_{Angle_beg}	K_{Angle_end}
5	θ_{beg}	θ_{end}
6	K_{Sbeg}	K_{Send}
7	S_{beg}	S_{end}

A.13 Fitted NURBS Curve (K_{ent} = 12)

The fitted NURBS curve entity fits a curve through the coordinates for the control points. The form of the input factors and the lines for the example input data block are the same as for Table A-10 shown above. However, for the fitted NURBS curve, $K_{ent} = 12$. The control point structure is also the same as shown in Table A-10.

A.14 Cosine-Sine Curve (K_{ent} = 13)

The cosine/sine curve entity generates a curve of a combination of the cosine and sine functions over an interval from X_{beg} to X_{end} of the form,

$$Y = A_C \cos \varphi_{pC} + A_S \sin \varphi_{pS} \quad \text{where} \quad \varphi_p = 2\pi \left(\frac{X}{X_p} \right) \tag{A-18}$$

The A_C and A_S are the amplitudes of the cosine and sine components, whereas the X_{pC} and X_{pS} are the periods of the cosine and sine variations, respectively. Table A-12 lists the input factors for the cosine-sine curve entity. Table A-12 also shows an example of the input lines needed to define the cosine-sine curve entity for the component input data block (DataID = 16), as well as the control point structure used within SUPIN.

TABLE A-12.—INPUT FACTORS, EXAMPLE LINES OF INPUT, AND CONTROL POINT STRUCTURE FOR THE COSINE-SINE CURVE ENTITY

Factor	Input	Description
X_{beg}	`Xbeg`	*X*-coordinate at the beginning of the curve
X_{end}	`Xend`	*X*-coordinate at the end of the curve
A_C	`AmpC`	Amplitude of the cosine wave term
A_S	`AmpS`	Amplitude of the sine wave term
X_{PC}	`PerC`	Period with respect to X for the cosine wave term
X_{PS}	`PerS`	Period with respect to X for the sine wave term

```
Kent  Ktrf  Kvgm  Ncps
 13     1     0     3
    Xbeg       Xend      AmpC     AmpS     PerC     PerS
 10.00000  22.00000  2.0000  2.0000  0.5000  0.5000
```

CP	X_{CP}	Y_{CP}
1	X_{beg}	X_{end}
2	A_C	X_{PC}
3	A_S	X_{PS}

A.15 Cosine-Sine-Squared Curve (K_{ent} = 14)

The cosine-sine-squared curve entity provides a variation from $(X,Y)_{beg}$ to $(X,Y)_{end}$ using cosine and sine functions of the form

$$Y = Y_{beg} \cos^2 \varphi + Y_{end} \sin^2 \varphi$$

$$\varphi = \left(\frac{X - X_{beg}}{X_{end} - X_{beg}} \right) \frac{\pi}{2} \tag{A-19}$$

Figure A-10 shows the variation of a cosine / sine squared entity from (0,0) to (0,1). This variation can be used to provide a smooth variation of a property. Table A-13 lists the input factors for the cosine-sine-squared curve entity. Table A-13 also shows an example of the input lines needed to define the cosine-sine-squared curve entity for the component input data block (DataID = 16), as well as the control point structure used within SUPIN.

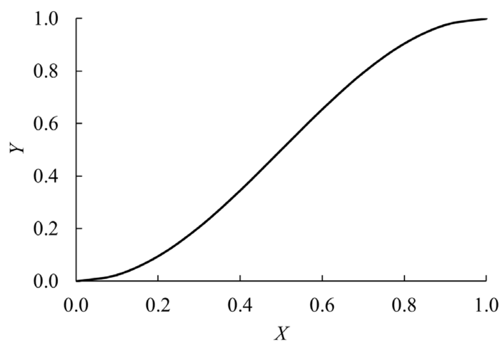

Figure A-10.—Cosine-sine-squared curve entity.

TABLE A-13.—INPUT FACTORS, EXAMPLE LINES OF INPUT, AND CONTROL POINT STRUCTURE FOR THE COSINE-SINE-SQUARED CURVE ENTITY

Factor	Input	Description
X_{beg}	`Xbeg`	X-coordinate at the beginning of the curve
Y_{beg}	`Ybeg`	Y-coordinate at the beginning of the curve
X_{end}	`Xend`	X-coordinate at the end of the curve
Y_{end}	`Yend`	Y-coordinate at the end of the curve

```
Kent  Ktrf  Kvgm  Ncps
 14     0     0     2
   Xbeg     Yend     Xend     Yend
 0.00000  1.00000  1.00000  1.00000
```

CP	X_{CP}	Y_{CP}
1	X_{beg}	Y_{beg}
2	X_{end}	Y_{end}

A.16 Annular Cross-Section (K_{ent} = 15)

The annular cross-section entity is defined by an inner radius (r_i), outer radius (r_o), angle of the beginning of the circumferential extent (ϕ_{beg}), and the amount of the circumferential extent ($\Delta\phi$). Figure A-11 shows the planar geometry of the annular cross-section entity. An annular cross-section entity with full circumferential extent has $\Delta\phi$ = 360 degrees. The annular cross-section entity is constructed from two circular arcs and two lines if the circumferential extent is less than 360 degrees. The direction of the one-dimensional curve parameter for the circular arc entities follows the right-hand rule with the normal extending out of the plane. The direction of the one-dimensional curve parameter for the lines is from the inner radius to the outer radius. The annular cross-section entity defines a closed curve enclosing an area, which is defined by Equation (A-20). Table A-14 lists the input factors for the annular cross-section entity. Table A-14 also shows an example of the input lines needed to define the annular cross-section entity for the component input data block (DataID = 16), as well as the control point structure used within SUPIN.

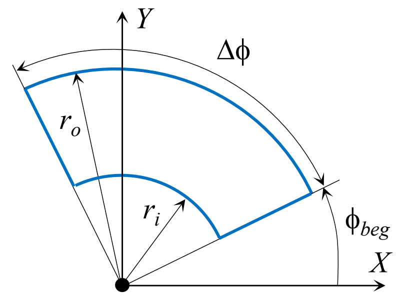

Figure A-11.—Annular cross-section entity.

$$A = \left(\frac{\Delta\phi}{2}\right)\left(r_o^2 - r_i^2\right) \tag{A-20}$$

TABLE A-14.—INPUT FACTORS, EXAMPLE LINES OF INPUT, AND CONTROL POINT STRUCTURE FOR THE ANNULAR CROSS-SECTION ENTITY

Factor	Input	Description
r_i	`Frinn`	Radius for inner circle
r_o	`Frout`	Radius for outer circle
ϕ_{beg}	`Phibeg`	Circumferential angle for start of the annular cross-section
$\Delta\phi$	`dPhi`	Angular extent of the annular cross-section

```
Kent  Ktrf  Kvgm  Ncps
 15     1     0     2
   Frinn    Frout   Phibeg    dPhi
 0.50000  1.00000   0.000  180.000
```

CP	X_{CP}	Y_{CP}
1	r_i	r_o
2	ϕ_{beg}	$\Delta\phi$

A.17 Super-Elliptical/Rectangular Cross-Section (K_{ent} = 16)

This entity creates a cross-section that can use both rectangular and super-elliptical shapes to define separate curves for the top and bottom of the cross-section. The cross-section is planar and centered at the origin of the local coordinate system (X,Y). The cross-section is also symmetric about a vertical line through the origin. The top and bottom planar curves connect at a horizontal line through the center point. The width of the cross section is specified by the input factor A_{widCS}. The heights of the top and bottom of the cross-sections at the center point are specified by the input factors B_{topCS} and B_{botCS}, which are ratios of the heights normalized by the width of the cross-section. The input factors p_{topCS} and p_{botCS} specify the super-ellipse parameter for the top and bottom, respectively. A negative value of p_{topCS} or p_{botCS} indicates that the respective curve is a rectangle rather than a super-ellipse. Table A-15 lists the input factors for the super-elliptical/rectangular cross-section entity. Table A-15 also shows an example of the input lines needed to define the super-elliptical/rectangular cross-section entity for the component input data block (DataID = 16), as well as the control point structure used within SUPIN.

TABLE A-15.—INPUT FACTORS, EXAMPLE LINES OF INPUT, AND CONTROL POINT STRUCTURE FOR THE SUPER-ELLIPTICAL/RECTANGULAR CROSS-SECTION ENTITY

Factor	Input	Description
A_{widCS}	AwidCS	Width for cross-section (ft)
B_{topCS}	BtopCS	Ratio of minor to major axis lengths for center of top of the cross-section
B_{botCS}	BbotCS	Ratio of minor to major axis lengths for center of bottom of the cross-section
p_{topCS}	ptopCS	Super-ellipse parameter for top ($p_{topCS} < 0$, then rectangular)
p_{botCS}	pbotCS	Super-ellipse parameter for bottom ($p_{botCS} < 0$, then rectangular)

```
Kent  Ktrf  Kvgm  Ncps
 16     1     0     3
  AwidCS   BtopCS   ptopCS   BbotCS   pbotCS
 2.00000   1.0000    2.000   0.5000    4.000
```

CP	X_{CP}	Y_{CP}
1	A_{widCS}	-
2	B_{topCS}	p_{topCS}
3	B_{botCS}	p_{botCS}

A.18 NURBS Curve Cross-Section (K_{ent} = 17)

This entity creates a planar cross-section that is defined by a NURBS curve specified by a list of N_{cps} control points in the local coordinate system (X,Y). The input factor of $K_{symCS} = 1$ is a flag indicating that the NURBS curve is symmetric with respect to the Y-axis. The default value is $K_{symCS} = 0$. A coordinate transformation specified by K_{trf} can be used to orient the cross-section within the global coordinate system. This cross-section can be used to create a series of cross-sectional shapes along the length of an inlet to define the interior ducting of the inlet or the cowl exterior. This entity could also be used to create a body or fuselage shape. A series of cross-sections would require a series of instances of this entity within the component structure. Table A-16 lists the input factors for the NURBS curve cross-section entity. Table A-16 also shows an example of the input lines needed to define the NURBS curve cross-section entity for the component input data block (DataID = 16), as well as the control point structure used within SUPIN.

TABLE A-16.—INPUT FACTORS, EXAMPLE LINES OF INPUT, AND CONTROL POINT STRUCTURE FOR THE NURBS CURVE CROSS-SECTION ENTITY

Factor	Input	Description
K_{symCS}	KsymCS	Flag indicating if the curve is symmetric wrt the *Y*-axis (=0 no, =1 yes)
X_{cpCS}	XcpCS	*X*-coordinate of control point
Y_{cpCS}	YcpCS	*Y*-coordinate of control point

```
Kent  Ktrf  Kvgm  Ncps
 17     1     0     7
 KsymCS
    1
     XcpCS       YcpCS
   0.00000  -1.50000
  -0.60000  -1.50000
  -0.80000  -0.40000
  -1.00000   0.00000
  -0.80000   0.40000
  -0.60000   1.00000
   0.00000   1.00000
```

CP	X_{CP}	Y_{CP}
1	K_{symCS}	-
2	X_1	Y_1
3	X_2	Y_2
4	X_3	Y_3
:	:	:
$N_{cps}+1$	X_{Ncps}	Y_{Ncps}

References

1. Beyer, W. H., CRC Standard Mathematical Tables, 27th Edition, CRC Press, Boca Raton, Florida, 1981.
2. Koncsek, J. L., “An Approach to Conformal Inlet Diffuser Design for Integrated Propulsion Systems,” AIAA Paper 1981-1395, July 1981.
3. Baals, D. D., Smith N. F., and Wright, J. B., “The Development and Application of High-Critical-Speed Nose Inlets,” NACA Report 920, January 1948.
4. Nichols, M. R. and Keith Jr., A. L., “Investigation of a Systematic Group of NASA 1-Series Cowlings with and without Spinners,” NACA Report 950, January 1949.
5. Re, R. J. and Abeyounis, W. K., “A Wind Tunnel Investigation of Three NASA 1-Series Inlets at Mach Numbers Up to 0.92,” NASA TM 110300, November 1996.
6. Piegl, L. and Tiller, W., *The NURBS Book*. Berlin: Springer-Verlag, 1997.

Appendix B.—Method of Characteristics for Planar Compressible Flow

This appendix discusses the method of characteristics (MOC) solution for steady inviscid adiabatic supersonic flow as applied to design and analyze of the external and internal supersonic diffusers of inlets. Reference 1 presented early MOC applications. References 2 and 3 discuss details on the MOC theory and application. References 4 and 5 discuss computer programs using the MOC approach for inlet design and analysis. The MOC methods available within SUPIN are based on the methods of Reference 5.

The quasi-linear, partial differential equations that govern steady inviscid adiabatic supersonic flow are hyperbolic equations. The quasi-linear nature indicates that the dependent variables can be non-linear, but that their first partial derivatives are linear within the equations. For hyperbolic equations, the flow properties at a point are only dependent on a small region of flow upstream of the point. This small region is known as the “domain of dependence”. The flow properties at a point are independent of the downstream flow conditions; however, the flow conditions at the point have a downstream “region of influence”. As it will be shown below, the upstream domain of dependence and the downstream range of influence are bounded by the characteristic curves passing through the point. The streamwise nature of the flow dependency leads to the use of space-marching methods for the solution of the flowfield. The method discussed here is the method of characteristics applied on a planar (x,y) domain which can be two-dimensional or axisymmetric. For an axisymmetric domain, the x-axis is assumed to be aligned with the axis-of-symmetry and the radial coordinate is denoted by y.

B.1 Characteristic Curves and Equations

Figure B-1 shows a point A in a flowfield on a plane (x,y) in which the Mach number at the point is supersonic ($M > 1$) with a local flow angle of θ. The streamline is shown through point A and curves as it extends downstream of point A in response to the local state of the flow at points along the streamline. Figure B-1 indicates two characteristic curves that pass through point A. The characteristic curves change slope if the flow conditions change as they pass through the flowfield.

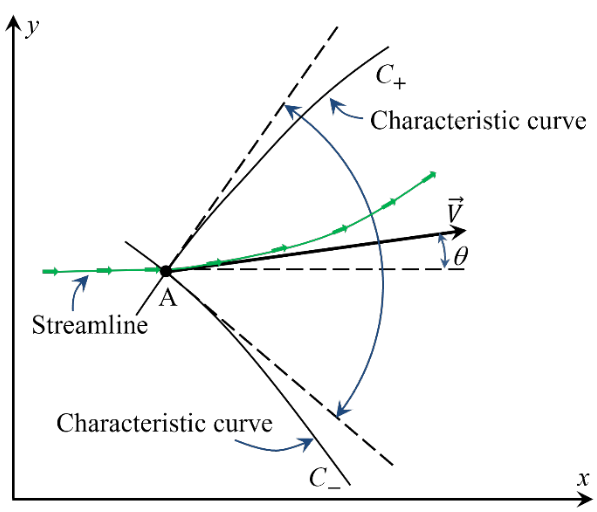

Figure B-1.—The streamline and characteristic curves associated with a point A in a supersonic flowfield.

In Figure B-1, the C_+ characteristic curve is also known as the left-running characteristic curve because from the viewpoint of an observer traveling in the direction of the streamline, the C_+ characteristic curve appears to go off to the left from point A. Likewise, the C_- characteristic curve is also known as the right-running characteristic curve because it appears to go off to the right of the observer at point A. The slope of a characteristic curve as a point is aligned with the slope of the Mach wave at that point. Thus, at point A, the magnitude of the slopes of these characteristic curves relative to the streamline is the Mach angle, $\mu = \pm\sin^{-1}(1/M)$. Thus, the C_+ characteristic curve has the slope $(\theta+\mu)$ in the planar frame of reference while the C_- characteristic curve has the slope $(\theta-\mu)$.

The derivation of the characteristic equations describing the path of the characteristic curves through the flow field can be found is the references below with the discussion by Anderson (Ref. 3, pp. 266-270) being a good presentation. At point A, the characteristic equations in a planar frame of reference are,

$$dy = \tan(\theta + \mu)\, dx = A\, dx \ \text{ Along } C_+ \tag{B-1}$$

$$dy = \tan(\theta - \mu)\, dx = B\, dx \ \text{ Along } C_- \tag{B-2}$$

The coefficients are defined as A = $\tan(\theta+\mu)$ and B = $\tan(\theta-\mu)$.

B.2 Compatibility Equations

The characteristic curves have the mathematical property that along the characteristics, flow properties are continuous; however, the derivatives of flow properties are indeterminate, and the derivatives may be discontinuous across the characteristic curves. Details on these properties of characteristic curves and derivations of equations can be found in the references listed below. The indeterminate nature of characteristic curves allows the partial differential equations defining planar, steady, adiabatic, irrotational supersonic flow to be changed to ordinary differential equations along the characteristic curves (Ref. 3). These ordinary differential equations are known as the compatibility equations and only are valid along the characteristic curves. The compatibility equations relate the velocity components and can be expressed as,

$$du = D\, dv + F\, dx \ \text{ Along } C_+ \tag{B-3}$$

$$du = E\, dv + G\, dx \ \text{ Along } C_- \tag{B-4}$$

where the coefficients are

$$D = -\tan(\theta - \mu) \tag{B-5}$$

$$E = -\tan(\theta + \mu) \tag{B-6}$$

$$F = G = \frac{c^2}{u^2 - c^2}\frac{v}{y} \tag{B-7}$$

For two-dimensional flows, $F = G = 0$.

The velocity components (u,v) and acoustic speed (c) listed above have been made nondimensional by the critical speed (c^*).

$$u = \frac{u^D}{c^*}, \quad v = \frac{v^D}{c^*}, \qquad c = \frac{c^D}{c^*} = \left[\frac{\gamma + 1}{2\left(1 + \frac{\gamma - 1}{2} M^2\right)}\right]^{1/2} \tag{B-8}$$

Where u^D, v^D, and c^D are the dimensional values of the velocity components and acoustic speed.

The characteristic curves form a characteristic net which encompasses the flowfield. The compatibility equations relate the propagation of flow properties along the characteristics. The intersections of the characteristics with each other, solid boundaries, and shock waves are possible and yield different solutions for the flow properties.

The general approach for solving for a flowfield using the method of characteristics is to start from a known flowfield at an upstream location and march downstream in the supersonic flow while integrating along the characteristic directions. The methods of Subsection 7.1 and 7.2 can be applied to determine these flowfields. For an external supersonic diffuser, the first stage is either a ramp for a two-dimensional diffuser that forms an oblique shock wave or a cone for an axisymmetric diffuser that creates a conical shock wave. The initial solutions define the flow variables up to the start of the second stage. The second and subsequent stages may create Mach or shock waves, as discussed in Section 7.0.

B.3 Method of Characteristics Solution Process

The process involves solving the characteristic and the compatibility equations simultaneously to determine the path of the characteristic curves and the flow solution along the characteristic curves. This creates a characteristic net through the flow field with the flow solution points located at the intersection of the characteristic curves, at boundaries, or at shock waves. These solution points are referred to as field, boundary, and shock wave points, respectively.

B.4 Field Point

A field point is at the intersection of C_- and C_+ characteristic curves within the flowfield and its solution illustrates the basic procedures for determining the non-linear flowfield. An illustration of a field point is shown in Figure B-2 where the field point is indicated as point 3. The known solutions on the C_+ and C_- characteristic curves are indicated as points 1 and 2, respectively.

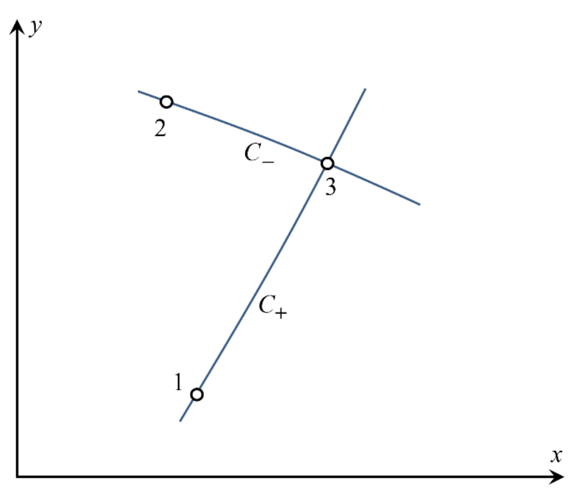

Figure B-2.—An illustration of a field point.

Solving for the solution at point 3 involves applying Equations (B-1) and (B-3) along the C_+ characteristic between points 1 and 3 simultaneously with Equations (B-2) and (B-4) along the C_- characteristic curve between points 2 and 3. Finite-differences can be used to approximate these equations as

$$y_3 - y_1 = \bar{A}\,(\,x_3 - x_1)\;\text{ Along } C_+ \tag{B-9}$$

$$y_3 - y_2 = \bar{B}\,(\,x_3 - x_2)\;\text{ Along } C_- \tag{B-10}$$

$$u_3 - u_1 = \bar{D}\,(\,v_3 - v_1) + \bar{F}\,(\,x_3 - x_1)\;\text{ Along } C_+ \tag{B-11}$$

$$u_3 - u_2 = \bar{E}\,(\,v_3 - v_2) + \bar{G}\,(\,x_3 - x_2)\;\text{ Along } C_- \tag{B-12}$$

The values ($\bar{A}$, $\bar{B}$, $\bar{D}$, $\bar{E}$, $\bar{F}$, and $\bar{G}$) are average values between the respective points along the respective characteristic curve. For example, $\bar{A}$ = ($A_1 + A_3$). Since the solution at point 3 is the unknown, a fixed-point iteration is performed to calculate x_3, y_3, u_3, and v_3. Equations (B-11) and (B-12) are solved simultaneously to obtain u_3, and v_3. The equations result in

$$v_3 = \frac{u_2 - u_1 + \bar{D}\,v_1 - \bar{E}\,v_2 + \bar{G}\,(\,x_3 - x_2) - \bar{F}\,(\,x_3 - x_1)}{\bar{D}\; - \bar{E}} \tag{B-13}$$

$$u_3 = u_2 + \bar{E}\,(\,v_3 - v_2) + \bar{G}\,(\,x_3 - x_2) \tag{B-14}$$

The coordinates x_3 and y_3 are determined by finding the intersection of the C_- and C_+ characteristic curves. It is assumed that between the points, the characteristics are straight lines in which the slopes of the lines are given by $\tan^{-1}(\bar{A})$ and $\tan^{-1}(\bar{B})$ along the C_+ and C_- characteristic curves, respectively.

B.5 Boundary Points

A boundary point is the intersection of a characteristic curve with a surface which forms part of the boundary of the flow domain for the flowfield. The MOC methods assume inviscid flow, and so at a surface, a slip-wall boundary condition is applied in which the flow is constrained to be parallel to the surface, which is equivalent to saying there is no flow normal to the boundary. This can be expressed mathematically as

$$v_3 = u_3 \tan\theta_3 \tag{B-15}$$

where point 3 is the unknown point on the boundary. An illustration of characteristics interacting with surfaces is shown in Figure B-3.

For the case of a C_+ characteristic curve intersecting a boundary, one can insert Equation (B-15) into Equation (B-11) and solve for u_3 to obtain,

$$u_3 = \frac{u_1 - \bar{D}\,v_1 + \bar{F}\,(\,x_3 - x_1)}{1.0 - \tan\theta_3\,\bar{D}} \tag{B-16}$$

Similarly, for the case of a C_- characteristic curve intersecting a boundary, one can insert Equation (B-15) into Equation (B-12) and solve for u_3 to obtain,

$$u_3 = \frac{u_2 - \bar{E}\,v_2 + \bar{G}\,(\,x_3 - x_2)}{1.0 - \tan\theta_3\,\bar{E}} \tag{B-17}$$

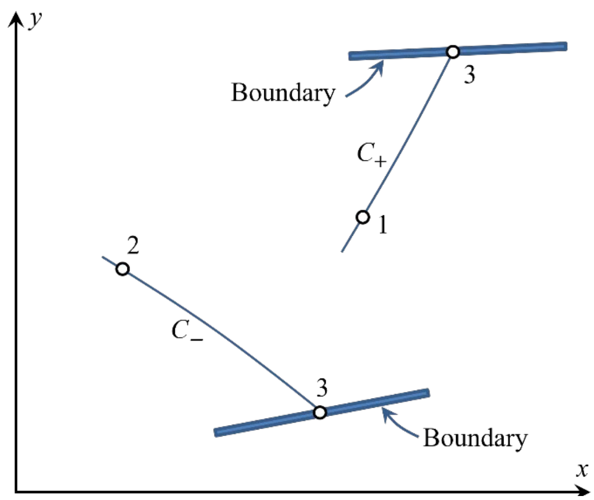

Figure B-3.—An illustration of boundary points.

The solutions of Equations (B-16) or (B-17) assume the coordinates and flow solution at points 1 and 2 are known. Additional information as to the nature of the boundary at point 3 is needed. It is first assumed that the boundary is fixed in space and that the planar profile of the boundary is known by some function $y(x)$. As with the field point, it is assumed that the characteristic curves are straight lines between the points, and so the coordinates x_3 and y_3 are determined as the intersection of the characteristic curve and the boundary defined by the known function $y(x)$. In addition, the function can provide the slope of the surface $\theta_3 = dy/dx$. The fixed boundary point problem is closed with the assumption of the Mach number at point 3 (M_3).

As for the solution of the field point, a fixed-point iteration can be performed to iterate on the values of u_3 and v_3. During this iteration, the boundary coordinates and slope are also updated as the intersection point of the characteristic curve and surface changes.

An alternative to the fixed-boundary problem described above is the free-boundary problem in which the coordinates and slope of the surface are computed as part of the solution of the equations. The solution to the free-boundary problem will be discussed in later subsections describing the design of curved surfaces that generate Mach waves for isentropic compression for both the external and internal supersonic compression. For both cases, the solution of the equations will involve consideration of the conservation of mass for the flowfield.

B.6 Shock Wave Points

A shock wave point is at the intersection of a characteristic curve with a shock wave and its properties of the point depend on whether the point is on the upstream or downstream side of the shock wave. The illustration on the left-hand-side of Figure B-4 shows a point 3 on the downstream side of a shock wave. The Mach number and flow angle on the upstream side of the shock wave are denoted as $(M_u,\theta_u)_3$, respectively, and are considered known from the solution of the flowfield upstream of the shock wave. Further, the coordinates of point 3 $(x,y)_3$ are also known from the upstream solution. It is also assumed that the solution point 1 at the downstream side of the shock wave $(M,\theta,x,y)_1$ and field point 2 $(M,\theta,x,y)_2$ are known. The objective of the shock wave boundary problem is to compute the solution point $(M,\theta)_3$ on the downstream side of the shock wave. The solution process is much like that discussed in the previous subsection for a point on a boundary. For the illustration of the left-hand-side of Figure B-4, a form of Equation (B-16) can be applied for the relationship between properties along a C_+ characteristic curve. In

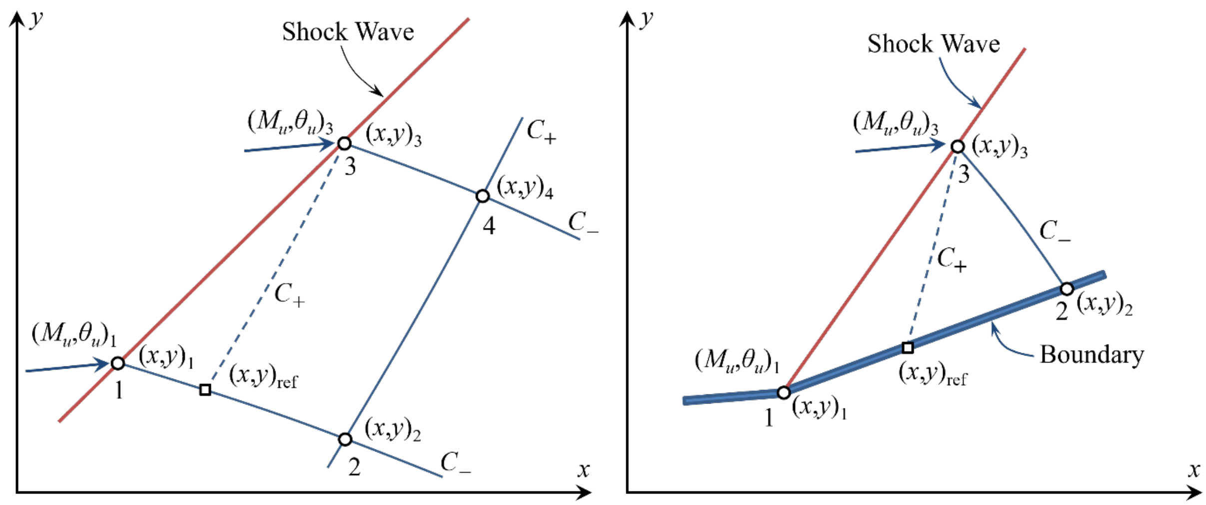

Figure B-4.—Illustrations of a shock wave point within the field (left) and a shock wave point near a boundary (right).

this case, as shown in Figure B-4, the C_+ characteristic curve is shown as a dashed line extending between a reference point labeled $(x,y)_{ref}$ and point 3. The properties at the reference point would take the place of the properties of point 1 as indicated in Equation (B-16) to form the equation,

$$u_3 = \frac{u_{ref} - \bar{D}\, v_{ref} + \bar{F}\left(x_3 - x_{ref}\right)}{1.0 - \tan\theta_3\, \bar{D}} \qquad \text{(B-18)}$$

The reference point is located along the C_- characteristic curve between points 1 and 2, whose solutions are known. The flow properties at the reference station $(M,\theta)_{ref}$ are determined from a linear interpolation of the flow solutions at points 1 and 2 once an estimate of the coordinates $(x,y)_{ref}$ are available. The average values of the coefficients $\bar{A}$, $\bar{D}$, and $\bar{F}$ are computed from the properties at the reference point and point 3. As with the solution of the boundary point discussed in the previous subsection, the values of the Mach number and flow angle $(M,\theta)_3$ at the solution point 3 are required and are obtained from the solution of the change in Mach number and flow angle across planar oblique shock wave. The solution of the oblique shock wave relations requires knowledge of the shock wave angle at point 3. The shock wave angle β_3 can be initialized from the value at β_1. With a value of the shock wave angle, the flow conditions downstream of the shock wave can be computed using the oblique shock wave relations. The solution process involves a fixed-point iteration for several iterations. Once the solution is known at point 3, the solution at point 4 can be obtained as a field point. The process then continues up the shock wave and into the downstream field.

For the case of a shock wave point near a boundary, as illustrated in the image on the right-hand-side of Figure B-4, the solution process is similar; however, now point 1 and the reference point are on the boundary, and so, the Mach number is prescribed, and the flow angle is equal to the slope of the surface at the point. An iteration is still performed to find the angle of the C_+ characteristic curve from the reference point to point 3. The flow solution at point 2 on the boundary is calculated as a boundary point on a C_- characteristic curve using the known flow solution at point 3.

B.7 MOC Flow Region A: Isentropic Compression

The use of the MOC solution processes discussed in the previous subsections for the design of the components of a supersonic inlet are described in this and the next few subsections. This subsection discusses the design of an isentropic second stage of a three-stage external supersonic diffuser. The flowfield of this isentropic second stage is designated as the MOC Flow region A and involves the isentropic compression of the supersonic flow through a series of Mach waves with a common focal point. Currently within SUPIN, the focal point for MOC region A is specified to be the cowl lip point. However, one could envision a design strategy in which the focal point is positioned away from the cowl lip. Figure B-5 shows the characteristic net for the MOC flowfield through the isentropic stage. The Mach waves are the C_+ characteristic curves with an index of i. The leading Mach wave has an index of $i = 1$ and the trailing Mach wave has an index of $i = N_{waves}$. The k index ranges from the focal point ($k = 1$) to the surface of the external supersonic diffuser. Each k index denotes a C_- characteristic curve. The solution variables for the MOC flow field are Mach number (M), flow angle (θ), planar coordinates (x,y). The values for these solution variables are stored in two-dimensional arrays with indices (i,k).

The starting solution for the flow region is specified along the leading Mach wave and corresponds to flow conditions at the outflow of the first stage, which is a wedge flow for a two-dimensional external supersonic diffuser and a conical flow for an axisymmetric diffuser. The wedge flow is established from planar oblique shock wave equations (as discussed in Subsection 7.1) with an inflow Mach number of M_L and a specified first-stage, ramp deflection angle of θ_1. For a two-dimensional ramp, the flow of the first stage has a uniform Mach number and flow angle equal to the ramp deflection angle. For an axisymmetric cone first stage, the conical flow is established through computational solution of the solution of the Taylor-Maccoll equations (as discussed in Subsection 7.2) with a conical half-angle for the first stage of the diffuser of θ_1. The conical flow is defined by conical rays focused about the vertex of the cone that range from the cone surface to the conical shock wave. The Mach number and flow angle are constant along each ray.

The coordinates (x,y) along the leading Mach wave are established by starting from the known focal point and solving the MOC field unit problems along the k-index from the focal point toward the surface of the first stage. This leading Mach wave is a C_+ characteristic curve. The Mach number and flow angle at the coordinates is obtained from interpolation of the flow solution of the first stage. The solution

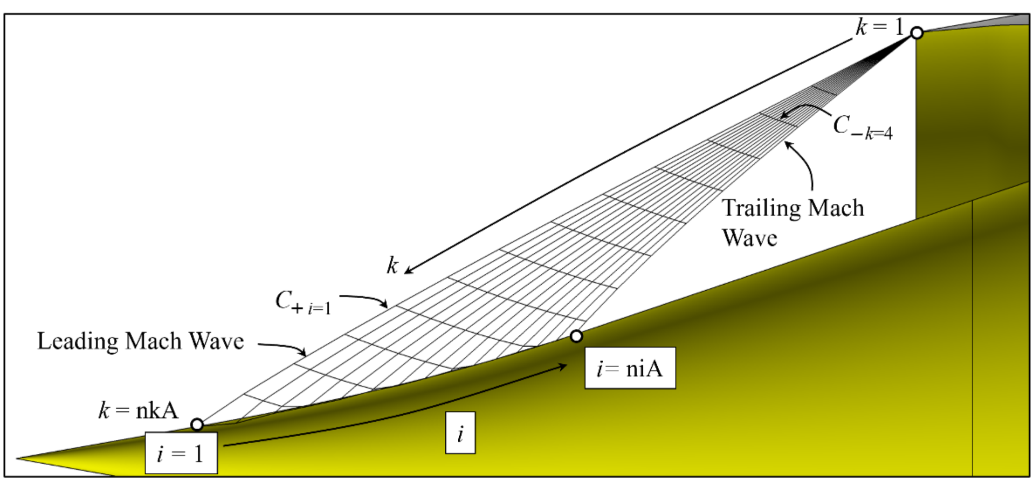

Figure B-5.—The characteristic net and features of the MOC region A.

process involves setting a step size between points and continuing the stepping until the surface of the external supersonic diffuser is reached, which becomes the end of the first stage $(x,y)_{stg1}$. For a two-dimensional external supersonic diffuser, the leading Mach wave is straight line because the flow solution for the first stage is uniform. For an axisymmetric external supersonic diffuser, the leading Mach wave is curved due to the decreasing of the Mach number and increasing of the flow angle as one approaches the cone surface. The leading Mach wave shown in Figure B-5 has a slightly curving leading Mach wave through the conical flow of the conical first stage of an axisymmetric external supersonic diffuser.

With the completion of the leading Mach wave, the stream function (ψ) can be evaluated for points along the leading Mach wave, which is a C_+ characteristic curve, between the focal point and the surface. The derivation of the equations for the stream function can be found in Reference 5. A value of $\psi = 1.0$ is assigned at the focal point, which has an index of $(i,k) = (1, 1)$, or $\psi_{k=1} = 1.0$. An integration of the stream function along the leading Mach wave for an axisymmetric flowfield takes the form of

$$\psi_{k+1} = \psi_k + \frac{1}{4}\left\{\left[\frac{\rho V}{M\sin(\mu+\theta)}\right]_k + \left[\frac{\rho V}{M\sin(\mu+\theta)}\right]_{k+1}\right\}\left(y_{k+1}^2 - y_k^2\right) \quad \text{(B-19)}$$

For a two-dimensional flowfield, the integration of the stream function along the C+ characteristic curve takes the form of

$$\psi_{k+1} = \psi_k + \frac{1}{2}\left\{\left[\frac{\rho V}{M\sin(\mu+\theta)}\right]_k + \left[\frac{\rho V}{M\sin(\mu+\theta)}\right]_{k+1}\right\}\left(y_{k+1} - y_k\right) \quad \text{(B-20)}$$

where,

$$V = \left(u^2 + v^2\right)^{1/2} \quad \text{(B-21)}$$

The integration continues until k = nkA at the surface of the external supersonic diffuser at the end of the first stage where the value is the stream function becomes the reference value (ψ_{ref}),

$$\psi_{ref} = \psi_{nkA} \quad \text{(B-22)}$$

which will be used for establishing the contour of the second stage that creates the Mach waves for the isentropic compression of the second stage.

The Mach wave structure of the second stage is initiated through the specification of a turning of the flow and expansion at the focal point ($k = 1$). Since the expansion is specified at a point, the flow turning and decrease in Mach number of the expansion are expressed in terms of the index i = 1, niA, where niA is the number of Mach waves. The process involves specifying the desired Mach number at the end of the expansion (M_{tw}) and linearly interpolating the Mach number with respect to the index i extending from the leading Mach wave ($i = 1$) to the trailing Mach wave (i = niA). With the Mach numbers known, a Prandtl-Meyer solution can be applied to compute the flow angles (θ) of each Mach wave at the focal point. The choice of the Mach number at the end of the isentropic compression of the second stage (M_{tw}) establishes much of the expansion of the external supersonic diffuser and the eventual distribution of Mach number across the end of the external supersonic diffuser at station 1. In designing the external supersonic diffuser, the value specified for M_{tw} may need to be iterated to obtain the desired Mach number distribution at station 1. Within SUPIN, the value of M_{tw} is specified by the input factor F_{mtexd} with $K_{mtexd} = 1$ and as discussed in Section 7.0. This may involve an iteration on M_{tw} to match the specified conditions.

The rest of the MOC flow field for region A is then computed by working along each Mach wave starting from the second Mach wave ($i = 2$) and proceeding from the focal point and solving the MOC field unit problems toward the diffuser surface while incrementing in the *k*-index. The stream function is evaluated along the way until the value of the reference stream function (ψ_{ref}) is bracketed. A linear interpolation of the bracketing solution points is then performed to establish the coordinates and flow solution of the Mach wave at the diffuser surface. As the solution proceeds for each Mach wave, *k*-index for the diffuser surface may be reduced as the surface turns into the MOC flowfield. The end of the second stage is reached upon solution of the trailing Mach wave at i = niA.

At the trailing Mach wave, the Mach number, flow angle, and coordinates are loaded into one-dimensional arrays (fsAma, fsAth, fsAx, and fsAy) with the index directed from the surface to the focal point. These arrays will provide the starting solution for the MOC region B.

B.8 MOC Flow Region B: Last Stage of the External Supersonic Diffuser

The MOC flow region B encompasses the last stage of the external supersonic diffuser, which ends at the station 1 cross-section. Two flowfields for region B are considered depending on the upstream flow of the external supersonic diffuser.

The first MOC region B flowfield is for the case of an isentropic second stage as discussed in the previous subsection for the MOC region A. The flow solution from the trailing Mach wave of region A serves as the starting solution for region B. Figure B-6 shows the characteristic net for this region B flowfield. The solution points are redistributed to evenly space the points along the inflow boundary. The lower bound of the region is the inlet surface for the third and last stage of the external supersonic diffuser, which has a constant slope as established at the end of the isentropic compression. The downstream boundary for the region is the planar cross-section for station 1. An *i*-index denotes a C_+ characteristic and a *k*-index denotes a C_- characteristic. The MOC solution process starts with a boundary point solution at $(i,k) = (2,2)$ followed by field point solutions along $i = 2$ until the station 1 plane is reached. The process is repeated for each characteristic in the *i*-index until station 1 is reached at the end of the external supersonic diffuser. The niB indicates the number of characteristics interacting with the inlet surface. The Mach number, flow angle, and coordinates are then loaded into arrays (fs1ma, fs1th, fs1x, fs1y) to provide for the starting solution for the MOC region C. The index for these arrays is directed from the diffuser surface toward the cowl lip. Figure B-6 shows the resultant characteristic net for this case for an axisymmetric spike inlet. For two-dimensional inlets, the flow conditions in region B are of uniform Mach number and flow angle.

The second MOC region B flowfield is for the case of a conical shock wave created by a bi-conic (axisymmetric spike) external supersonic diffuser. The MOC region B encompasses the flow of the second stage of the diffuser. Figure B-7 shows the characteristic net for this region B flowfield. The starting solution is obtained through solution of the shock wave boundary problem with the conditions upstream of the shock wave provided by the conical flowfield of the first stage. The solution process starts with the solution through an oblique shock wave at $(i,k) = (1,1)$. An iteration is then performed combining a shock wave-field problem at $(i,k) = (1,2)$ and boundary problem at $(i,k) = (2,2)$ for solution at these two points. The process then proceeds to an iteration combining a shock wave-field and a field problem while incrementing in the *k*-index until the cowl lip is reached. The shock wave will have a lower angle than the C_+ characteristics. The solution process must account for the collapse of C_+ characteristics into the shock wave with a change in which *i*-index provides the field point for the shock wave-field problem. In Figure B-7, the $i = 2$ C_+ characteristic is shown as collapsing into the shock wave. Once the solution process arrives at the cowl lip or focal point, the flow conditions downstream of the

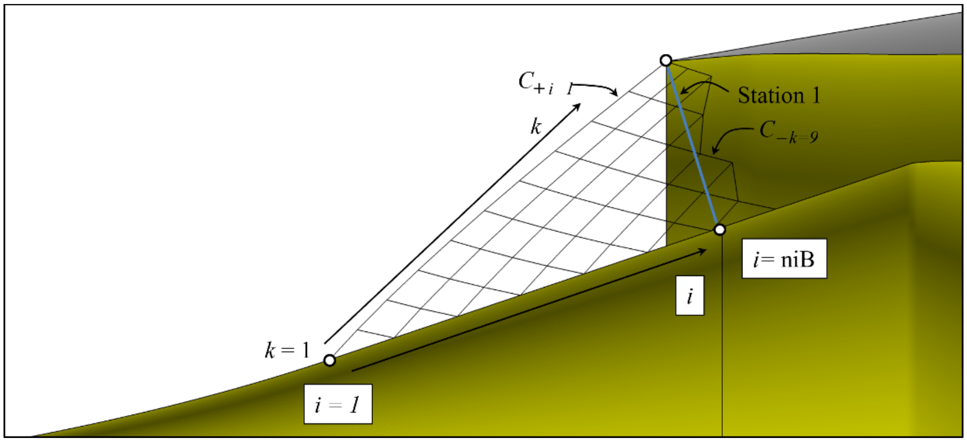

Figure B-6.—The characteristic net for the MOC region B downstream of an isentropic second stage.

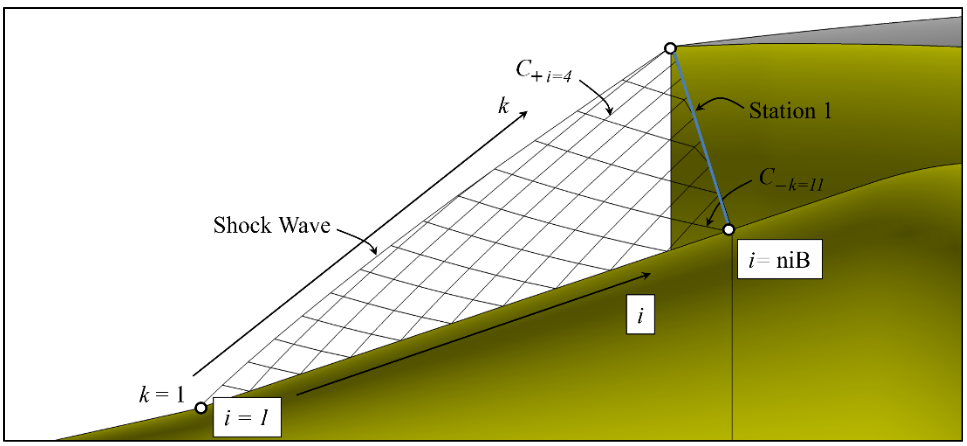

Figure B-7.—The characteristic net for the MOC region B downstream of an oblique shock.

shock wave and the coordinates of the shock wave are established. The solution of the remaining MOC flowfield for region B can be solved as discussed in the previous paragraph for the region B flowfield downstream of the isentropic second stage.

B.9 MOC Flow Region C: Internal Supersonic Diffuser Upstream of Cowl Interior Shock Wave

The MOC Flow region C encompasses the forward portion of the interior supersonic diffuser from station 1 as its inflow to the cowl interior shock wave as its outflow. The plane of station 1 and the cowl interior shock wave meet at the cowl lip, and so, constitute the upper boundary point of the flow region C. The bottom boundary of the flow region is the forward segment of the centerbody of the internal supersonic diffuser, which has a constant slope equal to the slope of the last stage of the external supersonic diffuser. The constant slope is intended to avoid introducing shock wave or Mach waves into the flow region. The downstream point of the region is the point at which the cowl interior shock wave intersects the centerbody, which is also the start of the shoulder. Figure B-8 shows the characteristic net for flow region C.

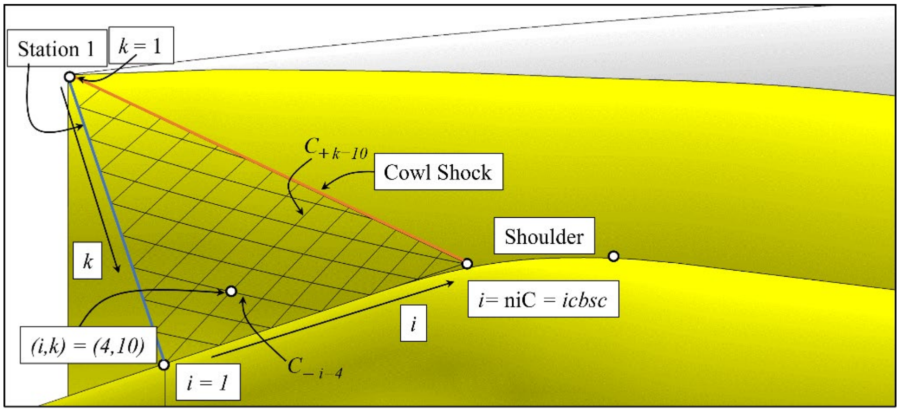

Figure B-8.—The characteristic net for the MOC flow region C of the internal supersonic diffuser upstream of the cowl interior shock.

The starting solution at the inflow to the region is obtained from the flow solution at station 1 obtained from the solution of the MOC flow region B. The solution points are redistributed to evenly space the points along the inflow boundary at station 1. For two-dimensional inlets, the Mach number and flow angle are uniform at the inflow. For axisymmetric spike inlets, the Mach number at the centerbody is lower than at the cowl lip. The local flow angle will be lower at the cowl lip than at the centerbody due to the isentropic compression created by the conical external supersonic diffuser.

The characteristic net associates the C_- characteristics with the *i*-index and C_+ characteristics with the *k*-index. The MOC solution process starts with the solution point at the cowl lip ($k = 1$) and computes the conditions across the oblique, cowl interior shock wave. The process then increments in the *k*-index to solve for solution points along each C_+ characteristic from station 1 toward the cowl shock wave as the *i* -index is incremented. If a field point solution indicates that the point coordinates are downstream of the cowl shock wave, then a shock wave-field solution is performed to compute the flow conditions upstream and downstream of the cowl shock wave along the characteristic. Eventually, the centerbody surface is reached. The MOC solution process then proceeds along a C_+ characteristic with a boundary point solution followed by field point solutions until the cowl shock wave is reached. As the process continues, the solution point is reached where the cowl shock wave intersects the centerbody surface, which marks the end of flow region C. The niC indicates the number of characteristics interacting with the centerbody.

B.10 MOC Flow Region D: Internal Supersonic Diffuser with Cancelled Cowl Interior Shock Wave

The MOC flow region D encompasses the aft portion of the internal supersonic diffuser downstream of the cowl interior shock wave to the end of the internal supersonic diffuser at the geometric throat station TH. The solution points on the downstream side of the cowl shock wave become the starting solution for the MOC solution of region D. The MOC solution process starts at the cowl just downstream of the cowl lip interior. The first segment of the cowl interior profile is a line with the slope equal to θ_{clin}. The MOC solution process marches in the downstream direction while solving the solid boundary, field point, and shock wave boundary unit problems. Eventually, a C_- characteristic is formed which extends from the cowl interior to the point on the centerbody on the downstream side of the cowl shock wave intersection with the centerbody. The stream function is evaluated along this C_- characteristic to obtain the reference stream function value for the streamline that will define the shape of the cowl interior between this reference C_- characteristic and station TH. Figure B-9 shows an example of a reference C_- characteristic.

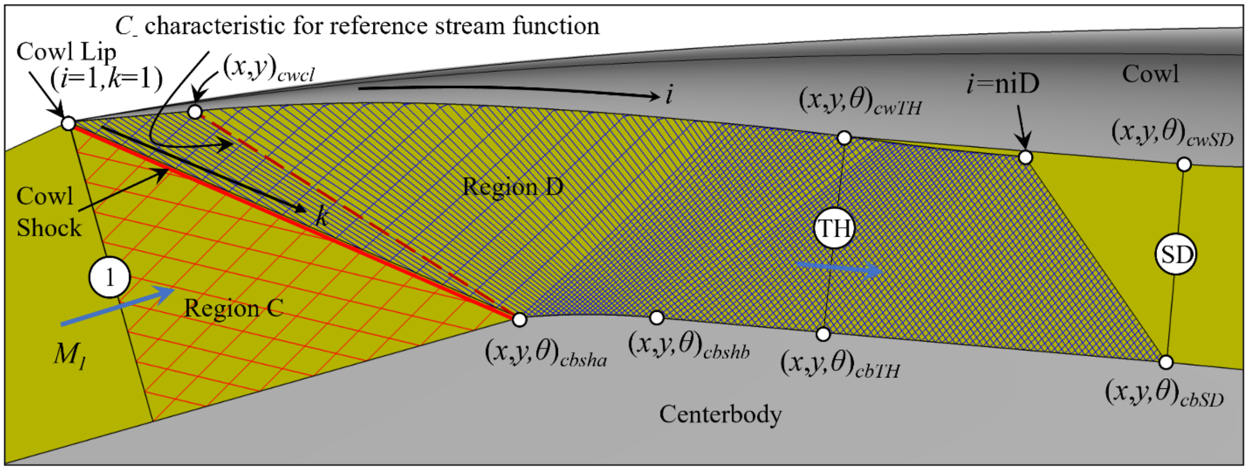

Figure B-9.—The characteristic net for the MOC region D of the internal supersonic diffuser downstream of the cowl interior shock.

The solution of the flow through the cowl shock wave at its interaction point with the centerbody yields a deflection of the flow through the shock wave. The interaction point is also the start of the shoulder of the centerbody and has the coordinates $(x,y)_{cbsha}$. The cowl shock wave can be cancelled at this interaction point to prevent a reflected shock wave from being generated. This requires that the slope of the start of the shoulder at the interaction point (θ_{cbsha}) be equal to the flow angle downstream of the interaction point. As discussed in Section 9.2, the shoulder facilitates the turning of the internal supersonic flow toward the engine face by forming a curved profile that matches to the slope of the aft portion of the internal supersonic diffuser (θ_{cbTH}).

The MOC solution process for region D downstream of the reference C_- characteristic constructs the (x,y) coordinates of the cowl interior as the streamline defined by the reference value of the stream function. The MOC solution process starts at the point on the centerbody which intersects the reference C_- characteristic. The specified centerbody profile of the shoulder and the third and fourth segments provides the needed (x,y) coordinates for the MOC solution along this boundary of the region D. Since the centerbody profile also defines a streamline, the flow angles for flowfield solution points can also be obtained from the centerbody profile. The Mach number distribution along the centerbody profile is needed to complete the boundary conditions for the MOC solution of region D. The Mach number (M_{cbsha}) is known at the point on the centerbody on the downstream side of the intersection of the interior cowl shock wave with the centerbody. The Mach number on the centerbody at station TH (M_{cbTH}) is specified as an input factor. A linear distribution ranging from M_{cbsh} to M_{cbTH} is used to calculate the Mach number at solution points on the centerbody between the interior cowl shock wave intersection point and station TH.

The MOC solution process within region D downstream of the reference C_- characteristic involve marching downstream through the throat section while solving a sequence of C_- characteristics that extend from the centerbody to the cowl interior. The solution along a C_- characteristic starts at the centerbody and works along the C_- characteristic toward the cowl interior. The niD indicates the number of characteristics that interact with the cowl interior. The values of the stream function are evaluated at each point along the C_- characteristic. Eventually, the values of the stream function bracket the reference value that define the cowl streamline. An interpolation is performed to find the (x,y) coordinates, Mach number, and flow angle for the solution point for the reference stream function value. This solution point then becomes the coordinates and flow solution at the cowl interior for that C_- characteristic. The characteristic net is solved in this manner in the downstream direction until station SD is reached on the centerbody. Figure B-9 shows a characteristic net for region D. The (x,y) coordinates of the characteristic net at the cowl interior are used to define the planar profile of the cowl interior between the interior cowl lip to station TH.

References

1. Ferri, A., "Application of the Method of Characteristics to Supersonic Rotational Flow," NACA Report 841, April 1946.
2. Zucrow, M. J. and Hoffman, J. D., *Gas Dynamics: Volume 1*, John Wiley & Sons, New York, 1976.
3. Anderson, J. D., Jr., *Modern Compressible Flow*, McGraw-Hill Book Company, New York, 1982.
4. Sorensen, V. L., "Computer Program for Calculating Flowfields in Supersonic Inlets," NASA TN D-2897, July 1965.
5. Anderson, B. H., "Design of Supersonic Inlets by a Computer Program Incorporating the Method of Characteristics," NASA TN D-4960, January 1969.

Appendix C.—Sample Cases for Pitot Inlets

Several sample cases are provided to demonstrate the use of SUPIN. This appendix provides sample cases for pitot inlets. Subsequence appendices will provide sample cases for the two-dimensional, axisymmetric spike, and streamline-traced inlets with differentiations for external- and mixed-compression inlets. The sample cases not only demonstrate the input and output of SUPIN, but the cases can also serve as starting points for other inlet design and analysis studies. For all sample cases, the input data files generate surface grids. For most cases, the input data files generate three-dimensional CFD grids. The distribution of SUPIN contains a folder of the sample input (*.in), output data file (*.out) and the Plot3D file of the surface grid (*.xyz).

C.1 SUPIN.K1.M065: Mach 0.65 Axisymmetric Pitot Inlet

This sample case involved the design of a subsonic, axisymmetric pitot inlet for $M_0 = M_L = 0.65$ at an altitude of $h_0 = 25000$ ft. The engine-face diameter was $D_2 = 3.5$ ft with an elliptical spinner with a hub-to-tip ratio of $D_{hub}/D_2 = 0.3$. The design engine-face Mach number was $M_2 = 0.5$, which corresponds to a corrected flow rate of $W_{C2} = 322.9$ lbm/s. The cowl lip interior profile was designed to produce a quasi-one-dimensional Mach number at the minimum cowl interior point of $M_{TH} = 0.85$ at station TH. The throat section was contained within the cowl lip interior, and so station SD starts at the end of the cowl lip interior point, $(x,y)_{clin}$. The inlet was formed with $\theta_{clip} = 7$ degrees and a subsonic diffuser with a length of $L_{subd} / D_2 = 1.0$, which placed the engine face station 2 at $x_{EF} = x_2 = 3.855$ ft. The profile of the cowl interior was formed using a NURBS curve between station SD and 2 in which input factors $K_{sdprp} = 0$ and $K_{sdvar} = 0$. This inlet was designated as inlet b00 based on the two digits indicated by K_{sdprp} and K_{sdvar}. Figure C-1 shows an image of the inlet b00.

Three additional inlets were generated that varied the options for the values of K_{sdprp} and K_{sdvar} so as to explore the design options for the cowl interior profile. Inlet b11 was designed using $K_{sdprp} = 1$ and $K_{sdvar} = 1$ to form a cowl interior profile with a linear variation in the cross-sectional area of the subsonic diffuser. The cowl lip interior angle was set to $\theta_{clin} = 4.8$ degrees to match the slope of the profile. Inlets b21 and b31 were similarly designed for linear Mach number and linear pressure distributions, respectively, through the subsonic diffuser. Table C-1 lists the values of θ_{clin} used for each inlet along with values of the capture area, inlet flow rate, and inlet total pressure recovery for each inlet as determined by SUPIN.

Viscous Wind-US CFD simulations were performed of the inlets at the design conditions. Figure C-2 shows Mach number contours on the plane of symmetry for each inlet. For the simulations, the Mach number at the downstream internal outflow boundary was adjusted until the design corrected flow rate of

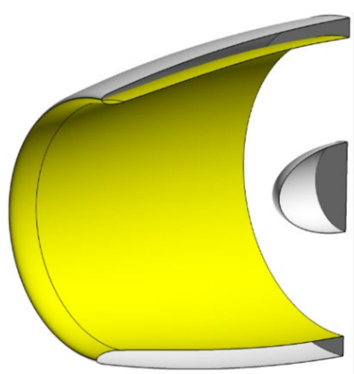

Figure C-1.—Subsonic, axisymmetric pitot inlet K1.M065.b00.

TABLE C-1.—PROPERTIES FOR THE K1.M065 SUBSONIC, AXISYMMETRIC PITOT INLETS

Inlet	θ_{clin} (deg)	A_{cap} (ft^2)	$(W_2)_{SUPIN}$ (lbm/s)	$(p_{t2}/p_{t0})_{SUPIN}$	$(M_2)_{CFD}$	$(W_2)_{CFD}$ (lbm/s)	$(p_{t2}/p_{t0})_{CFD}$
b00	7.0	7.3326	165.96	0.9881	0.5039	165.14	0.9827
b11	4.8	7.3066	165.37	0.9846	0.5051	165.18	0.9835
b21	0.0	7.2712	164.57	0.9799	0.5101	165.24	0.9827
b31	2.2	7.2796	164.76	0.9810	0.5074	165.14	0.9842

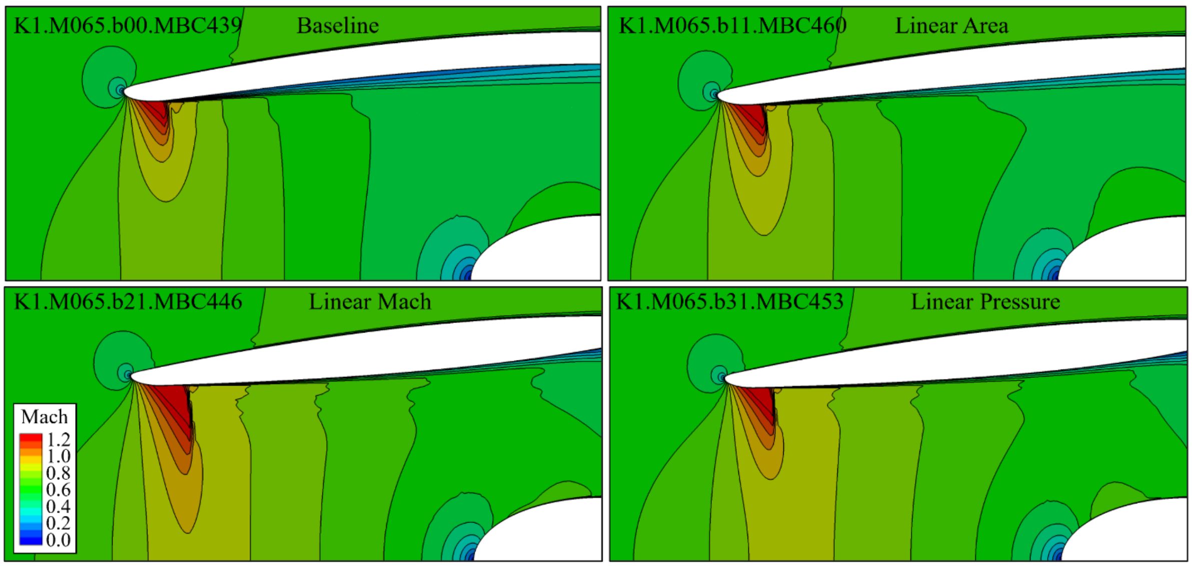

Figure C-2.—Mach number contours for the subsonic, axisymmetric pitot inlets for K1.M065.

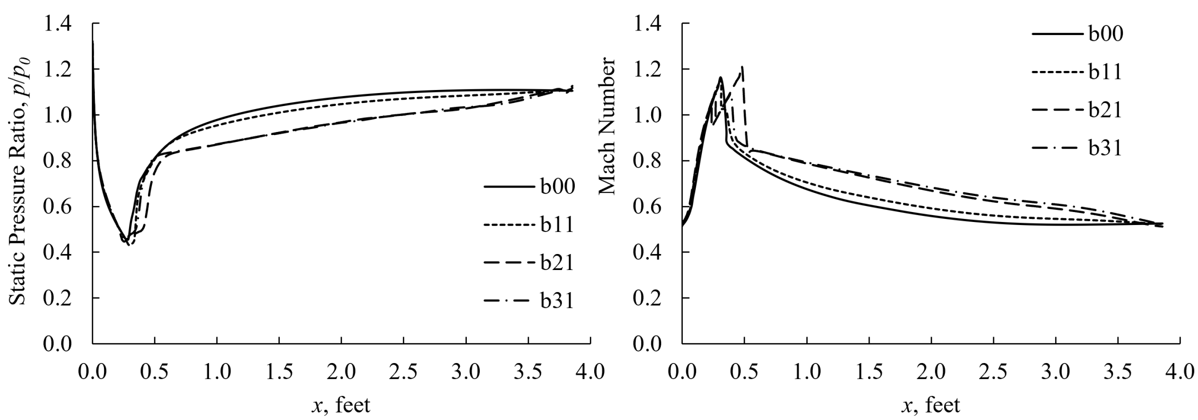

Figure C-3.—Variations of the static pressure ratio (left) and Mach numbers (right) along the cowl interior for the K1.M065 subsonic, axisymmetric pitot inlets.

W_{C2} = 322.9 lbm/s was achieved. A noticeable feature of the flowfields that a region of supersonic flow develops at the cowl lip interior as the captured flow accelerates upon entering the inlet. A small normal shock wave terminates the supersonic region. Inlet b00 with the NURBS curve for the cowl interior profile shows some low-momentum flow in the boundary layer downstream of the shock wave into the subsonic diffuser. The flowfields of inlets b21 and b31 have a more gradual diffusion rate along the subsonic diffuser which seems to remove the low-momentum flow observed for inlet b00. The extent of the supersonic region seems to be correlated to the value of θ_{clin} such that the size of the region is larger for smaller values of θ_{clin}. The plots of the static pressure ratio and Mach number along the cowl interior, which are plotted in Figure C-3, seem to verify that inlets b21 and b31 do result in linear distributions of

Mach number and static pressure, respectively, within the subsonic diffuser. Table C-1 lists the inlet performance as obtained from SUPIN and averages at the engine face from the CFD simulations. Overall, there is good agreement between SUPIN and the CFD simulations. The small variations in the total pressure recovery make it difficult to conclusively state that one design approach is better.

C.2 SUPIN.K1: Axisymmetric Pitot Inlets for Mach 1.4, 1.7, and 2.0

These sample cases involve the design of axisymmetric pitot inlets for $M_0 = M_L = 1.4$, 1.7, and 2.0. The engine-face diameter was $D_2 = 3.625$ ft with an elliptical spinner with a hub-to-tip ratio of $D_{hub}/D_2 = 0.3$. The inlets were designed with the freestream conditions corresponding to the altitudes (h_0) and engine-face corrected flow rates (W_{C2}) as listed in Table C-2. All three inlets were designed with the engine face at $x_{EF} = 2.54$ ft. The cowl lips was essentially sharp with an elliptic profile with a semi-minor axis length of 0.0005 ft and aspect ratio of 2. The cowl lip angle was specified to be $\theta_{clin} = \theta_{clip} = 3$ degrees with the cowl lip exterior angle of $\theta_{clex} = 7$ degrees. The inlets were designed with the normal shock wave at the cowl lip. The throat section and subsonic diffuser formed a diffusing with a total length of the inlets of $L_{inlet} / D_2 = 0.71$. The outer radius of the cowl exteriors were specified with $r_{cwex}/D_2 = 1.06$. Figure C-4 shows images of the Mach 1.4 inlet. The inlets for Mach 1.7 and 2.0 looked very similar with slightly smaller capture areas (A_{cap}) as listed in Table C-2. The right-hand-side image of Figure C-2 shows the Mach number contours from an axisymmetric, viscous Wind-US CFD simulation at the critical condition for Mach 1.4. The normal terminal shock wave is shown at the cowl lip and oblique shock waves forms on the cowl lip exterior. Table C-2 lists inlet performance metrics of the inlet as obtained from SUPIN and the CFD simulations. Overall good agreement was observed between SUPIN and CFD simulations.

TABLE C-2.—CASES FOR AXISYMMETRIC PITOT INLETS FOR M_0 = 1.4, 1.7, AND 2.0

M_0	h_0 (ft)	W_{C2} (lbm/s)	A_{cap} (ft^2)	Method	M_2	W_2 (lbm/s)	p_{t2}/p_{t0}	C_{Dwave}
1.4	50000	413	8.9047	SUPIN	0.6632	140.51	0.9556	0.05377
				CFD	0.6642	140.24	0.9547	0.05242
1.7	55000	383	8.8443	SUPIN	0.5810	133.26	0.8531	0.04279
				CFD	0.5812	133.10	0.8532	0.04249
2.0	60000	353	8.6669	SUPIN	0.5136	120.82	0.7190	0.04059
				CFD	0.5151	120.86	0.7188	0.04207

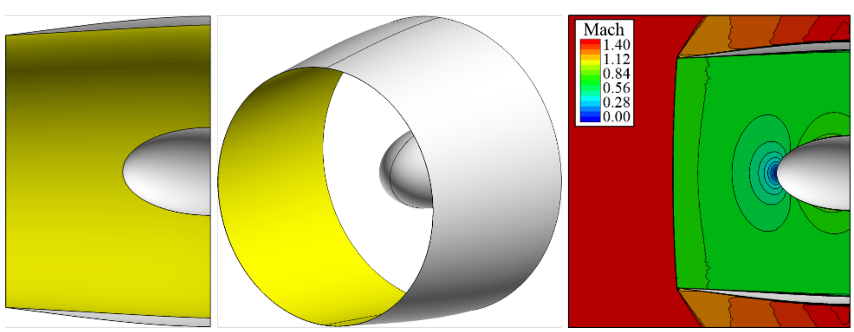

Figure C-4.—Mach 1.4 axisymmetric pitot inlet.

C.3 SUPIN.K6.M060: Mach 0.6 Three-Dimensional Pitot Inlet

This sample case involved the design of a subsonic three-dimensional pitot inlet for $M_0 = M_L = 0.60$ at an altitude of $h_0 = 30000$ ft. The engine-face diameter was $D_2 = 3.0$ ft with an elliptical spinner with a hub-to-tip ratio of $D_{hub}/D_2 = 0.3$. The design engine-face Mach number was specified to be $M_2 = 0.5$. The capture cross-section has a D-shape with the lower edge projected forward. The cowl lip dimensions yield a blunt cowl lip with $b_{clin} = b_{clex} = 0.05$ ft and these dimensions are uniform about the circumference of the capture cross-section. The elliptical cowl lips had an aspect ratio of 2. At the bottom of the capture cross-section the cowl lip angle is $\theta_{clip} = 0.0$ degrees, but about the circumference the cowl lip angle is varied to match the cowl lip angle of $\theta_{clip} = 5.0$ degrees at the top of the cross-section. The length of the throat section was $L_{thrt} / D_2 = 1.0$ with an area increase of $A_{SD}/A_1 = 1.02$. The subsonic diffuser was specified to have a length of $L_{subd} / D_2 = 2.5$. The engine face was offset below the inlet axis by $\Delta y_{EF} / D_2 = -0.5$. Figure C-5 show images of the inlet. Figure C-6 shows Mach contours on the symmetry plane from a CFD simulation for the design conditions. Some information on the inlet and performance results from SUPIN and the CFD simulation is summarized in Table C-3. SUPIN estimated a much lower inlet total pressure recovery than achieved from the CFD simulation. This seemed to be the result of SUPIN over-estimating the total pressure losses in the subsonic diffuser. This resulted in the inlet capture area being undersized. A redesign of the inlet could involve specifying Fpt2ptSD = 0.98 within the input data block for the subsonic diffuser, which results in an inlet total pressure recovery of $p_{t2}/p_{t0} = 0.9772$ and a new larger capture area of $A_{cap} = 5.5742$ ft^2.

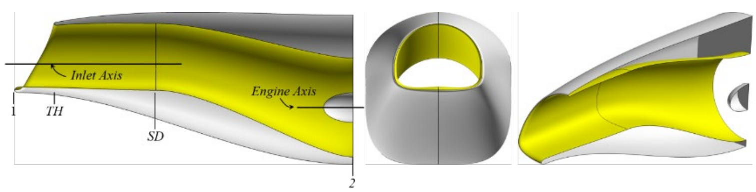

Figure C-5.—Subsonic three-dimensional pitot inlet for $M_0 = 0.6$.

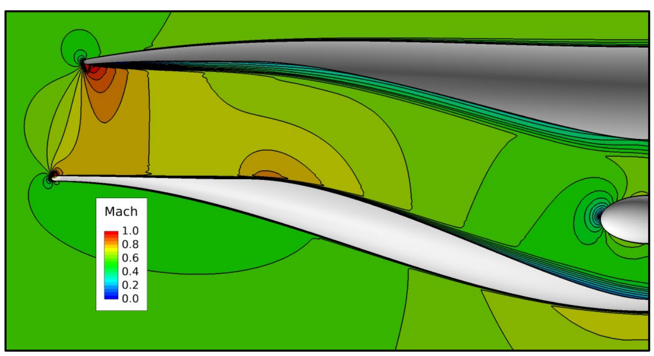

Figure C-6.—Mach number contours on the symmetry plane from a CFD simulation of the subsonic three-dimensional pitot inlet for $M_0 = 0.6$.

TABLE C-3.—COMPARISON OF INLET PERFORMANCE AS COMPUTED FROM SUPIN AND A CFD SIMULATION FOR THE THREE-DIMENSIONAL PITOT INLET

M_0	h_0 (ft)	M_2	A_{cap} (ft^2)	Method	M_2	W_2 (lbm/s)	p_{t2}/p_{t0}
0.6	30000	0.5	5.3117	SUPIN	0.5000	90.707	0.9312
				CFD	0.5091	95.344	0.9779

Appendix D.—Sample Cases for Two-Dimensional and Axisymmetric Spike External-Compression Inlets

These sample cases demonstrate the use of SUPIN for the design of axisymmetric spike and two-dimensional external-compression inlets.

D.1 SUPIN.K2.M14: Mach 1.4 External-Compression Two-Dimensional Inlet

This sample case involves an external-compression, two-dimensional single-duct inlet for $M_0 = M_L = 1.40$ and an altitude of $h_0 = 50000$ ft. This inlet was designed using the mission profile and engine model of the Supersonic Technology Concept Aeroplanes (STCA) (Ref. 1). The engine-face diameter was $D_2 = 3.625$ ft with an elliptical spinner with a hub-to-tip ratio of $D_{hub}/D_2 = 0.3$. The design engine-face corrected flow rate was specified to be $W_{C2} = 413$ lbm/s, which corresponded to an engine-face Mach number of $M_2 = 0.6632$. The external supersonic diffuser consists of a single ramp in which the Mach number at the end of the external supersonic diffuser was specified to be $M_{EX} = 1.25$. The design of the external supersonic diffuser included no supersonic spillage (i.e., $W_{spillage}/W_{cap} = 0.0$). The cowl lip was essentially sharp with an elliptic profile with a semi-minor axis length of 0.0005 ft and aspect ratio of 2. The cowl lip angle was specified to be $\theta_{clip} = 2$ degrees. The inlet was designed as an external-compression inlet with a normal shock wave at the cowl lip. The throat section was specified to have a total length of $L_{thrt} / D_2 = 0.523$ with the aft centerbody to have a slope of $\theta_{cbSD} = 0.0$ degrees. Station SD had an area ratio $A_{SD}/A_1 = 1.009$. The subsonic diffuser was had a length of $L_{subd} / D_2 = 1.5$. The vertical placement of the engine was specified such that the top surface of the subsonic diffuser at the symmetry plane was almost straight. Figure D-1 shows images of the inlet. Viscous CFD simulations were performed of the inlet using the Wind-US CFD solver. Figure D-2 shows images of the Mach number contours on the symmetry plane from a simulation near the critical operating point with the normal terminal shock wave at the cowl lip station. Table D-1 lists some properties of the inlet and the performance data obtained from SUPIN and averages at the engine face from the CFD flowfield. The dash in Table D-1 indicates that the cowl wave drag was not computed from the CFD simulation.

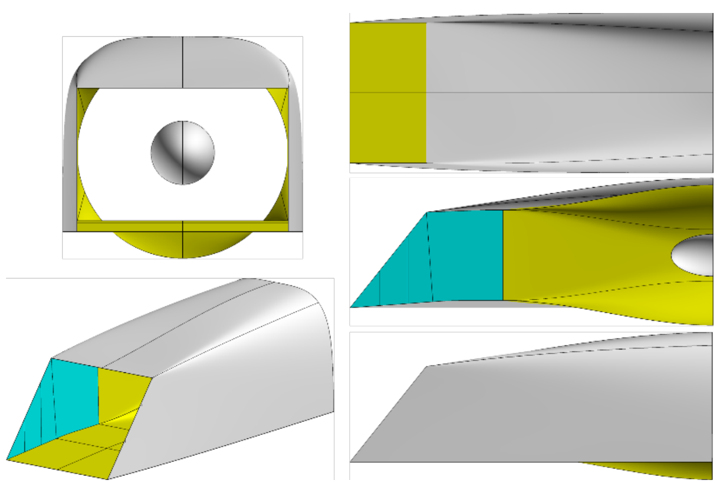

Figure D-1.—A Mach 1.4 external-compression, two-dimensional single-duct inlet.

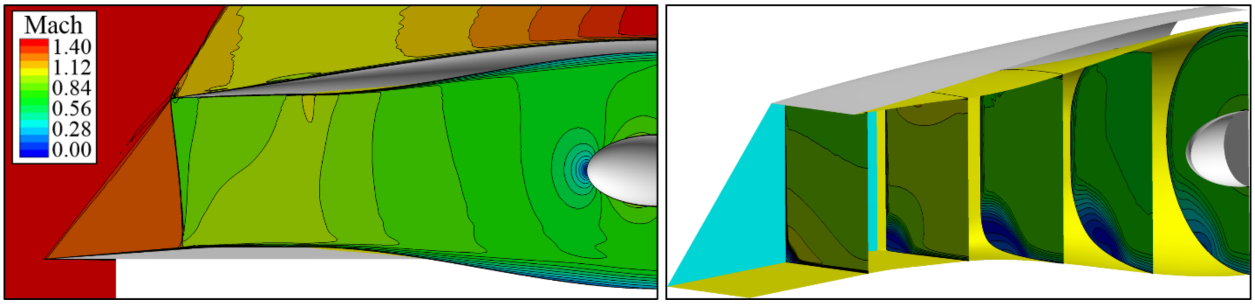

Figure D-2.—Mach number contours from a CFD simulation of a Mach 1.4 two-dimensional single-duct inlet.

TABLE D-1.—COMPARISON OF INLET PERFORMANCE FOR A MACH 1.4 TWO-DIMENSIONAL SINGLE-DUCT INLET

M_0	M_{EX}	A_{cap} (ft^2)	W_{cap} (lbm/s)	Method	M_2	W_2/W_{cap}	p_{t2}/p_{t0}	C_{Dwave}
1.40	1.25	8.95	141.22	SUPIN	0.6632	1.000	0.9785	0.1199
				CFD	0.6839	0.996	0.9547	0.1337

D.2 SUPIN.K2.M17: Mach 1.7 External-Compression Two-Dimensional Inlet

This sample case involves an external-compression, two-dimensional single-duct inlet for M_0 = M_L = 1.7 with the freestream conditions calculated using the standard atmosphere with an altitude of h_0 = 55000 ft. This inlet was designed using the mission profile and engine model of the Supersonic Technology Concept Aeroplanes (STCA) (Ref. 1). The engine-face diameter was D_2 = 3.625 ft with an elliptical spinner with a hub-to-tip ratio of D_{hub}/D_2 = 0.3. The design engine-face corrected flow rate was specified to be W_{C2} = 383 lbm/s, which corresponded to an engine-face Mach number of M_2 = 0.5810. The external supersonic diffuser consists of three stages in which the second stage is an isentropic compression stage. The Mach number at the end of the external supersonic diffuser was specified to be M_{EX} = 1.35. The design of the external supersonic diffuser included no supersonic spillage (i.e., $W_{spillage}/W_{cap}$ = 0.0). The cowl lip was essentially sharp with an elliptic profile with a semi-minor axis length of 0.0005 ft and aspect ratio of 2. The cowl lip angle was specified to be θ_{clip} = 6 degrees. The inlet was designed as an external-compression inlet with a normal shock wave at the cowl lip. The throat section was specified to have a total length of L_{thrt} / D_2 = 0.766 with the aft centerbody to have a slope of θ_{cbSD} = -5.0 degrees. A bleed slot was included at the shoulder and a bleed rate of W_{bleed}/W_{cap} = 3% was specified. Station SD was specified with an area ratio A_{SD}/A_1 = 1.12. The subsonic diffuser was specified to have a length of L_{subd} / D_2 = 1.5. The vertical placement of the engine was specified such that the top surface of the subsonic diffuser at the symmetry plane was almost straight. Figure D-3 shows images of the inlet. Viscous CFD simulations were performed of the inlet using the Wind-US CFD solver. Figure D-4 shows images of the Mach number contours on the symmetry plane from a simulation near the critical design condition. Table D-2 lists some properties of the inlet and the performance data obtained from SUPIN and averages of the CFD flowfield at the engine face.

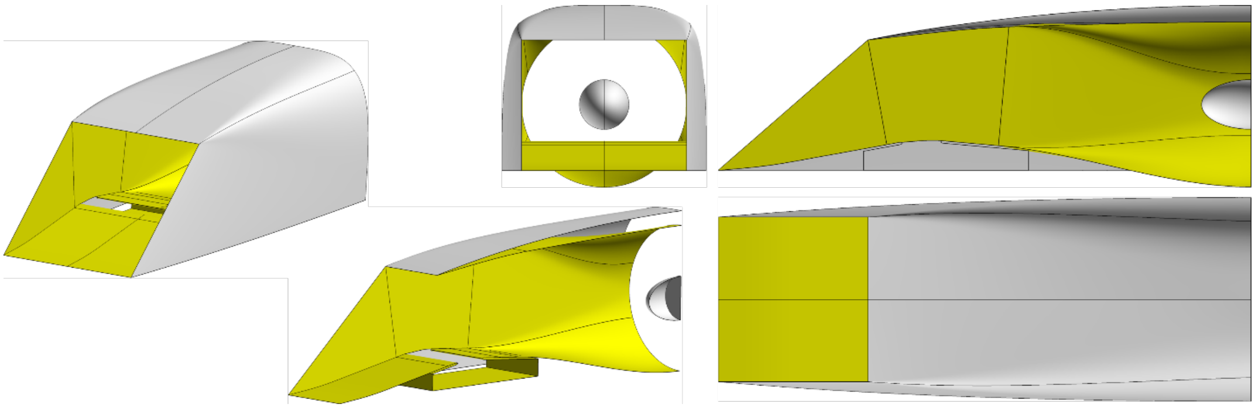

Figure D-3.—Mach 1.7 two-dimensional, single-duct external-compression inlet with a shoulder bleed slot.

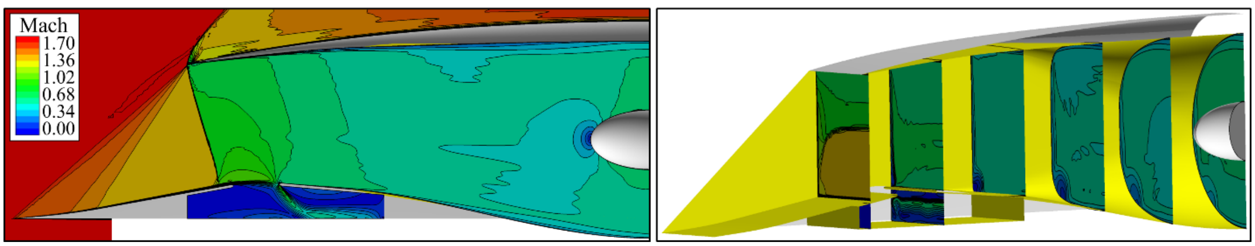

Figure D-4.—Mach 1.7 two-dimensional, single-duct external-compression inlet with a shoulder bleed slot and Mach number contours from a CFD simulation at the critical operating condition.

TABLE D-2.—COMPARISON OF INLET PERFORMANCE FOR A MACH 1.4 TWO-DIMENSIONAL SINGLE-DUCT INLET

M_0	M_{EX}	A_{cap} (ft^2)	W_{cap} (lbm/s)	Method	M_2	W_{bleed}/W_{cap}	W_2/W_{cap}	p_{t2}/p_{t0}	C_{Dwave}
1.70	1.35	10.4	156.703	SUPIN	0.5810	0.0300	0.9700	0.9446	0.0564
				CFD	0.5834	0.0314	0.9577	0.9611	0.0574

D.3 SUPIN.K2.Concorde: Mach 2 External-Compression, Two-Dimensional Inlet of the Concorde Aircraft

This sample case involves an external-compression, two-dimensional single-duct inlet that models the inlet of the Concorde aircraft. The dimensions and flow conditions for the model were obtained from data and reports available within the public domain and measurements of the Concorde inlet (Ref. 2). The local Mach number approaching the inlet was M_L = 1.915 and freestream conditions were calculated using the standard atmosphere with an altitude of h_0 = 60000 ft. The engine-face diameter was D_2 = 3.802 ft with a circular spinner with a hub-to-tip ratio of D_{hub}/D_2 = 0.314. The design engine-face Mach number was specified to be M_2 = 0.5. The external supersonic diffuser consists of three stages in which the second stage is an isentropic compression stage. The angle of the first stage was specified to be θ_{stg1} = 7.0 degrees. The Mach number at the end of the external supersonic diffuser was specified to be M_{EX} = 1.38. The design of the external supersonic diffuser included a supersonic spillage of $W_{spillage}/W_{cap}$ = 0.021 and a bleed rate of W_{bleed}/W_{cap} = 0.06. The Concorde inlet was indicated to have a square capture cross-section, which was specified through the SUPIN inputs using the input factor *Fwclip* = -1.0 to indicate the aspect ratio was unity. The cowl lip used an elliptic profile with a semi-minor axis length of 0.016 ft and aspect ratio of 4. The cowl lip angle was specified to be θ_{clip} = 12 degrees with a cowl lip exterior angle of θ_{clex} = 15 degrees. The inlet was designed as an external-compression inlet with a normal shock wave at the cowl lip. The throat section was modeled using the model described in Subsection 9.1 with K_{thrt} = 5. This throat section model placed station TH downstream of the shoulder station TS. For subsonic throat sections, it is recommended that the throat section model indicated by $K_{thrt} = 9$ as described in Subsection 8.3 be used. However, this case was first formulated before the model with $K_{thrt} = 9$ was available. The geometric throat of the inlet is near station 1 which should be the case for an external-compression inlet. The model with $K_{thrt} = 9$ essentially uses station TH as an intermediatory station between stations TS and SD rather than indicating the geometric throat of the inlet. The throat section was specified to have a total length of $L_{thrt} / D_2 = 1.127$ with the aft centerbody to have a slope of $\theta_{cbSD} = -6.10$ degrees. The throat section was specified to have a total length of $L_{thrt} / D_2 = 1.127$ with the aft centerbody to have a slope of $\theta_{cbTH} = -6.10$ degrees. Station TS was located at the shoulder and an area ratio of $A_{TS}/A_1 = 1.0$ was specified. The area ratios at stations TH and SD were $A_{TH}/A_1 = 1.07$ and $A_{SD}/A_{TH} = 1.035$. The subsonic diffuser was specified to have a length of $L_{subd} / D_2 = 2.0$. The shape of the throat section and subsonic diffuser, including the vertical placement of the engine face, was established through comparison with images of the Concorde inlet. The Concorde inlet featured a wide bleed slot, which SUPIN was able to approximate using the input data block with DataID = 15. Figure D-5 shows images of the inlet. Viscous CFD simulations were performed of the inlet using the Wind-US CFD solver. Figure D-6 shows images of the Mach number

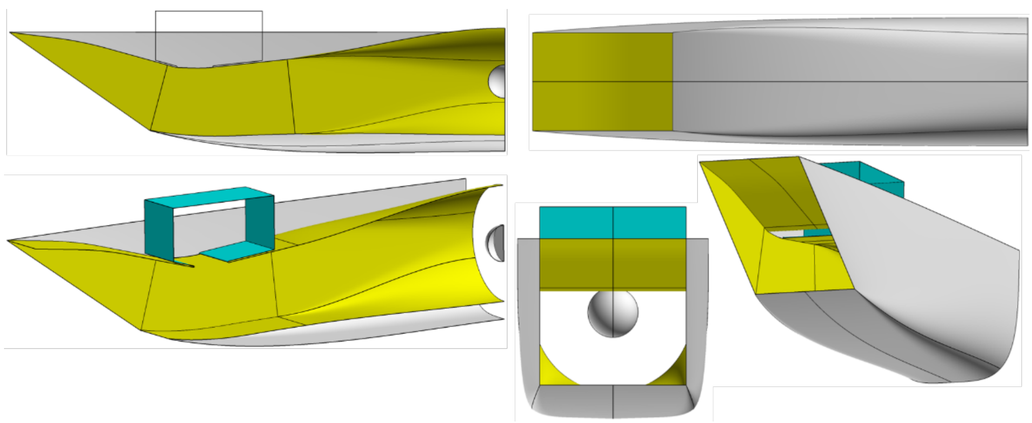

Figure D-5.—Two-dimensional, external-compression inlet model of the Concorde inlet for Mach 1.915.

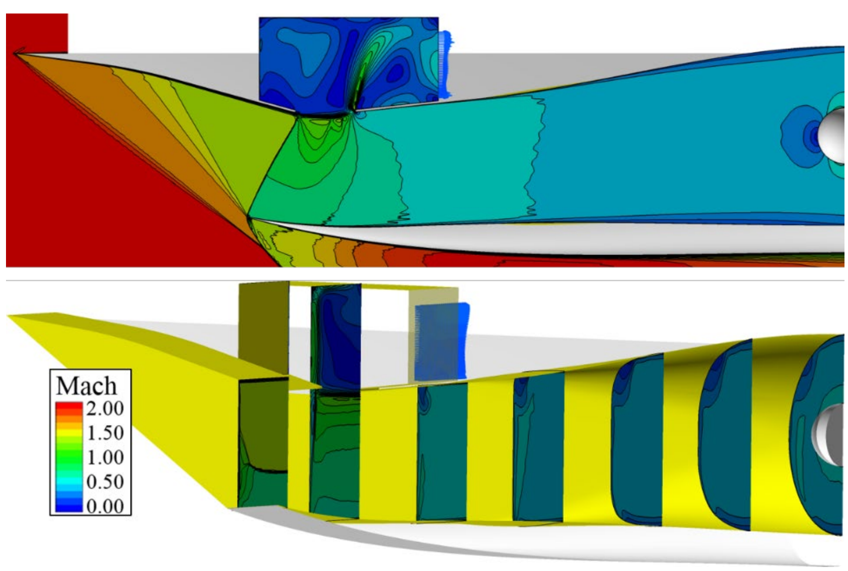

Figure D-6.—Mach number contours on the symmetry plane and on axial stations for the model of the Concorde inlet.

TABLE D-3.—COMPARISON OF INLET PERFORMANCE FOR THE SUPERSONIC, TWO-DIMENSIONAL INLET OF THE CONCORDE AIRCRAFT

M_0	M_{EX}	A_{cap} (ft^2)	W_{cap} (lbm/s)	Method	M_2	$W_{spillage}/W_{cap}$	W_{bleed}/W_{cap}	W_2/W_{cap}	p_{t2}/p_{t0}	C_{Dwave}
1.915	1.38	11.399	152.15	Test	0.5	0.021	0.06	0.919	0.96	-
				SUPIN	0.5000	0.021	0.06	0.919	0.9283	0.08305
				CFD	0.4668	0.0375	0.071	0.8915	0.9538	-

contours on the symmetry plane and along axial stations from a simulation with the terminal shock wave near the critical operating condition. The engine-face Mach number for this condition was $M_2 = 0.4668$, which was less than the design condition of $M_2 = 0.5$. This suggests that the capture area of the inlet was too small. The terminal shock wave exhibits the strong oblique shock wave structure reported for the Concorde inlet. The CFD simulation resulted in a total pressure recovery of $p_{t2}/p_{t0} = 0.9538$, which is close to the reported critical recovery of $p_{t2}/p_{t0} = 0.96$ for the Concorde inlet. In the simulation, the bleed flow exited the bleed slot plenum at the back face of the plenum, which is illustrated by the blue arrows. It was reported for the Concorde inlet that the bleed flow into the bleed slot featured a supersonic jet into the bleed plenum, which is captured in the CFD simulation shown in Figure D-6. Table D-3 lists some properties of the inlet and the performance data obtained from SUPIN and averages of the CFD flowfield at the engine face.

D.4 SUPIN.K3.M14: Mach 1.4 Axisymmetric Spike, External-Compression Inlet

This sample case involves an external-compression, axisymmetric spike inlet for $M_0 = M_L = 1.4$ at an altitude of $h_0 = 50000$ ft. This inlet was designed using the mission profile and engine model of the Supersonic Technology Concept Aeroplanes (STCA) (Ref. 1). The engine-face diameter was $D_2 = 3.625$ ft with an elliptical spinner with a hub-to-tip ratio of $D_{hub}/D_2 = 0.3$. The design engine-face corrected flow rate was specified to be $W_{C2} = 413$ lbm/s, which corresponded to an engine-face Mach number of $M_2 = 0.6632$. The external supersonic diffuser consists of a single stage cone in which the Mach number at the end of the external supersonic diffuser was specified to be $M_{EX} = 1.2825$, which resulted in a cone with a half-angle of $\theta_{stg1} = 15.149$ degrees. The choice of M_{EX} was based on the desire that the maximum diameter of the centerbody within the throat section matched the diameter of the engine-face hub. The design of the external supersonic diffuser included no supersonic spillage ($W_{spillage}/W_{cap} = 0.0$). The cowl lip was essentially sharp with an elliptic profile with a semi-minor axis length of 0.0005 ft and aspect ratio of 2. The cowl lip angle was specified to be $\theta_{clip} = \theta_{clin} = 4.0$ degrees. This angle was greater than the local flow angle of 2.56 degrees but needed to provide a monotonically decreasing slope of the cowl interior and a monotonically increasing cross-section area through the throat section. The inlet was designed as an external-compression inlet with a normal shock wave at the cowl lip. The throat section was specified to have a total length of $L_{thrt} / D_2 = 0.154$ with the centerbody to have a slope of $\theta_{cbSD} = 0.0$ degrees. Stations SD had an area ratio of $A_{SD}/A_1 = 1.0$. The subsonic diffuser had a length of $L_{subd} / D_2 = 0.5$. The inlet included four support struts. Figure D-7 shows images of the inlet. Viscous CFD simulations were performed of the inlet using the Wind-US CFD solver. The multi-block, structured CFD grid was generated by SUPIN. Figure D-8 shows images of the Mach number contours on the symmetry plane and along axial stations from a CFD simulation near the critical design condition. The normal terminal shock wave is shown at the cowl lip plane. Table D-4 lists some properties of the inlet and the performance data obtained from SUPIN and averages of the CFD flowfield at the engine face.

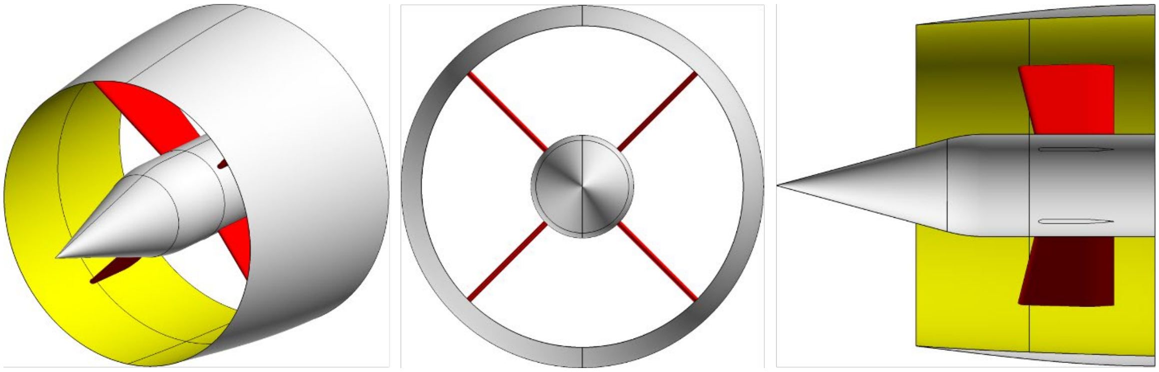

Figure D-7.—The Mach 1.4 external-compression, axisymmetric spike inlet.

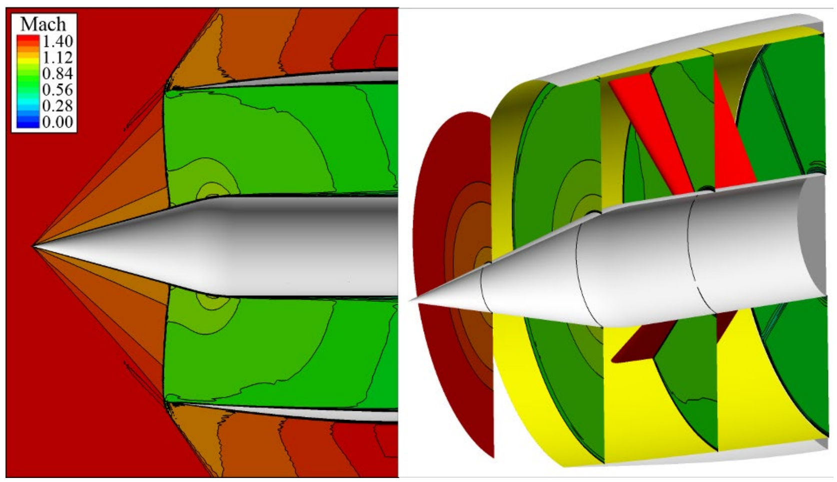

Figure D-8.—Mach number contours on the symmetry plane and axial stations through the Mach 1.4 axisymmetric spike inlet.

TABLE D-4.—COMPARISON OF INLET PERFORMANCE FOR A MACH 1.4 EXTERNAL-COMPRESSION, AXISYMMETRIC SPIKE INLET

M_0	M_{EX}	A_{cap} (ft^2)	W_{cap} (lbm/s)	Method	M_2	W_2/W_{cap}	p_{t2}/p_{t0}	C_{Dwave}
1.40	1.2825	9.15	144.382	SUPIN	0.6667	1.0000	0.9793	0.04422
				CFD	0.6683	0.9934	0.9756	0.04384

D.5 SUPIN.K3.M17 Inlet: Mach 1.7 Axisymmetric Spike, External-Compression Inlet

This sample case involves an external-compression, axisymmetric spike inlet with a freestream Mach number of $M_0 = M_L = 1.7$ at an altitude of $h_0 = 55000$ ft. This inlet was designed using the mission profile and engine model of the Supersonic Technology Concept Aeroplanes (STCA) (Ref. 1). The engine-face diameter was $D_2 = 3.625$ ft with an elliptical spinner with a hub-to-tip ratio of $D_{hub}/D_2 = 0.3$. The design engine-face corrected flow rate was specified to be $W_{C2} = 383$ lbm/s, which corresponded to an engine-face Mach number of $M_2 = 0.5810$. The external supersonic diffuser consists of three stages. The first stage was specified to have no supersonic spillage ($W_{spillage}/W_{cap} = 0.0$) and a conical angle of $\theta_{stg1} = 15$ degrees. The second stage was an isentropic stage whose Mach waves focus onto the cowl lip. The Mach number at the end of the external supersonic diffuser was specified to be $M_{EX} = 1.38$. The cowl lip was essentially sharp with an elliptic profile with a semi-minor axis length of 0.0005 ft and aspect ratio of 2. The cowl lip angle was specified to be aligned with the local flow angle with $\theta_{clip} = \theta_{clin} = 8.106$ degrees. The inlet was designed as an external-compression inlet with a normal shock wave at the cowl lip. The throat section was specified to have a total length of $L_{thrt} / D_2 = 0.254$ with the aft centerbody to have a slope of $\theta_{cbSD} = -2.0$ degrees. Station SD had an area ratio $A_{SD}/A_1 = 1.0237$, which was intended to provide a linearly decreasing Mach number through the throat section. The engine face was positioned at x2 = 4.0 ft, which resulted in the subsonic diffuser having a length of $L_{subd} / D_2 = 0.8$ and an equivalent conical angle of $\theta_{eq} = 3.465$ degrees. The inlet contained four support struts off-set from the vertical by 45 degrees and equally spaced about the circumference of the inlet. The centerbody contained a constant diameter segment ahead of the engine face to allow for translation of the centerbody for off-design conditions. Images of the inlet geometry are provided in Figure D-9. Viscous CFD simulations were performed of the inlet using the Wind-US CFD solver. Figure D-10 shows images of the Mach number contours on the axisymmetric plane from a CFD simulation at the Mach 1.7 critical design condition ($W_{C2} \approx 383$ lbm/s). The normal terminal shock wave is shown at the cowl lip plane. Table D-5 lists some properties of the inlet and the performance data obtained from SUPIN and averages of the CFD flowfield at the engine face.

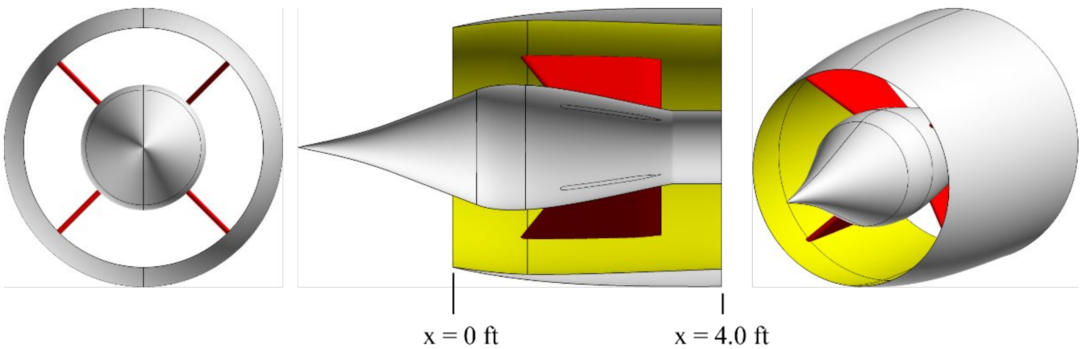

Figure D-9.—The external-compression, axisymmetric spike inlet for Mach 1.7.

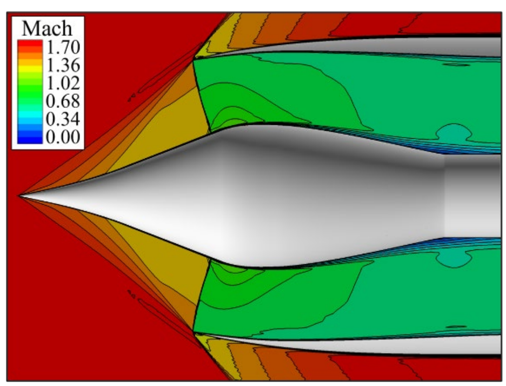

Figure D-10.—Mach number contours on a symmetry plane through the Mach 1.7 axisymmetric spike inlet.

TABLE D-5.— COMPARISON OF INLET PERFORMANCE FOR A MACH 1.7 EXTERNAL-COMPRESSION, AXISYMMETRIC SPIKE INLET

M_0	M_{EX}	A_{cap} (ft^2)	W_{cap} (lbm/s)	Method	M_2	W_2/W_{cap}	p_{t2}/p_{t0}	C_{Dwave}
1.7	1.38	9.96	150.073	SUPIN	0.5810	1.0000	0.9598	0.06106
				CFD	0.5844	0.9945	0.9552	0.06295

D.6 SUPIN.K3.M166.LBSS: Gulfstream Low-Boom Single-Stream (LBSS) Inlet

This sample case models the Mach 1.7 Gulfstream Low-Boom Single-Stream (LBSS) axisymmetric spike, external-compression inlet that was tested in the NASA Glenn 8x6-foot supersonic wind tunnel during 2010 and 2011 (Refs. 3 and 4). The geometry of the inlet was specified with axial and radial coordinates for the planar profiles of the centerbody and the cowl interior, as mentioned in Subsection 4.15. SUPIN is used in geometry mode with K_{mode} = 1 to model the LBSS inlet. The external supersonic diffuser had an initial cone angle of θ_{stg1} = 13.65 degrees and a planar profile that created a distributed or relaxed field of Mach waves rather than being focused on the cowl lip. This reduced the flow angle at the cowl lip such that a zero-cowl lip interior angle (θ_{clin} = 0 deg) could be used to minimize cowl wave drag. The cowl lip was essentially sharp with an elliptic profile with a semi-minor axis length of b_{clin} = 0.001 ft and aspect ratio of 4. Station TS was located at the shoulder and the resulting area ratio was A_{TH}/A_1 = 0.9616. The slope of the centerbody downstream of the shoulder was θ_{cbTH} = -5.023 degrees. Station SD was at an area ratio A_{SD}/A_1 = 1.0308. The inlet included four support struts. The geometry inputs for the struts were obtained from drawings of the struts. Figure D-11 shows views of the inlet.

Viscous CFD simulations were performed using the Wind-US CFD solver and a flow domain that contained the starboard half of the inlet with symmetry assumed. SUPIN generated the three-dimensional, multi-block CFD grid that included the struts. The freestream conditions were selected to match the conditions of a test in the NASA Glenn 8x6 supersonic wind tunnel. The conditions were a Mach number of M_0 = 1.670, a total pressure of p_{t0} = 21.658 psi, and total temperature of T_{t0} = 634.93 °R. Figure D-12 shows an image of the Mach number contours on the symmetry plane of the inlet at the critical condition of maximum total pressure recovery. The terminal shock wave is curved in the downstream direction at the shoulder and some local acceleration of the flow is observed at the shoulder. The inlet performance from the CFD simulation is presented in Table D-6 along with the results from the wind-tunnel test.

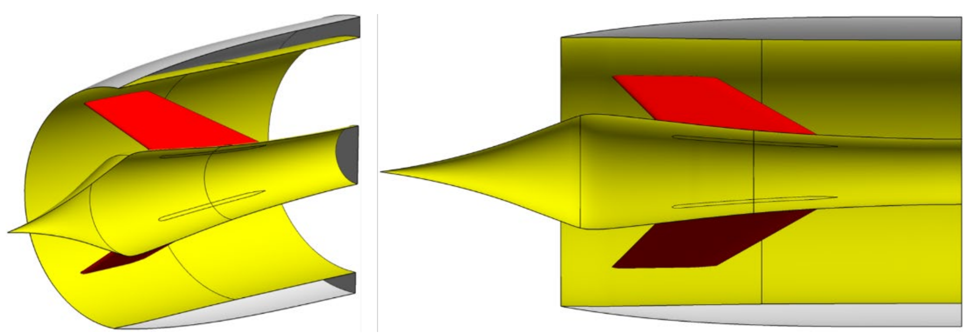

Figure D-11.—Gulfstream Low-Boom Single-Stream (LBSS) external-compression, axisymmetric spike inlet for Mach 1.7.

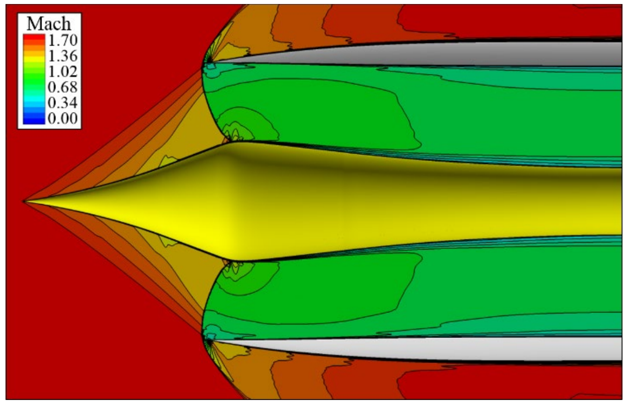

Figure D-12.—Mach number contours on the symmetry plane through the Gulfstream LBSS inlet at Mach 1.664.

TABLE D-6.—CASE K3.M166.LBSS FOR THE MACH 1.664 GULFSTREAM LOW-BOOM SINGLE-STREAM (LBSS) AXISYMMETRIC SPIKE INLET

M_0	θ_{stg1} (deg)	M_{EX}	A_{cap} (ft^2)	θ_{cbSD} (deg)	L_{subd} / D_2	M_2	D_2 (ft)	D_{hub}/D_2
1.664	13.65	-	0.7870	-6.783	1.010	-	0.9793	0.2479
			W_{cap} (lbm/s)	Method	M_2	W_2/W_{cap}	p_{t2}/p_{t0}	C_{Dwave}
			31.4339	Test	---	---	0.9470	--
				CFD	0.6735	0.988	0.9389	0.0927

References

1. Berton, J. J., Huff, D. L., Seidel, J. A., and Geiselhart, K. A., “Supersonic Technology Concept Aeroplanes for Environmental Studies,” AIAA Paper 2020-0263, January 2020.
2. Slater, J. W., “A Study of the Internal Aerodynamics of the Concorde Inlet,” AIAA Paper 2020-3770, August 2020.
3. Conners, T. R. and Wayman, T. R., “The Feasibility of High-Flow Nacelle Bypass for Low Sonic Boom Propulsion System Design,” AIAA-2011-3797, June 2011.
4. Hirt, S. M., Chima, R. V., Vyas, M. A., Conners, T. R., Wayman, T. R., and Reger, R. W., “Experimental Investigation of a Large-Scale Low-Boom Inlet Concept,” AIAA-2011-3796, June 2011.

Appendix E.—Sample Cases for Mixed-Compression Inlets

These sample cases demonstrate the use of SUPIN for the design of axisymmetric spike and two-dimensional mixed-compression inlets.

E.1 SUPIN.K2.M30: Mach 3.0 Two-Dimensional, Mixed-Compression Inlet

This sample case involved the design of a two-dimensional, mixed-compression inlet using methods of characteristics. The Mach number approaching the inlet is $M_0 = M_L = 3.0$ with the freestream corresponding to an altitude of $h_0 = 70000$ ft from the Standard Atmosphere model. The engine face diameter was $D_2 = 4.0$ ft with an axisymmetric spinner with an elliptic profile with an aspect ratio of 2. The ratio of the diameter of the spinner at the engine face to the diameter of the engine face was $D_{hub}/D_2 = 0.35$. The engine-face Mach number was specified to be $M_2 = 0.2$. The external supersonic diffusers of the inlet consisted of three stages with the second stage being an isentropic stage. The angle of the first stage was specified to be $\theta_{stg1} = 5.0$ degrees. The Mach number at the end of the external supersonic diffuser was specified to be $M_{EX} = 2.505$ to yield a supersonic compression split of 50% external and 50% internal supersonic compression. The design of the external supersonic diffuser included no supersonic spillage (i.e., $W_{spill}/W_{cap} = 0.0$). The aspect ratio of the capture cross-section was specified to be $w_{clip} / D_2 = 1.0$. The cowl lip was essentially sharp with an elliptic profile with a semi-minor axis length of 0.0005 ft and aspect ratio of 2. The cowl lip angle was specified to be $\theta_{clip} = \theta_{clin} = 1.2$ degrees, which resulted in a static pressure rise across the cowl shock of 1.785. The method-of-characteristics were used to design the isentropic section of the external supersonic diffuser and the throat cowl interior profile. The centerbody profile in the internal supersonic diffuser was specified to have the length of the shoulder to be $\Delta x_{cbsh} / D_2 = 0.15$ with the aft centerbody to have a slope of $\theta_{cbTH} = -5.0$ degrees. The length from the shoulder to station TH on the centerbody was specified to be $L_{shTH} / D_2 = 0.4$. The length from station TH to station SD on the centerbody was specified to be $L_{THSD} / D_2 = 1.0$. The methods-of-characteristics solution established the slope at the shoulder such that the cowl shock wave was cancelled at the shoulder. The Mach number on the centerbody at the downstream side of the cancellation was Mach = 2.122. The Mach number on the centerbody at station TH was specified to be $M_{cbTH} = 1.3$. A linear distribution of the Mach number on the centerbody was assumed between the shoulder and station TH. This provided a boundary condition along the centerbody for the methods-of-characteristics. A streamline-tracing created the profile of the throat cowl interior from the cowl lip to station TH on the cowl interior. The area ratio between stations TH and SD was specified to be $A_{SD}/A_{TH} = 1.02$. The subsonic diffuser was specified to have a length of $L_{subd} / D_2 = 3.0$. The throat section did not incorporate any smoothing of the shoulder or adjustment of the cowl interior for the boundary layer (i.e., $F_{cbds} = 0.0$ and $F_{cwds} = 0.0$). Figure E-1 shows images of the inlet. The characteristic net from the MOC solution for the internal supersonic diffuser is shown in the top image of Figure E-2. The middle image shows the Mach number contours for the planar flowfield through the internal supersonic diffuser from the MOC solution. As a means of verifying the MOC method, a planar inviscid CFD simulation was performed with a flow domain with supersonic outflow specified at station SD. The bottom images of Figure E-2 shows the Mach number contours through the internal supersonic diffuser. Some small differences from the MOC solution are noticeable in the image of the CFD solutions, but overall, the images are similar and Mach 1.3 flow is created within the throat section downstream of station TH. SUPIN estimated the total pressure recovery at station TH to be $p_{tTH}/p_{t0} = 0.9753$. From the CFD simulation, the average Mach number at station TH was $M_{TH} = 1.286$ with a recovery of $p_{tTH}/p_{t0} = 0.9745$.

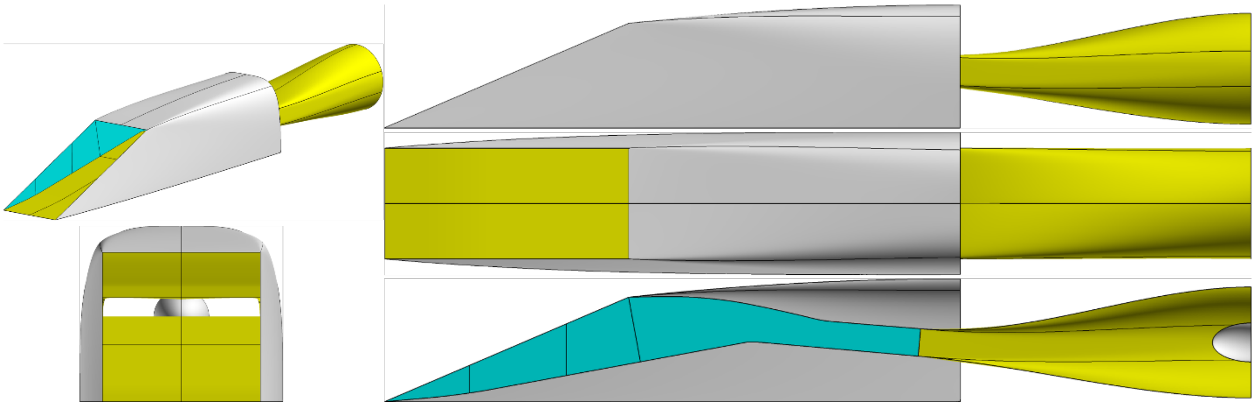

Figure E-1.—A Mach 3 two-dimensional, mixed-compression inlet designed using the method-of-characteristics.

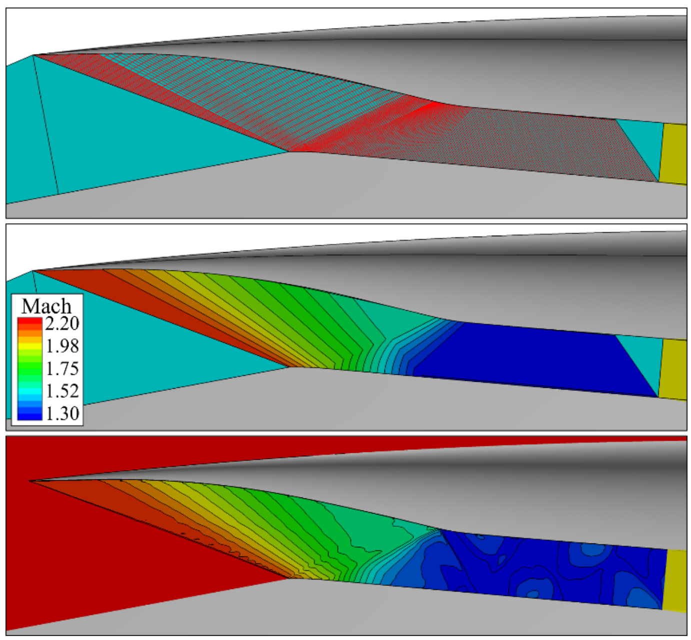

Figure E-2.—Characteristic net (top) and Mach number contours from the MOC solution (middle) and inviscid CFD simulation (bottom) for the Mach 3 two-dimensional, mixed-compression inlet.

E.2 SUPIN.K3.M30: Mach 3 Axisymmetric Spike, Mixed-Compression Inlet

This sample case involved the design of an axisymmetric spike, mixed-compression inlet for $M_0 = 3.0$ using the method-of-characteristics. The freestream corresponding to an altitude of $h_0 = 70000$ ft from the Standard Atmosphere model. The engine face had a diameter of $D_2 = 3.833$ ft. The centerbody covered the hub of the engine face with a hub-to-top ratio of $D_{hub}/D_2 = 0.365$. The engine-face Mach number was specified to be $M_2 = 0.2$. The inlet had an external supersonic diffuser with three stages with an isentropic second stage. The first stage cone was specified to have a semi-vertex angle of $\theta_{stg1} = 10$ degrees and its conical shock wave was specified to be focused on the cowl lip for no supersonic spillage (i.e., $W_{spill}/W_{cap} = 0.0$). The external supersonic diffuser decelerated the flow to a Mach number of $M_{EX} = 2.503$ to yield a supersonic compression split of 50% external and 50% internal supersonic compression. The cowl lip was essentially sharp with an elliptic profile with a semi-minor axis length of 0.0005 ft and aspect ratio of 2.

The cowl lip angle was specified to be $\theta_{clip} = \theta_{clin} = 1.4$ degrees, which resulted in a static pressure rise across the cowl shock of 1.794. The method-of-characteristics were used to design the isentropic section of the external supersonic diffuser and the throat cowl interior profile. The centerbody profile in the internal supersonic diffuser was specified to have the length of the shoulder to be $\Delta x_{cbsh} / D_2 = 0.1345$ with the aft centerbody to have a slope of $\theta_{cbTH} = -8.0$ degrees. The shoulder of the centerbody included a 9.463-degree deflection that cancelled the cowl shock wave. The length from the shoulder to station TH on the centerbody was specified to be $L_{shTH} / D_2 = 0.15$. The length from station TH to station SD on the centerbody was specified to be $L_{THSD} / D_2 = 0.2$. The Mach number on the centerbody at the downstream side of the cancellation was Mach = 2.075. The Mach number on the centerbody at station TH was specified to be $M_{cbTH} = 1.25$. A linear distribution of the Mach number on the centerbody was assumed between the shoulder and station TH. This provided a boundary condition along the centerbody for the methods-of-characteristics. A streamline-tracing created the profile of the throat cowl interior from the cowl lip to station TH on the cowl interior. The area ratio between stations TH and SD was specified to be $A_{SD}/A_{TH} = 1.01$. The subsonic diffuser was specified to have a length of $L_{subd} / D_2 = 1.0$. The throat section did not incorporate any smoothing of the shoulder or adjustment of the cowl interior for the boundary layer (i.e., $F_{cbds} = 0.0$ and $F_{cwds} = 0.0$). Figure E-3 shows images of the inlet. The characteristic net from the MOC solution for the internal supersonic diffuser is shown in the top image of Figure E-4. The middle image shows the Mach number contours for the planar flowfield through the internal supersonic diffuser from the MOC solution. As a means of verifying the MOC method, a planar inviscid CFD simulation was performed with a flow domain with supersonic outflow specified at station SD. The bottom images of Figure E-4 shows the Mach number contours through the internal supersonic diffuser. Some small differences from the MOC solution are noticeable in the image of the CFD solutions, but overall, the images are similar and Mach 1.25 flow is created within the throat section downstream of station TH. SUPIN estimated the total pressure recovery at station TH to be $p_{tTH}/p_{t0} = 0.9823$. From the CFD simulation, the average Mach number at station TH was $M_{TH} = 1.204$ with a recovery of $p_{tTH}/p_{t0} = 0.9799$. The cowl interior profile within the internal supersonic diffuser had to be slightly modified to position the cowl shock wave so that it mostly cancelled. This required dthcbeg = 0.5 degrees, FNcbeg = 0.38, FNcend = 0.15, and dthcend = 0.0 degrees.

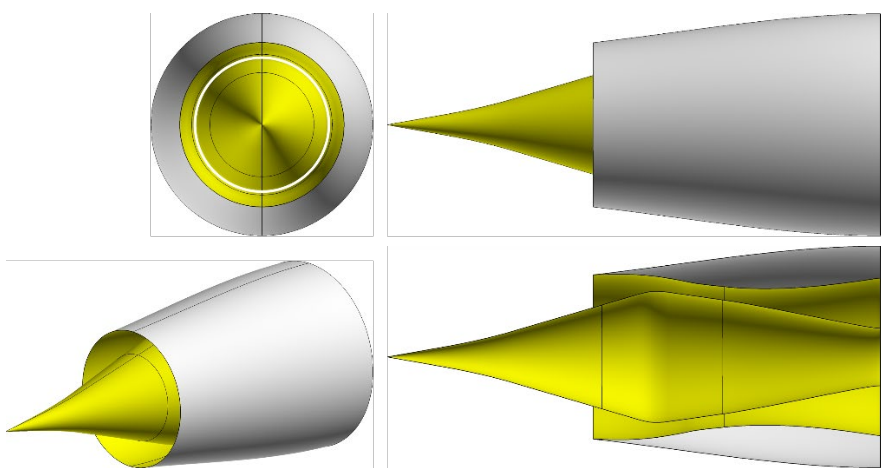

Figure E-3.—Mach 3.0 axisymmetric spike, mixed-compression inlet designed using the method-of-characteristics (MOC).

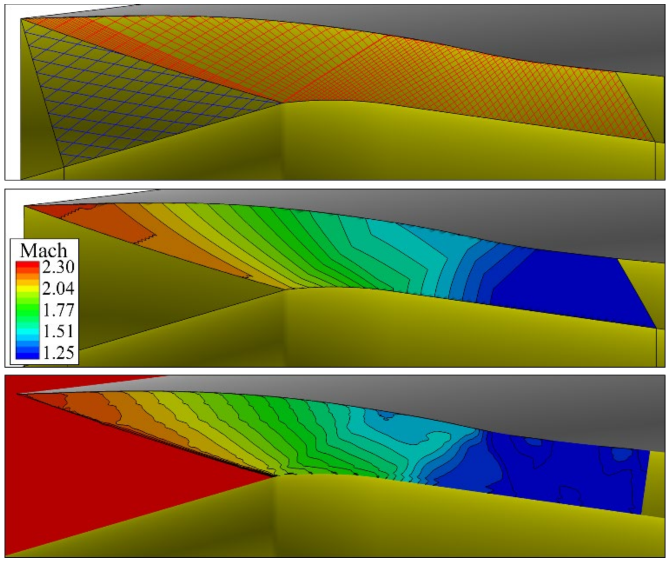

Figure E-4.—Characteristic net (top) and Mach number contours from the MOC solution (middle) and inviscid CFD simulation (bottom) for the Mach 3 axisymmetric spike, mixed-compression inlet.

E.3 SUPIN.K3.M30.NASA1507: Mach 3 NASA 1507 Axisymmetric Spike, Mixed-Compression Inlet

This sample case involved the modeling of a Mach 3 axisymmetric spike, mixed-compression inlet that was designed and tested in a wind tunnel in the 1960s at the NASA Ames Research Center (Ref. 1). Aspects of this inlet were previously discussed in Subsection 11.3 involving the specification of bleed regions within inlets. An image of the inlet was shown previously in Figure 11.4. Figure E-5 shows an image of the inlet geometry as modeled within SUPIN.

This inlet was the subject of a test case for the AIAA Propulsion Aerodynamics Workshop (PAW) in January 2023 and information and grids for the test case can be found at the webpage https://paw.larc.nasa.gov/paw-6-inlet-test-case. Reference 2 presented a summary of the modeling and CFD simulations involving the Wind-US CFD solver.

The freestream conditions were those of the wind tunnel test section and involved M_0 = 3.0, p_{t0} = 15.0 psi, and T_{t0} = 616 °R corresponding to a Reynolds number of 2.0x10^6 /ft. The diameter of the capture cross-section was D_{cap} = 20 inches, which resulted in A_{cap} = 2.182 ft^2. The diameter of the engine face was D_2 = 1.375 ft and included no spinner.

The planar profile of the centerbody and cowl interior was provided within Reference 1 in the form of (x,r) coordinates. For the SUPIN modeling, these coordinates were represented by lines and four-point NURBS curves as part of the specification of the components and entities as described in Subsection 4.15. The input data file provides an example of the input data blocks for the specification of the components and entities. Also involved in the modeling, is an input data block for transforming the entities for the forward part of the cowl as described by Subsection 14.3. Such a cowl translation was the variable-geometry used in the wind-tunnel model. The cowl lip was essentially sharp with an elliptic profile with a semi-minor axis length of 0.0001 ft and aspect ratio of 1. The cowl lip angle was specified to be θ_{clip} = θ_{clin} = 0.0 degrees. The input data file for this case also includes a block for specification of the bleed regions as discussed in Subsection 11.3. The cowl exterior geometry was approximated since the focus of the modeling and CFD simulations was the internal flow. CFD simulations were performed

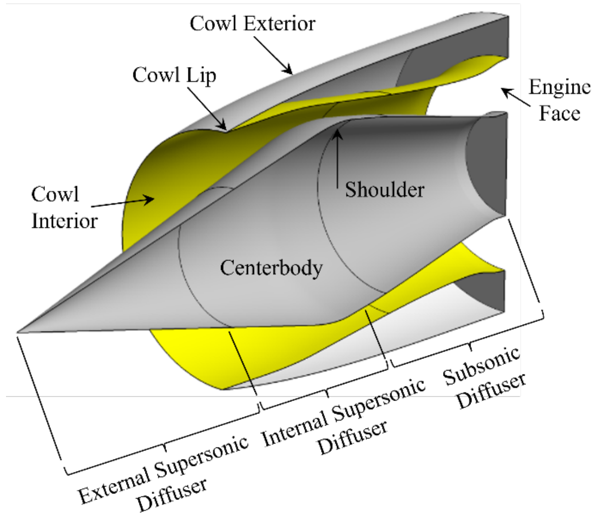

Figure E-5. Mach 3.0 NASA 1507 axisymmetric spike, mixed-compression inlet.

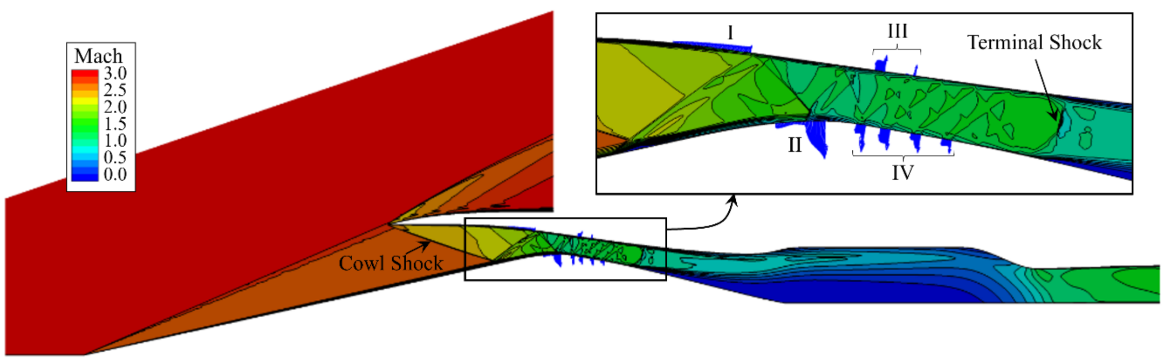

Figure E-6.—Mach number contours from a planar CFD simulation of the Mach 3.0 NASA 1507 axisymmetric spike, mixed-compression inlet.

and Figure E-6 provides some images from those simulations. The flow through the bleed regions is represented by the blue arrows indicating the bleed flow momentum vector at grid points within each bleed region. Reference 2 summarizes the CFD simulations. The images show the flow for the supercritical condition in which the terminal shock is well downstream of the throat section.

References

1. Sorensen, N. E., and Smeltzer, D. B., "Investigation of a Large-Scale Mixed-Compression Axisymmetric Inlet System Capable of High Performance at Mach Numbers 0.6 to 3.0," NASA TM X-1507, February 1968.
2. Slater, J. W., "Wind-US Simulations of the NASA 1507 Inlet Test Case," AIAA Paper 2024-0981, January 2024.

Appendix F.—Sample Cases for Two-Dimensional and Axisymmetric Spike Mahoney Ramjet Inlets

These sample cases demonstrate the use of the Mahoney throat section model as discussed in Subsection 8.5 for the design of axisymmetric spike and two-dimensional external-compression inlets.

F.1 SUPIN.K2.Mahon: Two-Dimensional Mahoney Inlets

These sample cases involved two-dimensional, external-compression inlets for Mach 2, 3, and 4 using the throat section design methods of Mahoney (Ref. 1) as described in Subsection 8.5. The altitude for the freestream was specified to be h_0 = 40000 ft. The engine faces were square with a width and height of 1.0 ft with an engine face Mach number of M_2 = 0.3 for all three inlets. The inlets had a rectangular cross-section with a constant width of 1.0 ft throughout the lengths of the inlets. The external supersonic diffusers of the inlets all consist of three stages with the second stage being an isentropic stage. Table F-1 lists the angles of the initial ramp and the supersonic Mach number at the end of the external supersonic diffusers (M_{EX}) for each inlet. The throat section uses a circular arc to turn the flow from the external supersonic diffuser to the axial direction as described in Subsection 8.5. The throat section was constructed with F_{rcirc} = 4.0. The values for the throat length F_{Lthrt} are listed in Table F-1. The Mach 2.0 inlet ends the throat section at the end of the circular arc while the Mach 3.0 and Mach 4.0 inlets add an additional diffusing isolator based on the length guidelines of Mahoney. The throat section was specified to be a constant area duct with FA_{TS}/A_1 = 1.0 and FA_{SD}/A_{TS} = 1.0. The length of the subsonic diffuser was calculated such that the equivalent conical angle was 5.0 degrees. SUPIN designed and sized the inlets and estimated the inlet flow rate and total pressure recoveries for each of the inlets, which are listed in Table F-1. Figure F-1 shows images of each of the three inlets. Viscous CFD simulations were performed using the Wind-US CFD flow solver for each of the inlets using planar CFD grids generated by SUPIN. The simulations were performed to match, as best possible, the engine face Mach number of M_2 = 0.3. Table F-1 lists the values of the engine-face Mach number, inlet flow rate, and engine-face total pressure recovery obtained from the CFD simulations. Figure F-2 shows the Mach number contours on the planar cross-section of the inlets. The image for the Mach 2.0 inlet shows that a normal terminal shock wave was formed with subsonic flow within the throat section and subsonic diffuser. At the foot of the shock, a small bifurcation exists due to a small-scale boundary layer separation region. The image for the Mach 3.0 inlet shows a terminal shock wave formed with oblique shock wave waves caused by a boundary-layer separation at foot of the shock wave. The image for the Mach 4.0 inlet shows a terminal shock wave with a much greater separated region at the foot of the terminal shock wave on the external supersonic diffuser. Further, the shock about the cowl lip is detached. The simulation at Mach 4.0 exhibited some unsteadiness, which made it difficult to match the desired M_2 = 0.3.

TABLE F-1.—TWO-DIMENSIONAL MAHONEY INLETS FOR MACH 2, 3, AND 4

M_0	θ_{stg1}	M_{EX}	FL_{thrt}	M_2	$(W_2)_{SUPIN}$ (lbm/s)	$(p_{t2}/p_{t0})_{SUPIN}$	$(M_2)_{CFD}$	$(W_2)_{CFD}$ (lbm/s)	$(p_{t2}/p_{t0})_{CFD}$
2.0	5.0	1.47	0.0	0.3	26.53	0.8775	0.3003	26.32	0.8874
3.0	5.0	1.99	4.0	0.3	78.34	0.6886	0.3027	79.66	0.6962
4.0	5.0	2.52	8.0	0.3	179.37	0.4671	0.3146	186.44	0.4686

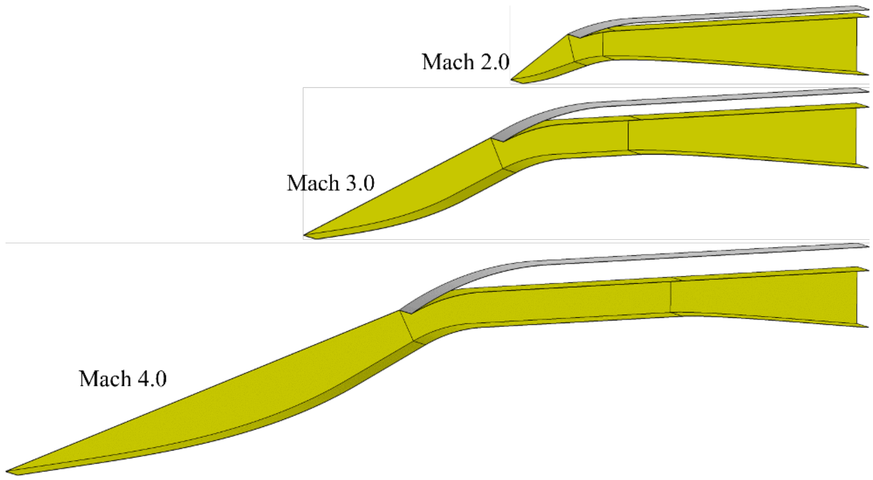

Figure F-1.—Two-dimensional Mahoney inlets for Mach 2, 3, and 4.

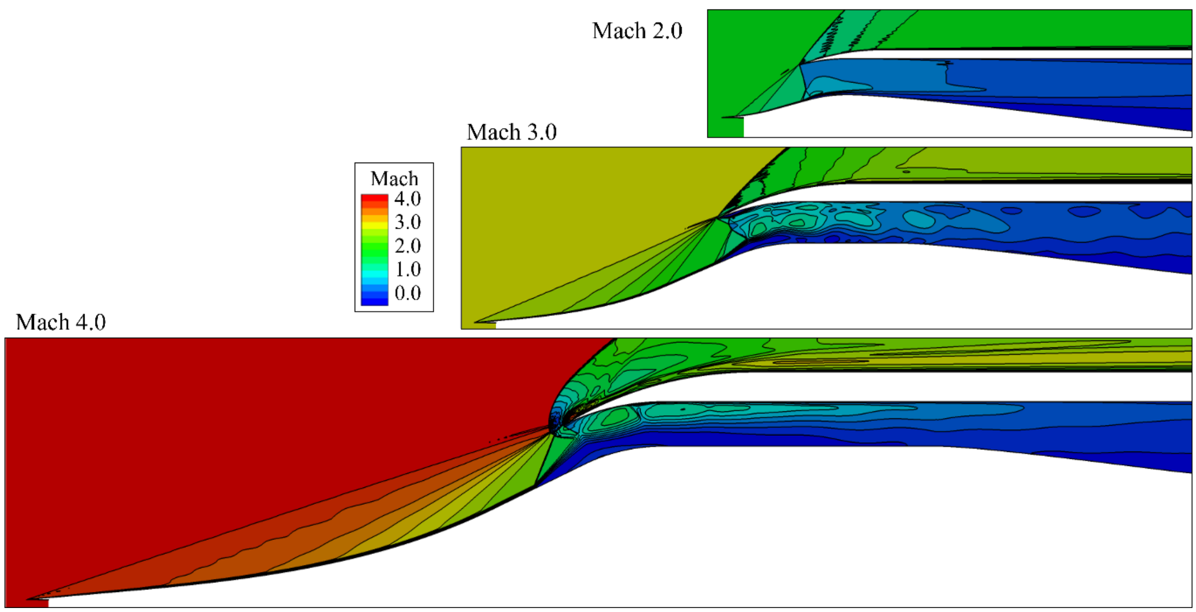

Figure F-2.—Mach number contours from Wind-US CFD simulations of the two-dimensional Mahoney inlets for Mach 2, 3, and 4.

F.2 SUPIN.K3.Mahon: Axisymmetric Spike Mahoney Inlets

These sample cases involved axisymmetric spike, external-compression inlets for Mach 2, 3, and 4 using the throat section design methods of Mahoney (Ref. 1) as described in Subsection 8.5. The altitude for the freestream was specified to be h_0 = 40000 ft. The engine faces were annular with an outer diameter of 1.0 foot. The diameter of the hub expressed as a hub-to-tip ratio for each inlet is listed in Table F-2. The engine-face Mach number was specified to be M_2 = 0.3 for all three inlets. The external supersonic diffusers of the inlets consisted of three stages with the second stage being an isentropic stage. Table F-2 lists the angle of the initial cone and the supersonic Mach number at the end of the external supersonic diffuser (M_{EX}). The throat section uses a circular arc to turn the flow from the external supersonic diffuser to the axial direction. The throat section was constructed with F_{rcirc} = 4.0. The values for the throat length F_{Lthrt} as listed in Table F-2. The Mach 2 inlet ends the throat section at the end of the circular arc while the Mach 3 and 4 inlets add an additional length for the diffusing isolator based on the length guidelines of Mahoney. The throat section was specified to be a constant area duct with FA_{TS}/A_1 = 1.0 and FA_{SD}/A_{TS} = 1.0. The length of the subsonic diffuser was calculated such that the equivalent conical angle was 5.0 degrees. SUPIN designed and sized the inlets and estimated the inlet flow rate and total pressure recoveries for each of the inlets, which are listed in Table F-2. Figure F-3 shows images of each of the three inlets. Viscous CFD simulations were performed using the Wind-US CFD flow solver for each of

TABLE F-2.—AXISYMMETRIC SPIKE MAHONEY INLETS FOR MACH 2, 3, AND 4

M_0	θ_{stg1}	M_{EX}	FL_{thrt}	M_2	D_{hub}/D_2	$(W_2)_{SUPIN}$	$(p_{t2}/p_{t0})_{SUPIN}$	$(M_2)_{CFD}$	$(W_2)_{CFD}$	$(p_{t2}/p_{t0})_{CFD}$
2.0	12.0	1.47	0.0	0.3	0.30	19.81	0.9170	0.3003	19.59	0.9121
3.0	10.0	1.99	4.0	0.3	0.70	32.40	0.7109	0.3045	31.68	0.6827

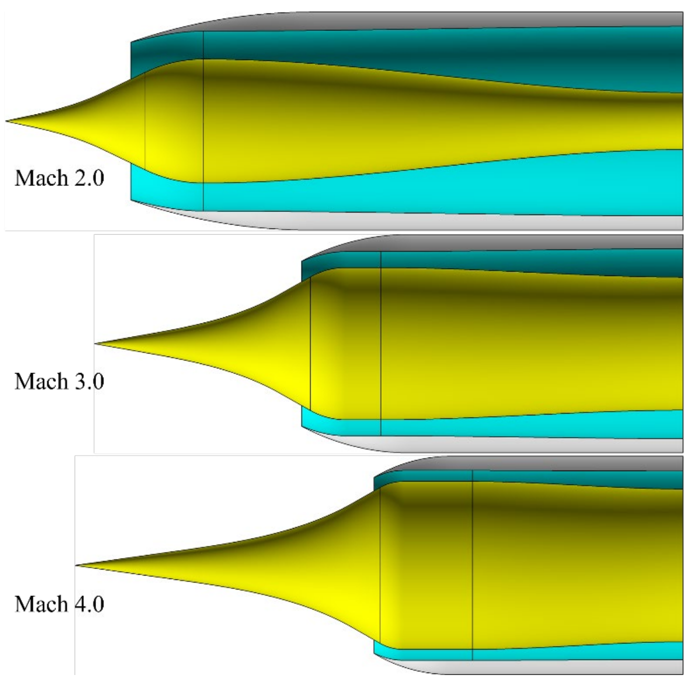

Figure F-3.—Axisymmetric spike Mahoney inlets for Mach 2, 3, and 4.

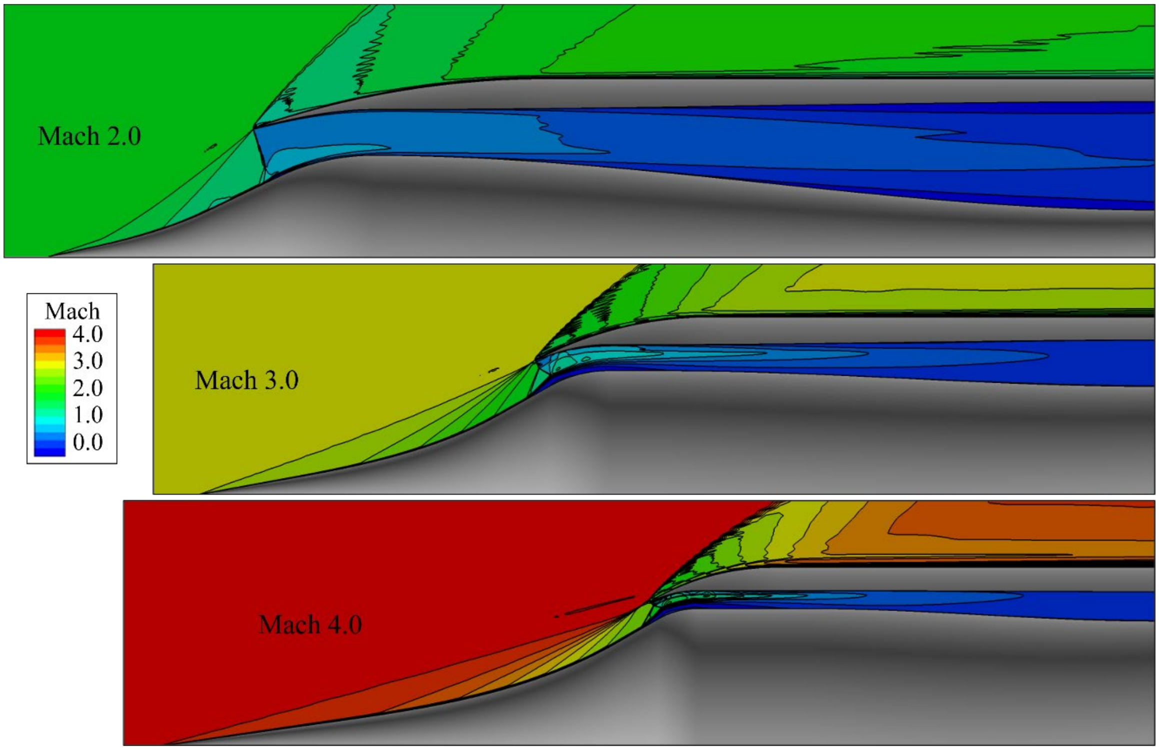

Figure F-4.—Mach number contours from Wind-US CFD simulations of the axisymmetric spike Mahoney inlets for Mach 2, 3, and 4.

the inlets using planar CFD grids generated by SUPIN. The simulations were performed to match, as best possible, the engine face Mach number of $M_2 = 0.3$. Table F-2 lists the values of the engine-face Mach number, inlet flow rate, and engine-face total pressure recovery obtained from the CFD simulations. Figure F-4 shows the Mach number contours on the planar cross-section of the inlets. The image for the Mach 2 inlet shows that a normal terminal shock wave was formed with subsonic flow within the throat section and subsonic diffuser. The image for the Mach 3.0 inlet shows a terminal shock wave formed with oblique shock wave waves caused by a boundary-layer separation at foot of the shock wave. The image for the Mach 4.0 inlet shows a terminal shock wave with a much greater separated region at the foot of the terminal shock wave on the external supersonic diffuser.

References

1. Mahoney, J. J., *Inlets for Supersonic Missiles*, AIAA Education Series, Washington, DC, 1990.

Appendix G.—Sample Cases for Streamline-Traced Inlets

Sample cases for streamline-traced inlets is provided.

G.1 SUPIN.K5.M166

This sample involves a streamline-traced, external-compression (STEX) inlet designed for flow conditions ahead of the inlet with a Mach number of M_0 = 1.664, a total pressure of p_{t0} = 21.535 psi, and total temperature of T_{t0} = 622.5 °R. These conditions correspond to those of the nominal Mach 1.7 test point of the NASA Glenn 8x6-foot supersonic wind tunnel. Figure G-1 shows views of the STEX inlet. Table G-1 summarizes some of the properties of the inlet and its performance as calculated by SUPIN and from CFD simulation. The engine face has a diameter of 0.9793 ft with an axisymmetric spinner with an elliptic profile with an aspect ratio of 2. The ratio of the diameter of the spinner at the engine face to the diameter of the engine face is 0.315. The engine corrected flow rate at the engine face corresponds to a mass-averaged Mach number of M_2 = 0.4776. The axisymmetric parent flowfield for the STEX inlet was established using the ICFA-Otto-Busemann method as discussed in Subsection 10.3. The internal angle of the leading edge was θ_{stle} = -5.0 degrees. The parent flowfield contained a leading, weak oblique shock wave followed by an isentropic supersonic compression which ended with a strong oblique shock wave with a shock wave angle of β_{stex} which decelerated the flow to M_{stex} = 0.9 and turned the flow into the axial direction. The surface of the external supersonic diffuser was created by tracing streamlines in the upstream direction through the parent flowfield starting from circular tracing curves located at the outflow of the parent flowfield. The center of the circular tracing curves was offset from the axis-of-symmetry of the parent flowfield, which resulted in a scarfed leading edge for the external supersonic diffuser. The shoulder of the inlet indicated the start of the subsonic diffuser at x = 0.387 ft. The origin of the coordinate system (x = 0.0 ft) was located at the origin of the axisymmetric parent flowfield. The circumferential black curve shown in Figure G-1 indicates the location of the shoulder and start of the subsonic diffuser. The shoulder was rounded slightly to aid the turning of the subsonic flow into the subsonic diffuser. In addition, the cross-sectional area at the shoulder was increased to account for the displacement thickness of the boundary layer. The throat also featured a “cut-out” at the bottom of the leading edge of the inlet. This cut-out allowed for greater subsonic spillage downstream of the terminal

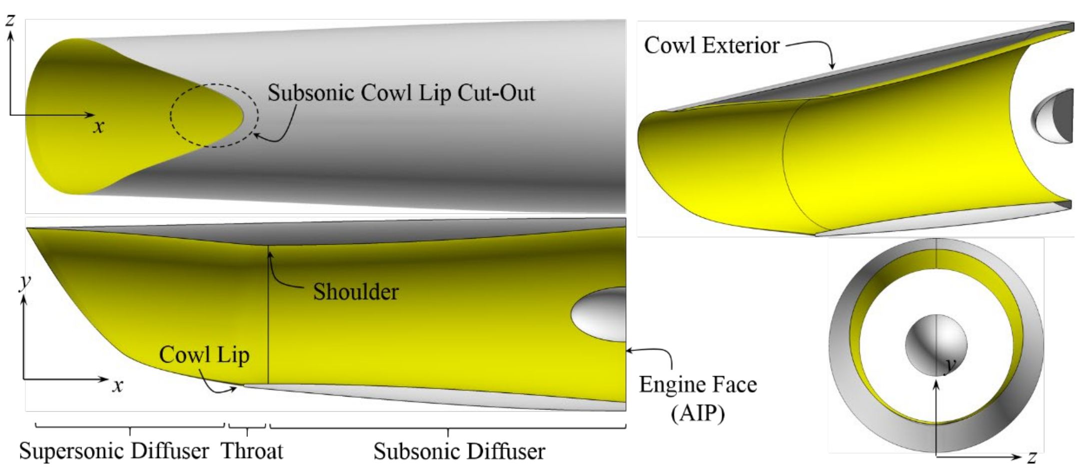

Figure G-1.—Streamline-traced, external-compression (STEX) inlet for Mach 1.664.

TABLE G-1.—STREAMLINE-TRACED, EXTERNAL-COMPRESSION INLET FOR MACH 1.664

M_0	M_{EX}	A_{cap} (ft^2)	W_{cap} (lbm/s)	Method	M_2	W_2/W_{cap}	p_{t2}/p_{t0}	C_{Dwave}
1.664	1.3	0.6006	30.427	SUPIN	0.4776	1.0000	0.9397	0.02115
				CFD	0.4772	0.9704	0.9352	0.01274

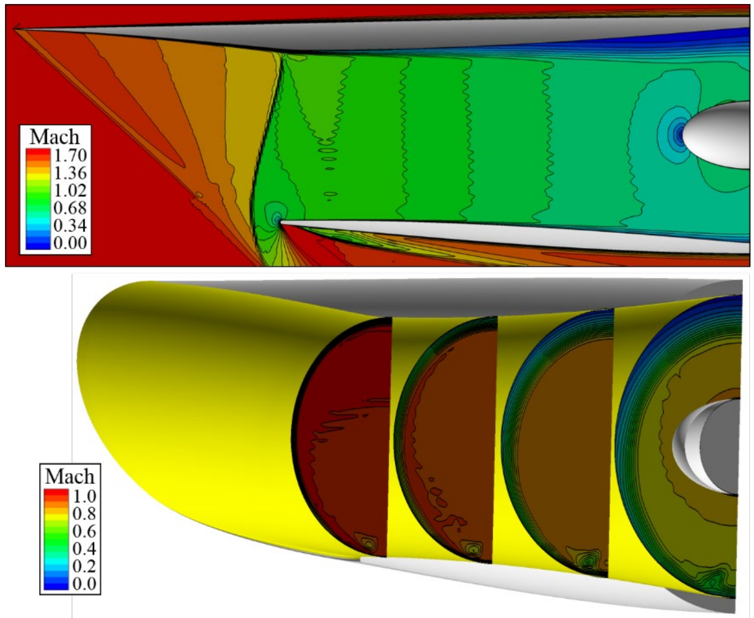

Figure G-2.—Mach number contours for a CFD simulation of the streamline-traced, external-compression (STEX) inlet for Mach 1.664.

shock wave, which allowed for the smooth positioning of the terminal shock wave with change in inlet flow rate. The subsonic diffuser was axisymmetric about the inlet axis and had a length of 2.0 ft. The equivalent conical angle for the subsonic diffuser was 2.94 degrees. The inlet had a blunter cowl lip at the cut-out than the rest of the leading edge. The cowl lip thickness was increased from 0.001 ft to 0.016 ft to improve the flow as it spilled past the cowl lip. The STEX inlet had a capture area of A_{cap} = 0.6006 square-ft and inlet length of 3.353 ft. The reference capture flow rate was computed as W_{cap} = 30.427 lbm/s. The engine flow rate (W_2) at the design conditions equaled the reference capture flow rate. The inlet total pressure recovery computed by SUPIN was p_{t2}/p_{t0} = 0.9397 and accounted for losses in the total pressure through the shock waves and subsonic viscous dissipation.

The inlet is classified as an external-compression inlet because the terminal shock wave is detached from the cowl lip and subsonic flow downstream of the terminal shock wave can spill past the cowl lip at all inlet operating conditions. However, it is recognized that the streamline-traced, external supersonic diffuser envelopes much of the exterior supersonic compression, which suggests some internal-compression character for the inlet.

A viscous CFD simulation was performed using the Wind-US CFD solver with the inlet operating near the critical condition. Figure G-2 shows images of the Mach number contours on the symmetry plane and along axial stations from a CFD simulation near the critical design condition with the resulting mass-averaged Mach number at the engine face of M_2 = 0.4772. The terminal shock wave stood ahead of the cowl lip and intersects the upper surface of the inlet slightly upstream of the shoulder. The CFD simulation resulted in a total pressure recovery of p_{t2}/p_{t0} = 0.9352 with an inlet flow rate of W_2 = 29.53 lbm/s, which indicated a subsonic spillage of 2.96% of W_{cap}.

G.2 Sample Case for Mach 2.0 Streamline-Traced, External-Compression Inlet with Bleed Slot

This sample case involved a streamline-traced, external-compression (STEX) inlet for $M_0 = M_L = 2.0$ at an altitude of $h_0 = 60000$ ft. The engine-face diameter was $D_2 = 3.625$ ft with an elliptical spinner with a hub-to-tip ratio of $D_{hub}/D_2 = 0.3$. The design engine-face corrected flow rate was specified to be $W_{C2} =$ 353 lbm/s, which corresponded to an engine-face Mach number of $M_2 = 0.5136$. The inlet was designed assuming no supersonic spillage ($W_{spillage}/W_{cap} = 0.0$) and a bleed rate of $W_{bleed}/W_{cap} = 0.05$. The axisymmetric parent flowfield for the STEX inlet was established using the ICFA-Otto-Busemann method as discussed in Subsection 10.3. The internal angle of the leading edge was $\theta_{stle} = -5.0$ degrees. The parent flowfield contained a leading, weak oblique shock wave followed by an isentropic supersonic compression which ended with a strong oblique shock wave with a shock wave angle of β_{stex} which decelerated the flow to $M_{stex} = 0.9$ and turned the flow into the axial direction. The surface of the external supersonic diffuser was created by tracing streamlines in the upstream direction through the parent flowfield starting from circular tracing curves located at the outflow of the parent flowfield. The center of the circular tracing curves was offset from the axis-of-symmetry of the parent flowfield, which resulted in a scarfed leading edge for the external supersonic diffuser. Images of the inlet are shown in Figure G-3. The shoulder of the inlet indicated the start of the subsonic diffuser at $x = 2.397$ ft. The origin of the coordinate system ($x = 0.0$ ft) was located at the origin of the axisymmetric parent flowfield. A bleed slot was integrated into the shoulder as shown in Figure G-4. The axial length of the bleed slot was 1.27 ft and extended over half of the circumference of the inlet. The bleed slot worked to match the inlet capture flow with the engine flow by removing excess inlet flow unable to be accepted by the engine. The inlet featured a “cut-out” at the bottom of the leading edge of the inlet. This cut-out allowed for greater subsonic spillage downstream of the terminal shock wave. The subsonic diffuser had a length of $L_{subd} / D_2 = 1.5$. The equivalent conical angle for the subsonic diffuser was 2.42 degrees. The inlet had a blunter cowl lip at the cut-out than the rest of the leading edge. The cowl lip thickness was increased from 0.0005 ft in the supersonic region to 0.01 ft in the subsonic spillage region to improve the flow as it

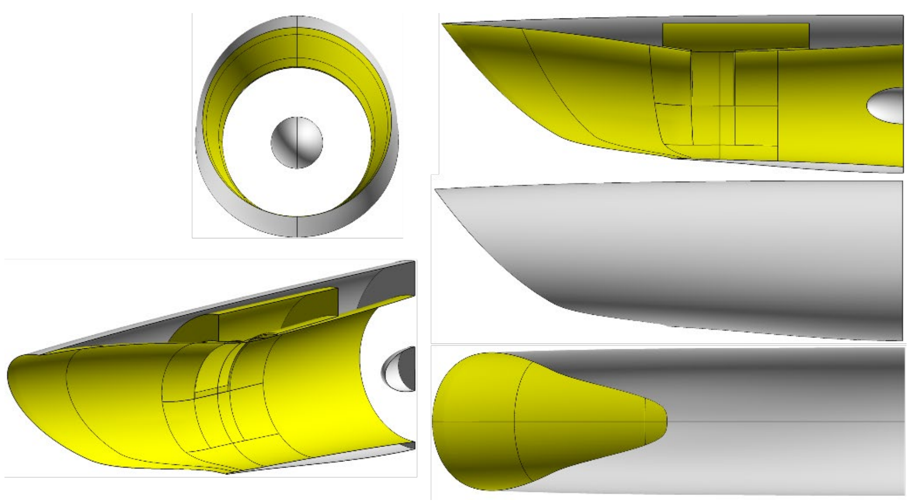

Figure G-3.—Streamline-traced, external-compression (STEX) inlet with a bleed slot for Mach 2.0.

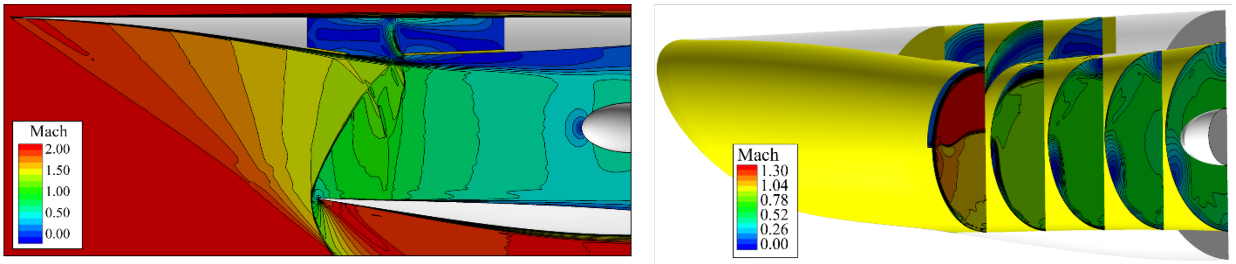

Figure G-4.—Mach number contours on the symmetry plane (left) and at stations through the inlet (right) from a Wind-US CFD simulation of the Mach 2 STEX inlet with a bleed slot.

TABLE G-2.—STREAMLINE-TRACED, EXTERNAL-COMPRESSION INLET FOR MACH 2.0

M_0	M_{EX}	A_{cap} (ft^2)	W_{cap} (lbm/s)	Method	M_2	W_2/W_{cap}	p_{t2}/p_{t0}	C_{Dwave}
2.0	1.3	12.3	164.60	SUPIN	0.5253	0.9600	0.9292	0.01244
				CFD	0.4772	0.9162	0.9495	0.01871

spilled past the cowl lip. The leading edge used an elliptical profile with an aspect ratio of 2. The STEX inlet had a capture area of A_{cap} = 12.5 ft^2 and inlet length of L_{inlet} / D_2 = 3.775. The reference capture flow rate was computed as W_{cap} = 174.25 lbm/s. The inlet total pressure recovery computed by SUPIN was p_{t2}/p_{t0} = 0.9717 and accounted for losses in the total pressure through the shock waves and subsonic viscous dissipation.

Viscous CFD simulations were performed of the inlet using the Wind-US CFD solver. The multi-block, structured CFD grid was generated by SUPIN. Figure G-4 shows images of the Mach number contours on the symmetry plane and along axial stations from a CFD simulation near the critical design condition. The strong oblique terminal shock wave is shown about the cowl lip and extending into the inlet to interact with the bleed slot. Below the bleed slot the flow there is a supersonic region and shocks that complete the deceleration of the flow to subsonic conditions. Table G-2 lists some properties of the inlet and the performance data obtained from SUPIN and averages of the CFD flowfield at the engine face.

G.3 Sample Cases for Mach 4 Axisymmetric Streamline-Traced Inlets

These sample cases involved two streamline-traced inlets for $M_0 = M_L$ = 4.0 that decelerated the flow to M_{stex} = 1.5. These inlets were introduced in Subsection 10.7. The first inlet used the axisymmetric Busemann parent flowfield (K_{stex} = 0) as discussed in Subsection 10.2. The second inlet used the axisymmetric ICFA-Otto-Busemann parent flowfield (K_{stex} = 1) as discussed in Subsection 10.3. Both inlets used circular tracing curves positioned with their centers coincident with the axis-of-symmetry of the parent flowfields. Thus, the streamlined shapes resulted in axisymmetric inlets. The first inlet with the Busemann parent flowfield creates the classic Busemann inward-turning inlet. Both inlets can be classified as fully internal-compression inlets. The engine face was specified to be circular with a diameter of D_2 = 1.0 ft. The outflow of the inlet was specified to be supersonic (K_{comp} = 3). A constant-area duct was specified downstream of the streamline-traced supersonic diffuser. The geometry of the inlets was shown in Figure 10.9 and is repeated here in Figure G-5. The comparison of the two inlet geometries was discussed in Subsection 10.7 and Figure 10.10 showed images of both inlets together. Inviscid CFD simulations were performed for both inlets and Figure 10.11 showed images of the Mach number contours on the symmetry plane as obtained from those CFD simulations. The simulations mostly verified that the inlet designs established the desired flowfields. For the axisymmetric Busemann inlet, the isentropic supersonic compression was established on the supersonic diffuser and the conical oblique

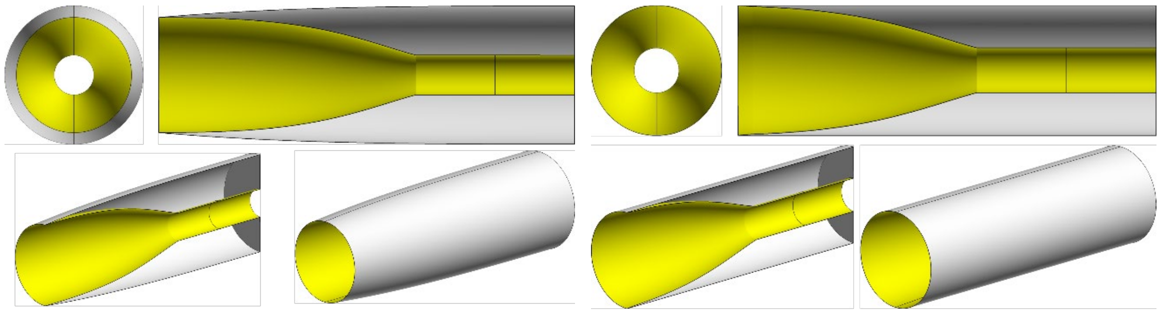

Figure G-5.—Axisymmetric streamline-traced, internal-compression inlets for Mach 4.

TABLE G-3.—STREAMLINE-TRACED, INTERNAL-COMPRESSION INLETS FOR MACH 4.0

K_{stex}	M_0	M_{stex}	A_{cap} (ft^2)	W_{cap} (lbm/s)	Method	M_2	W_2/W_{cap}	p_{t2}/p_{t0}	C_{Dwave}
0	4.0	1.5	6.5793	164.013	SUPIN	1.5000	1.000	0.9192	0.01014
					CFD	1.5340	1.000	0.9435	0.01052
1	4.0	1.5	6.6043	164.636	SUPIN	1.5000	1.000	0.9227	0.00170
					CFD	1.5269	1.000	0.9417	0.00000

shock was formed that intersected the end of the diffuser and start of the constant area duct of the inlet. The axisymmetric ICFA-Otto-Busemann inlet created the leading-edge oblique shock and ICFA flowfield followed by the isentropic Mach waves on the diffuser. The conical outflow shock also intersected the inlet close to the end of the diffuser and start of the constant-area section. For both inlets some differences from the ideal parent flowfield were seen due to the resolution of the grid and numerical effects. Some reflected waves can be seen within the constant-area duct and the flow was slightly greater than the desired Mach 1.5 flow. Table G-3 list some of the geometric properties of the inlets along with performance metrics as computed by SUPIN and inviscid CFD simulations.

Appendix H.—Sample Cases for Scheduling, Flowpath Analysis, and Unit Problem Mode

Several sample cases demonstrate the input factor scheduling, flowpath analysis, and unit problem mode within SUPIN.

H.1 Sample Cases for Scheduling

The scheduling of input factors, which was discussed in Subsection 14.2, is demonstrated by two sample cases involving two-dimensional, external-compression inlets:

- SUPIN.K2.Sched.A. This case designs two-dimensional inlets for a sequence of five freestream Mach numbers from M_0 = 1.4 to 1.6 in steps of 0.05. The schedule also contains two two-factor schedules that set the altitude and engine-face corrected flow rate based on the freestream Mach number.
- SUPIN.K2.Sched.B. This case designs two-dimensional inlets for a sequence of five freestream Mach numbers from M_0 = 1.4 to 1.6 in steps of 0.05 and three freestream altitudes. This creates a total of 15 inlet designs. The schedule also contains two two-factor schedules that set the engine-face corrected flow rate based on the freestream Mach number.

H.2 Sample Cases for the Flowpath Analysis

The quasi-one-dimensional flowpath analysis, which was discussed in Subsection 4.16, is demonstrated by three sample cases:

- SUPIN.K0.FPA.M075. This case is a subsonic inlet with M_0 = 0.75.
- SUPIN.K0.FPA.M170. This case is an external-compression inlet for M_0 = 1.7.
- SUPIN.K0.FPA.M250. This case is a mixed-compression inlet for M_0 = 2.5.

H.3 Sample Cases for the SUPIN Unit Problem Mode

These sample input files use the K_{mode} = 0 capabilities to perform various unit problem calculations using SUPIN. Some of the input files provide examples of the scheduling capability of SUPIN to execute through a range of input factors.

- SUPIN.Km01.in. This case computes the freestream properties for a schedule of altitudes.
- SUPIN.Km02.in. This case computes the freestream properties for a constant dynamic pressure over a schedule of Mach numbers.
- SUPIN.Km03.in. This case computes the approach flow consisting of two ramps of 10 and 8 degrees in a Mach 2.5 freestream.
- SUPIN.Km04.in. This case computes the approach flow for a cone of an angle of 15 degrees in a Mach 2.5 freestream.
- SUPIN.Km05.in. This case computes and writes out the flowfield about a cone of an angle of 15 degrees in a Mach 2.5 freestream.
- SUPIN.Km06.in. This case computes a table of isentropic flow ratios over a schedule of Mach numbers from 0.2 to 2.0.

- SUPIN.Km07.in. This case computes the properties across a normal shock wave over a schedule of Mach numbers from 1.0 to 5.0.
- SUPIN.Km08.in. This case computes the Prandtl-Meyer function and Mach wave angle over a schedule of Mach numbers from 1.0 to 5.0.
- SUPIN.Km09.in. This case computes the freestream properties when the freestream Reynolds number per foot and static temperature are specified.
- SUPIN.Km10.in. This case uses Moeckel's model to compute the stand-off distance for a shock wave from the cowl lip of an axisymmetric inlet for a schedule of inlet flow ratios.

Appendix I.—Quick Reference for SUPIN Factors

DataID	Description	DataID	Description
0	Main Control of SUPIN	16	Components and Entities
1	Freestream Conditions	17	Geometry Transformations
2	Approach Flow	18	Variable Geometry
3	*Capture Cross-Section*	19	Schedules
4	External Supersonic Diffuser	20	*Not assigned*
5	Uniform Cowl Lip	21	*Inlet surface grid input*
6	Cowl Exterior	22	*Vortex generators*
7	Three-Dimensional Cowl Lip	23	Unit Problem Calculations
8	Throat Section	24	Reference Dimension
9	Support Struts	25	Forebody Step Diverter
10	Subsonic Diffuser	26	Forebody Geometry Model
11	Engine Face	27	*Sidewall Geometry*
12	Bleed and Bypass	28	*Auxiliary Intake*
13	Flow Domain and Grid Spacing	29	Global Geometry Transformations
14	Variations	30	Output Summary Table
15	Shoulder Bleed Slot	31	*3D Engine Face*

K_{mode}	Design and Analysis Mode
0	Unit Problem Mode
1	Inlet Geometry Mode
2	Inlet Design Mode
3	Inlet Analysis Mode
4	Inlet Flowpath Analysis Mode

K_{typ}	Type of Inlet
0	Generic Quasi-1D Inlet for Flowpath Analysis
1	Axisymmetric Pitot Inlet
2	Two-Dimensional Inlet
3	Axisymmetric Spike Inlet
4	Two-Dimensional, Bifurcated-Duct Inlet
5	Streamline-Traced Inlet
6	Three-Dimensional Pitot Inlet

K_{comp}	Type of Supersonic Compression
0	Subsonic inlet
1	External-compression inlet
2	Mixed-compression inlet with subsonic outflow
3	Mixed-compression inlet with supersonic outflow

Factor	Input	Description
K_{Winp}	`KWinp`	Flag indicating nature of the flow rate input [0] = 0 no flow rate information specified = 1 specify actual engine flow rate W_2 (F_{Winp} *is* W_2) = 2 specify corrected engine flow rate W_{C2} (F_{Winp} *is* W_{C2}) = 3 specify average engine face Mach M_2 (F_{Winp} *is* M_2) = 4 specify capture flow rate W_{cap} (F_{Winp} *is* W_{cap}) = 5 specify capture area A_{cap} then compute W_{cap} (F_{Acap} *is* A_{cap})
F_{Winp}	`FWinp`	Input for flow rate (see K_{Winp})
K_{Wunit}	`KWunit`	Flag indicated the units of the flow rate = 0 non-dimensional. = 1 slug/s. = 2 lbm/s.
F_{wclip}	`Fwclip`	Width or circumferential extent of the capture cross-section For K_{typ} = 2 and 4, F_{wclip} is the cross-stream width normalized by D_{ref} For K_{typ} = 2 and $F_{wclip} < 0$, $\mid F_{wclip} \mid$ is the capture aspect ratio (w_{cap}/h_{cap}) For K_{typ} = 1, 3 5, and 6, F_{wclip} = 1.0 for full extent of the circumference

Factor	Input	Description
K_{surf}	`Ksurf`	Flag indicating whether the inlet surface grids are calculated [0] = 0 do not calculate the inlet surface grids = 1 calculate the inlet surface grids and output grids in Plot3D format = 2 calculate the inlet surface grids and output grids in STL format = 3 calculate the inlet surface grids and output grids in Plot3D and STL formats
K_{gCFD}	`KgCFD`	Flag indicating whether the CFD grids are to be generated [0] = 0 do not generate CFD grids = 2 generate the two-dimensional CFD grid = 3 generate the three-dimensional CFD grid

Factor	Input	Description
K_{fs}	`Kfs`	Flag indicating the manner of specification of p and T [1] = 1 specify altitude (h_0) and use atmospheric models = 2 specify static pressure (p_0) and static temperature (T_0) = 3 specify total pressure (p_{t0}) and total temperature (T_{t0}) = 4 specify dynamic pressure (q_0) and calculate altitude (h_0) = 5 specify total pressure (p_{t0}) and calculate altitude (h_0) = 6 specify Reynolds number (/ft) and static temperature (T_0)
K_{atm}	`Katm`	Flag indicating the atmospheric model [0] = 0 standard model = 2 hot day model = 1 cold day model = 3 tropical day model

Factor	Input	Description
K_{app}	`Kapp`	Flag for the approach flow [0] = 0 no approach flow conditions are to be set = 1 approach flow is defined by N_{sapp} flow segments = 2 specify the Mach number, total pressure ratio, and angles at station L = 3 use code defined in subroutine `FlowApproachCode` = 4 use freestream conditions for station L
K_{sapp}	`Ksapp`	Flag for the type of flow process for each stage [0] = 1 2D oblique shock wave compression or isentropic expansion = 2 conical shock wave compression = 3 isentropic compression or expansion

Factor	Input	Description
K_{exd}	`Kexd`	Flag indicating how the external supersonic diffuser geometry is created [0] = 0 no external supersonic diffuser is specified = 1 simple quasi-one-dimensional external supersonic diffuser model = 2 single stage ramp or single cone (K_{typ} = 2, 3, or 4) = 3 two-stage ramp or bi-cone (K_{typ} = 2, 3, or 4) = 4 three-stage ramp or triple-cone (K_{typ} = 2, 3, or 4) = 5 three-stage ramp or triple-cone with isentropic second stage (K_{typ} = 2, 3, or 4) = 6 streamline-traced external supersonic diffusers (K_{typ} = 5) = 7 simplified design inputs for planar inlets (K_{typ} = 2, 3, or 4, and K_{mode} = 2) = 8 external supersonic diffuser geometry is specified using entities
p_{tEX}/p_{tL}	`FptEXptL`	Total pressure ratio between stations L and EX
p_{t1}/p_{tEX}	`Fpt1ptEX`	Total pressure ratio between stations EX and 1

Factor	Input	Description
K_{mtexd}	`Kmtexd`	Flag indicating the flow condition to match at the supersonic outflow [0] = 0 do not match a flow property, use stage angles explicitly = 1 F_{mtexd} is the outflow Mach number = 2 F_{mtexd} is the static pressure ratio, p_{EX} / p_L = 3 F_{mtexd} is the flow angle at station EX, θ_{EX} (degrees)
F_{mtexd}	`Fmtexd`	Flow condition value at diffuser outflow to be matched
K_{focal}	`Kfocal`	Flag indicating how focal points are used [0] = 1 use shock-on-lip condition for all focal points (Δy_{focal} = 0 ft) = 2 use the first-stage offset (Δy_{focal}) for all focal points = 3 use specified offsets (Δy_{focal}) for each stage = 4 focal points are linearly interpolated between first and last stage points = 5 the offsets (Δy_{focal}) are specified as a factor of y_{clip} = 6 a single focal point is placed to provide for specified supersonic spillage
K_{nose}	`Knose`	Flag for the shape of the nose [1] = 1 sharp = 2 circular
Fr_{nose}	`Frnose`	Radius of a circular nose (ft)
Fx_{nose}	`Fxnose`	*x*-coordinates for the start of the nose (ft)
θ_{stexd}	`thstexd`	Angle at the end of the stage (deg)
x_{stexd}	`xstexd`	Axial x-coordinate at the end of a stage (ft)
Δy_{focal}	`dyfocal`	Offset in *y*-direction from y_{clip} for focal point for a stage [0.0 ft]

Factor	Input	Description
K_{cwex}	`Kcwex`	Method for constructing the cowl exterior geometry [0] = 0 No cowl exterior is modeled = 1 Create cowl exterior curves using planar NURBS curves = 2 Create cowl exterior curves using planar ogive curves = 3 Create cowl exterior curves using the NACA-1 profile = 4 Use entities to define the cowl exterior (K_{comt} = 18)
F_{xcwex}	`Fxcwex`	Factor for axial placement of the end of the cowl exterior
F_{rcwex}	`Frcwex`	Factor for radial placement of the cowl exterior
θ_{swex}	`thswex`	Angle of the sidewall (deg) (For K_{typ} = 2 and 4 only)

Factor	Input	Description
K_{thrt}	`Kthrt`	Flag indicating the geometry model [0] = 0 no model = 1 quasi-one-dimensional Mach-area flowpath analysis = 2 throat section for an axisymmetric pitot inlet (K_{typ} = 1) = 3 throat section for a three-dimensional pitot inlet (K_{typ} = 6) = 4 throat section for a Mahoney inlet (K_{typ} = 2, 3) = 5 2D and axisymmetric spike, mixed-compression inlets (K_{typ} = 2, 3, 4) = 6 2D and axisymmetric spike, mixed-compression inlets using MOC (K_{typ} = 2, 3, 4) = 7 throat section for a streamline-traced inlet (K_{typ} = 5) = 8 throat section geometry is specified using entities = 9 throat section for external-compression 2D and axi-spike inlets (K_{typ} = 2, 3, 4)
p_{tsegA}	`FptsegA`	Ratio of total pressures for segment A
p_{tsegB}	`FptsegB`	Ratio of total pressures for segment B
p_{tsegC}	`FptsegC`	Ratio of total pressures for segment C

Factor	Input	Description
K_{subd}	`Ksubd`	Flag for the model of the subsonic diffuser [0] = 0 undefined. Subsonic diffuser is not modeled. = 1 simple quasi-one-dimensional subsonic diffuser model (All inlets). = 2 subsonic diffuser for axisymmetric pitot inlets (K_{typ} = 1). = 3 subsonic diffuser for an axisymmetric spike inlet (K_{typ} = 3). = 4 subsonic diffuser for a two-dimensional inlet (K_{typ} = 2). = 5 subsonic diffuser for a two-dimensional, bifurcated-duct inlet (K_{typ} = 4). = 6 subsonic diffuser as a sequence of super-elliptical cross-sections. = 7 subsonic diffuser as a network of NURBS curves (K_{typ} = 5 and 6). = 8 subsonic diffuser for a rectangular engine face (K_{typ} = 2, K_{thrt} = 8). = 15 entities for centerbody and cowl interior components (K_{comt} = 16 & 17).
K_{Lsubd}	`KLsubd`	Flag indicating how the length of the subsonic diffuser is computed. = 1 $F_{Lsubd} = L_{subd}$ (ft) = 2 $F_{Lsubd} = L_{subd} / D_{ref}$ = 3 L_{subd} is computed as the distance between x_{SD} and the specified value of x_{EF} = 4 L_{inlet} is specified (F_{Lsubd}) and L_{subd} is remaining distance between x_{SD} to x_{EF} = 5 L_{subd} is computed based on cross-sectional areas and conical angle θ_{eqsd}
F_{Lsubd}	`FLsubd`	Input defining the length of the subsonic diffuser (value based on K_{Lsubd}).
θ_{eqsd}	`theqsd`	Equivalent conical angle of the subsonic diffuser (deg)
p_{t2}/p_{tSD}	`Fpt2ptSD`	Factor specifying the total pressure ratio within the subsonic diffuser

Factor	Input	Description
K_{sdprp}	`Ksdprp`	Property establishing the area distribution [0]. = 0 no area distribution is used. = 1 specify the axial distribution of the cross-sectional area. = 2 specify the axial distribution of Mach number. = 3 specify the axial distribution of static pressure.
K_{sdvar}	`Ksdvar`	Type of variation [0]. = 0 no area distribution is used. = 1 linear variation. = 2 cosine-sine-squared variation. = 3 four-point NURBS variation with 1/3rd weighting.

Factor	Input	Description
K_{xEF}	`KxEF`	Flag for determining x_{EF} [2] = 1 x_{EF} is an input through F_{xEF} (ft) = 2 x_{EF} is placed at the end of the subsonic diffuser
F_{xEF}	`FxEF`	Input for the axial position of the center of the engine face (ft)
K_{yEF}	`KyEF`	Flag for determining y_{EF} [3] = 1 y_{EF} is specified by F_{yEF} (ft) = 2 y_{EF} is the offset from y_{inlet} by the value of F_{yEF} (normalized by D_{ref}) = 3 $y_{EF} = y_{inlet}$ = 4 y_{EF} is computed to reduce cowl drag (K_{typ} = 2) = 5 y_{EF} is placed to make flat top for subsonic diffuser (K_{typ} = 2) = 6 $y_{EF} = y_{SD}$, center of station SD (K_{typ} = 2, 5, 6) = 7 $y_{EF} = y_{SD} + F_{yEF}\, L_{subd}$. So, $F_{yEF} = \Delta y_{EF} / L_{subd}$. ($K_{typ}$ = 2, 5, 6)
F_{yEF}	`FyEF`	Input for the vertical position of the center of the engine face
θ_{EF}	`thetEF`	Angle of the engine face within the (x,y) plane about the z-axis (deg)

Factor	Input	Description
K_{EF}	`KEF`	Flag for the cross-sectional, planar shape of the engine face [1] = 1 circular engine face = 2 circular engine face with a spinner or centerbody (co-annular) = 3 super-elliptical engine face = 4 rectangular engine face
D_{EF}	`diamEF`	Diameter of a circular or co-annular engine face (ft) [1.0]
r_{hub} / r_{EF}	`HubTip`	Ratio of the radii of the hub to the tip of a co-annular circular engine face
a_{seEF}	`aseEF`	Length of semi-major axis of super-elliptical engine face (ft)
AR_{seEF}	`ARseEF`	Aspect ratio of a super-elliptical engine face ($AR_{seEF} = a_{seEF} / b_{seEF}$)
p_{seEF}	`pseEF`	Parameter for super-elliptical engine face
h_{EF}	`hEF`	Height of a rectangular engine face (ft)
w_{EF}	`wEF`	Width of a rectangular engine face (ft)

Factor	Input	Description
K_{spin}	`Kspin`	Flag for the shape of the nose of an axisymmetric spinner [3] =0 no spinner =1 conical spinner (specify θ_{spin}) =2 circular spinner ($r_{spin} = r_{hub}$) =3 elliptical ($b_{spin} = r_{hub}$, specify AR_{spin}) =4 conical spinner with circular nose (specify r_{spin} and θ_{spin})
θ_{spin}	`thspin`	Half-angle of the conical spinner (deg) (K_{spin} = 1 and 4)
Fr_{spin}	`Frspin`	Fraction for the nose radius of a conical spinner, $Fr_{spin} = r_{spin} / r_{hub}$ (K_{spin} = 4)
AR_{spin}	`ARspin`	Aspect ratio of the spinner ($AR_{spin} = L_{spin} / b_{spin}$) [2.0] (K_{spin} = 3)

K_{comt}	Component Description	K_{comt}	Component Description
1	External Supersonic Diffuser	14	*Engine Face*
2	*External Diffuser Sidewall*	15	*Spinner*
3	*Capture Cross-Section*	16	Centerbody
4	*Cowl Lip Interior*	17	Cowl Interior
5	*Cowl Lip Exterior*	18	Cowl Exterior
6	*Throat Section Duct*	19	*Bleed Slot and Plenum*
7	Throat Section Centerbody	20	*Support Struts*
8	Throat Section Cowl Interior	21	*Outflow Nozzle*
9	*Throat Section Sidewall*	22	Planar Forebody
10	*Subsonic Diffuser Duct*	23	
11	Subsonic Diffuser Centerbody	24	
12	Subsonic Diffuser Cowl Interior	25	
13	*Subsonic Diffuser Sidewall*	26	

K_{ent}	Entity Type	K_{ent}	Entity Type
0	Point	13	Cosine-Sine Curve
1	Line	14	Cosine-Sine-Squared Curve
2	Circular Curve	15	Annular Cross-Section
3	Ogive Curve	16	Super-Elliptical / Rectangular Cross-Section
4	Elliptical Curve	17	NURBS Cross-Section
5	Super-Elliptical Curve	18	*Transfinite Interpolation (TFI) Surface*
6	NACA-1 Series Curve	19	*NURBS Surface*
7	Polynomial Curve	20	
8	Piecewise Linear Curve	21	
9	Fitted Cubic Spline Curve	22	
10	NURBS Curve	23	
11	Four-Point NURBS Curve	24	
12	*Fitted NURBS Curve*	25	

Factor	Input	Description
K_{comt}	`Kcomt`	Type of component (see Table 4.33)
N_{ents}	`Nents`	Number of entities in the component
K_{part}	`Kpart`	Flag for further defining the component
K_{ent}	`Kent`	Type of entity (see Table 4.34)
K_{trf}	`Ktrf`	Pointer to the geometric transformation information for an entity (=0, none)
K_{vgm}	`Kvgm`	Pointer to the variable geometry schedule for an entity (=0, entity is static)
N_{cps}	`Ncps`	Number of control points for the entity

Factor	Input	Description
K_{stex}	`Kstex`	Type of parent flowfield used for streamline tracing = 0 Axisymmetric Busemann flowfield = 1 Axisymmetric ICFA-Busemann flowfield = 2 Two-dimensional wedge flowfield
M_{stex}	`Mstex`	Mach number at the outflow of the parent flowfield
F_{stle}	`Fstle`	Slope at the leading edge of the streamline-traced surface (deg)
F_{strunc}	`Fstrunc`	Factor for the truncation of the axisymmetric Busemann flowfield